# ANALYSIS OF SHEAR WALL COUPLING BEAMS

# WITH TWO TYPES OF REINFORCEMENT

by

**SADDEK ABID, Ingeniorat, MSc.**

**THESIS SUBMITTED TO HERIOT-WATT**

**UNIVERSITY FOR THE DEGREE OF**

**DOCTOR OF PHILOSOPHY**

**December 1995**

**Faculty of Engineering**

**Department of Civil and Offshore Engineering**

**Heriot-Watt University**

# CERTIFICATE OF RESEARCH

This is to certify that except where specific reference to the other investigations is made, the work described in this thesis is the result of the investigation carried out by the candidate.

Supervisor Mr. David Haldane

# DEDICATION

To my father (may Allah bless his soul) and my family

# ACKNOWLEDGEMENTS

I wish to express my appreciation for the way in which my supervisor Mr. David Haldane has contributed to the completion of this thesis. His continual help, guidance, encouragement and many useful discussions have made the completion of this project possible.

My many thanks are due:

To Dr. A. Irwin for his continual help and to the head of the Department of Civil and Offshore Engineering, for providing the various facilities.

To the Algerian Government and British Council for their financial support.

To the technical staff in the workshop for their support during the laboratory based part of this programme of research, in particular Graham Sorley and Stevie Ritch.

Finally I would like to thank my family and my wife for their encouragement, understanding and for their constant moral support during this project.

# Contents

# List of Tables

# List of Figures

# Notations

Linear Dimensions

| | |
|---|---|
| $a_1$ | Distance between the centroids of the two sections of shear walls. |
| $a_2$ | Distance between the centre lines of the connecting beams |
| $L_1$ | Cantilever length of shear wall |
| $L_2$ | Clear span of the connecting beams |
| $A_1$ | Cross section of each shear wall |
| LW | Longitudinal dimension of the expanded metal mesh |
| SW | Transversal dimension of the expanded metal mesh |
| W | Width of strand of the expanded metal mesh |
| $ts$ | Thickness of the strand from the expanded metal mesh |
| n | Number of strands crossing the diagonal crack |
| L | Shear span of the beam |
| L-1/L-2 | Dimensions of the two end blocks |
| b | Span of the coupling beams |
| d | Depth of the beam |
| t | Thickness of the specimen |
| H | Height of the end blocks |
| h' | Effective height of the beam |
| l | Effective length of the beam |
| bw | Width of the rectangular beam |

## Moments, Forces and Parameters

| | |
|---|---|
| $q_x$ | Laminar shear force |
| $V_x$ | Shear forces in the coupling beam at location x |
| $M_a$ | Applied bending moment |
| $M_c$ | Moment corresponding to shear failure |
| $M_f$ | Flexural capacity of the beam |
| Pv,Ph | Vertical and horizontal contributions of the web reinforcement |
| Pm,Td | Contribution forces of the expanded metal mesh and diagonal bars |
| V | Shear force in compressive corners of the beam |
| H,Vs | Horizontal and vertical components of the web splitting force |
| C | Crushing strength of the concrete |
| Va | Maximum applied load |
| $Q_{flex}$ | Flexural capacity |
| $Q_{shear}$ | Shear capacity |
| $Q_u$ | Ultimate capacity of the beam |
| $\alpha$ | Geometry parameter used in laminar analysis |
| $\rho$ | Density of steel |
| $\alpha_c$ | Angle of the assumed crack with the horizontal |
| $\beta$ | Angle of the expanded metal mesh with the horizontal |

Areas and Stresses

| | |
|---|---|
| $I_1$ | Moment of inertia of each shear wall |
| $S_1, S_2, S_3$ | Areas of the expanded metal mesh used as stirrups |
| $A_{st}$ | Area of stirrup reinforcement |
| $A_d$ | Area of the diagonal reinforcing bar |
| $A_m$ | Area of the strand of the expanded metal mesh |
| Ah | Area of web reinforcement (Vertical) |
| Av | Area of web reinforcement (Horizontal) |
| z | Lever arm |
| E | Young's modulus |
| f'cu | Cube strength of concrete |
| f'cu | Cylinder strength of concrete |
| f'y | Yield strength of longitudinal bars |
| f'u | Ultimate strength of longitudinal bars |
| $f'y_{st}$ | Yield strength of stirrup steel |
| $f'u_{st}$ | Ultimate strength of stirrup steel |
| $f'y_m$ | Yield strength of expanded metal mesh steel |
| $f'u_m$ | Ultimate strength of expanded metal mesh steel |
| $f'y_d$ | Yield strength of diagonal bars |
| $f'u_d$ | Ultimate strength of diagonal bars |
| $f_{tc}$ | Tensile strength of concrete |

## Abstract

This project was undertaken as an attempt to obtain improvements in the strength of coupling beams between shear walls and in particular to investigate ways of suppressing the shear mode of failure. The tests mainly addressed the influence of the use of expanded metal mesh and its positioning within coupling beams, with a range of shear span to depth ratios.

The development of effective design procedures for this type of reinforcement was also addressed in the investigation. The investigation included tests on thirteen large scale models, in which a number of different reinforcement arrangements were examined in the coupling beams whose shear span to depth ratios were in the range from 1.1 to 2.0. The test specimens were carefully instrumented and tested under reversed cyclic loading in order to produce large post-elastic deformations.

Two beams in each test series were reinforced with four additional diagonal reinforcement bars which intersected at midspan. The diagonal reinforcement bars were intended to supplement the strength of the web reinforcement which consisted mainly of either stirrups or expanded metal mesh.

The introduction of the two different forms of reinforcement was intended to be consistent with the perceived system of internal forces. The combination of expanded metal mesh and diagonal reinforcement bars in the beam was found to be effective and resulted in the development of a reinforcement arrangement which was superior to those in current use. The investigation also addressed the development of an analytical approach to predict the ultimate load which can be sustained by the beams. The approach which was developed was based on the approaches put forward by Kotsovos and Subedi.

The results obtained confirmed both the applicability and effectiveness of both approaches in the context of coupling beam structures.

# Chapter 1

# SHEAR WALLS IN TALL BUILDING STRUCTURES

## 1.1 INTRODUCTION

Structural engineers have long recognised the usefulness of wall systems in the overall planning of multistorey buildings. The positioning of such wall systems either externally or internally can lead to structures which are extremely efficient in resisting lateral loads originating, from either storms or earthquakes, in addition to their other functions such as transmission of vertical loads, weather protection and insulation.

The more sophisticated science and technology becomes the greater the requirement for more precise information to be obtained from research in order to maximise economy and efficiency in engineering design. The development of the high-rise construction industry has transpired partly because of the prestigious nature

of such developments and partly for egoistic purposes, however, the main driving force is the necessity to utilize the full potential of available land. This trend in multistorey building has helped solve some problems of urbanisation, such as the increasing use of various types of tall buildings for compactness of office accommodation, for residential housing and, in some instances, for industrial manufacturing processes. The performance of coupled shear wall structures in high rise buildings has been studied by a number of researchers. Most of these studies have focussed attention on the elastic behaviour of these major lateral load resisting structures. To evaluate the full potential of shear wall structures it is necessary to examine their post-elastic behaviour since during severe ground motion the attainment of the ultimate capacity and subsequent elasto-plastic energy absorbing deformations become a reality. Therefore, it is necessary to quantify the magnitudes of the post-elastic deformations in the elements of the structure at various stages leading up to their ultimate capacities in order to facilitate accurate analysis of the coupled wall units in survival conditions. In recent years there has been a rapid increase in the number of tall buildings under construction for both commercial and residential purposes throughout the world and especially in areas prone to high winds and earthquakes. This increase has highlighted the necessity for a greater knowledge of the behaviour of these structures and, in particular, the necessity to develop methods of analysis capable of giving rapid and accurate assessment of their overall strength and stiffness as well as detailed information about any local stress concentrations. The behaviour of reinforced concrete members and structural systems under various loadings has been the

subject of intensive investigation since the beginning of the present century. The present-day design methods continue, in many respects, to be based on empirical approaches which use the results from a large number of laboratory based investigations because of the complexities associated with the development of rational analytical procedures. In spite of hundreds of research investigations, no fully rational method for shear design has been developed. Codified methods continue to include expressions for shear resistance based on fitting curves to results obtained from laboratory based investigations. Such an approach has been necessary in the past, and may continue to be the most convenient for ordinary design. The finite element method can offer, however, a powerful and general purpose analytical tool for studying the behaviour of reinforced concrete members and can be used to analyse many effects previously ignored or treated in a very approximate way. Nevertheless, there is a continuing need for laboratory based research both to provide a firm basis for empirically derived relationships and to provide much needed information for the validation of the more refined analytical methods. It is also necessary to obtain laboratory derived information on material properties and on the behaviour at interfaces between materials, since both of these aspects represent fundamental input data for the analytical approaches.

## 1.2 AIM OF THE RESEARCH PROGRAMME

This programme of research was aimed at advancing the understanding of the behaviour of shear wall structures subjected to combined vertical and severe lateral loadings.

The principal aim of the work was to formulate a reliable method for the prediction of the elastic and plastic behaviour of coupling beam structures containing four different approaches to the detailing of the reinforcement. The next task which was undertaken was to examine experimentally how reinforced concrete coupling beams would behave and how they could meet the demand for strength when reinforced with either expanded metal mesh or conventional reinforcement. Included in this aim was the requirement to provide suitable performance criteria for use with the coupling beams reinforced with the expanded metal mesh such that they could be incorporated in normal design procedures.

Three groups of four coupling beams were tested to examine the influence of the variations in the span to depth ratios of the beams, the percentage of conventional beam reinforcement present, and the amount of expanded metal mesh reinforcement included in the beams when subjected to lateral reversed loading.

## 1.3 LAYOUT OF THESIS

The programme of research, which is the subject of this thesis, has been presented in eight Chapters. The introduction and the overall objective of the study is given in Chapter 1. A review of the literature relating to coupling beams in shear wall structures is described in Chapter 2.

Chapter 3, contains details of the test specimens, loadings and the properties of the materials used in the laboratory based investigation. It also includes a description of the test procedures which were adopted.

Chapter 4, describes the analytical work which was based on the ultimate strength

analysis of the two types of specimens containing the different forms of reinforcement using the Compressive Force Path concept [1] and the approach put forward by Subedi [2].

Chapter 5, contains the analysis and the discussion of the experimental results obtained from the eight coupling beams with different span to depth ratios and different percentages of reinforcement. Particular attention was made to the failure mechanisms experienced in each case.

Chapter 6, presents in detail the results from the tests on the two beams, with the same span to depth ratio, reinforced with the two types of steel (conventional and expanded metal mesh). The test programme investigated the principal aspects of the behaviour of the coupling beams. Correspondingly the behaviour of the flexural reinforcement over the entire span, and that of the web reinforcement over the major portion of the depth of the beams, has been assessed. The compression strains in the cracked and uncracked concrete were also measured in the specimens. The deformations, rotations, elongations, transverse expansions and the deflections of the beams were determined during three loading cycles.

The development of the cracks is discussed and the nature of the failure mechanism is presented.

Chapter 7, contains a comparison between the results obtained from the laboratory based investigation and the analytical investigation for all the test specimens.

In Chapter 8, a summary is given of the major points of discussion together with the conclusions which have resulted from the study. Recommendations for further research are also presented in this Chapter.

Finally, three Appendices have been included at the end of the thesis. Appendix A contains a photograhic record of significant parts of the investigation. Appendix B describes in detail the application of the two analytical approaches to the design and analysis of the coupling beams. Appendix C contains the results, in tabular form, obtained during the first and second loading cycles.

## 1.4 PRESENTATION OF THE RESULTS

In general the results from the laboratory based investigation have been presented graphically rather than in tabular form. Wherever possible a comparison is drawn with existing theories. In order to achieve a concise presentation, only the essential and typical laboratory based results are reproduced here. However, all the evidence necessary to make valid conclusions within the scope of the project has been provided.

To enable the reader to examine easily the results and their quantitative interpretations while reading the text, all the relevant illustrations and Figures have been presented at the end of each Chapter. The photographs are presented in Appendix A.

## 1.5 PROBLEMS ASSOCIATED WITH COUPLED SHEAR WALLS

There are many problems associated with the analysis and detailed design of coupled shear wall structures. Multistorey buildings are continually being designed in taller and more slender forms, incorporating coupled shear wall structures, which often emerge as the critical design item. New building techniques, such as lift slab construction, often rely entirely for stability on the lateral stiffness and strength of shear walls.

It has also become evident that the accepted methods of structural analysis used in the design of rigid jointed frames are inadequate for the accurate analysis of complex shear wall structures.

Deformation due to axial and shear stresses, which were thought of as being insignificant in comparison with flexural deformations in beam and column structures, must be taken into account. This has necessitated the search for new techniques to provide accurate analysis of coupled shear wall structures, while making only manageable demands on computational time and other resources required from a design office.

Deep structural members, such as coupling beams, do not obey the laws of classical flexural theory. To avoid cumbersome stress functions in the assessment of the nonlinear stress patterns in deep members, more attention has been directed towards photoelastic methods in structural model studies. Unfortunately the validity of the results from such studies are often limited to a specific structure.

Theoretical or experimental results, however successful the projects are from which they originated, still need to be related to the actual structural material to be used. Since the majority of tall buildings use reinforced concrete as the primary construction material, attention is focussed on another source of problems associated with the relationships used in the classical methods of elastic analysis, namely the behaviour of cracked reinforced concrete members under load.

## 1.6 STRUCTURAL SYSTEMS FOR TALL BUILDINGS

Early structural systems, utilizing frames, gave good stability at an economical cost for structures of moderate height. These frames however, required columns and beams of large proportions for tall reinforced concrete building structures which resulted in a requirement for high percentages of expensive reinforcing steel. The extent of column free space required in office buildings is another demanding requirement.

Various steel frame designs have been used in tall building frames and often these structures rely on shear cores for stability. The idea of utilizing shear walls in tall structures is not new, in fact European engineers pioneered the construction of residential apartments of up to 20 storeys. In the early 1920's these buildings, comprising cross walls and floors for the basic structures, were used to house those rendered homeless by the first World War. This form of construction lends itself to the utilisation of precast units, or sliding shutter-methods, for speedy erection

of the cross walls and floors, which combine to form an efficient system for the resistance of horizontal and vertical forces, division of space, acoustic and fire insulation.

For weight saving, economy of materials and the provision of reasonable open shells for periodical reorganisation of the interior, staggered shear walls or wall beams have been combined with bracing provided by service shafts for building structures of up to 40 storeys.

Top-down or suspended floors construction has been developed and used for structures of up to 35 storeys thus making full use of the strength of the concrete in compression and steel in tension.

Framed tube buildings can provide spacious office accommodation and sufficient lateral stiffness to resist environmental loadings for up to 40 storeys in elevation and many such buildings are now in existence. In this type of construction, the exterior columns are very closely spaced and joined with rigidly connected spandrel girders resulting in a rigid exterior wall to provide lateral stability.

Tube in tube buildings in which the service core is used to resist lateral loads thus absorbing the shear forces and the perimeter columns or mullions acting as the flanges of the beam to resist the bending moments have been constructed to more than 70 storeys.

The demand for very tall buildings in excess of 100 storeys has resulted in the development of several new structural systems such as the cantilevered core, pierced tube, braced frame and bundled tubes structures. The structural design process for tall buildings was developed in response to a wide range of imposed condi-

tions and restraints. The final solution must be practical, utilitarian, aesthetically acceptable and in many cases will result in a building comprising several of the structural forms mentioned above interacting with each other to resist all the imposed loads.

Figures 1.1 and 1.2 show several basic forms of the structures used in tall buildings.

## 1.7 SHEAR WALL CONSTRUCTION IN SYSTEM BUILDINGS

In seismically active areas, the structure must be designed and constructed in such a manner that it will be able to resist moderate loadings without suffering significant damage and also be able to resist severe loadings without complete collapse.

The current interest in shear wall construction is derived from two factors:

- The realisation that for economy in building construction every element must be used as efficiently as possible.

- The increase in system or "industrialised" building.

The first factor has led to the widespread use of shear walls in high rise apartment buildings. In these buildings partition walls must be solidly constructed to provide the necessary fire and sound resistance and for economy the walls are also

used to carry vertical and lateral loads.

The second factor has resulted in the increased use of precast concrete elements. In this type of construction tension joints are difficult to form, although many methods have been used, such as conventional lapped reinforcement, welded or bolted connections, and prestressing tendons. Efficient horizontal and vertical shear transfer is also difficult in precast construction.

All of these methods tend to become complicated and expensive. A wall system, in which vertical compressive stresses are always greater than tensile stresses due to bending under lateral loads, will avoid the necessity for tension joints and is likely to be more economical than a framed structure.

The speed of construction of shear wall buildings is normally controlled by the concreting and subsequent depropping of the floor slabs. Props must be left in place until the slab has achieved adequate strength to resist further propping and construction loads. Where speed is important, permanent formwork methods are often used. Composite steel-concrete framed structures surrounding service cores, are especially popular in northern areas of the U.S.A.

The use of repetitive structural elements which maintain uniform dimensions throughout a building, has created a demand for more sophisticated formwork using larger, re-usable assemblies.

Prefabricated and prestressed elements are widely used to simplify and reduce shuttering and are available in a variety of shapes. These include rectangular, T or double T shaped joists, flat or ribbed slab panels, spandrel beams, facade panels, flights of stairs and many other panels for structural and non-structural

units.

Erection procedures using new types of equipment such as creeper stiff-leg derricks and tower cranes, have reduced the time and the cost of construction.

The most common method of erecting steel framed structures is the tier by tier method in which each tier represents a column height of two or three building floors. Some medium height structures have been erected using "push up" construction. In this process the top floor is erected first at about ground level, jacked upwards, and additional steel placed underneath and attached to the previously completed floor slab.

Hybrid frame construction offers an unlimited combination of concrete and steel frames. Such structures can have a steel frame braced by concrete cores; concrete cores and walls with steel floor framing; and many other combinations.

In top down construction a concrete core is first constructed and the floor systems are subsequently suspended from the core top. In this form of construction, creep and shrinkage in the concrete and differential expansion are especially important. Allowances must be made for tolerances permitted in both steel and concrete construction when designing connections in these hybrid structures.

## 1.8 SERVICE SYSTEMS

The service system for tall buildings are mainly:

- Mechanical system;

- Electrical system;
- Safety system;
- Other technical services: water supply systems, plumbing systems, sewerage and draining systems, cleaning and waste disposal system.

The technical development and the standard of all these service systems, and their influence on tall building construction has to be part of the architectural layout at the very preliminary design stage of the architectural and structural concepts. Of these, vertical transportation is of prime importance, without elevator transportation, high rise buildings would be impractical and uneconomical. The structural concept, floor plan layout and architecture in general are strongly influenced by the elevator core systems and their inherent space requirements. As the height of the building increases, the conventional elevator rapidly becomes inefficient due to limited elevator speeds and increasing core area. This necessitates the use of some other cost effective transport system. A double-deck elevator system has been used effectively but has the disadvantage that all floor to floor heights must be exactly the same in order to permit accurate floor leveling.

Technology offers a wide choice of heating, ventilation and air-conditioning systems, energy sources and distribution schemes, suitable for tall buildings. The optimum combination for any particular building is dependent on the potential use of the building, for example; apartments, offices, manufacturing facilities, laboratories, hospitals or a combination of several of these functions. The general design of environmental systems such as those mentioned above, although more

complex, is not vastly different from that of other buildings. There are several features which require special consideration due to the height of the structure and they are; the hydrostatic pressure on piping systems and equipment; the exhaust air flows, the weight and space requirements of vertical risers and location of the mechanical plant. None of these problems have proved insurmountable but may become more significant with future generations of taller buildings. Fire-safety is one of the major criteria for the planning design and management of high rise buildings.

## 1.9 LOADINGS AND BEHAVIOURAL CHARACTERISTICS

In contrast to low-rise buildings where the dominant loadings are vertical dead and live loadings. Horizontal loading often assumes greater importance than vertical loadings in tall building structures.

It is convenient to divide the principal force actions on shear walls in buildings into the following three main groupings:-

- **Loadings**: construction loads, dead loads, imposed loads, impact loads, earth pressures, liquid pressures, dynamic loads from internal and external sources, collision loads, internal and external blast loads, fire and chemical attack and loadings from debris.

- **Environmental actions**: snow, icing, wind, earthquake.

- **Constraints**: creep, shrinkage, temperature, settlements.

In the assessment of the action of these forces in limit state design we require to know the principal characteristic value in each case. This is defined as the magnitude of that force which has a selected probability of being exceeded during the useful life of a structure. This is difficult to apply if insufficient data is available or if unusual loadings are likely to be encountered. In load factor design for limit states, combinations of characteristic values multiplied by their load factors are used and for conditions where temporary overstress is allowed then load factors of less than unity may apply.

### 1.9.1 Loadings

Shear wall structures are subjected to several types of loading and are summarised as follows:

- **Dead loads**: Contrary to popular belief dead loads acting on shear walls are frequently not easily determined accurately.

  Variations in formwork and site control give deviations of (+) or (-) 6 to 12 mm from plan dimensions which results in differences from predicted loadings as do additions or alterations to the design of fixings and services late in the design process or even during construction. Questions also arise such as, what are the contributory dead loading areas for a wall and where it is not specified by the appropriate Code, are partitions to be regarded as live or dead loadings since these may be moved, removed altogether or added too. Many of these factors are taken into account in arriving at load

factors for design but their influences on the dynamic response may cause problems in response predictions.

- **Construction loads**: Normal construction forces include shoring, pouring and support of in-situ units and attachment of services and fixings but often the most severe forces arise from concentrated storage of materials such as reinforcement. This form of loading is only temporary but may be much greater locally than the design live loading. It is doubly severe considering the fact that design life loads may be fully realised rarely in the life of a structure and generally only act some months after pouring of the concrete when it has achieved a strength somewhat greater than its 28 day design strength whereas construction storage loads may closely follow the stripping of formwork. Loading on shear walls can also arise from construction tolerances resulting in the structure being out-of-plumb. This can cause both in-plane and out-of-plane bending of walls and could affect structural stability. There is also the possibility of the cumulative addition of fabrication tolerances resulting in bending and axial force actions on shear walls.

- **Live loads**: Imposed floor loadings stipulated in Codes of Practice usually consist of uniformly distributed and concentrated loads. In some Codes it is not made clear if these loads are intended to be applied concurrently or not. The intensity of prescribed loading depends upon the use of the building and in cases of change of use a reappraisal of the structure may be required.

Again a difficulty with live loading is the estimation of the areas which contribute to the vertical loading on particular walls. Vertical force actions can also result in bending of the walls within a building due to the transfer of forces from slabs to beams and from uneven vertical load distribution causing differential axial movements of vertical load bearing elements.

- **Impact loads**: An impact load is defined as a single collision of a mass in motion with a second mass which may either be in motion or at rest. Impact loads on shear walls can arise simply by movement of equipment, personnel or elevators. Their effect on a structure depends upon the magnitude of the force, structural stiffness and damping. A collision represents a major impact loading.

- **Dynamic loads** External dynamic loadings arise from either traffic, piling or similar operations while internal sources of dynamic loadings include air flows, out of balance motors and repetitious manufacturing or duplicating processes. Estimation of such forces and the frequency of the force input and even the source of dynamic input are often difficult to determine therefore bases and footings for motorised machines in buildings should be isolated or damped. To avoid vibration input to the building from known external sources isolated footings may be used. In many Codes, static loadings are factored upwards to take account of dynamic effects and this approach often works but resonance movements and vibration associated noises can result in adverse comments from occupants of buildings.

- **Earth pressure**: This form of loading may act on shear walls at basement levels. It is largely dependent upon the soil type and the prevailing conditions. It generally takes the form of out-of-plane bending and shear in walls resulting from back filling which is additive to the effects caused by shrinkage of the first storey slabs, active pressure on basement walls or negative earth pressures bending basement floors and the effects being transferred to the walls or to the base of the wall.

- **Blast loads**: External blast loads from an underground source cause both horizontal and vertical vibrations to the foundations of a building. The amplitudes of vibration may be magnified by structural action. Surface blasting causes initial ground motion to be input to a structure followed by air pressure waves. Internal blast loadings have been the subject of recent studies [3] following actual occurrences of destructive blasts in shear wall buildings. These studies have shown that large negative floor loads can result and provisions for alternate load paths are required to cater for the possibility of wall blow out.

- **Fire**: Much of the available fire load and temperature data is based on wood fire studies and complete burn-out of a room or the contents of the building. This data base is generally in need of updating. Fire resistance is mostly described in terms of protection times for a given wall thickness and percentages of reinforcement and cover to reinforcement. A two-hour fire rating is a common requirement for shear walls and four hours may

be required in certain structures where shear walls enclose arterial escape routes.

- **Chemical attack**: This form of loading may arise in shear walls resulting in a reduction in strength caused by internal alkali attack on the matrix or from adverse external atmospheric pollution often combined with alternating wet/dry conditions. Such attacks can result in spalling of the concrete cover and in extreme cases in subsequent buckling of the compression steel if it is not totally bound by horizontal reinforcement.

- **Loading from debris**: This form of loading results from the falling of floor slabs and imposed loads onto parts of a structure which remain intact after a blast, collision, earthquake or other occurrence which has resulted in partial failure of a structure. For example blow out of a wall section may cause debris from the storeys above to fall onto the floor at the level of the occurrence thus causing an impact load in addition to the added mass.

## 1.9.2 Environmental Effects

### Behaviour of Shear Wall Structures During Earthquakes

Over the last few years it has been shown [4], [5], [6] and [7] that coupled shear walls can be used in buildings to restrict lateral drift and to minimise earthquake damage and repair costs. This has been proved during the earthquakes at Hicheng in China in February 1975, Mexico in 1985 [8], and in Armenia in 1988.

These examples and more have demonstrated that the twin requirements of safety

and damage control can be improved by utilisation of the strength and stiffness inherent in well designed and constructed shear walls.

Earthquakes are one of natures greatest hazards to life on this planet. It is evident that even the successful prediction of such occurrences cannot eliminate the earthquake hazard. Even if all the people are evacuated safely it is often the structures which largely determine the standard of living of the community. Destruction of the building can thus be a disastrous loss to the economy of the region. Also it may not be practical to evacuate a whole region.

This aspect of earthquakes can be countered only by the design and construction of earthquake resistant structures. Even a completely successful earthquake prediction programme would not eliminate the need for effective earthquake engineering. On the other hand, with the effective application of earthquake engineering knowledge, the collapse of structures and the resulting hazard to life can be avoided or at least minimised.

Two characteristics, considered essential in structural design for the resistance to seismic forces, are:

- The ability to sustain high deformations without appreciable loss of strength or the provision of sufficient strength to resist the seismic forces with minimum damage at low deformations in stiff structures.

- The ability to dissipate as quickly as possible high levels of input energy.

The analysis and design of tall buildings in a seismically active area depends on the local surface and the nature of the earthquakes in the area.

The design is normally dependent on the premise that the walls supporting gravity loads will be the last ones to be damaged. Several studies involving coupled shear walls have indicated that in order to achieve this, much higher stiffnesses are required by individual structural members especially beams coupling shear walls. The coupling beam, which is the weak point in shear wall structures, needs to be very stiff and ductile to ensure that it can sustain the significant level of shear forces which need to be transferred by them during such loading cycles.

## Earthquake Characteristics

Following a major earthquake, it is usually possible to retrace the build up and dissipation of the stored energy through the record of seismic shocks and tectonic movements over an extended period. This period may cover several weeks or even years, and the record will usually show several shocks preceding and following the major one. Some of the minor shocks may be of significant magnitude themselves, as well as being the foreshocks and aftershocks of the major earthquake. The major earthquake is usually rather short in duration, often lasting only a few seconds and seldom more than minute.

During the general earthquake, there are usually one or more major peaks in the magnitude of the motions. These peaks represent the maximum effect of the earthquake. Although the intensity of the earthquake is measured in terms of the energy release at the location of the ground fault, the critical effect on a given structure is determined by the ground movements at the location of the structure.

Modern recording equipment and procedures for the interpretation of such data provide representations of the ground movements at various locations. This allows the simulation of the effects of major earthquakes.

Although it may seem like a gruesome way to achieve it, we advance our level of competency in design every time there is an earthquake which results in some major structural damage to buildings as well as from structures which successfully resist such an event. Engineering societies and other groups routinely send investigating teams to the sites of major earthquakes to report on the effects on buildings in the area. The structures which fail are of interest but more information can be obtained from those which suffer least damage. Recently built structures are of particular interest because these buildings incorporate the latest seismic resistance techniques. Each new edition of the Building Codes usually reflect some of the results of the cumulative growth in knowledge obtained from the latest disasters.

## Consequences of Earthquake Damage

There are two basic adverse results from earthquakes:

- Loss and impairment of human life.

- Destruction and damage to the natural and built environment.

The basic design aims are therefore confined to the reduction of the loss of life in any earthquake, either resulting from a structural collapse or through secondary damage, such as from falling debris or fire and to the reduction of damage and loss of use of the built environment.

The choice of an acceptable level of seismic risk is a complex problem, involving consideration of the financial implications, as well as the probable degree of physical risk that is inherent in the seismic history of the site.

## Wind Effects on Building Structures

The effects of wind on stationary objects in its path can be generalized as follows:

- Direction of positive pressure.
- Aerodynamic drag.
- Negative pressure.
- Rocking effects.
- Harmonic effects.
- Clean-off effects.
- Effects of vortices.

These effects, shown in Figure 1.3, are translated into building design criteria as explained in the following paragraphs:

- **Inward pressure on exterior walls**

  Surfaces directly facing the wind are generally required to be designed for the full base pressure, although this is somewhat conservative, because the windward force usually accounts for only about 60% of the total force on a building.

- **Suction on exterior walls**

  Most Codes also require suction on exterior walls to be the full base pressure, although the comment above about inward pressure generally applies in areas not affected by the action of vortices.

- **Overall horizontal force on the building**

  The overall horizontal force is calculated using the horizontal pressure distribution on the building silhouette, with adjustments made for height above the ground. The lateral resistive structural system of the building is designed either for this force or the force resulting from seismic action.

- **Overturning effect**

  As with horizontal sliding, the dead weight tends to resist the overturning, or toppling effect. In practice the overturning effect is usually analysed in terms of the influence of bending and shear on the individual vertical elements of the lateral resistive system, rather than for overturning of the building as a whole.

- **Harmonic effect**

  Design for vibration, flutter, whipping and swaying requires a dynamic analysis to be carried out and cannot be accounted for using the equivalent static load method. Alternate shedding of vortices has also a build up effect over a period of time depending upon building plan shape, mass and stiffness.

- **Torsional effect**

If the building is not symmetrical in terms of its wind silhouette, or if the lateral resistive system is not symmetrical within the building, the wind force may produce a twisting effect. Although there may be a prevailing direction of wind in an area, the wind must be considered to be capable of blowing in any direction. Depending on the building shape and the arrangement of its structure, an analysis for wind from several possible directions may be required.

## Human Response to the Wind Induced Motion of Tall Buildings

An important criterion to be considered in the design of tall buildings is the comfort of the occupants, which includes the problem of vibrations induced by wind forces. When little damping is present then there is an increase in the dynamic response.

Experimental evidence has shown that human perception to horizontal linear and rotational motion can be caused by stimulation of the central nervous system through various perceptions and by visual contact with the environment.

In the last few years Irwin [9] reviewed and analysed existing and new data on human perception and produced a series of curves which give acceptable values of building acceleration for the peak of the worst wind-storm with a return period of at least five years, for vibrations in the range of 0.063 Hz to 80Hz. The peak periods of the storms are usually assumed to be fully developed for longer than 10 minutes, when the extreme motions are experienced.

Torsional and translational components of motion can be combined to give an

equivalent translational motion on plan. It may be necessary to adopt more severe criteria where this is the dominant motion because of the visual perception of twisting.

### 1.9.3 Influence of Constraints

**Creep**

Creep of shear walls including differential movements between reinforcement and concrete, can take place over long periods (25 years and more). In conjunction with shrinkage, reduction in storey heights sufficient to cause distress in tight fitting non-structural units is possible.

**Shrinkage**

Foundations to shear wall structures are generally relatively rigid, poured in situ formations and are cured in below-ground conditions such that shrinkage is minimised to a greater extent than in successive storeys of the building cured above ground. Horizontal differential shrinkage especially between the foundation and first storey levels and to a certain extent at higher levels when continuous pouring methods are not employed gives rise to out-of-plane bending of shear wall assemblies. Normally slip joints are provided when the length or width of a structure exceeds 45 - 60m. Otherwise extra reinforcement is required to restrict predetermined amounts of movement.

### Temperature movements

Differential temperature movement between interior and exterior structural elements can be significant and may need to be considered in a similar manner to creep and shrinkage. Relative movement between elements such as mullions and windows should be taken into account in the detailing of the joints. Differential creep of vertical structural elements can cause effects similar to temperature movements. In the case of a 150m high building with exterior walls at the extreme temperature sides of a building, a differential movement of about 40 mm or more between the two sides of the building is possible assuming an expansion coefficient of 1.1 x $10^{-5} per^{o}C$.

### Settlement

Rotation resulting from foundation or differential settlements may deform floor slabs between rows of walls to cause out-of-plane bending of walls or set up shear forces in slabs or beams coupling shear walls in line. This adds to the stresses caused by other loadings and can radically alter both the dynamic response and ultimate capacities of shear wall structures. In coupled shear wall structures all of the above forms of loading result in shear and bending of the beams and slabs connecting the walls. Although wind and earthquakes are predominant dynamic actions other sources of loading are generally additive.

## 1.10 PROBLEMS OF ULTIMATE BEHAVIOUR OF COUPLED SHEAR WALLS

The strength capacity of a coupled shear wall subject to lateral loading is reached when a collapse mechanism is formed. Two plastic hinges in each coupling beam are required to terminate its ability to accept additional shear. In addition one plastic hinge needs to be developed in each of the cantilever walls, normally at their base, to complete the collapse mechanism. The sequence of hinge formation for a given loading will depend on the relative strength and stiffness of the component parts. The behaviour of some coupled shear walls that have been exposed to more severe lateral loads, indicated that all or most coupling beams failed before the ultimate strength of the coupled walls was attained.

Relatively few analytical studies on the plastic behaviour of shear walls have been reported. Winokur and Gluck [10] proposed an approach based on the uniform distribution of the flexural strength of the coupling systems. These coupling beams often short and relatively deep, may be subjected to high shearing stresses when the ultimate flexural strength is to be developed. In deep spandrel beams, these shear forces not only inhibit the full development of the flexural capacity, they also restrict the ductility which can be obtained. It is therefore important to assess the ductility demand on the coupling system when the overall ultimate strength of the coupled shear wall structure is being determined. Apart from the strengths of the coupled walls at foundation level, three critical areas of the behaviour require the attention of the designer. These are discussed in the next

section.

## 1.11 CRITICAL ASPECTS OF COUPLED SHEAR WALL BEHAVIOUR IN EARTHQUAKES

There are three areas in ductile coupled shear wall structures which have to be detailed carefully where critical conditions may arise during a strong ground motion as shown in Figure 1.4.

- **Coupling beam**

  The damage suffered by the coupling beams during known earthquakes and the experiments carried out by investigators in particular Paulay [11] show that these beams, conventionally designed for shear and flexure with stirrups and horizontal flexural reinforcement respectively, cannot sustain the flexural yield load generated during high intensity cyclic loading. These experiments revealed that the shear deformation greatly overshadowed the deformation resulting from flexure. Even when the stirrup reinforcement provided was in excess of that required for the maximum possible shear force, which would develop when the flexural steel yields, it has been found by Paulay [11] that after a few cycles, causing alternate yielding in the top and bottom flexural reinforcement, the beam may fail in sliding shear. When the flexural steel yields at the face of the wall almost all of the shear force is transferred across the concrete in the compression zone. However, this concrete is likely to have been cracked during previous loading cycles

and its frictional shear resistance will have greatly diminished as a result of repeated opening and closing of the cracks and the smoothing or grinding of the contact surfaces. This shows that even a drastic increase in stirrup steel cannot improve the behaviour as sliding shear may occur between the two adjacent stirrups. Such a sliding shear failure in coupling beams cannot be considered as a satisfactory mode of failure for the purposes of seismic resistance, moreover, sliding shear means a considerable loss of strength. The concern for the provision of coupling beams with adequate strength led to the present investigation into a different type and arrangement of reinforcement.

- **Tension wall**

  The shear strength of a wall may be seriously affected by axial tension generated by the earthquake induced overturning moments. It is important to realise that under these conditions, the contribution of the concrete to the overall shear resistance becomes negligible.

- **Compression wall**

  The axial compression generated by earthquake induced forces and by gravity loads on the structure may limit the ductility attainable in the compression wall. Apart from this, construction joints in shear walls (shown as broken lines in Figure 1.4 may become the weakest link in the sequential chain of resistance.

## 1.12 CONCLUSIONS

This Chapter examines the different structural aspects to be considered in coupled shear wall structures and confirms that present day problems relating to the resistance to shear loadings is mainly associated with the coupling beams. It is believed that a satisfactory solution to the problem can only be achieved through a better understanding of the mechanism of diagonal failures. Shear wall structures frequently require changes in their internal planning, extensive improvements to their environment services, possible increases in their load capacity, and often a significant extension of their life expectancy. Essential to each of these, are the questions of strength, stability and durability of shear wall structures.

Research efforts are required to be directed to investigate the overall structural behaviour of the weakest links in the lateral load resisting system in coupled shear wall structures which are the coupling beams. Their relative dimensions suggest that their behaviour is not likely to obey the classical concepts of flexure. These commonly occurring structural members are important enough to warrant the undertaking of a detailed study into their behaviour.

To ensure satisfactory performance when coupled shear wall structures are exposed to severe lateral loads, it is necessary to be able to assess the behaviour of the structure in both the elastic and plastic range of loadings. It should be noted, however, that with proper attention to reinforcement details, the failure of the coupling beams can be either delayed or completely eliminated and a more ductile failure can be obtained.

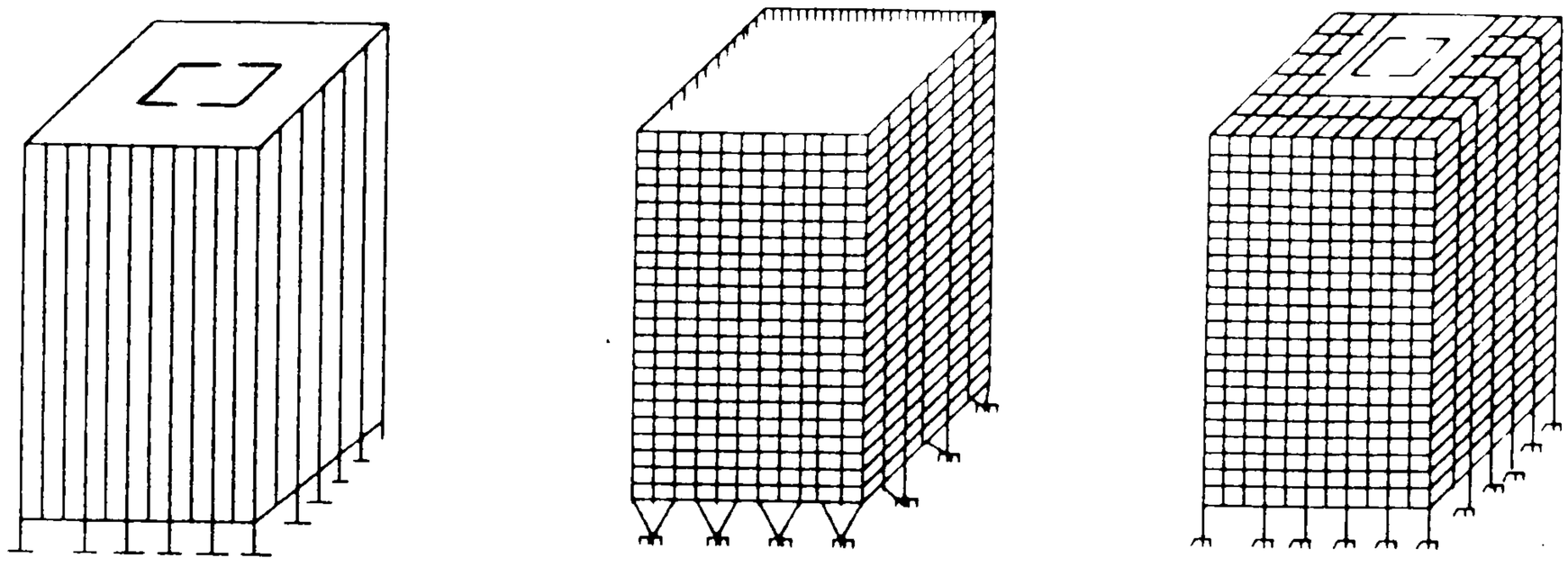


Figure 1.1: Basic structural form of tall buildings. Irwin [7]

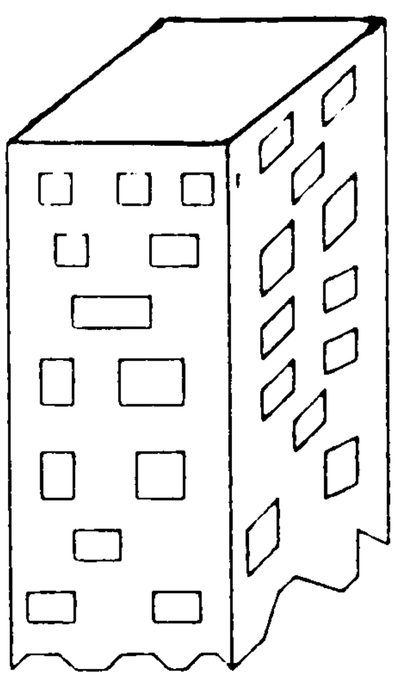

Pierced tube

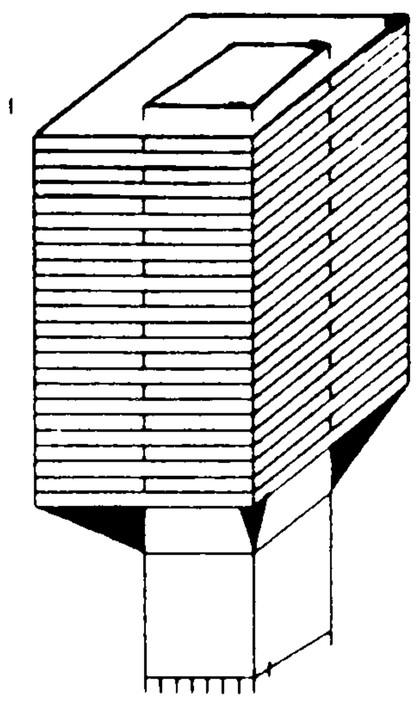

Cantilevered core structure

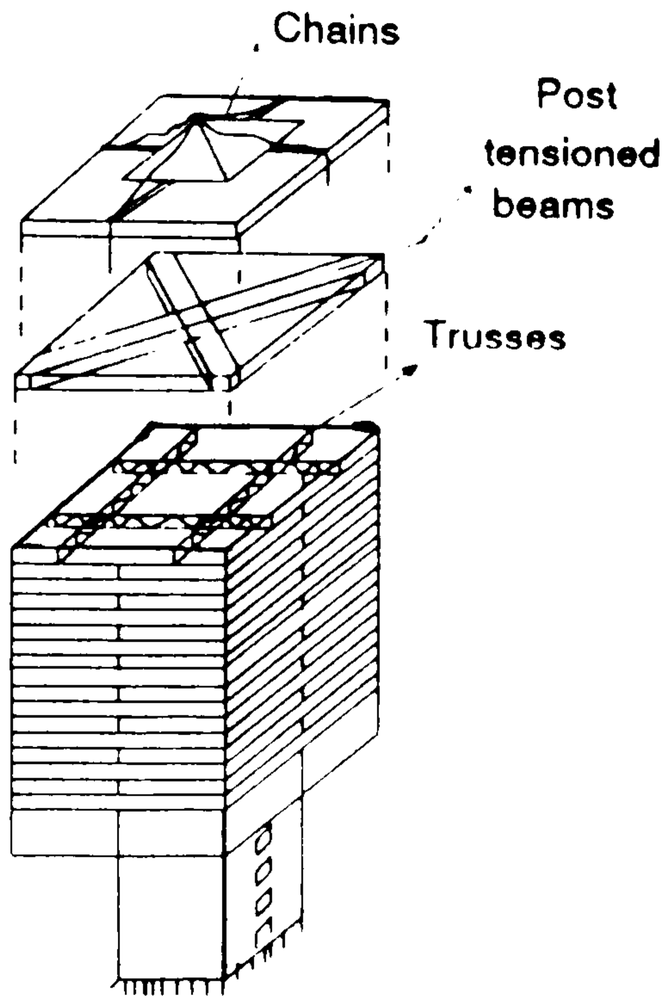


Top down construction
or suspended floor system

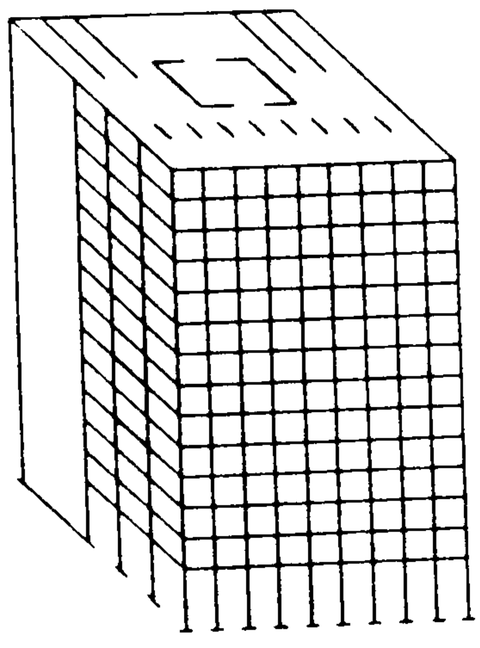

Frame wall interaction

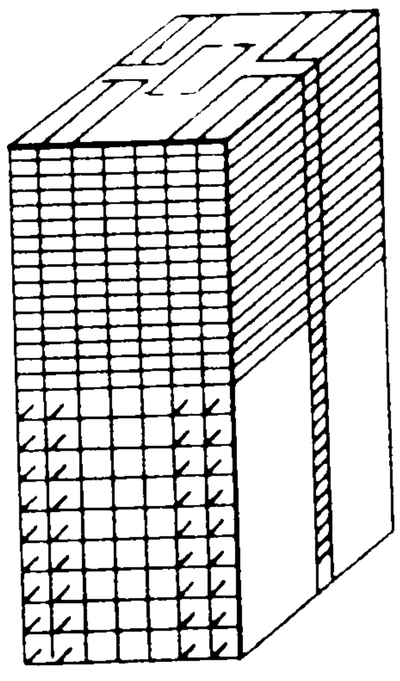

Frame on shear wall

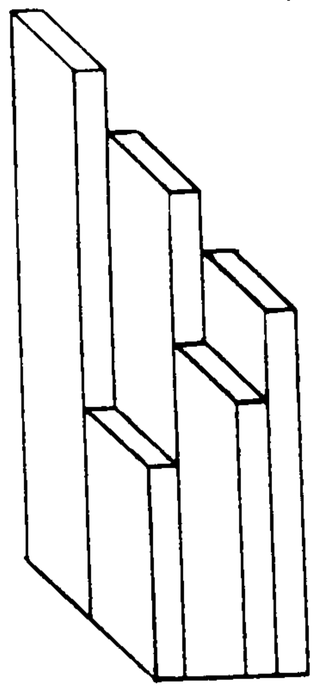

Bundled tube

Figure 1.2: Basic structural form of tall buildings. Irwin [7]

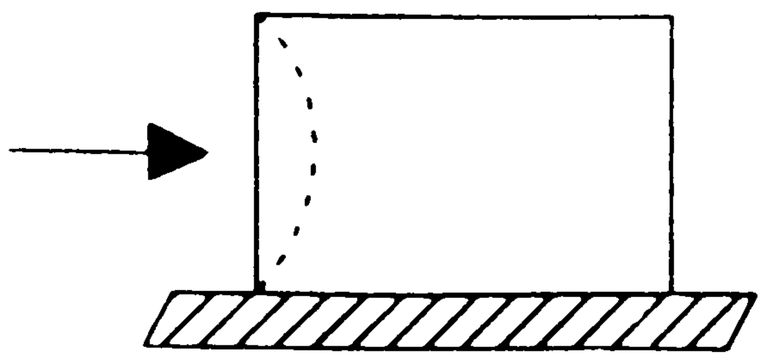

(a) Direction of positive pressure

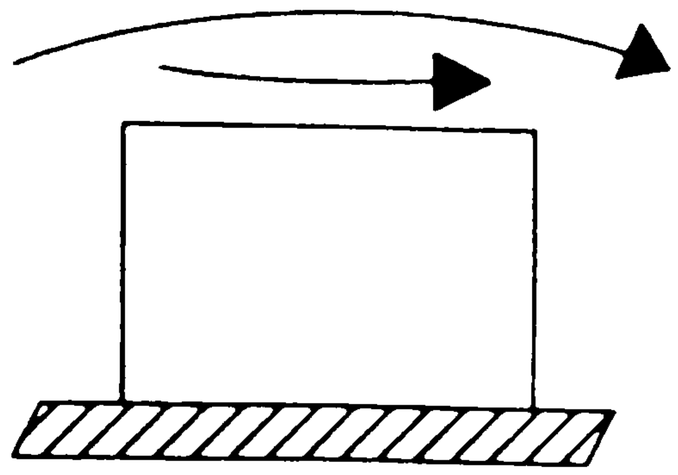

(b) Aerodynamic drag

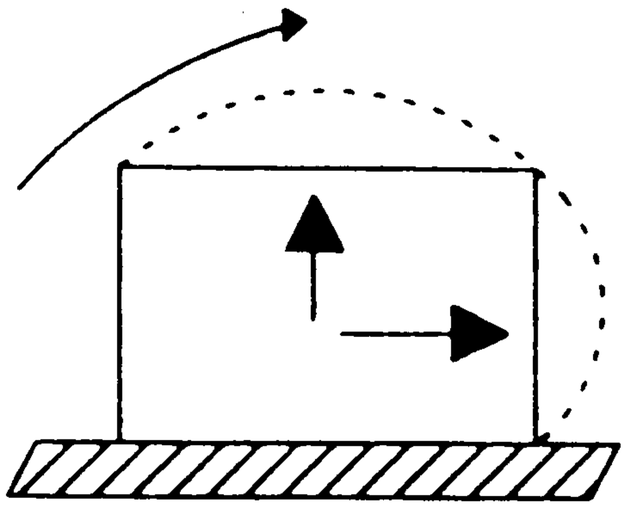

(c) Negative pressure

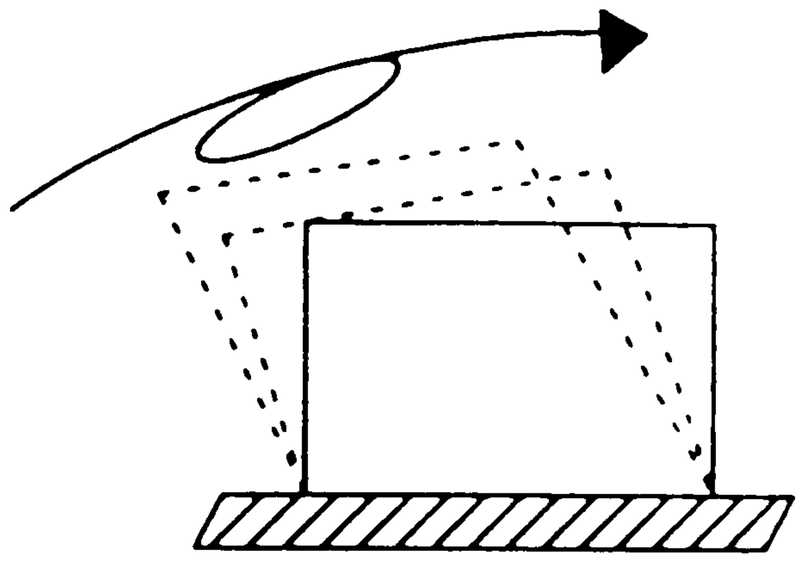

(d) Rocking effects

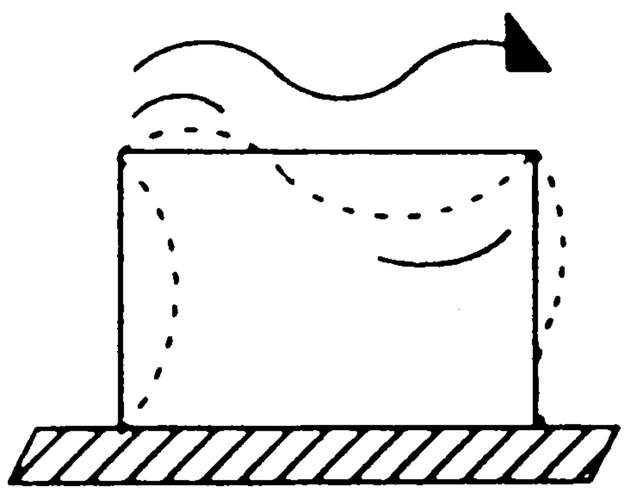

(e) Harmonic effects

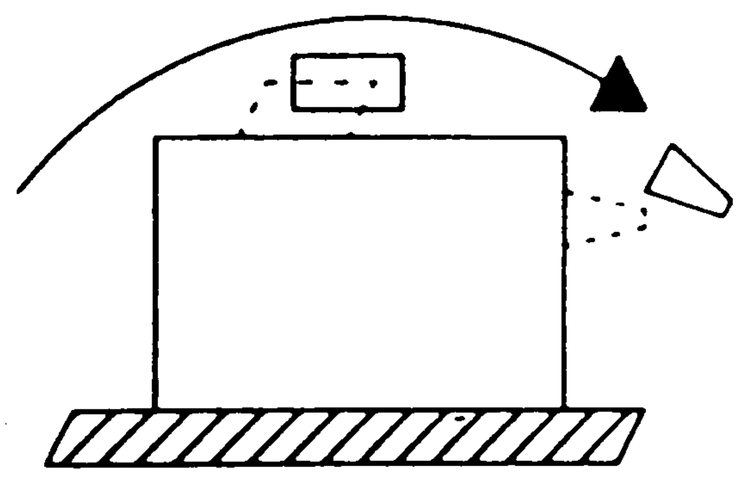

(f) Clean off effects

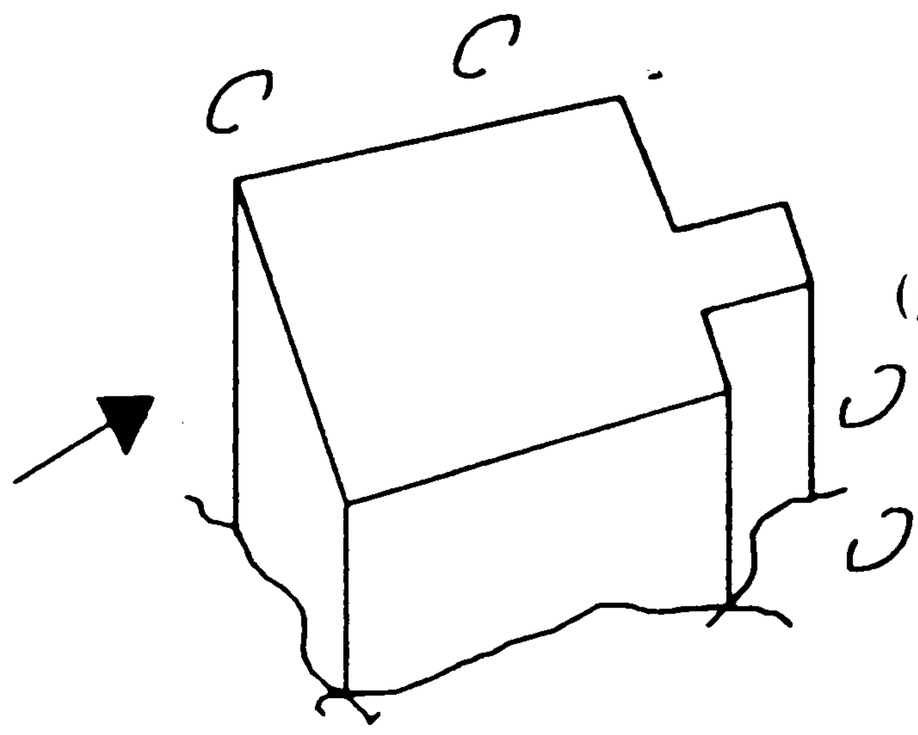

(g) Effects of vortices

Figure 1.3: Wind and earthquake effects on building structures. Irwin [7]

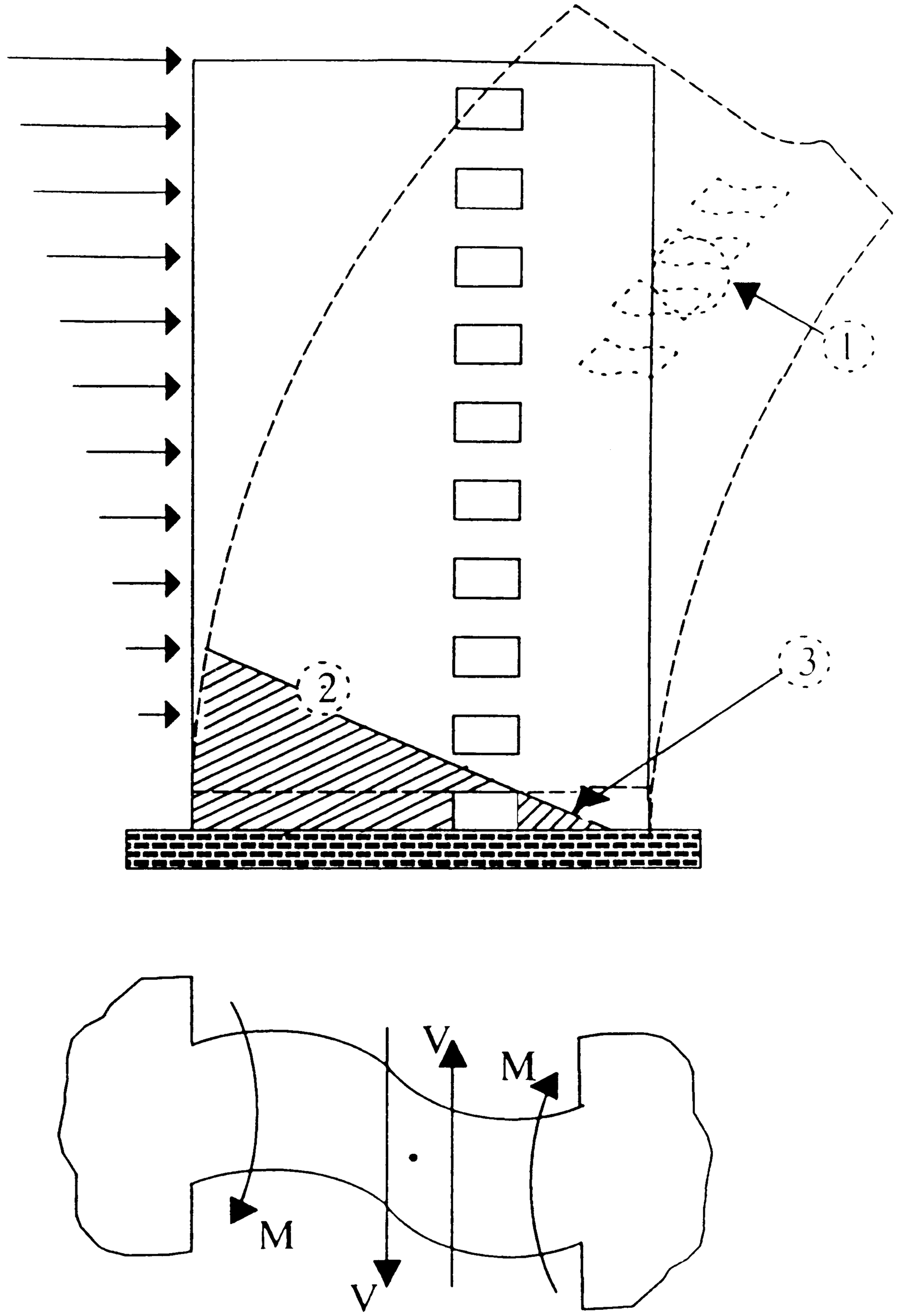


Enlargement of coupling beam

Figure 1.4: Typical laterally loaded ductile coupled shear wall. Paulay [52]

# Chapter 2

# LITERATURE REVIEW

## 2.1 INTRODUCTION

Bronze rods were used to reinforce concrete in Roman times. More recently, calculated amounts of iron, and later steel, rods have been employed to enhance the compressive strength and buckling resistance of concrete sections and to overcome problems presented by the low tensile strength of the concrete in flexural applications. It is only in the last 100 years that there has been a systematic study to determine the influence of shear and flexure in these anisotropic structures. The behaviour of reinforced concrete members and structural systems, specifically their response to sustained loads, and other actions, has been the subject of intensive investigation since the beginning of the present century. The rapid increase in the use of shear walls, and in particular coupled shear walls, has highlighted the necessity for a better understanding of their behaviour. This stimulant for research has produced an extensive and comprehensive bibliography covering

the elastic behaviour of two-dimensional shear wall structures.

In buildings it is common practice to provide the required rigidity by utilising the internal and external walls, which are normally necessary for functional reasons. These walls normally contain openings for doors, windows and corridors, and may even be discontinued completely at lower levels to allow large uninterrupted areas for a concourse. Local stress concentrations inevitably occur near such openings and discontinuities, and some knowledge of these stresses is necessary to enable the designers to provide adequate reinforcement.

The contributions of researchers towards the problem relating to the behaviour and design of the coupling beams in shear wall structures is examined in this Chapter. The aim of this Chapter is also to provide a summary of the current knowledge relating to shear wall structures, by reviewing briefly the relevant research papers, and by compiling a comprehensive bibliography.

The most important conclusions that have emerged from each part of the published literature are presented at the end of the Chapter.

## 2.2 REVIEW OF PREVIOUS WORK

The large dimensions often encountered in shear wall structures, seriously limit the efficient application of the conventional techniques of structural matrix analysis. It is for this reason that numerous attempts were made to develop analytical methods which were able to predict more accurately the behaviour of this type of structure.

This review is restricted to an examination of such theories put forward to assess

the strength and behaviour of coupled shear walls. Investigations related to the behaviour of reinforced concrete coupled shear walls subjected to static loading and including elastic analysis, elasto-plastic analysis and laboratory based investigations are included.

This survey is divided into the following three parts:

1-Elastic analysis.

2-Elasto-plastic analysis.

3-Experimental investigations.

### 2.2.1 Elastic Analysis

The following three approaches have been used in the analysis of coupling shear walls:

a) Laminar and frame analytical approaches.

b) Finite element analysis.

#### a) Laminar and Frame Analytical approaches

Both the laminar and frame analytical approaches have been used in the elastic analysis of coupled shear walls. The laminar approach, by which the statically indeterminate problem of coupled shear walls is reduced to relatively simple analysis was first developed by Chitty [12] in 1947. In this investigation the behaviour of a number of parallel cantilevers which were rigidly interconnected by cross-bars was

studied. These bars were replaced by an equivalent continuous elastic medium capable of transmitting the same actions as the cross bars. Chitty [12] correctly assessed the equilibrium and compatibility requirements but neglected the effects of shear. A differential equation expressed in terms of the continuously varying moment applied by the connecting medium to the cantilever beam was proposed. The solution of the problem is completed by satisfying the boundary conditions for the cantilever.

In a paper by Green [13] in the early fifties, an approximate method of analysis was put forward which was applicable to frames with deep beams. This approach was similar to the "portal method" which was extensively used to determine the approximate actions in a building frame subjected to lateral static loading. The axial deformations in columns were neglected but the significance of shear deformations in deep members was emphasised. Although the inflection point in the piers of a bracing wall will usually be close to the mid-height of the windows as assumed in portal theory, the inflection points in the spandrels will not be at their centre unless the width and stiffness of the piers and spandrel lengths comply with specific requirements. This analytical approach is based on the assumption that the lengths of the piers and spandrels do not change. Furthermore, the inflection points in the spandrels must be at the centre of their lengths, which establishes certain requirements for the elastic properties of the wall.

The structure was analysed as a type of frame in which the walls between the windows correspond to the columns of the frame and the spandrels constitute the

beams. The only essential difference is that the walls and spandrels are relatively wide, which changes the deformed shape and necessitates that effects of shear stress as well as bending stress be included in stress analysis. A detailed description of the method of analysis including a worked example using the approach are provided.

Beck [14] studied the behaviour of wall panels containing one or more rows of openings. In 1962, Beck [15] presented an approximate method of analysis where a continuous system was used to replace the discontinuous frame system. Simple formulae for the determination of statically redundant values of the forces were developed. The basis of this method of analysis was to combine all redundant values in one single unknown function q(x) dx, instead of having a set of linear functions. Only one differential equation for the determination of the unknown function has therefore to be solved. The results from this method can be improved if large numbers of unknown values are replaced by the function q(x). The resulting accuracy is sufficient for all practical purposes. A series of curves was presented for practical use to allow shear forces for connecting beams and the bending moment in the shear walls to be obtained without the need for extensive numerical work. The simplification used by Beck [14] allowed an easier treatment of the problem and is justified only for practical purposes where there is a limited number of connecting beams each one of which having the same stiffness, being equidistant from each other and being only subjected to a constant linear horizontal force. This method is not valid for use in situations where the parameter

$\alpha$ is higher than 20, which can be determined thus:

$$\alpha = (6a_1^2 L_1^2 I_2)/(6a_2 L_2^3 I_1).$$

The internal forces can be found to an acceptable level of accuracy which is comparable to an exact solution because such systems in this case will act as a homogeneous beam.

$$q_x = \frac{S}{I} V_x$$

where $q_x$: is the shear force.

and

$$V_x = 2\frac{dM_0}{d_x}; \qquad S = A_1(a_1)/2$$

$A_1$=cross section of each shear wall.

$M_0$=bending moment applied to one shear wall.

$a_1$=distance between the centroid of the cross section of shear.

$V_x$=shear force of the connecting beam at location x.

Rosman [16] who was a most prolific theoretical researcher on the subject of the analysis of shear wall structures first published in 1960. The fundamental Eulerian differential equation to represent this problem was established by making use of the laminar system and by using strain energy considerations. A solution was chosen in terms of the axial force on the walls and expressed as a trigonometric series. By applying this approach to a shear wall with two vertical rows

of openings, it was shown that the solution of the set of second order differential equations with constant coefficients, yield the required static quantities. In this mathematical approach, Rosman [16] neither allowed for shear deformations nor considered the separation forces which are exerted by the coupling beams. In 1964, Rosman [17] presented a simple approximate method of analysis for various types of shear walls loaded with a concentrated load at the top. The approach used the continuous system method and the integral shear forces in the continuous connections of individual walls were chosen as statically redundant functions. The deformations due to the bending moment were taken into consideration, as were the contributions of the normal forces in the walls, and the shear in the connecting beams. The formulae used in this approach were derived using a mathematically exact solution. The resulting algorithm is therefore the same for all types of shear walls. It was proved that the variation in the rigidities in the direction of the height of the wall had a negligeable effect on the statically redundant functions. The method was validated using the results from a programme of experimental work performed by Naumann and Walter [18].

This approach, which is widely used in Europe will give more realistic results if the dimensions and the properties of the members are constant throughout the full height of the building.

The only difference between the methods put forward by Beck [15] and Rosman [17] is the use of the shear force as a statically redundant function instead of the integral shear force. This appears to lead to a more complicated expression for the integration constant and the numerical procedure becomes tedious. The

assumptions used in the method developed by Beck [15] are the same as those used by Rosman [17]. Hence both methods give the same results, but only the simplest type of wall is treated by Beck [15] i.e. the wall is weakened by a single symmetrically arranged line of openings with the walls fixed in a common perfectly rigid footing.

In 1964 Decauchy [19] continued the theoretical work initiated by Albiges and Goulet [20] in France on "the lateral bracing of buildings" in which they presented a method to calculate the stress due to the horizontal load in walls pierced with openings arranged in one or several vertical alignments. The rigidity of the foundation was one of the main assumptions. Decauchy [19] addressed the problem of foundation tilting and presented a family of curves to be used as design aids. It was shown that taking such deformations into account modifies considerably the distribution of stresses in the various elements of the walls and makes it possible, in particular, to determine according to the case being considered, an upper limit for each of these types of stresses.

In 1967 Coull and Choudhury [21] used the basic assumptions underlying shear connection techniques i.e. both walls deflect equally with the point of contraflexure at midspan of the connecting beams and the discrete system of connecting beams may be replaced by a continuous medium of equivalent stiffness. The origins of this approach are contained in an earlier paper [22] in which the stresses and maximum deflections in a system of coupled shear walls subject to uniformly

distributed lateral loading were analysed directly. A series of curves were presented for the determination of the wall bending stress factors and the connecting beam stress factors for both point loads at the top and for triangularly distributed loading as shown in Figures 2.1 and 2.2 and Figures 2.3 and 2.4 respectively to enable rapid design calculations to be performed for any shape of shear wall structure. Although the curves produced in the paper are intended to be of a general nature, since the cross-sectional properties may include the influence of cross walls acting as flanges to the shear walls, they refer only to walls of rectangular cross section. The method of analysis may readily be adapted to deal with shear walls of variable thickness.

Coull and Puri [23] extended the approximate analysis to account for shearing deformations in the walls. The relative importance of these shearing deformations is indicated by a comparison of the theoretical values of deflections and stresses with the results from tests on model coupled wall structures having one and two bands of openings. The influence of the flexibility of the wall-beam connection was also considered, and the relative influence of the two effects compared.
Two different methods have been employed in the analysis of coupled shear walls, the frame analogy and the continuous connection technique. In the first method the deep wall was replaced by a line column at the centroid, the finite depth being incorporated by the use of rigid arms to link the ends of the connecting beams to the columns. The analysis is then carried out using a computer program which was pre-requisite for the method. In the second method the discrete system is

replaced by a continuous medium of equivalent stiffness.

The test programme was performed on four 21 storey models, two of these models had a single band of openings, one being symmetrical and other asymmetrical, while the others had two symmetrical bands of openings. The dimensions and other details of the models are given in Figure 2.26. The results presented in the paper emphasized the accuracy of the continuous connection technique for the analysis of coupled shear walls. Good agreement was reached between the theoretical and the experimental values for the deflections and the stresses even when the depths of the connecting beam are comparable with that of the opening. In all cases the greatest accuracy was achieved when the influence of the flexibility of the wall-beam connection was included in the analysis. The results indicated that the inclusion in the analysis of shearing deformations in the wall had little effect on the stresses and increased the deflection by only a few percent. Better agreement between theoretical and experimental stresses can be achieved if the wall-beam connection is included in the analysis, although the distinction between the two is not so significant in the case of the deflections.

An approximate method for the analysis of the distribution of the load between the shear walls in a three dimensional multistorey building subjected to bending and torsion was carried out by Coull and Irwin [24]. The method was based on the continuous connection technique. It was aimed particularly at buildings with uniformity of structure throughout the height. They assumed that bending was the dominant overall mode of behaviour of the structure. The effects of the axial

deformation in the vertical members were included as well as the effect of the bending stiffness of the floor slabs in the coupling action between wall assemblies. A series of graphs presented in Figure 2.5 shows that the results from the proposed method and the experimental investigation were in very close agreement. These results were obtained from a fifteen storey model constructed from sheet perplex clamped horizontally in a test frame and loaded by means of dead weights applied to hangers suspended from the floor slabs. In general they showed that the continuous connection technique is capable of yielding accurate results in the analysis of complete three-dimensional shear wall structures. The only disadvantage of this approach is that the accuracy of the results is dependent on the height of building i.e. the method is more accurate as the number of storeys increases.

A new technique introduced by Coull [25] considered the influence of the top stiffening beam on the structural behaviour of a pair of coupled shear walls situated on a deformable foundation. The analytical approach used in this investigation was based on the continuous connection technique which enabled a closed solution to the problem to be achieved. The top beam used in this analysis has the effect of including axial tensile forces at the top of the windward wall, where the gravitational stresses to counteract them are least. However, the stresses are relatively small and would be resisted by the reinforcement required in the top wall-beam joint. A numerical example was presented for the pair of shear walls shown in plan in Figure 2.6 for a 20 storey building, total height of 60m, and assumed to be connected at each storey by coupling beams. The results indicate that under

certain conditions a considerable increase in structural efficiency may readily be achieved by the provision of the top beam. It appears that the stiffening top beam would be uneconomic in the case where the connecting beams are relatively stiff. The elastic analysis used by Coull [25] has considerably oversimplified the real properties of soil in order to produce a simple solution to the problem. If this analytical approach is to be used, due care must be exercised in allocating realistic stiffness properties to the foundations and the soil.

In more recent years Chan and Kuang [26] presented a method of analysis to investigate the beneficial effect of a large stiffening beam on the performance of coupled shear walls supported on either rigid or flexible foundations using the continuum approach. The behaviour of such a structure under lateral loading was also investigated. The work consisted of determining the optimum location of the stiffening beam to achieve the maximum reduction in the deflection at the top of the walls and the bending moments in the walls at the base level and the shear forces in the lintel beams. The results from the investigation which included different flexural rigidities of the stiffening beam showed that the optimum location of a stiffening beam should be at a level of about 0.4 of the structural height in order to achieve the greatest reduction in the maximum shear force in the coupling beams and about 0.5 of the height for achieving the minimum top deflection. Depending on the flexural stiffness of the coupling beams, the minimum base moment in the wall is generally obtained when the stiffening beam is located at a lower level of approximately 0.2 or less of the structural height. In

a comparison with a structure without stiffening, it was shown that at least a 10% improvement in the laminar shear and base moment in the walls and 15% improvement in the top drift can be achieved by the installation of a stiffening beam at a range of levels of between 0.2 to 0.5 of the overall height in coupled shear wall structures. The results of the analysis presented by Coull [25] and Chan and Kuang [26] demonstrated that the introduction of the stiffening beam into coupled shear walls supported on flexible foundations was an effective means of reducing the bending moments in the walls at the base level and in enhancing the lateral rigidity of the structure. It will also alleviate the effects of foundation deformations on the structure. The only difference between the two approaches is that the approach by Chan and Kuang [26] was more realistic and economical in comparison with the approach developed by Coull [25].

**Summary**

The analysis of the coupling between shear walls described in the previous Section can be summarised as follows:

The methods presented which are based on elastic analysis have proved to be suitable for the analysis of multistorey shear walls, coupled by beams, subjected to any pattern of lateral loading.

The results obtained by several researchers [27], [25], and Beck [15] emphasized the accuracy of the continuous technique for the analysis of coupled shear wall structures.

The results also indicate that these approaches are capable of yielding accurate results in the analysis of complete shear wall structures. Indeed, the elastic theory can give some useful information about the behaviour of reinforced coupled shear walls, but, by itself, it will in most cases only provide an approximate solution to the complete behaviour of the structure.

Laminar analysis can be readily extended to assess the elastic behaviour of coupled shear wall structures at various stages of cracking by making due allowance for the loss of stiffness in the component parts. Significant changes in critical moments can occur as a result of cracking.

### b) Finite Element Method

The finite element method offers a convenient and versatile tool to assist in the understanding of the behaviour of structural systems. This method has been applied with considerable success to various static and dynamic problems.

Ngo and Scordelis [28], first demonstrated the feasibility of the approach and explored its potential as well as the difficulties of using the finite element method with the ultimate aim of developing a general analytical method for the study of reinforced concrete members under load. The reinforced concrete beam shown in Figure 2.7 with defined crack patterns was analysed assuming that the concrete and the steel followed a linearly elastic stress-strain relationship.

The concrete and the steel were represented by two dimensional triangular finite elements and account was taken of bond slip between the two using finite springs. The results from several examples of reinforced concrete beams on simple supports under third point loading were presented. All the beams studied were identical in all aspects except for the assumed idealized crack patterns and the stiffness values of the bond links. The results from their investigation gave a detailed picture of the stress distribution throughout the beams which cannot readily be obtained using other analytical or experimental methods. The effect of nonlinearities which plays an important role in reinforced concrete was not included in the approach.

Cervenka and Gerstle [29], [30] used the finite element method for the analysis of reinforced concrete panels including the influence of cracking and plasticity effects. The influence of these approximations was studied analytically and ex-

perimentally. Two series of laboratory tests were included in the investigation. The first test series which was intended to simulate the action of shear walls, was conducted on two panels combined to form one beam-like specimen as shown in Figure 2.8. The type of test arrangement used enabled the beam specimens to be tested as a simply supported beam loaded at the midpoint. The two square panels were always tested simultaneously but each panel acted independently of the other because of the statically determinate supports. The second test series shown in Figure 2.9 was performed by Paulay [11] in an investigation into the coupling of shear walls. The first test specimen was subjected to cyclic loading and the results were presented only for the first four load cycles. The analytical results indicate changes due to crack formation only in the first two cycles, whereas the experimental results show some residual displacement even under this low load. The results from the second test specimen detailing the load-rotation characteristics show the over estimation of the real stiffness of the member. In the analysis of the results considerable differences were found between the predicted and actual failure mechanisms. In the experiment, the opening of the diagonal crack led to an abrupt instability failure whereas the analysis showed plasticity of the cracked concrete in the vicinity of the diagonal crack which added to the displacement capacity of the panel. This difference may be caused by the short comings in the finite element method idealisation of the cracked concrete since the cracks in the analytical model were not smoothly continuous from one element to another. In this investigation very good agreement was found between the results obtained from the experimental and the analytical studies.

In 1973 Yuzugullu and Schnobrich [31] described a procedure for the determination of the behaviour of shear wall and frame systems using the finite element method. The finite element method was used to predict the behaviour of the shear wall and frame systems in the cracked state. The method used in the analysis was of the displacement type and was applied in incremental form. A new grid with nonrectangular elements to provide a finer mesh in the critical compression zones was also used.

The shear wall structure studied was from a series of prototype models which was tested at the University of Tokyo in 1964 [32]. The panel of the shear wall frame was divided into finite elements and a quadrilateral element composed of four constant strain triangles was chosen to represent the wall element. The separation of the wall from the frame was provided by link elements similar to those used by Ngo and Scordelis [28] with very large values assigned to the spring constant to represent the stiffness of the link element.

A comparison of the predicted and the actual results shows good agreement for the load-displacement relationship up to a specific load which was a third of the failure load. The approach could have been made more efficient if the reinforced concrete shear wall frame system had been analysed as a simple integral unit rather than the wall and a frame using the link element.

Darwin and Pecknold [33] presented a nonlinear constitutive model for plain concrete subjected to cyclic biaxial stress. Its successful application in the case of

cyclic loading was demonstrated by presenting numerical solutions for the two shear panels tested and analysed by Cervenka and Gerstle [29], [30]. The first model was loaded monotonically and the second was subjected to large cyclic load reversals. The finite element used in the analysis was a four noded isoparametric quadrilateral with four extra nonconforming modes to soften the element and to improve its behaviour in flexure. The element tangent stiffness was formed numerically using a three by three grid of Gaussian integration points by calculating the current orthotropic constitutive matrix and then rotating to global coordinates. A combined incremental iterative numerical solution was used in which the effects of nonlinear material behaviour are included in load terms. In a comparison with the work of Cervenka and Gestle [29], [30] the predicted results were found to be in good agreement for both monotonic loads as shown in Figure 2.10. Improvements could be achieved in a number of ways: first, the elasto plastic model remains elastic in compression until the yield surface is reached, whereas the proposed model is significantly softer for stresses above 0.7 $f'_c$. Second, the model allowed for only one open crack. It was found that a significant portion of cracks remained open, even when the cyclic loading was reversed which agrees with the experimental evidence. Cervenka and Gerstle [30] also refer to the omission of the bond slip relationship as a possible cause of the discrepancy. However, the model was able to simulate the experimental results reasonably well without including a bond slip relationship which does not appear to be a major factor for deep shear walls. More realistic results can be obtained if the method is applied to a large scale model.

In a report published by McGill University, Mamet and Mufti [34] presented a new finite element procedure for the static analysis of tall buildings in the form of shear walls. A common formulation with linear and bilinear displacement fields was used for the floor slabs and the shear walls. Fictitious beams were included for the transmission of moments in the plane of the elements. The floors were treated as substructures. The stiffness matrix and load vectors were condensed prior to the solution of the system of equilibrium equations. A reduced structure consisting of columns, shear walls and equivalent floor stiffnesses was used. An extension of the work to earthquake analysis was also outlined.

The main shortcoming of this work was that there was no validation presented either in terms of experimental test results or by comparison to results from earlier investigations.

In 1973, Bhatt [35] carried out a study into the problem of beam-shear wall junctions using slightly finer finite element meshes than those used by Hall [36]. Three alternative methods of allowing for the joint deformations were proposed. The first method, which may be referred to as the deflection factor method, is to use the deflection factor, i, to increase the flexibility of the coupling beam so as to account for the joint deformations. Actually this i-factor also allows for the shear deformations of the beam. It was presented as a function of the wall width/beam depth and cantilever span/beam depth ratio in the form of a small scale plot. The second method was to increase the effective length of the beam by a factor of

$0.5\ \sqrt[3]{i}$ at each end. This equivalent length allows for both local deformations at the joints and shear deformation of the beam. In other words, the shear deformations of the beam are not allowed for by incorporating a shear deformation factor in the stiffness matrix but rather by extending the length of the beam beyond that required for taking into account joint deformation effects. The third method was to add rotational springs at the ends of the beam as put forward by MacLeod [37].

More recently, Cheung [38] used quadratic elements to analyse the joint deformations of the coupling beam and the wall. Details of the finite element analysis were not given, but theoretically quadratic elements should be able to give more accurate results than the lower order element. Cheung [38] proposed to increase the length l, of the beam to $\beta$ l, where values of $\beta$ are presented in tabular form, to allow for joint deformations. As in the case of the approach put forward by Bhatt [35] the equivalent length $\beta$ l, allows for both local deformation at the joints and shear deformation of the beam.

Macleod [37] and Macleod and Hosny [39] adopted a more fundamental approach to modelling of the non-planar shear walls as assemblies of interconnected planar wall units, with the warping displacement of the non-planar walls evaluated as an integral part of the solution. Determination of the shear centres and sectorial coordinates of the non-planar walls is no longer required, and the Vlasov theory [40] is dispensed with all together. Figure 2.11 shows the planar wall element used by Macleod and Hosny [39]. The wall elements shown in Figure 2.11(a) are

just normal column elements with rotational degrees of freedom at the nodes, whereby the finite widths of the walls are taken into account by incorporating rigid arms in the corresponding beam elements. This type of element is most suitable where there are coupling beams (e.g. in a wall with openings) but is not applicable if the wall is connected to other walls at both edges, in which case the solid wall element shown in Figure 2.11(b) is needed. Unlike the column element, the solid wall element has rigid arms incorporated in the wall itself rather than the beams. However, since there are no rotational degrees of freedom, the solid wall element is not suitable if coupling with beams is required. Therefore, for wall units connected to beams along one edge and the wall at the other, the special arrangement shown in Figure 2.12 is necessary. The use of the wall elements put forward by Macleod and Hosny [39] is reasonably complicated for the following reasons: firstly, it requires a mixture of the two types of element to be used; secondly, some of the nodes would have rotational degrees of freedom while others would have none. Shear deformation can be incorporated theoretically by including shear flexibility in the derivation of the stiffness matrices of the frame members. However, this needs to be considered in conjunction with the rotational degrees of freedom of the nodes. Figure 2.13 shows the difference in deformation of the coupling beams for two common definitions of nodal rotations. In Figure 2.13(a), the nodal rotations are defined as the rotation of the horizontal fibres (axis of the rigid arms or beams), while in Figure 2.13(b), they are taken as those of the vertical fibres (axis of the walls). It can be noted that the difference in rotations of the horizontal and vertical fibres is actually the shear strain. The

arrangement put forward by Macleod and Hosny [39] in Figure 2.12 is, in fact, equivalent to defining the nodal rotations as those of the rigid arms i.e. the horizontal fibres. This is incorrect, as illustrated for the particular case shown in Figure 2.13, in which case according to Macleod and Hosny [39], the coupling beams should not be stressed at any stage.

Figure 2.13 also shows that incompatibility at the wall-beam joints would arise if nodal rotations are taken as those of the horizontal fibres.

In 1981 Nobuaki [41] presented a finite element formulation capable of clarifying inelastic behaviour of reinforced concrete shear wall structures. Inelastic effects such as tensile cracking of concrete, nonlinear stress strain response of concrete and steel, bond between steel and concrete, aggregate interlock between cracked concrete surfaces and dowel action of the reinforcement bars, were considered. Particular attention was given to constitutive modeling of these effects which have an important influence upon the hysteresis characteristics of reinforced concrete structures. The concrete was assumed to be a homogeneous isotropic material when it was uncracked and anisotropic when it was cracked. The Von Mises yield criterion for plasticity was used to simulate compressive behaviour. The reinforcement bars were distributed uniformly within the respective concrete elements and were subjected to a uniaxial stress state. The procedure used in this approach to solve the governing equations was the incremental initial stress approach or an incremental self-correcting approach. No attempt was made to validate the approach.

In 1985 Duen and Chi [42] proposed a method to analyse the shear wall and the shear core assemblies subjected to general loading using a combination of the finite strip method and the continuum method. Firstly, in the finite strip method, the structure was divided into a number of finite strips. Displacements at each strip were represented by a set of given functions. Formulation is in terms of a number of nodal parameters which define the displacements of the structure. The second method i.e. continuum method, which assumes the shear core acts as a cantilever and replaces the different bands of lintel beams by a set of continuous laminates of equivalent shear stiffness. The proposed method was based on the following points:

a) The structure is divided into a number of rectangular wall strips. As a result, the calculation of the sectional properties of the wall elements is considerably simplified.

b) A modification of the shear stiffness of the continuous laminates and the inclusion of the out-of-plane bending stiffness of the wall strips.

c) Slight modification of the boundary conditions results in an approximate solution for structures with dimensions varying along the height of the building.

Simplification of the continuum method and the flexibility of the finite strip method which is the basis of the proposed method, can lead to several assumptions:

The floor slab is assumed to be infinitely rigid in its own plane and the wall strip is assumed to be infinitely stiff in bending. Secondly, plane sections are assumed

to remain plane. All joints are considered to be rigid and the structure is founded on a rigid foundation. Although the formulation appears to be rather complex, the advantage is that the actual numerical calculation can readily be carried out using a micro-computer and it is applicable to the analysis of all core walls with variable cross sections thoughout the height of the structure, and to the analysis of frames and frame-tubes. No comparisons were attempted in the investigation.

Ha and Desbois [43] studied a tall building using both displacement-based and strain based approaches within the finite element method. In the analysis the actual structure was replaced by a set of equivalent orthotropic membranes. Each membrane may represent a gridwork of the beams and columns, a band of coupling beams, or a solid facade such as a shear wall. The continuum is then discretised into macro-elements interconnected at their nodes. The mesh of macro-elements is subsequently analysed for nodal displacements and stresses. A series of formulae were derived for both displacements and strains for the four noded element. A 40 storey frame and 15 storey core supported structure were analysed numerically which showed that the macro-element technique together with the simple strain-based element can model the stiffness of a tall building. Its simplicity and ease of use make it particularly well suited for preliminary analysis and design.

The phenomenon of local deformation at beam-wall joints can significantly reduce the effective stiffness of coupled shear wall structures and was studied by Kwan [44], [45] in the early 1990's. The analytical approach used in this inves-

tigation is based on the problem of incompatibility between the beam and wall elements. In an attempt to resolve these problems it was postulated that in order to ensure compatibility between the wall and beam elements, the joint rotations should be defined as the rotations of the beam interfaces. The modifications necessary for the existing methods to allow for joint deformations after changing the definition of joint rotations to the rotation of the beam-wall interfaces were studied. It was found that they all have shortcomings and that a better method is to use joint elements to model the joint deformations.

A parametric study of the local deformations around the beam-wall joints was carried out using the finite element method of analysis and a very fine mesh of rectangular bilinear elements as shown in Figure 2.14. The structural parameters studied are the half wall width/beam depth ratio, (w/2d), and the cantilever span/beam depth ratio (c/d). In this investigation the problem was analysed in which both ratios varied from 0.5 to 4.0 i.e. (4.0, 3.0, 2.0, 1.0 and 0.5). All together 25 combinations of the two parameters were studied. Poisson's ratio was taken to be 0.25 throughout. The resulting deformed shape of the structure is shown in Figure 2.15 which also gives the position of the maximum principal stress. The results of the finite element analysis are presented in the form of flexibility coefficients and equivalent lengths. Two alternative beam elements, one in which joint deformation was allowed for by means of flexibility coefficients as shown in Figure 2.16 and the other by means of equivalent length, were developed. The first element is more general and can give more accurate results but its implementation on a computer is more involved. The second approach is easier to

use. The main problem with this method is restricted only to those cases in which the walls and the beams are of the same material and thickness and is slightly less accurate than the first element.

## Summary

The findings from the research work discussed above can be summarised under several points:

- The introduction of the finite element analysis was found to have a significant influence in the analysis of coupled shear wall structures.

- The findings of the investigators reviewed in this Section confirmed that the application of the finite element method to coupled shear walls was very accurate in cases involving either changes of geometry or at beam-wall joints.

- The finite element method has been developed to study the behaviour, strength and ductility of coupled shear wall structures. This technique can be extended to structures containing more than two shear walls and with complex geometries.

- The finite element method was able to predict the behaviour of coupled shear wall structures well into the cracked state. It has been shown by Yuzugullu [31] that, in advanced stages of loading the solution becomes sensitive to the behaviour of a limited number of elements located in the critical compression zones.

- The results of the finite element method indicate that this type of analysis will be valuable to the design engineer as it offers a complete picture of the stress distribution both in the concrete and the steel.

- No tool is perfect in itself, and this is also true of the finite element method of analysis. Several factors should be kept in mind. First, the method is an approximate analytical procedure, whose accuracy depends on the fineness of the mesh size used. Second, the accuracy of the analytical results, when referred to the actual reinforced concrete member, is dependent on including all of the major influences in the analytical idealisation of the actual member. Third, as more and more of these influences are incorporated into the analytical model the computational effort become so great that it begins to tax even the largest modern digital computers in terms of computation time and storage requirements.

### 2.2.2 Elasto-plastic Analysis

In 1968 Winokur and Gluck [10] presented an approach for the ultimate lateral load analysis of coupled shear walls. The assumption on which the work was based was that the collapse mechanism had plastic hinges at the points of contact between the connecting beams and the shear wall and at the bottom of the shear wall. The analytical procedure comprised of the following two main steps:

The first step consisted of the determination of the ultimate moments in the connecting beam which was considered to be a doubly reinforced concrete cross section. These moments were dependent on the percentage of reinforcement in the beam.

The second step considered the ultimate lateral load acting on the vertical cantilever and the ultimate moments acting at floor levels. The distribution of the external ultimate lateral load between the two shear walls is obtained by equating the deflections at the floor levels. In the analysis the indeterminate statical system was replaced with a continuous system subjected to distributed moments. The approach provided an effective means for the structural analysis of shear walls using simple formulae which can also be used for structures consisting of several simple or coupled shear walls with or without abrupt changes in cross section. A design method based on such a collapse mechanism was proposed and procedures were put forward to simplify the analysis and to achieve economy in reinforcement materials. In certain cases the resulting ultimate strength design procedure may be misleading e.g. it does not show the ability of the component parts of the system to contribute to its ductility associated with the overall mechanism

required to resist shear forces. Therefore, it is important to be able to assess the order of magnitude of the ductilities, particularly in the coupling beams, which are needed to develop in order to obtain the ultimate strength of a shear wall structure.

This work was extended by Paulay [46] in which an elasto-plastic analysis of a coupled shear wall was presented with more emphasis placed on the ductilities particularly in coupling beams where high shear forces may inhibit large postelastic deformations. It was shown that the laminar analysis can be readily extended to assess the elasto-plastic behaviour of coupled shear wall structures at various stages of cracking. A step by step procedure was suggested for the evaluation of the post-elastic performance of the structure. The need to check the ductility requirement in assessing the ultimate strength of a coupled shear wall was also emphasised. Paulay [46] also showed that the demands for laminar ductility were affected by the relative stiffness of the coupled shear wall and that the ultimate load of coupled shear wall structures needs to be compared with the strength of its foundation. In most cases, the aforementioned approaches are not applicable in practice because the coupling beams may not supply the required rotational ductility factor to allow the formation of the collapse mechanism.

In order to assess the significance of this problem Gluck [47] presented an elasto plastic procedure of lateral load analysis of coupled shear walls based on the continuum approach in which plastic hinges at the ends of coupling beams are allowed

to develop only in part of the height of the wall as shown in Figure 2.17. The structure was divided up into three zones where it was assumed in the analysis that the upper and lower zones behaved elastically and the middle zone behaved plastically. An upper triangular lateral load pattern was assumed and a series of plots were presented for the determination of the overall ductility factor and the associated rotational ductility of the coupling beam for various design characteristics which may be used in practice directly to design coupled shear walls in a more rational and economic way.

The analytical procedure and the plots which were presented are valid for only part of the height of the wall and are very often used to simulate the dynamic effect of earthquake motion.

To provide a basic treatment of the problem of yielding in the component parts of coupled shear wall structures a simplified elasto-plastic procedure was presented by Pekau [48]. In this case an attempt was made to examine the complete history of the response of laterally loaded coupled shear wall structures from the initial application of loading until overall collapse. The elastic continuum method was modified to allow for plastic action in coupling beams as well as in the two walls. The loading pattern which was adopted consisted of upper triangular loading together with a concentrated top load. Numerical examples were presented to demonstrate the application of the method and also a comparison was made with the results using three other approaches.

The first comparison was with the frame analogy method using the 20 storey

building examined in the study. Good agreement was noted at all stages of loading including final collapse in the case of the load-displacement relationship also for the magnitude of the internal forces in the beams and walls as shown in Figures 2.18 to 2.25. The beam shear force used in the proposed approach shown in Figure 2.18 is obtained by integrating the coupling beam shear between mid-height of adjacent storeys, whereas the curves for the wall bending moment shown in Figure 2.20 represent the average values at floor levels in the case of the frame solution.

The second comparison with the approach put forward by Gluck [47] using the 18 storey building described previously showed close agreement over the applicable ranges of behaviour as shown in Figures 2.23 and 2.24. The procedure developed by Gluck [47] gave a solution which was more accurate over this range of behaviour.

In the final comparison the results for the 18 storey structure reported by Paulay [46] were used in order to demonstrate the accuracy of this approach during each stage of behaviour. All the coupling beams yielded prior to the formation of plastic hinges at the base of the structure. The results from this investigation show that the displacements in Figure 2.25 and the internal forces agree closely for the two methods. It should be noted that the procedure developed by Paulay [46] assumes yielding of the upper connecting beams prior to formation of plastic hinges in the wall. The analysis proposed by Pekau [48] is not confined to a fixed sequence of yielding in the structure. In general, the method developed by Pekau [48] predicts results within an acceptable level of accuracy when the structure is

entirely elastic as well as in the nonlinear case when the beam has yielded locally within the overall structure.

## Summary

The most important investigations reviewed in this Section, relevant to the elasto-plastic analysis of coupled shear walls were as follows:

Modest overall plastic deformations in coupled shear walls may require the coupling beam system to possess a very large rotational capability. It is insufficient and unsafe to assess ultimate strength using the laws of equilibrium, behavioural mechanisms and yield criteria only. Ductility requirements also need to be checked.

Significant improvements in the analysis of coupled shear wall structures in the ultimate state were presented by Winokur and Gluck [10]. This approach provided an effective means for the structural analysis of shear walls with the aid of simple formulae. The approach can be also used for structures consisting of several simple or coupled shear walls with or without abrupt changes in cross section.

The investigation carried out by Paulay [46] was essentially an extension of the work carried out by Winokur and Gluck [10]. The proposed method of analysis showed how laminar analysis can be extended to assess the elasto-plastic behaviour of the structure.

Gluck [47] showed the beneficial use of the continuum approach in the analysis of coupled shear walls in the elasto-plastic state. Several relationships were presented [47] for a range of design characteristics which may be used directly for practical design including the determination of the ultimate load for a given rotational factor. It can be concluded that the proposed approach leads to a more rational and economic design of coupled shear wall structures.

Finally, Pekau [48] developed a simplified elasto-plastic procedure to be used to examine the complete load history of coupled shear walls. The modification of the elastic continuum method was adopted in this investigation and three comparisons were made. The results from the investigation confirmed that the approach was capable of predicting the magnitude of the load with a reasonable degree of accuracy.

### 2.2.3 Experimental Investigations

The first test on a large scale reinforced concrete coupled shear wall was reported from Rumania [49]. These models were studied under monotonic loading. As part of a research programme on shear walls an investigation into the behaviour of coupling beams was undertaken by Paulay [11] in 1971. In this study the nature of the interaction between flexural and shear in cracked deep beams, the mechanism of the shear resistance, the deformation characteristics and stiffnesses were investigated. The effects of alternating cyclic loading was examined but this is not the subject of the present programme of research. Nine coupling beams were tested with different span to depth ratios. The dimensions and the properties of these test beams are given in Figure 2.26 and Table 2.1. An analytical study was carried out on the use of the equilibrium requirement of the free body shown in Figure 2.27. It was shown that no matter how much stirrup reinforcement was provided, the flexural reinforcement will always be subjected to tension in the compression zone of the diagonally cracked coupling beam. Secondary horizontal reinforcement was used in these test beams to increase their ultimate capacity and to control the crack patterns. However, in the design, the area of the additional secondary reinforcement was not included but will be capable of providing at least a 15% increase in the strength of the beams. In all these tests the deflection measurements showed that the shear distortions greatly overshadow those produced by flexural effects. The loss of stiffness of the test beams after cracking, was considerably more than the loss encountered in normally proportioned reinforced concrete flexural members. It was also less than that predicted using

elastic analysis assuming homogeneous sections when shear deformations are also considered. The test measurements and the results from the analytical studies indicate that in the beams included in this investigation the loss of stiffness caused by diagonal cracking was of the order of at least 80%. In general it was observed that the structural behaviour of relatively deep beams differs significantly from that of beams based on the conventional concept of double curvature bending.

In the same year Paulay [11] presented a detailed study of spandrel beams, with the aim of establishing experimentally all aspects of their behaviour under conditions which are likely to occur during a severe earthquake and to enable reasonable analytical predictions to be made. Fourteen spandrel beams from typical coupled shear walls were tested in the investigation. The span to depth ratios of these approximately half full size specimens were 2.0, 1.29, and 1.03. Detailed information on the investigation was published earlier [11]. In order to ensure the maximum shear resistance, separation of the beam along the main diagonal must and can be suppressed. This may be achieved by providing stirrup reinforcement to resist the whole of the shear developed when the flexural capacity is attained. The introduction of a plate by Subedi [2] for shear reinforcement to minimise the damage from the coupling shear force is a feasible solution. Paulay [11] also showed that the cause of failure in spandrels adequately reinforced for shear, is crushing of the concrete due to the presence of the flexural and diagonal compressions, or it is a shear slip in the compression zone across previously formed cracks because of the break-down of aggregate interlock friction. Commonly both effects occur

simultaneously.

The research work carried out by Paulay and Binney [50] in 1975 consisted of the analysis of conventionally reinforced coupled beams containing horizontal flexural reinforcement and vertical stirrups to provide resistance to shear. The investigation was aimed at improving the ductility of these coupling beams and in particular in suppressing the shear failure mode. Three beams were instrumented and tested under reversed cyclic loading so as to impose large post elastic deformations i.e. ductilities. The conventional flexural reinforcement normally consisting of a group of horizontal bars in the top and the bottom of the beams, was omitted. Instead groups of diagonal bars were used which intersected at the midspan of the beam. The objective was not to supplement the strength of the conventional web reinforcement, consisting of vertical stirrups but to provide reinforcement consistent with an entirely different internal resisting system of forces. The approach was included to simulate the behaviour of cross bracing. The two types of beams used in the experimental investigation are shown in Figure 2.28 and the rotation of the coupling beam is shown in Figure 2.29. It was difficult to accommodate two symmetrical sets of diagonal bars because all the beams were 152 mm wide. Four 22 mm diameter bars were used in two layers in one direction and between these three 25 mm diameter bars were placed in a single layer in the centre of the 152 mm width of the beams to overcome this problem. Load was applied to the beams in approximately ten increments during each cycle and then it was reduced in two to three increments to zero. The strain readings along the four diagonal

bars were recorded. The results from the investigation showed that the use of diagonal bars in coupled shear walls can increase the stiffness of the beam and prolong their effective contribution during catastrophic earthquakes. A detailed design procedure for diagonally reinforced coupling beams was described and put forward by Paulay and Binney [50].

Yamada and Kawamura [51] in 1975 aimed to clarify by means of Laboratory based tests, the elasto-plastic deformation behaviour of a confined concrete shear wall unit with openings. They also tried to clarify analytically the strength and deformation related behavioural mechanisms in this form of shear wall. These tests were carried out mainly on the effects of the width and depth ratio of the opening to the inside width and depth of the surrounding frame upon the resisting characteristics of the shear walls. In the investigation the main resisting factors are the shear deformation of the side walls with the columns and the bending deformation of the beams. Therefore, the beams are idealised such that they comprise of shear compressive resisting elements in the form of an equivalent brace and the flexural resisting element as a T-section. The results obtained by the investigators show that the computed values resulting from the idealised analysis agree reasonably well with the test results. Two main types of failure modes were identical i.e. a brittle mode caused by the shear compressive fracture of the concrete in the side walls and a ductile mode caused by flexural yielding of the beam with the T-section. It was found that the critical condition between these two main fracture modes was mainly influenced by the reinforcement surrounding

the opening and the thickness of the walls, i.e.

- An increase in the reinforcement surrounding the openings resulted in an increase in the resistances of the flexural elements.
- A decrease in the thickness of the walls, resulted in a decrease in the strength of the shear compressive element.

A detailed study of the ductility of reinforced concrete coupling beams was described in a report by Paulay and Santhkumar [52]. This investigation was aimed at verifying the behaviour of the coupling beams which had been studied by Paulay and Binney [50], as part of the complete coupled shear wall structures. The results of the study, were reported briefly and compared to the more interesting features of the behaviour of two-one quarter full size seven storey reinforced concrete coupled shear wall models, with different reinforced coupling beams, when subjected to high intensity alternating cyclic loading simulating seismic effects. The two models used in the investigation into different coupling beam reinforcement arrangements are shown in Figure 2.30, and were tested in the horizontal position. The triangular distributed load commonly used in Building Codes was modelled by the investigators by applying three point loads of equal intensity in the third, fifth and seven floors. It was found that all the coupling beams in the conventionally reinforced wall failed by sliding shear after several cycles. In contrast, the diagonally reinforced coupling beams in wall B shown in Figure

2.30 indicated no sign of distress under similar loadings despite the presence of large measured strains. The investigators emphasised that the energy absorbed by the diagonal reinforcement was considerably larger particularly at low loads. The shaded area in Figure 2.31 shows that the extra energy absorbed along the instrumented lengths of the diagonal reinforcement was approximately 50% of the corresponding total energy absorbed by the beam in wall A shown in Figure 2.30. The performance of the two models when subjected to very severe displacements were compared in terms of stiffness degradation, ductilities attained and energy absorbtion capacity. In every respect the investigation showed the superior performance of the coupling beam reinforced diagonally. In general the results from the investigation indicate that with careful detailing, particularly in the area where yielding can occur, coupling shear wall structures can be made to possess all the desirable features of an effective earthquake resistant structure.

Detailed studies were conducted on 1:25 models of complete shear wall buildings in 1976 by Irwin and Young [53]. These studies were used to determine the overall behaviour of complete buildings subjected to lateral loading resulting in elastic and elasto-plastic behaviour of the structure. Larger scale model tests on walls coupled by beams were carried out by Paulay [54] in 1975 to determine the sequence of hinge formations and the failure patterns for a range of wall geometries. In 1975 Irwin [4] also carried out combined torsion and vertical load tests on reinforced concrete shear wall structures at a scale of 1:25.

A limited number of experiments were carried out by Chana [55] in 1988. These tests were used to give an insight into the behaviour of reinforced beams, with particular reference to the shear failure mechanisms. A series of beams, 200mm deep and 100mm wide with four 10mm diameter (1.8%) high yield steel bars as the main reinforcement and nominal compression steel were included in the investigation. These results showed that in the case of the beams which were reinforced against dowel failures, the shear failures were accompanied by yielding of the main reinforcement. This reinforcement is, however, unable to develop its full flexural potential owing to the presence of dowel action and the reduced neutral axis depth observed in the case of shear failures. During the investigation, it was noted that in the beams with large stirrup spacings, failure was attributable to splitting at the level of the reinforcement without yielding of the reinforcement.

A new approach to reinforcing shear wall coupling beams, where shear is dominant, was introduced by Subedi [2] in the late 1980's. The approach involved the replacement of stirrups by vertical plates to absorb the shear stresses and ordinary reinforcement bars to resist the bending moments. In parallel with the experimental work an analytical approach based on the equilibrium of a half beam was adopted. A total of six beams were tested in this investigation; four beams were reinforced with a restricted depth plate and two other with a full depth plate. Three different thicknesses of plate reinforcement (2.0, 4.0 and 6.0 mm) were also used. The experimental models consisted of two beams arranged symmetrically and cast monolithically with the reinforced concrete columns as shown in Figure

2.32. All the beams tested contained two 16 or 20mm diameter reinforcement bars in the top and the bottom for flexural resistance and a profiled plate as shown in Figure 2.33. The shear resistance of the profiled plate was provided by incorporating semi-circular cut-outs along the edges to ensure the full composite action and to avoid slippage in the longitudinal direction.

It was shown that the failure of the beam containing the thinnest plate (2mm) was characterised by a large shear crack running at an angle of approximately $45^0$ and a large horizontal crack indicating that there was no transfer of horizontal shear between the top of the plate and the main reinforcement bars. The second type of beam reinforced with a 4mm thick plate failed in a similar manner except that the failure load was closer to the predicted failure load. The failure of the beams containing full depth 4.0 and 6.0 mm thick plates was characterised by splitting of the concrete along the compressive diagonal. The investigation showed that the main problem associated with this type of construction was the possibility of slippage at a premature stage, caused by the horizontal shear at the interface between the main bars and the top of the plate. It was also shown that higher values of shear stress can be achieved by using a thick plate. In all cases the results obtained from the programme of experimental work were compared with those obtained from the analytical studies and good agreement was achieved as shown in Table 2.2.

A mathematical failure model to predict the ultimate strength of reinforced concrete coupling beams was proposed by Subedi [56] in 1990. This method was

used to verify the results from nine beams previously tested by Paulay [11]. The proposed method was based on the equilibrium of a triangular section of the beam subjected to flexural and shear stress actions in which the structural behaviour is governed by shear. The method was found to give a satisfactory prediction of the mode of failure, the ultimate strength and the distribution of the forces in the main reinforcement bars.

In the late 1980's Kotsovos [57] also introduced a new and simplified model representing the ultimate limit state of simply supported reinforced beams subjected to transverse in-plane loading. The model referred to as the Compressive Force Path concept was in the form of a simple design procedure which was shown to yield design solutions that were both safer and significantly more economical compared to those obtained using other widely used approaches. The implementation of the Compressive Force Path concept in beam design has been based on modeling a beam at its ultimate limit state as a frame with inclined legs tied together by the tension reinforcement, with a frame providing a simplified yet realistic representation of the beam in the region of the path of the compressive force. A full description and verification of the method have been published in [1], [58], [59]. It was demonstrated that the proposed model and ensuing design method can be extended easily to apply to any type of skeletal structural concrete configuration [60], where the model represents the structural elements between consecutive points of inflection with the interaction between the elements in the region of such points being modeled as an "internal hinged support" affected by

the provision of transverse reinforcement.

There is a clear need for further testing in the areas where the structure is indeterminate, enabling the development and validation of realistic models. For the present, the proposed method is limited to very simple tests of simply supported beams and consists of empirical fits to test data.

## Summary

The most important findings from the research work discussed in this Section can be summarised as follows:

The need for diagonal reinforcement bars to resist the large diagonal tension force resultant was recognised by Paulay [11]. In the response to this need, a new reinforcement arrangement was developed in which diagonal bars crossed the shear span diagonally from one support to the other. The introduction of these reinforcement bars in the coupling beam was found to have a significant influence on the strength and stiffness. The provision of such reinforcement bars was also found to improve the ductility of the beam.

Subedi [2] attempted to improve the strength of coupling beams by introducing a new type of reinforcement. The introduction of a plate to provide resistance to shear was found to be a feasible solution to this crucial problem in these structures. It must be pointed out that the use of plate reinforcement has potential and can lead to a practical solution to the design of coupling beams. It was found that the overall strength of the coupling beams can be increased significantly by varying the thickness of the plate. The proposed design procedure was presented in a straight forward way so that it can be readily adopted by practicing structural engineers. The procedure is also applicable to coupling beams regardless of the type and the percentage of the reinforcement present in the structure.

The design approach proposed by Kotsovos [61], [58], [1] has been developed based on an understanding of the actual structural behaviour of the beams under transverse loading. It was shown that the collapse of a beam occurs as a result of the

development of transverse tensile stresses along the compressive force path which consists of horizontal and inclined leg regions. The model did not deal specifically with the design of coupling beams, but resulted in a moment redistribution in continuous beams which made the coupling beams less critical.

It can be concluded that the Compressive Force Path concept has the advantage of considering the overall behaviour of the beam. It also offers a realistic explanation based on a better understanding of the concrete at the material level [1], [62], [63] of the causes of diagonal failure which in this context, is related to the actual state of stress in the compression zone of the beam structure in which the transverse tensile stress initiates the failure.

On the basis of the Compressive Force Path concept, the load-carrying capacity of the structural member is associated with the strength of the concrete in the region of the path along which compressive forces are transmitted to the support.

## 2.3 CONCLUSIONS

In attempting to summarise the many publications in the field of shear wall structures, the papers which were particularly relevant to the present study were selected. The papers included in this Chapter describe the likely behaviour of shear walls in multistorey buildings when subjected to lateral loading, for both elastic and plastic conditions. These studies have considerably advanced our understanding of the behaviour of shear walls and have resulted in the development of approaches which can be used to assess the behaviour of these major lateral load resisting structures in multistorey buildings. The main conclusions which can be drawn from this review can be summarised as follows:

- The main problem in reinforced concrete coupling beams is the presence of a large diagonal crack crossing the beam from one corner to the other. This critical shear force must be resisted by reinforcement in order to prevent the brittle failure of the coupling beams. Such reinforcement which is provided to absorb the shear should be of a practical form in order not to give rise to any difficulties during construction. Another major problem in coupling beams is the need to effectively anchor the main reinforcement in the adjoining structural members.

- The contribution of the majority of researchers [11] [52] [50][10][2] has taken the form of theoretical and experimental investigations conducted on test beams containing different reinforcement arrangements. These investigations have resulted in the presentation of test results accompanied by a

number of conclusions and recommendations based on the behaviour of the beams observed during the tests. Several investigations have also attempted to develop a rational set of design recommendations for coupling shear wall structures.

- A considerable amount of research work has investigated the effect of lateral loading on the shear strength of coupled shear walls. The results have tended to be of a practical nature.

- To date, there has been an absence of an understanding of the actual behaviour of such structures. As a result of this, no effective, design procedures currently exist in a Code of Practice.

- The problem of coupling beams has been addressed by setting limitations on the the percentage of the web reinforcement which can be used to resist the shear force.

- All the different approaches used by investigators have been used as a basis for the present programme of research which has attempted to develop new ideas for the reinforcement of coupling beams with expanded metal mesh and also to develop a design approach which can be used with this new type of reinforcement.

The above statement highlights the extent of the absence of work in the literature relating to reinforced coupling beams, which emphasises the need for the development of a more rational and unified design procedure for different types of web reinforcement.

| Beam number[a] (1) | Concrete strength when tested, in pounds per square inch (2) | Flexural steel content, as a percentage[b] (3) | Yield strength of flexural reinforcement, in kips per square inch (4) | Web steel content, as a percentage (5) | Yield strength of stirrups, in kips per square inch (6) | Horizontal secondary reinforcement, number and size of bars (7) | Yield strength of horizontal reinforcement, in kips per square inch (8) |
|---|---|---|---|---|---|---|---|
| 311 | 5,330 | 1.58 | 44.5—46.5 | 0.88 | 56.0 | None | — |
| 312 | 5,100 | | | 1.65 | 41.3 | None | — |
| 313 | 6,450 | | | 2.52 | 45.5 | None | — |
| 314 | 6,490 | | | 2.52 | 45.5 | 4—No. 5 | 45.5 |
| 315 | 5,500 | | | 2.43 | 46.5 | 4—No. 5 | 46.5 |
| 391 | 4,570 | 1.06 | 45.8 | 0.88 | 59.0 | 6—No. 3 | 59.0 |
| 392 | 5,460 | | | 0.88 | 59.0 | 6—No. 3 | 59.0 |
| 393 | 4,460 | | | 1.62 | 47.5 | 6—No. 4 | 47.5 |
| 394 | 6,260 | | | 2.52 | 45.5 | (4—No. 5)<br>(2—No. 4) | (45.5)<br>(47.5) |

[a] The effective depths of the beams were 28.1 in. and 36.1 in., respectively.
[b] $100 A_s/bd$.

Table 2.1: Properties of the test beams. Paulay [11]

| Beam | Test | | | Analysis | | | | | Predicted | | | |
|---|---|---|---|---|---|---|---|---|---|---|---|---|
| | Observed behaviour | Failure load $P_{e\,test}$: kN | Average shear stress $v$: N/mm$^2$ | Flexural failure $P_{e1}$: kN‡ | Shear (diagonal splitting) failure | | | | Composite deep girder $P_{e3}$: kN | Mode of failure: kN | Ultimate strength $P_{e\,analysis}$: kN | $\frac{P_{e\,analysis}}{P_{e\,test}}$ | $\frac{P_{e3}}{P_{e\,test}}$ |
| | | | | | Concrete splitting force: kN* | Shear capacity of plate: kN† | Control of web | $P_{e2}$: kN¶ | | | | | |
| 1SP2 | Shear crack at 45° followed by separation at the interface between plate and main bars | 96 | 2·12 | 170 | 168 | 109 | Concrete | 145 | — | Shear (diagonal splitting) | 145 | 1·51 | — |
| 2SP2 | As for 1SP2 | 108 | 2·39 | 178 | 166 | 73 | Concrete | 147 | — | As above | 147 | 1·36 | — |
| 3SP4 | Shear crack at 45° separation at the interface at the final stages | 144 | 3·19 | 178 | 159 | 156 | Concrete/ plate | 135 | — | As above | 135 | 0·94 | — |
| 4SP6 | Shear (diagonal splitting and crushing at the compressions corners) | 174 | 3·88 | 264 | 211 | 224 | Concrete/ plate | 173 | — | As above | 173 | 0·99 | — |
| 5FP4 | As for 4SP6 | 220 | 4·87 | 253 | 212 | 372 | Plate | 185 | 209 | As above | 185 | 0·84 | 0·95 |
| 6FP6 | As for 4SP6 | 222 | 5·29 | 359 | 201 | 611 | Plate | 218 | 305 | As above | 218 | 0·98 | 1·38 |

* Concrete splitting force = $f_{cu}\, b\sqrt{[l^2 + (h')^2]}$.
† Shear capacity of plate = $(f_w/2)z\sqrt{[D^2 + s^2]}$, where $s = D(l/h')$.
‡ $P_{e1} = 2 \times P_{e\,test}$ for the double beam test specimens.
¶ $P_{e2} = 2 \times P_{e\,test}$ for the double beam test specimens.

Table 2.2: Comparison of results. Subedi [2]

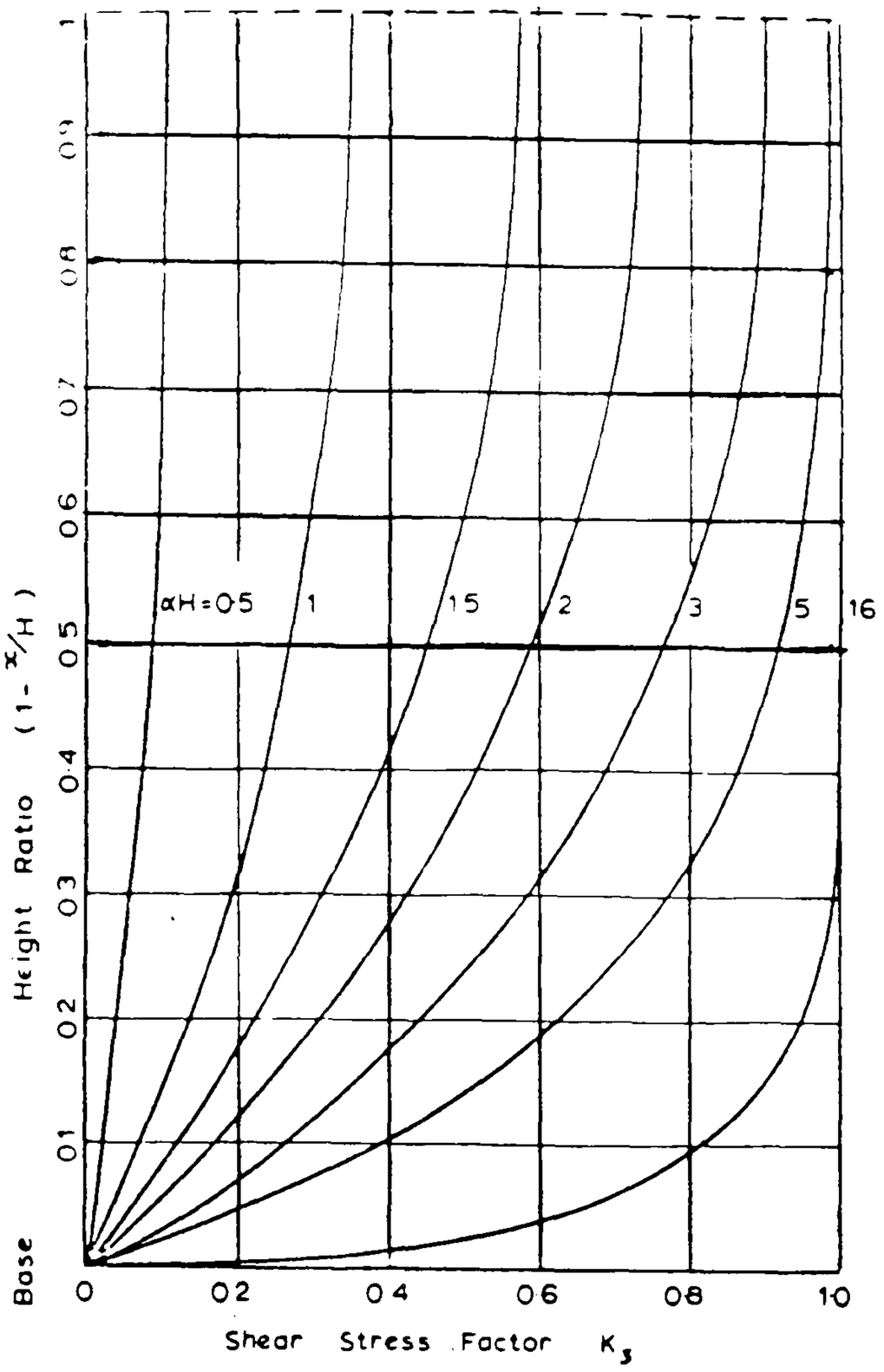


Figure 2.1: Variation of the connecting beam stress factor $k_3$ for point load at the top. Coull and Choudhury [27]

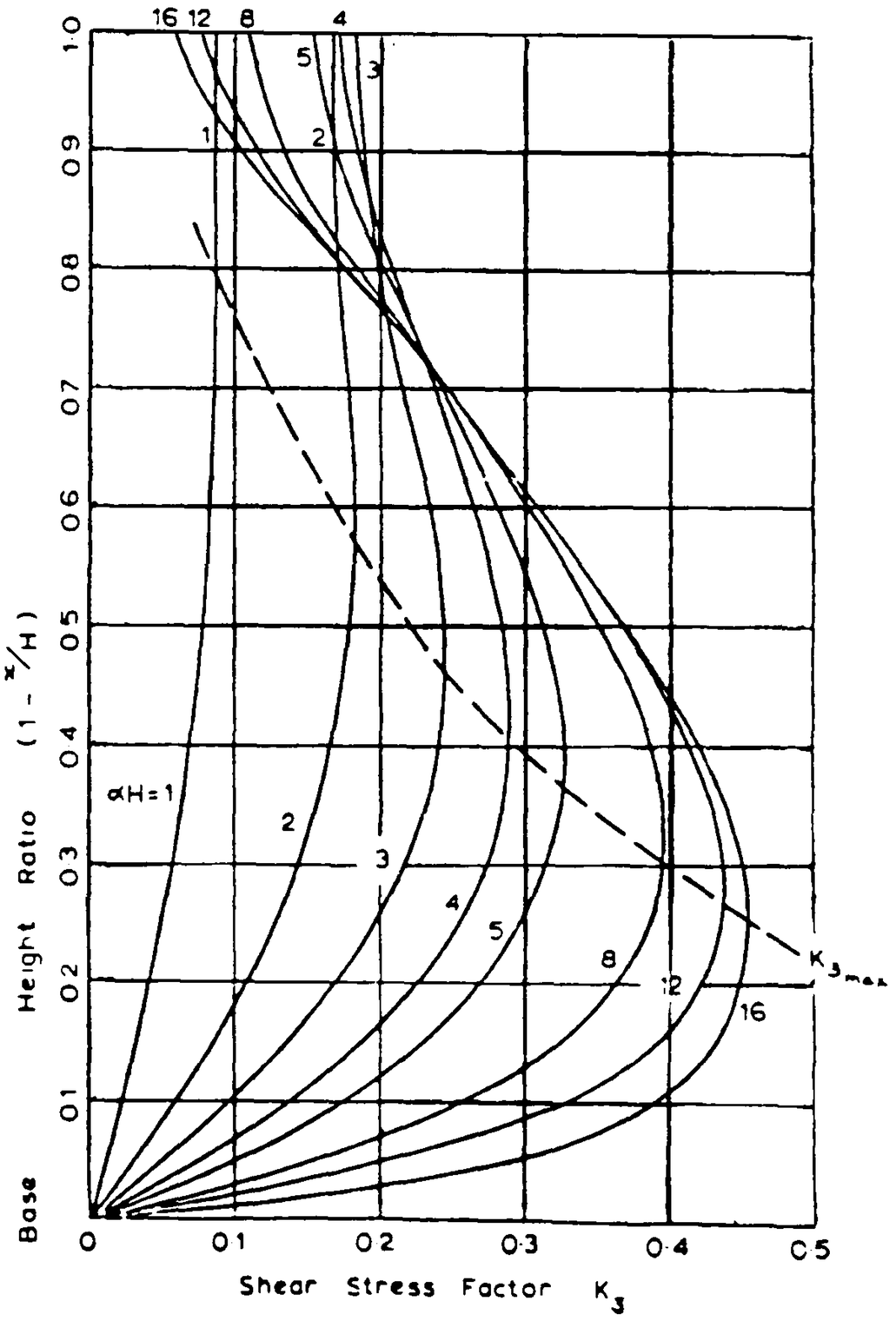


Figure 2.2: Variation of the connecting beam stress factor $k_3$ for triangular distributed load. Coull and Choudhury [27]

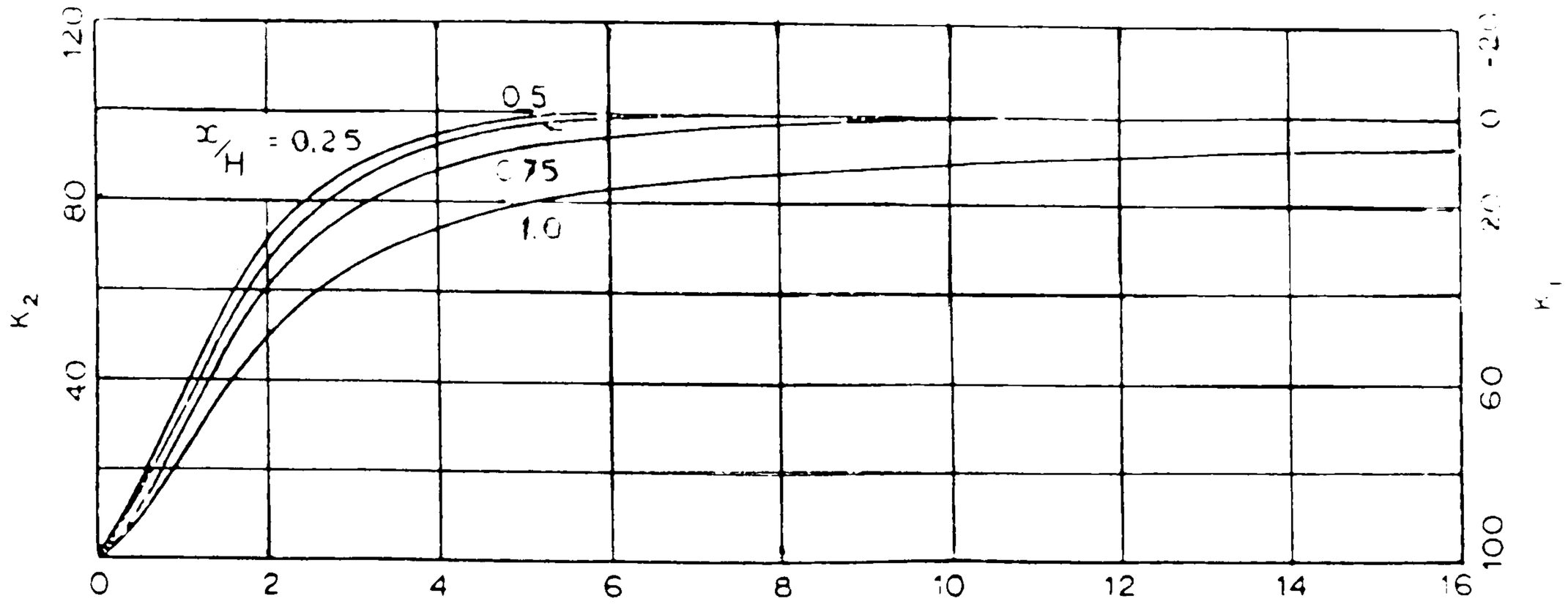


Figure 2.3: Variation of the wall bending stress factors $k_1, k_2$ for point load at the top. Coull and Choudhury [27]

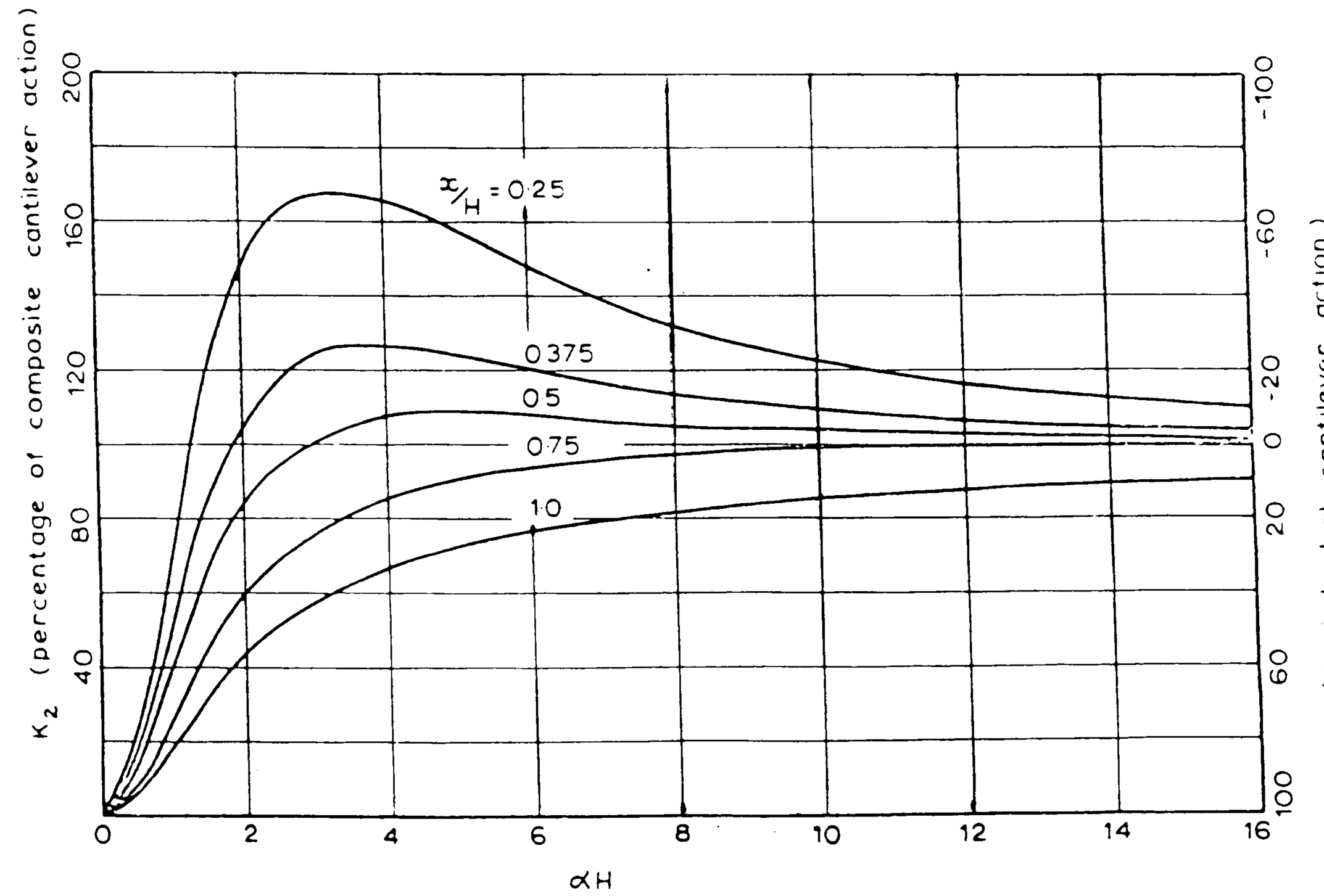


Figure 2.4: Variation of the wall bending stress factors $k_1, k_2$ for triangular distributed load. Coull and Choudhury [27]

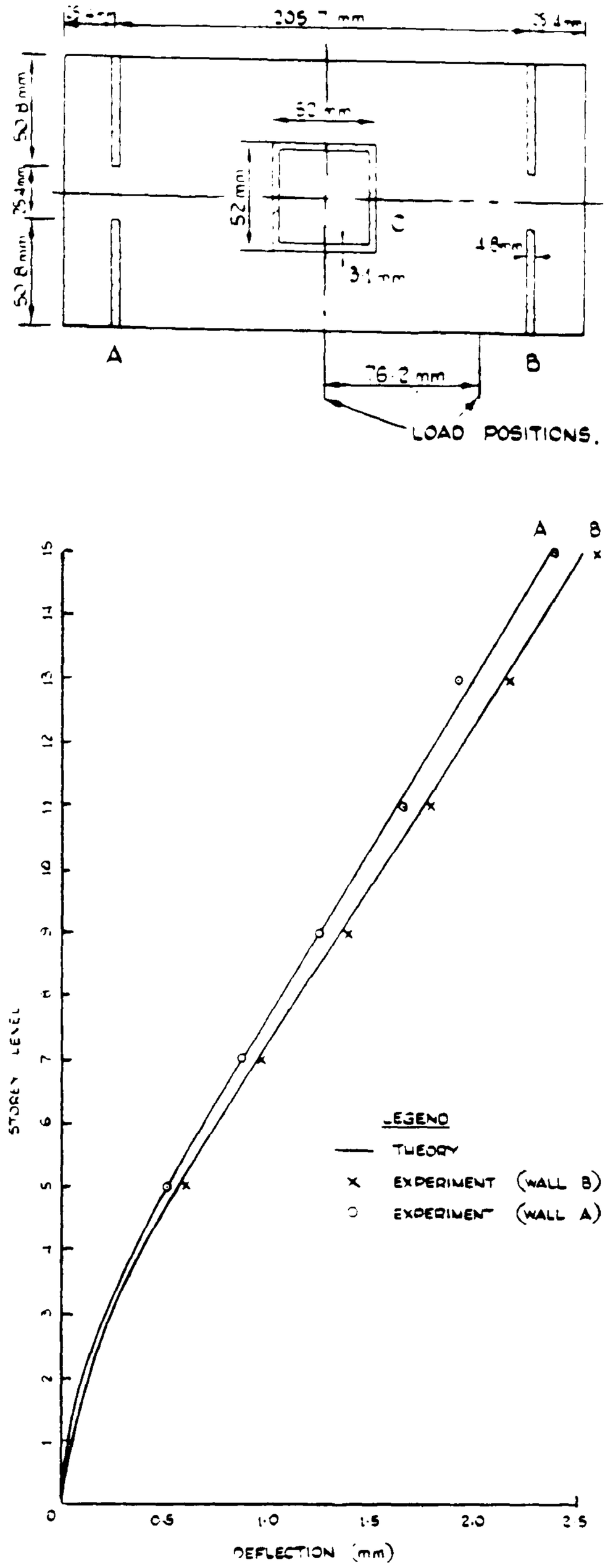


Figure 2.5: Deflection profile of walls A and B under uniform load. Coull and Irwin [24]

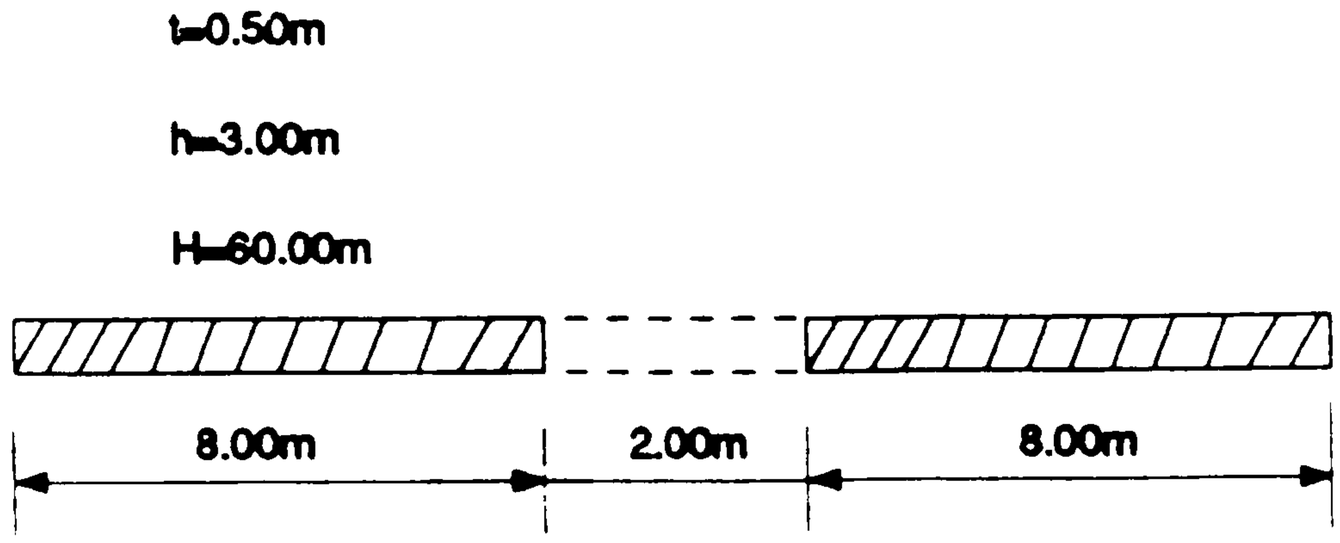


Figure 2.6: Design of the top stiffening beam on shear wall structure. Coull [25]

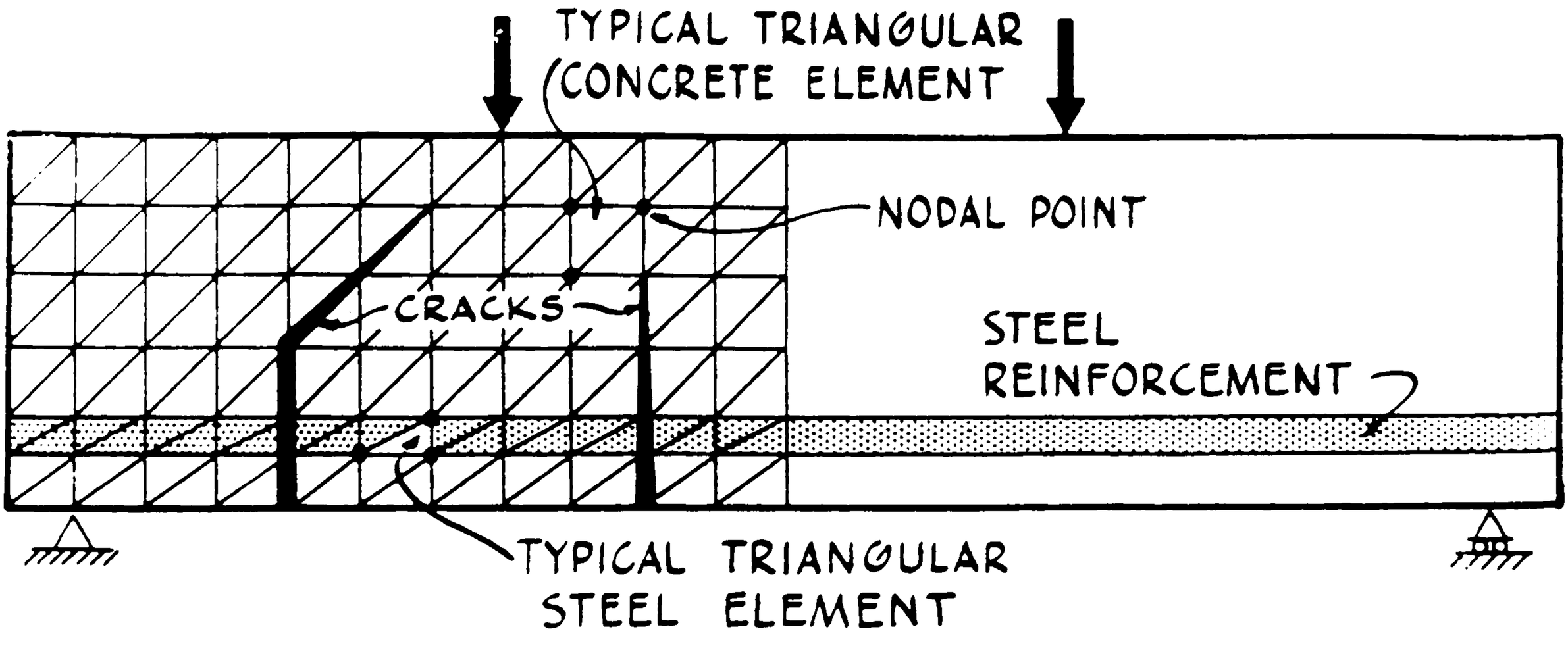


Figure 2.7: Finite element idealisation. Ngo and Scordelis [28]

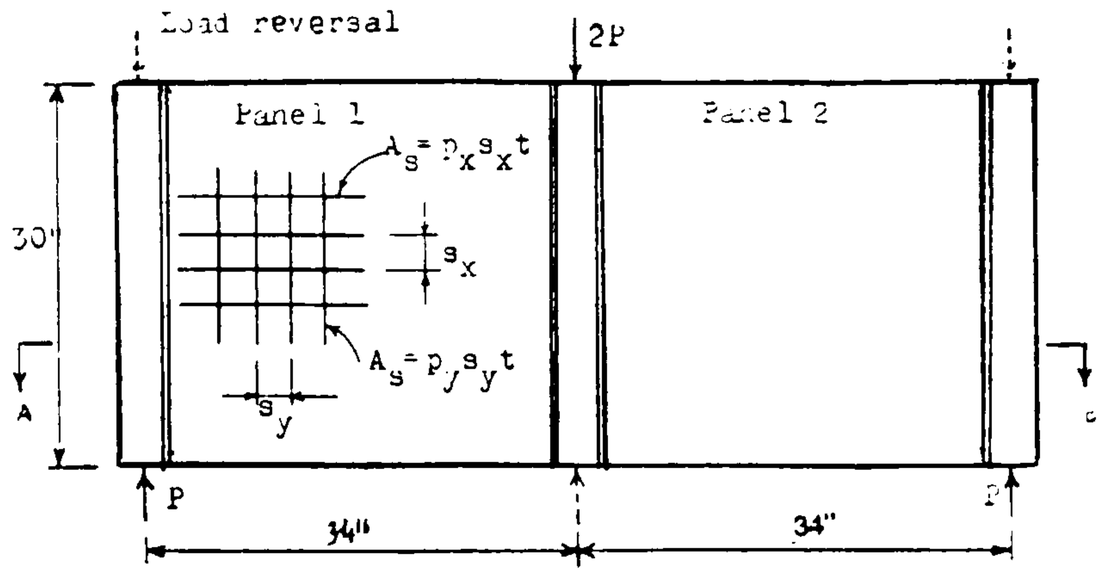


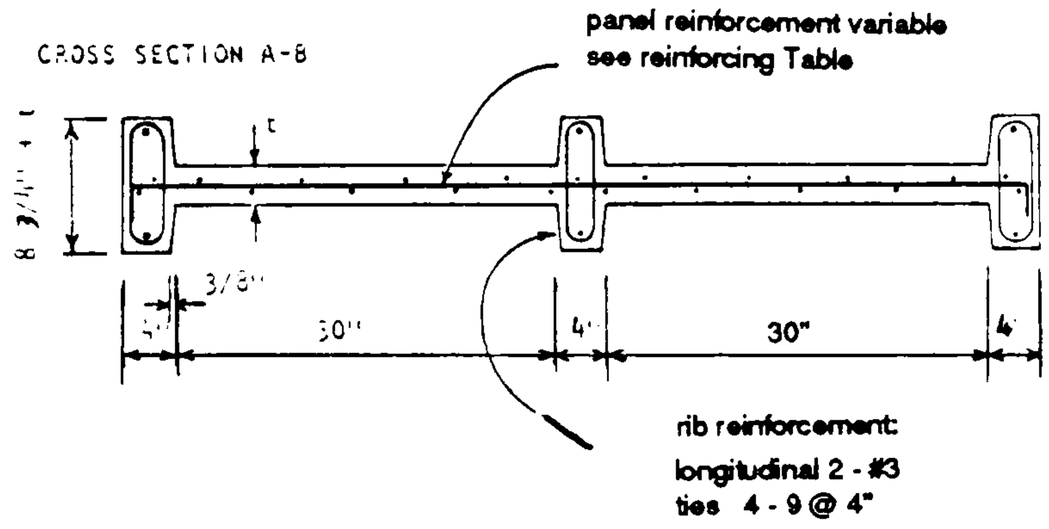


Figure 2.8: Cervenka [29] test specimen

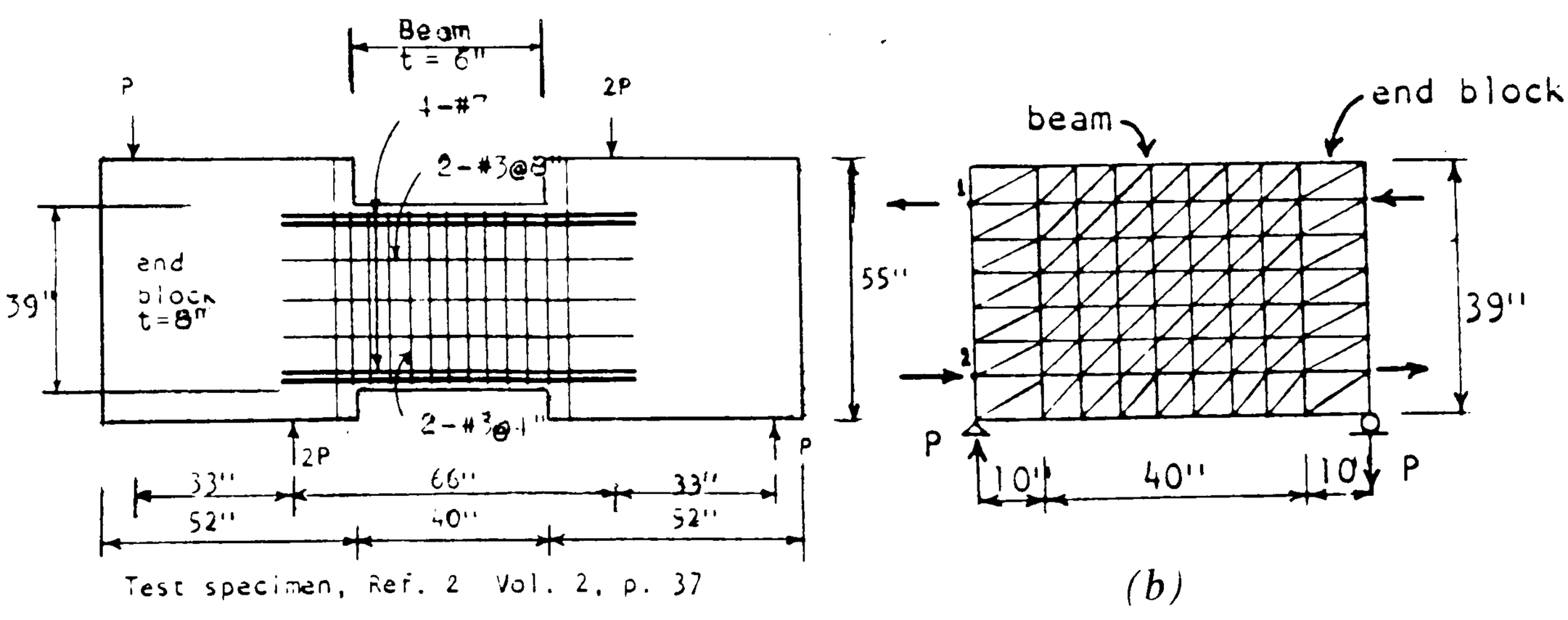


Figure 2.9: (a)Paulay [11] test specimen (b) the layout of the mesh

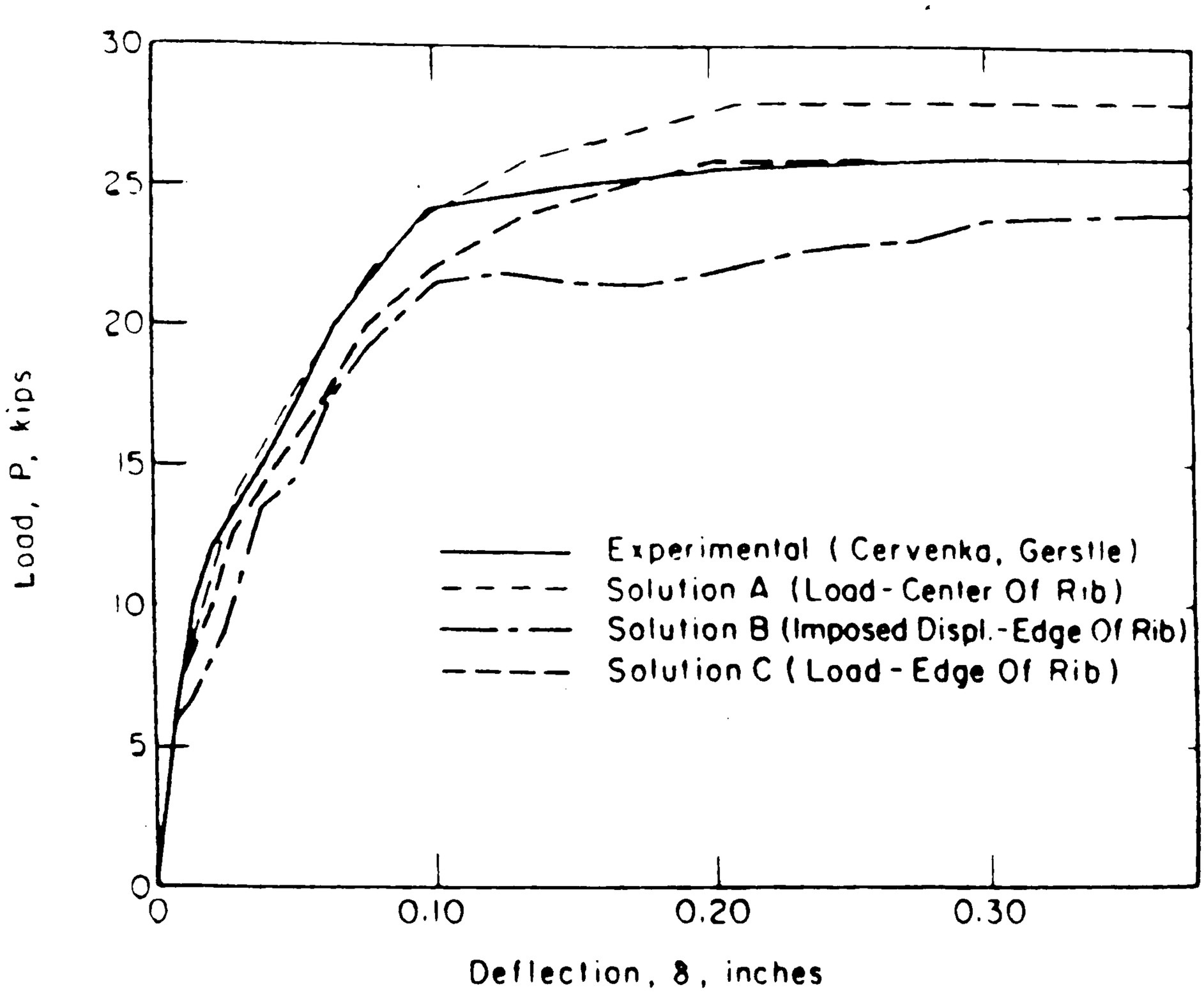


Figure 2.10: Load deflection curves for shear panel W-2. Darwin [33]

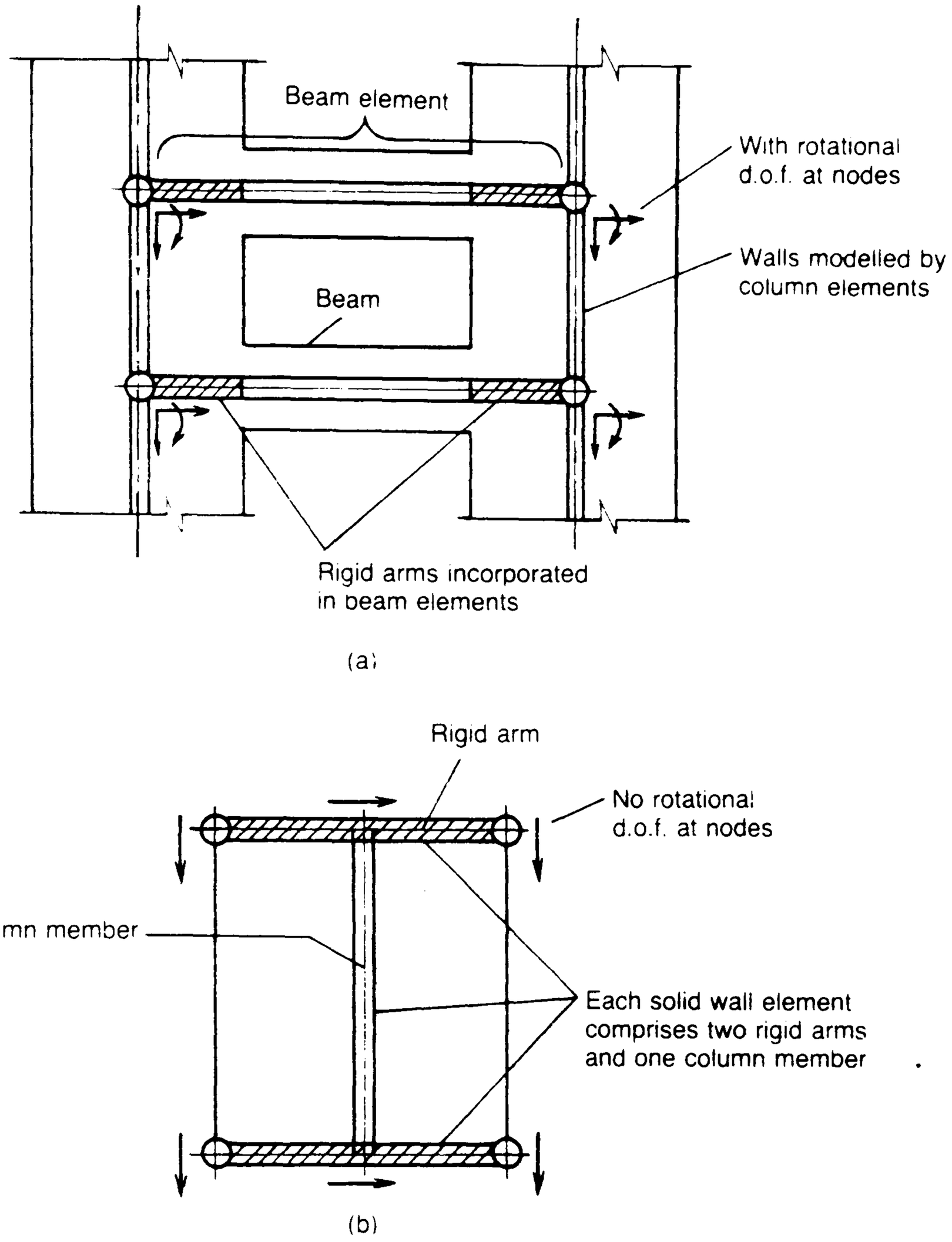


Figure 2.11: Wall elements used by Macleod and Hosny [39]: (a) wide column frame elements; (b) solid wall element (arrows designate degrees of freedom)

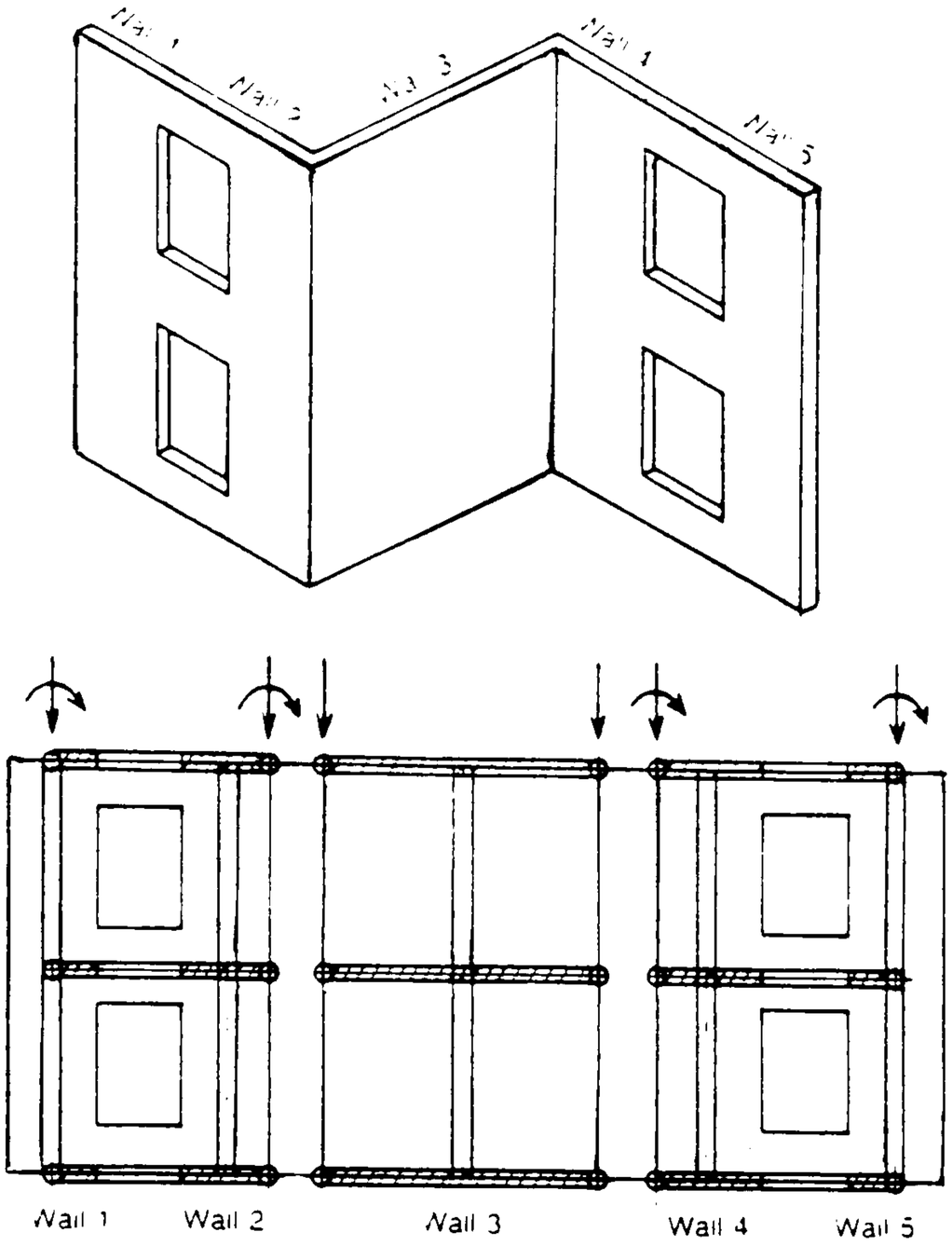


Figure 2.12: Macleod and Hosny's [39] test arrangement for wall connected to beams at one edge and another wall at another edge

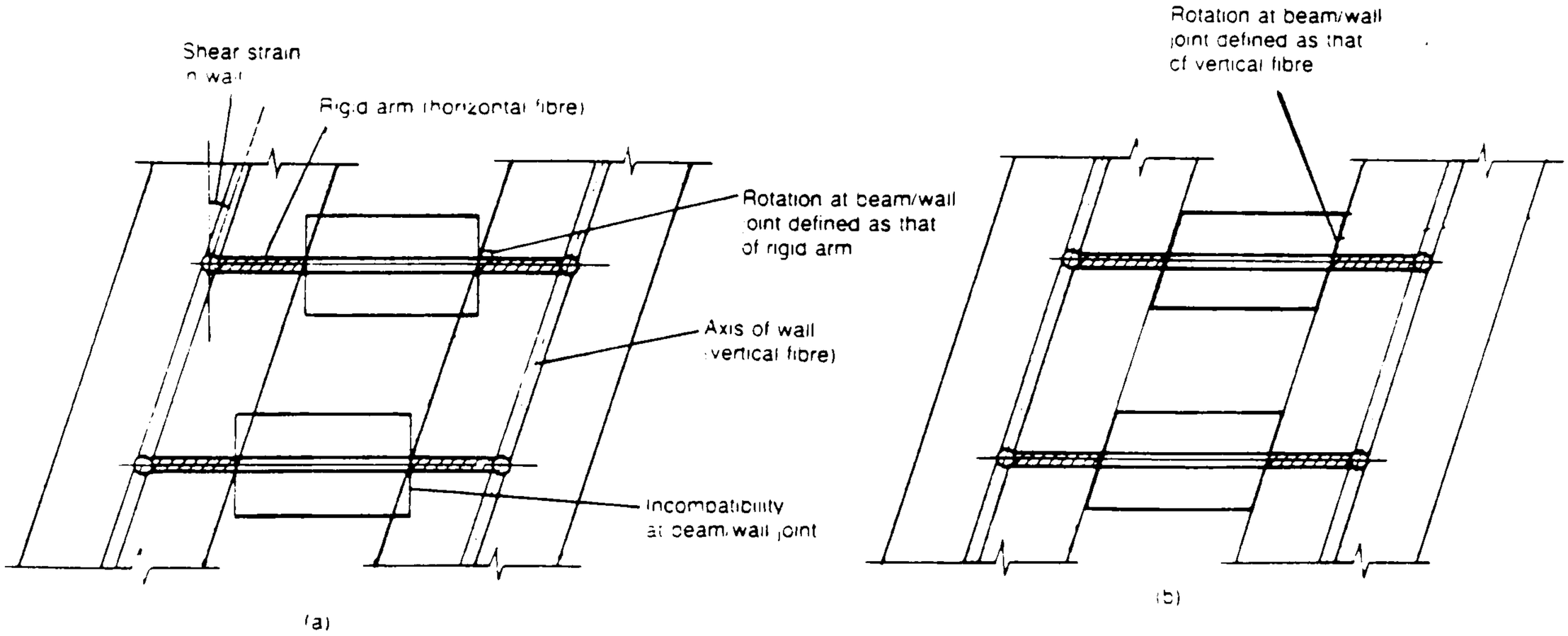


Figure 2.13: Two common definitions of nodal rotation degrees of freedom: (a) nodal rotation defined as rotation of horizontal fibre; (b) nodal rotation defined as rotation of vertical fibre

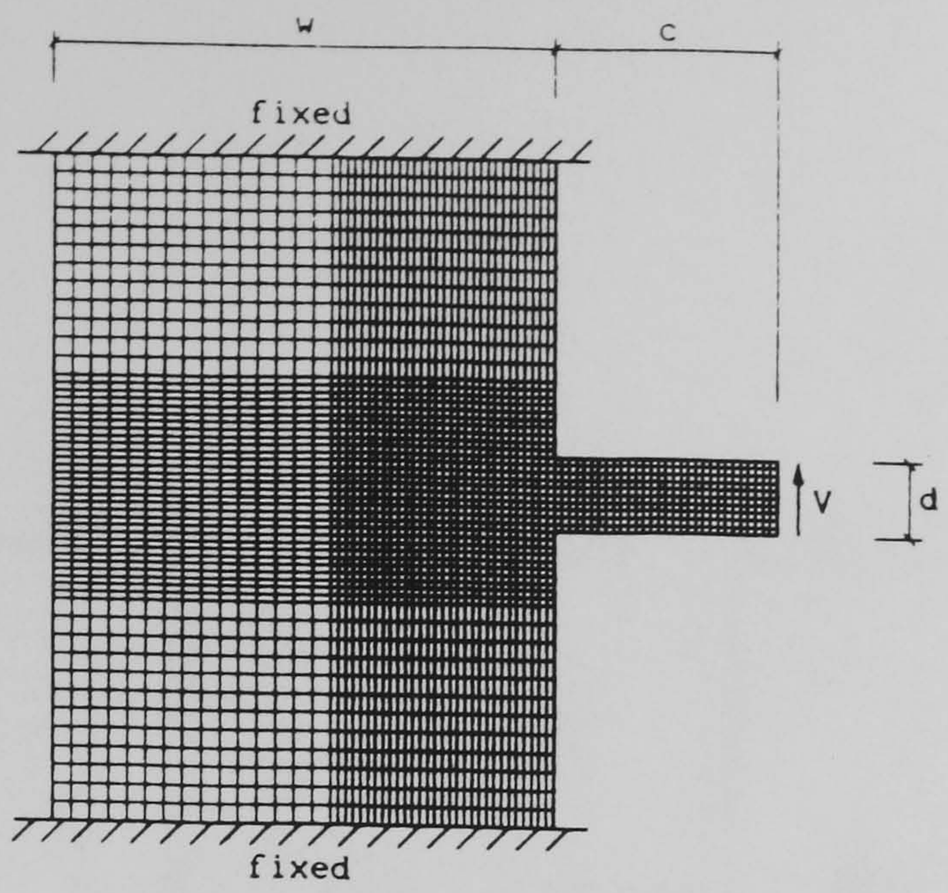


Figure 2.14: Finite element analysis of local deformations around beam-wall. Kwan [45]

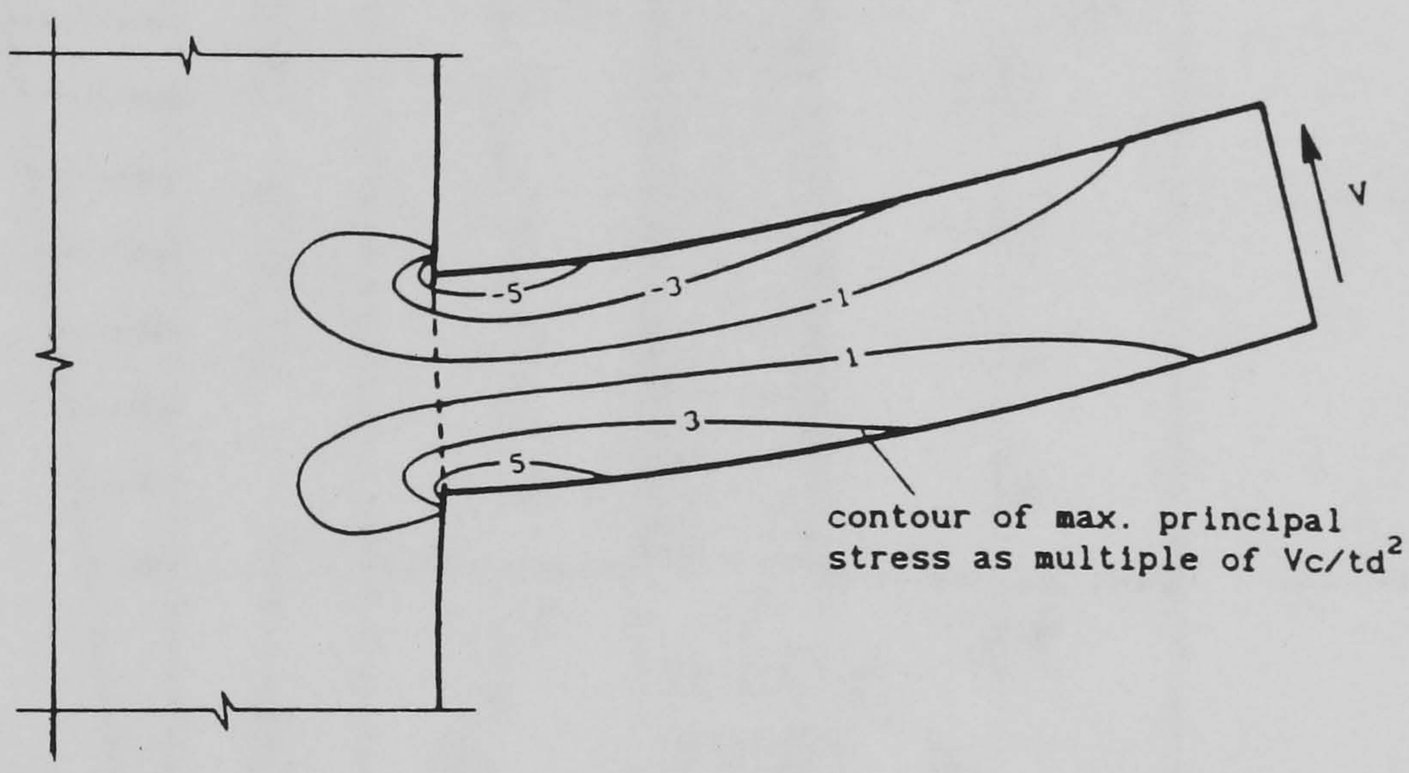


Figure 2.15: Local deformations and stress concentrations around beam-wall joint. Kwan [45]

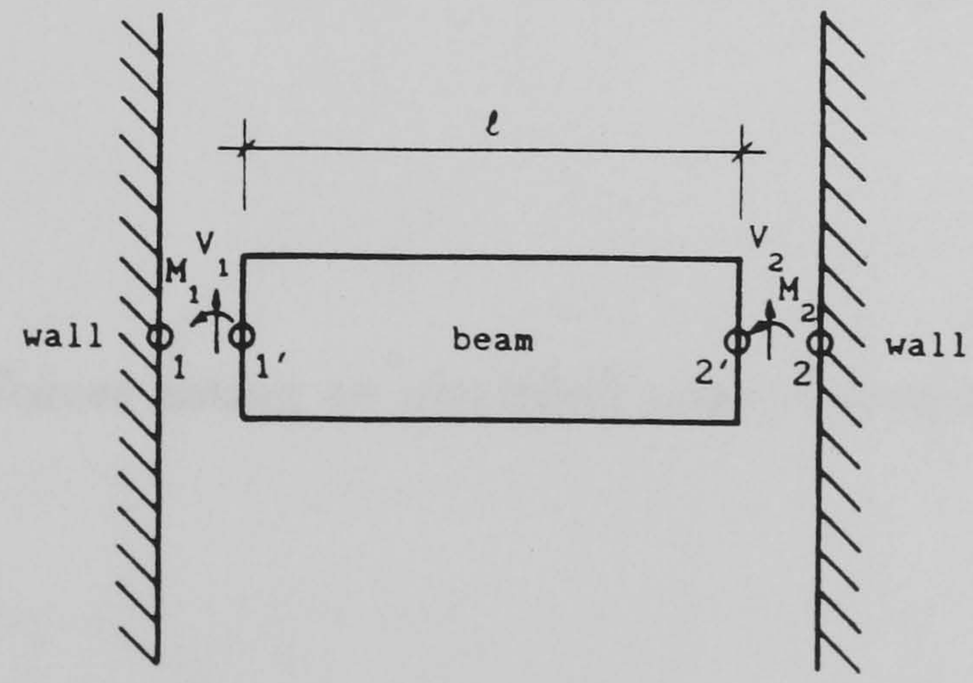


Figure 2.16: A beam element with allowance for joint deformations. Kwan [45]

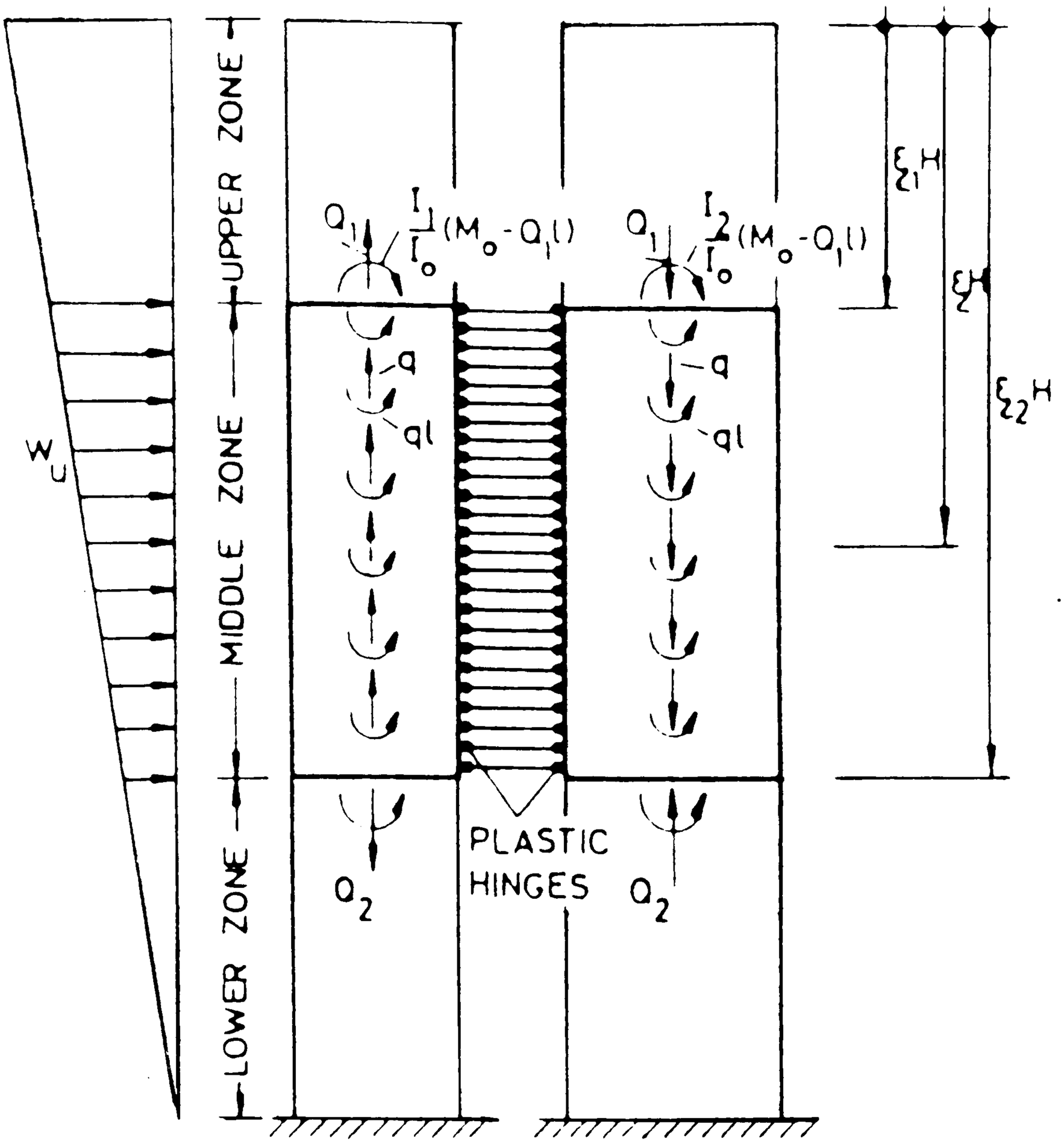


Figure 2.17: Forces acting on plastified zone of coupled shear wall. Gluck [47]

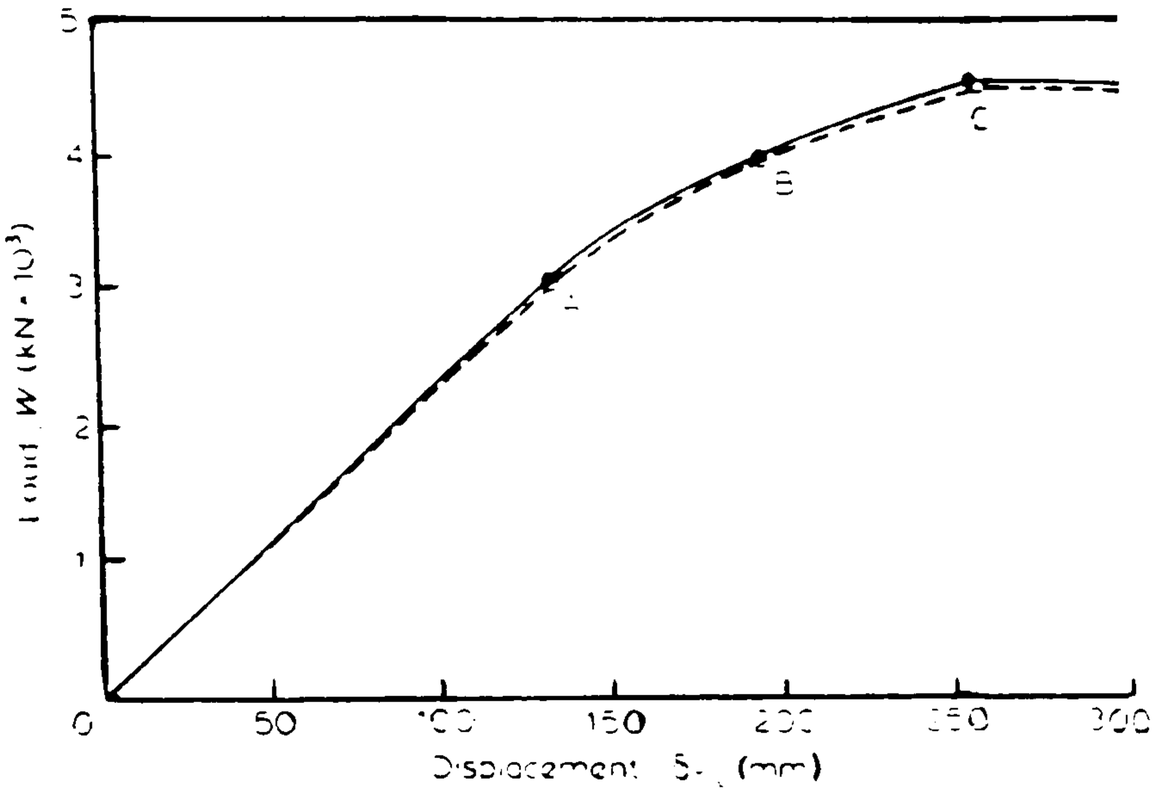


Figure 2.18: Proposed analysis versus frame analogy load-displacement. Pekau [48]. A, first yield; B, wall 1 yields; C wall 2 yields. (— ), proposed analysis; (- - - -), frame analogy

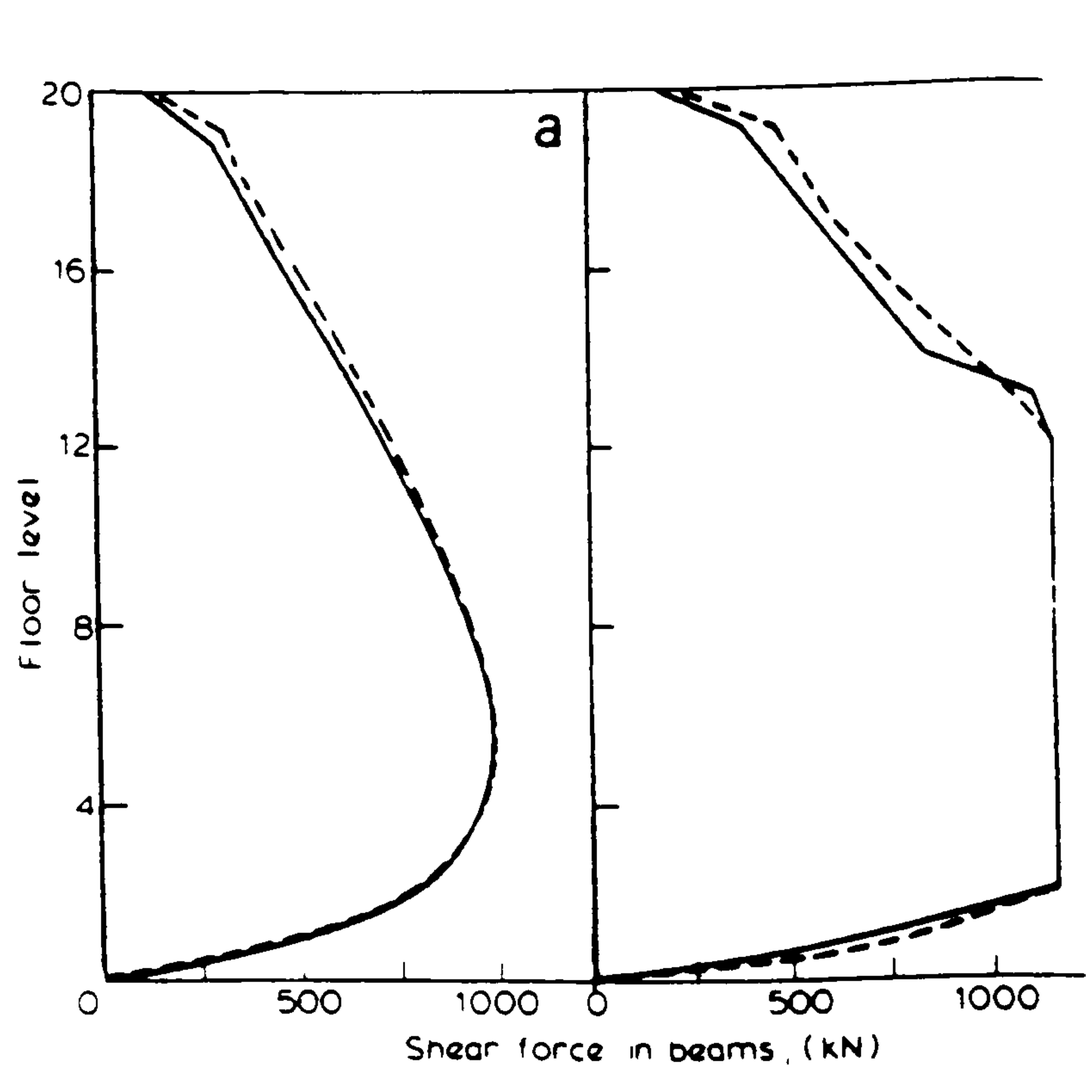


Figure 2.19: Proposed analysis versus frame analogy. Pekau [48]:distribution of shear force in beams. (a), elastic state, W=2760 kN. (b) Partial plastic state, W= 3700 kN. (— ), proposed analysis, (- - - -), frame analogy.

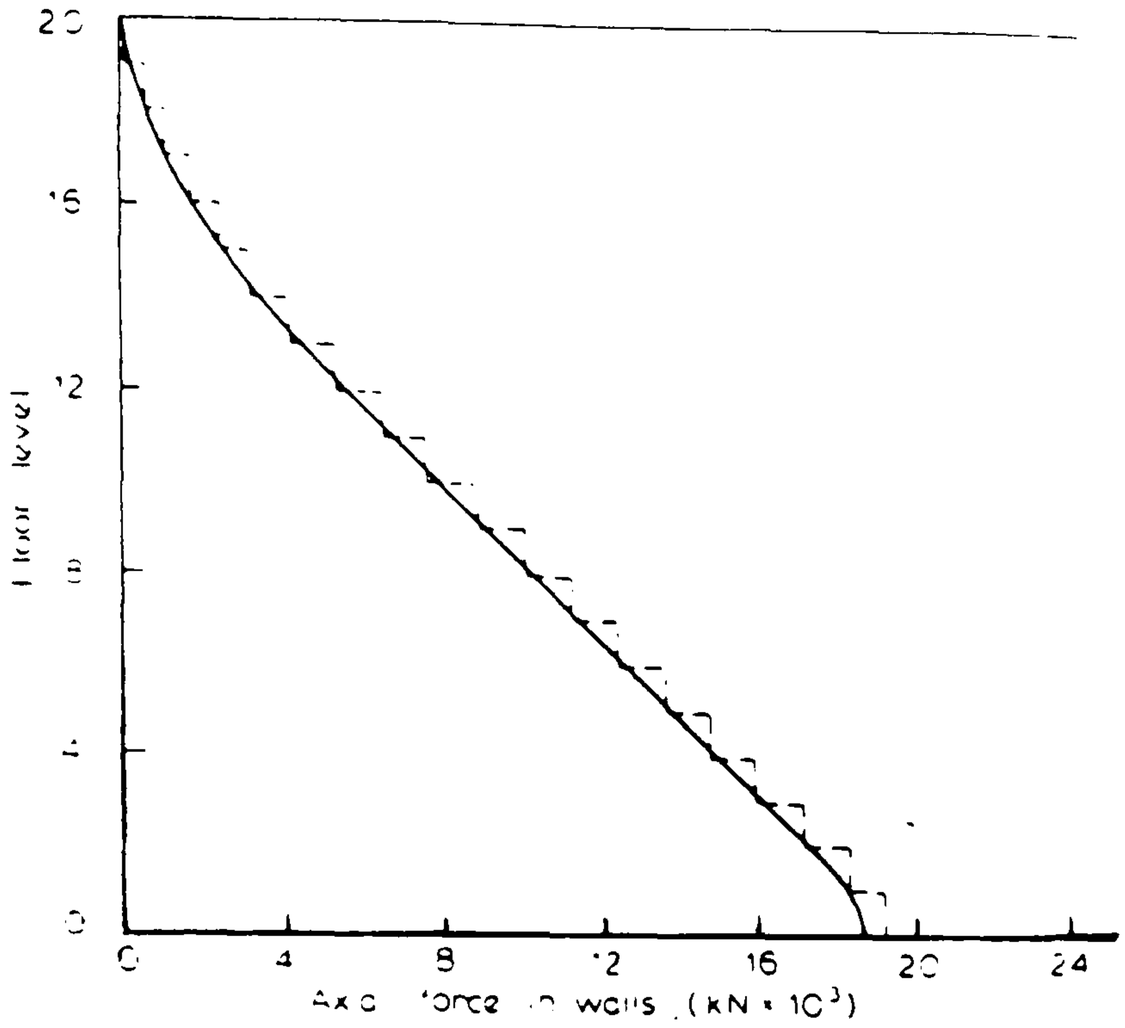


Figure 2.20: Proposed analysis versus frame analogy. Pekau [48]:distribution of axial force in walls (W=3700 kN).(— ), proposed analysis, (- - - -), frame analogy.

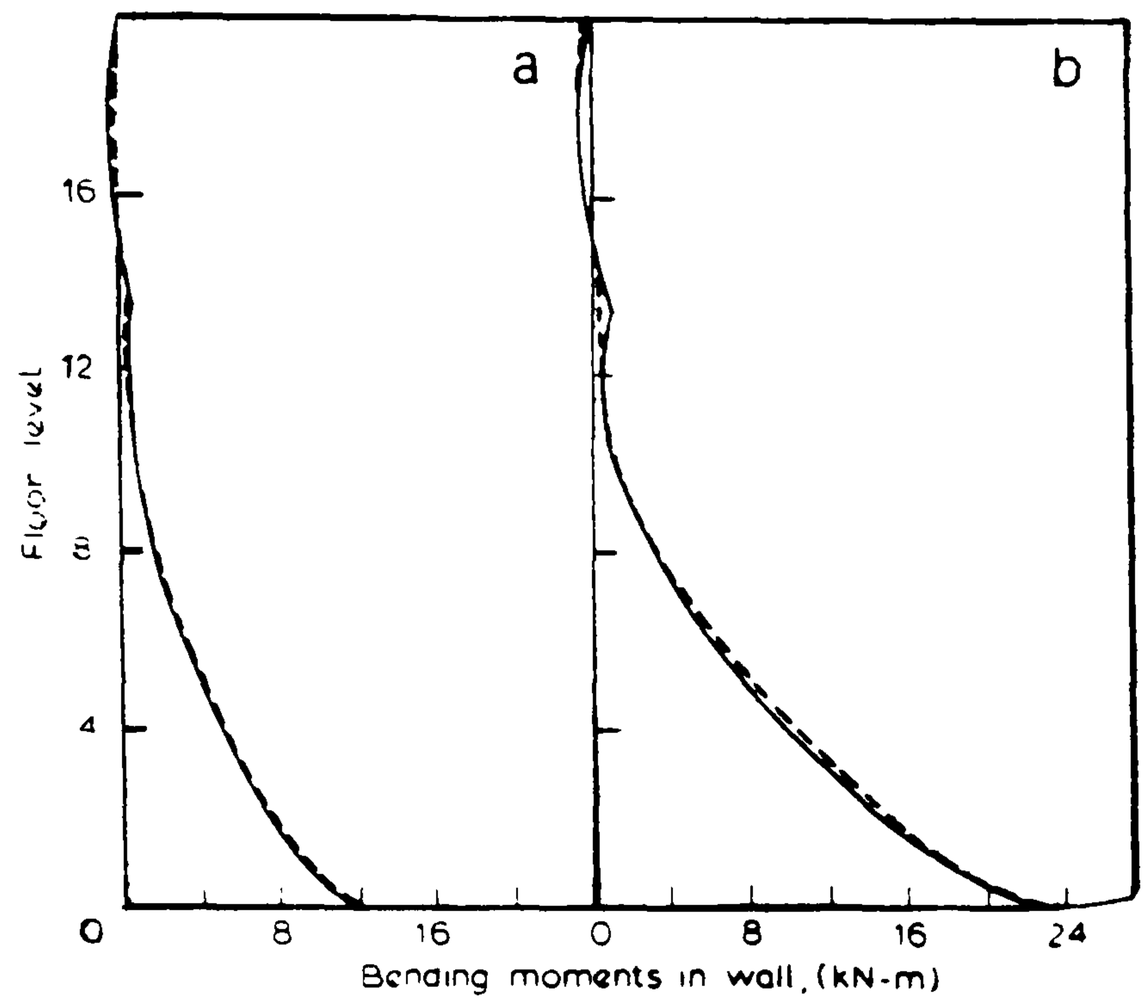


Figure 2.21: Proposed analysis versus frame analogy. Pekau [48]:distribution of bending moment in walls (W= 3700 kN). (a), Wall 1; (b), wall 2. (— ), proposed analysis, (- - - -), frame analogy.

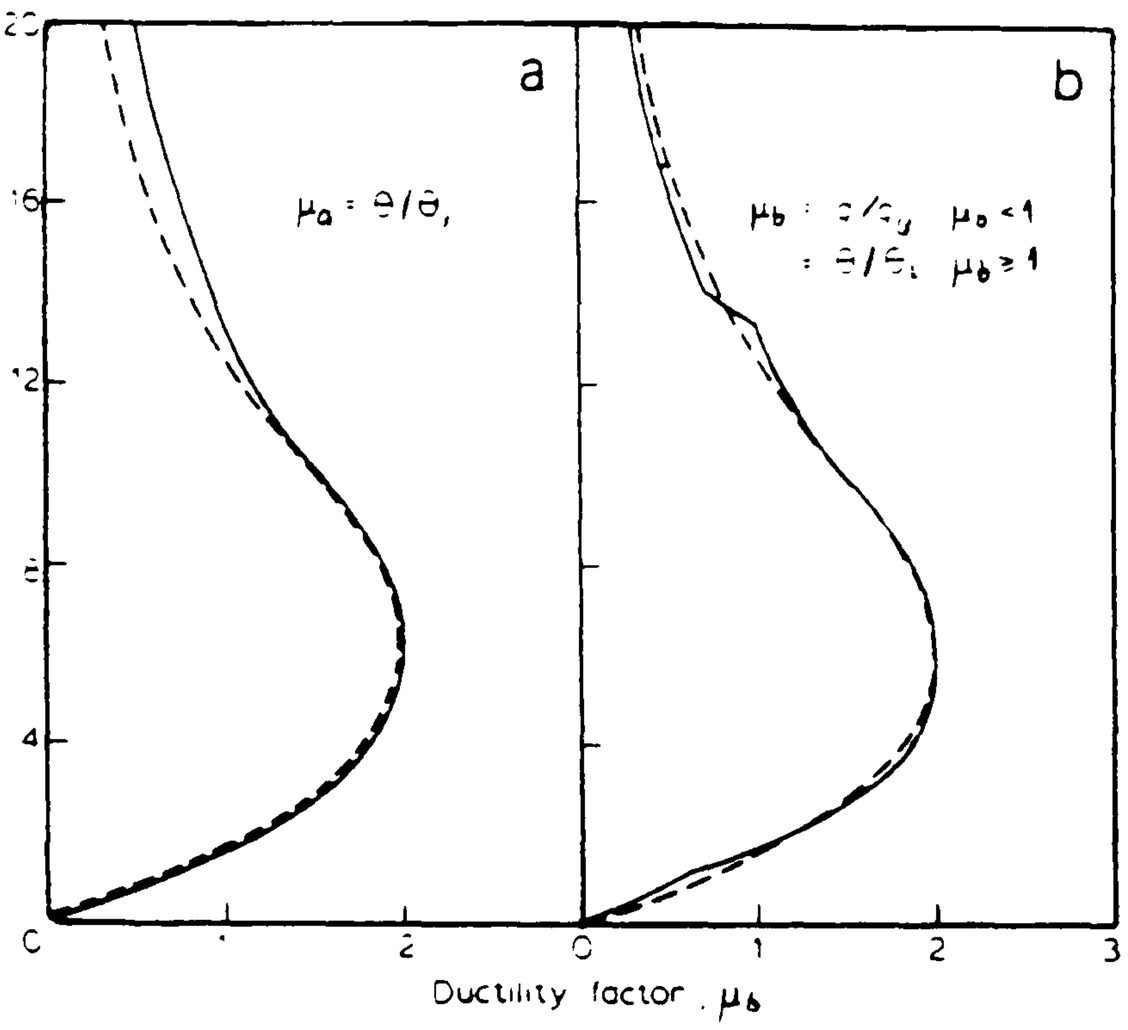


Figure 2.22: Proposed analysis versus frame analogy. Pekau [48]: distribution of beam ductility factors (W= 3700 kN). (— ), proposed analysis, (- - - -), frame analogy.

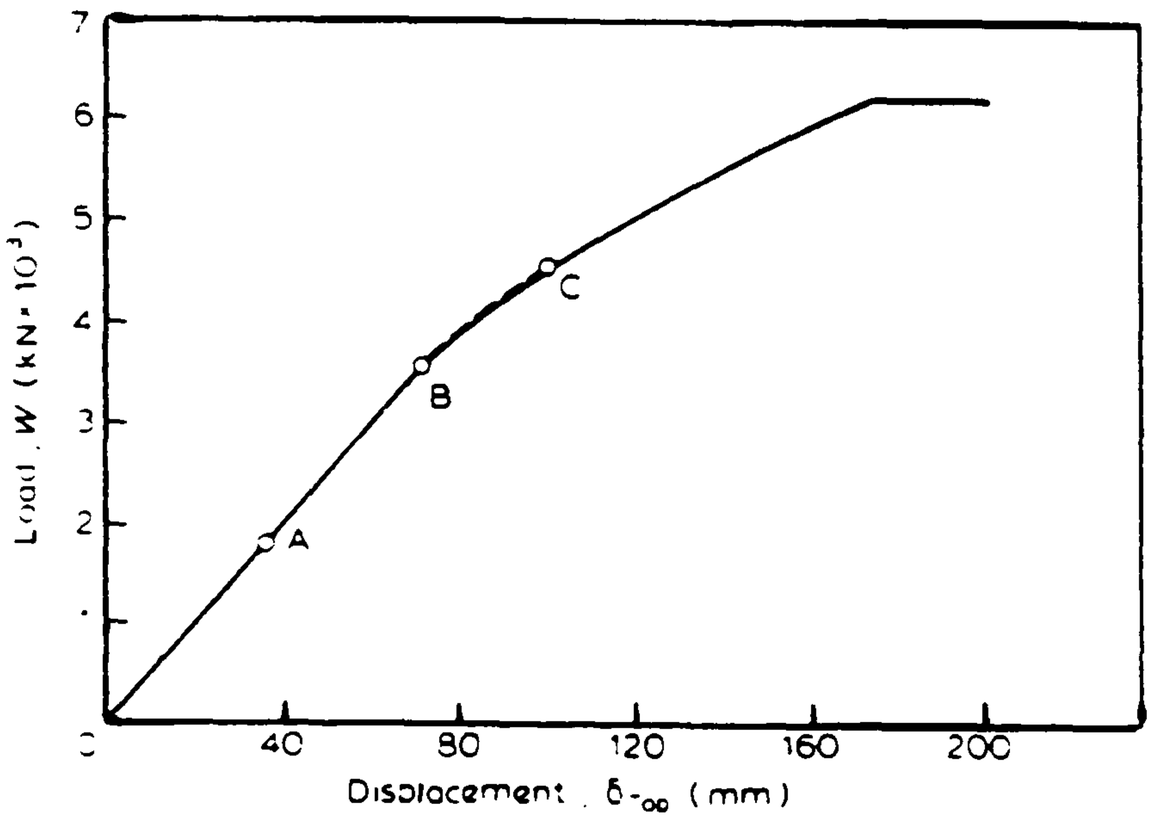


Figure 2.23: Proposed analysis versus Gluck's solution. Pekau [48]: load-displacement diagram. A, elastic; B, first yield; C, wall 1 yields. (— ), proposed analysis, (- - - -), Gluck's solution.

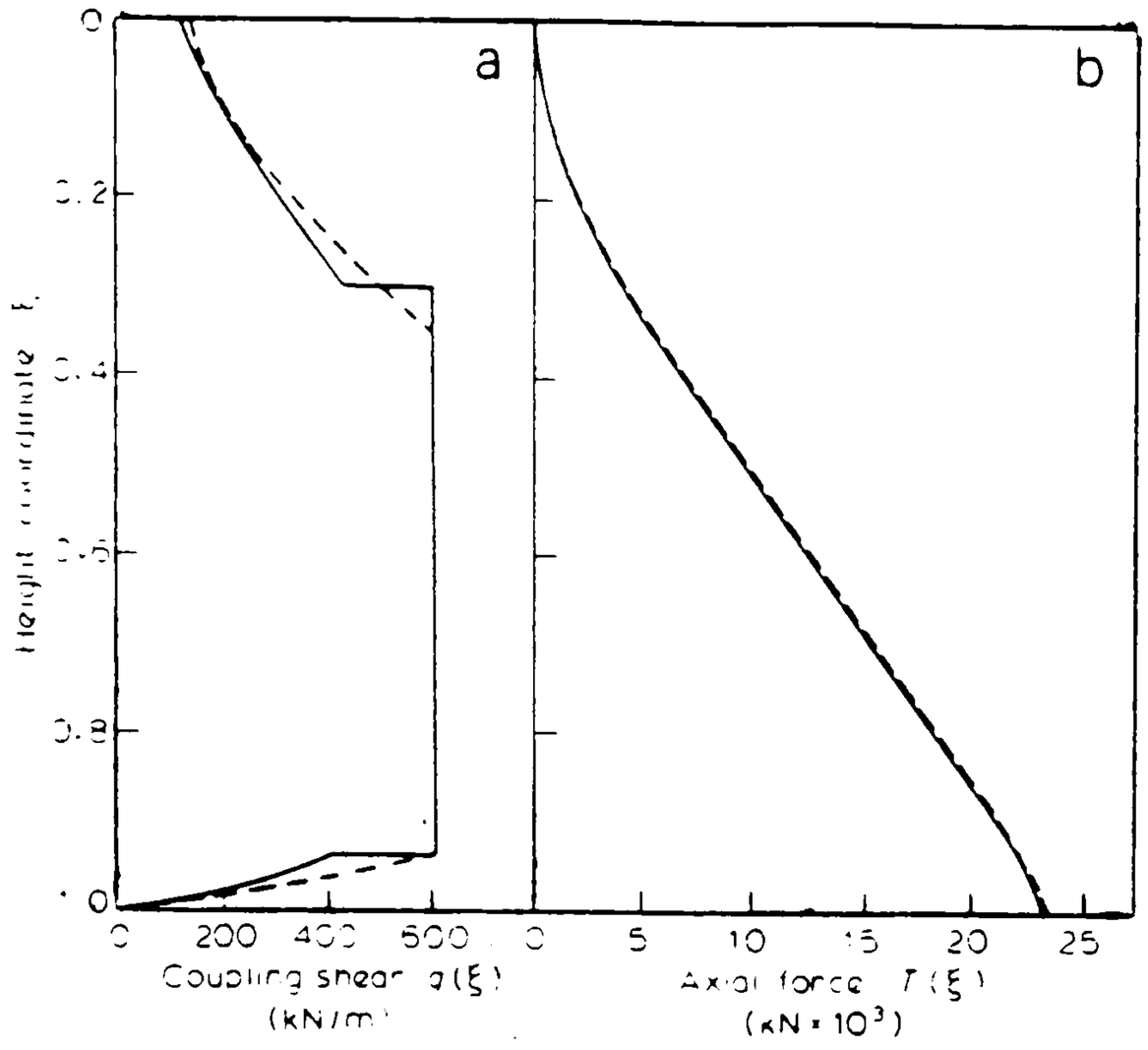


Figure 2.24: Proposed analysis versus Gluck's solution. Pekau [48]: (a) distribution of coupling shear;(b) distribution of axial load force in walls (W=4435 kN). (— ), proposed analysis, (- - - -), Gluck's solution.

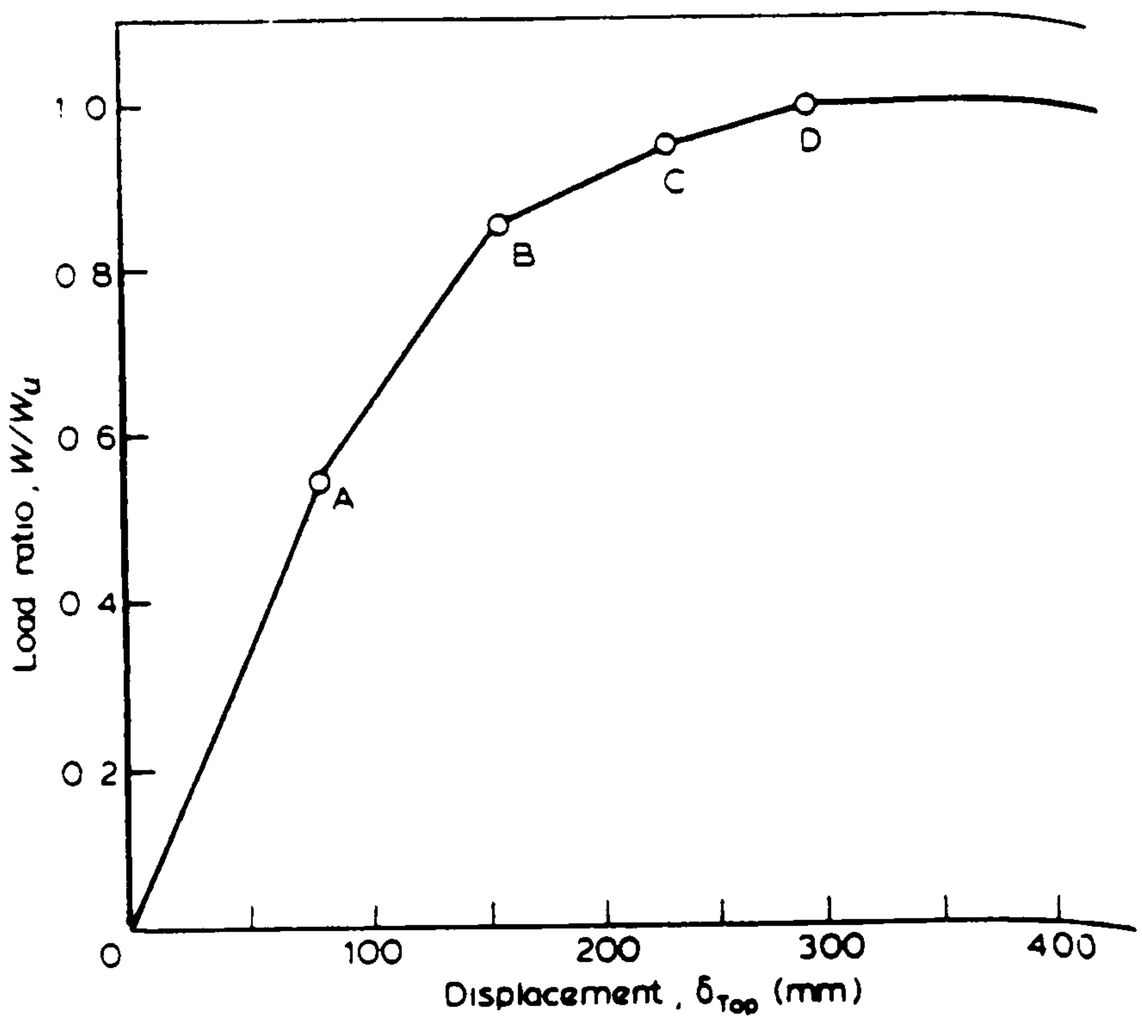


Figure 2.25: Proposed analysis versus Paulay's solution. Pekau [48]: load-displacement diagram. A, first yield; B, topmost beam yields; C, wall 1 yields; D wall 2 yields. (— ), proposed analysis, (o), Paulay's solution.

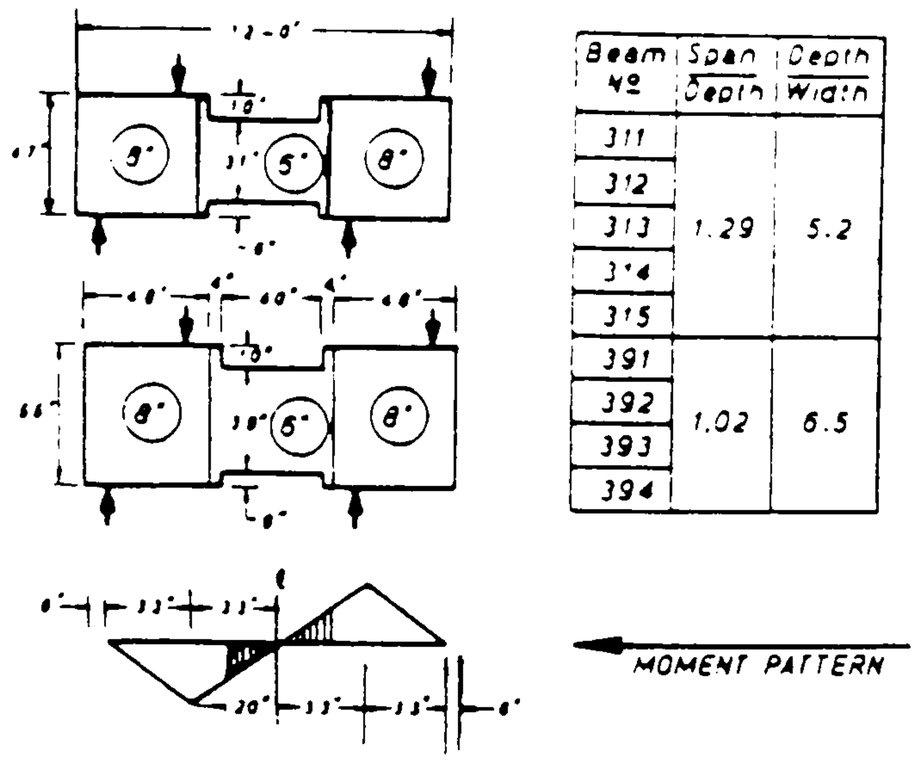


| Beam No | Span / Depth | Depth / Width |
|---|---|---|
| 311 | 1.29 | 5.2 |
| 312 | | |
| 313 | | |
| 314 | | |
| 315 | | |
| 391 | 1.02 | 6.5 |
| 392 | | |
| 393 | | |
| 394 | | |

Figure 2.26: Dimension and loading of test beams. Paulay [11]

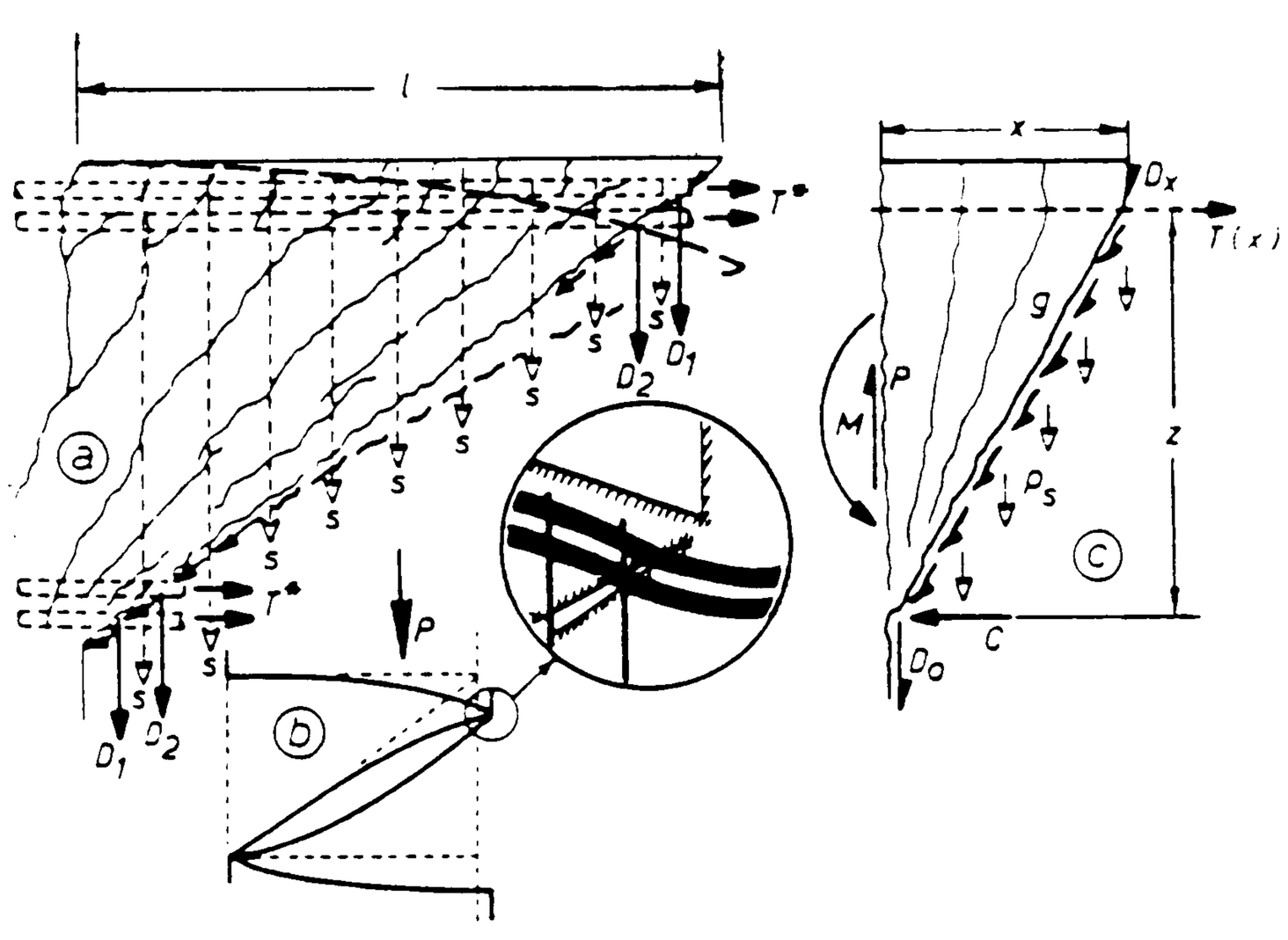


Figure 2.27: Diagonal tension failure mechanism and internal forces. Paulay [11]

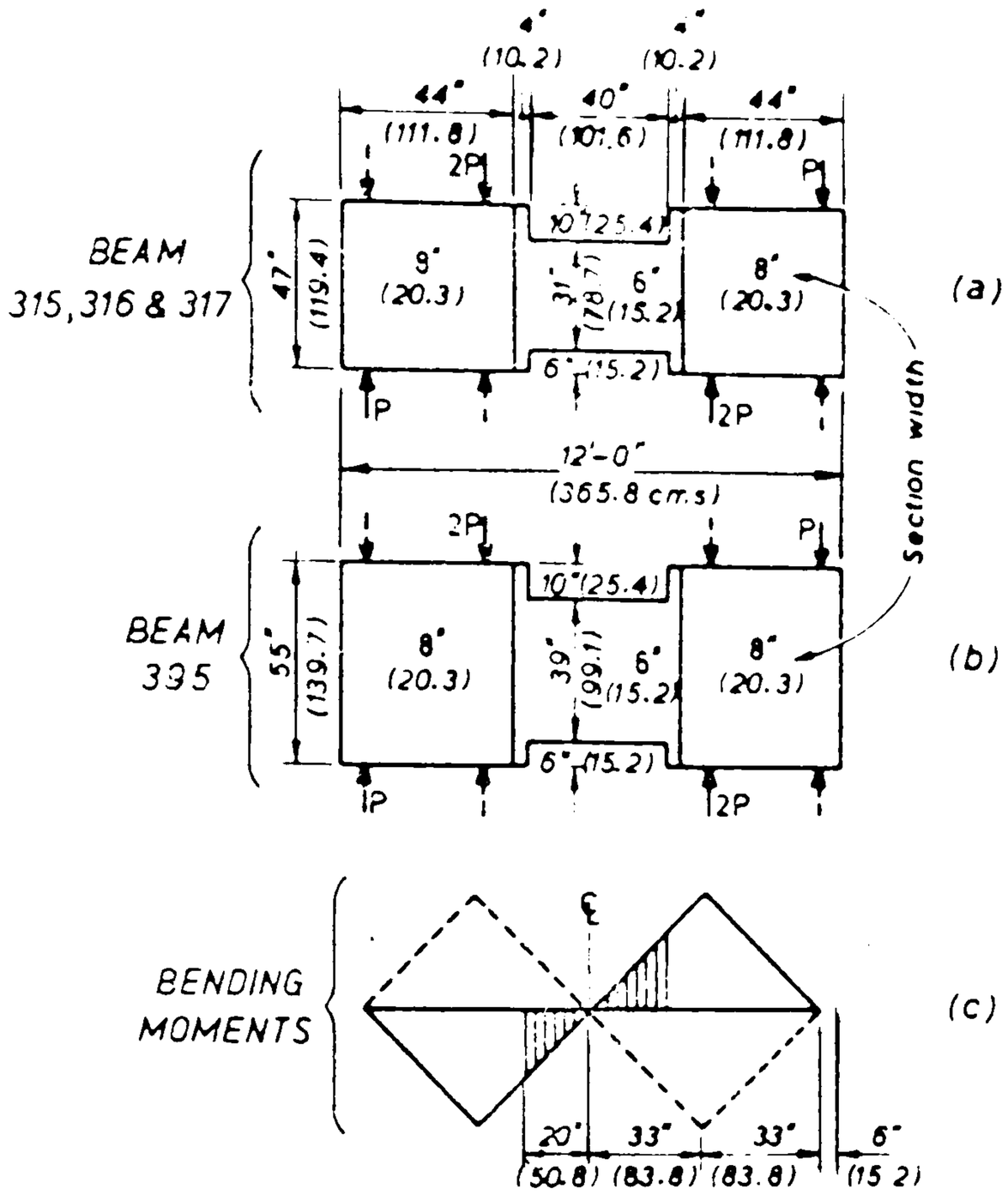


Figure 2.28: Principal dimensions and load pattern of test beams. Paulay and Binney [50]

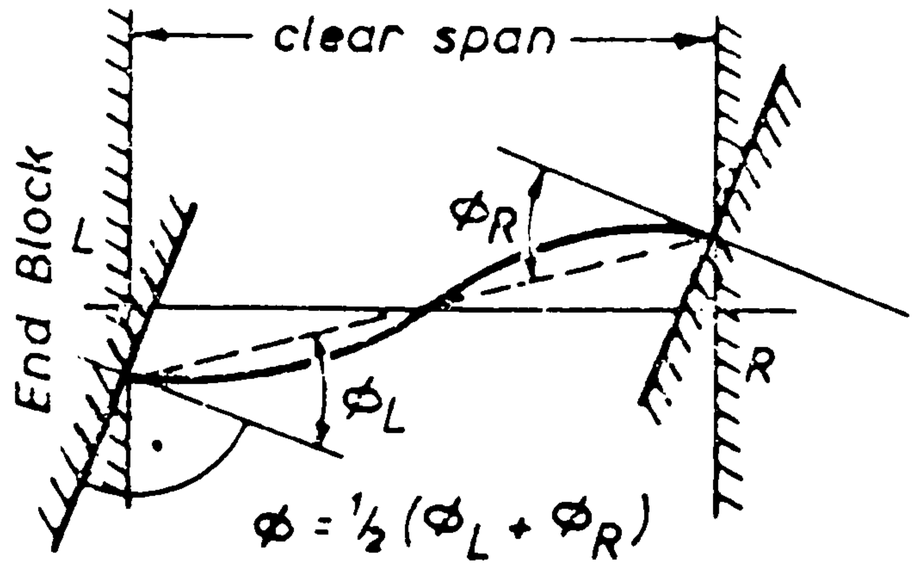


Figure 2.29: The mean support rotation of coupling beams. Paulay and Binney [50]

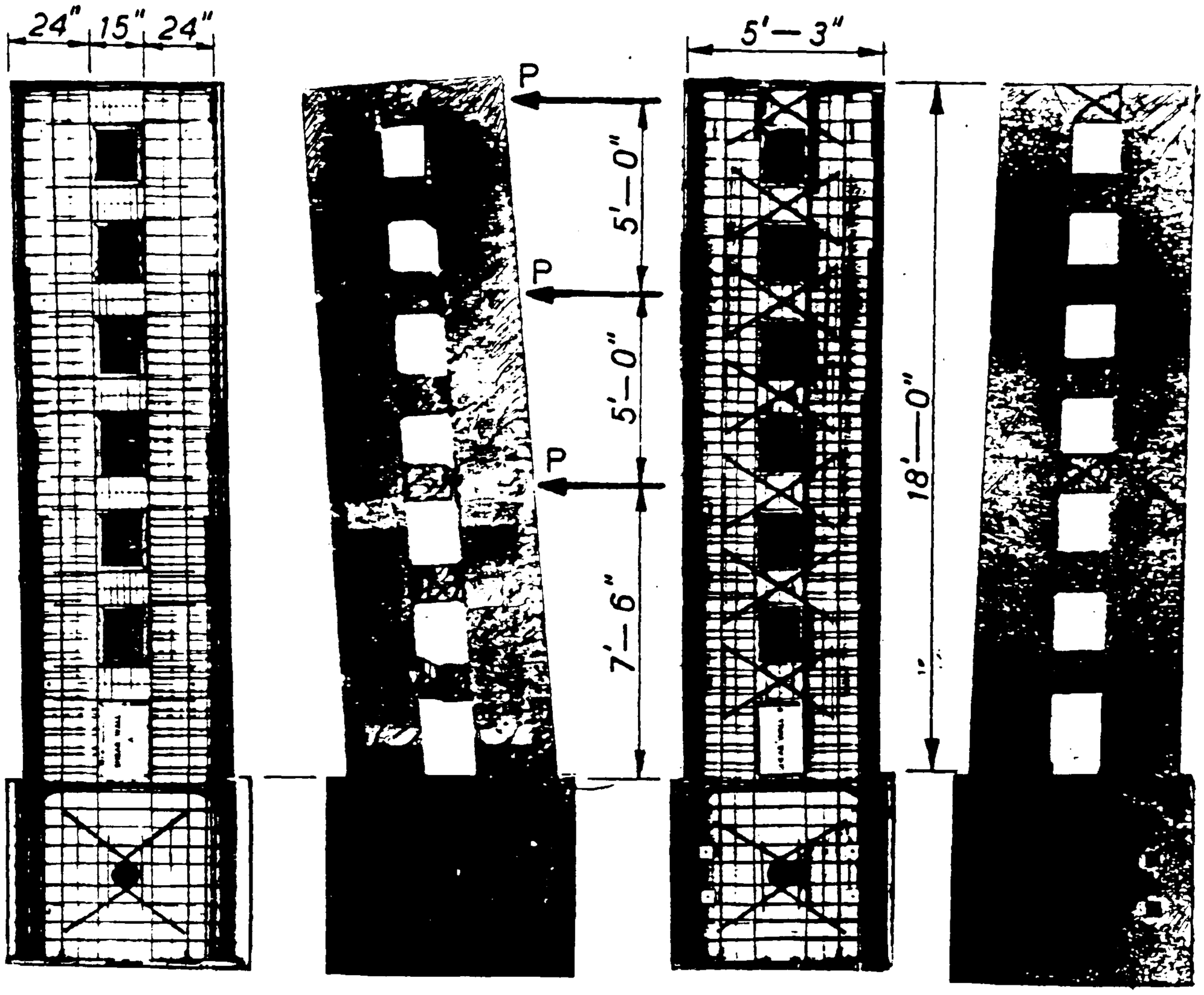


Figure 2.30: Reinforcement and crack pattern in two quarter full size shear wall models subjected to reversed cyclic loading. Paulay and Sunthkumar [52]

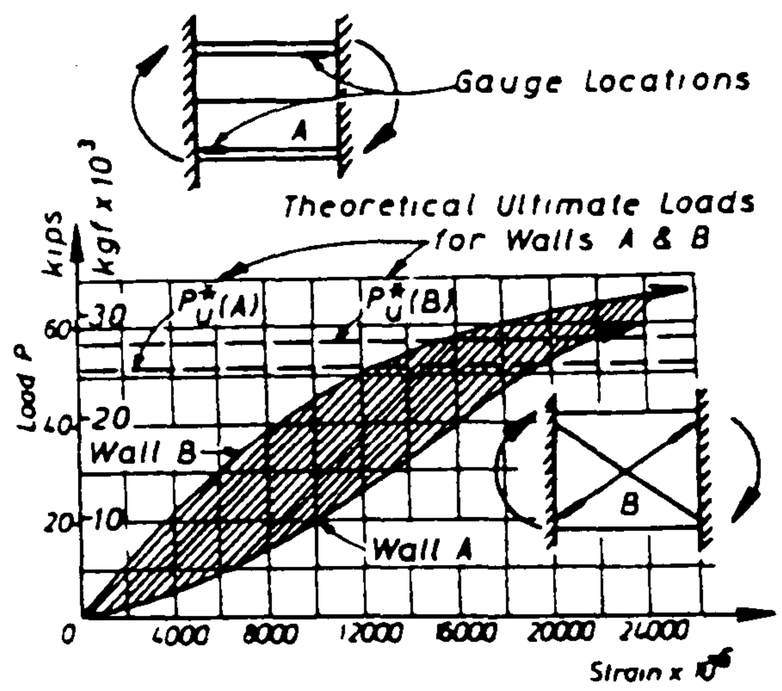


Figure 2.31: Comparison of the steel strain history of second floor beams of models and load-roof deflection. Paulay and Santhkumar [52]

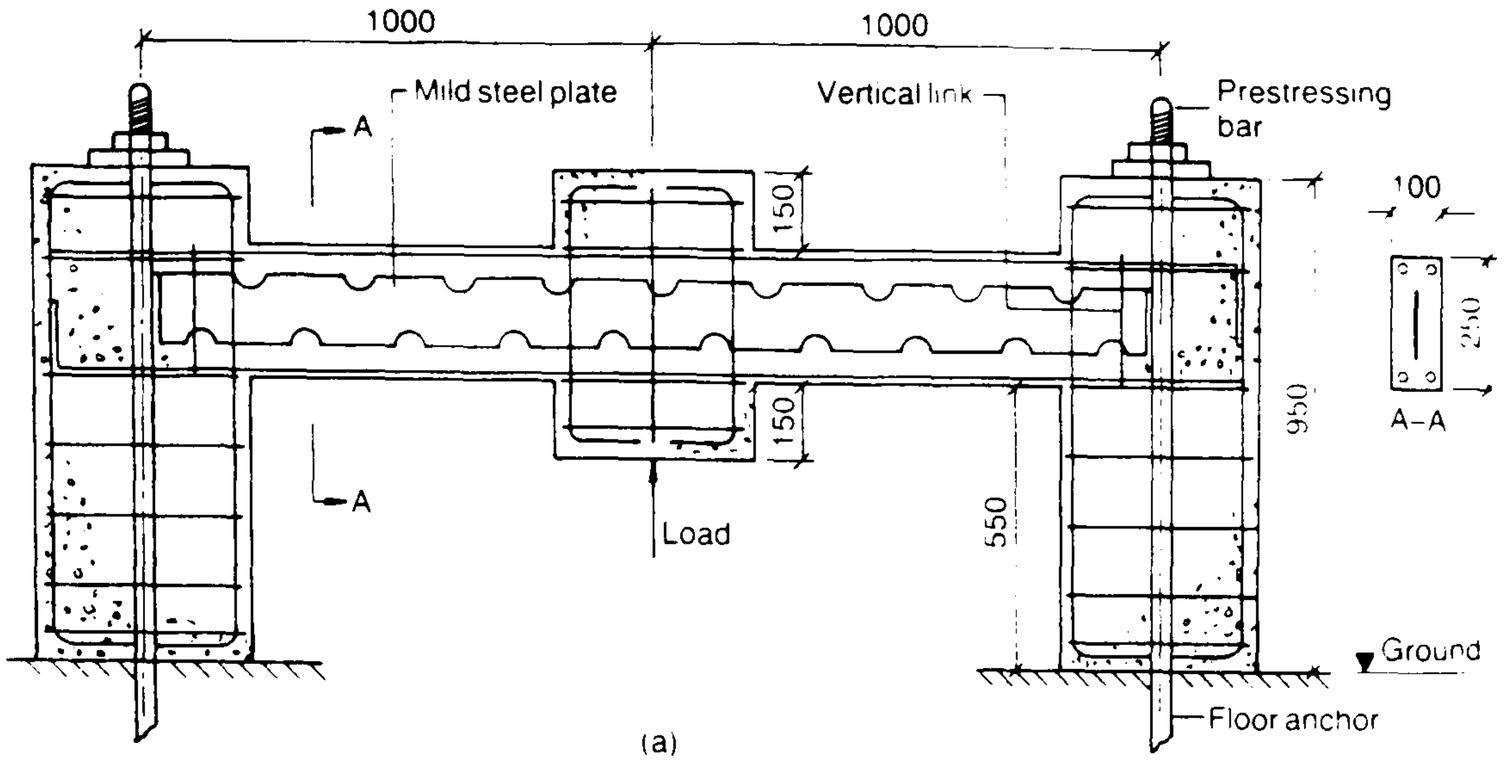


Figure 2.32: Detail of the test beams: a) longitudinal section; b) plan; c) loading arrangement. Subedi [2]

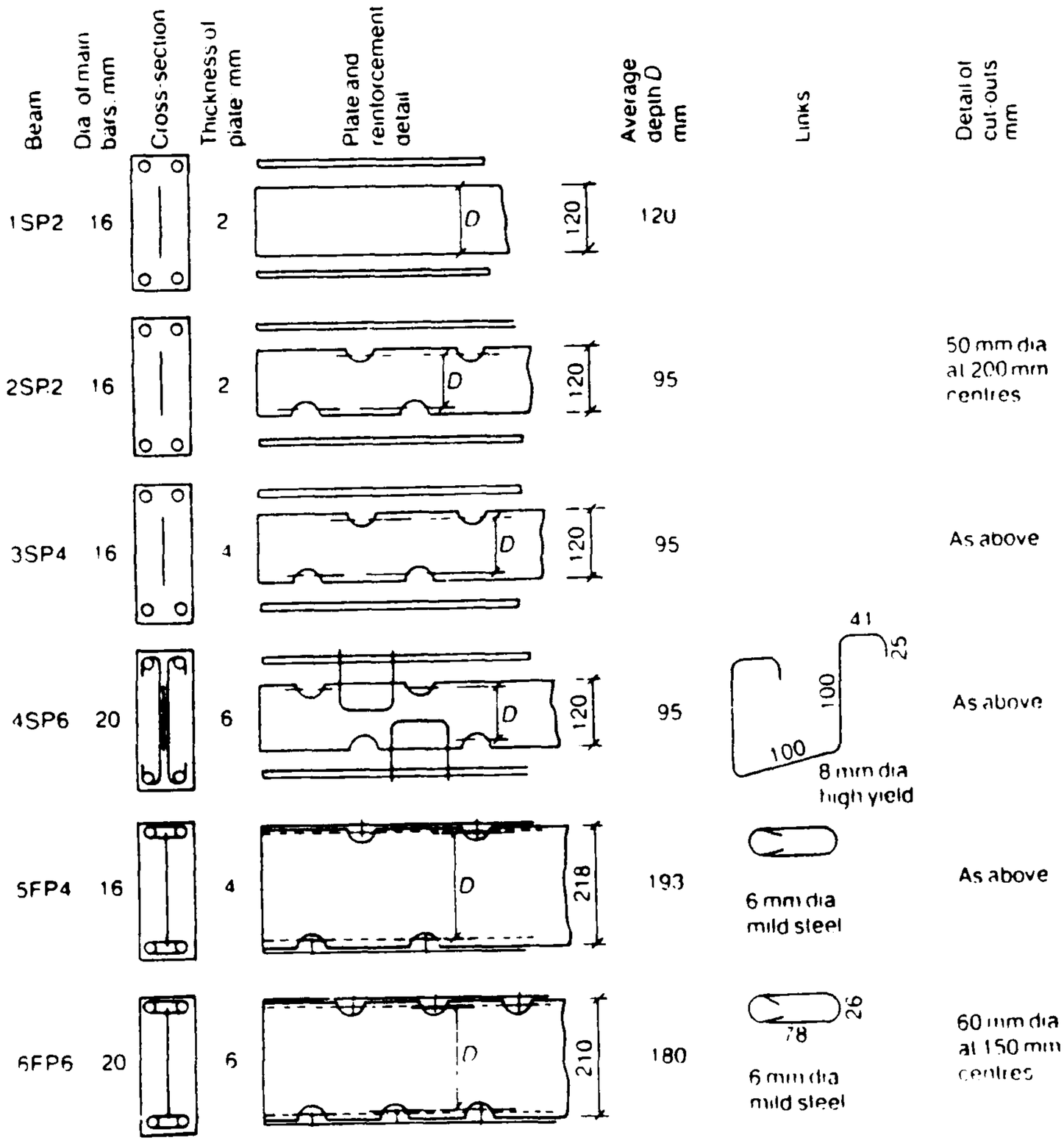


Figure 2.33: Profiles of plates and links. Subedi [2]

# Chapter 3

# LABORATORY BASED INVESTIGATION

## 3.1 INTRODUCTION

Wood, brick, concrete and steel are the most common load bearing materials used in the construction of tall buildings. The primary structure of multi-storey buildings is generally of steel, reinforced concrete or a mixture of both but reinforced brickwork has also been used for structures up to about ten storeys high. Steel sections are manufactured under carefully controlled conditions, the material properties are determined in a laboratory and described in a certificate from the manufacturer such that quality control can normally be guaranteed.

On a construction site where concrete is the main building material the situation is totally different. It is true that the quality of cement is guaranteed by the manufacturer in a manner similar to that of steel and, provided a suitable cement

is chosen, it is hardly ever the cause of faults in a structure. It is the concrete and not the cement that is the building material. Structural concrete members are more often than not made in-situ, and the quality of the concrete is almost exclusively dependent on workmanship including production, degree of compaction and curing regime.

It must not be concluded from the above that making good concrete can be difficult. "Bad" concrete or concrete of unsuitable consistency which hardens into a honeycombed, non-homogeneous mass is made simply by mixing cement, aggregate and water. Surprisingly, the ingredients of a good concrete are exactly the same. The difference is only in the "know-how" and site control rather than the economic constraints such as additional labour costs or the requirements for sophisticated equipment. Shear walls made of reinforced concrete may therefore vary greatly in strength and ductility resulting from either their basic design or from the quality of construction. It is therefore essential to maintain good quality control in a laboratory based investigation.

This Chapter describes the basic steps undertaken in the construction, instrumentation and testing of the various structural forms of coupling beams investigated in this research programme. However, in the case of the expanded metal mesh reinforcement specimens, there will, of course, be a difference in the amount and the form of the steel.

This Chapter, as such, can be considered as the basis of all the experimental work undertaken in this programme of reseach.

## 3.2 TEST SPECIMENS

The investigation reported herein was designed to study the behaviour of lintel beams in coupled shear walls subjected to lateral wind, earthquake or other loads of sufficient magnitude to result in elasto-plastic deformations of these beams. To be able to reproduce, on an economic basis, the loadings and boundary conditions which are likely to occur in coupling beams present in actual shear wall structures; test specimens of the form shown in Figure 3.1 and Figure 3.2 were selected. The overall dimensions of the specimens were made large enough so that no scale effects need be considered in the analysis of the results. The relatively large specimens also enabled numerous strain measurements to be recorded with relative ease on the actual surface of the beam. The dimensions of the specimens used in the laboratory based tests were selected so as to correspond to either a half or a quarter of the full size elevation as shown in Table 3.1. The thickness of each test specimen was 120 mm. The beam was cast integrally with two 120 mm thick rectangular shaped end-blocks to represent the coupled shear walls. The 120 mm thick walls were reinforced in such a manner that they would resist buckling when the ultimate strength of the coupling beam was attained and their behaviour during the test was not monitored. The beams were cast horizontally through one face. Therefore, the bond conditions for both the top and bottom reinforcement were the same. The load was applied through one of the end-blocks as shown in Figure 3.3. The loads were applied to the wall at points which were considered to be located far enough away from the junction between the wall and the coupling beam so as not to result in stress concentrations at the boundaries

of the coupling beams, where were significantly different from that which occurs in an actual shear wall structure. Cycles of loading in alternate directions were applied in 6 increments until the desired maximum intensity was attained. These were then reduced in three to four increments to zero to complete each load cycle. At the third load cycle the load was taken to failure. The hydraulic jacks were then repositioned so that the load could be applied in the opposite direction.

## 3.3 TEST ARRANGEMENT AND LOADING SYSTEM

Figure 3.3 shows the test arrangement including the loading system. The restraints on the specimens shown in Figure 3.4 consisted of welded 25 mm thick steel plates and box sections bolted to the structural floor of the laboratory. The test arrangement was designed to allow the application of monotonic and cyclic loadings.

In the design of the reaction frames the following requirements were considered:

- the minimisation of the bolt loads and the elimination of movement under load;
- all the required loadings to be allowed to be applied using only two 1000 kN capacity hydraulic rams in the case of specimens CBD1 and EBD1, and one hydraulic ram of 800 kN capacity for the remaining test specimens;
- specimens of different dimensions should be easy to accommodate;

- allow rapid reversal of the direction of loading;
- allow mobilisation and demobilisation of the test arrangement in minimum time.

The operation of the test arrangement may be summarised as follows:

- The load was applied using the 800 kN capacity hydraulic jack, which was positioned on the unconstrained end-block of the test specimen. This location was chosen to avoid stress concentrations around the beam ends, and to generate equal moments at both ends of the beam and to enable a known constant shearing force to be applied.
- The load applied to the test beams was transmitted through the stiffened steel bearing plates.
- The friction between the laboratory floor and the underside of the test specimens was minimised using a series of 20 mm diameter rollers positioned between each test specimen and the laboratory floor.

## 3.4 CONCRETE MIX

### 3.4.1 Mix Design

Mix design may be defined as the determination of the most suitable proportion of the constituents for a particular concrete taking into account the properties of these constituents to provide the desired workability, strength, durability and finished appearance required of the concrete. The limited laboratory facilities

available to produce large volumes of concrete for one complete beam resulted in the concrete being supplied in three separate batches for specimens of half full size storey height and, two separate batches for specimens of quarter full size storey height. The value for the concrete cube crushing strength for each specimen was obtained from an average of three cubes and three cylinders taken from each batch of concrete. The target 28 day cube crushing strength was $30N/mm^2$. It was in fact difficult to obtain a concrete strength less than $30N/mm^2$, when not less than 250 kg of cement per cube metre of concrete was used and when the workability required was approximately a slump of 120 mm. The unit weight of the concrete was found to be between 23 and 25 $kN/m^3$. No additives were used in the mix. Ordinary portland cement was used in all of the batches of concrete. The relative proportions of the constituents and other relevant data for all mixes used during the test programme are given in Table 3.2.

### 3.4.2 Concrete Placement and Compaction

The base of each shutter was suitably prepared before placement of the concrete. Special precautions were taken to remove all foreign matter from the inside of the shutter. Some of the sides of the shuttering were oiled and the remaining sides were covered with a sheet of polythene in order to reduce the adherence of the concrete to the shuttering. These operations provide a simple and effective means of sealing the surface of the wooden form to eliminate local variations in surface absorbency.

The concrete was mixed in the laboratory batching plant using accurately weighed

quantities and was placed into the shutter immediately after delivery. The concrete was deposited in uniform horizontal layers and was vibrated to achieve compaction, thus filling all the voids and expelling any entrapped air. Care was taken to avoid segregation within the concrete and to ensure that the concrete would be homogeneous.

An immersion poker type vibrator of 25.4 mm diameter was used to compact the concrete in each case. Vibration was terminated when mortar began to flow to the surface adjacent to the vibrator, and when air ceased to be expelled.

A smooth finish was produced on the test specimens using a steel trowel once compaction of the concrete was completed. Three standard cylinders and three cubes were compacted on a vibrating table for each batch of concrete.

### 3.4.3 Curing

The last step, and an exceedingly important one in the manufacture of concrete, is the curing operation. As hydration of cement takes place only in the presence of moisture and favourable temperatures, these conditions have to be maintained for a suitable time interval called the curing period. Specifications [64] usually require that the surfaces of the concrete be protected to prevent loss of moisture for at least 7 days where normal cement is used. In the case of special mixes 14 days or more may be required.

In the present investigation each specimen was cured for 10 days under hessian soaked with water and covered with polythene sheeting. The cylinders and cubes were removed from their steel moulds approximately 48 hours after casting and

were stored in water for 7 days and then kept under similar conditions to the test specimens in a curing room until tested.

### 3.4.4 Removal of Shuttering

The formwork for each specimen was loosened after 24 hours and completely removed after 21 days. This allowed the concrete to harden sufficiently and gain strength to approximately 90% of its final value such that the specimen could be handled without damage.

## 3.5 TESTING OF HARDENED CONCRETE

The properties of the concrete are a function of the degree of maturity including ambient humidity and this is why, in order to be of value, tests on concrete have to be performed under specified controlled conditions. The most common of all tests on hardened concrete is the compressive strength test. Additional tests are also commonly performed to determine values for the elastic modulus and Poisson's ratio which are often essential input data for analytical approaches.

Both cubes and cylinders were tested in compression to determine the crushing strength and the corresponding elastic modulus of the concrete used in the construction of the specimens. The values are presented in Tables 3.3 - 3.5.

## 3.6 CONCRETE STRENGTH PROPERTIES

The sets of standard test specimens were crushed either during or at the end of the corresponding test on the shear wall units. The tests on the shear wall units tended to last up to five days. The values for each test specimen presented in Tables 3.3 - 3.5 mentioned above were normally derived from the average values of three cubes and three cylinders for each batch of concrete used to form each test specimen.

### 3.6.1 Cube Tests

These specimens were cast in 100 mm steel cube moulds which conformed to the prescribed dimensions and tolerances required by the relevant British Standard [65]. All the cubes were kept under water for a period of at least seven days. The test specimens were than stored undisturbed in laboratory curing room at a controlled temperature until the test date.

The loading of the cubes was carried out in accordance with the appropriate British Standard [65].

### 3.6.2 Cylinder Tests

The same procedure as described above was repeated for the cylinders which had a diameter of 150 mm and were 300 mm long. These cylindrical specimens were also made in accordance with the appropriate British Standard [65].

## 3.7 REINFORCEMENT

### 3.7.1 Introduction

The uses of metals in civil engineering are many and varied, ranging from their use as the main structural material to their use for fastenings and bearing materials and even for decoration.

All reinforcement used for the stirrups and expanded metal meshes in the coupling beams was made from mild steel. The steel mesh was manufactured and supplied by Expamet [66], [67] in the UK. This reinforcement is marketed as being guaranteed to be free from corrosion and of a very high strength in terms of flexural loading. A series of tensile tests was carried out on single strands of the mesh to obtain the actual yield strength of this material. The yield point was determined from the graphical output from the testing machine for both the conventional reinforcement bars and the strands of expanded metal mesh.

Typical stress-strain curves for the two types of steel included in the investigation are shown in Figure 3.5. The strength properties of the reinforcement and other relevant data are tabulated in Table 3.6.

## 3.8 EXPANDED METAL MESH

### 3.8.1 Introduction

The expanded metal mesh reinforcement used in this investigation consisted of the group of meshes formed from a single piece of metal. The process is not wasteful

of material, a particular useful feature where high value metals are considered or where reduced weight is required.

The meshes are expanded from carbon steel in accordance with BS 1449: Part 1:1972 [66], [67] in which the dimensions are given for each specific mesh. The standard meshes in the 700-4000 series are deburred using wire brushing and are coated with oil as an anti-corrosion measure. The diamond-shaped mesh provides an excellent bond between the steel and the concrete and it has also been confirmed by the suppliers that the shape of the mesh assists in the distribution of stresses in concrete arising from shrinkage and changes in temperature.

### 3.8.2 Dimensions and Characteristics of the Expanded Metal Mesh

Recently steel in expanded metal mesh, as shown in Figure 3.6, has been adopted in construction as a simple way to repair concrete damage mainly because of the simplicity of its placement, the high bond characteristics, and excellent corrosion resistance. The properties of the expanded metal mesh reference 4095 used in this investigation given by the manufacturers are as follows:

LW = 101.60 mm

SW = 50.80 mm

Percentage of open area :

Nor = 80%

Max = 84%

Size of the strand :

W = 5.029 mm

ts = 3.0 mm

$\rho = 4.659 kg/m^3$

The test specimen included in the experimental investigation demonstrates the importance of testing the strand of the expanded metal mesh in order to get the actual value of its yield strength. A test machine was used to load the strand in direct tension. The specimens were subjected to monotonic loading up to failure. The stress strain relationship recorded using the plot from the test machine is shown in Figure 3.5 together with the plot for the 8 mm diameter steel bar.

## 3.9 DESIGN WITH EXPANDED METAL MESH

This Section reflects advances in the design of coupling beams present in tall buildings in which a new type of reinforcement "expanded metal mesh" replaces the vertical stirrups as a method of reinforcing against a shear failure. Basically, the expanded metal mesh is intended to carry all the shear forces although this will depend on its geometry and its strength characteristics. No Code to date has addressed the use of expanded metal mesh to accommodate shear or flexural behaviour in composite construction.

The design of the coupling beam reinforced with expanded metal mesh depends on the distribution of the forces on each strand of the expanded metal mesh which in term depends on two major parameters:

a) The assumed direction of the crack at the failure of the coupling beam.

b) The angle of the strand in the expanded metal mesh with respect to the crack

direction.

To solve the second parameter, two cases can arise in the determination of the number of strands crossing the diagonal crack in coupling beam structures as shown in Figure 3.7 and Figure 3.8:

1) The angle of the assumed crack $\alpha_c$ is less than the expanded metal mesh angle $\theta$.

$$\text{AB} = \sqrt{(OA)^2 + (OB)^2}$$

Consider the triangle ABC as shown in Figure 3.7:

$$sin\gamma_2/AB = sin\gamma_3/CB = sin\gamma_1/AC$$

where

$$\gamma_1 = \theta - \alpha_c$$

$$\gamma_2 = 180 - (\theta + \alpha_c)$$

$$\gamma_3 = 180 - (\gamma_1 + \gamma_2)$$

Then :

$$\text{CB} = sin\gamma_3 AB/sin\gamma_2$$

The horizontal projection of CB is CB $cos\alpha_c$

The number of strands of the expanded metal mesh crossing the crack along the beam of shear span L can be calculated as follows:

$$\text{n} = L/CBcos\alpha_c$$

2) The angle of the assumed crack $\alpha_c$ is greater than the expanded metal mesh angle $\theta$.

Consider the triangle ABC as shown in Figure 3.8:

$$sin\gamma_2/AB = sin\gamma_3/CB = sin\gamma_1/AC$$

where

$\gamma_1 = \alpha_c - \theta$

$\gamma_2 = 180 - (\gamma_1 + \gamma_3)$

$\gamma_3 = 180 - (\gamma_4)$

$\gamma_4 = 180 - (2\theta)$

$\gamma_3 = (2\theta)$

The number of strands of the expanded metal mesh crossing the crack along the beam of shear span L can be calculated as described above.

## 3.10 BASIS OF COMPARISON BETWEEN THE TWO TYPES OF STEEL

A major difficulty in the development of a basis of comparison for the two types of steel used to absorb the shearing force was identified because of a lack of information on expanded metal mesh. The basis of comparison between the two types of reinforcement was related to the weight, the area and the characteristics of the steel used in both specimens in the form of expanded metal mesh and stirrups.

### 3.10.1 Design of the Specimens

One series of coupling beams with a ratio b/d=1.43 was used to calculate the amount of reinforcement in the form of both the expanded metal mesh and the conventional reinforcement as shown in Figure 3.9 and Figure 3.10.

a)**Beam reinforced with expanded metal mesh**

Area of two sides (A) ... $S_1$= 2(0.08 x 0.5) = $0.08m^2$

Area of two sides (B) ... $S_2$= 2(0.31 x 0.75) = $0.465m^2$

Total area of expanded metal mesh used:

$S_t$= 0.08 + 0.465 = 0.545 $m^2$

Weight of expanded metal mesh used in the beam:

$P_1$ = 0.545 x 4.659 = 2.539 kg

b)**Beam reinforced with stirrups**

Length of the eight stirrups used in the beam:

8[(0.31 + 0.08) 2] = 6.24 m.bar

Allowance for 10% overlap:

6.24 + (6.24 x 10)/100 = 6.864 m.bar

Weight of 8mm diameter for 1.00m length and density of 7.8g/$cm^3$:

$[(0.8^2\pi)/4]$ 100 x 7.8 = 391.872g/m length

Total weight for 8 stirrups:

$P_2$= 0.3918 x 6.864 = 2.689 kg

## 3.10.2 Design Conclusions

- When the weight of conventional stirrups and the expanded metal mesh are compared, the calculation shows that the weight of the eight stirrups used in the specimen is higher than the weight of the expanded metal mesh required to absorb the shear force. The difference between the two was found to be

15.9%.

- The time required to make the reinforcement cage using expanded metal mesh is less than the time required to form the cage with conventional stirrups.

- The price for one tonne of expanded metal mesh is greater than that of 8 mm diameter mild steel reinforcement bars.

- The yield strength of a strand from expanded metal mesh of reference 4095 used in the investigation is approximately equal to that for the 8 mm diameter mild steel reinforcement bars.

## 3.11 ASSEMBLY OF REINFORCEMENT CAGES

The reinforcement cages for all the beams were carefully assembled as shown in Figures 3.15 to 3.18 for both forms of reinforcement, so that the main bars and the stirrups or the expanded metal mesh were always (+) or (-) 5 mm from their specified positions. In order to maintain the relative positions of the reinforcement bars during concreting, either the stirrups or the expanded metal mesh were tied to the main bars using 2 mm diameter mild steel tie wires. On completion of the cage for each beam, the cages for the two end-blocks were correctly positioned in the shutter with the full bond length of the main reinforcement of the beam tied to the reinforcement in the walls.

The strain gauge installations on all deformed longitudinal bars, stirrups, and the sections of expanded metal mesh were coated with a protective sealant before

the commencement of the assembly of the cages for beams CBM3 and EBM3. This arrangement ensured that the surrounding concrete did not interfere with the strain measurements in the steel even when the strain hardening region was encountered.

The dimensions and the details of the four types of coupling beams containing the conventional and the expanded metal mesh reinforcement included in this programme of research are given in Figures 3.15, 3.16, 3.17, and 3.18.

## 3.12 INSTRUMENTATION

### 3.12.1 Steel Strain Measurements

The strains in the stirrups and the expanded metal mesh in the coupling beams were measured in order to determine the level to which they were stressed and thus their effectiveness in absorbing shear in the coupling beams during each test. Twelve strain gauges were used to measure the elongation of the 12 mm diameter flexural reinforcement bars positioned in the top and bottom regions at the supports and the middle of the beam. All the stirrups were instrumented with two strain gauges positioned at points in from the corners of the stiruups along the longest legs. The second stirrup in from each support was instrumented with four strain gauges at both sides of the beams to identify any tendency to twist or warp. The same approach was used for positioning the strain gauges on the expanded metal mesh as can be noted in Figure 3.11.

The strain gauges had a resistance of 120Ω (ohm) and a gauge length of 10 mm.

The gauge factor was 2.10.

The reinforcement bars and the strand in the expanded metal mesh were cleaned using a wire brush attached to a portable drill and then blasted with compressed air prior to installation of the strain gauges. The specially prepared surfaces were then examined under a microscope. The gauges were bonded to the specially prepared surfaces of the reinforcement bars using an epoxy adhesive. Once the epoxy adhesive had hardened, the strain gauges were coated with a water proofing compound. Each strain gauge was connected up into a quarter-bridge circuit.

A small number of strain gauges proved to be unreliable because of their unstable behaviour before testing of the beams, possibly due to the formation of dry joints or loose connections.

### 3.12.2 Data Retrieval

The data logging system, as shown in Plate A.1 in Appendix A, was used to record the strain gauge measurements in test specimens CBM3 and EBM3. Readings were taken at each load step and were output in printed form by the data logger. The data were then transferred in the form of a linear array to a mainframe computer for further processing and subsequently presentation in graphical form.

### 3.12.3 Concrete Strain Measurements

Sets of demec buttons 50 mm and occasionally 150 mm apart were positioned on the upper face of the beams.

The concrete surface was cleaned with a wire brush and the dust was removed using a compressed air source. The demec buttons were bonded to the surface of the test specimen using an epoxy resin adhesive either before commencement of the test or after the formation of the cracks. The demec buttons were positioned along sections passing through the supports, the quarter span points and the midspan of the beam as shown in Figure 3.12. All the readings were manually recorded.

### 3.12.4 Rotation Measurements

The horizontal displacements along the vertical reference line were measured using three dial gauges. The readings near the top and the bottom edges of the end blocks were used to determine the absolute rotations. Any twisting, which may have occurred could be detected from these measurements along both the top and bottom edges of the test specimen. Readings taken at the centre point of the end block, which was situated on the horizontal axis of the beam proper, enabled the displacement of one end-block relative to the other to be determined. The accuracy of the readings from the dial gauges was approximately 0.06 mm. The measured displacements were subsequently converted into angular measurements. The measurements were recorded after each loading increment during each test.

### 3.12.5 Deflection Measurements

In order to get the general picture of the deformations of the beam, three dial gauges were normally placed under the centre of its soffit. This may be noted

from Figure 3.13. The accuracy of the readings on these dial gauges was the same as the dial gauges used to measure the rotation of the test specimens.

### 3.12.6 Elongation and Expansion Measurements

If the length of a rectangular reinforced concrete beam, subjected to combined bending and shear is measured along its axis at mid-depth, then it is readily noted that all such beams increase in length along this axis under load, after cracking. The reason for this is the movement of the neutral axis away from the central geometrical axis such that the latter is located at a level where tensile strain is induced.

The elongations and the expansions of the beams were measured between two pairs of demec buttons placed in positions A - A' and B - B' respectively on the same axis of each beam as shown in Figure 3.14.

### 3.12.7 Recording of Crack Patterns

After application of an increment of loading each specimen was carefully examined to identify the presence of any new cracks and to detect any growth in the existing cracks. Whenever significant changes occurred in the crack pattern a photograph was also taken. The cracks were coloured in green, red and blue to trace their propagation during the first, second and third load cycles respectively. These coupling beams were considered as parts of an "earthquake resistant" structure. The performance of the coupling beams with respect to the serviceability limit state was not studied in depth. No attempt was made to accurately ob-

serve the development of the widths of the cracks in the majority of the beams. The width of the most significant cracks within the beam in each test specimen was measured at predetermined loading levels using a crack microscope with an accuracy of 0.10 mm.

### 3.12.8 Temperature Control

As constant temperature could not be maintained in the laboratory, it was necessary to compensate for the effects of the variable temperature environment upon the readings from the strain gauges using a dummy gauge in the circuit.

One strain gauge with a gauge length of 10 mm was bonded to a concrete control block (100x100x100 mm) to act as the dummy gauge and to compensate for temperature variations.

## 3.13 TEST PROCEDURE

The principal objective of the programme of experimental work was to provide data on the behaviour of reinforced concrete shear wall coupling beams under in-plane loads sufficient to cause elasto-plastic behaviour. These results were then to be compared with the results obtained from analytical studies. The following main aspects were investigated:

- to determine the behaviour of the coupling beams under cyclic loading conditions;
- to plot the crack pattern and crack propagation for each beam;

- to determine the failure mechanism, and reserve of strength in each test specimen.

Each coupling beam specimen was placed in position on the test floor of the laboratory at least one week before testing. After the surface of the specimen was painted, the positions of the loading and monitoring points were marked on it.

Two days before testing the data logger was connected up to the strain gauges and calibrated. Since the failure load was one of the most important parameters studied in this test programme, great care was taken to ensure that the load was applied correctly to each test specimen.

Each strain gauge and dial gauge was repeatedly read to accurately establish the mean value under the "no load" condition before the commencement of each test.

The testing procedure adopted in the first two load cycles consisted of applying the load in six increments up to a predetermined level of 50kN and then unloading took place in stages. In the third load cycle, the load was increased in steps up to the maximum value which the test beam could sustain. Attempts to increase the load further resulted in a sudden drop in load and was accompanied by large deformations when the beam had suffered extensive cracking. This observation assisted in the characterisation of the failure mechanism in the beam. The strains and the displacements were measured at each increment of load during the three load cycles in each test. However, the results presented here refer only to the third and final load cycles.

After an increment of loading was applied to each test specimen the measurements and observations were taken in the following sequence:

1. The line of action of the load was checked.

2. The temperature and time were noted.

3. Demec gauge readings were checked.

4. Dial gauge readings and rotational measurements were recorded.

5. Strains along the flexural reinforcement were recorded.

6. Strain in the stirrups or in the expanded metal mesh were recorded.

7. Concrete strains were recorded.

8. Dial gauge readings and the displacement of the beam and the wall were recorded.

9. The readings were repeated for confirmation purposes.

10. Specimen was examined for new cracks and growth of existing cracks in the beam and walls.

11. Crack width measurements were taken.

12. Photographs were taken as required.

At each load increment the load was held constant for approximately 3 to 4 minutes in order to monitor all the points described above.

All readings from the dial and demec buttons were manually recorded on standard data sheets. The steel strains were measured and processed using a data logger.

## 3.14 CONCLUSIONS

This Chapter summarises the experimental procedures which were adopted in the present investigation. It describes the properties of the materials which have been used in the production of the test specimens, the casting process, the curing regimes, the instrumentation used and the test procedure.

It also describes the new reinforcement arrangement, involving the use of expanded metal mesh which has been developed in an attempt to overcome the inefficiencies which exist in coupling shear wall structures with respect to the behaviour and detailing of reinforcement in such structures. Two form of reinforcement have been used in this investigation. The first one consisted of the use of expanded metal mesh only. The second approach was similar to the technique used already by Paulay [11] to overcome the problem of ductility in coupling beams.

It must be emphasised that the effectiveness of the use of expanded metal mesh will be based on tests carried out on coupling beams containing both reinforcement approaches. The beneficial effect of using expanded metal mesh was taken into consideration in the design.

| Dimension of the specimens (mm) | | | | | | |
|---|---|---|---|---|---|---|
| Beam specimen | t | b | d | H | $L_1$ | $L_2$ |
| Quarter scale | 120 | 500 | 250/300 | 750 | 500 | 500 |
| Half scale | 120 | 1000 | 900 | 1500 | 1000 | 1000 |
| Double storey | 120 | 500 | 250 | 750 | 500 | 500 |

Table 3.1: Dimensions of the specimens

| Characteristics of concrete mix | | |
|---|---|---|
| 1 | Water-cement ratio | 0.55 |
| 2 | Cement content | 400 $kg/m^3$ |
| 3 | Moraine gravel aggregates | 1200 $kg/m^3$ |
| 4 | Sand | 600 $kg/m^3$ |
| 5 | Minimum aggregate size | 10 mm |
| 6 | Workability | medium |
| 7 | Slump | 120 mm |

Table 3.2: Concrete mix proportions

| Parameter | Symbol | Units | CBD1 | EBD1 | DBS2 |
|---|---|---|---|---|---|
| Cube strength | f'cu | $N/mm^2$ | 31.33 | 32.26 | 36.16 |
| Cylinder strength | f'c | $N/mm^2$ | 25.30 | 27.29 | 30.45 |
| Strength ratio | f'c/f'cu | - | 0.807 | 0.845 | 0.842 |
| Elastic modulus | E | $N/mm^2$ | 205598 | 23542 | 29546 |
| Density | $\rho$ | $kg/m^3$ | 2378 | 2410 | 2362 |

Table 3.3: Concrete properties for beams with shear span to depth ratios of 1.1 and 2.0

| Parameter | Symbol | Units | CBS1 | CBS2 | EBS1 | EBS2 |
|---|---|---|---|---|---|---|
| Cube strength | f'cu | $N/mm^2$ | 36.06 | 35.04 | 40.20 | 40.00 |
| Cylinder strength | f'c | $N/mm^2$ | 30.10 | 29.56 | 31.87 | 31.98 |
| Strength ratio | f'c/f'cu | - | 0.834 | 0.843 | 0.813 | 0.799 |
| Elastic modulus | E | $N/mm^2$ | 27964 | 26874 | 32422 | 33928 |
| Density | $\rho$ | $kg/m^3$ | 2360 | 2355 | 2320 | 2375 |

Table 3.4: Concrete properties for beams with shear span to depth ratio of 2.0

| Parameter | Symbol/Units | CBM1 | CBM2 | EBM1 | EBM2 | CBM3 | EBM3 |
|---|---|---|---|---|---|---|---|
| Cube strength | f'cu($N/mm^2$) | 33.90 | 35.23 | 40.20 | 36.40 | 35.40 | 36.20 |
| Cylinder strength | f'c($N/mm^2$) | 28.04 | 29.48 | 31.19 | 30.57 | 30.90 | 30.15 |
| Strength ratio | f'c/f'cu | 0.827 | 0.836 | 0.810 | 0.839 | 0.826 | 0.835 |
| Elastic modulus | E ($N/mm^2$) | 22919 | 24289 | 30273 | 28843 | 29950 | 28150 |
| Density | $\rho$ ($kg/m^3$) | 2375 | 2410 | 2350 | 2375 | 2405 | 2390 |

Table 3.5: Concrete properties for beams with shear span to depth ratio of 1.43

| Ultimate/Yield strength for both types reinforcement ($N/mm^2$) | | | | | | | | |
|---|---|---|---|---|---|---|---|---|
| Beams | f'y | f'u | $f'y_{st}$ | $f'u_{st}$ | $f'y_m$ | $f'u_m$ | $f'y_d$ | $f'u_d$ |
| CBD1 | 415 | 520 | 305 | 400 | - | - | 350 | 465 |
| EBD1 | 400 | 500 | - | - | 285 | 360 | 355 | 470 |
| DBS2 | 410 | 520 | 310 | 410 | - | - | - | |
| CBS1 | 400 | 485 | 300 | 395 | - | - | 350 | 470 |
| CBS2 | 400 | 495 | 295 | 405 | - | - | - | - |
| EBS1 | 410 | 480 | - | - | 290 | 360 | 345 | 440 |
| EBS2 | 410 | 490 | - | - | 295 | 370 | - | - |
| CBM1 | 405 | 490 | 295 | 380 | - | - | 375 | 450 |
| CBM2 | 410 | 495 | 290 | 395 | - | - | - | - |
| CBM3 | 405 | 490 | 290 | 385 | - | - | - | - |
| EBM1 | 400 | 500 | - | - | 285 | 370 | 350 | 460 |
| EBM2 | 400 | 480 | - | - | 285 | 360 | - | - |
| EBM3 | 400 | 485 | - | - | 290 | 370 | - | - |

Table 3.6: Properties of the reinforcement for all the coupling beams

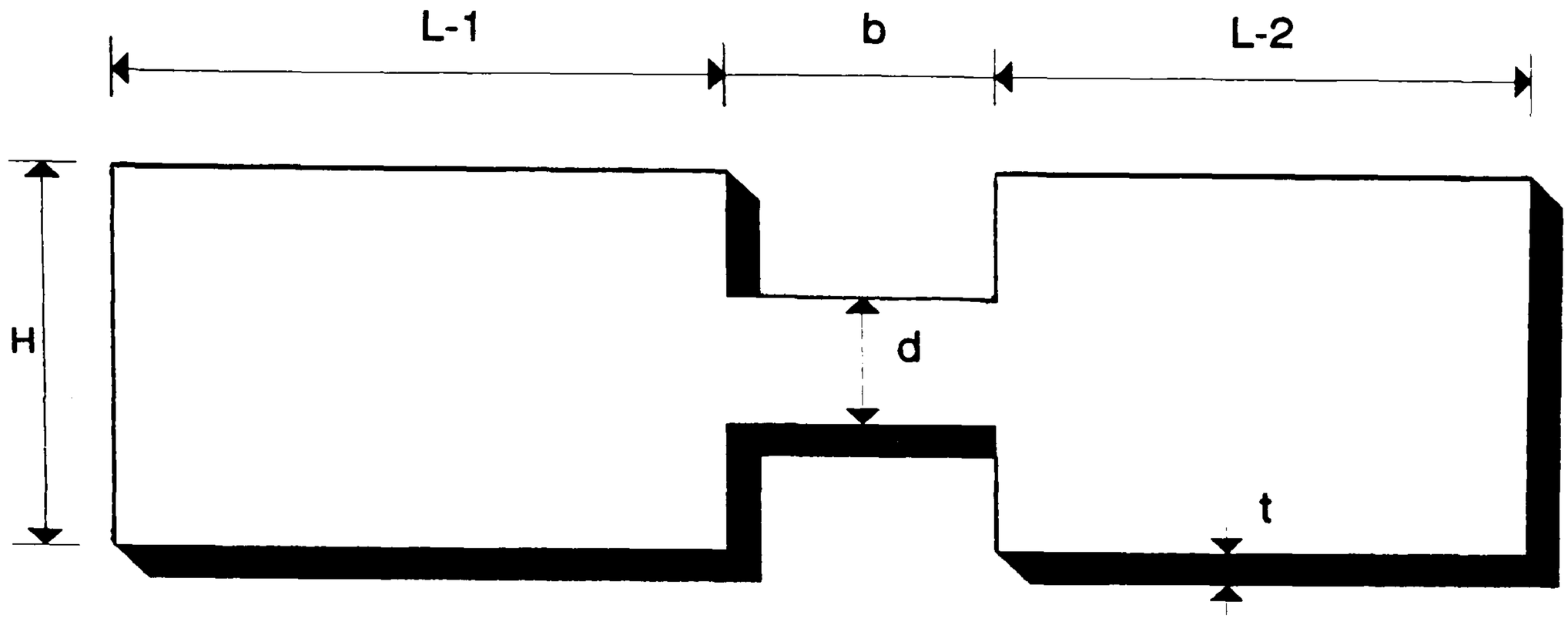


Figure 3.1: Single storey specimen

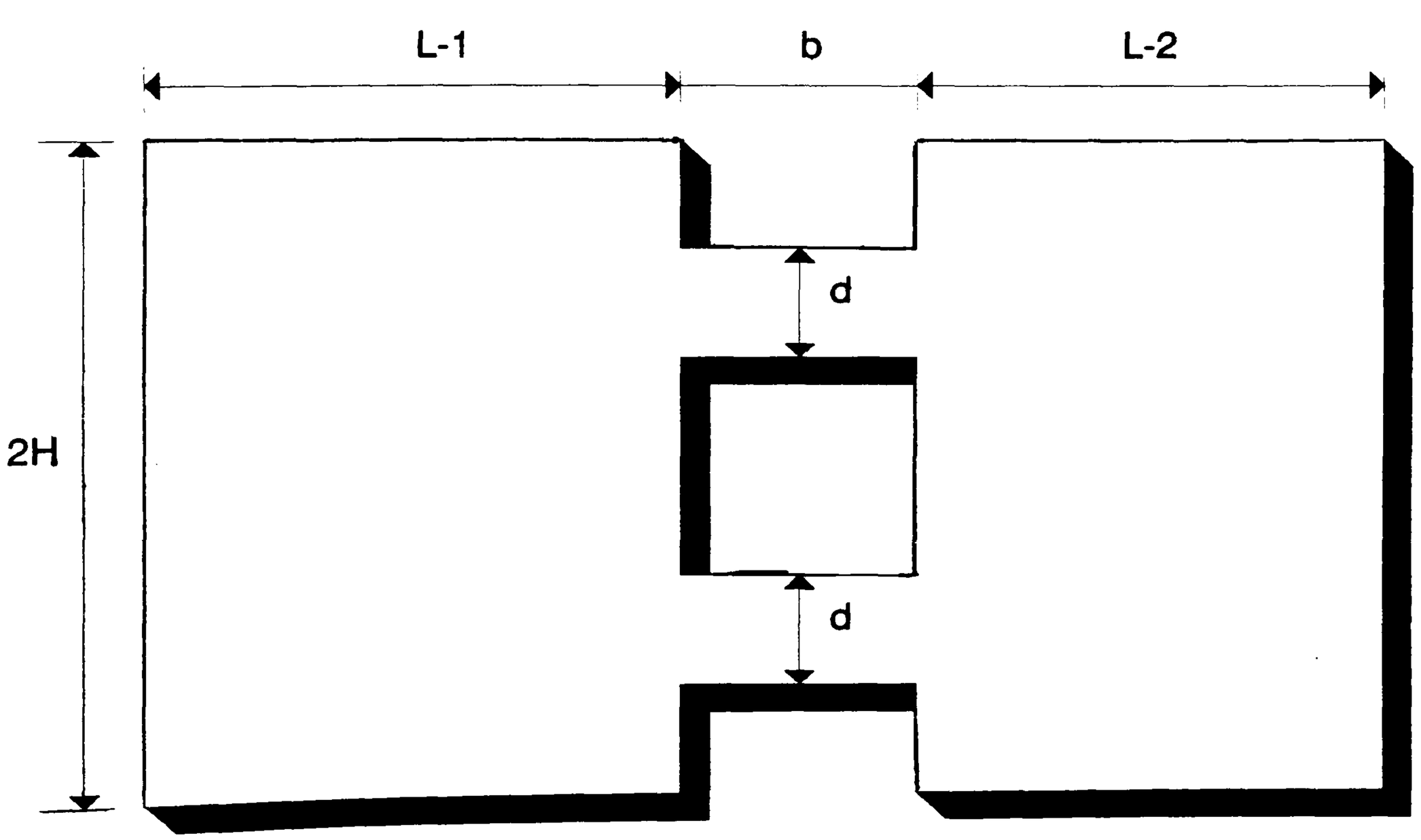


Figure 3.2: Double storey specimen

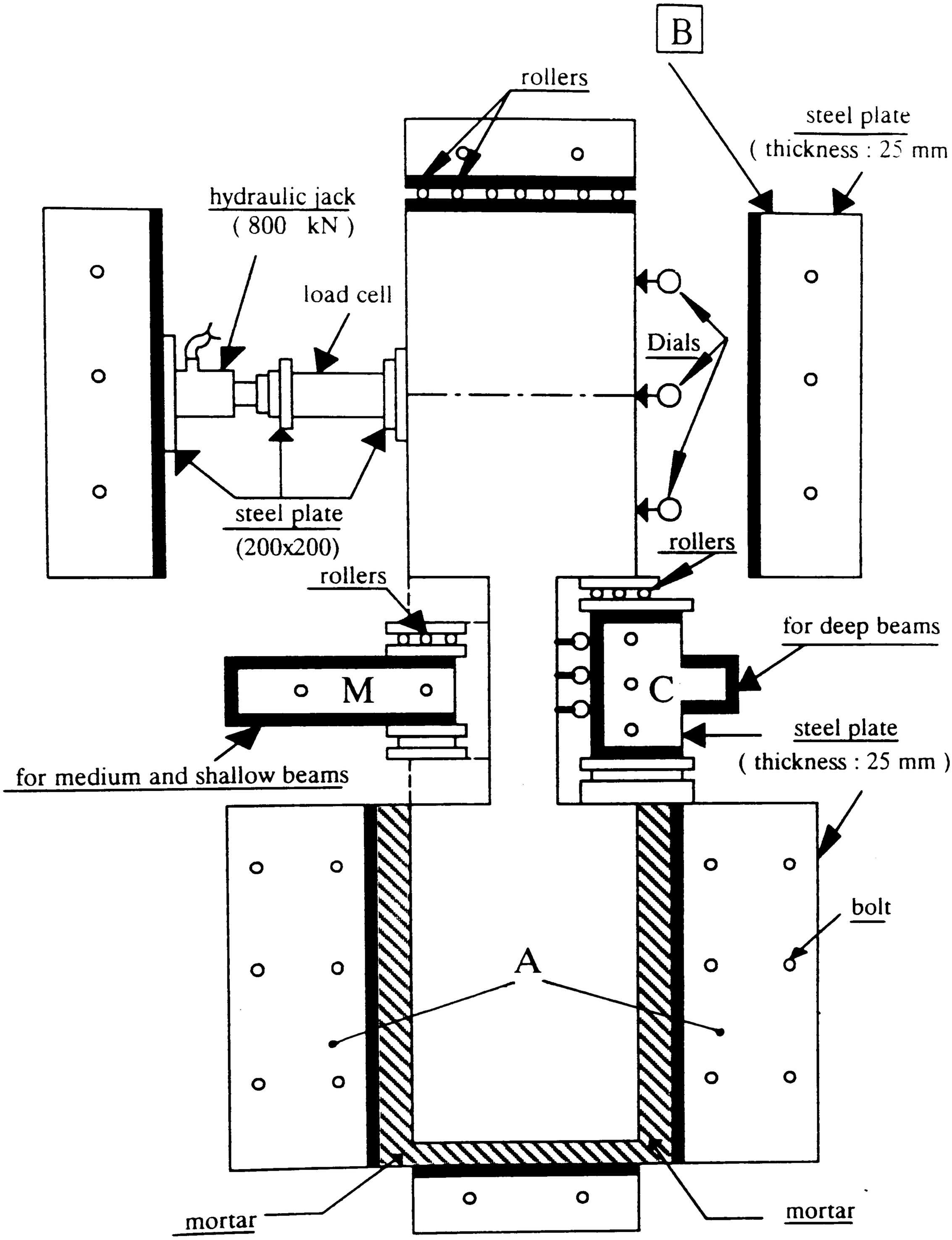


Figure 3.3: Test arrangement and loading system

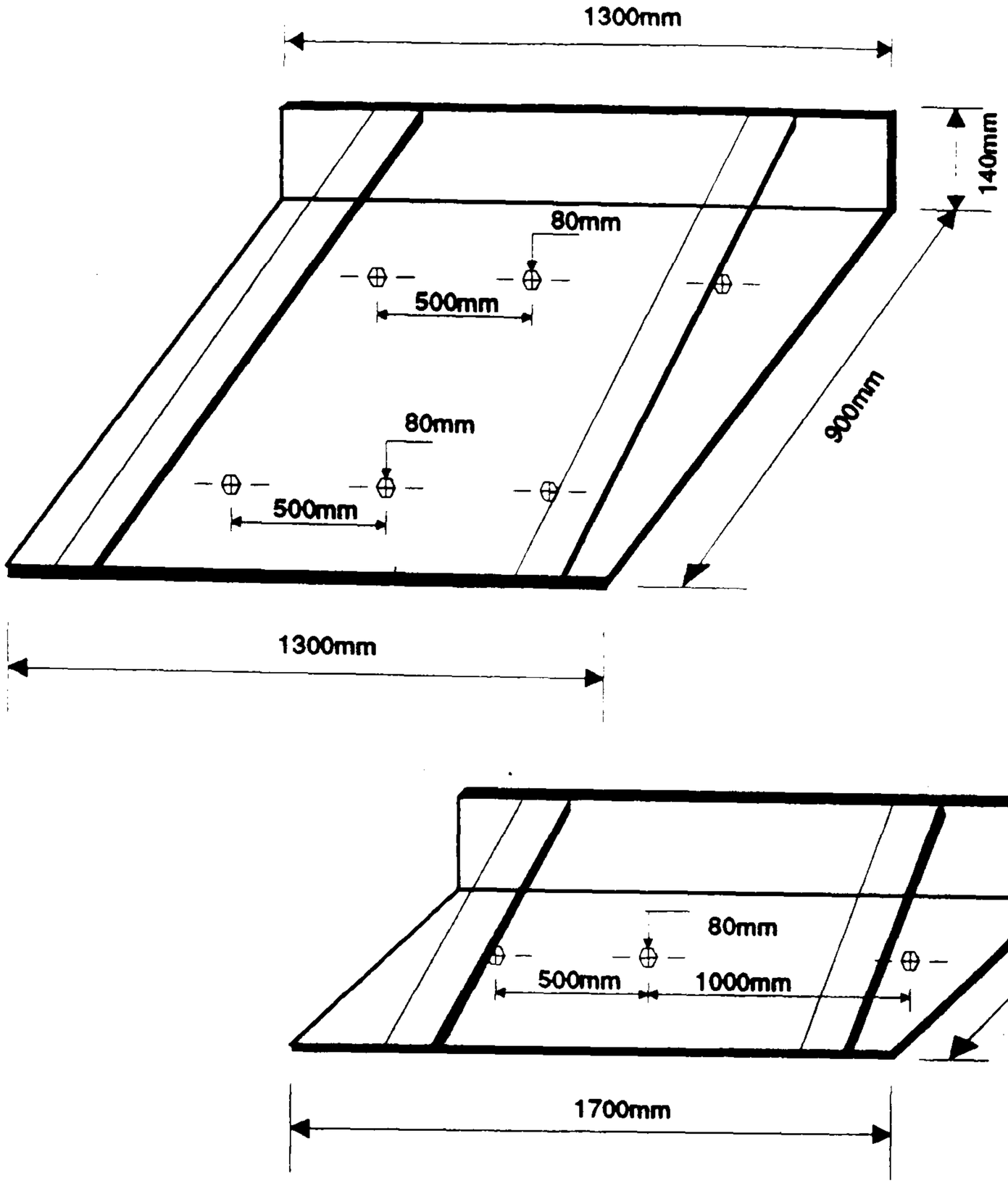


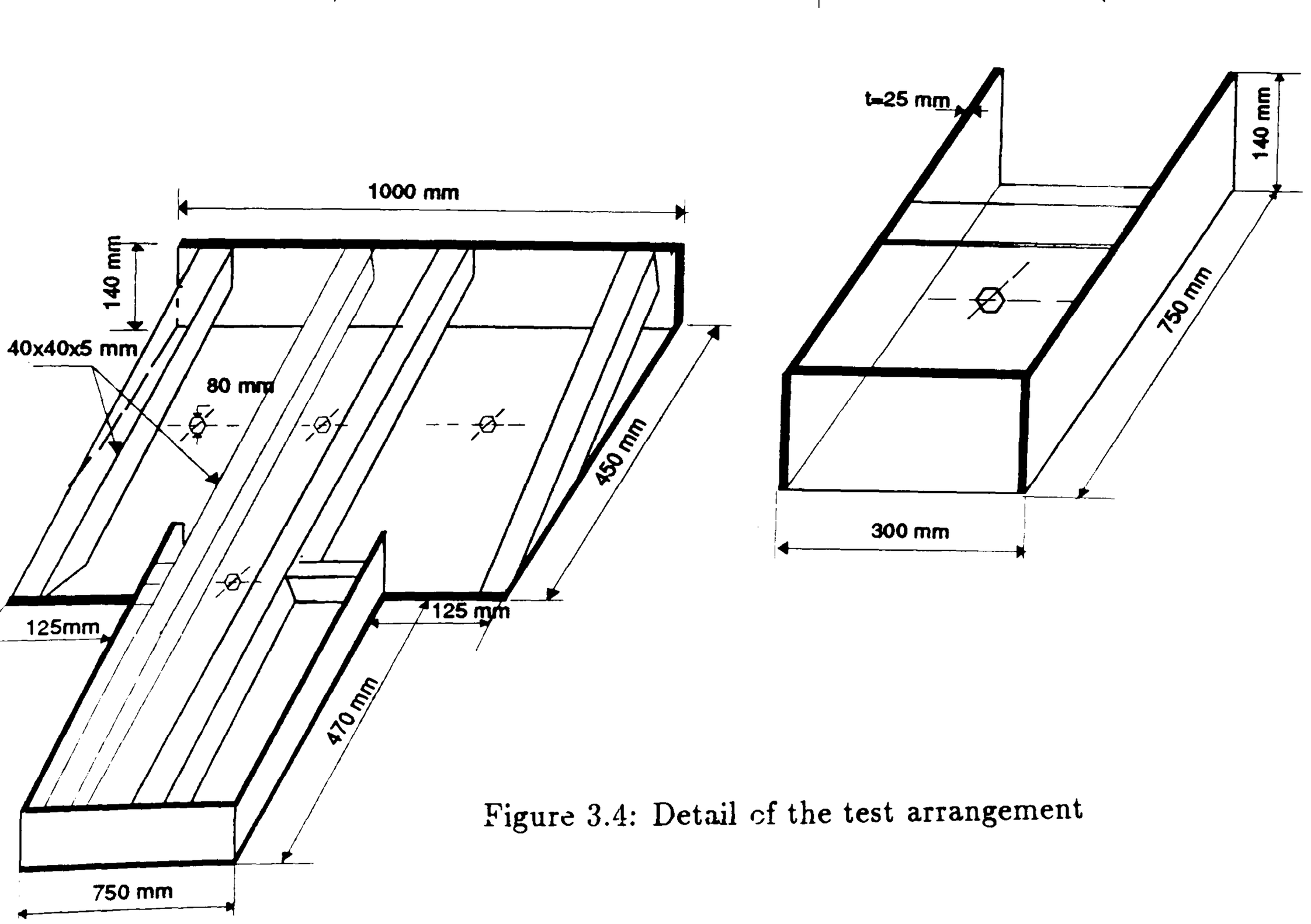


Figure 3.4: Detail of the test arrangement

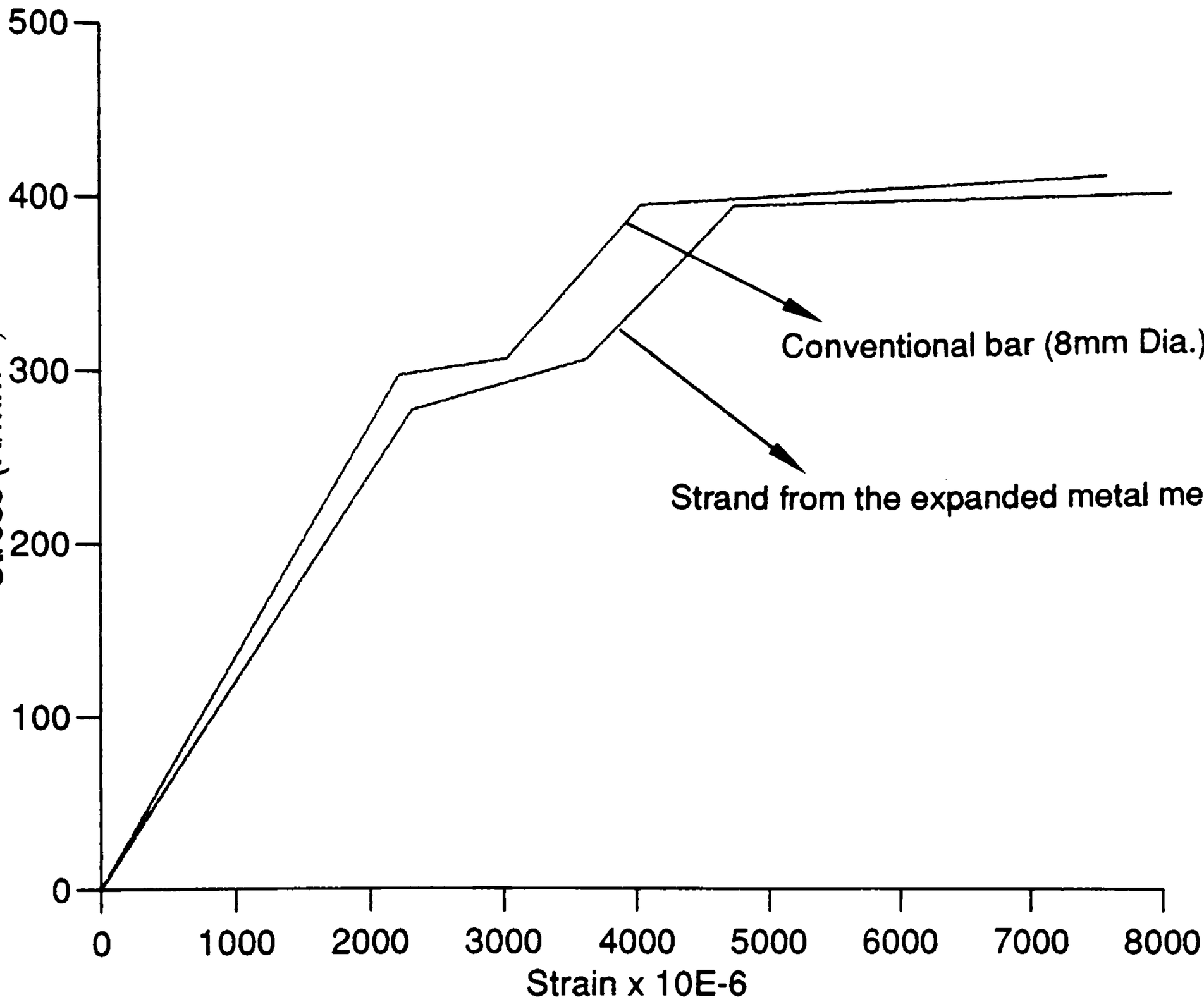


Figure 3.5: Stress-strain curve for both types of reinforcement

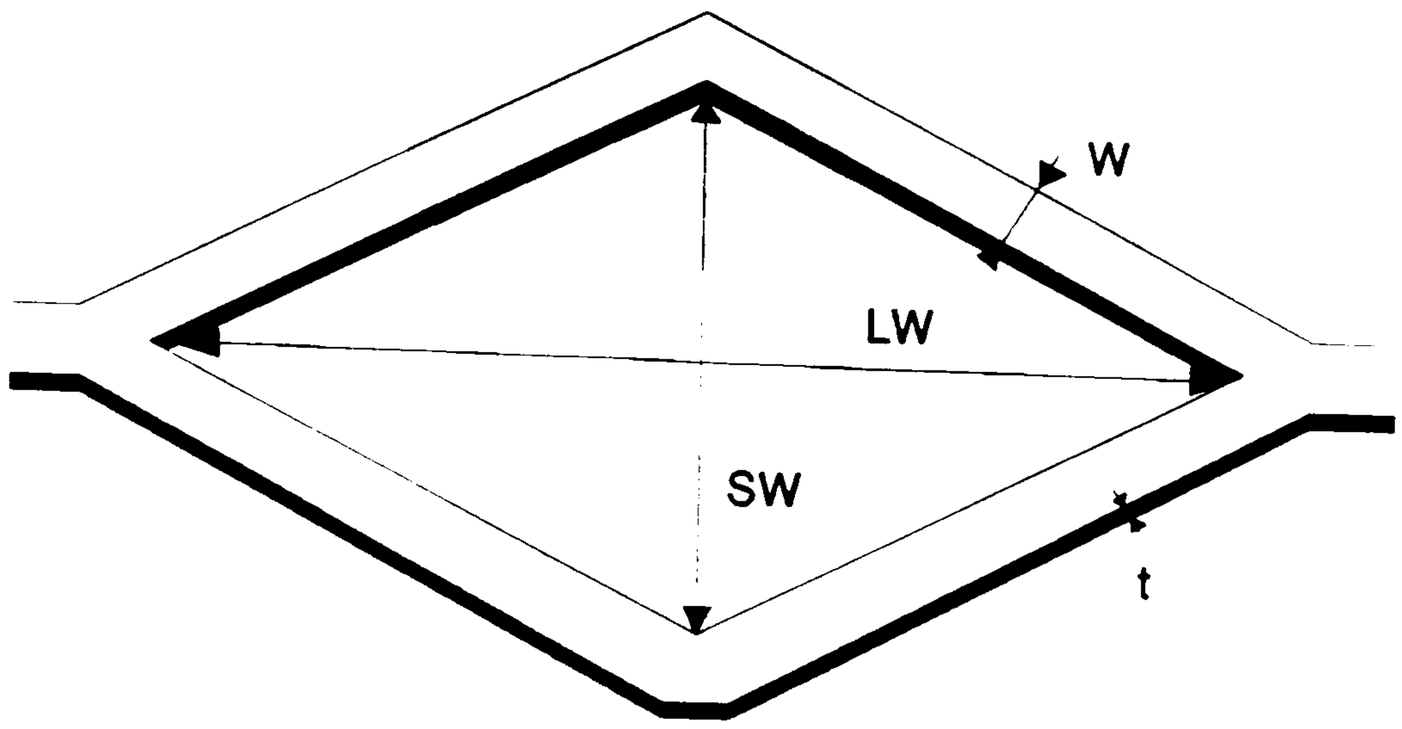


Figure 3.6: Representation of expanded metal mesh

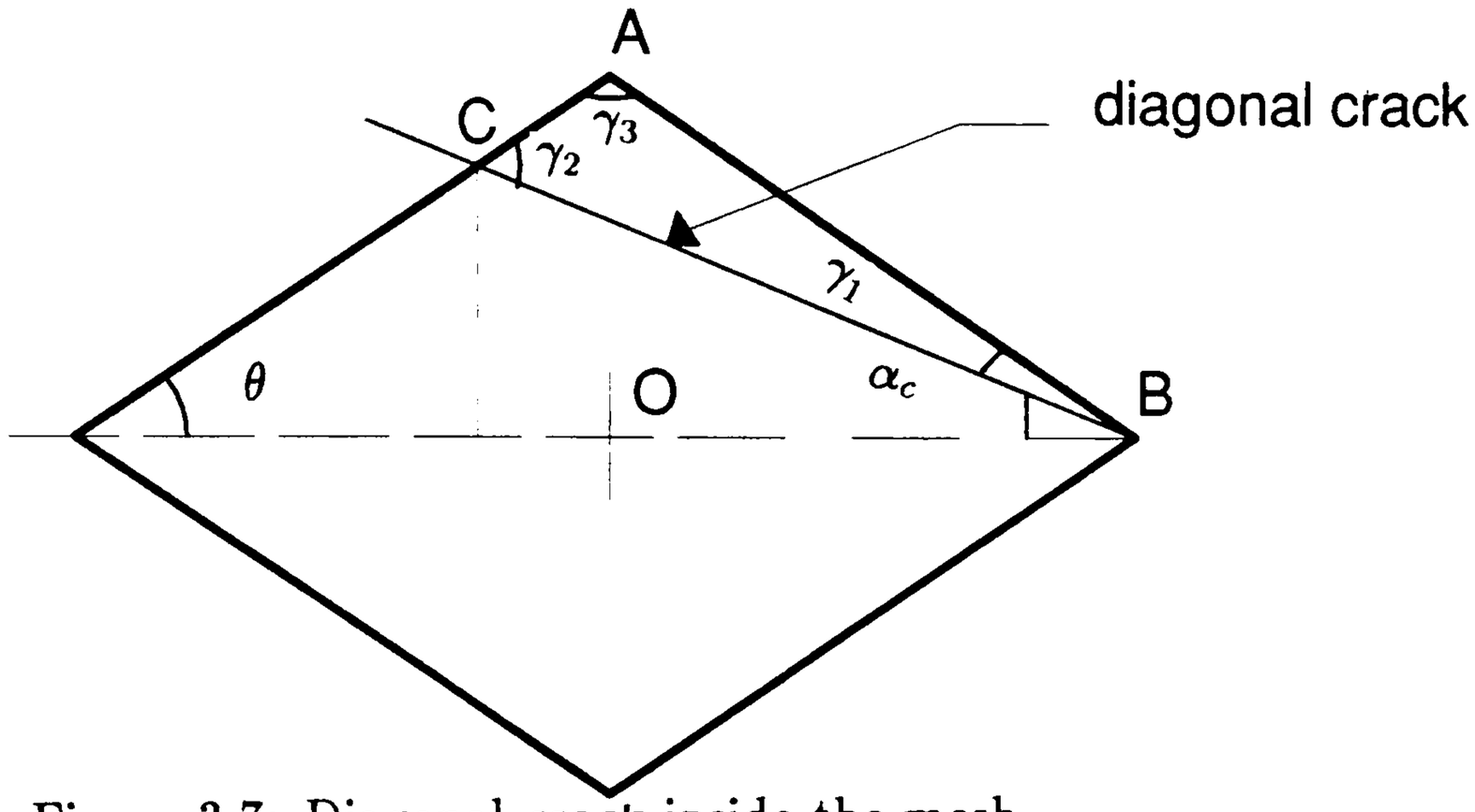


Figure 3.7: Diagonal crack inside the mesh

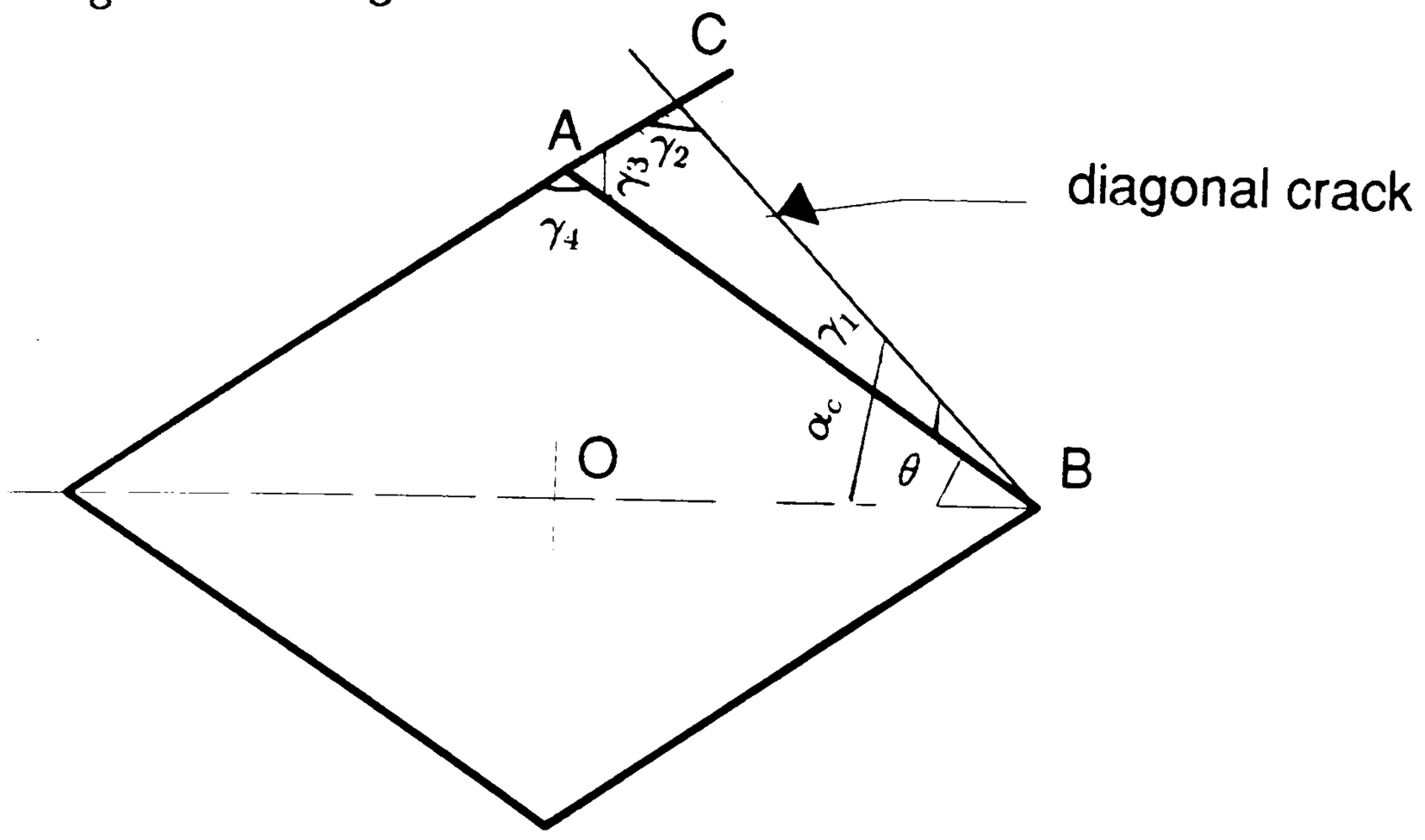


Figure 3.8: Diagonal crack outside the mesh

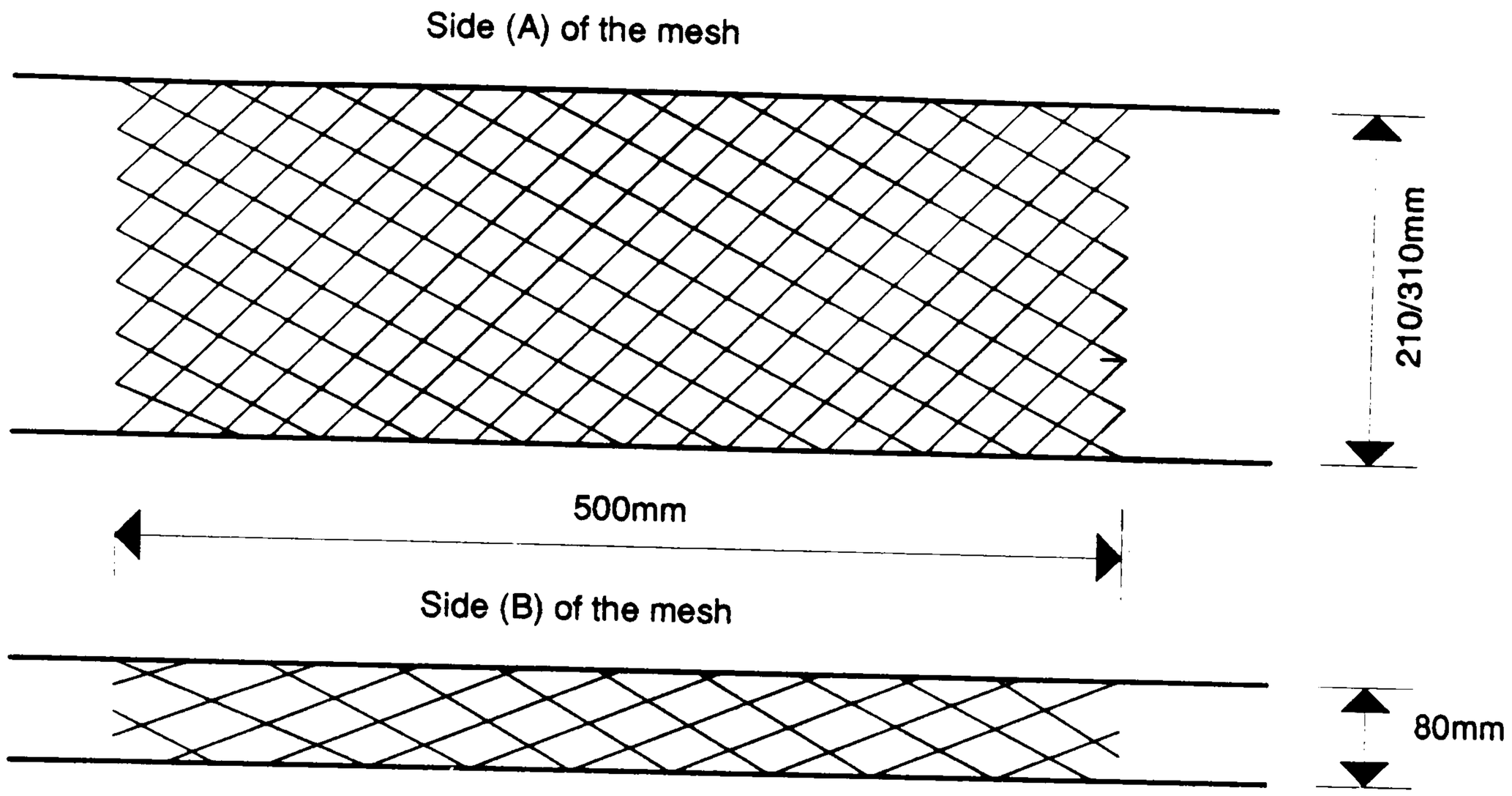


Figure 3.9: Dimensions of the mesh used as stirrups

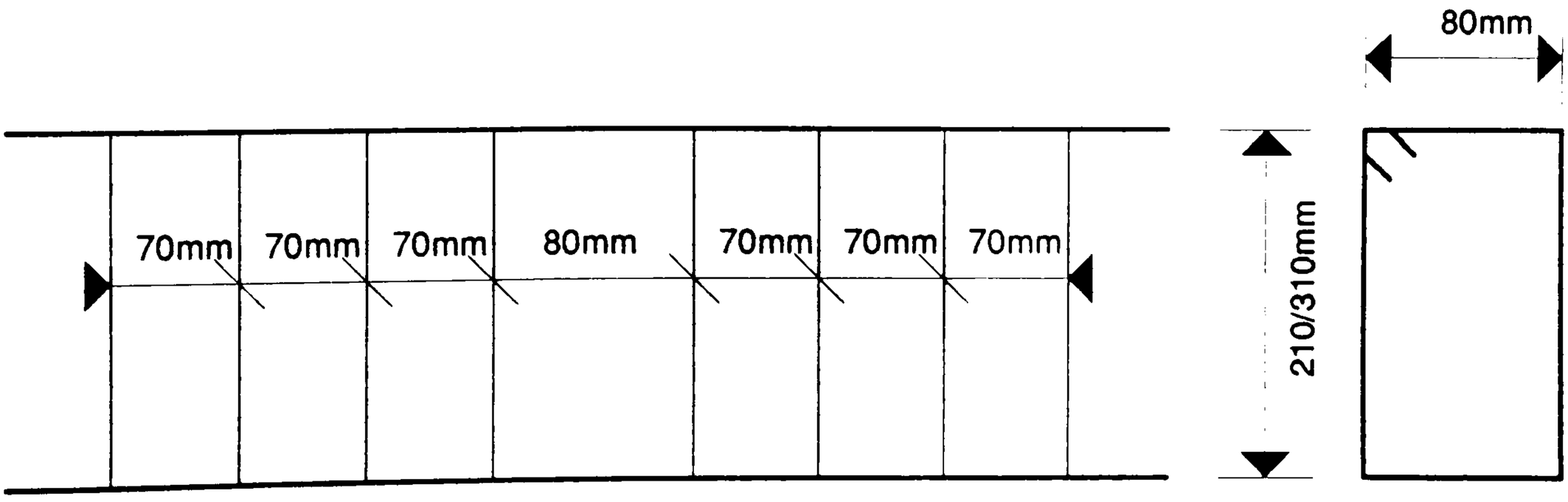


Figure 3.10: Dimensions of the conventional reinforced beam

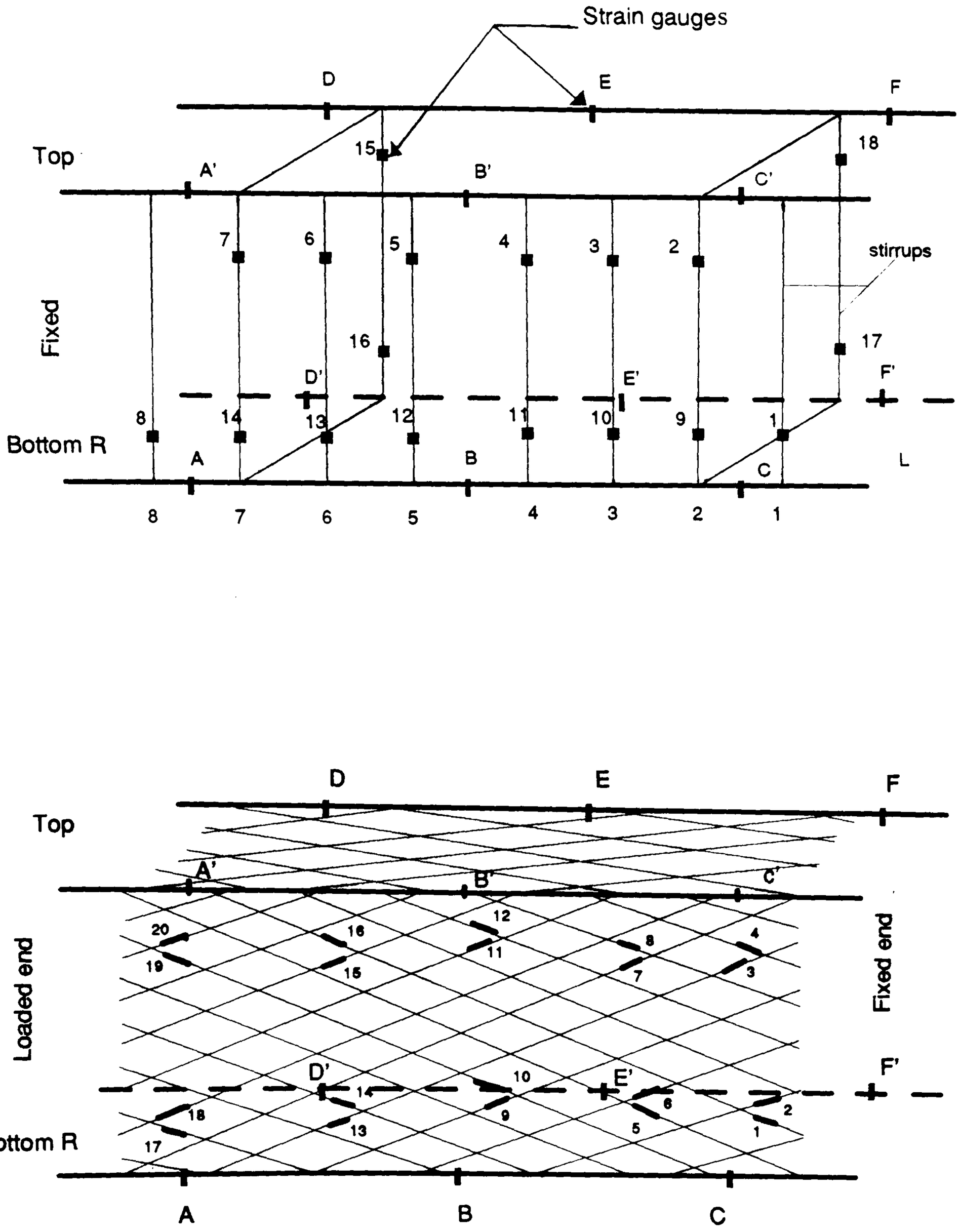


Figure 3.11: Positions of strain gauges for both types of reinforcement

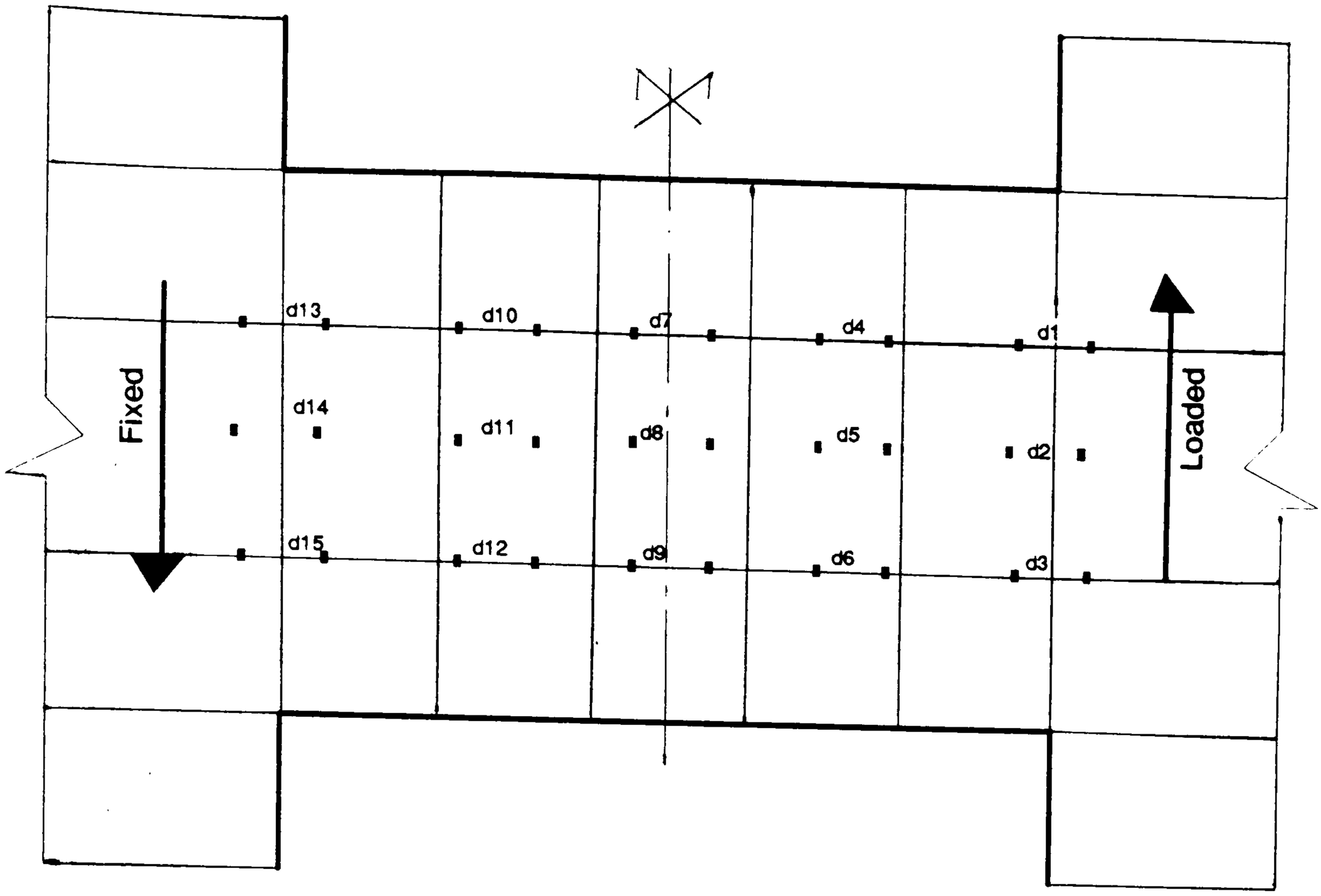


Figure 3.12: Positions of demec buttons on the concrete

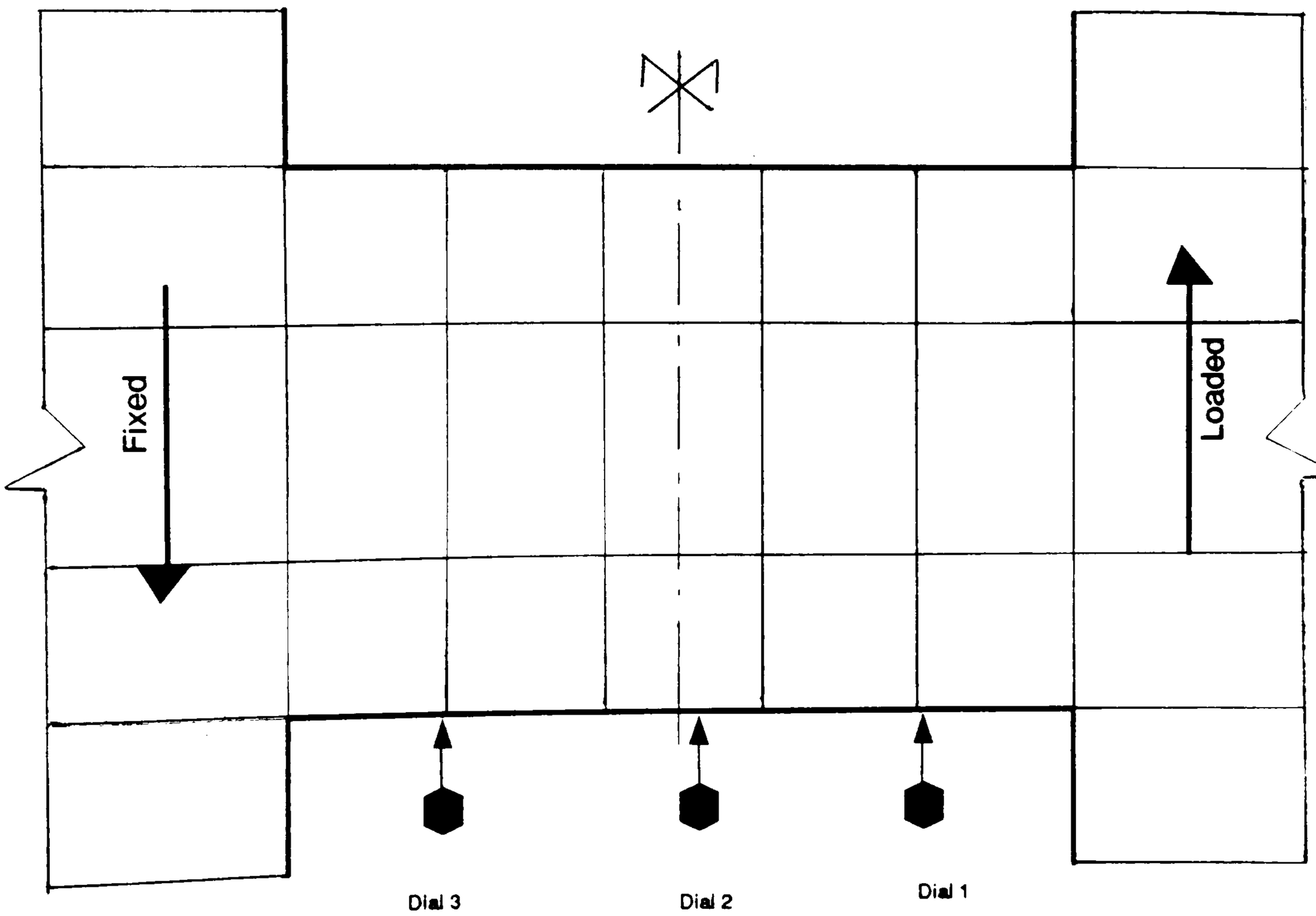


Figure 3.13: Positions of dial gauges on the beam

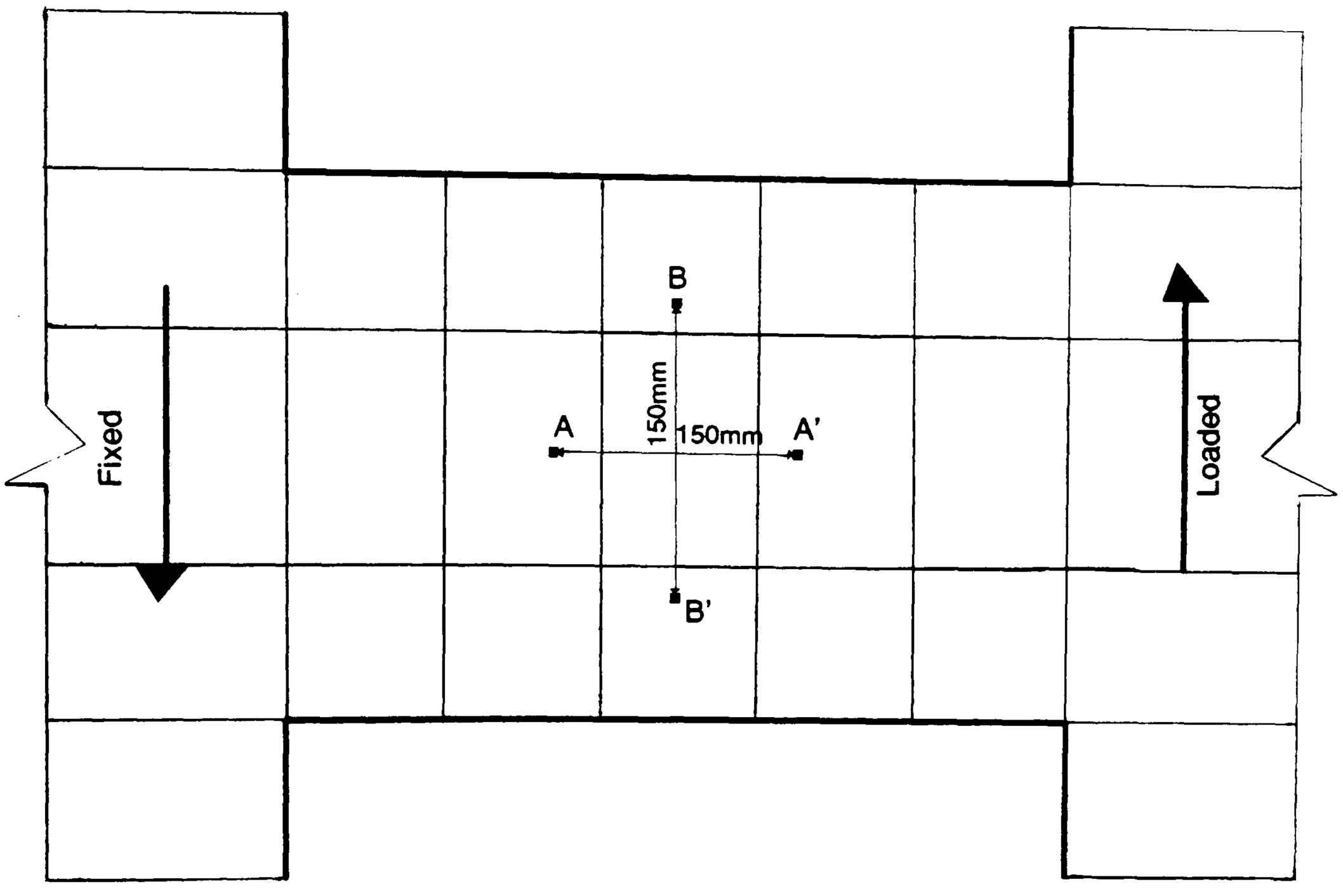


Figure 3.14: Positions of demec demec on side of the beam

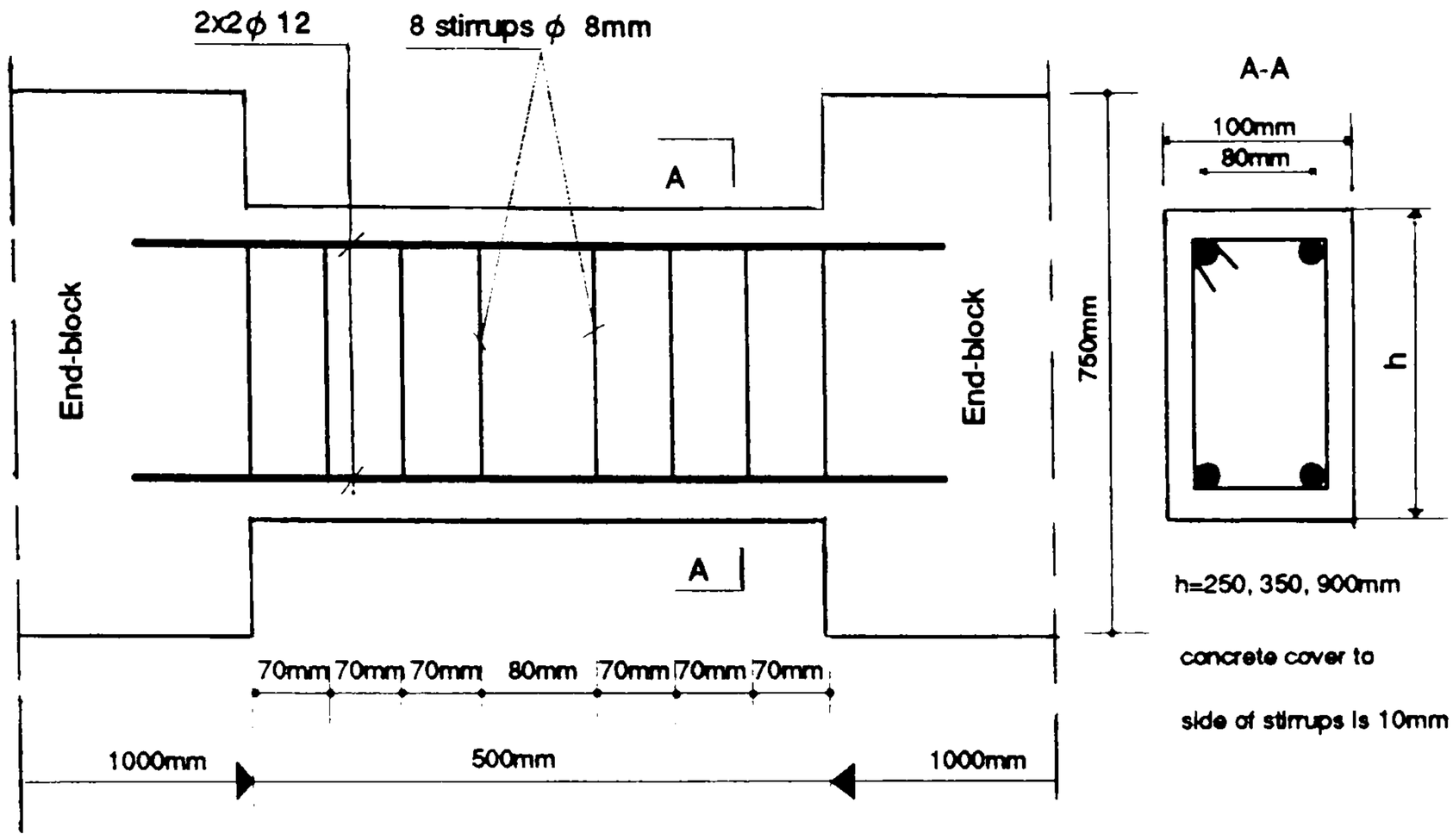


Figure 3.15: Dimensions of the coupling beam reinforced only with stirrups

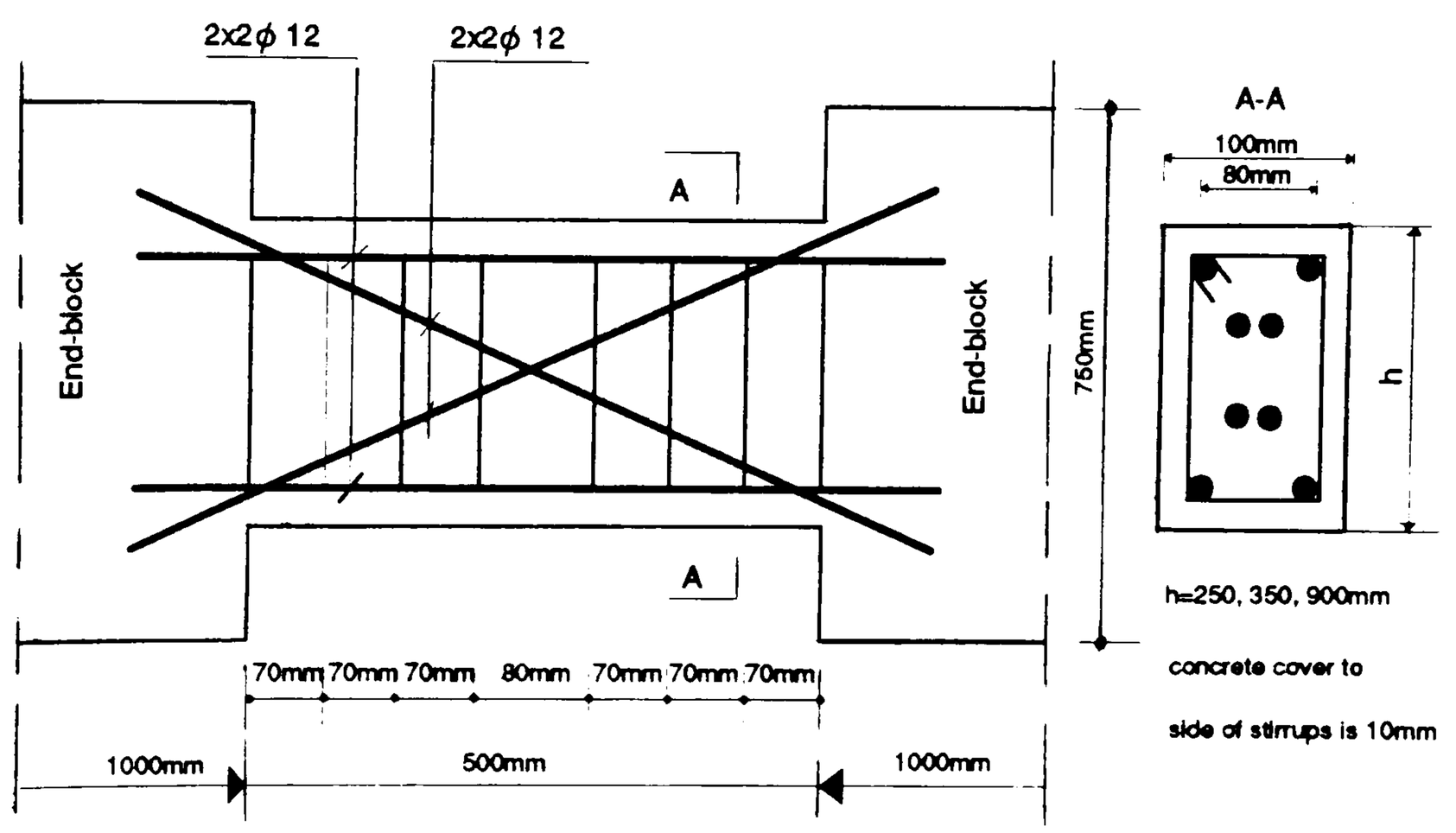


Figure 3.16: Dimensions of the coupling beam reinforced with stirrups and diagonal bars

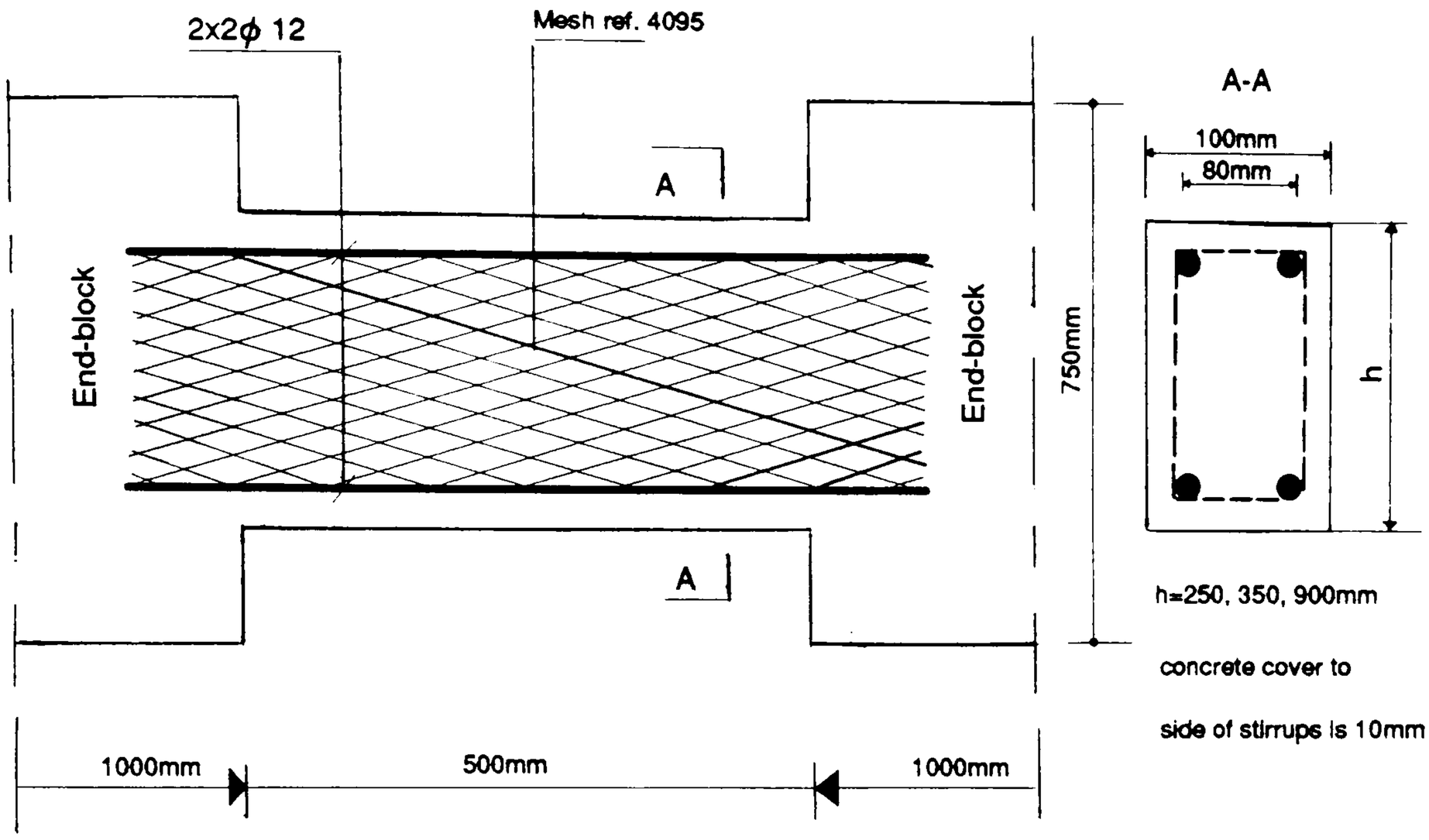


Figure 3.17: Dimensions of the coupling beam reinforced only with mesh

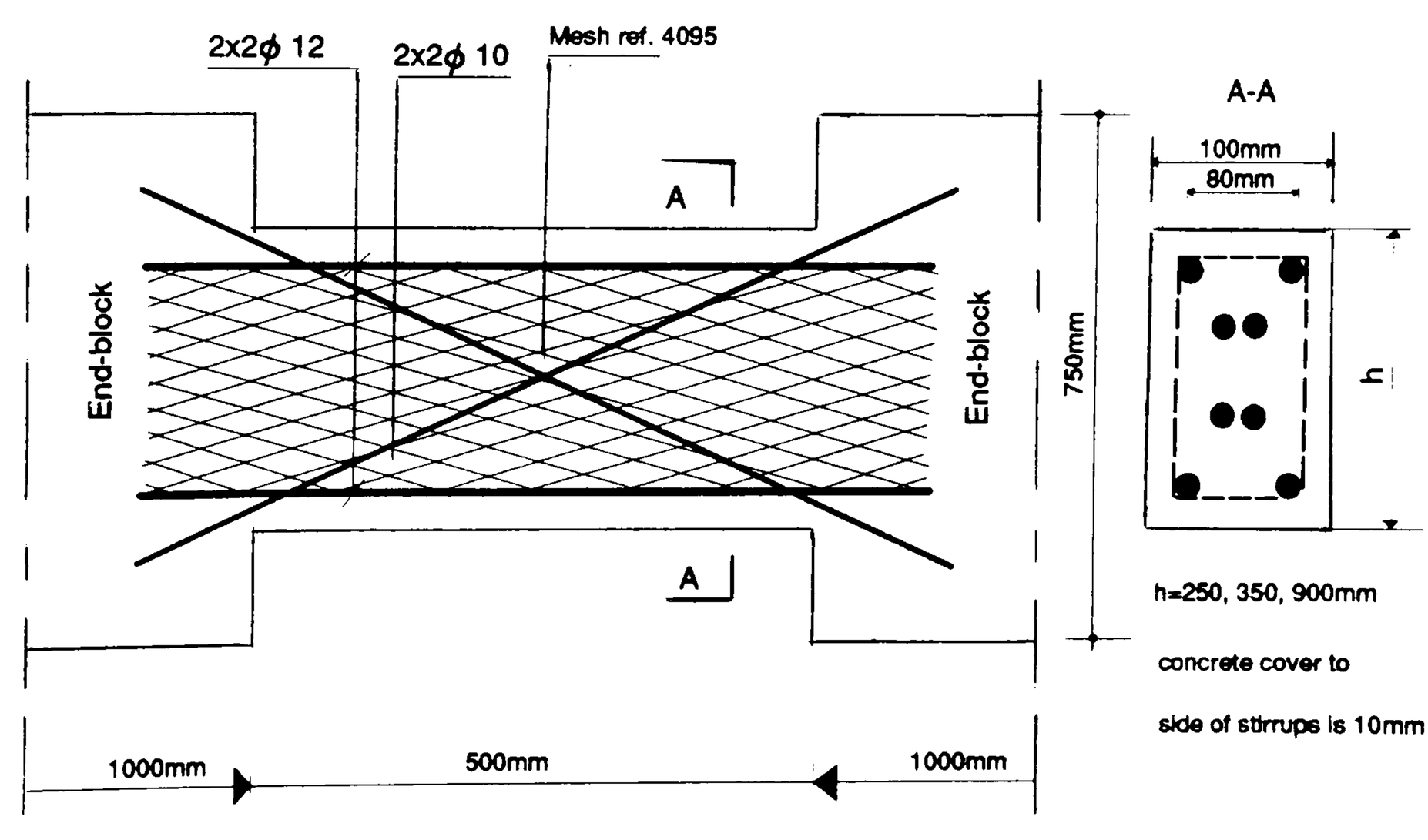


Figure 3.18: Dimensions of the coupling beam reinforced with mesh and diagonal bars

# Chapter 4

# THEORETICAL ANALYSIS OF COUPLING BEAMS

## 4.1 INTRODUCTION

In many tall buildings coupled shear walls provide the stiffness and strength required to resist lateral loading resulting from wind and earthquake effects. Currently, the analysis of coupled shear wall structures is normally carried out using elastic methods, such as the continuous connection technique, modified frame, and the finite element approaches. Design of the shear wall structure is not covered by any British Standards. Up-to date information on available analytical techniques and recommendations for design and detailing of shear wall structures are presented in a report published in 1984 by CIRIA [68].

The structural design of tall buildings continues to advance and this advance is reflected primarily in better knowledge of the lateral loads that tall buildings must

resist, the use of simpler and more effective approaches to the detailing of the reinforcement, better quality concrete, and more efficient construction methods as well as refinement in structural forms.

The objective of this Chapter is to develop an analytical method which can be reasonably and rapidly performed in the field to predict the failure mechanism of the coupling beams and to provide guidance on the design of coupled beams reinforced both with expanded metal mesh and conventional reinforcement. It is based largely on existing published information which has been assessed critically and presented in a form suitable for application in practice.

The approaches included in this Chapter, which were put forward by Subedi [69] and Kotsovos [1], are capable of predicting the ultimate strength of coupling beams. These two approaches were tested against the results obtained from tests on thirteen coupling beams with shear span to depth ratios in the range of 1.1 to 2.0 incorporating several forms of reinforcement. The aims of these approach reflect advances in the design approach based on the ultimate load method for the analysis of reinforced coupling beams. These methods were developed to analyse the beams containing expanded metal mesh examined in this investigation.

The application of these methods to the analysis of coupling beams will permit the load at which the structure will fail to be accurately determined, and the structure can be designed so that the working load is some chosen fraction of the failure load.

Many countries have now introduced ultimate load analysis into their design approaches, and there is little doubt that eventually it will become the accepted

method of analysis. Indeed, it is the only permitted method in many parts of eastern Europe.

## 4.2 ANALYSIS OF THE COUPLED BEAMS USING THE C.F.P APPROACH

It has been shown that the causes of shear failure in reinforced concrete beams in general and coupling beams in shear wall construction in particular are associated with the strength of the concrete in the region of the path along which the compressive force is transmitted to the supports.

Most of the current design concepts are based on uniaxial stress-strain characteristics. Recent work [78] has shown quite conclusively that the ultimate limit-state behaviour of reinforced concrete beams, can only be explained in terms of multiaxial effects which are always present in a structure. It is the consideration of the multiaxial effects that has led to the introduction of the Compressive Force Path concept (C.F.P) [1] which has been shown not only to provide a realistic description of the causes of failure of structural concrete, but can also form a suitable basis for the development of models capable of providing safe and efficient design solutions.

This approach to the design of beams put forward by Kotsovos [1] brought fresh ideas to the age-old design concepts for concrete structures which fail to promote an adequate explanation of the behaviour of such structures.

method of analysis. Indeed, it is the only permitted method in many parts of eastern Europe.

## 4.2 ANALYSIS OF THE COUPLED BEAMS USING THE C.F.P APPROACH

It has been shown that the causes of shear failure in reinforced concrete beams in general and coupling beams in shear wall construction in particular are associated with the strength of the concrete in the region of the path along which the compressive force is transmitted to the supports.

Most of the current design concepts are based on uniaxial stress-strain characteristics. Recent work [78] has shown quite conclusively that the ultimate limit-state behaviour of reinforced concrete beams, can only be explained in terms of multiaxial effects which are always present in a structure. It is the consideration of the multiaxial effects that has led to the introduction of the Compressive Force Path concept (C.F.P) [1] which has been shown not only to provide a realistic description of the causes of failure of structural concrete, but can also form a suitable basis for the development of models capable of providing safe and efficient design solutions.

This approach to the design of beams put forward by Kotsovos [1] brought fresh ideas to the age-old design concepts for concrete structures which fail to promote an adequate explanation of the behaviour of such structures.

This concept is based on a proper understanding of concrete at the material level and thus, appears to be resourceful enough to overcome the deficiencies of present-day design concepts.

Many investigators have attempted to apply the C.F.P method to simply supported reinforced and prestressed beams made from a wide range of concrete strengths. However, it has been suggested that the proposed method can be applied, not only to simply supported normally reinforced and prestressed structural concrete members, but also to any form of skeletal structural configuration.

It has been observed that the strength of the concrete present along the compressive force trajectory of the structural concrete member plays an important role in its overall behaviour at the ultimate limit state. It was perceived that the design of concrete structures should be based on realistic models, and one such model is based on the Compressive Force Path concept. The extension of this concept to reinforced concrete coupling beams will be addressed.

### 4.2.1 Shear Resistance of the Concrete

The most crucial problem in a shear wall structure is associated with a shear failure. It may be argued that the concrete is unlikely to sustain by itself, the high tensile stress caused by the presence of shear forces when the depth of the compressive zone is small. Such an argument is normally based on the assumption that concrete within the compressive zone of a reinforced concrete beam at its ultimate limit state can realistically be described using uniaxial stress-strain

characteristics. This assumption is in conflict with experimental evidence which has indicated that the compressive zone is subjected to triaxial stress conditions. In fact the stress state has been found [58] to be wholly compressive in the region of the sections containing deep cracks where the tensile stresses due to the shear force are expected to be critical.

It appears therefore, that a part of the vertical component of this compressive stress state counteracts the tensile stresses which develop due to the presence of shear forces. Hence in spite of the presence of such forces, the stress state can remain compressive, and this causes a significant enhancement in the local strength of the member. A schematic representation of the mechanism which provides the resistance to shear is shown in Figure 4.1.

### 4.2.2 Shear Capacity of Critical Section

The shear capacity of the cross section is normally defined in Codes of Practice in terms of the nominal shear stress $v = V/bd$, where $V$ is the shear force and b and d are the width and the depth of the cross section, respectively.

A reinforced concrete coupling beam with insufficient shear reinforcement is considered to fail in shear when the nominal shear stress, $v$, at a critical section exceeds a critical value, $v_c$, before the flexural capacity of the beam is attained. According to this reasoning, any section within the shear span of a reinforced concrete beam without shear reinforcement subjected to a four point loading system is critical: therefore, the beam should fail in shear when the shear capacity of the

shear span is exceeded before the flexural capacity of the beam is attained. Hence, shear failure can be prevented only by placing shear reinforcement throughout the shear span.

### 4.2.3 Factors Affecting Coupling Beam Shear Strength

Experimental studies of the factors affecting the shear strength of reinforced concrete coupling beams have been presented by many investigators [70]. Some of these factors are concrete strength, shear span-to-depth ratio, web reinforcement ratio, longitudinal and diagonal steel ratio, spacing and angle of inclination of the stirrups, cross-sectional properties of the coupling beams such as the breadth and depth of the beam, aggregate interlock, and dowel action.

Many equations [70] based on experimental test results have been proposed for predicting the shear strength of beams taking into consideration the effect of some of the factors above.

## 4.3 EVALUATION OF THE C.F.P CONCEPT FOR ANALYSIS AND DESIGN

It is clear from the literature survey that, despite the very considerable efforts exerted by a number of researchers over the last few decades, an understanding of the behaviour of concrete structures in general is still in disarray particularly for coupling beams. Despite the fact that over the last few years, promising new

ideas and concepts have emerged in this field, most of them are in reality based on the traditional way of thinking.

The new theories or models, like the compressive field theory [74], the modified compression field theory [75] [76], or the strut-and-tie model [77], are no exception, because the truss-analogy forms the core of all these concepts.

The Compressive Force Path concept on the other hand, is significantly different from such approaches. However, in the recent past, the widely held view that concrete exhibits strain-softening material characteristics under any state of stress has been challenged by Kotsovos [71] using the results from a laboratory based investigation which has indicated that concrete as a material is brittle in nature. He showed [71] that the conventional strain-softening response is not a material characteristic as widely believed, but merely a descriptor of secondary testing effects. Clearly the above finding has significant implications on current approaches to analysis and design.

The shallowness of present-day design concepts becomes evident by looking at the extensive number of design equations put forward by researchers or by the same individuals on different occasions. Incidentally, most of the investigators seldom deviate from the truss-analogy, yet fail to put forward a generalised design solution. The design equations are validated using the results from a set of experiments and thus have significant limitations in their application.

## 4.4 VALIDITY OF THE C.F.P

The deformational response of the compressive zone can be established by testing a reinforced concrete beam under four point loading and measuring the longitudinal and the transversal strains at the top and the bottom face of the coupling beam within the middle zone region.

The validity of the present approach is tested by comparing the behaviour predicted by the C.F.P with that found from the tests included in the present investigation i.e. coupling beam structures reinforced with conventional and expanded metal mesh reinforcement. The approach was also tested by comparing it to Subedi's proposed method presented in Section 4.9.

To be able to apply the Compressive Force Path concept to the coupling beam models, several assumptions have to be made:

a) It is considered that coupling beam structures are composed of two cantilevers loaded independently at their free end.

b) The conditions at a section in the middle of the span of the simply supported beam are the same as at the fixed ends of the coupling beams.

c) The reaction of the simply supported beam can be taken as the force in the middle section of the coupling beam.

## 4.5 PROPOSED PHYSICAL MODEL FOR COUPLING BEAMS

It has been suggested that the Compressive Force Path concept may be introduced into design by developing physical models of structural concrete members at the ultimate limit state, which are capable of providing a realistic description of the principal features of the reinforced structural concrete members.

In the case of indeterminate reinforced concrete members such as beams coupling two structural walls, i.e. with fixed-ends, it is argued that they can also be designed in accordance with the proposed method, since the coupling beam can be divided into two portions between the fixed end and the section through the point of contraflexure (inflection), each of them being essentially a cantilever beam.

A cantilever beam subjected to a point load at its free end can be designed as a simply supported beam subjected to point loading at the midspan, since the fixed-end conditions of the cantilever beam are similar to the conditions of the midspan cross section of the simply supported beam, as can be noted in Figure 4.2(a).

In this case, however, the design should allow for the interaction between the two portions of the coupling beams. The latter may be modelled as an internal support where the reaction is equal to the shear force that develops in the section through the point of inflection.

The provision of the web reinforcement in the form of stirrups or expanded metal mesh by an amount sufficient to sustain the action of the shear force should be

considered and for such reinforcement to extend over a length equal to "2d" to either side of the point of inflection.

It can be noted in Figure 4.2(b) that the design of the internal support involves the provision of transverse reinforcement to counteract the tensile forces acting in that region. Considering the fact that the concrete is very weak in tension, it is proposed that only a minor contribution, of the order of $0.5N/mm^2$, from the concrete can be considered in the design of such internal supports, and only in uncracked sections.

This approach has been adopted in the present context for modelling coupling beams which have initially been transformed into a number of determinate structural elements. The coupling beams used in the experimental work are classified as being in the range of type II members ( 2d> a> d ) which indicates that brittle failure of the beam [1] is associated with the failure of the horizontal member of the frame in the region of the joint as shown in Figure 4.3.

## 4.6 FAILURE CRITERIA

It is essential to provide the model described above with a failure criterion before it can be adopted in design.

It has been proposed that a shear failure in a coupling beam is associated with the presence of tensile stresses which develop in the region of the Compressive Force Path. The tensile stresses may develop perpendicular to the path because of a number of causes.

The main causes include the following:

a)-Change in the path direction: a tensile stress resultant $T$ as shown in Figure 4.4 is necessary for equilibrium purposes at locations where the path changes direction.

b)-Varying intensity of the compressive stress field along the path. The compressive stress will reach a critical level at the narrowest section along the path, where stress intensity is therefore highest, before this level is reached in an adjacent section. This level marks the start of an abrupt and large material dilation that induces tensile stresses $t_1$ as shown in Figure 4.4 in the surrounding concrete.

c)-The tip of the inclined cracks: it is well known from a consideration of fracture mechanics that a large tensile stress $t_2$ as shown in Figure 4.4 develops perpendicular to the direction of the maximum principal compressive stress in the region of the crack tip.

d)-Bond failure: bond failure at the level of the tension reinforcement between two consecutive flexural cracks changes the stress conditions in the compressive zone of the beam element between these cracks, as indicated in Figure 4.5.

It can be noted from Figure 4.5, that the loss of the bond force results in an extension of the flexural crack which is sufficient to cause an increase $\Delta z$ in the lever arm z, such that C $\Delta z$ = V a. The extension of the flexural crack reduces the depth of the neutral axis and thus increases locally the intensity of the compressive stress block. This change in the stress intensity should give rise to a tensile stress in a similar manner to that described in (b) above.

Such a criterion may take the form of a well established relationship between the strength of a reinforced concrete beam expressed in terms of a moment corre-

sponding to the failure load and the shear span to depth ratio.

The failure in the coupling beam occurs within the shear span and is brittle in nature at a load which corresponds to the ultimate bending moment which is not normally significantly different from the value of the flexural capacity $M_f$. In particular, there is a definite need for the development of an understanding of the behaviour and strength of coupling beams. The main factors affecting the behaviour and the performance of the coupling beams require to be analysed very carefully and include:

a) span to depth ratio;

b) cross-section properties;

c) amount and location of the main reinforcement;

d) amount, type and location of the web reinforcement;

e) shear span to depth ratio;

f) type and position of loading;

In order to prevent such a failure, the legs of the frame may be designed in accordance with C.F.P approach put forward by Kotsovos [1].

## 4.7 DESIGN METHOD

### 4.7.1 Introduction

The design method adopted in the investigation into the behaviour of the coupling beams is based on the Compressive Force Path concept which has been fully described by Kotsovos [1] and further developed by Ziara [73]. The Compressive

Force Path concept, stipulates that the load-carrying capacity of a normally reinforced structural concrete member is highly dependent on the strength of the concrete in the region of the path along which compressive forces are transmitted to the supports.

The above concept has been implemented in design by modelling a reinforced concrete beam as a frame with inclined legs tied by tension reinforcement with the frame providing a simplified representation of the Compressive Force Path. According to the concept, shear reinforcement is only required at the intersection between the horizontal and the inclined members of the frame. A nominal amount of reinforcement is assumed to be sufficient in the remainder of the beam. The shear reinforcement is designed to be able to sustain the portion of the tensile force balancing the action of the compressive force acting in the direction of the members that cannot be sustained by the concrete alone.

### 4.7.2 Method of Calculation

The method has been used to assess the load carrying capacity of the large coupling beams whose behaviour has already been established in the laboratory based part of the investigation. The correlations between the predicted and the measured values presented in the next Chapters are shown in Table 7.1. The investigation covers a wide range of coupling beams reinforced differently in shear. The distinction has been drawn between beams with web reinforcement since the effect of such reinforcement on the load carrying capacity appears to be significant. As

discussed in Section 4.2, the coupling beams can be designed in compliance with the C.F.P, since it can be divided into two equal portions between fixed ends and the section through the point of contraflexure.

The design of beams subjected to reversed load can be designed according to current Codes of Practice as a doubly reinforced section. In order for the beam to remain within safe design limits, the bending moment $M$ can only go on increasing until either:

- steel reaches its ultimate strength;

or

- the compressive zone extends down to half of the effective depth i.e. $x = d/2$;

When either of these conditions is reached. The applied bending moment $M_a$ will have reached the ultimate moment of resistance $M_u$ of the beam. Thus $M_u$ is the lower of the two values, one depending on the steel and the other depending on the concrete.

The ultimate moment of resistance can be calculated by considering the steel using the relationship:

$$M_{us} = T_u z = 0.875 A_{st} f_y z \tag{4.1}$$

The ultimate moment of resistance can be calculated by considering the concrete using the relationship:

$$M_{uc} = C z = 0.45 f_{cu} b x z \tag{4.2}$$

As $M_{us} = M_{uc}$ the compressive depth can be calculated from Equations 4.1 and 4.2.

$$x = 0.875 f_y A_{st} / 0.45 f_{cu} b \tag{4.3}$$

then, the lever arms of the internal forces acting horizontally can be evaluated from:

$$z = d - 0.45x \tag{4.4}$$

The maximum applied shear force $V_a$ can be found by dividing the flexural capacity $M_f$ (using the ultimate characteristic strength of the steel) by the shear span (s) between two point loads.

$$V_a = M_f / s \tag{4.5}$$

The failure in coupling beams occurs within the shear span and is usually brittle in nature under a failure load corresponding to the maximum bending moment which is not usually significantly different from the value of the flexural capacity $M_f$. In order to prevent such a failure, the legs of the frame may be designed using the approach put forward by Kotsovos [1].

An analytical expression for the bending moment in type II beams corresponding to shear failure of the inclined portion of the coupling beam was derived by Bobrowski and Badhan-Roy [59]. This expression was modified slightly by Kotsovos [61] as detailed below:

$$M_c = 0.875 s d (0.342 b + 0.3 M_f / d^2 \sqrt[4]{z/s} \sqrt{16.66/(\rho_w f_y}) (N.mm) \tag{4.6}$$

where

s is the distance of the cross-section from the support.

z is the lever arm.

b is the effective width.

then

$$V_c = M_c/s \tag{4.7}$$

The applied load $V_a$ at the critical cross section is checked to determine if it is larger or smaller than $V_c$.

- If $V_a$ is less than or equal to $V_c$; only nominal web reinforcement is required which will be similar to that specified in current design practice.

- If $V_a$ is greater than $V_c$; web reinforcement should be designed in accordance with the requirements described in Section 4.8

## 4.8 PROVISION OF TRANSVERSE REINFORCEMENT

In accordance with the C.F.P concept, failure of the idealised coupling beam should occur as a result of failure of either the horizontal or the inclined members of the frame or at the joint between these members.

If the failure of the beam occurs before a flexural failure occurs, a design solution which will allow the coupling beam to attain its flexural capacity will require the provision of transverse reinforcement. Such reinforcement is provided to sustain

that portion of the internal tensile actions that cannot be sustained by the concrete alone in the region of the Compressive Force Path.

The transverse reinforcement required to sustain the portion of the first of the actions described above, in excess of that which can be sustained by the concrete alone will modify the comb-like model shown in Figure 4.2(a) to that shown in Figure 4.6. Figure 4.6 shows the region where the inclined and horizontal members of the model intersect and indicates that the transverse reinforcement not only sustains the action of the vertical component, $V$, of the inclined compression, but also subjects the shaded concrete block of the beam web where it is anchored, to a compressive force, $D$. This force balances the shear force, $V$, acting at the block.

The transverse reinforcement may also be required horizontally in portions of the beam to sustain tensile stresses which may develop when bond failure occurs between two adjacent flexural or inclined cracks.

Apparently, the penetration of the inclined crack deep into the compressive zone reduces the cross sectional area of the zone and thus leads to a reduction in both the load carrying capacity of the zone as well as the moment which can be sustained by the section. Failure can be prevented by increasing the moment resistance to the level of the applied bending moment through the provision of web reinforcement in the form of stirrups or the segments of expanded metal mesh uniformly distributed throughout the portion of the idealised model between the support and the area where the frame members intersect.

Such reinforcement should be designed such that at yield, it will be capable of

sustaining a total tensile force acting between the support and the intersection point.

The total amount of transverse reinforcement required to provide the critical section with a moment of resistance larger than or equal to the applied moment will be:

$$A_{st} = T/f_y = 2[(M_a) - (M_c)]/(af_y) \tag{4.8}$$

Once the area of transverse reinforcement is found, the type of expanded metal mesh required is determined using the design procedure presented in Chapter 3. It is recommended [58] that shear reinforcement should be extended beyond the shear span region for a distance equal to the depth of the neutral axis.

## 4.9 ANALYSIS OF THE COUPLED BEAMS USING SUBEDI'S APPROACH

### 4.9.1 Background to the Design Approach

It is common design practice to first design a coupling beam to have the required flexural capacity and then to ensure that any type of failure, other than a flexural failure which would occur when the flexural capacity is attained, is prevented. The flexural capacity is assessed on the basis of the plane sections theory which not only is generally considered to describe realistically the deformational response of the beams, but it is also formulated so that it provides a design tool which is recognised for both its effectiveness and simplicity. However, a reinforced concrete coupling beam experiences a shear failure which normally occurs before the flexural capacity of the beam is attained. This Section presents an overview of the lateral resistant provisions for the ultimate limit state design of reinforced concrete shear wall structures. The description will focuss on how the flexural and shear strengths are determined. It should be noted, as stated by Subedi [2], that the desirable design philosophy for coupling beam structures is to ensure the combined action (flexural and shear deformations) which the beam undergoes when it is subjected to any lateral load.

The approach to the analysis is based on a simple concept of the equilibrium of forces in a section of the beam between the two diagonally opposite end supports prior to collapse. The main assumption of this approach is that the reinforced concrete coupling beams fail predominantly through the development of the di-

agonal cracks.

The actual deformation of the coupling beam is a combination of the flexural and the shear deformations.

### 4.9.2 Flexural Behaviour

Flexural failures may be recognised by the inelastic yielding and final fracture of the flexural reinforcement along the span. Vertical cracks propagate from the soffit and extend with increasing load to almost the full effective height. This type of failure usually occurs because the reinforcement fractures and only rarely is it due to crushing of the concrete. In flexure, the beam bends in double curvature with a point of contraflexure at the centre of the span. The shear force acting through the point of contraflexure produces maximum bending moments at the end supports, and is accompanied by the development of the flexural cracks.

When the applied shear force is increased, the flexural cracks progress towards the compression corners. Eventually, crushing will take place in the compression corners, leading to the ultimate failure of the beam.

To ensure that the ultimate flexural strength of the beam is achieved, the capacity of the reinforcement must be sufficient to satisfy the equilibrium requirements of the internal and the external forces:

$$Ql/2 = h' A_{st} f_y \tag{4.9}$$

$A_{st} f_y$ is the capacity of the main reinforcement, and $h'$ and $l$ are the effective height and the shear span of the beam respectively.

### 4.9.3 Shear Behaviour

The provision of shear reinforcement in reinforced concrete coupling beams is based on the traditional assumption that diagonal cracks form from one corner to the other and the stirrups or the expanded metal mesh crossing these cracks are capable of resisting that fraction of the transverse force which is not resisted by the concrete. The shear carried by the concrete is transferred through the compressive zone of the beam, through dowel action of the flexural reinforcement and by means of aggregate interlock across the crack. It is essential that the shear be transferred entirely by the web reinforcement, and that no reliance is placed on other mechanisms which may assist in the provision of shear resistance, to prevent a separation failure along a main diagonal i.e. diagonal tension failure.

The pure shear deformation requires both top and bottom surfaces of the beam, all along its length, to be in tension. Tension and compression is present in the diagonal axis of the beam. An element near the midspan is subjected to a biaxial compression-tension state of stress. The mode of failure in shear will be characterised by the extension of the diagonal crack from one corner to the other and by the inability of the beam to carry any further load due to yielding of the reinforcement.

## 4.10 DESIGN METHOD FOR ULTIMATE STRENGTH OF THE BEAM

### 4.10.1 Equilibrium

The conditions that must be obeyed if the structure is to be in equilibrium are :

- The sum of the forces acting vertically or horizontally on the structure must be zero.

- The sum of the moments about any arbitrary point of the forces acting on the structure, together with any externally applied moment must be zero.

The design method based on the equilibrium of forces at failure of the triangular shaped section of the beam was used to analyse the coupling beam containing the expanded metal mesh and conventional reinforcement in order to predict the mode of failure and ultimate strength of the beam. Basically the expanded metal mesh is assumed to carry all the shear forces although this will depend on the geometry and the strength characteristics of the expanded metal mesh. No Code of Practice to date covers the use of expanded metal mesh in any type of structural concrete member.

The analytical method consists of the analysis of four types of beams which contained different forms of reinforcement to resist shear as shown in Figures 4.7 to 4.10.

## 4.11 DESIGN OF THE BEAM REINFORCED WITH CONVENTIONAL REINFORCEMENT

The reinforced concrete coupling beams subjected to flexural and shear stress actions and in which the structural behaviour is governed by shear can be analysed by considering the equilibrium of forces of a triangular shaped section of the beam as shown in Figure 4.7. The forces which are present are as follows:

- The shear force,$V$, in the compressive corners of the beam.
- The ultimate load of the beam, $Q_u$.
- The crushing strength of the concrete, $C$.
- The contribution of the stirrups, $P$.
- The tensile strength of the concrete, $f_{tc}$.

Consider the equilibrium of the forces acting on the beam reinforced only with stirrups for shear.

$\sum$ of horizontal forces $= 0$

$$T = C + f_{tc}bh' \tag{4.10}$$

$\sum$ of vertical forces $= 0$

$$Q = 2V + P_v + f_{tc}bl \tag{4.11}$$

$\sum$ of moment/A $= 0$

$$Th' = Vl + 1/2P_v + f_{tc}b(l^2 + h'^2/2 \tag{4.12}$$

The ultimate strength and the predicted mode of failure of any coupling beam structure is determined by comparing the magnitude of the shear and the flexural strengths of the beam. Two assumed modes of failure can be considered:

### 4.11.1 Flexural Mode of Failure

The flexural capacity of the beam can be evaluated by taking into account only the main reinforcement:

$$Q_{flex} = 2h'/l[f_y A_{st}] \tag{4.13}$$

The ultimate capacity of the beam is:

$$Q_u = 2Q_{flex} \tag{4.14}$$

### 4.11.2 Shear Mode of Failure

The most important parameter in this mode of failure is the control of the behaviour of the web and the contribution of the reinforcement.

The control of the web depends on the magnitude of the following:

$H = f_{tc}bh + A_h f_s$ against the capacity of the horizontal web bars $A_h f_{yw}$, and

$V = f_{tc}bl + A_v f_s$ against the capacity of the vertical web bars $A_v f_{yw}$.

The governing requirements to check the control of the web by the concrete or the reinforcement are given in Table 4.1. The following criteria, put forward by Subedi [2], can be applied to coupling beams by comparing two cases:

When the strength of the web is controlled by the reinforcement, the contribution of the concrete will be equal to zero ($f_{tc} = 0$). The contributions from the reinforcement are $P_h = \lambda_1 A_h f_{ys}$ and $P_v = \lambda_2 A_v f_{ys}$. Here $\lambda_1, \lambda_2 = 1$.

When the strength of the web is controlled by the concrete $f_{tc}$ will contribute. Here $f_s$ = modular ratio x $f_{tc}$ and $\lambda_1, \lambda_2$ are factors which depend on the geometric parameters and $P_v = A_v f_s$ and $P_h = A_h f_s$.

For this type of beam:

The horizontal component of the web splitting force is given by:

$$H = f_{tc} b h' + A_h f_s \tag{4.15}$$

and

$$A_h f_{yw} = 0 \tag{4.16}$$

The vertical component of the web splitting force is given by:

$$V s = f_{tc} b l + A_v f_s \tag{4.17}$$

and

$$A_v f_{yw} = A_s f_{ys} \tag{4.18}$$

Finally from Equations 4.10 to 4.12 for equilibrium, the ultimate shear capacity can be expressed as :

$$Q_{u_{shear}} = 2Q_{shear} = 2[f_{tc} b h' + 2C]h'/l \tag{4.19}$$

where

$$C = 0.67 f_{cu} b \frac{(h-h')}{2}$$

a comparison between the two values for the ultimate flexural and the ultimate shear behaviour given by Equations 4.14 and 4.19 will predict the mode of failure

of the beam. The governing ultimate load from the analysis will be taken as the smallest of the two values detailed above.

## 4.12 DESIGN OF THE BEAM REINFORCED WITH CONVENTIONAL AND DIAGONAL REINFORCEMENT

The use of the diagonal bars in reinforced concrete coupling beams results in increases in the ductility and the strength of the beam.

The same approach will be considered here taking into consideration the additional diagonal bars as shown in Figure 4.8.

Consider the equilibrium of the forces acting on the structure as shown in Figure 4.8.

$\sum$ of horizontal forces $=0$

$$T = C + f_{tc}bh' + P_h \tag{4.20}$$

where

$$P_h = T_d cos\alpha$$

$\sum$ of vertical forces $= 0$

$$Q = 2V + P_v + f_{tc}bl + P_v \tag{4.21}$$

where

$$P_v = T_d sin\alpha + T_{stirrups}$$

$\sum$ of moment/A $= 0$

$$Th' = Vl + L/2P_v + f_{tc}b(l^2 + h'^2)/2 + P_h(h'/2) \tag{4.22}$$

### 4.12.1 Flexural Mode of Failure

In this case the flexural capacity of the beam can be evaluated by taking into account the presence of the main reinforcement as well as the diagonal reinforcement bars:

$$Q_{flex} = h'/l[2f_y A_{st} + f_{yd} A_d cos\alpha] \tag{4.23}$$

The ultimate capacity of the beam is:

$$Q_u = 2Q_{flex} \tag{4.24}$$

### 4.12.2 Shear Mode of Failure

The horizontal component of the web splitting force:

$$H = f_{tc}bh' + A_d cos\alpha f_s \tag{4.25}$$

and

$$A_h f_{yw} = A_d cos\alpha f_{yd} \tag{4.26}$$

The vertical component of the web splitting force:

$$Vs = f_{tc}bl + A_d sin\alpha f_s \tag{4.27}$$

and

$$A_v f_{yw} = A_d sin\alpha f_{yd} + A_s f_{ys} \tag{4.28}$$

In a comparison of Equations 4.25 and 4.27 with their corresponding capacities given by Equations 4.26 and 4.28, the control of the web can be found using the criteria test in Table 4.1.

Finally from Equations 4.20 to 4.22 the ultimate shear capacity of the beam can be obtained:

$$Q_{u_{shear}} = 2Q_{shear} = 2[f_{tc}bh' + 2C + T_d cos\alpha]h'/l \tag{4.29}$$

## 4.13 DESIGN OF THE BEAM REINFORCED WITH EXPANDED METAL MESH ONLY

The most important point here is that the expanded metal mesh normally provided to resist only shear will also act to resist flexural actions and hence will contribute in both directions in the web. The same approach will be considered here again as shown in Figure 4.9.

Consider the equilibrium of the forces acting on the structure in Figure 4.9.

$\sum$ of horizontal forces = 0:

$$T = C + f_{tc}bh' + P_h \tag{4.30}$$

where

$$P_h = P_m cos\theta$$

then

$$T = C + f_{tc}bh' + P_m cos\theta \tag{4.31}$$

$\sum$ of vertical forces $= 0$

$$Q = 2V + P_v + f_{tc}bl \tag{4.32}$$

$$Q = 2V + P_m sin\theta + f_{tc}bl \tag{4.33}$$

$\sum$ of moment/A $= 0$

$$Th' = Vl + P_m/2[lsin\theta + h'cos\theta] + f_{tc}b(l^2 + h'^2)/2 \tag{4.34}$$

### 4.13.1 Flexural Mode of Failure

The flexural capacity of the beam can be evaluated by taking into account the main reinforcement as well as the expanded metal mesh.

Then the flexural capacity of the beam can be found as :

$$Q_{flex} = (h'/l)[2f_y A_{st} + f_{ym} n A_m cos\theta] \tag{4.35}$$

The ultimate flexural capacity of the beam is:

$$Q_u = 2Q_{flex} \tag{4.36}$$

### 4.13.2 Shear Mode of Failure

The horizontal component of the web splitting force.

$$H = f_{tc}bh' + 2nA_m cos\theta f_s \tag{4.37}$$

and

$$A_h f_{yw} = 2nA_m cos\theta f_{ym} \tag{4.38}$$

The vertical component of the web splitting force.

$$Vs = f_{tc}bl + 2nA_m sin\theta f_s \tag{4.39}$$

and

$$A_v fyw = 2nA_m sin\theta f_{ym} \tag{4.40}$$

In a comparison of Equations 4.37 and 4.39 with their corresponding capacities given in Equations 4.38 and 4.40, the control of the web strength can be found using the criteria test in Table 4.1

Finally from Equations 4.30 to 4.34, the ultimate shear capacity of the beam can be obtained.

$$Q_{u_{shear}} = (f_{tc}bh' + 2C + P_m cos\theta)h'/l \tag{4.41}$$

## 4.14 DESIGN OF THE BEAM REINFORCED WITH EXPANDED METAL MESH AND DIAGONAL REINFORCEMENT

The final type of beam to be analysed is the one in which the diagonal bars and the expanded metal mesh are combined as shown in Figure 4.10.

Consider the equilibrium of the forces acting on the structure shown in Figure 4.10

$\sum$ of horizontal forces $= 0$

$$T = C + f_{tc}bh' + P_h \tag{4.42}$$

where

$$P_h = P_m cos\theta + T_d cos\alpha$$

then

$$T = C + f_{tc} b h' + P_m cos\theta + T_d cos\alpha \tag{4.43}$$

$\sum$ of vertical forces= 0

$$Q = 2V + P_m sin\theta + f_{tc} b l + T_d sin\alpha \tag{4.44}$$

$$Q = 2V + f_{tc} b l + P_v \tag{4.45}$$

where

$$P_v = P_m sin\theta + T_d sin\alpha$$

then

$\sum$ of moment/A = 0

$$Th' = Vl + f_{tc} b(l^2 + h'^2)/2 + P_h(h'/2) + P_v(l/2) \tag{4.46}$$

$$Th' = Vl + f_{tc} b(l^2 + h'^2)/2 + [P_m cos\theta + T_d cos\alpha](h'/2) + [P_m sin\theta + T_d sin\alpha](l/2)$$

(4.47)

### 4.14.1 Flexural Mode of Failure

The flexural capacity of the beam can be evaluated by taking into account the main reinforcement bars as well as the expanded metal mesh and the diagonal bars, using:

$$Q_{flex} = (h'/l)[2 f_y A_{st} + 2n f_{ym} A_m cos\theta + A_d f_{yd} cos\alpha]. \tag{4.48}$$

The ultimate capacity of the beam is:

$$Q_u = 2Q_{flex} \tag{4.49}$$

### 4.14.2 Shear Mode of Failure

The horizontal component of the web splitting force.

$$H = f_{tc}bh' + [A_d cos\alpha + 2nA_m cos\theta]f_s \tag{4.50}$$

and

$$A_h f_{yw} = A_d cos\alpha f_{yd} + 2nA_m cos\theta f_{ym} \tag{4.51}$$

The vertical component of the web splitting force.

$$Vs = f_{tc}bl + [A_d sin\alpha + 2nA_m sin\theta]f_s \tag{4.52}$$

and

$$A_v f_{yw} = A_d sin\alpha f_{yd} + 2nA_m sin\theta f_{ym} \tag{4.53}$$

In a comparison of Equations 4.50 and 4.52 with their corresponding capacities given by Equations 4.51 and 4.53, the control of the web can be found using the criteria test in Table 4.1.

Finally, the ultimate shear capacity of the beam can be obtained from Equations 4.42 to 4.47.

$$Q_{u_{shear}} = 2[f_{tc}bh' + 2C + 2nA_m f_s cos\theta + A_d f_{yd} cos\alpha]h'/l \tag{4.54}$$

## 4.15 CONCLUSIONS

The design procedures described in this Chapter have only been used to assess the load-carrying capacity of the coupling beams reinforced with the two types of reinforcement (conventional and expanded metal mesh). The two approaches were based on the Compressive Force Path concept and the equilibrium of forces. The numerical calculations based on these approaches are presented in Appendix B for all the coupling beams with different shear span to depth ratios.

It can also be concluded that the Compressive Force Path concept has the advantage of considering the overall behaviour of the beam. It also offers a realistic explanation, based on a better understanding of concrete at the material level, of the causes of diagonal failure. The failure, in this context, is related to the actual state of stress in the compression zone of the beam structure in which the transverse tensile stresses initiate failure. Therefore, a new detailing arrangement for the prevention of diagonal failures was proposed such that the expanded metal mesh is positioned in such a way as to confine the compression concrete along the load path within the beam.

In the idealised model, the role of expanded metal mesh is also to restrain the development of the secondary transverse tensile stresses which cause failure. This can be regarded as enhancing the tensile strength of the concrete.

On the other hand, the approach put forward by Subedi [2] has suggested a simplified method for calculating the ultimate load capacity of the beam. In this method the ultimate strength of the beam is found to be the sum of the contribution from the web concrete $f_{tc}$ and the main and web reinforcement. It should be

noted, that the contribution of the main reinforcement is based on the magnitude of the diagonal and splitting forces.

The proposed procedures were presented in a straight forward way so they can be readily adopted by practicing structural engineers. The two methods are suitable for use with both conventional and expanded metal mesh reinforcement as described in this Chapter.

In the present Chapter emphasis has been placed on determining the ultimate load capacity which can be sustained by the beams.

| Test criteria | | | |
|---|---|---|---|
| Test | $f_{tc}bh' + A_h f_s$ | $f_{tc}bh' + A_h f_s$ | Web strength control |
| 1 | $< A_h f_{yw}$ | $< A_v f_{yw}$ | Reinforcement |
| | $> A_h f_{yw}$ | $> A_v f_{yw}$ | Reinforcement |
| 2 | or $> A_h f_{yw}$ | $< A_v f_{yw}$ | Concrete |
| | or $< A_h f_{yw}$ | $> A_v f_{yw}$ | Concrete |

Table 4.1: Test control criteria

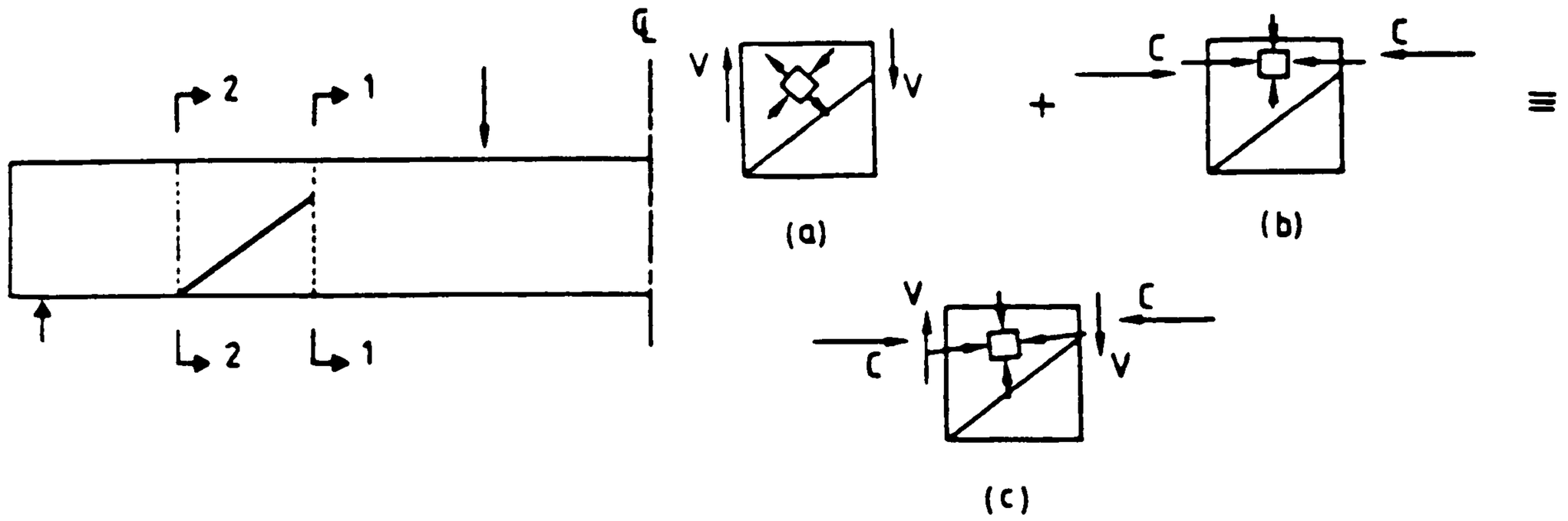


Figure 4.1: Schematic representation of the mechanism providing shear resistance to the compressive zone of the element between sections 1-1 and 2-2 stress conditions to (a) **V**, (b) **C** and (c) Combined **C** and **V**. Kotsovos [58]

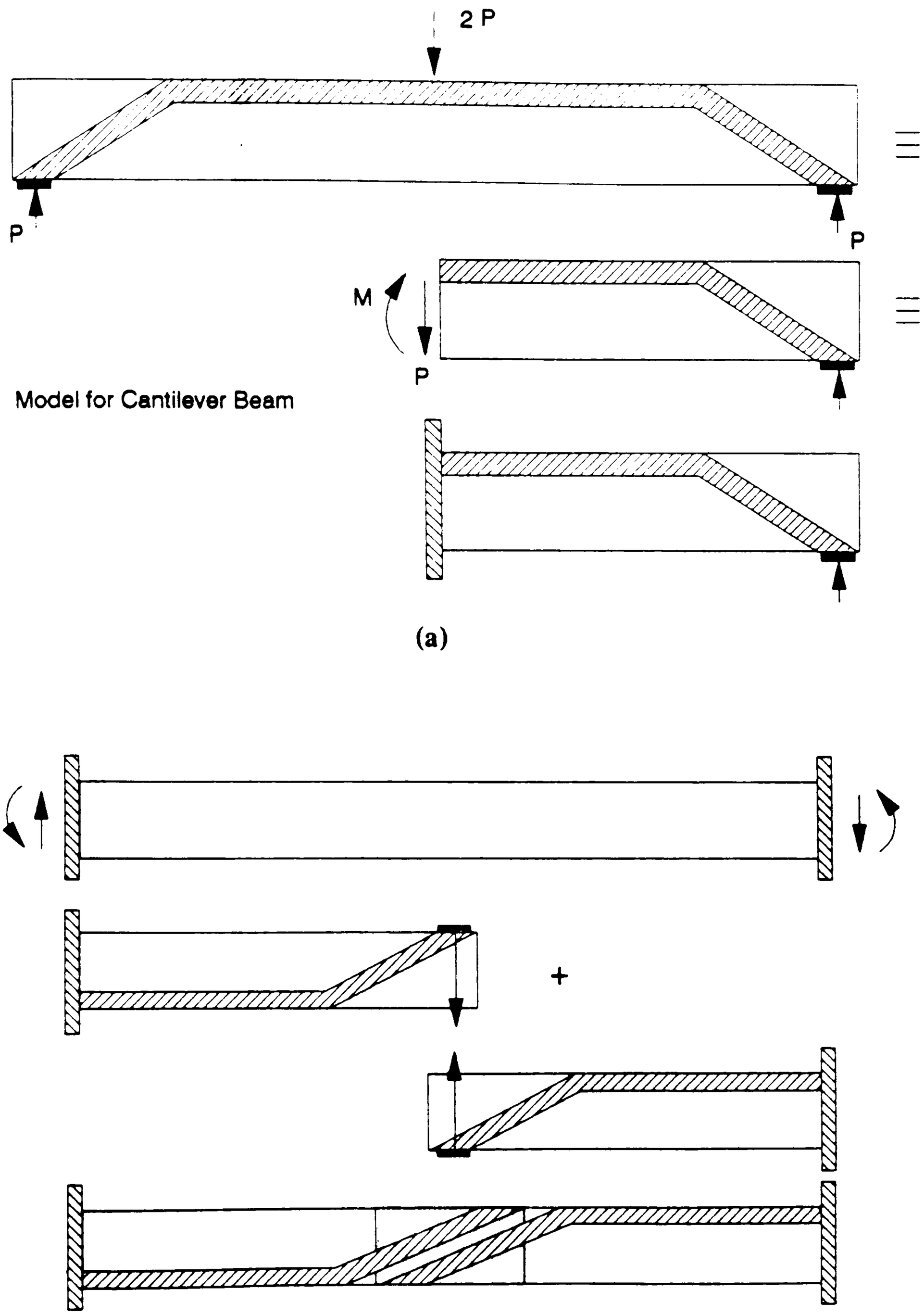


Model for Cantilever Beam

Figure 4.2: Proposed model for (a) cantilever beam, and (b) coupling beam.

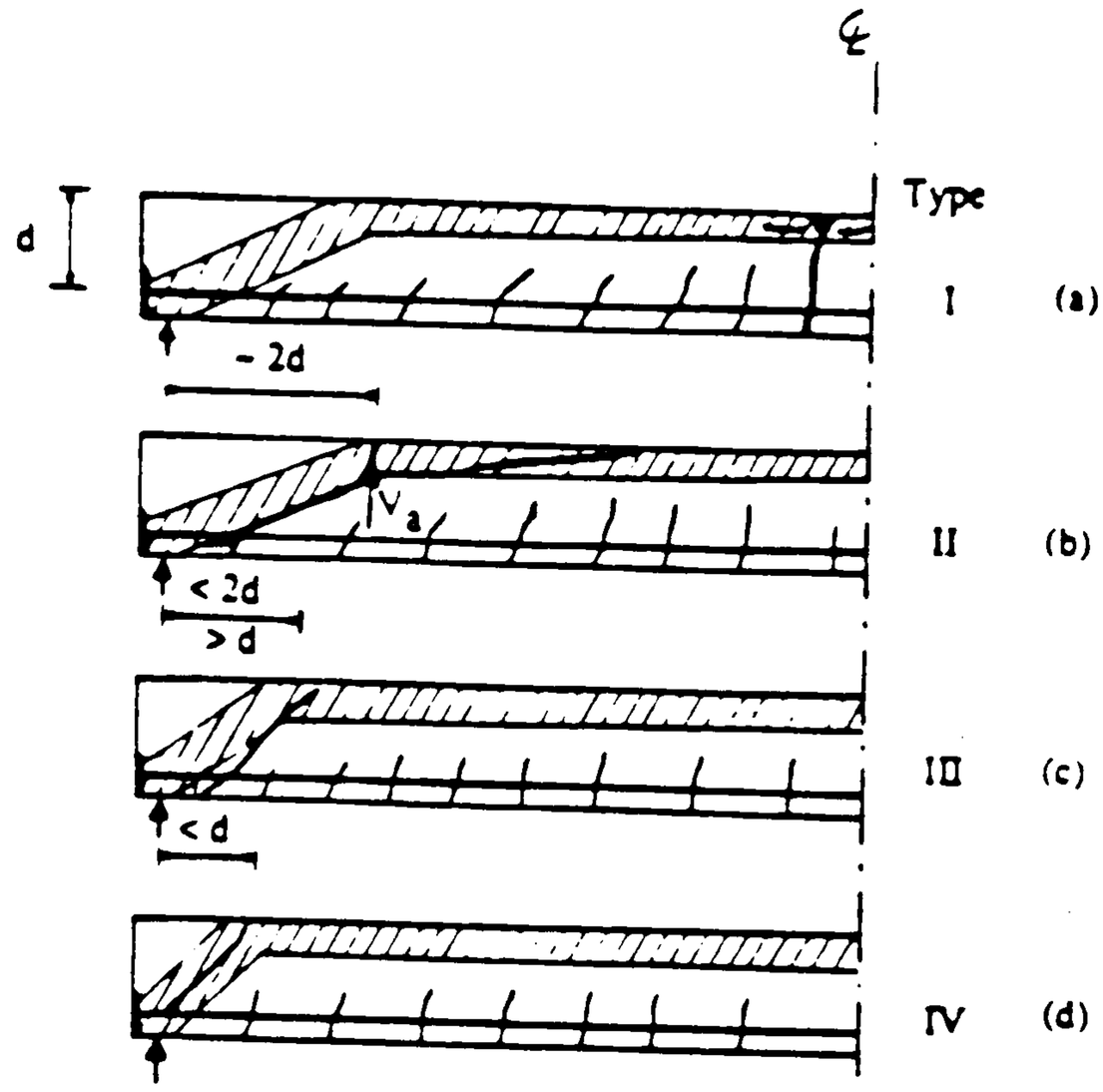


Figure 4.3: Typical types of behaviour exhibited by reinforced concrete beams without shear reinforcement. Kotsovos [60]

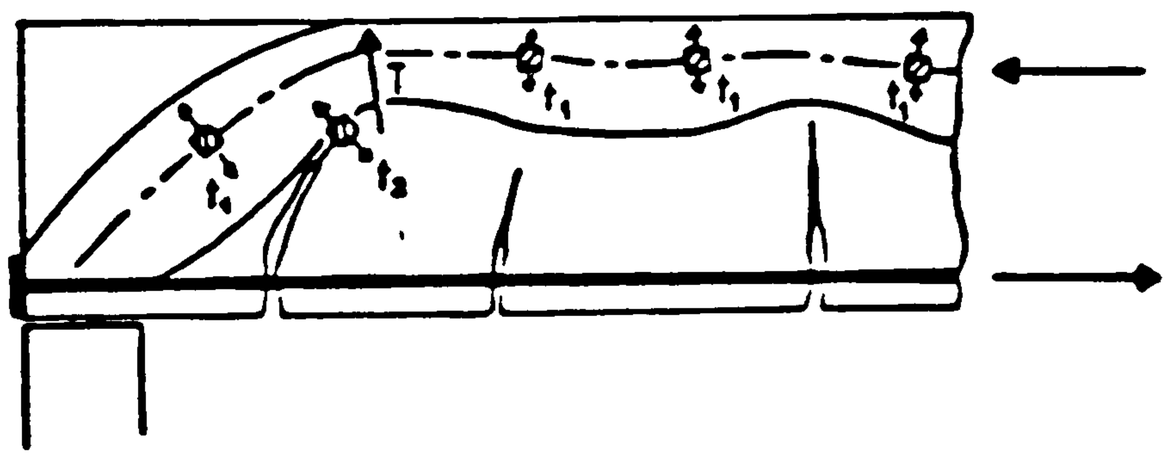


Figure 4.4: Schematic representation of the Compressive Force Path. Kotsovos [60]

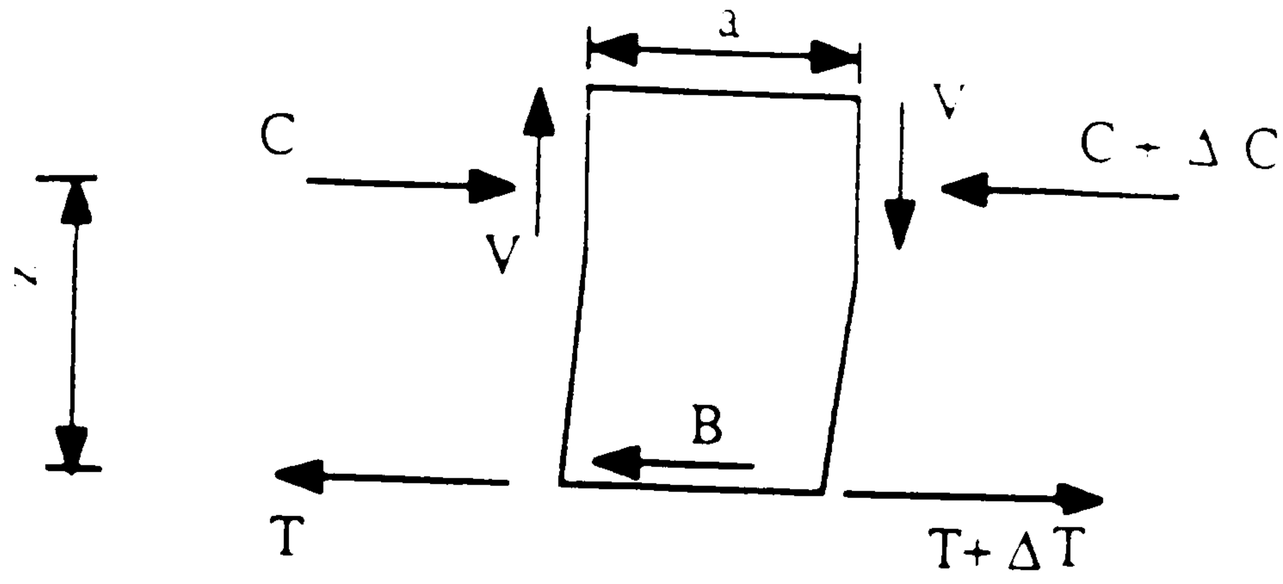


$$V.a = \Delta T.z$$

Before bond failure

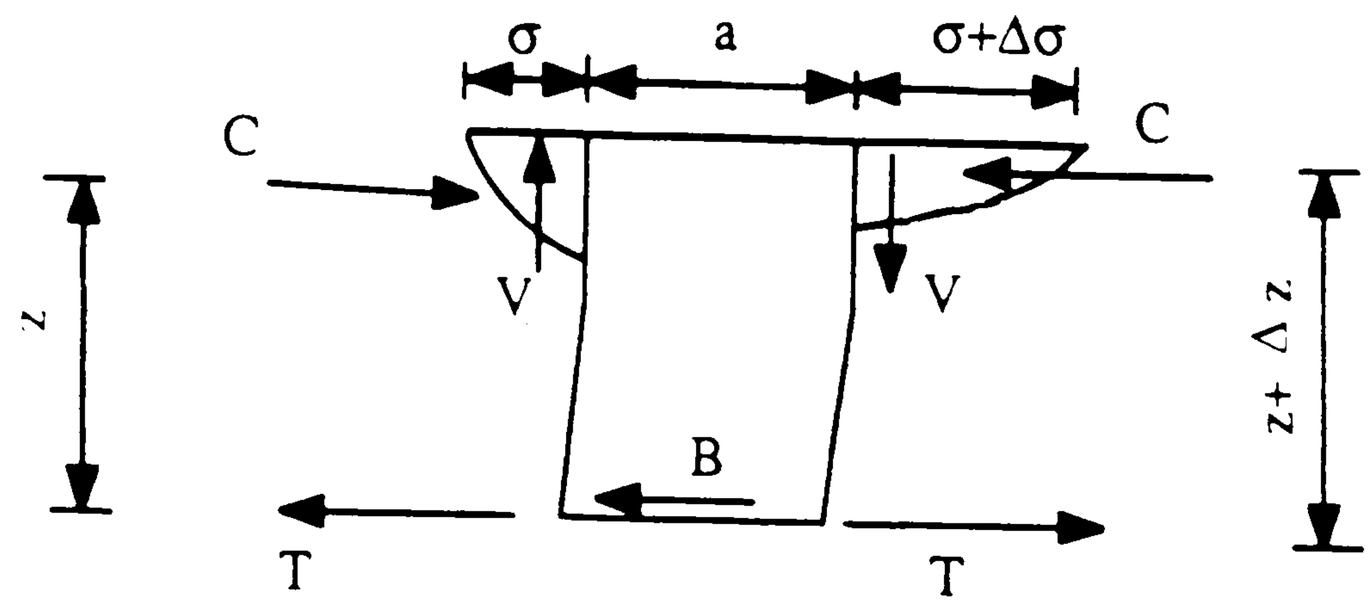


$$V.a = T.\Delta z$$

After bond failure

Figure 4.5: Effect of the bond failure on stress conditions in compressive zone.

Kotsovos [1]

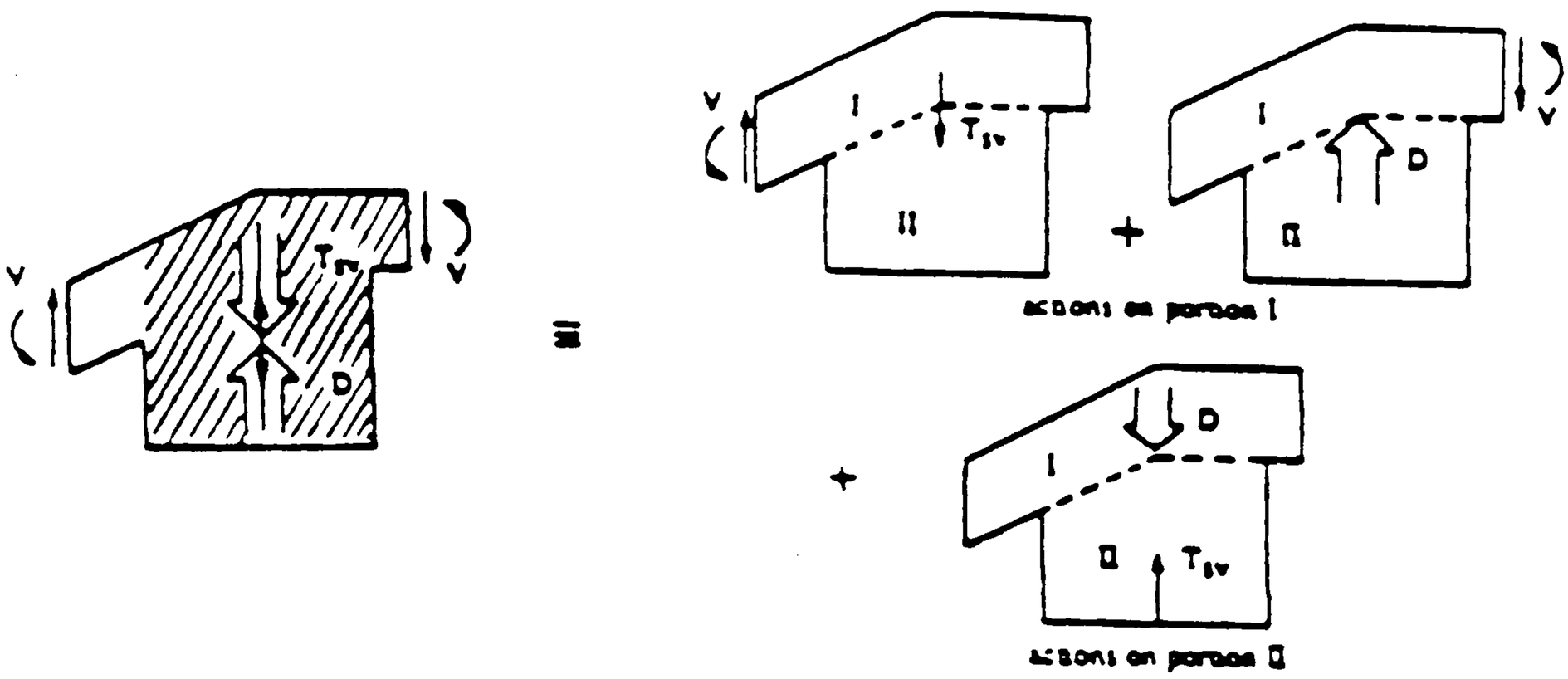


Figure 4.6: (a)Frame model of Kotsovos, and effect of transverse reinforcement on local internal action. Kotsovos [1]

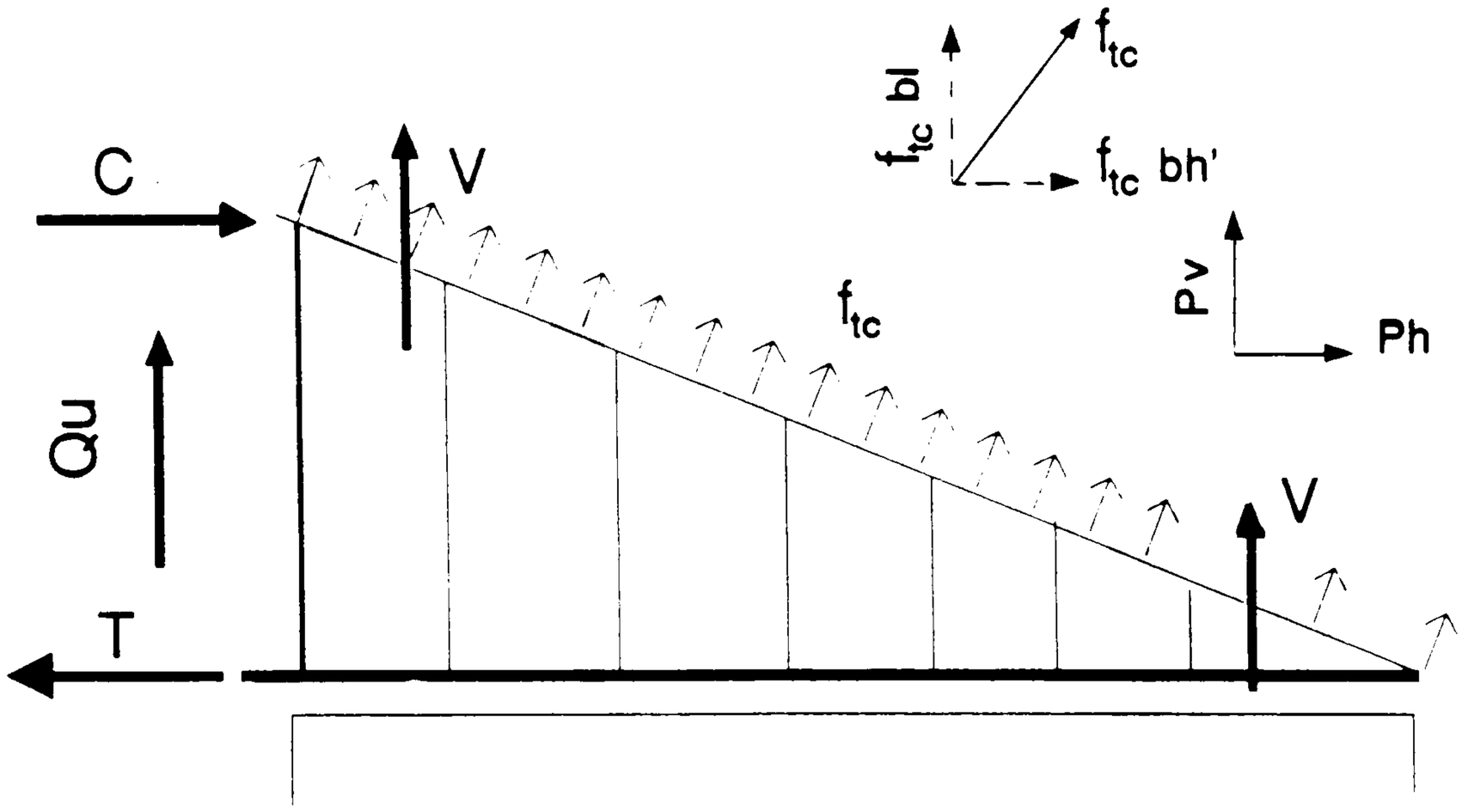


Figure 4.7: Beam with only conventional reinforcement

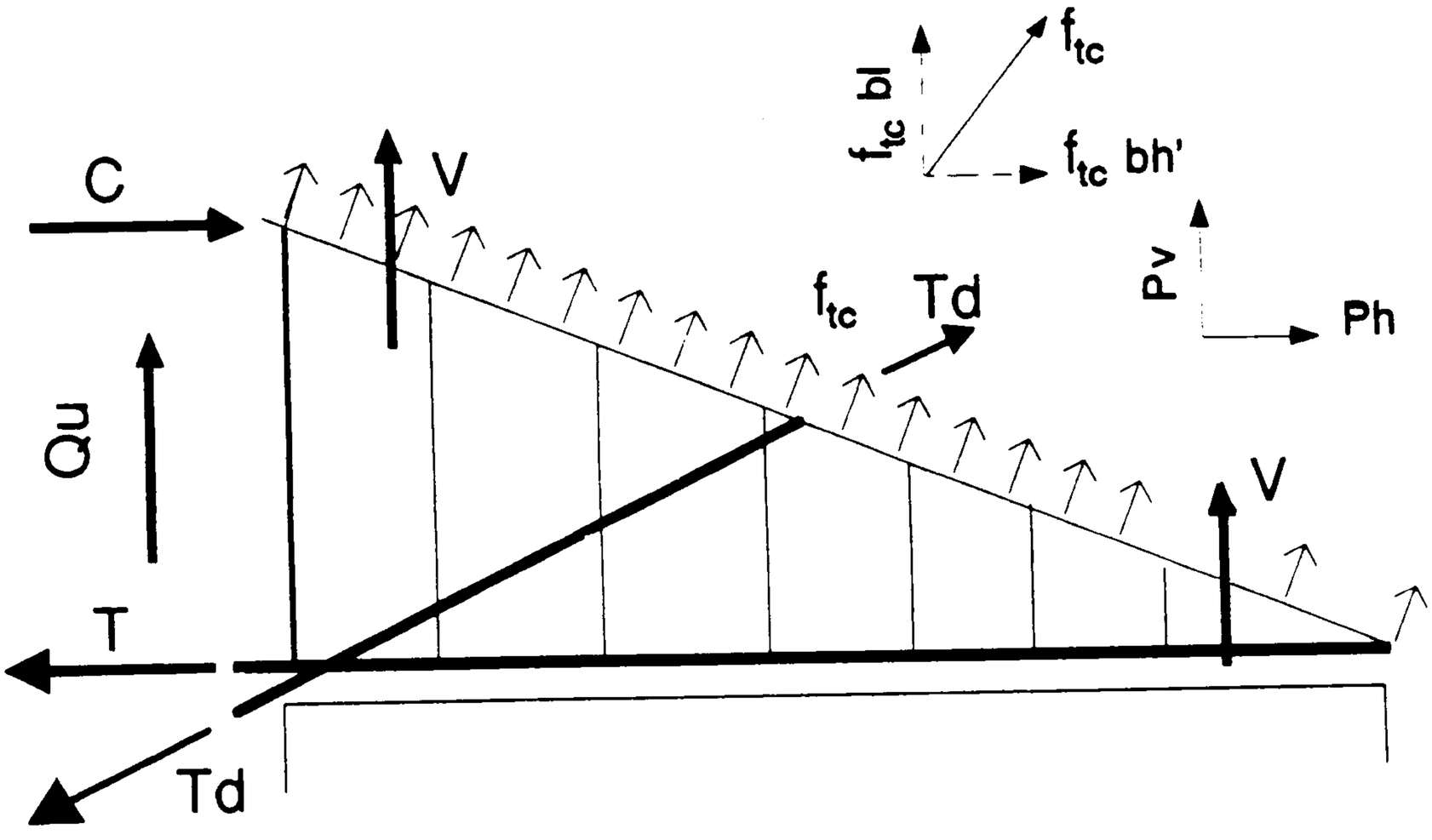


Figure 4.8: Beam with conventional and diagonal reinforcement bars

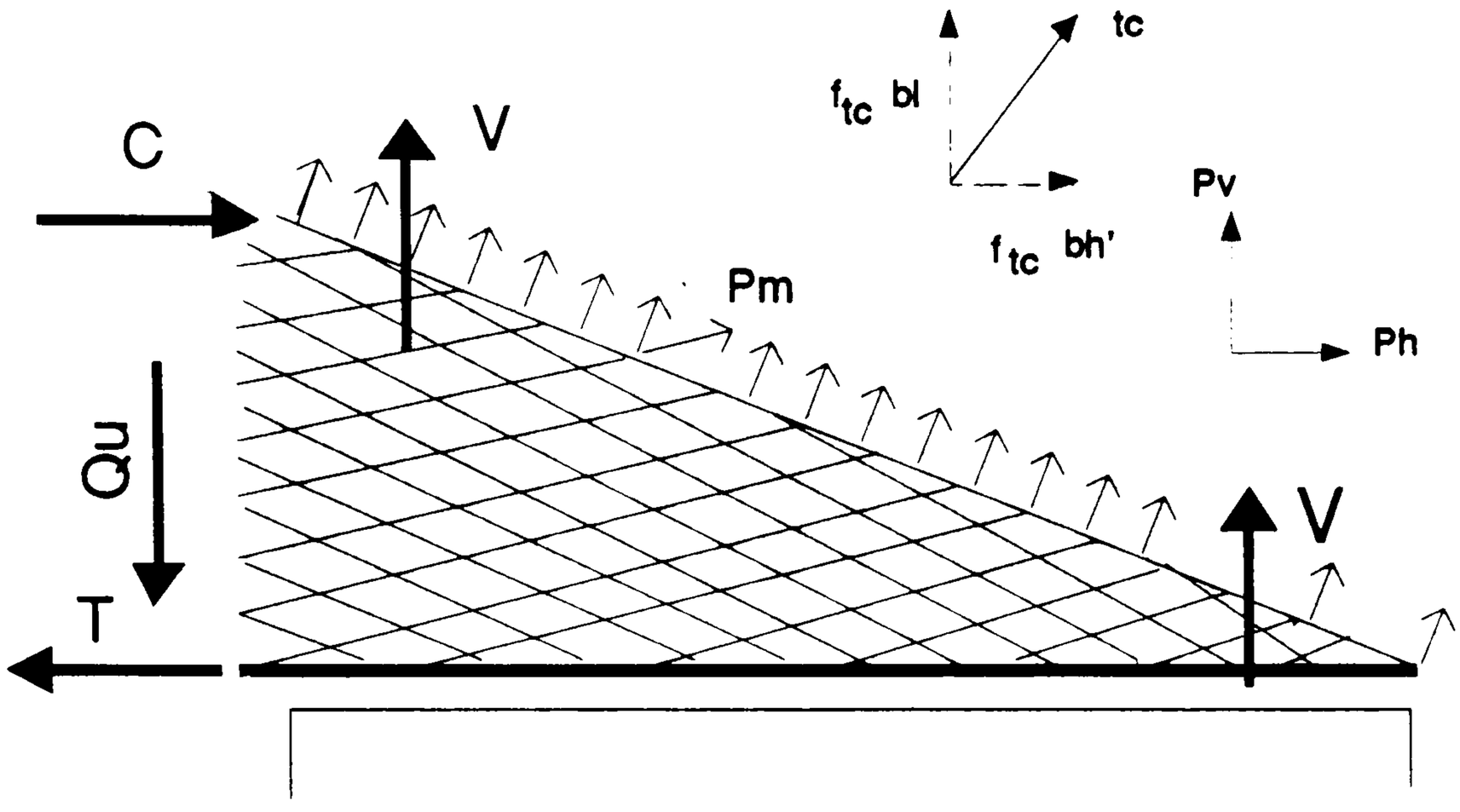


Figure 4.9: Beam with only mesh reinforcement

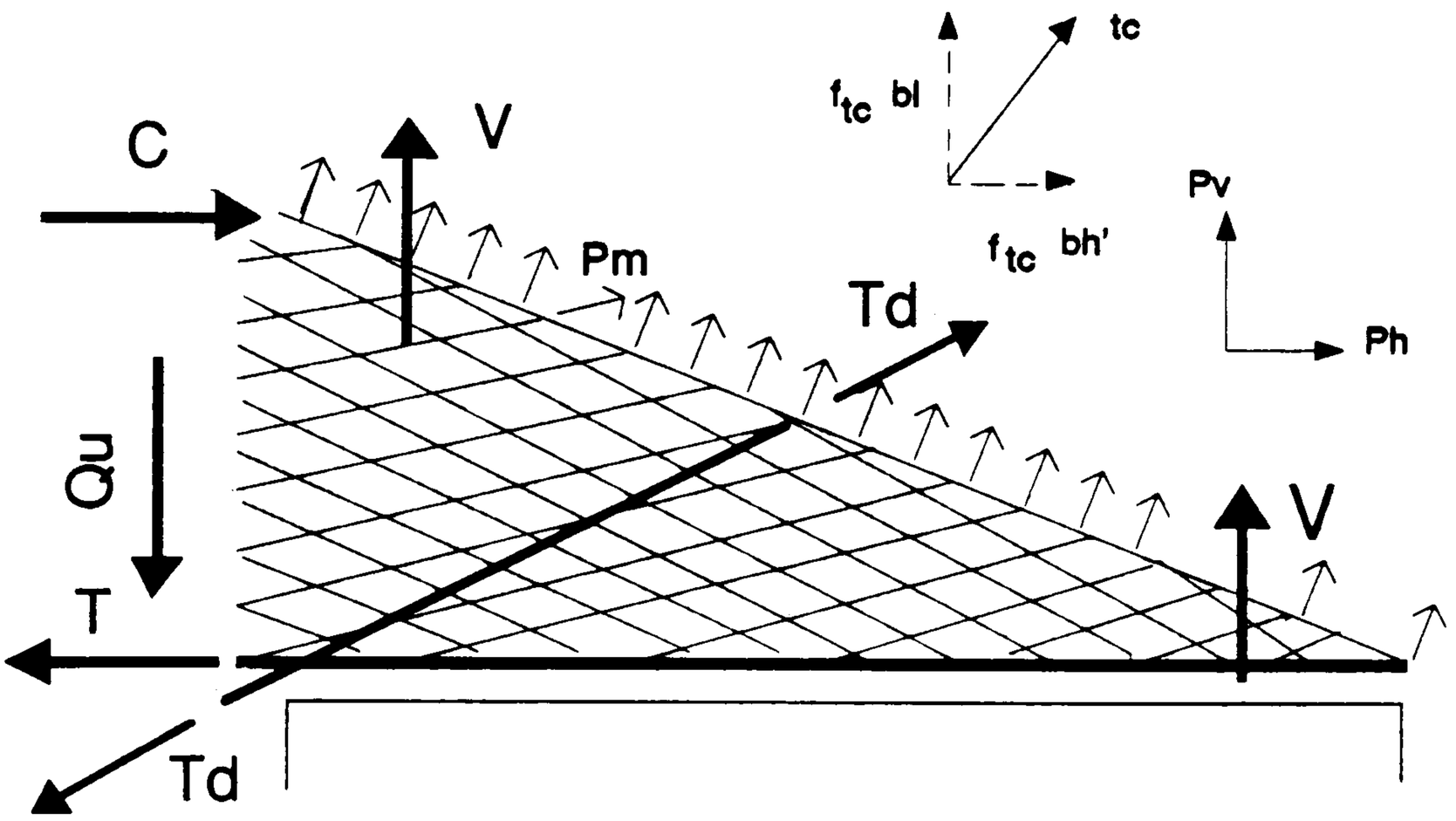


Figure 4.10: Beam with mesh reinforcement and diagonal reinforcement bars

# Chapter 5

# EXPERIMENTAL BEHAVIOUR OF THE FIRST SERIES OF BEAMS

## 5.1 INTRODUCTION

Earthquake damage has repeatedly shown itself to be in the form of diagonal tension failures of coupling beams containing insufficient web reinforcement. Clearly such failures, normally of a brittle nature resulting in a high rate of strength degradation under cyclic loading, must be suppressed if satisfactory seismic resistance is to be provided. Irrespective of design loads the shear strength of coupling beams must be equal to or larger than its flexural capacity. This requirement may impose an upper limit on the flexural steel content in such beams, particularly when they are regarded as deep relative to their span. To ensure satisfactory perfor-

mance when coupled shear wall structures are exposed to severe lateral loadings, it is necessary to be able to assess, at least approximately, the behaviour of the structure in both the elastic and plastic range of loadings. From the point of view of damage control, and possible repair, it is desirable that the parts of the wall are the last to fail as ultimate load conditions are approached.

In this Chapter, an experimental study of the response of eleven reinforced concrete coupling beam systems subjected to lateral loading is presented. The test beams are identified as CBMi, CBSi, EBMi, EBSi, CBDi and EBDi. The first two letters (CB) or (EB) indicate the type of reinforcement present in the beams (Conventional or Expanded metal mesh reinforcement). The third letter (M), (S) and (D) refers to the shear span to depth ratio of the beams, (1.43), (2.0) and (1.1) respectively. The last letter (i) indicates the presence or absence of diagonal bars i.e. (1 = with reinforcement bars, 2 = without reinforcement bars). The final test beam referred to as (DBS2) is the double storey specimen. The overall geometry and the method of loading remained the same for all coupling beams as described in Chapter 3.

This Chapter, also describes the actual behaviour of the test beams, observed during the final load cycle, including the failure mechanism, the deflections, the rotations, the crack patterns and in particular the performance of the expanded metal mesh. No attempt was made to measure the strains in this series of coupling beams.

## 5.2 BEHAVIOUR OF COUPLING BEAMS WITH A SPAN/DEPTH RATIO OF 1.43

This group of tests consists of four coupling beams CBM1, CBM2, EBM1, and EBM2 each with a different type of reinforcement, as shown in Figures 3.15 to 3.18. The properties and dimensions of the beams were described previously in Chapter 3.

The purpose of this group of tests was to investigate the effect of parameters such as the shear span to depth ratio, the beam strength, and the overall behaviour of the structure.

### 5.2.1 Beam CBM1

**Loading and test procedure**

Beam CBM1 was reinforced with conventional reinforcement to resist the shear and flexural loadings as shown in Figure 3.16. The walls were reinforced with two layers of 8.0 mm diameter reinforcement bars arranged vertically at a spacing of 100 mm and 12 mm diameter reinforcement bars arranged horizontally at a spacing of 150 mm. The beam was reinforced, top and bottom, with two 12 mm diameter high yield steel bars which were extended into the end walls to provide the necessary anchorage. Four additional mild steel bars of the same diameter were placed diagonally. Eight 8 mm diameter stirrups were also used.

In relation to the tests a load cycle was defined as a loading sequence in which the load was increased in increments from zero to the specified level of 50 kN

and then reduced in steps back down to zero. The next cycle followed the same sequence, normally with the load being applied in the opposite direction. The testing procedure for the first and second cycles consisted of applying the load in steps of a predetermined magnitude and then unloading in steps of a similar magnitude. In the third cycle, the load was increased in steps up to the maximum value the test beam could sustain. When the test beam had suffered extensive cracking, any attempt to increase the load further resulted in a sudden drop in the applied load accompanied by large deformations. This indicates that the beam had reached its maximum capacity and that the beam had failed. This failure criterion was applied in every case to determine the ultimate capacity of a beam. The results presented in this Chapter refer only to the measurements recorded during the third load cycle.

### Elongation of the beam

The load-elongation curve for the coupling beam is shown in Figure 5.1. After the occurrence of diagonal cracking, the beam was in a state of tension over its entire span. It is thus evident that the beam must have tended to lengthen. This phenomenon becomes more obvious when the position of the coupling beam is examined in relation to the adjoining shear wall. If the coupling beam is incompressible the two shear walls would not have moved a distance apart. However, to preserve continuity, the beam shortens along the diagonal and extends in the horizontal direction.

The elongation of the beam could also be determined from the rotational mea-

surements. The elongation observed in the wall was larger than the extension along the span of the beam because it includes the extension of one half of each block. The elongation of beam CBM1 shown in Figure 5.1 confirms that it had behaved in a more ductile manner which can only be attributed to the presence of the diagonal bars. At a load of 50 kN, the total elongation was of the order of 5.50 mm and at 70% of the failure load, the elongation measured was 11.20 mm.

**Transverse expansion**

The load-transverse expansion relationship at mid-span of beam CBM1 shown in Figure 5.2 indicates that considerable transverse deformation occurred during the last load cycle. It appears that this is a more reliable way of defining diagonal cracking than the customary practice of visual inspection. The curve also confirmed that the behaviour of beam CBM1 was more ductile. It was noted that after the appearance of the major diagonal crack during the third load cycle at a load of 40 kN, the transverse expansion increased dramatically. This may be due to the expansion of the middle stirrups. The maximum expansion measured during the third load cycle at a load of 50 kN was of the order of 2.50 mm. An increase of approximately 25% was also observed at 70% of the failure load.

**Deflection**

The results from the deflection measurements, taken along the soffit of coupling beam CBM1 as shown in Figure 3.13 in Chapter 3 are presented in Figure 5.3

for the three dial gauge positions. The curves D1, D2 and D3 indicate that during the first increment of loading up to 20 kN, during the last load cycle, a large deformation of approximately of 8.0 mm was measured. In the following increments the deformations were increasing in proportion to the applied load up to 50 kN. At this stage, the measured deformations were 12.10 mm, 15.30 mm and 19.36 mm for dial gauge positions D1, D2 and D3 respectively. At 70% of the failure load, a large deformation of 35.00 mm was recorded at dial gauge position D3, this was accompanied by an increase in the width of the diagonal crack.

**Rotation**

An important piece of information, which these experiments was expected to supply, was the load-rotation characteristics of the coupling beams. It was anticipated that the actual rotation of the vertical sections of the beam along its boundary should be related to the load. It was decided to establish a vertical reference line, the horizontal displacement of which was to be measured at two points remote from the horizontal axis of the beam. The vertical reference line was chosen to coincide with the edge of the end-blocks along which dial gauge position D4 was established at an equal distance from the horizontal axis of the beam to detect any rotation of the end block.

To obtain the desired beam rotation $\theta$ in a simple way, it was necessary to assume that the end-blocks behaved as infinitely rigid bodies. The error involved led to an overestimation of the rotation capacity of the beams. The overestimation could be significant during the first load cycle before the cracks start to develop but it

reduced as the stiffness of the beam relative to the end-block was reduced with progressive cracking. The rotation of the end-blocks should be identical, because the structure is symmetrical, but differences can arise because of uneven crack formation and the uneven distribution of the material properties. These differences were assumed to be very small.

The load-rotation relationship for beam CBM1, based upon the measurements is presented in Figure 5.4 which indicates a permanent deformation during the third load cycle. At all stages of loading during the third load cycle, the measured rotation was almost linear and the increase was proportional to the applied load. At a load of 50 kN, the rotation was estimated to be 11.30 x $10^{-3}$ radians. At 70% of the failure load when the diagonal crack opened, a 50% increase in rotation was recorded.

**Crack formation and crack width**

Figure 5.5 and Plate A.2 in Appendix A show the crack pattern in beam CBM1. As expected, the first major cracks formed at the tension corners of the beam. The propagation of the secondary cracks was almost perpendicular to the spanning direction of the beam. These cracks appeared at an early loading level and continued to develop as the load was increased. During the first load cycle the width of these cracks was less than 0.3 mm at a load of 50 kN. During the second load cycle most of the cracks which developed during the first load cycle closed and new ones appeared which were less than 0.2 mm in width at a load of 50 kN. At the third load cycle most of the cracks started to extend in length and

propagate into the depth of the beam. The main diagonal crack only fully developed at 40% of the failure load. At 70% of the failure load, the width of the major crack running along the main diagonal accounted for 112% of the measured transverse expansion which occurred at a load of 50 kN. The width of the second crack which extended from the top right hand corner across the depth of the beam was estimated to be 1.10 mm at a load of 50 kN. The cracks, which propagated into the end-blocks at the tension corners of the beam, suggest the presence of high bond stresses in these regions. These cracks were only few in number and it appeared that the minimum anchorage length of 0.5m for the flexural reinforcement was ample. The width of the secondary diagonal cracks did not increase proportionally with load but remained nearly constant over a large range of loading.

**Failure of beam CBM1**

It is apparent from Figure 5.5 and Plate A.2 in Appendix A taken at failure of beam CBM1 that the beam was separated into two halves along the main diagonal.

The failure of this beam was characterised by the formation of a large shear crack extending from the top right hand corner to the lower left hand corner of the beam and another vertical crack running down the depth of the beam indicating the presence of a high bending moment.

During the first and second load cycles, the width of the diagonal crack was very small and was of the same order of magnitude as the width of the flexural crack.

Therefore, shear forces could be transmitted across the cracks in this area by the interlocking of the aggregate particles. During the third load cycle; the cracks which appeared during the first load cycle increased in width and new cracks also appeared. In the centre of the beam the width of the crack was so large that no shear forces could be expected to be transmitted in this region by the aggregate interlock mechanism. Beam CBM1 in which diagonal bars were present failed at a load of 225 kN which was 24% higher than the theoretical value for the beam calculated using the Compressive Force Path concept. It is believed that the presence of the diagonal reinforcement contributed to this enhancement in strength.

### 5.2.2 Beam CBM2

Beam CBM2 was similar to beam CBM1, described previously, except that no diagonal reinforcement bars were included.

#### Loading and test procedure

The loading and test procedure were essentially the same as that adopted for beam CBM1 and for this reason only new features are described below.

#### Rotation

The rotations of the plane sections passing through the boundaries of the coupling beam were calculated, as described previously for beam CBM1, from the measurement of the displacements of the end-block. The following observations

were made from the load-rotation relationship obtained for the third and final load cycles as shown in Figure 5.6:

1. At a load of 20 kN during the first load increment of the final load cycle a large rotation corresponding to 30% of the measured value at 50 kN was observed.

2. At a load of 30 kN the rotation of the beam increased by a further 15%.

3. A small increase in rotation between 5 and 10% was recorded during the first increments of loading up to 50 kN where the rotation was of the order of 13.5 x $10^{-3}$ radians.

4. The curve was mostly linear up to a load of 50 kN.

5. As the failure load was approached, the instruments had to be removed because of contact between the test arrangement and the beam due to the large rotations which accompanied the formation of the vertical crack.

**Elongation**

During loading in two directions the end-blocks of the test specimens gradually moved further apart. The major part of this movement was due to the elastic and plastic elongations of the coupling beam. The elongation increased with the extension of the top and bottom reinforcement, in the tension zones. The curve in Figure 5.7 clearly shows that at the beginning of the third load cycle a permanent elongation was present in the beam. Apart from when the load was at 35 kN, this permanent deformation was equal to the elongation that occurred at the end

of the first load cycle which was 30% of the elongation measured at a load of 50 kN during the final load cycle. The magnitude of this elongation was 7.00 mm at a load of 50 kN. At 70% of the failure load, the elongation of beam CBM2 was 13.40 mm. This large increase was due to the opening of the vertical crack crossing the depth of the beam.

**Transverse expansion**

The transverse expansion was measured in exactly the same way as in the case of beam CBM1. In the third load cycle, it was noticeable that the behaviour of the beam deteriorated mainly in the upper left hand corner. This was due in part to contact between the beam and the test arrangement as can be noted in Plate A.3 in Appendix A and is also shown diagrammatically in Figure 5.10. The expansion of beam CBM2 was slightly greater than that found in the previous beam as shown in Figure 5.8 because of the reduced percentage of reinforcement. The expansion measured at a load of 50 kN during the final load cycle was of the order of 3.00 mm. At a load approaching failure the expansion of the beam increased dramatically.

**Deflection**

The results obtained from the three dial gauge positions i.e. D1, D2, and D3, during loading are shown in Figures 5.9. It is interesting to note that the estimated axis of the beam was only slightly deformed during the final load cycle at a load of 50 kN. The measured deflections were of the order of 13.80 mm, 16.70 mm and

20.75 mm for dial gauge positions D1, D2 and D3 respectively. At 70% of the failure load the total deflections increased to more than 75% i.e. 32.80 mm, of the corresponding value at a load of 50 kN for dial gauge position D3.

**Failure mechanism and crack patterns**

The behaviour of beam CBM2 was similar to that of beam CBM1. During the third load cycle, the load was increased in small increments until failure occurred at a load of 153 kN, which was at least 10% higher than the theoretical strength of the beam. It is necessary to point out that the third load cycle was applied in the same positive direction as the first load cycle i.e. in the direction in which the beam first failed. The width of the crack in the left hand corner of the beam was 4.00 mm at failure and was influenced by contact between the test beam and the test arrangement. This is shown in Plate A.3 in Appendix A and is shown diagrammatically in Figure 5.10.

It is doubtful whether the load on the beam could have been increased much further at the end of the third load cycle, if there had been no contact between the test arrangement and the test beam. A number of cracks developed in the unrestrained end-block where the load was applied which may have been due to the concentration of stresses at the loading points. The width of the principal crack at a load of 70% of the failure load was of the order of 3.10 mm. The crack extending from the top right hand corner to the bottom right hand corner of the beam resulted from the applied bending moment and was found to be 1.20 mm wide at failure. Beam CBM2 failed in shear before the appearance of the flexural

cracks along a crack which extended from the top left hand corner across the depth of the beam due to contact with the test arrangement.

### 5.2.3 Beam EBM1

The third beam in this group, EBM1, differed from beam CBM1 in respect of the form of the reinforcement. In this case expanded metal mesh was used in conjunction with conventional reinforcement as shown in Figure 3.18 in Chapter 3. To examine the influence of the expanded metal mesh reinforcement with respect to shear behaviour, two sheets of expanded metal mesh, reference 4095, were placed symmetrically about the horizontal axis of the beam to replace the conventional steel stirrups. The contribution of the expanded metal mesh to the ultimate load capacity of the beam will be discussed in Chapter 7.

#### Loading and test procedure

The loading and the test procedure were identical to that used in beams CBM1 and CBM2.

#### Rotation

The load-rotation relationship for the third load cycle is shown in Figure 5.11. The gradual loss of stiffness of the beam is evident from the changing slope of the curve. The plot of the variation in rotation of beam EBM1 confirms that only small plastic rotations had occurred during the third load cycle. These were significantly smaller than those found in previous specimens in this group.

The curve indicates that the small increase in rotation up to a load of 35 kN was proportional to the increase in load, thus indicating linear behaviour. This increase was estimated to be between 5 to 10% for each of the load increments. The slight increase in the rotation can be explained in terms of the increase in the maximum stiffness of the beam observed in the third load cycle, i.e. when the cracks had already fully developed.

It was very difficult to assess whether this was due to the presence of expanded metal mesh together with the diagonal bars reinforcement or due to the smaller plastic deformations which were found in the beam during the first two load cycles. In any event the reduction in plastic deformation would most likely be attributable to the presence of diagonal bars together with the expanded metal mesh.

At a load of 50 kN the rotation of beam EBM1 was only 9.1 x $10^{-3}$ radians. The resulting plots will be further discussed when they are compared with the relationships obtained from the other test beams in the same group of tests in Chapter 7.

**Elongation**

The elongation curve obtained from the displacements of the beam and the end-blocks, reproduced in Figure 5.12, is similar in form to those obtained for the other beams in this group.

The loading branches of the curve are somewhat steeper than those for beams CBM1 and CBM2, thus indicating a greater stiffness. The expanded metal mesh and the extra diagonal bars, which restrain the elongation of the beam were

responsible for this. This was expected as there were no large deformations of the beam during the first two load cycles. The increase in elongation of the beam was found to be between 10 and 15% up to a load of 40 kN. At a load of 50 kN during the third load cycle, the elongation of the beam was of the order of 4.90 mm and at 70% of the failure load, the total elongation was of the order of 8.50 mm.

**Transverse expansion**

The transverse expansion was measured in the same way as for beams CBM1 and CBM2. A very small deformation of only 2.0 mm was observed in this case under a loading of 50 kN. The absence of deterioration of the beam can be noted from Figure 5.13. The transverse expansion was measured up to a load of 50 kN during the third load cycle and the resulting relationship is shown in Figure 5.13. At a load of 30 kN the maximum expansion of the beam was less than 1.0 mm, which confirms the high stiffness of the test beam. This was also due to the closure of the cracks which formed during previous load cycles. After the load reached 40 kN the corresponding expansion increased to more than 40% during this loading increment. At a load of 50 kN the transverse expansion was of the order of 2.00 mm and no large increase was observed as failure was approached.

**Deflection**

The deflections, which were measured in the same manner to that adopted previously, revealed no significant new features. Figure 5.14 shows that up to a load

of 50 kN during the third load cycle, the variations in the deformations recorded at the three dial gauge positions were almost linear. At a load of 50 kN, the deflections recorded at the three dial gauge positions D1, D2, and D3 were 10.20 mm, 13.90 and 16.30 mm respectively. At 70% of the failure load the deflections increased by 65% compared to the values found at a load of 50 kN. The superior performance of the diagonal reinforcement supplementing the expanded metal mesh was apparent from the smoothness of the curve for this coupling beam.

**Failure of the beam and cracks patterns**

The significantly higher amounts of reinforcement in beam EBM1, did not change the basic crack pattern, as can be noted in Plate A.4 in Appendix A and shown diagrammatically in Figure 5.15. A small number of cracks running at approximately right angles to the diagonal crack along which failure occurred were observed in the first and second load cycles. These flexural cracks almost reached the mid-depth of the beam and their width did not exceed 0.10 mm. Failure occurred when the width of the major diagonal crack was 2.30 mm at a load of 280 kN which was at least 15% higher than the predicted values. The damage resulting from the alternating opening and closing of the cracks in this beam which contained the combined expanded metal mesh and diagonal reinforcement arrangement, was much less than that found in the conventionally reinforced beams.

The test demonstrated the superior characteristics of beams with this type of reinforcement arrangement compared with conventionally reinforced coupling beams i.e.

- Higher stiffness of the complete structure at low load levels.
- Significantly reduced shear deformations.
- Larger energy absorption capacities.
- Much less overall damage to the beam.

### 5.2.4 Beam EBM2

The final beam in this group was identical to beam EBM1, except that no diagonal reinforcement was present.

#### Loading and test procedure

The loading procedure used was identical to that used for the other beams in the group.

The behaviour of this beam under load is presented below:

#### Rotation

The load-rotation relationship for beam EBM2 is shown in Figure 5.16. It can be noted from this curve which is for the third load cycle that in early stages of loading i.e. up to a load of 30 kN, the beam behaved elastically as characterised by the linear load-rotation relationship. This may be explained by the ability of the expanded metal mesh to resist rotation during the early stages of loading. The rotation measured at a load of 50 kN was of the order of 12.9 x $10^{-3}$ radians. 30% of this rotation occurred during the last increment of loading before

the application of a load of 50 kN. At the end of the first and second load cycles, the rotation of beam EBM2 was 35% of that measured at a load of 50 kN during the third load cycle. In the third load cycle the beam developed a large plastic rotation as the failure load was approached.

**Elongation**

The elongations obtained at all load levels during the last load cycle are shown in Figure 5.17. After the formation of the failure mechanism, the beam started to contract. This contraction was due to a sliding shear failure as shown in Plate A.5 in Appendix A. The curve in Figure 5.17 shows that the elongation increased proportionally with respect to the applied loading and the relationship was nonlinear. The major increase in the elongation was detected after a load of 35 kN was reached during the third load cycle. This indicates that at this stage the cracks had widened. This may be due to the deterioration of the bond between the concrete and the reinforcement. The maximum elongations noted were 6.30 mm at a load of 50 kN and 11.30 mm at 70% of the failure load. During the first two load cycles, the elongation was very small and of order of 1.90 mm at a load of 50 kN.

**Transverse expansion**

The maximum transverse expansion of this beam, was recorded for each increment of load during the last load cycle and is compared to the expansions for the

remaining beams from the same group in Chapter 7. The transverse expansion measurements for beam EBM2 are given in Figure 5.18. The curve shows that the expansion of the beam increased linearly up to a load of 30 kN. At a load of 50 kN the expansion of the beam was 2.80 mm. However, the elastic behavioural properties of the concrete may have influenced the expansion of the beam more significantly in the cracked state. A significant expansion was observed near ultimate when the cracks started to widen.

**Deflection**

Typical load-deflection relationships at the three dial gauge positions D1, D2 and D3, are given in Figures 5.19. These curves indicate that the beam deflection increased proportionally with the applied load until a load of 50 kN was reached in the third load cycle. The readings obtained at dial gauge positions D1, D2 and D3, positioned on the soffit of the beam varied linearly up to a load of 40 kN and then the gradient of the curve changed. The commencement of a change in slope of the curve may be explained by the appearance of the cracks which may have had some influence on the readings recorded at dial gauge position D2. The measured deflections at the three dial gauge positions D1, D2 and D3 at a load of 50 kN were 11.30 mm, 14.20 mm and 17.55 mm respectively. At 70% of the failure load when the major diagonal crack had widened, the deflections recorded at the three dial gauge positions increased by 70% compared to the set of measurements taken at a load of 50 kN.

### Failure mechanism and crack patterns

The development of the failure mechanism in beam EBM2 was essentially the same as that described previously for beam EBM1. The failure of the beam is shown in Plate A.5 in Appendix A and shown diagrammatically in Figure 5.20, and is characterised by a large shear crack crossing the beam diagonally.

During the elastic loading range only a few cracks developed. These initial cracks occurred at the tension corners in the beam at a load of 35 kN during the first load cycle. During the second load cycle new cracks developed at a load of between 40 and 50 kN. These cracks were almost perpendicular to the diagonal crack and were of a flexural nature. The width of these cracks did not exceed 0.30 mm. At the junction of the wall and the beam the cracks propagated along the length of the beam. These were then followed by the formation of the diagonal cracks within the beam.

The top left hand corner cracks shown in Figure 5.20 near the joint appeared at an early load level during the first load cycle and continued to increase in length and width as the load was increased. The width of the major diagonal crack was 2.90 mm at 70% of the failure load. Beam EBM2 failed in shear at a load of 185 kN.

## 5.2.5 Summary

The following conclusions can be drawn from the test results obtained from this series of beams:

No significant change in failure mode was observed between the different beams examined in this group of tests. The crack patterns were essentially the same for the four beams irrespective of whether diagonal reinforcement bars were present or not for both types of reinforcement. However, less damage at failure was observed in beams CBM1 and EBM1.

A significant decrease in beam stiffness was observed when the major inclined crack formed in the shear span in all the beams. The presence of expanded metal mesh was very effective in reducing crack widths and deflections after the appearance of inclined cracking. Therefore, the expanded metal mesh present in beams EBM1 and EBM2 should also be used for crack control.

The use of expanded metal mesh as web reinforcement appears to have had an influence on the ultimate shear strength of the beams. Its influence is more noticeable in this series of beams.

The results obtained from the first test series indicate that with very careful detailing, particularly in the areas where yielding can occur, coupled shear wall structures can be made to possess all the desirable features of an effective earthquake resistance structure.

## 5.3 BEHAVIOUR OF COUPLING BEAMS WITH A SPAN/DEPTH RATIO OF 1.1

This second group of tests examined the behaviour of coupling beams CBD1 and EBD1. The properties of these beams were summarised in Chapter 3. Beams CBD1 and EBD1 were made at the beginning of this programme of research. Several faults in the instrumentation and testing procedure were identified during the preliminary phase of the investigation. These faults were subsequently overcome before the coupling beams with shear span to depth ratios of 1.43 and 2.0 were subsequently tested. The coupling beams included in this group of beams were half scale and the overall dimensions of both beams were identical and are shown in Chapter 3. The shear span to depth ratio of these two beams was equal to 1.1.

### 5.3.1 Beam CBD1

The aim of this test group was the same as that for the previous group of coupling beams with a shear span to depth ratio of 1.43 described in Section 5.2. The reinforcement arrangement in the beam and the walls was the same for all the beams as shown in Figures 3.15 to 3.18 in Chapter 3. Both beams contained diagonal reinforcement bars.

#### Loading and test procedure

The beams were loaded using two high capacity hydraulic jacks i.e. maximum

load of 1000 kN as shown in Plate A.6 in Appendix A. The load was applied in thirteen increments for the first and second load cycles and to failure in the final load cycle. During each increment the load was held constant while the cracks were marked, photographs taken and the displacements were measured.

**Failure mechanism and crack patterns**

The failure of beam CBD1 was different to that of the previous group of beams with a shear span to depth ratio of 1.43. The previous tests on the beams resulted in a failure by separation along the main diagonal cracks which divided the beam into two halves. In this beam, vertical cracks appeared unexpectedly near a support and caused the failure of the beam during the third load cycle. This was due in part to the test arrangement which moved slightly when the beam was subjected to the high load levels. This movement resulted in an eccentricity in the loading which produced very high bending moments in the beam. The failure of the beam occurred at a load of 360 kN. The location of the failure was at the right hand support, as shown in Plate A.6 in Appendix A and shown diagrammatically in Figure 5.21. The widening of the crack running in a vertical direction near the support was considerably greater than in other areas of the beam and its value was 5.0 mm at failure. The failure of the beam was sudden with little or no plastic deformation. The cracks appeared to be very severe during the third load cycle even although the load was only 50% of the failure load. The decision was taken to redesign and replace the test arrangement on completion of the test.

## Deflection

The deflections recorded during the third load cycle at the three dial gauge positions D1, D2 and D3 are presented in Figure 5.22. The resultant behaviour of beam CBD1 during the first and second load cycles was similar with respect to cracking. When the major crack developed running in a vertical direction at the support the deflection recorded was significant. The deflection measurements taken at a load of 120 kN during the last load cycle were 34.45 mm, 39.85 mm and 48.68 mm for dial gauge positions D1, D2 and D3 respectively. At the beginning of the third load cycle at a load of 20% of the failure load, deflections 30 to 40% higher than the above values were recorded. After these large increases, the increase in the deflections were proportional to the increase in load up to failure. No significant plastic deformations were found in beam CBD1 during the third load cycle. Consequently, the loss in stiffness appeared to be significantly higher when the vertical crack appeared.

## Elongation

The effect of the presence of diagonal reinforcement in the beam was characterised by large elongations in the beam before failure. The elongation was very high as a result of the appearance of the vertical crack which tended to elongate the beam along its longitudinal axis. The elongations of the beam varied linearly up to 33% of the failure load as shown in Figure 5.23. At a load of 120 kN, the total elongation found in beam CBD1 was 10.10 mm. When the load approached failure a large elongation was experienced by the beam when the vertical crack

increased in width above 3.0 mm.

### Transverse expansion

The behaviour of beam CBD1, is shown by the slope of the load-transverse expansion relationship in Figure 5.24, up to 33% of the load failure. The transverse expansions of this beam were larger than those observed in the previous group of beams, because of the presence of the larger forces and longer stirrup lengths. The nonlinearity of the load-expansion relationship immediately after the cracks had developed during the first load stage of the third load cycle is also evident in this beam. At a load of 120 kN just before failure during the third load cycle the measured expansion of the beam was of the order of 4.80 mm.

## 5.3.2 Beam EBD1

In order to avoid a diagonal tension failure and to increase the stiffness of the beam the stirrups in beam CBD1 were replaced by an expanded metal mesh within the beam and in the end-blocks. An overall view of the reinforcement arrangement in this beam is shown in Figure 3.18 in Chapter 3.

### Loading and test procedure

This new test arrangement was adopted for all subsequent beams, as shown in Figure 3.3 in the Chapter 3.

### Failure mechanism and crack patterns

The development of the failure mechanism in this beam was essentially the same as for beam CBM1 described previously in Section 5.2.1. The failure of this beam occurred at a load of 480 kN at which point a 45° (approximately) crack developed on the surface of the beam. This crack divided the beam into two halves and was followed by the development of another crack which ran through the thickness of the beam at the level of the main reinforcement bars.

The bond between the concrete and expanded metal mesh did not prove entirely sufficient. This may have been because of the size of the expanded metal mesh. The widening of the cracks along the main diagonal was greater than that in other areas of the beam. The width of the major diagonal crack was estimated to be 3.80 mm when the beam failed. The failure of the beam is shown in Plate A.7 in Appendix A and also shown diagrammatically in Figure 5.25. It can be noted that several cracks running in a horizontal direction, developed at the four corners of the beam indicating the possible presence of stress concentrations at these locations. The cracks during the second load cycle formed approximately at right angles to the previous ones but were very small in magnitude. The width of the widest crack which formed during the first two load cycles was less than 0.3 mm. The considerably higher percentage of web reinforcement present in beam EBD1 did not influence the crack pattern in the coupling beam.

## Deflection

The load-displacement relationships for the third load cycle are given in Figure 5.26. This curve indicates an increase in the strength and stiffness when expanded metal mesh was used compared with the beam in which only conventional reinforcement was present i.e. beam CBD1. The marked increase in the strength of beam EBD1 was due to the presence at the corners of the confining influence of this type of reinforcement and the use of new test arrangement. It was noted that the displacements of beam EBD1 were decreased by at least by 20 to 30% compared with the previous test. The confining influence of the presence of the expanded metal mesh placed across the whole span of the beam together with diagonal bars, prevented the rapid deterioration of the beam and resulted in significant increase in ductility. The deflections measured in beam EBD1 at a load of 25% of the failure load during the third load cycle were 23.66 mm, 28.59 mm and 37.86 mm for dial gauge positions D1, D2 and D3 respectively.

## Elongation

If the overall length of a rectangular reinforced concrete beam is measured along its longitudinal axis at mid-depth, then it may be said that all such beams increase in length under the action of applied load after the onset of flexural and shear cracking. The reason for this is related to the upward movement of the neutral axis. The presence of the expanded metal mesh and the diagonal reinforcement bars resulted in a reduction in the elongation of beam EBD1 compared to that of beam CBD1. Figure 5.27 shows that the elongation of beam EBD1 varied

linearly with respect to the applied load except during the early stage of loading between 50 and 60 kN where the elongations were significant. At 25% of the failure load the elongation measured was of the order of 9.20 mm. An increase in the elongation was noted at each load increment until failure occurred.

**Transverse expansion**

The stiffening effect of replacing stirrups with the expanded metal mesh can be noted in Figure 5.28 which show the load-expansion curve, at the mid-span of the beam. The results from beam EBD1 indicate that the introduction of expanded metal mesh led to a reduction in the transverse expansion and maximised the load carrying capacity of the beam. The expanded metal mesh did not prevent the beam from separating into two halves. The total transverse expansion measured during the third load cycle at a load of 120 kN was of the order of 4.40 mm.

### 5.3.3 Summary

Two major conclusions can be made:

1 - Several faults were observed in the test on beam CBD1 as far as the instrumentation, loading procedure and test arrangement are concerned.

It was found that beam CBD1 failed more in flexure due to the resulting movement of the test arrangement. A decision was then made to re-design the test arrangement and to make it adaptable to all types of beams with different shear span to depth ratios.

2 - Beam EBD1 with the same shear span to depth ratio failed by sliding shear after a few load reversals which caused yielding of the flexural reinforcement.

The performances of the two test beams upon which very severe displacements were imposed, were compared in terms of deformations and the failure loads. In every aspect the superior performance of beam EBD1 containing expanded metal mesh, was identified. The reason for this was the arrangement of reinforcement in the test beam, particularly in the beam which enabled the major critical internal force components to be carried by the reinforcement rather than the concrete.

## 5.4 BEHAVIOUR OF COUPLING BEAMS WITH A SPAN/DEPTH RATIO OF 2.00

The purpose of this group of tests was to determine the effect of a decrease in the depth of beams which had the same form of reinforcement as those described in the earlier Sections in this Chapter. The four beams CBS1, CBS2, EBS1, and EBS2, had a shear span to depth ratio of 2.0. They were tested in the same manner as the beams with a shear span to depth ratio of 1.43. The dimensions of this group of beams were selected to be similar to those investigated previously. All the beams had a shear span, depth and thickness of 500 mm, 250 mm and 100 mm respectively. A different reinforcement arrangement was used in each of the beams. The properties of each beam are summarised in Tables 3.3 to 3.6 in Chapter 3.

### 5.4.1 Beam CBS1

The loading test procedure for beam CBS1 in this group were essentially the same as that used for beam CBM1 and described in Section 5.2.1. The only difference was the shear span to depth ratio.

**Failure of the beam and crack patterns**

It was expected that failure of this beam would occur along one of the diagonals across the beam. Plate A.8 in Appendix A and Figure 5.29 indicates that the inclined crack formed within the span of beam CBS1 under increasing load at

approximately 30% of the failure load during the third load cycle. It was also observed that after the load reached 50% of the failure load, the crack pattern did not change significantly and only the inclined crack extended within the beam towards the supports as failure was approached. Collapse of the beam occurred at a load of 142 kN during the final load cycle due to the development of the major diagonal crack. It is interesting to note in Figure 5.29 that at failure the width of the major inclined crack was very significant. The width of the crack was estimated to be 3.00 mm. It is argued that when the width of a crack is 3.00 mm aggregate interlock will be negligible. The absence of aggregate interlock action will result in little or no resistance to shear stresses.

**Elongation**

The load-elongation relationships for beam CBS1 are shown in Figure 5.30. The curve showed that the beam behaved nonlinearly. The increase in the elongation of the beam was approximately proportional to increase in the load during the first and second load cycles. In the third load cycle they were small increases in elongation during each load increment up to 30% of the failure load. At a load of 50 kN the estimated elongation was 6.00 mm. A large portion of this increase in the elongation was recorded when the load was between 40 and 50 kN. At 70% of the failure load an increase in the elongation of more than 100% was found i.e. at this stage of loading the measured elongation was of the order of 12.30 mm. This sudden increase in elongation appeared to reflect the presence of the inclined web crack, which extended through the whole depth of the beam.

### Transverse expansion

The transverse expansion along the beam is shown in Figure 5.31 for the third load cycle. The curve indicates that the expansion of the beam was approximately proportional to the applied load, up to a load of 30 kN during the last load cycle. At approximately 50% of the failure load, the total expansion was found to be of the order of 2.80 mm. Figure 5.31 shows that at a load of 30% of the failure load, a permanent increase in the expansion of the beam was comparable to the increase in the crack widths.

### Rotation

The load-rotation relationship for beam CBS1 is shown in Figure 5.32. The curve for the third load cycle indicates degradation in the stiffness of the beam due to yielding of the coupling beam in the critical end region and the formation of the diagonal cracks. The lack of stiffness at the commencement of the third load cycle was due to closing of the cracks which had opened during the previous load cycle. When these cracks closed an improvement in stiffness resulted from the development of the contact stresses present between the cracked surfaces in the concrete. After reaching a maximum stiffness before the failure load was reached, the stiffness began to fall off, due to yielding of the main reinforcement in the beam. The rotation measured at a load of 50 kN during the final load cycle was of the order of 12.30 x $10^{-3}$ radians. A large increase in rotation was noted as failure was approached.

### Deflection

The deflection measurements taken along the soffit of the beam, as shown in Figure 5.33 for dial gauge positions D1, D2 and D3, showed that the beam was subject to significant deformations in both flexural and shear behavioural modes. The nonlinearity of the behaviour of the beam can be noted from the readings obtained from each dial gauge during the third load cycle. During this loading cycle at a load of 50 kN, the deflection measurements were 14.20 mm, 17.10 mm, and 21.60 mm for dial gauge positions D1, D2 and D3 respectively. Approximately 20 to 30% of the measured deflections at a load of 50 kN found during the first stage of loading in the final load cycle was due either to the change of loading direction or to the closure of the cracks formed during the previous load cycle.

## 5.4.2 Beam CBS2

The only differences between beam CBM1 and beam CBS2 was that beam CBS2 did not contain any diagonal bars and was reinforced with stirrups to prevent shear failure and also the shear span to depth ratios.

### Loading and test procedure

The loading and the test procedure for beam CBS2 were essentially the same as those described in earlier Sections for beam CBM1.

### Rotation

The gradual loss in the stiffness was evident at a load of approximately 30 kN, from the load-rotation curve shown in Figure 5.34. The low stiffness of the beam was due to the poor performance of the reinforcement. The stiffness of beam CBS2 gradually decreased with increasing load and the stiffness approached zero at failure when yielding of the main reinforcement bars occurred. At a load of 50 kN, the measured rotation was of the order of 14.50 x $10^{-3}$ radians. A large increase in rotation was also observed in this beam as the load approached failure. The curve indicated that the behaviour of the beam was mainly nonlinear.

### Elongation

The load-elongation relationships shown in Figure 5.35 showed that the beam had undergone elongation as the whole structure increased in length. It was noted that the elongation of the beam during the elastic range was very small and was of the order of 2.35 mm during the last increment of the first load cycle i.e. at a load of 50 kN. It also shows that the increase in elongation was proportional to the increase in load up to 30% of the failure load. A large elongation of 8.00 mm was found at a load of 55% of the failure load after the appearance of the crack which eventually led to failure of the beam. Prior to failure at a load of 70% of the failure load the elongation was of the order of 14.50 mm. Such a large elongation was due to the unexpected appearance of a vertical crack which resulted in elongation of the beam along its longitudinal axis.

### Transverse expansion

Figure 5.36 demonstrates the influence of the presence of the strength of the stirrups in the vertical direction found in beam CBS2. The high transverse expansion of 4.00 mm measured at only 55% of the failure load was due either to the absence of the diagonal reinforcement bars or to the failure mechanism of this beam. During the third load cycle, at a load of 25 to 35% of the failure load, a large expansion of 25% of the value measured at a load of 50 kN was observed. In addition, in this beam the expansion of the stirrups was very high, as anticipated from the absence of diagonal reinforcement bars which provided some resistance to the resulting expansion of the beam.

### Deflection

The load-displacement relationship is given for the three dial gauge positions in Figure 5.37. During the last load cycle, the beam was loaded until yielding occurred, but the measurements were recorded up to 55% of the failure load. The curves show that the three measurements taken during the third loading cycle at a load of 45% of the failure load were 15.60 mm, 18.30 mm and 23.10 mm for dial gauge positions D1, D2 and D3 respectively. A large increase in the deflections of the beam occurred when the vertical crack increased in width at a load of 70% of the failure load. This caused a considerable loss of strength in beam CBS2.

### Failure mechanism and crack patterns

The mode of failure observed in this beam was not as expected. The first visible inclined crack in this beam occurred at the joint between the wall and the beam at a load of about 30 to 40% of the failure load. At each loading increment these cracks, initially limited in length, tended to propagate slowly in their respective diagonal directions. In the loading range of 40 to 70% of the failure load, typical vertical cracks, longer than the initial ones, suddenly developed. These cracks could be attributed to flexural action. The absence of the diagonal reinforcement allowed the beam to fail more in a flexural rather than a shear mode. The failure of the beam occurred when the load reached 115 kN when the largest crack width was of the order of 3.80 mm. The mode of failure of this beam is shown in Plate A.9 in Appendix A and is also shown diagrammatically in Figure 5.38.

## 5.4.3 Beam EBS1

In general, beam EBS1 was reinforced in the same manner as beam EBM1 which is described in Section 5.2.3. The only difference between the two beams was in their shear span to depth ratios.

### Loading and test procedure

The loading and test procedure were identical for both beams.

## Deflection

The load-deflection relationship presented in Figure 5.39 shows no significant new features other than confirmation of the superior performance of the diagonal reinforcement bars in conjunction with expanded metal mesh when compared to that of beams containing horizontal flexural reinforcement and normal vertical stirrups. The curves obtained from the test on the beam shown in Figure 5.39 gave deflections for beam EBS1 at a load of 50 kN of 13.10 mm, 15.40 mm and 19.40 mm for three dial gauge positions D1, D2 and D3 respectively. The curves indicate that, when the beam was subjected to gradually increasing load, the observed deflections behaved nonlinearly up to a load of 50 kN for dial gauge positions D1, D2 and D3.

## Rotation

The load-rotation characteristics of beam EBS1, are given in Figure 5.40. The most significant aspects of this curve have previously been discussed for beams with a shear span to depth ratio of 1.43. It should be recalled that the rotations at the supports of the beam are based on the assumption that the end-blocks are rigid. In fact small rotations of the end-blocks also occurred and these mearsurements were subsequently used to correct the deflection results in conjunction with the results from the two storey test beam DBS2, described in Section 5.4.5. A gradual loss in the stiffness is evident from the changing slope of the load-rotation relationship. At a load of 50 kN during the final load cycle, the rotation of this beam was 10.8 x $10^{-3}$ radians which corresponds to a failure load of less than

30%. It was confirmed from Figure 5.40 and by observations made during the test that the reduction in stiffness of beam EBS1, was accelerated when the beam was subjected to reverse loading. This may be explained by the development of the cracks during the previous load cycles.

**Elongation**

The load-elongation characteristics of beam EBS1 are shown in Figure 5.41. These were found to be very similar to those for beams with a shear span to depth ratio of 1.43. The progressive yielding and accumulation of plastic deformations during the load cycles were evident. At approximately 30% of the failure load, the elongation of beam EBS1 was of the order of 5.20 mm. This small elongation showed the superiority of the expanded metal mesh when used together with diagonal reinforcement bars. It was noted that the residual elongation of the beam increased after each load cycle. This was due to the opening of the cracks resulting from yielding of the flexural reinforcement. Progressive elongation of the beam after each load cycle showed that the cracks had widened. This was due to the deterioration of the bond between the concrete and the web reinforcement. During the final load cycle, when the load was removed, the beam experienced a significant contraction and closure of the cracks.

**Transverse expansion**

The maximum transverse expansion of this beam was of the order of 2.20 mm at a load of 50 kN during the third load cycle. This can be attributed to the

presence of the expanded metal mesh, acting to confine the concrete and also acting as shear reinforcement, thus expanding less than the conventional stirrup reinforcement. The curve presented in Figure 5.42 confirms that the degree of expansion of the beam was much smaller at all loading stages than that of the corresponding curve obtained from beam CBS1.

**Failure mechanism and crack pattern**

As anticipated failure occurred as a result of diagonal cracking in the beam, which extended from the top right hand support to the lower left hand support of the beam at a load of 175 kN.

Beam EBS1 failed by separation of the beam into two triangular shaped blocks at failure. This type of failure was generally characteristic of a typical shear failure. A number of vertical and inclined cracks with a width of less 0.40 mm were found to be evenly distributed over the entire length of the beam. The pattern of these cracks changed as the load increased. The cracks extended progressively higher into the beam, finally forming into a diagonal crack. At failure the width of the major diagonal crack was of the order of 2.50 mm. The failure mode of beam EBS1 is shown in Plate A.10 in Appendix A and is also shown diagrammatically in Figure 5.43.

### 5.4.4 Beam EBS2

The loading and test procedure for beam EBS2, was identical to that adopted for the other beams in this group of tests.

## Deflection

The deflection of beam EBS2, was similar to that observed in the other beams in this group of tests as can be noted from the load-deflection curves for the three dial gauge positions shown in Figure 5.44. In the earlier stages of the third load cycle the load-deflection relationships were linear up to a load of 30 kN during which the beam remained intact with the exception of a few cracks. The beam deformed significantly, possibly due to the absence of the diagonal reinforcement bars, when it was loaded up to 50% of the failure load. The deflections measured at a load of 50 kN during the final load cycle were 14.90 mm, 17.20 mm and 21.95 mm for dial gauge positions D1, D2, and D3 respectively.

## Elongation

Figure 5.45 shows non linear behaviour of the beam at all points along the span. Observations made during the third load cycle at a load of 50 kN indicated that the elongations increased more rapidly than in the case of beam EBS1. The results obtained during the initial load increments during the final load cycle show that the behaviour of the beam remained essentially elastic and the elongation varied in proportion to the increase in the applied load up to a load of 30 kN. At a load of 50 kN during the final load cycle the elongation was found to be of the order of 7.00 mm. When the load was increased the elongation of the beam increased rapidly and the increase was of the order of 30% of that measured at a load of 50 kN. Some recovery did occur when the load was reduced after reaching the failure load. The larger contraction of the beam at low loads during the third load cycle

resulted from the closure of the wider cracks which had formed during the first and second load cycles of the beam. This is in agreement with the crack width measurements.

### Transverse expansion

The transverse expansion measurements, shown in Figure 5.46 indicate that the beam behaved similarly to beam EBS1. These results further emphasised the efficiency of the use of expanded metal mesh as reinforcement against shear loading. The total transverse expansion of this beam was of the order of 3.40 mm at a load of 50 kN during the final load cycle.

### Rotation

The load-rotation characteristics of beam EBS2, are shown in Figure 5.47. The most significant features of these curves have previously been discussed for the beams in the same test series. At a load of 50 kN the corresponding rotation was of the order of 13.20 x $10^{-3}$ radians. During the first load increment of the final load cycle, a rotation of 30% of the rotation measured at a load of 50 kN was experienced by the beam. This rotation was due to the closure of the cracks which had formed during the second load cycle. The loss in stiffness of beam EBS2 during the three load cycles was considerably higher than that found in beam EBS1 as confirmed by the curve shown in Figure 5.47 where a rotation of 5.0 x $10^{-3}$ radians was measured during the initial load increments.

### Failure mechanism and Crack patterns

The failure mechanism found in beam EBS2 was similar to that obtained previously in beam EBS1 as shown in Plate A.11 in Appendix A and shown diagrammatically in Figure 5.48. The type of cracks which formed at the junction between the beam and the walls propagated diagonally. The increases in the lengths were proportional to the increases in the applied load until the major crack appeared, which led to failure of the beam.

It was also noted that the flexural cracks first appeared after the initiation of the diagonal cracks at a load of 15 to 25% of the failure load. The flexural cracks almost reached mid-depth of the beam and their widths did not exceed 0.30 mm. A further increase in load caused the existing cracks to widen and to extend whilst, simultaneously, new diagonal cracks developed more or less parallel to the existing ones. The width of the widest diagonal crack was of the order of 3.60 mm at the failure load of 145 kN.

## 5.4.5 Beam DBS2

### Introduction

To minimise the costs of the laboratory based programme of tests the majority of beams comprised of single beams with end blocks. These units were either held rigidly, or were constrained to move in predetermined directions. However, it is inevitable that some rotation and slippage of the test beam will occur during

the test. Since such movements are inevitable a double beam unit was made and subjected to the same form of loading as the single beam models included in the earlier test series. The results from this test were then available to check the accuracy of the single beam tests and to provide data to permit the adjustment of the results from the previous test series. The dimensions of the beams in the double beam unit were the same as the beams in the second group of test beams with a shear span to depth ratio equal to 2.0.

The double beam test specimen DBS2, was reinforced in the same manner as beam CBS2, details of which are given in Chapter 3.

### Loading and test procedure

The loading and the test procedures were also the same as those described in Section 5.2.1. In this case the presence of the two beams acting together to restrain the rotation of the wall blocks. The test arrangement for beam DBS2 was the same as the beams tested previously.

### Transverse expansion

The transverse expansion along the beam is shown in Figure 5.49, for the six loading increments applied during the third load cycle.

During the test, the expansion of beam B1 was found to be 2.30 mm at a load of 50 kN, and it was observed that a small increase occurred at 70% of the failure load. For the same load, the expansion of coupling beam B2 was larger due to appearance of a crack with a width in excess of 3.0 mm. This variation may have

been due either to small differences in the concrete matrix, the relative positions of the beams or their location relative to the points at which the loading was applied.

### Elongation

The variation in the elongation of the beam under load during this test is shown in Figure 5.50. As was noted for the expansion of the beam, the elongation of beam B1 was slightly smaller than that for beam B2. This was obvious when the positioning of the coupling beams was examined in relation to the adjoining shear wall.

The elongation of each beam increased as the top and bottom reinforcement was being stressed which were generally found to be experiencing tension and compression actions. The measured elongations found in beam B1 at a load of 50 kN was found to be 4.20 mm and it was noted that the elongation of B2 was larger.

### Rotation

The average end rotation of the beam at all loading stages was very small. The load-rotation relationship for the beam is presented in Figure 5.51. As the rotations increased the loss in stiffness became greater and it was difficult to maintain the position of the load. This introduced an unintentional shift of the point of zero moment away from the centre line of the beam and resulted in the generation of a large bending moment at the ends of the beams where they were attached to

the wall. The maximum rotation, obtained during the third load cycle at a load of 50 kN, was 6.10 x $10^{-3}$radians. Towards the end of the test severe buckling was observed in the reinforcement, which reduced the strength of beam B2.

**Deflection**

The load-deflection relationships for beam B1 in double storey specimen DBS2 are given in Figure 5.52. It can be noted from these curves that the beam was subjected to severe shear forces. The nonlinearity in the behaviour of the beam can be noted from the deflection measurements taken at the three dial gauge positions D1, D2, and D3. At a very early stage of loading, the beams started to deform in a normal flexural mode. At this stage the beams had double curvature with a point of contraflexure at the centre of each span. However, the intensity of the shear loading soon became sufficiently large to lead to the formation of a diagonal crack in beam B2 and a change in its flexural behaviour. When the diagonal splitting of the concrete started along the main compression diagonal, the behaviour was identical to that of the single shallow beams with a shear span to depth ratio of 2.0. The total deflections measured at a load of 50 kN were of the order of 6.85 mm, 8.58 mm, and 9.75 mm for dial gauge positions D1, D2, D3 respectively. The small deflections accounting for 50% of those found in the single test beam reflect the increase in rigidity obtained when the beams act together.

## Failure Mechanism and Crack Patterns

The crack pattern for beam DBS2 at failure shown in Plate A.12 in Appendix A and is also shown diagrammatically in Figure 5.53, suggest that a shear mode of failure was associated with the major presence of the cracks which separated the beams B1 and B2 along their main diagonals. The failure load was applied in the same direction as in the first load cycle i.e. in the direction in which beams B1 and B2 were first forced to yield. The cracks at failure in beams B1 and B2 were at an angle of approximately $27^o$ with the horizontal axis and were 2.60 mm and 4.50 mm in width respectively at a load of 290 kN.

In the top right hand corner of beam B2 the width of the crack was such that no shearing forces could be expected to be transmitted by an aggregate interlock mechanism in that region.

A limited number of cracks, 0.10 mm in width, were observed in the first and second load cycles in beam B1 and no significant cracks were found in beam B2.

## 5.5 CONCLUSIONS

The results obtained from the tests on coupling beams have been presented separately, because of the large number of coupling beams included in this part of the investigation and in order to simplify the presentation and discussion of the test results.

The findings have shown that the strength of coupling beam structures can be enhanced very significantly by the introduction of additional diagonal reinforcement bars together with expanded metal mesh along the span of the beam. The main aim of diagonal reinforcement bars is to transmit the load to the walls. The observed increase in strength using this technique i.e. diagonal reinforcement bars and expanded metal mesh compared to a similar beam of the same shear span to depth ratio reinforced conventionally was at least 18 to 20 % for the beams with a span to depth ratio of 1.43 and 19 to 21% for the beams with a shear span to depth ratio of 2.0.

It must be emphasised, however, that the average 20% increase in strength did accurately reflect the actual contribution of the expanded metal mesh. The beneficial influence of the expanded metal mesh is attributed to its role in reducing the extent of both the flexure and shear cracks. Another improvement in strength of the coupling beams can be achieved by increasing the depth of the beams.

The behaviour of beams EBM1, EBM2, EBS1, EBS2 and EBM3 was found to be satisfactory under load. The introduction of the expanded metal mesh does not contribute only to shear resistance but also contributes to the flexural resistance of the beams by increasing their flexural capacities.

The ductility of the beams reinforced with expanded metal mesh was higher than the conventionally reinforced beams. This was due to the influence of the confining effect of the expanded metal mesh on ductility.

The provision of the expanded metal mesh in the beams appeared from the test results to have improved the load carrying capacity of the beams. However, providing the mid-span region with expanded metal mesh clearly indicates how much improvement in the ductility had occurred in the beams which failed by diagonal cracking.

The performance of beams containing expanded metal mesh could have been improved if extra stirrups have been included at the supports, this type of detail was not investigated further because it was likely to prove not to be cost effective.

The beams reinforced with expanded metal mesh prevented the occurence of brittle failure and resulted in much improved behaviour. The behaviour of the conventionally reinforced beams was characterised by the early appearance of the diagonal crack within the central region of the beam.

The superior behaviour of the beams reinforced with diagonal reinforcement bars together with expanded metal mesh was evident. Although these beams were capable of significant improvements in their behaviour, their deformation characteristics and crack widths could have been improved further. Such improvements can be achieved either by increasing the dimensions of the expanded metal mesh or by introducing extra stirrups at the supports.

The beams generally failed in shear and the measured ultimate loads were considerably higher than the ultimate loads predicted by the two design approaches

described in Chapter 4.

The strength of the beams was enhanced by increasing the concrete strength. This increase appeared to be more pronounced in beams with lower span to depth ratios.

The test results show that the inclined cracking loads normally occured between 40 and 50% of the failure load.

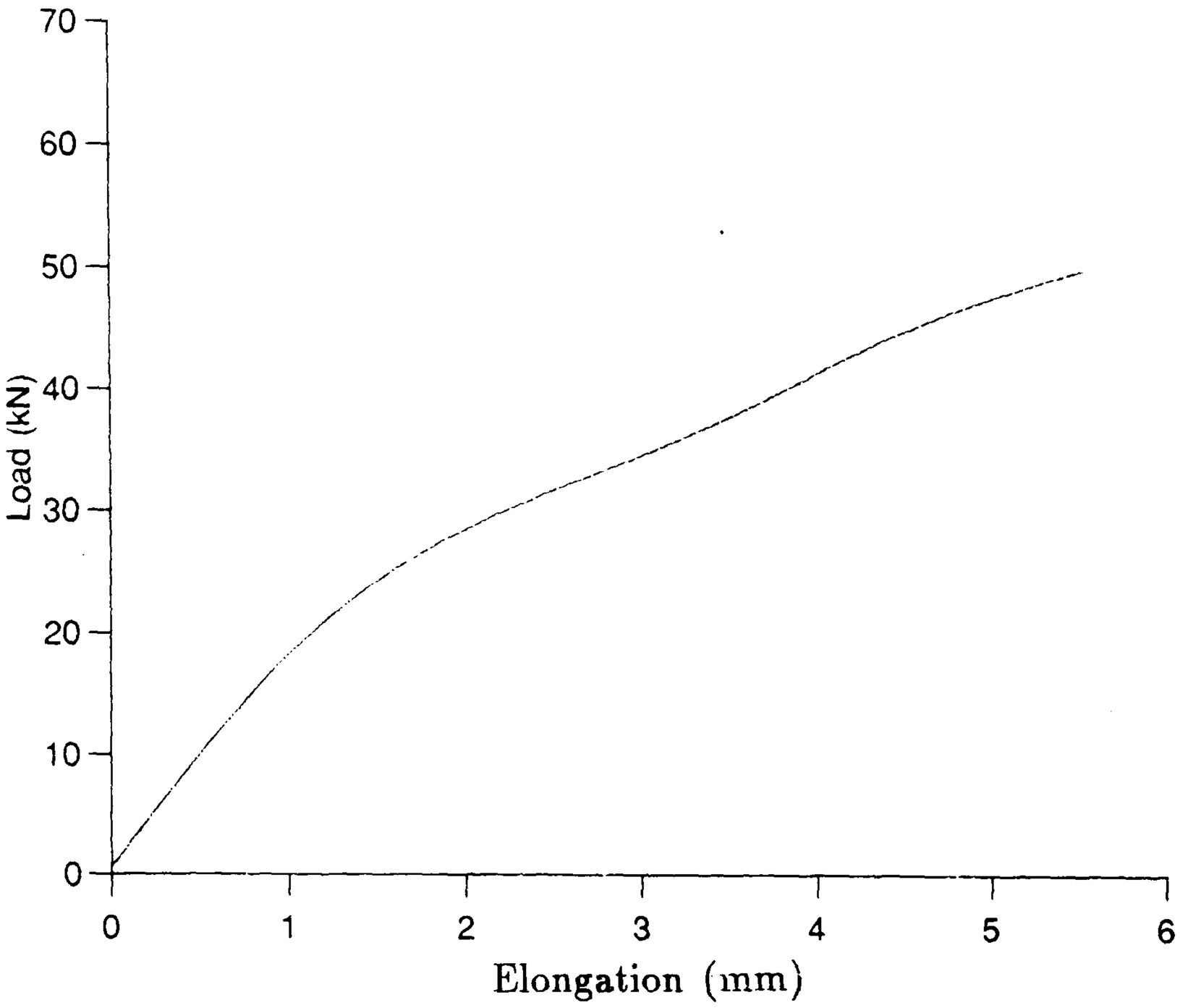


Figure 5.1: Load-elongation relationship for beam CBM1

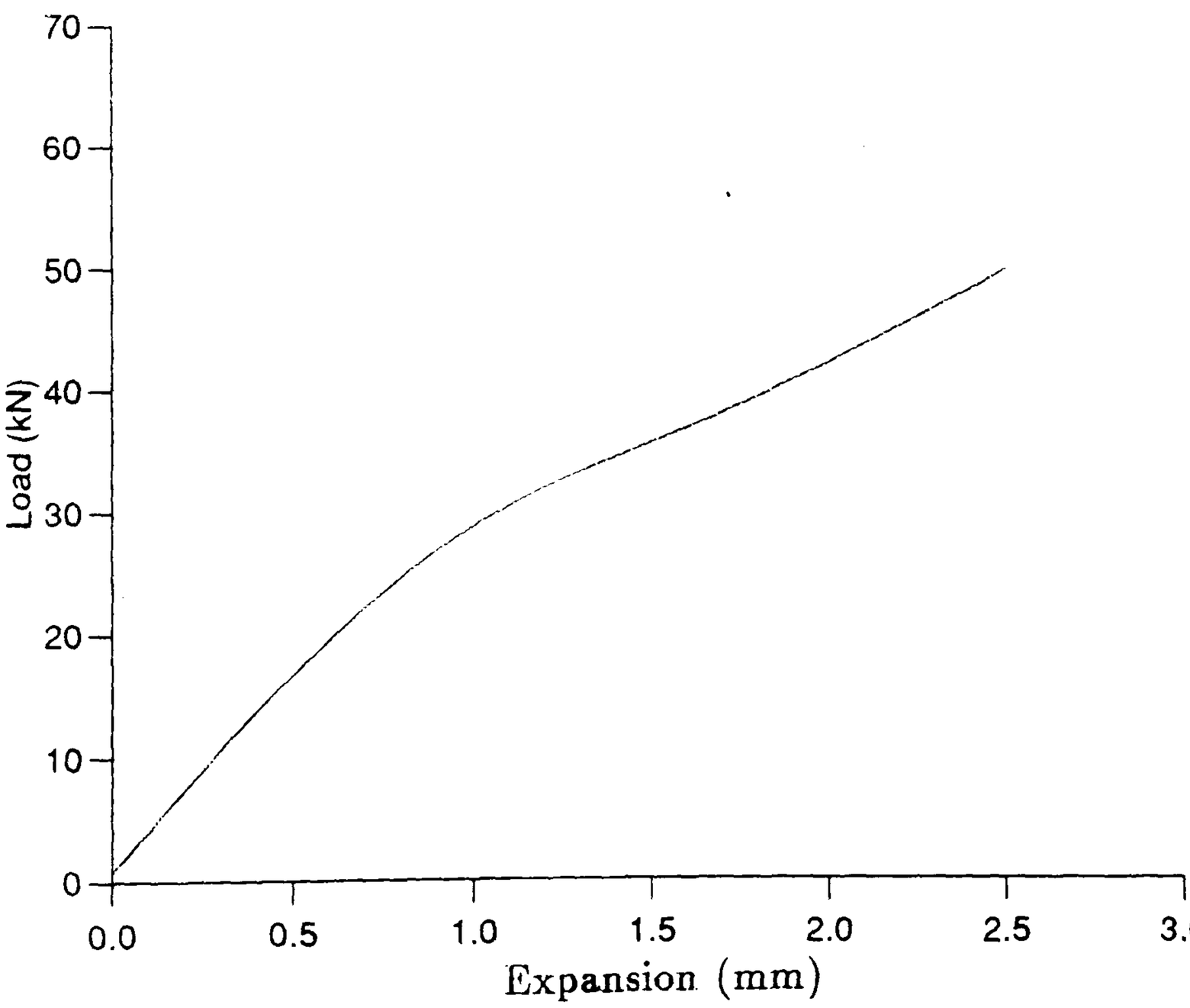


Figure 5.2: Load-expansion relationship for beam CBM1

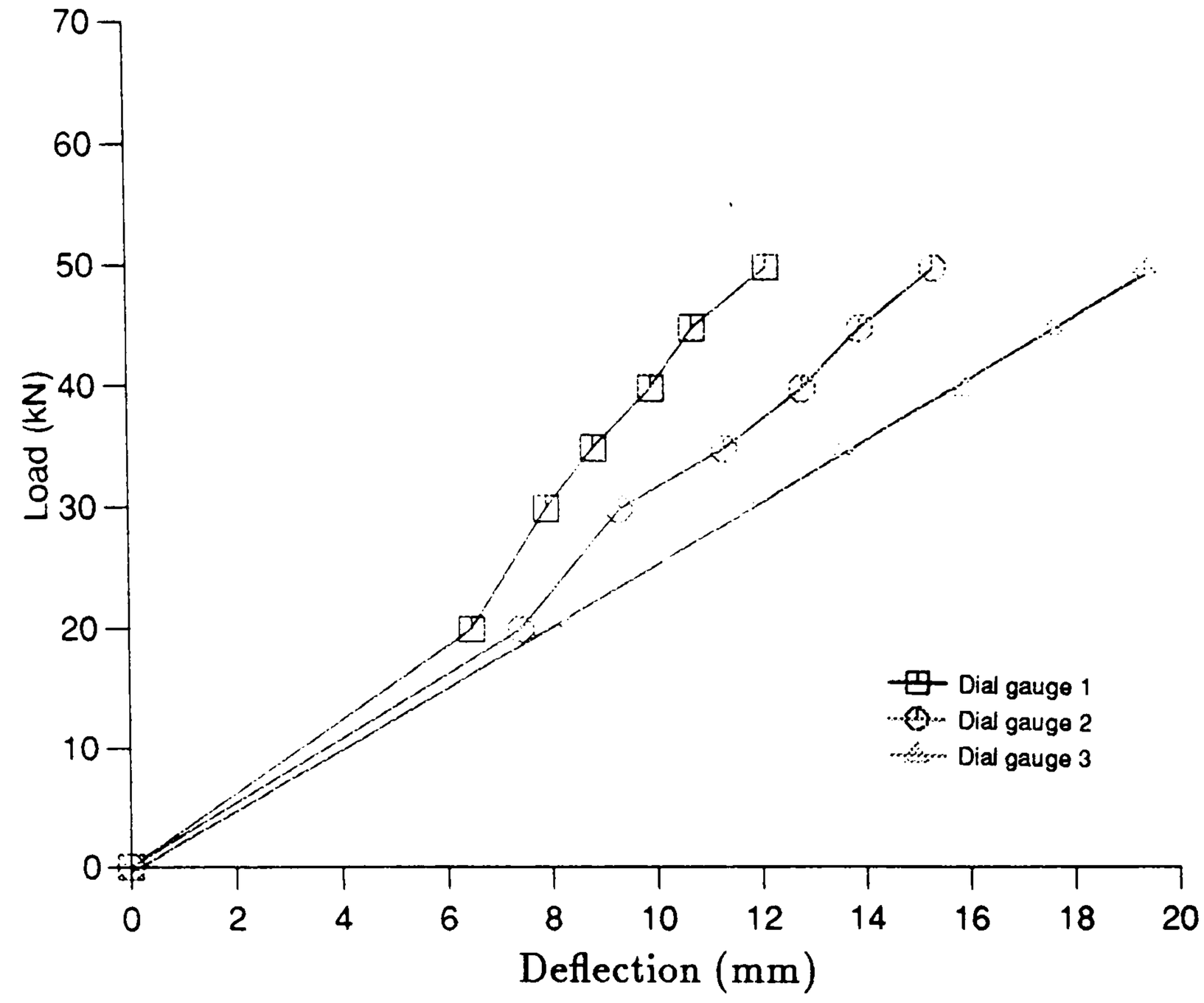


Figure 5.3: Load-deflection relationships for beam CBM1

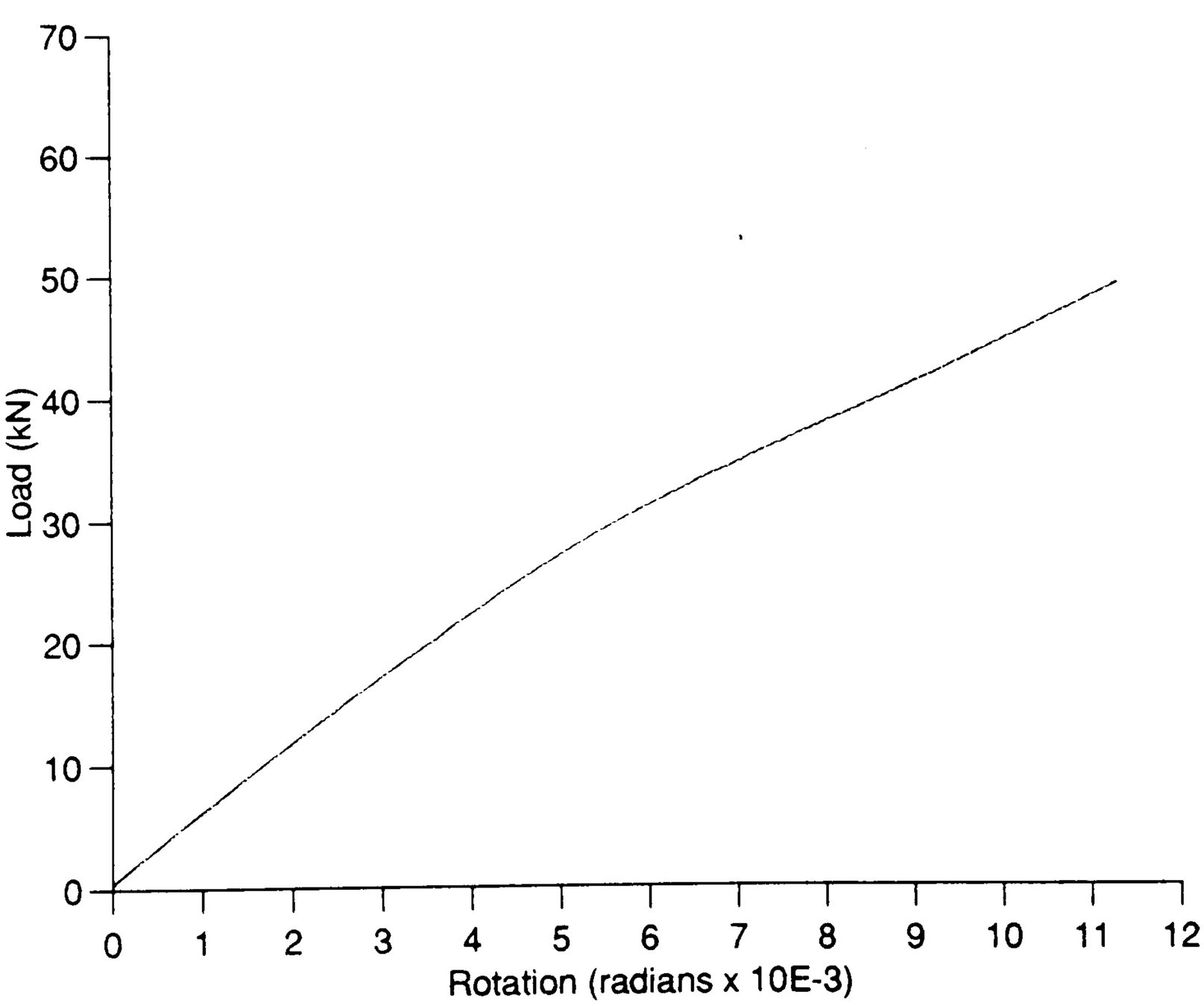


Figure 5.4: Load-rotation relationship for beam CBM1

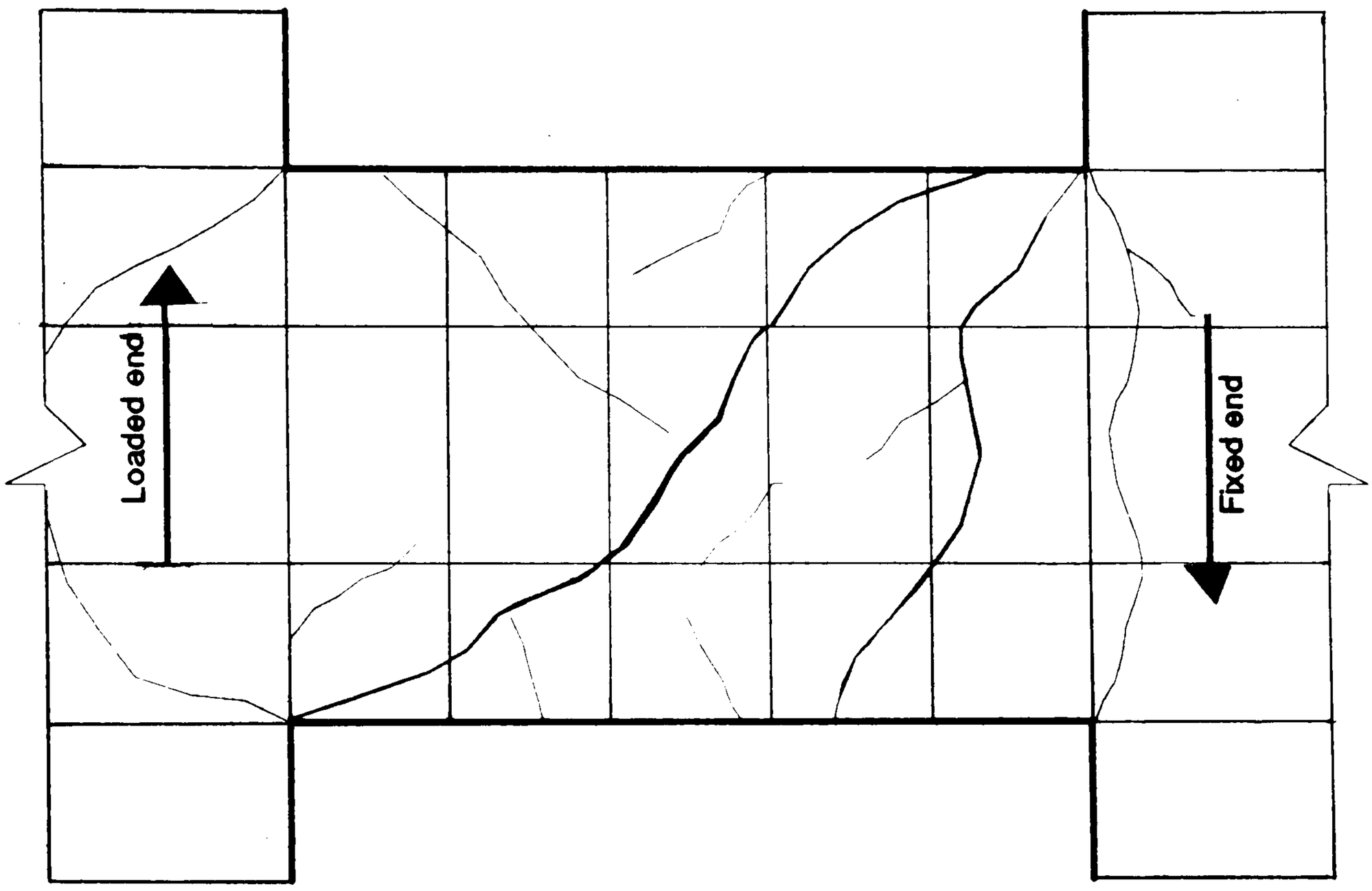


Figure 5.5: Failure mechanism and crack pattern for beam CBM1

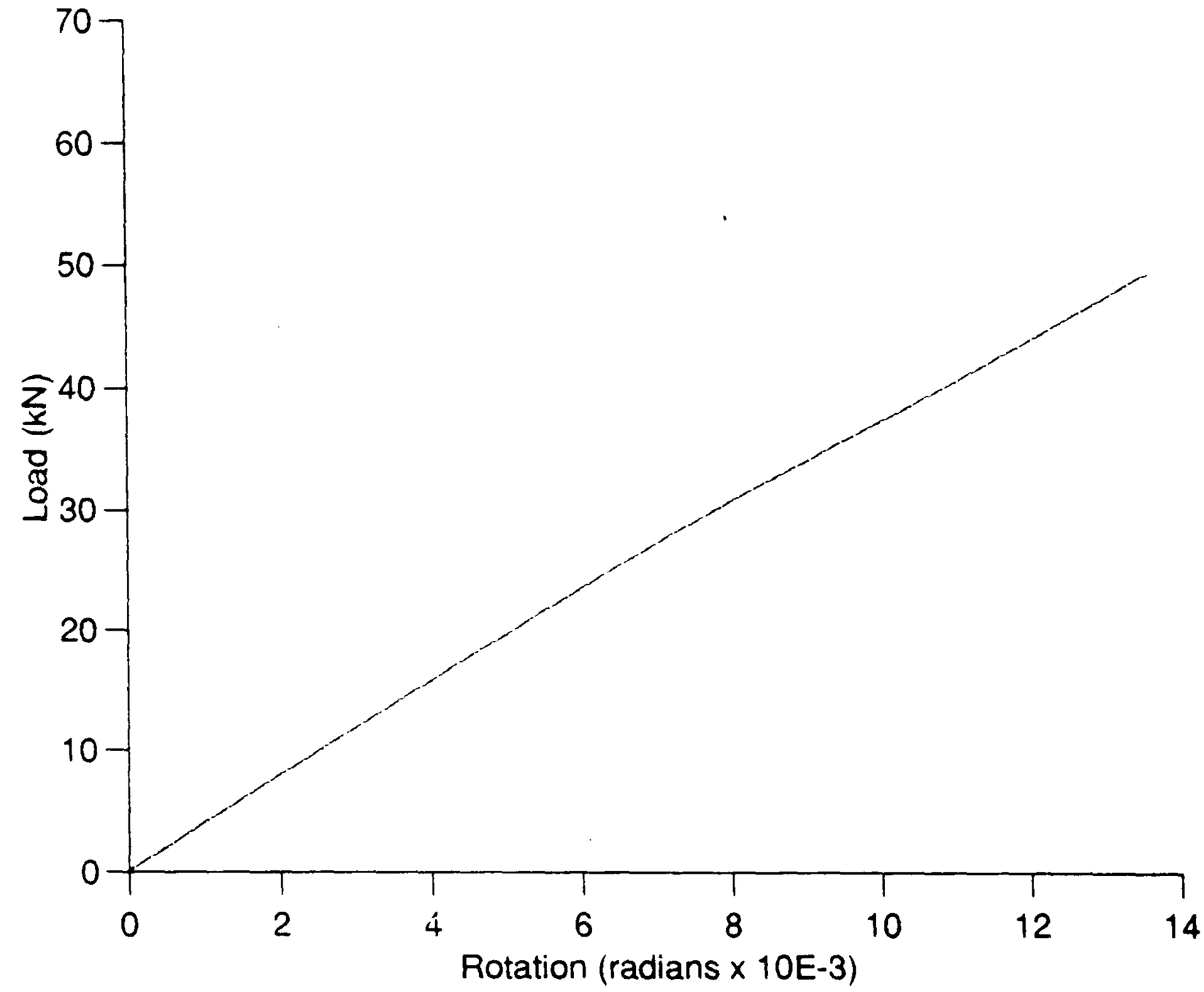


Figure 5.6: Load-rotation relationship for beam CBM2

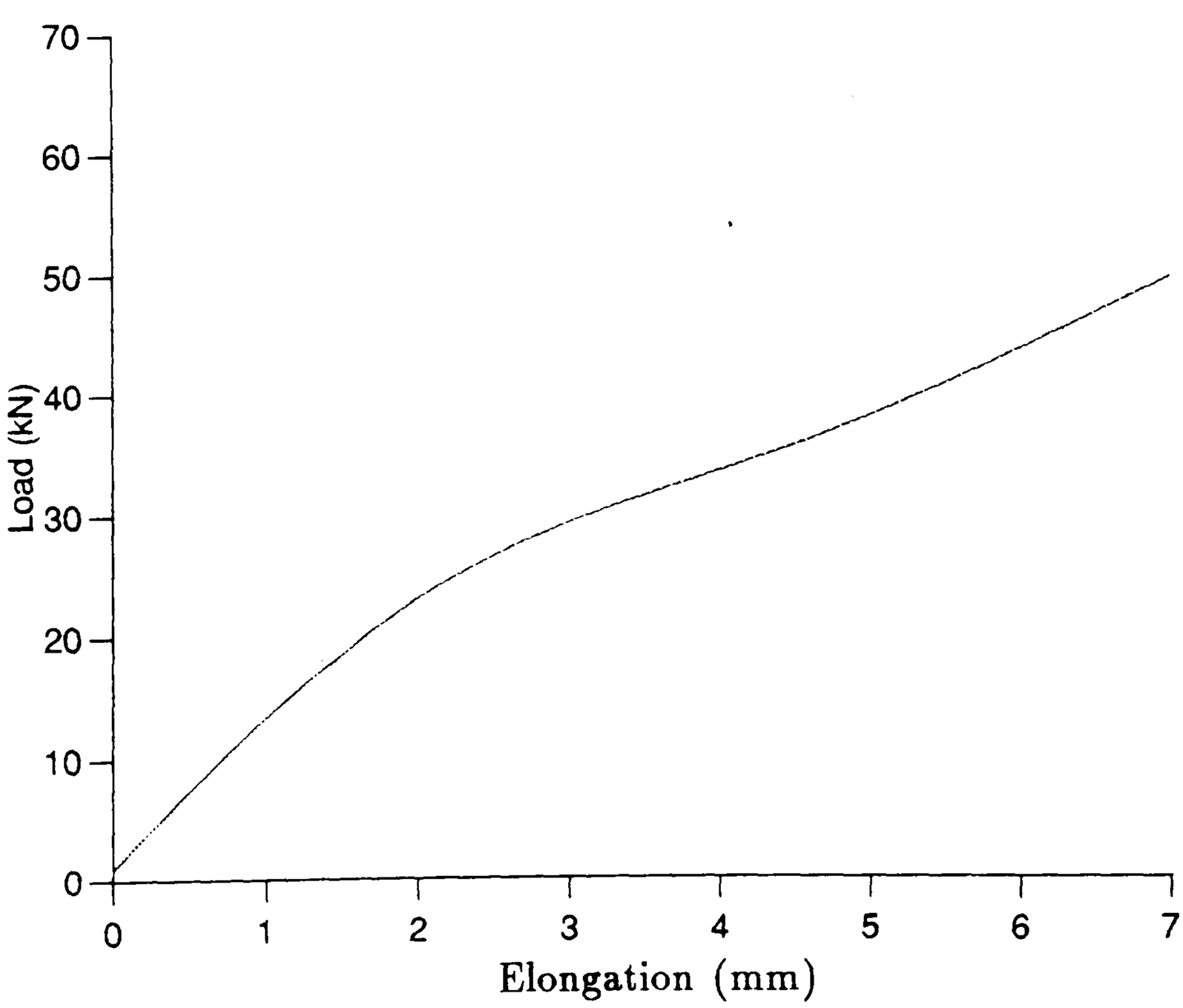


Figure 5.7: Load-elongation relationship for beam CBM2

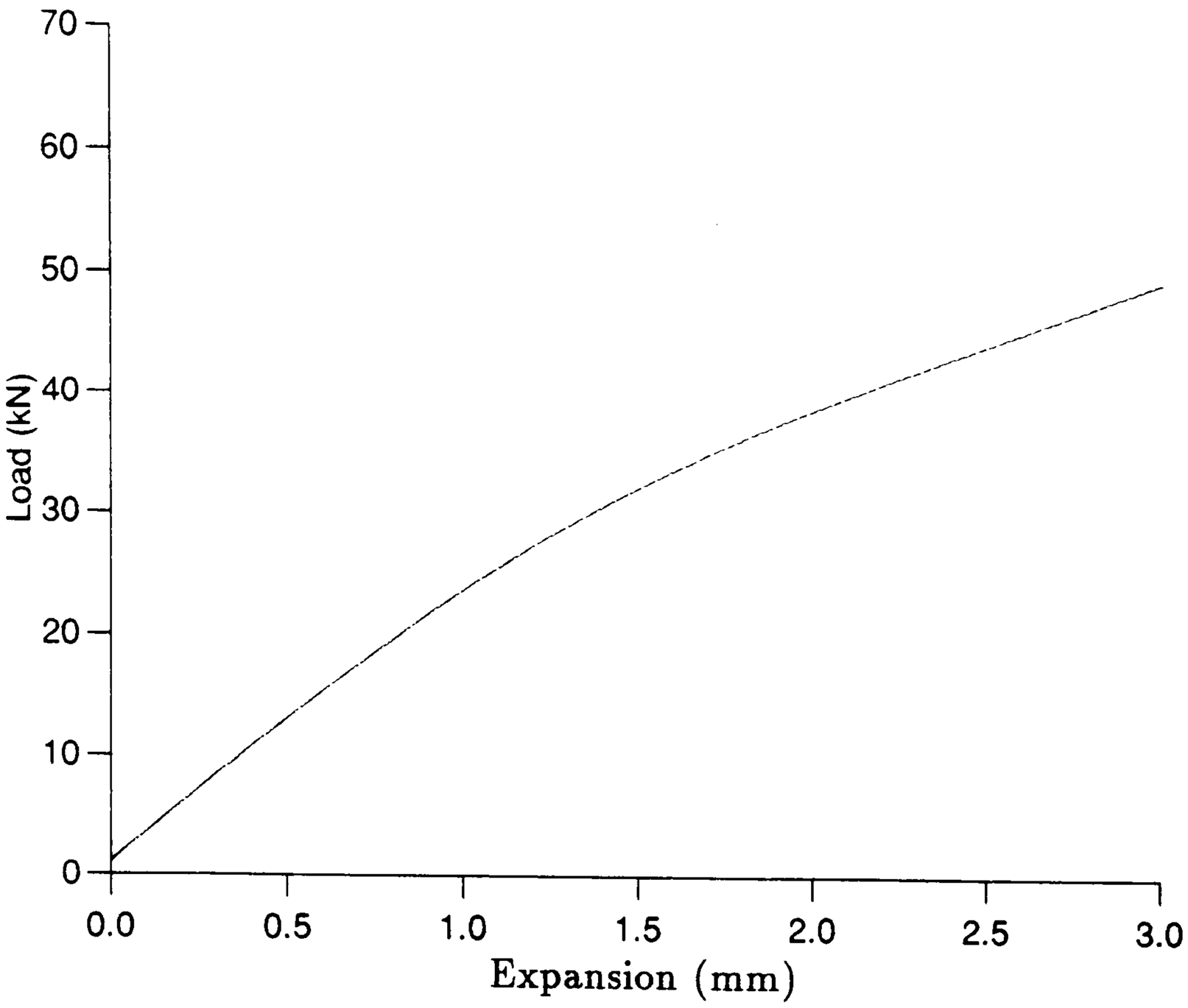


Figure 5.8: Load-expansion relationship for beam CBM2

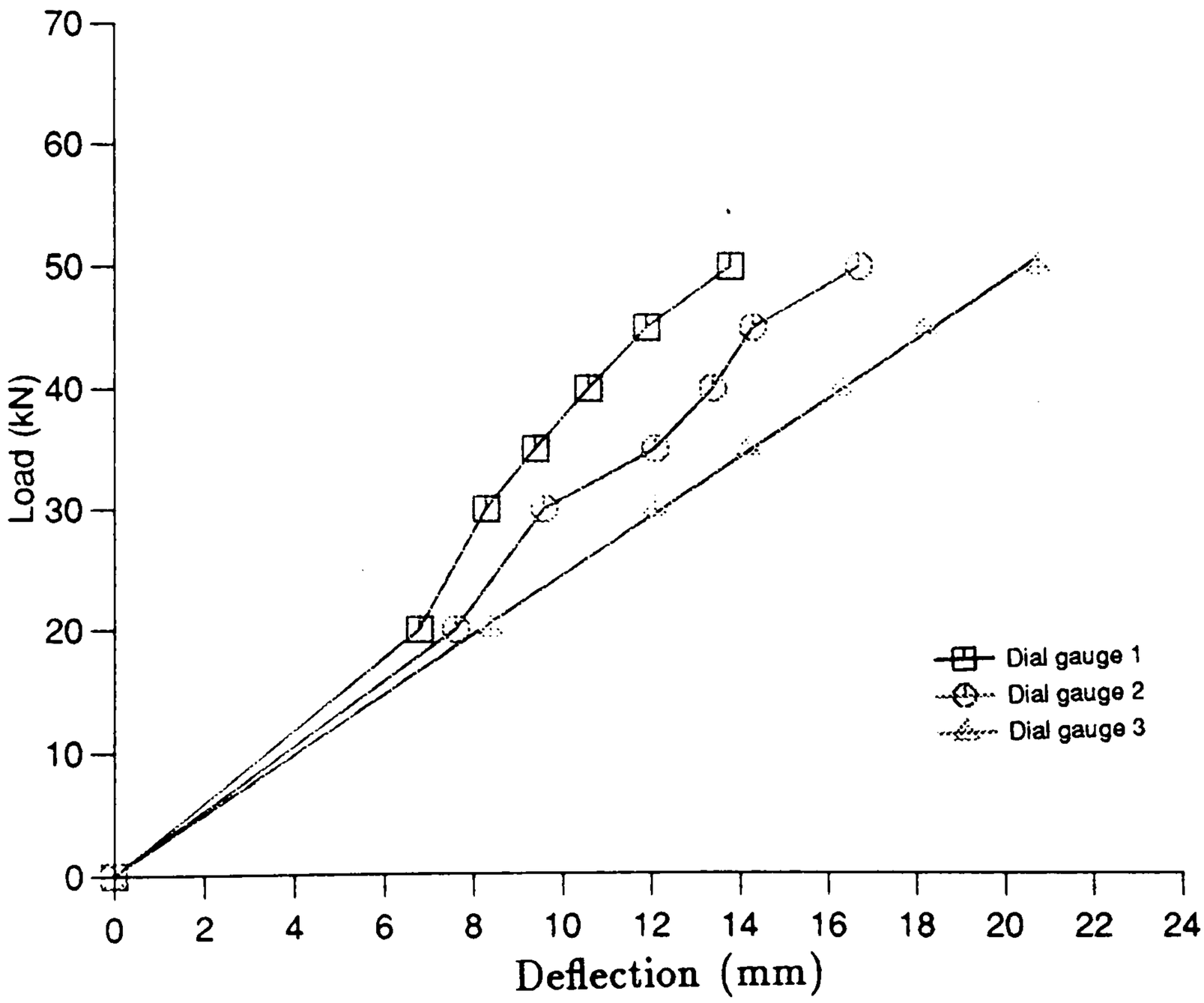


Figure 5.9: Load-deflection relationships for beam CBM2

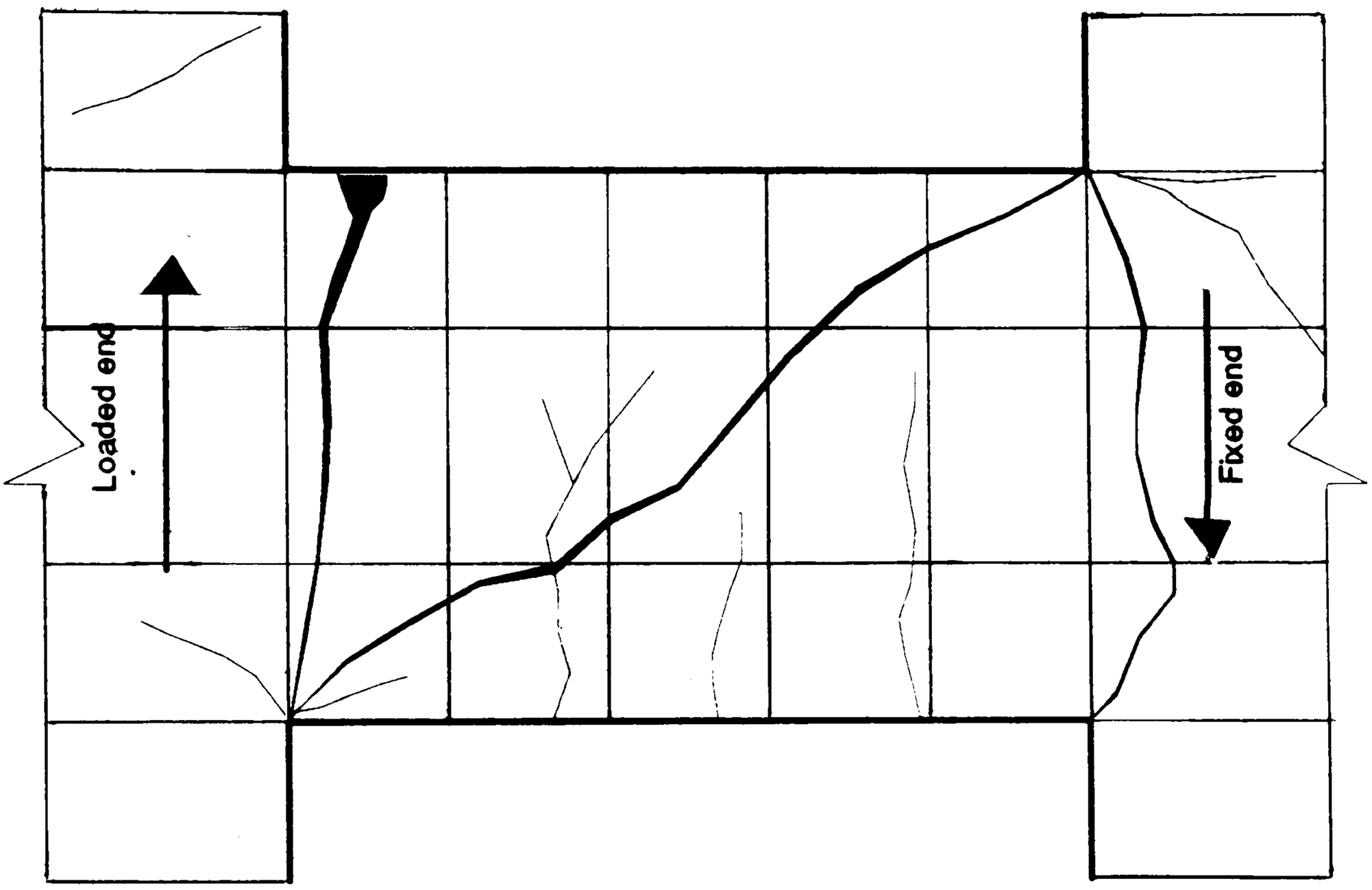


Figure 5.10: Failure mechanism and crack pattern for beam CBM2

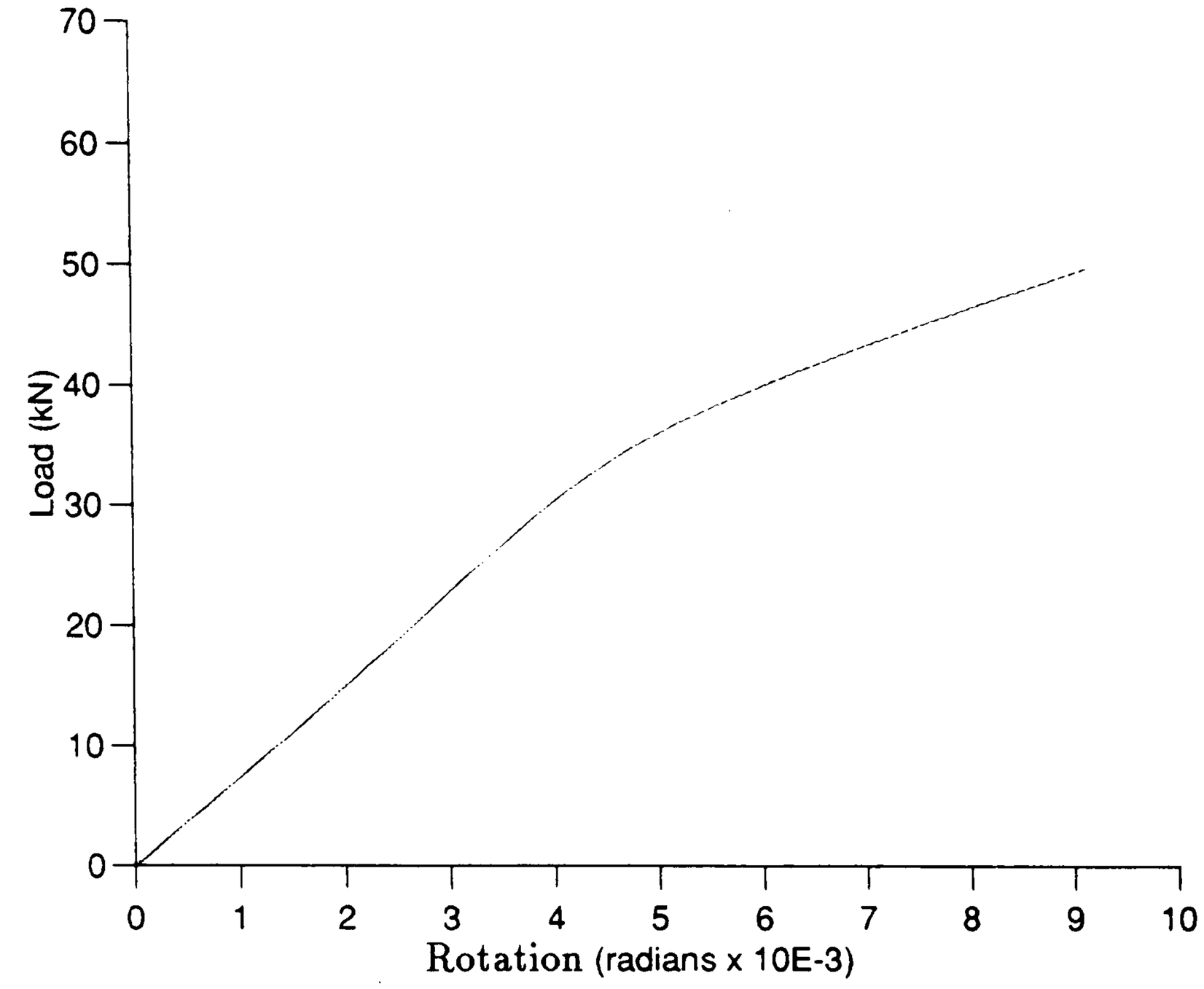


Figure 5.11: Load-rotation relationship for beam EBM1

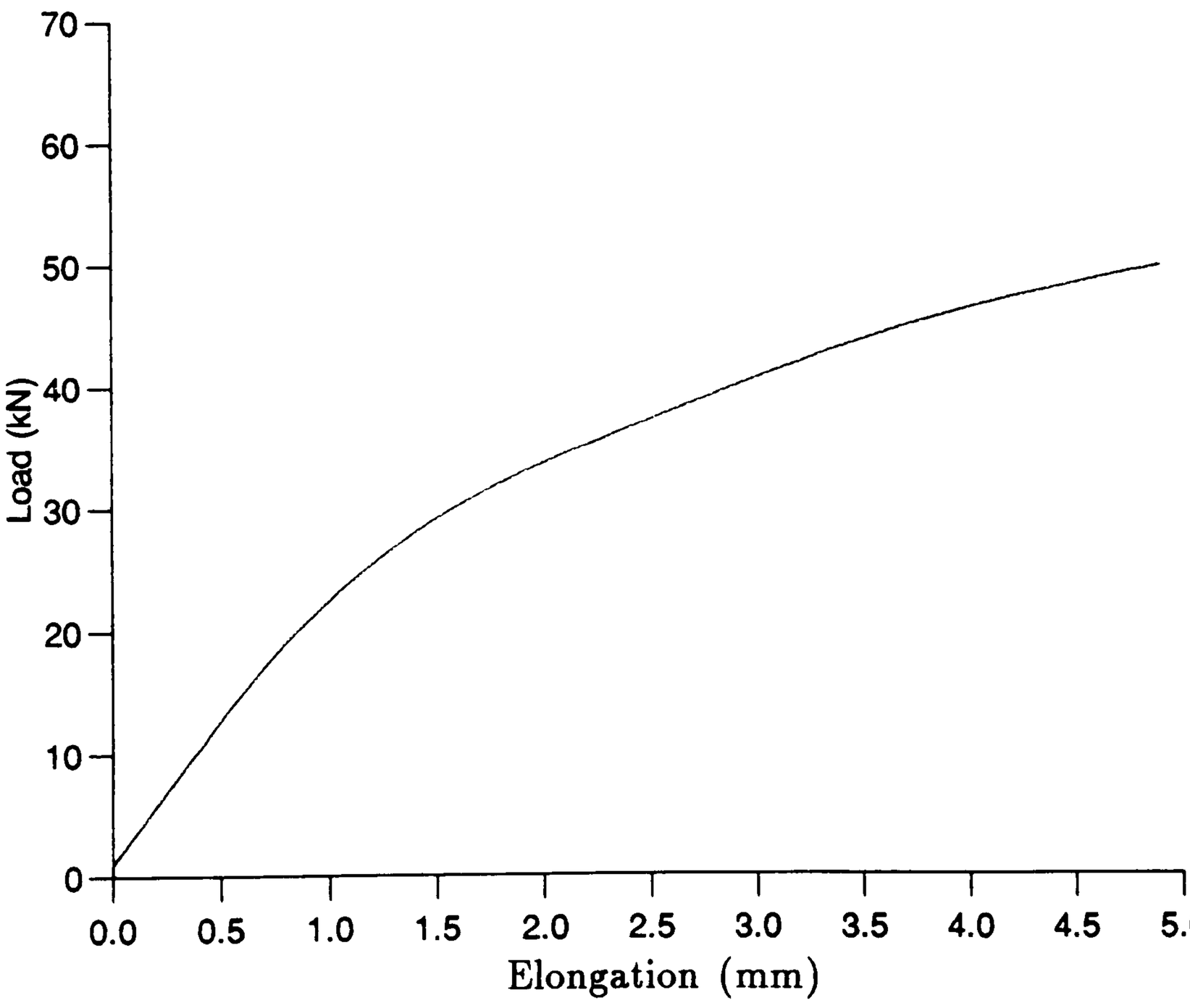


Figure 5.12: Load-elongation relationship for beam EBM1

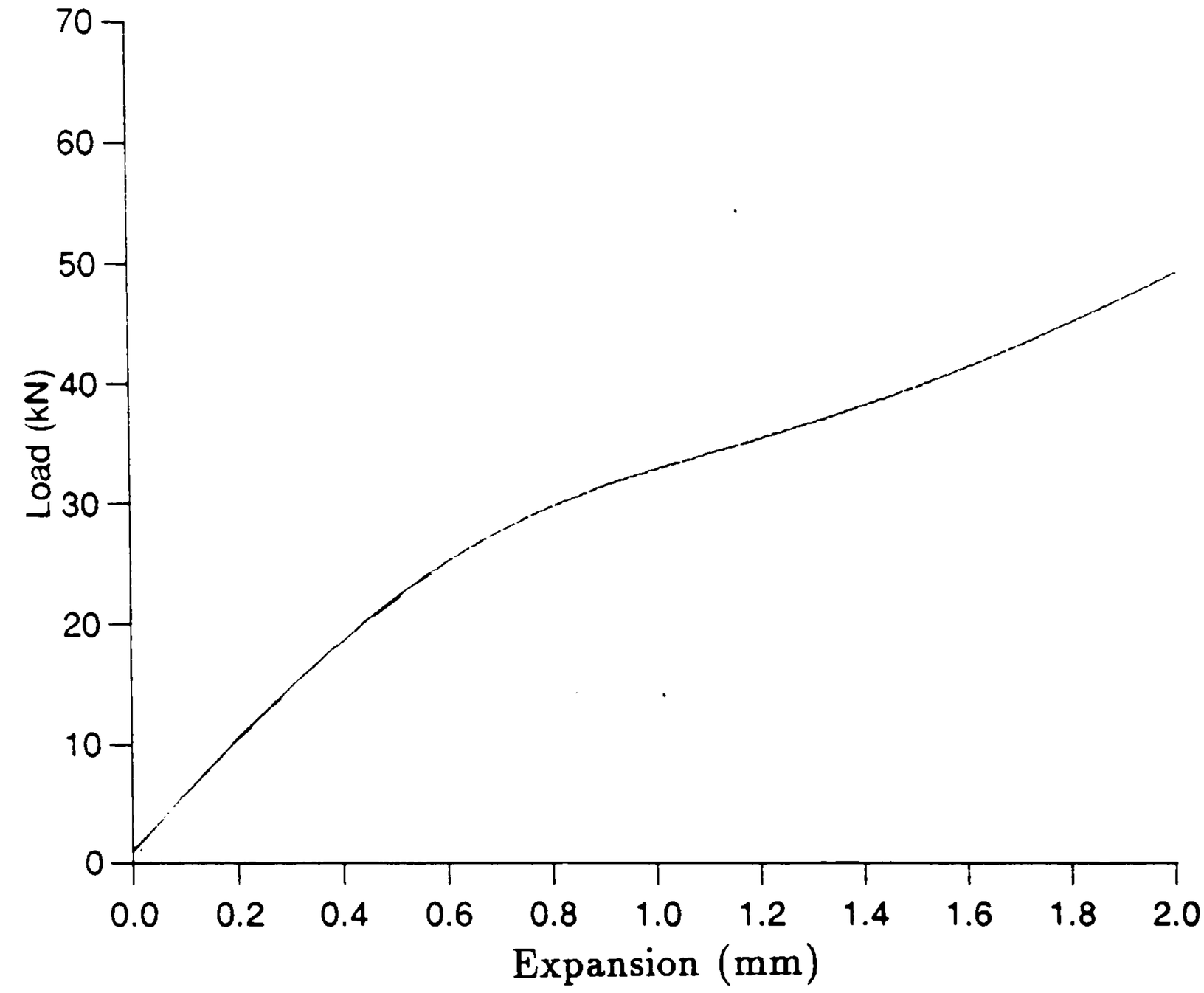


Figure 5.13: Load-expansion relationship for beam EBM1

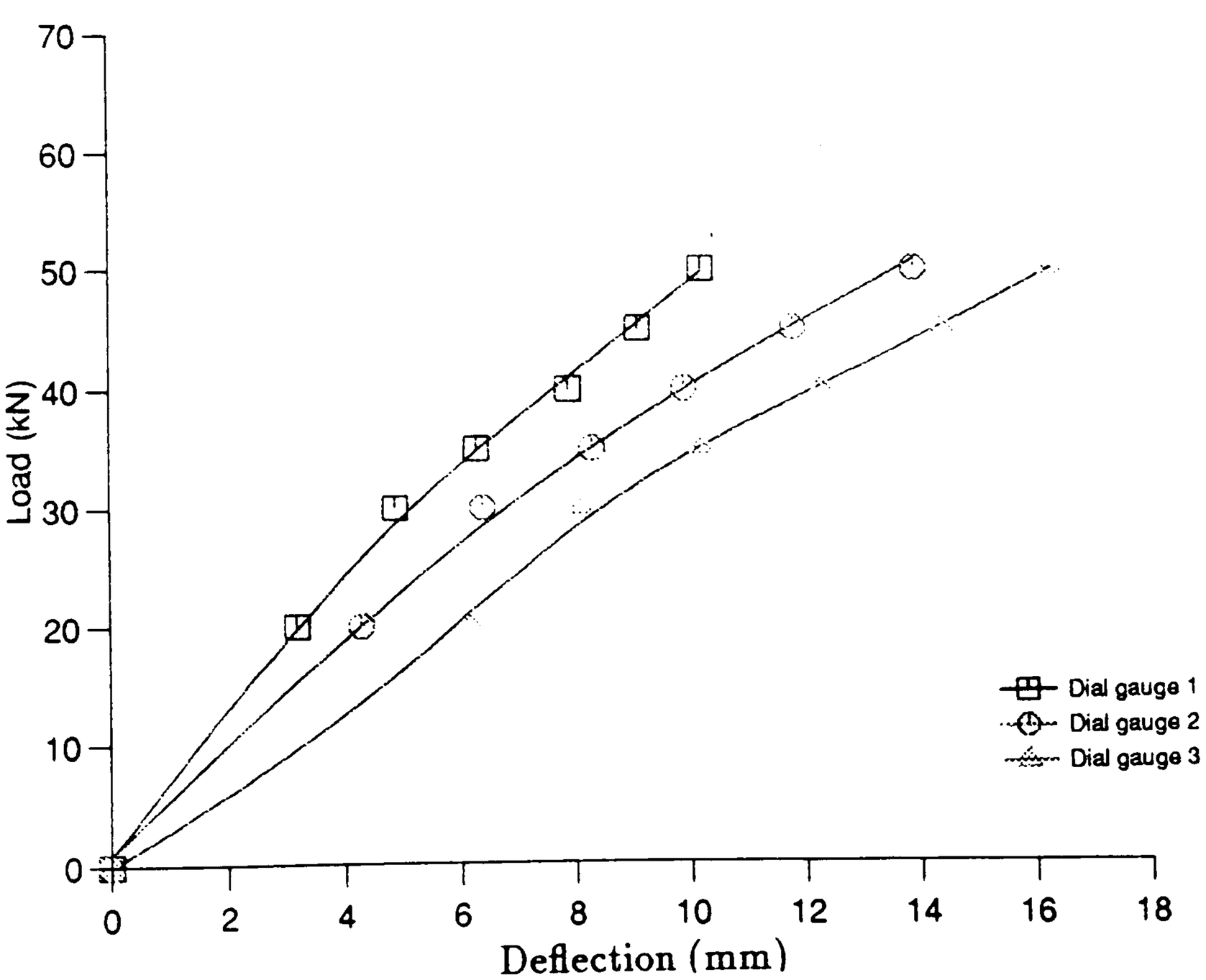


Figure 5.14: Load-deflection relationships for beam EBM1

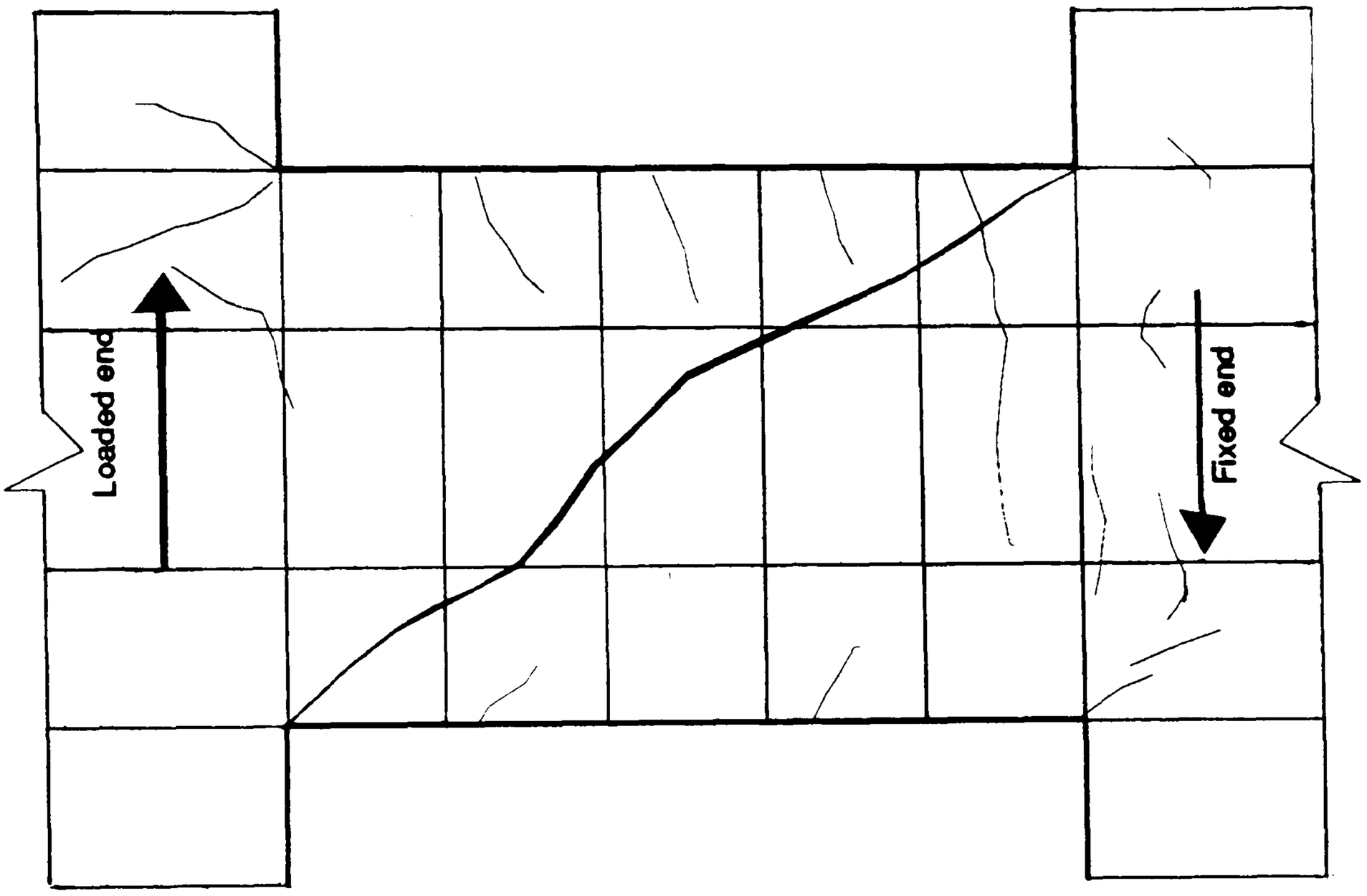


Figure 5.15: Failure mechanism and crack pattern for beam EBM1

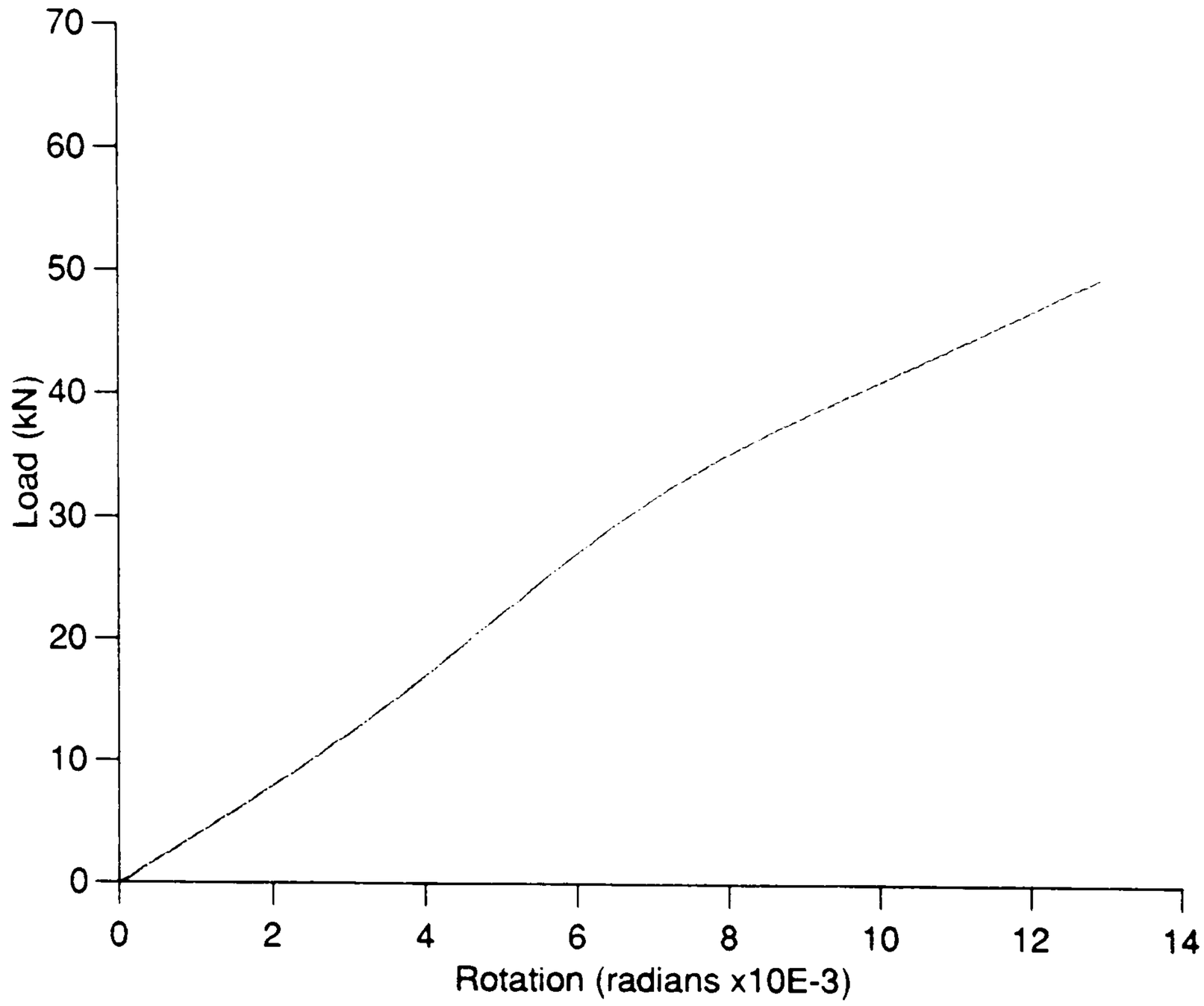


Figure 5.16: Load-rotation relationship for beam EBM2

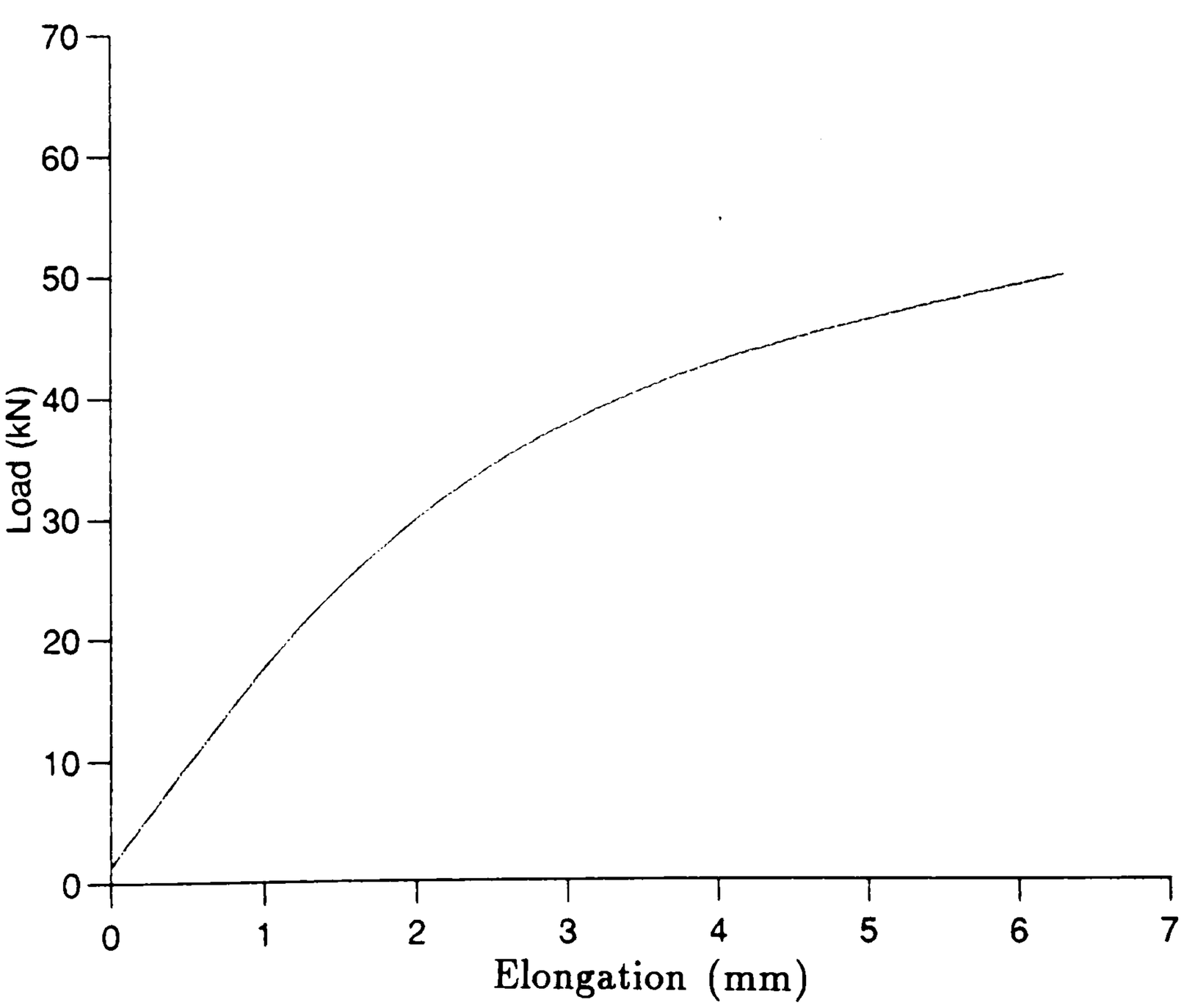


Figure 5.17: Load-elongation relationship for beam EBM2

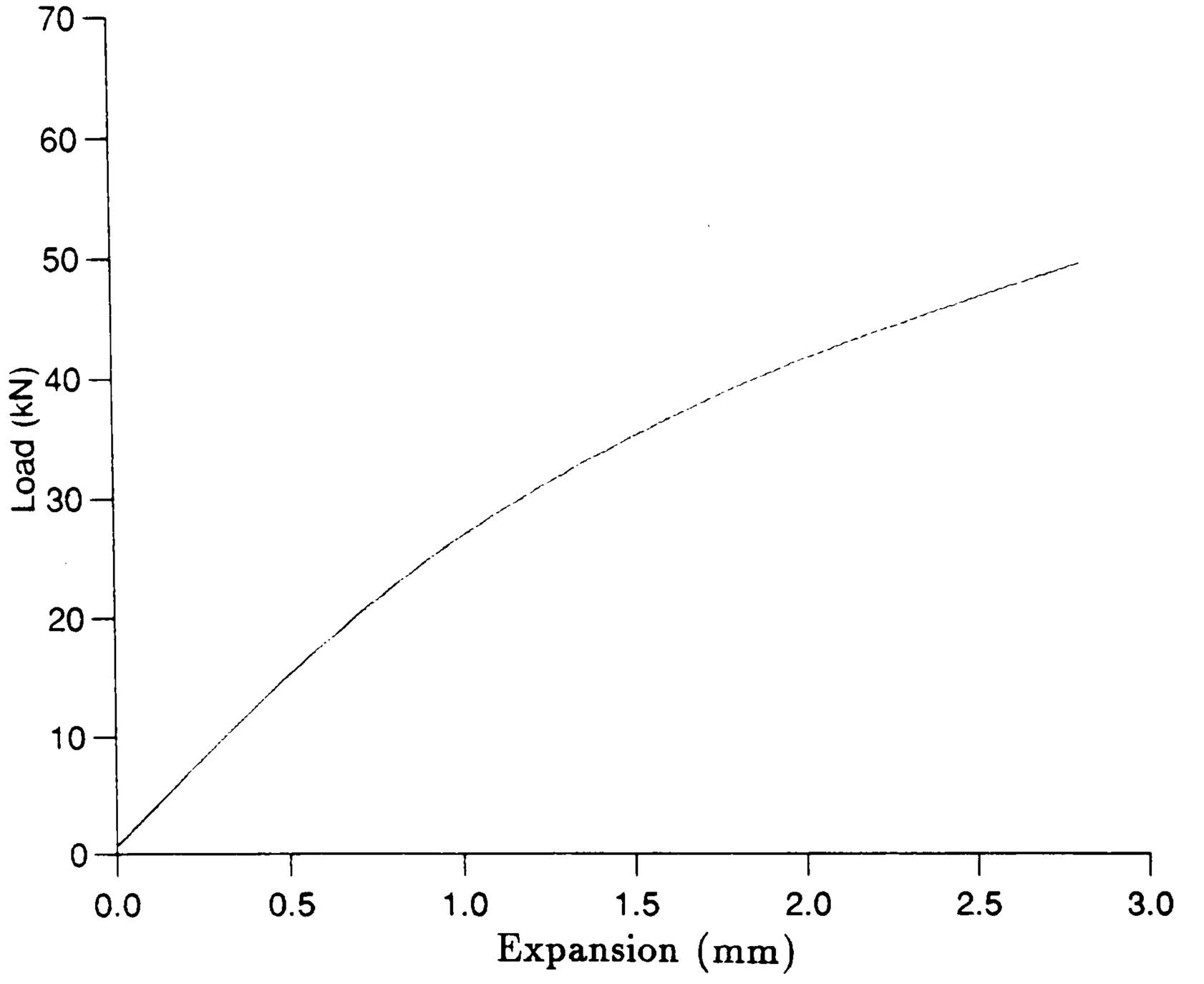


Figure 5.18: Load-expansion relationship for beam EBM2

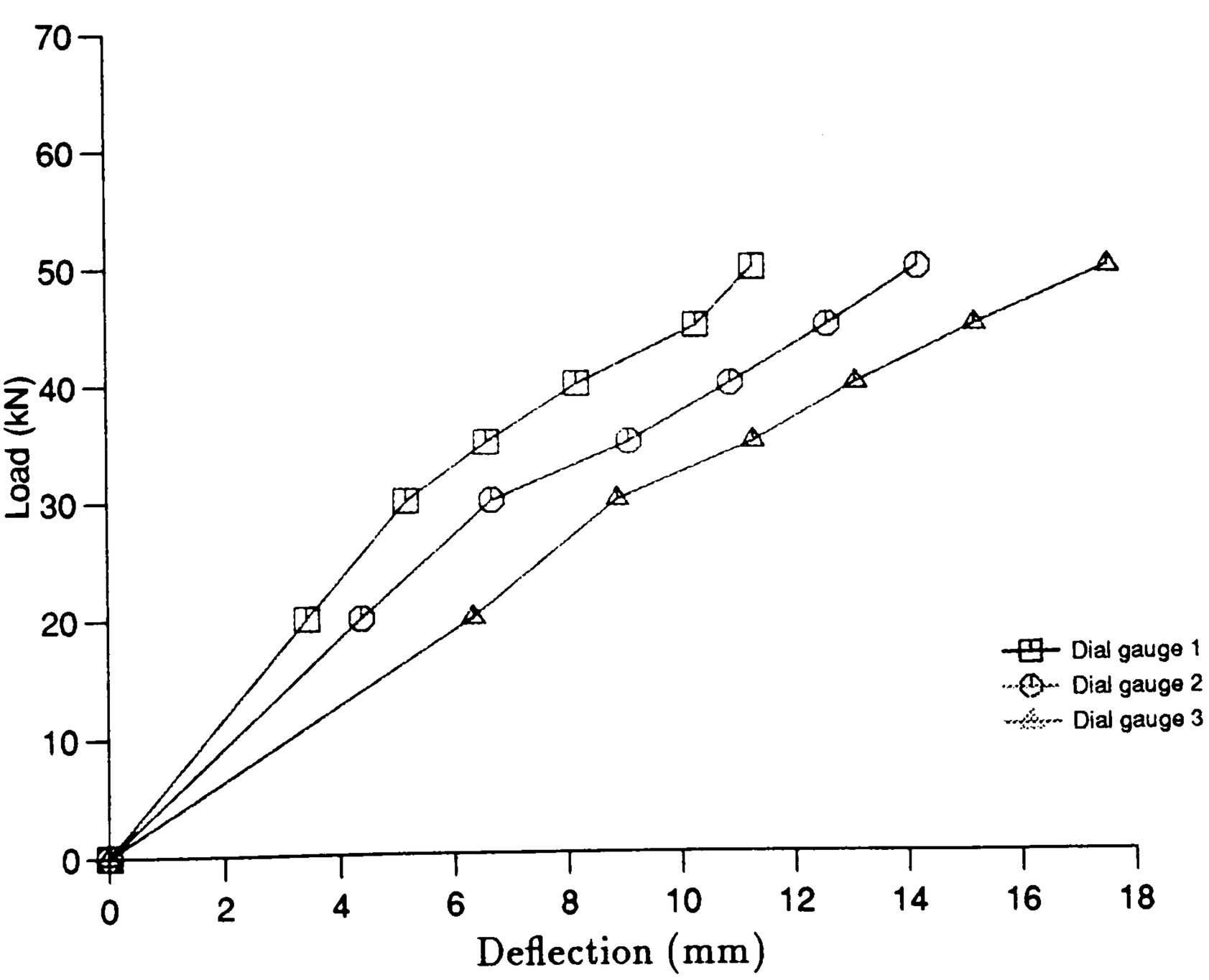


Figure 5.19: Load-deflection relationships for beam EBM2

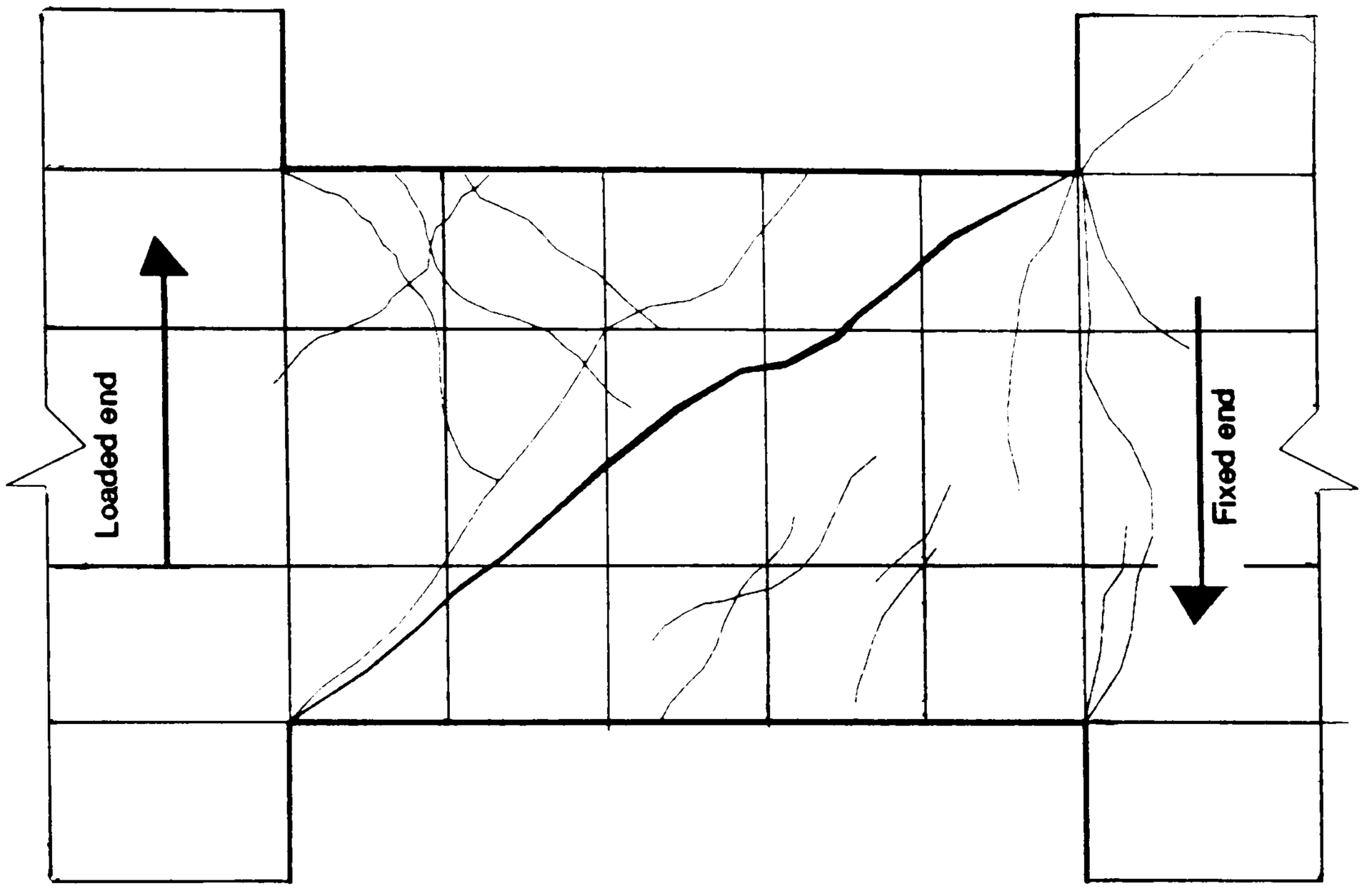


Figure 5.20: Failure mechanism and crack pattern for beam EBM2

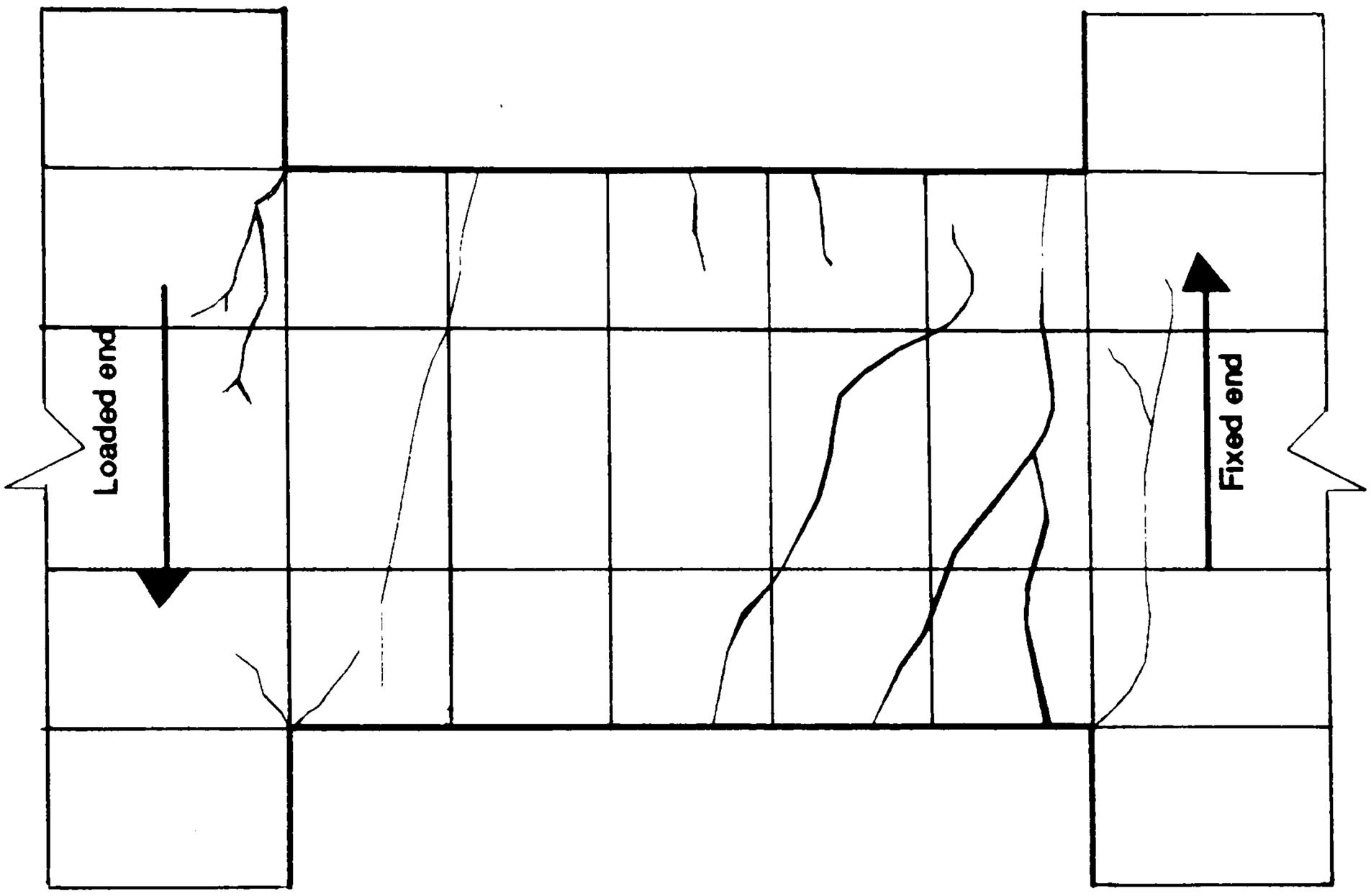


Figure 5.21: Failure mechanism and crack pattern for beam CBD1

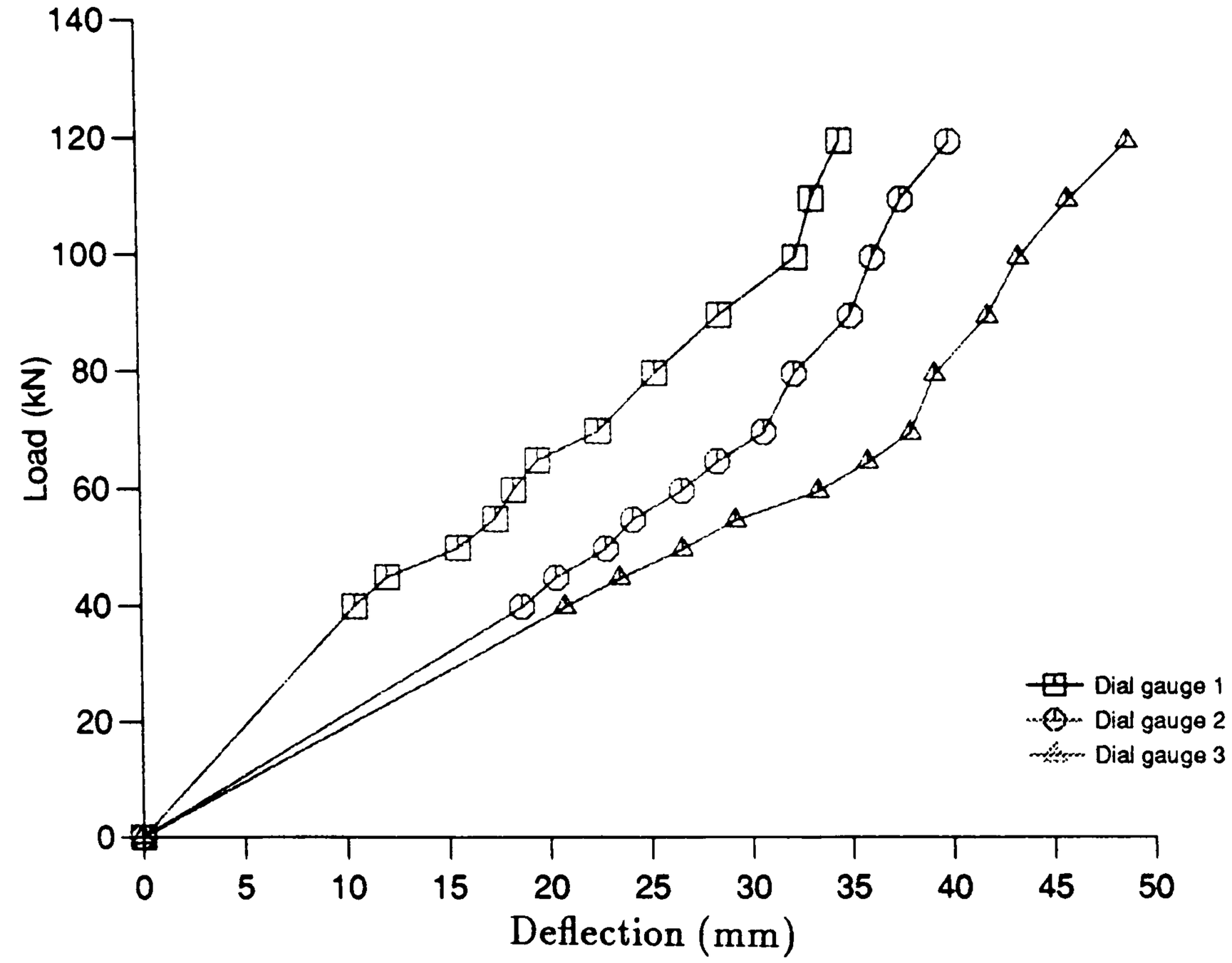


Figure 5.22: Load-deflection relationships for beam CBD1

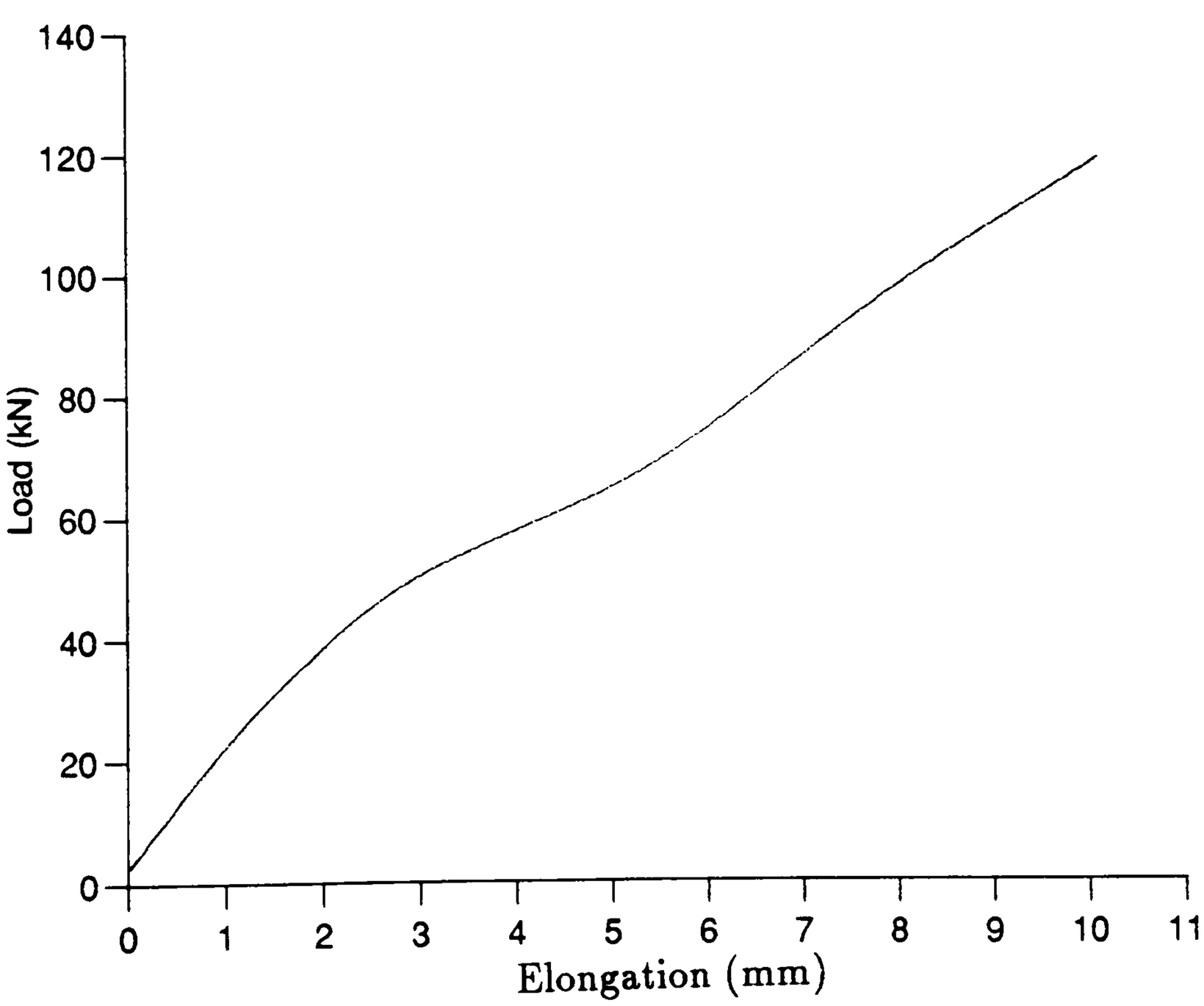


Figure 5.23: Load-elongation relationship for beam CBD1

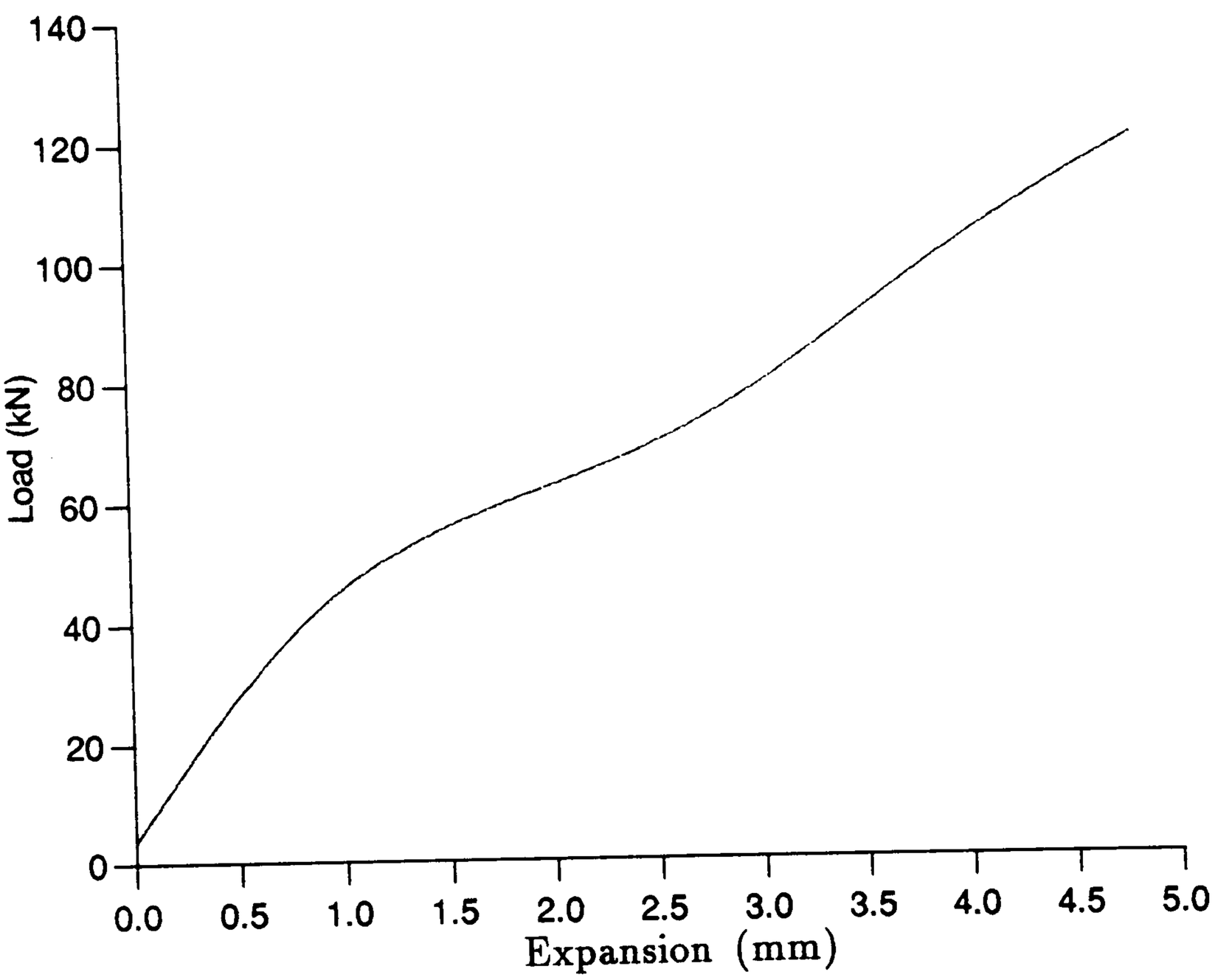


Figure 5.24: Load-expansion relationship for beam CBD1

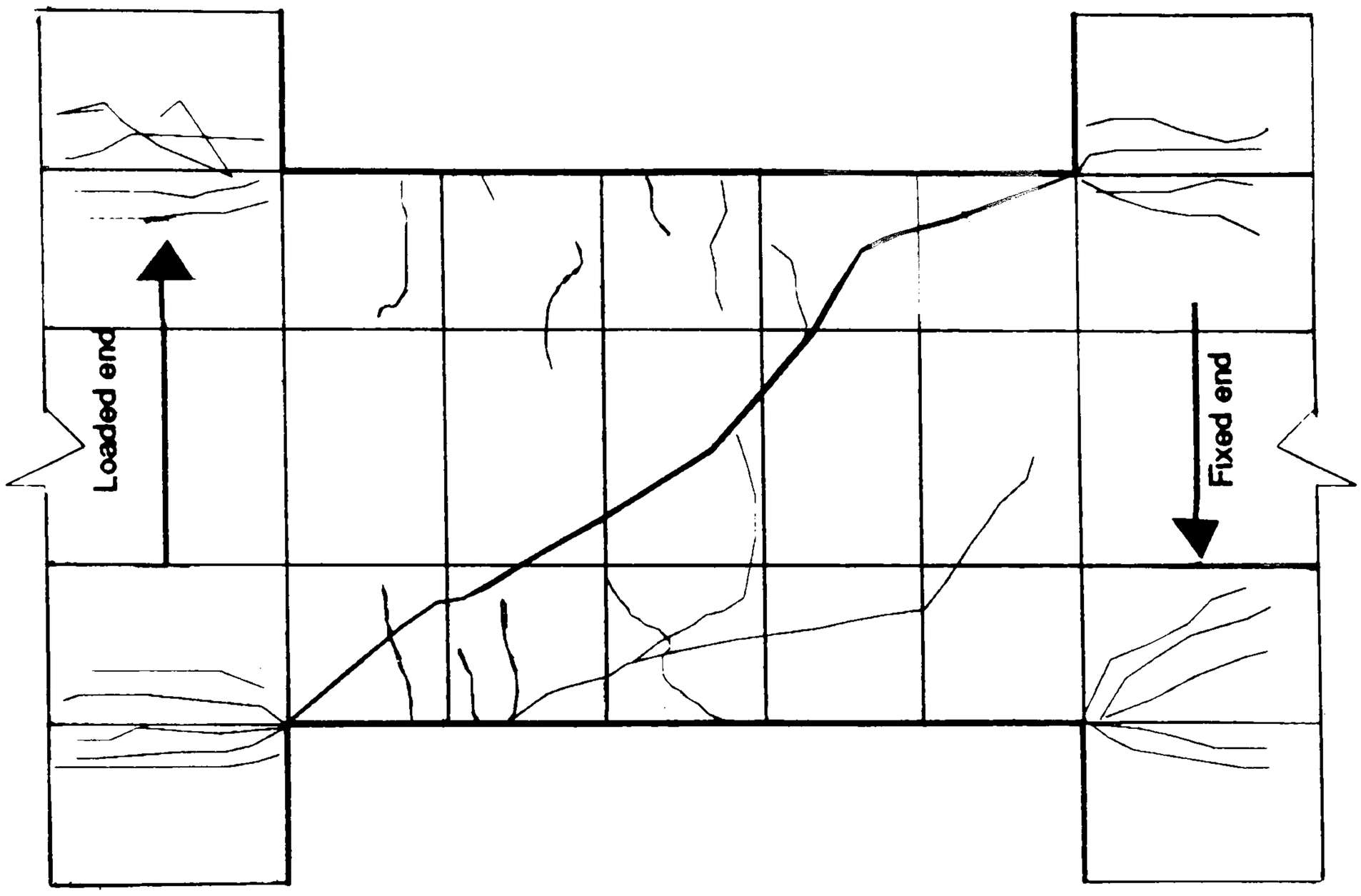


Figure 5.25: Failure mechanism and crack pattern for beam EBD1

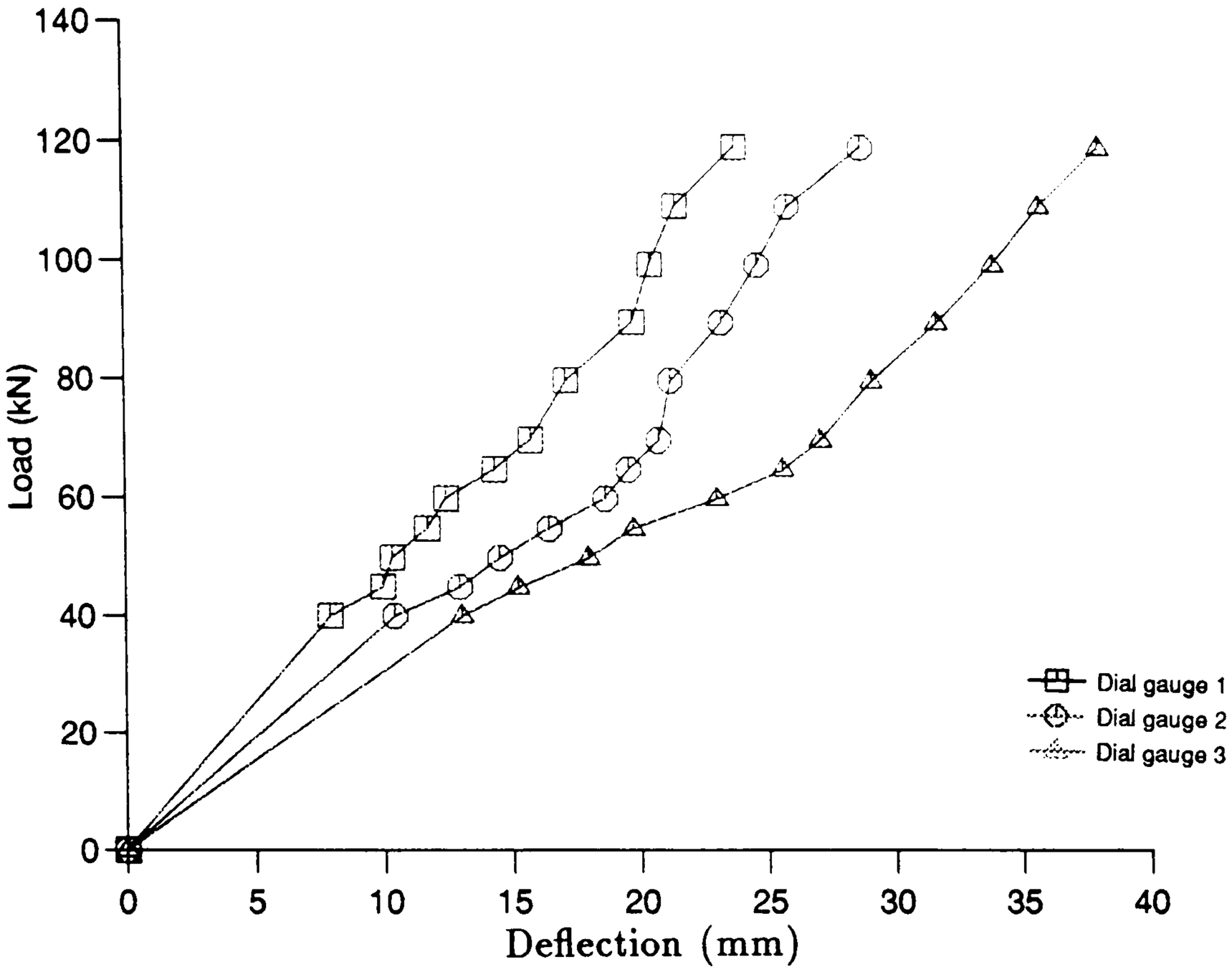


Figure 5.26: Load-deflection relationships for beam EBD1

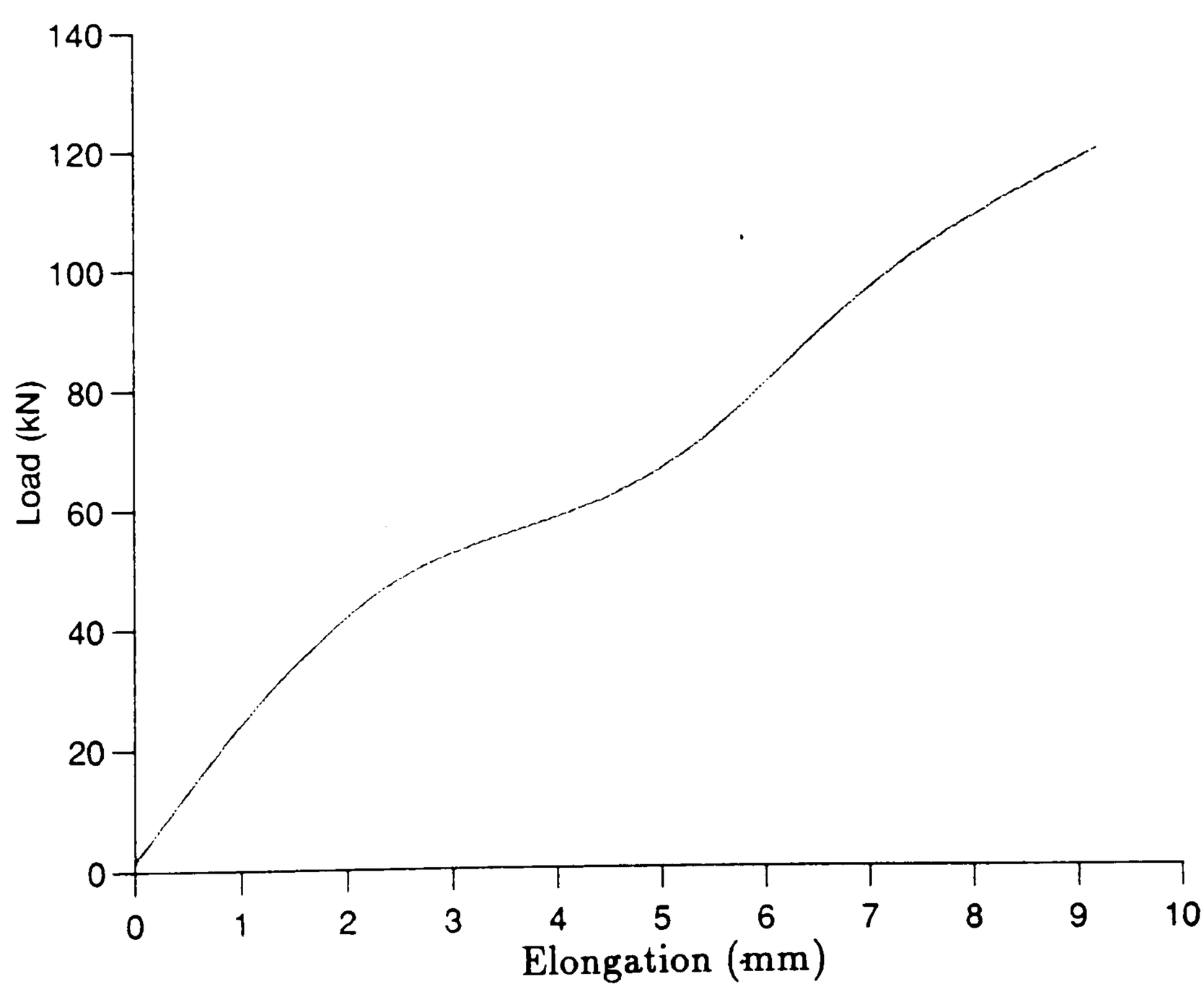


Figure 5.27: Load-elongation relationship for beam CBD1

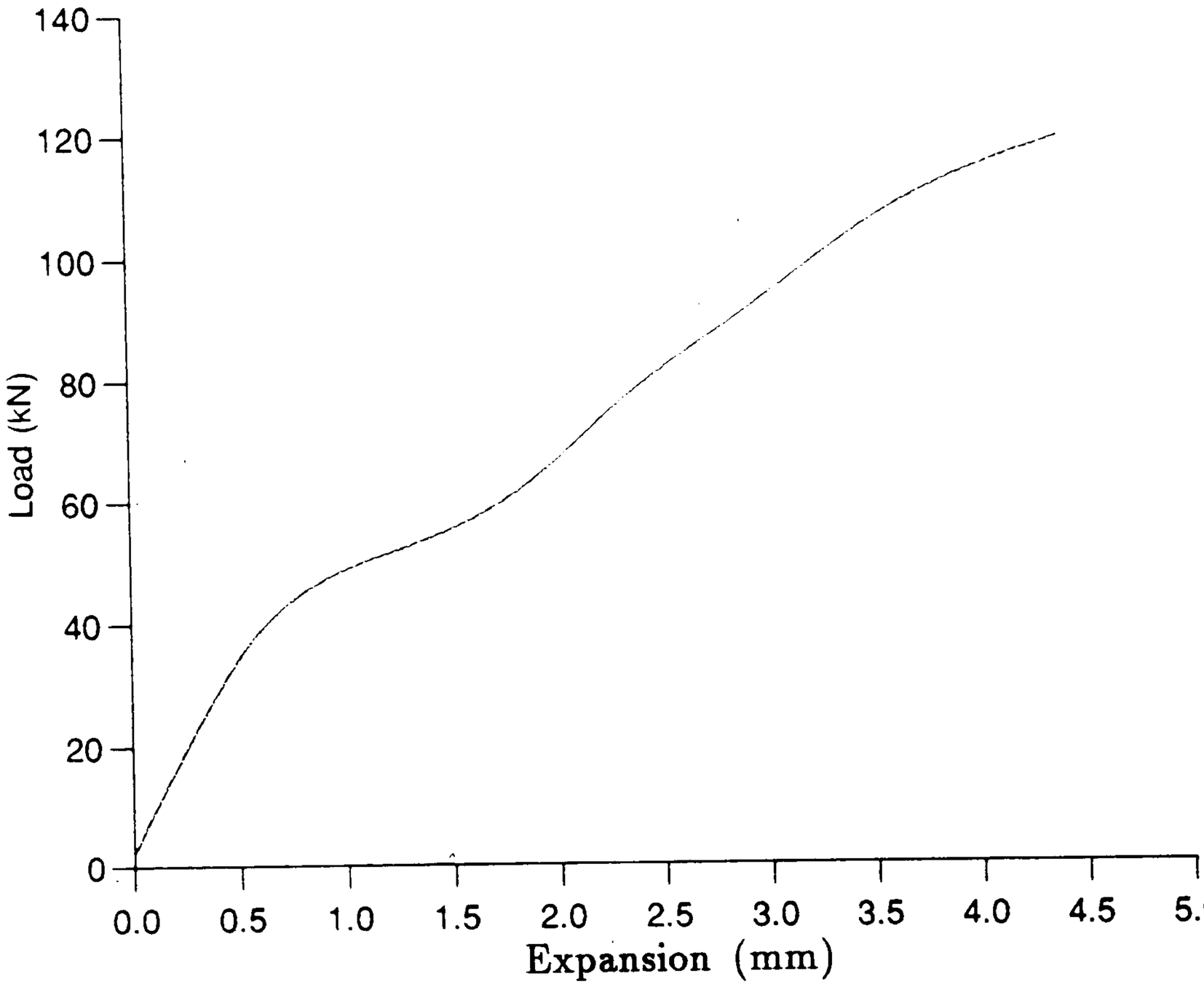


Figure 5.28: Load-Expansion relationship for beam CBD1

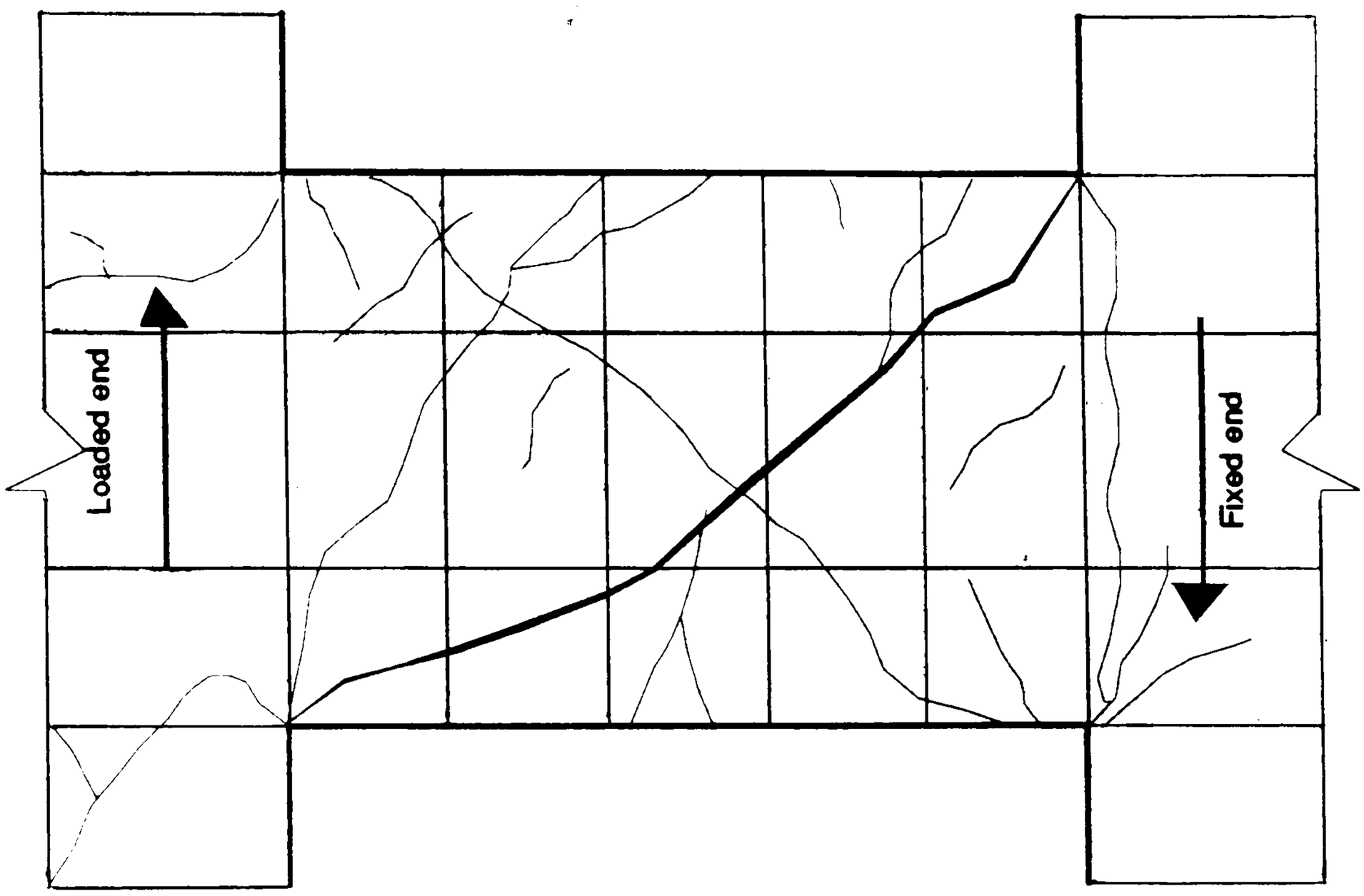


Figure 5.29: Failure mechanism and crack pattern for beam CBS1

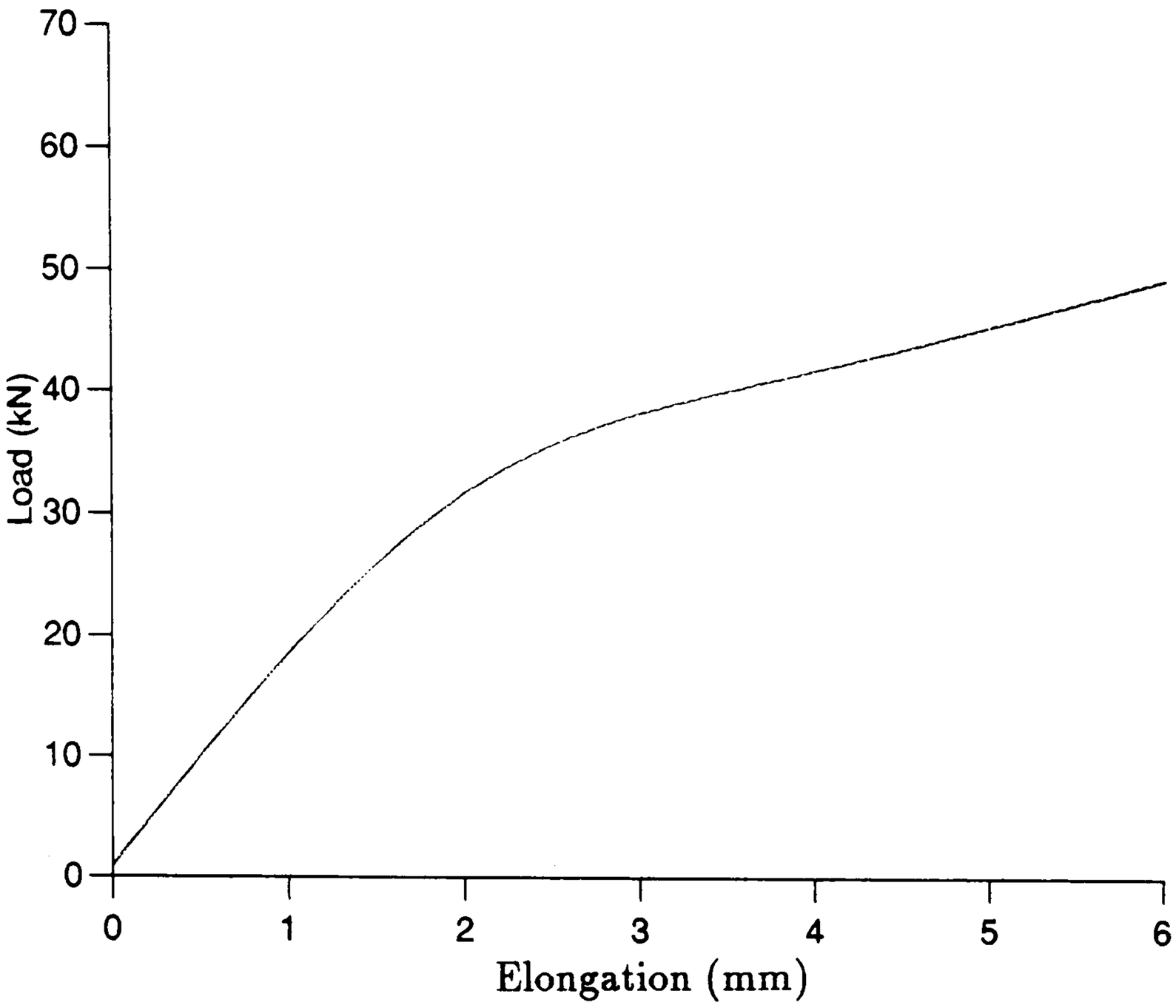


Figure 5.30: Load-elongation relationship for beam CBS1

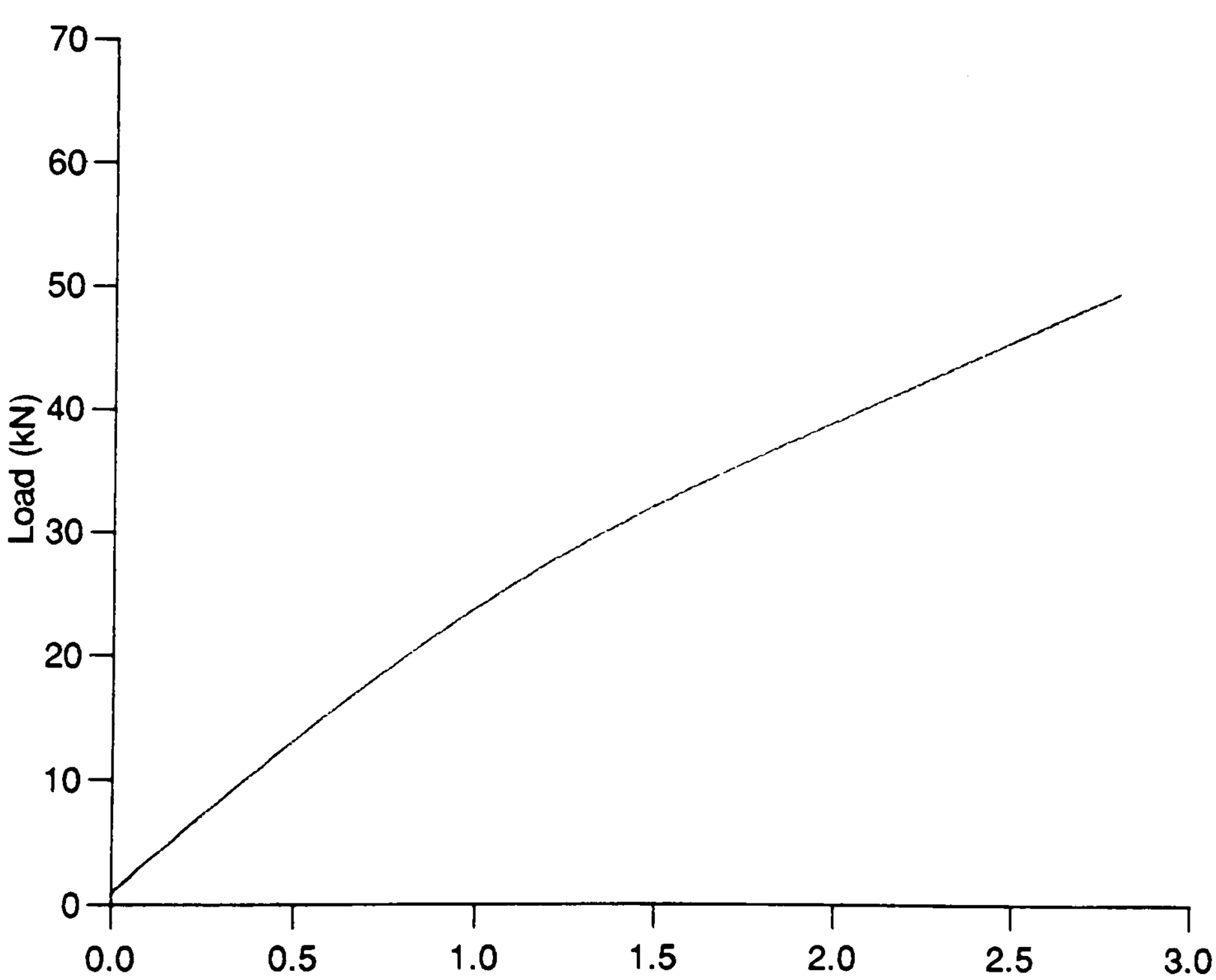


Figure 5.31: Load-expansion relationship for beam CBS1

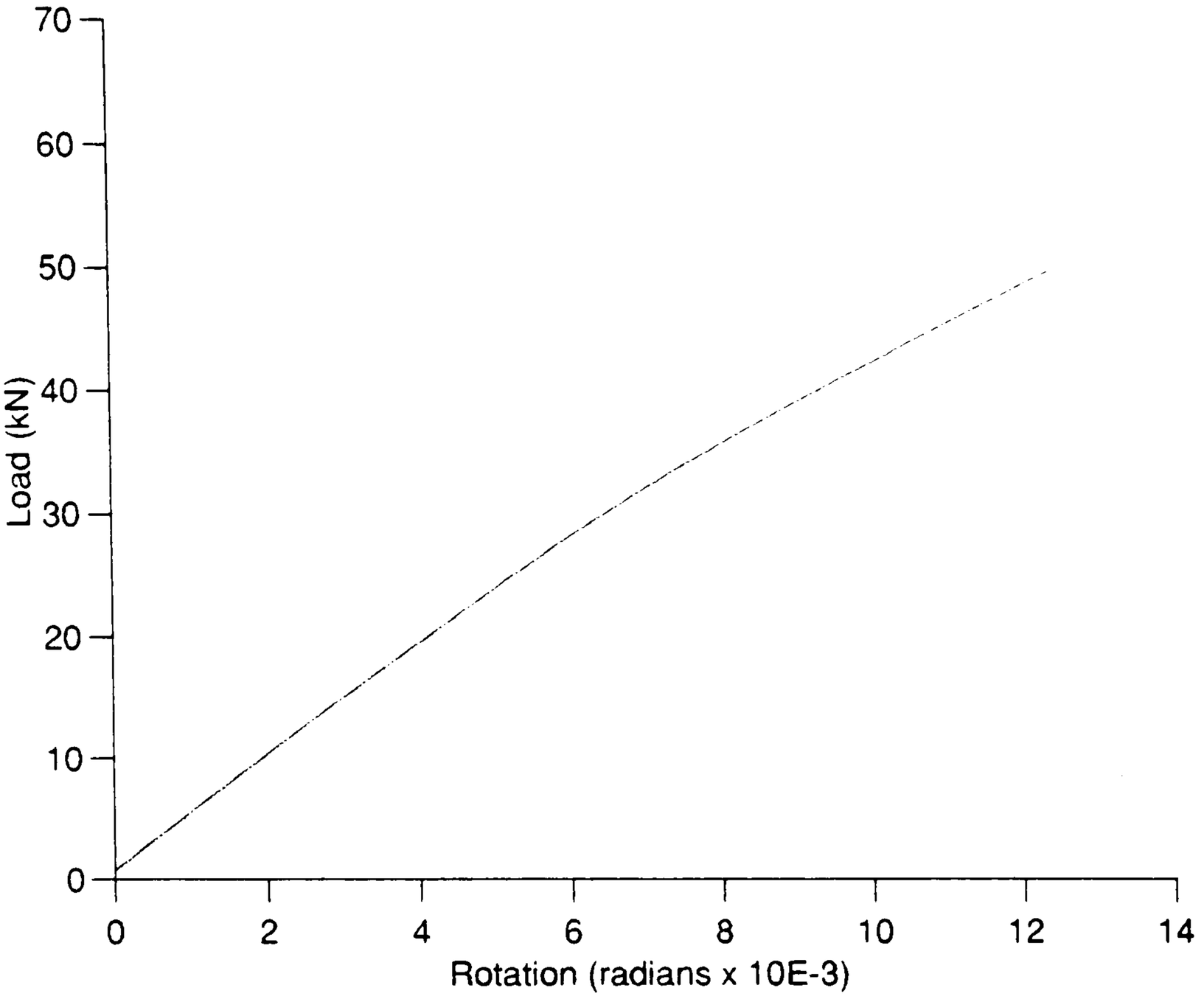


Figure 5.32: Load-rotation relationship for beam CBS1

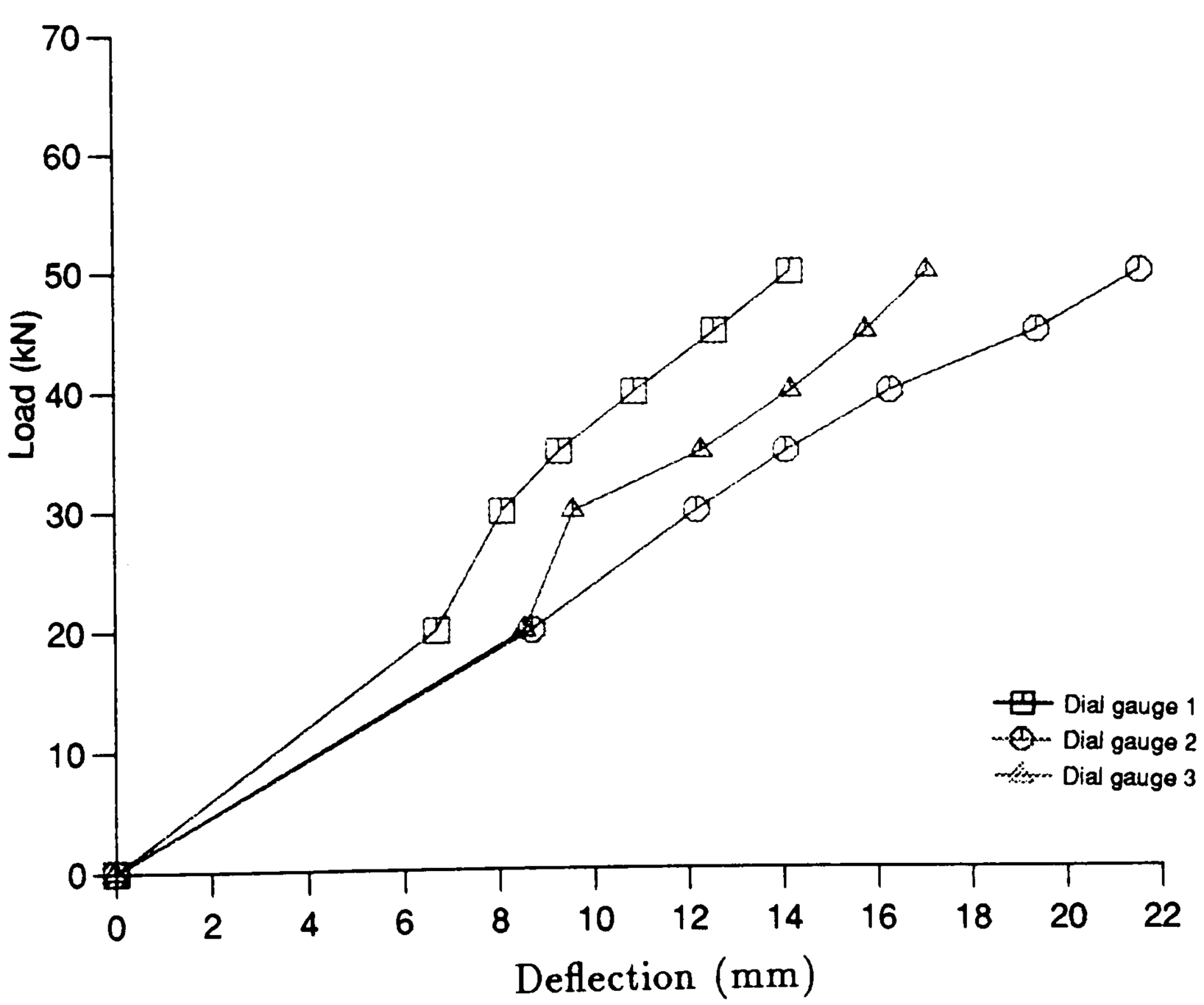


Figure 5.33: Load-deflection relationships for beam CBS1

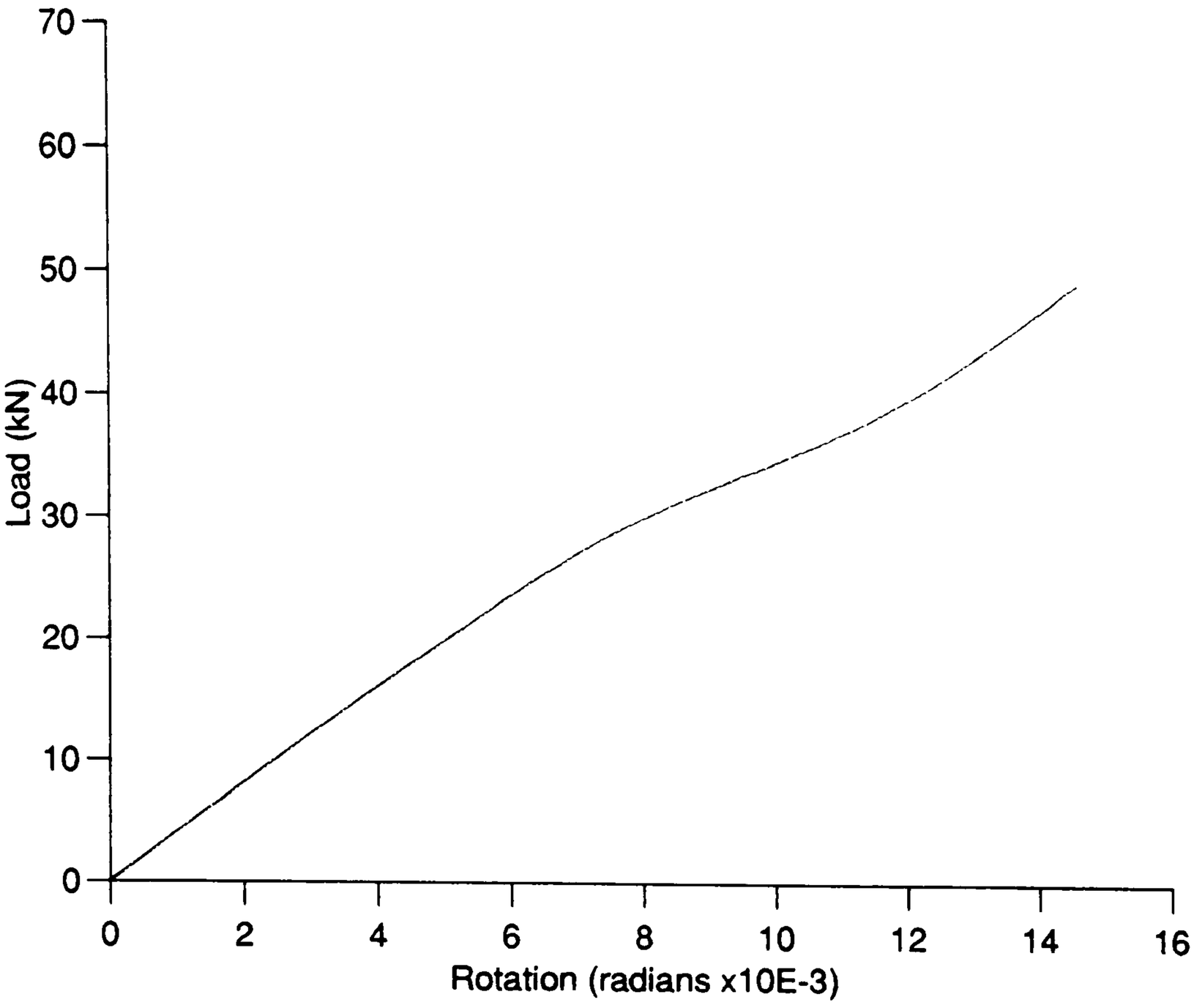


Figure 5.34: Load-rotation relationship for beam CBS2

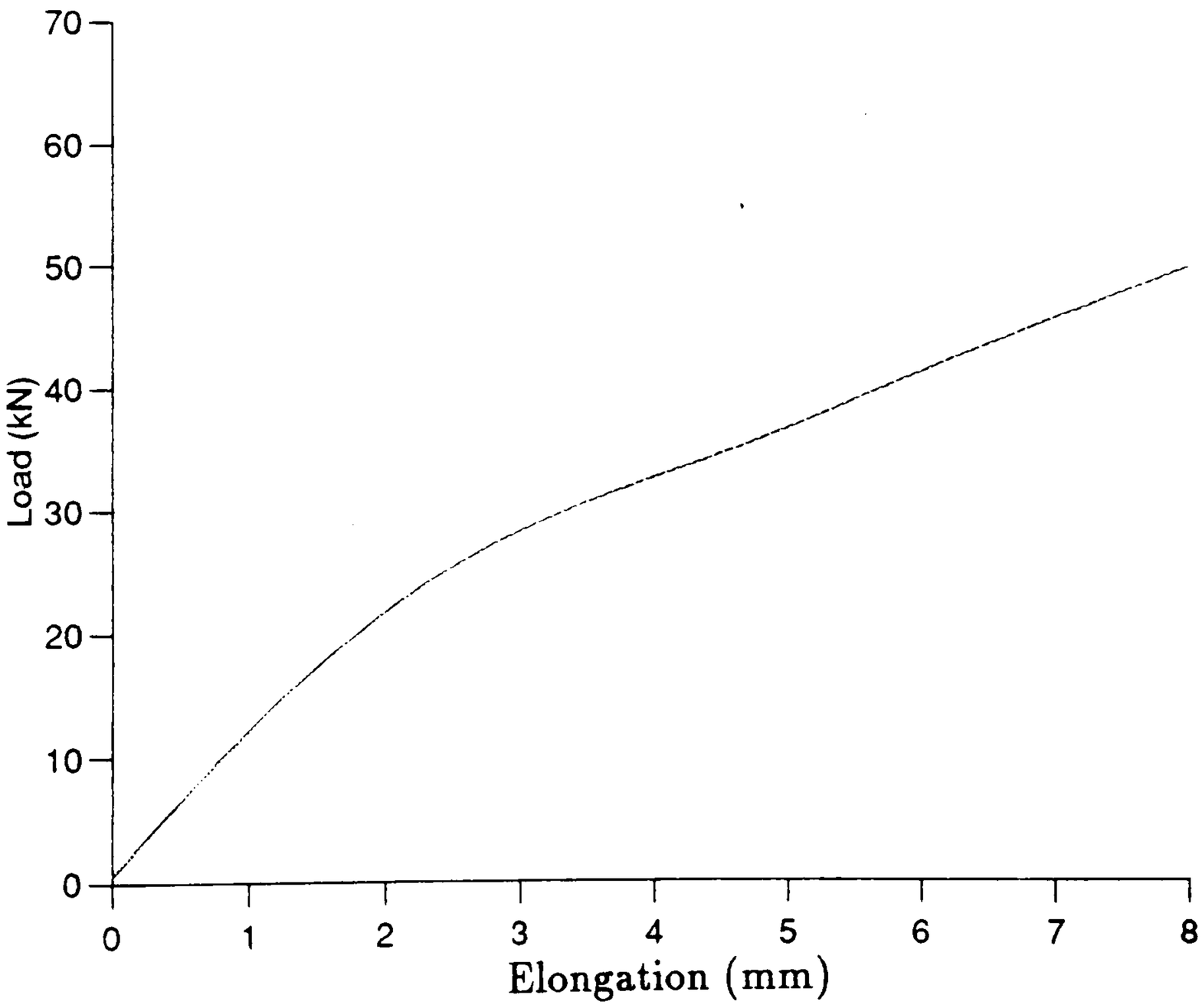


Figure 5.35: Load-elongation relationship for beam CBS2

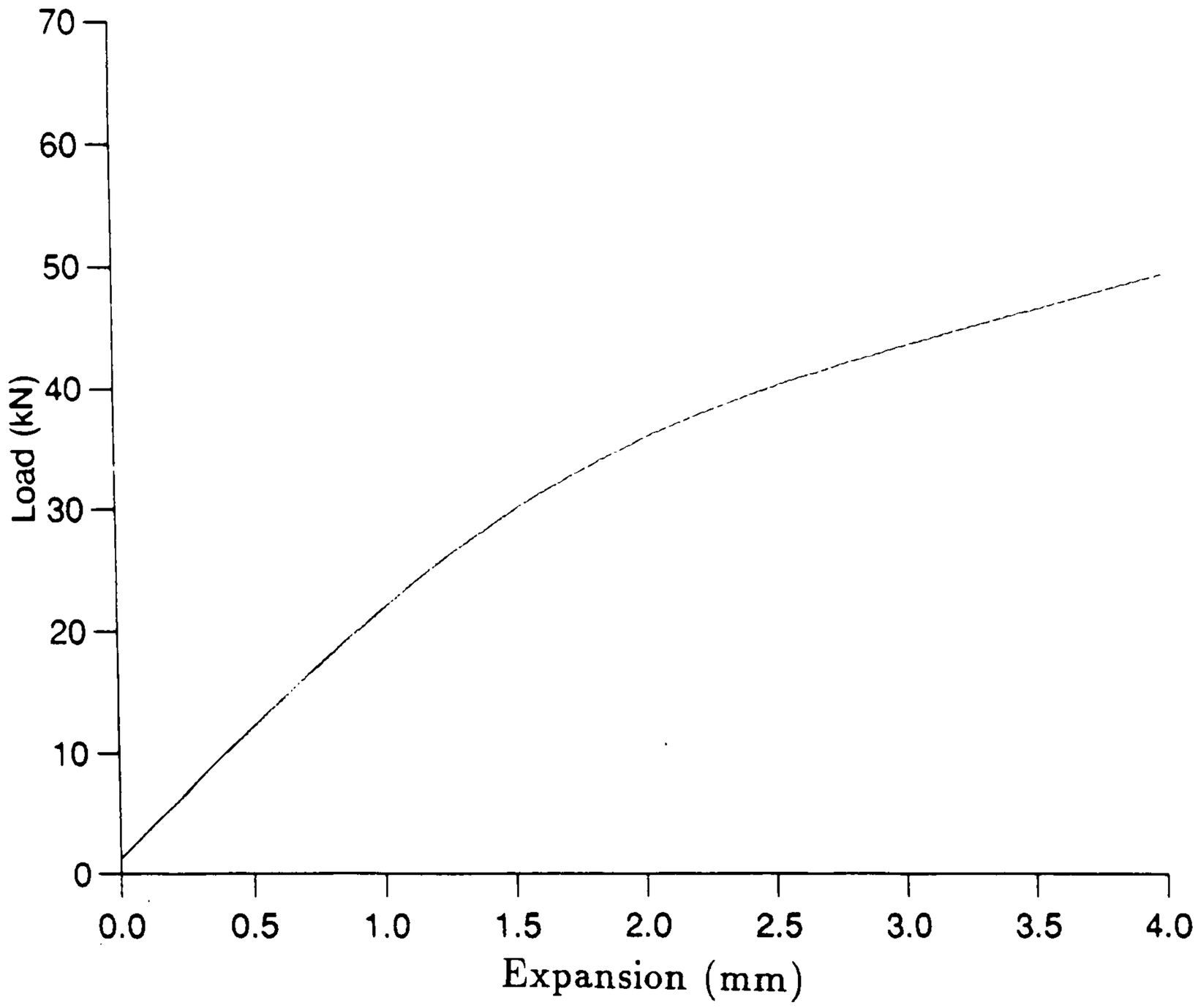


Figure 5.36: Load-expansion relationship for beam CBS2

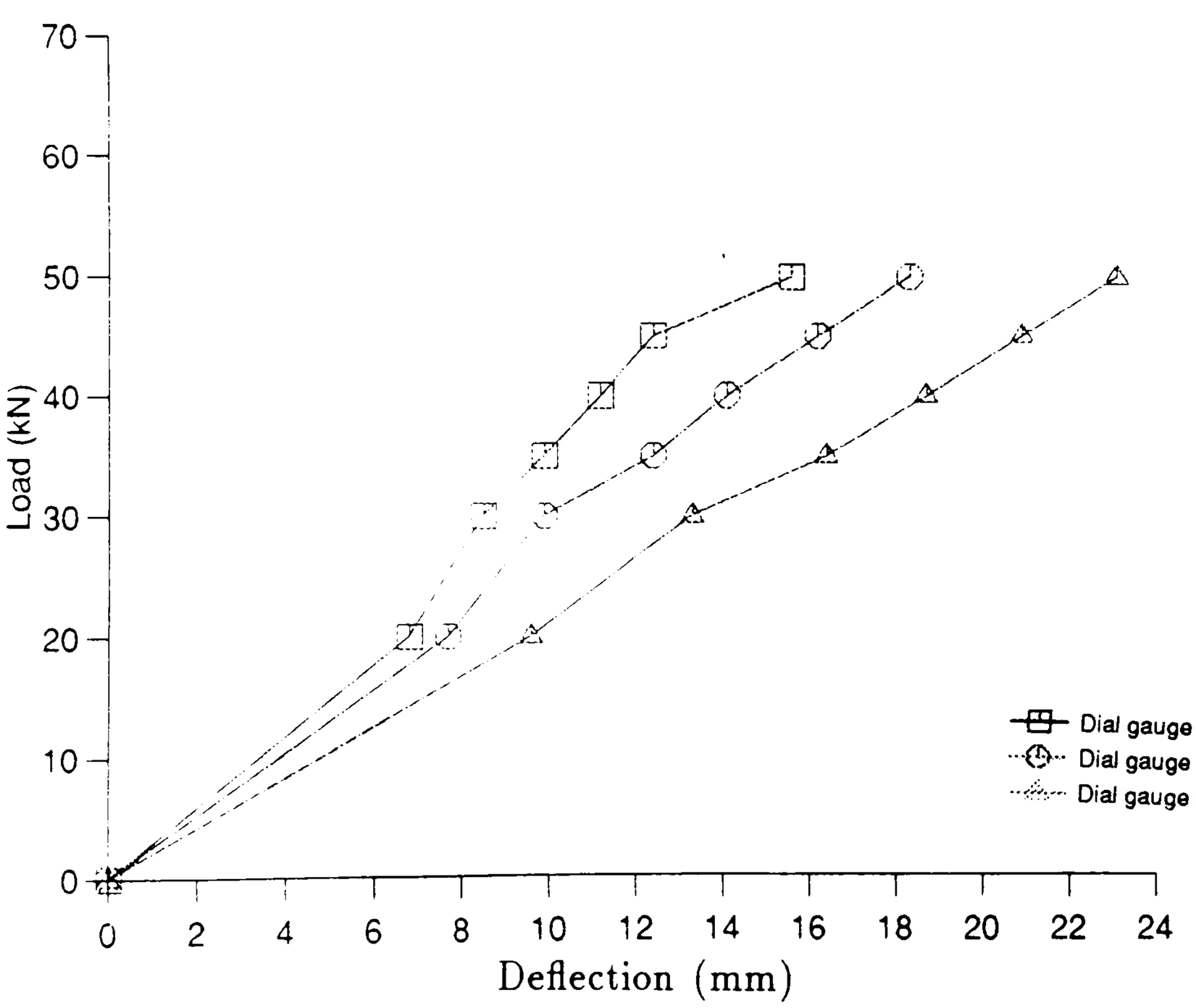


Figure 5.37: Load-deflection relationships for beam CBS2

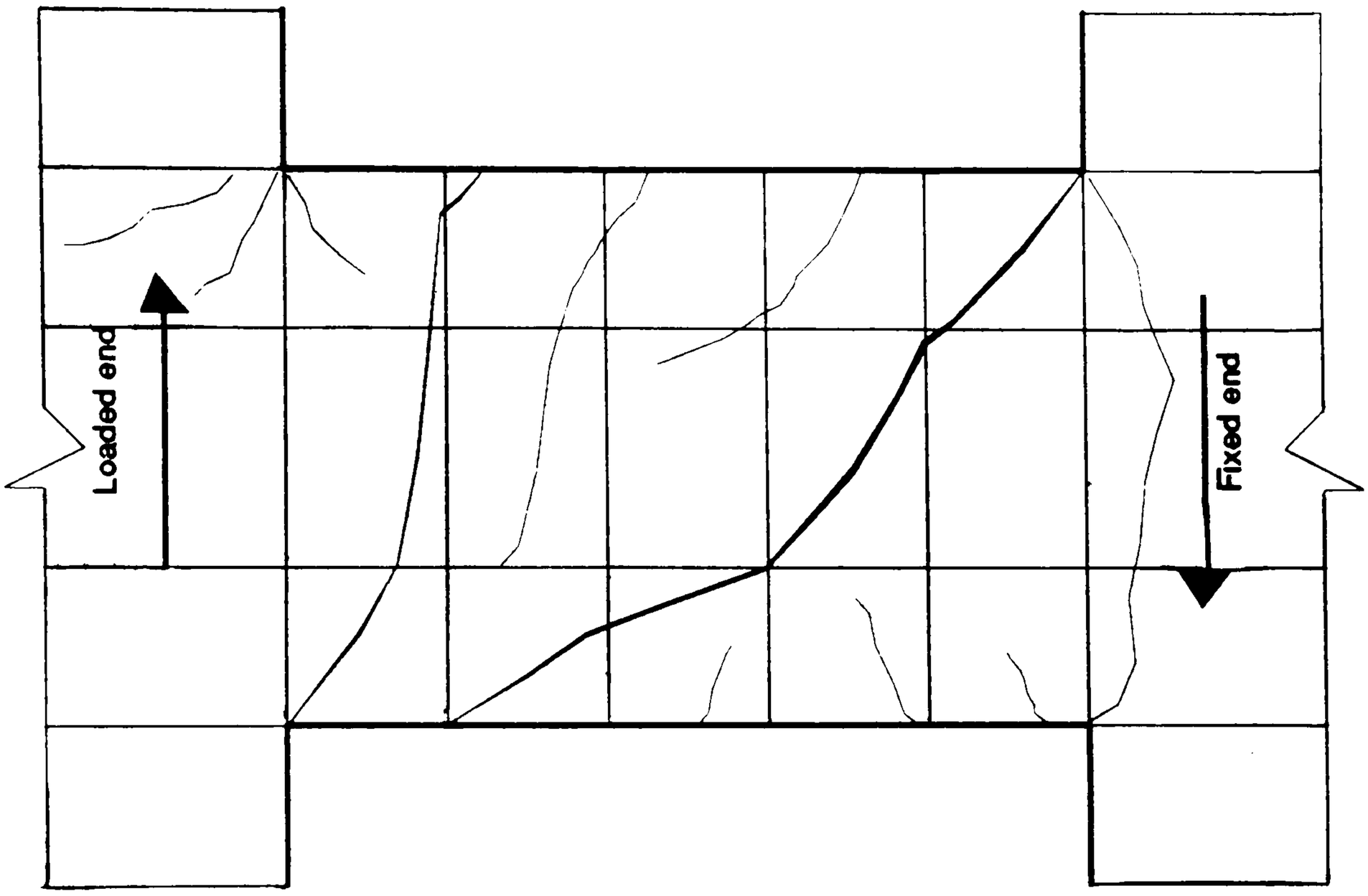


Figure 5.38: Failure mechanism and crack pattern for beam CBS2

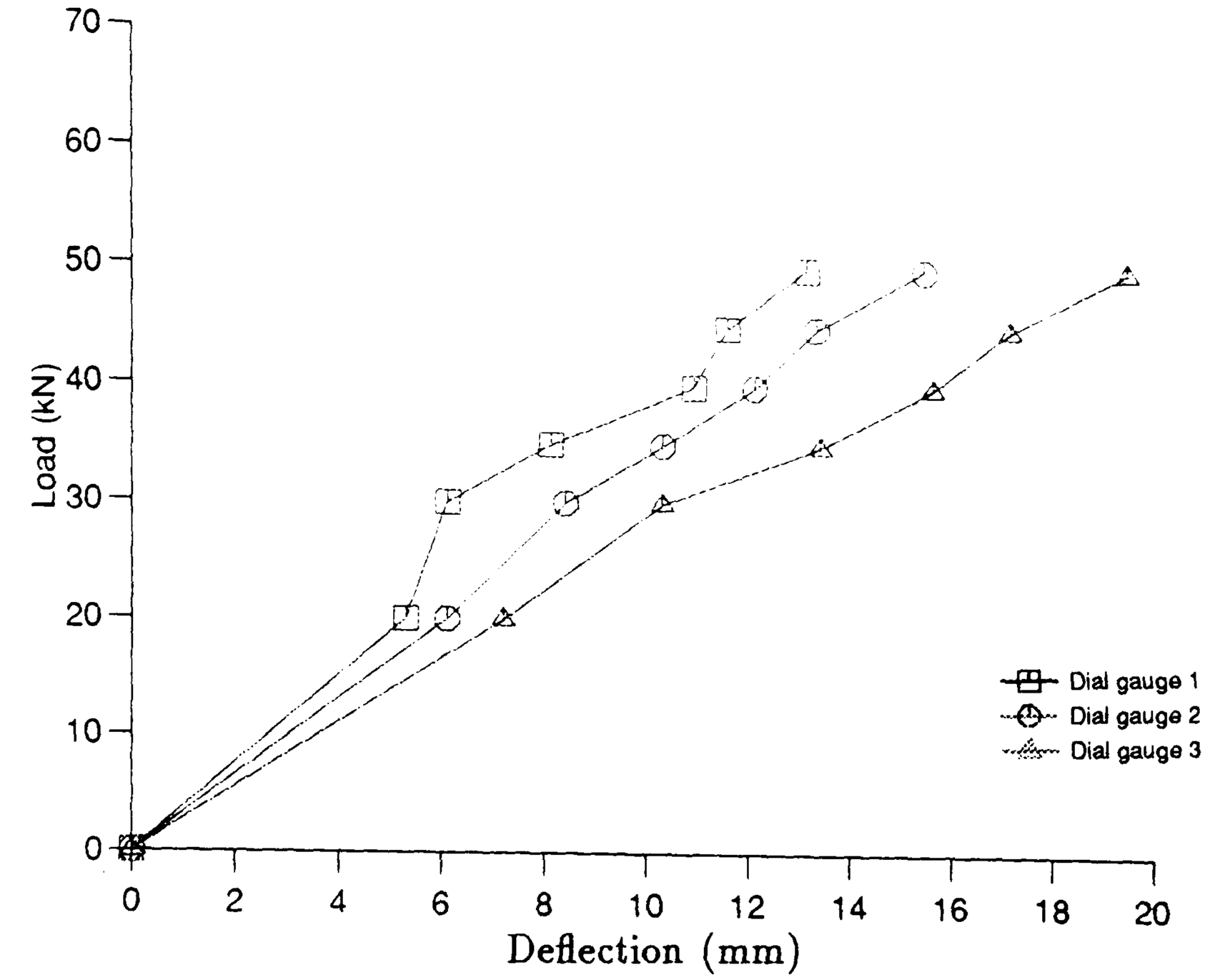


Figure 5.39: Load-deflection relationships for beam EBS1

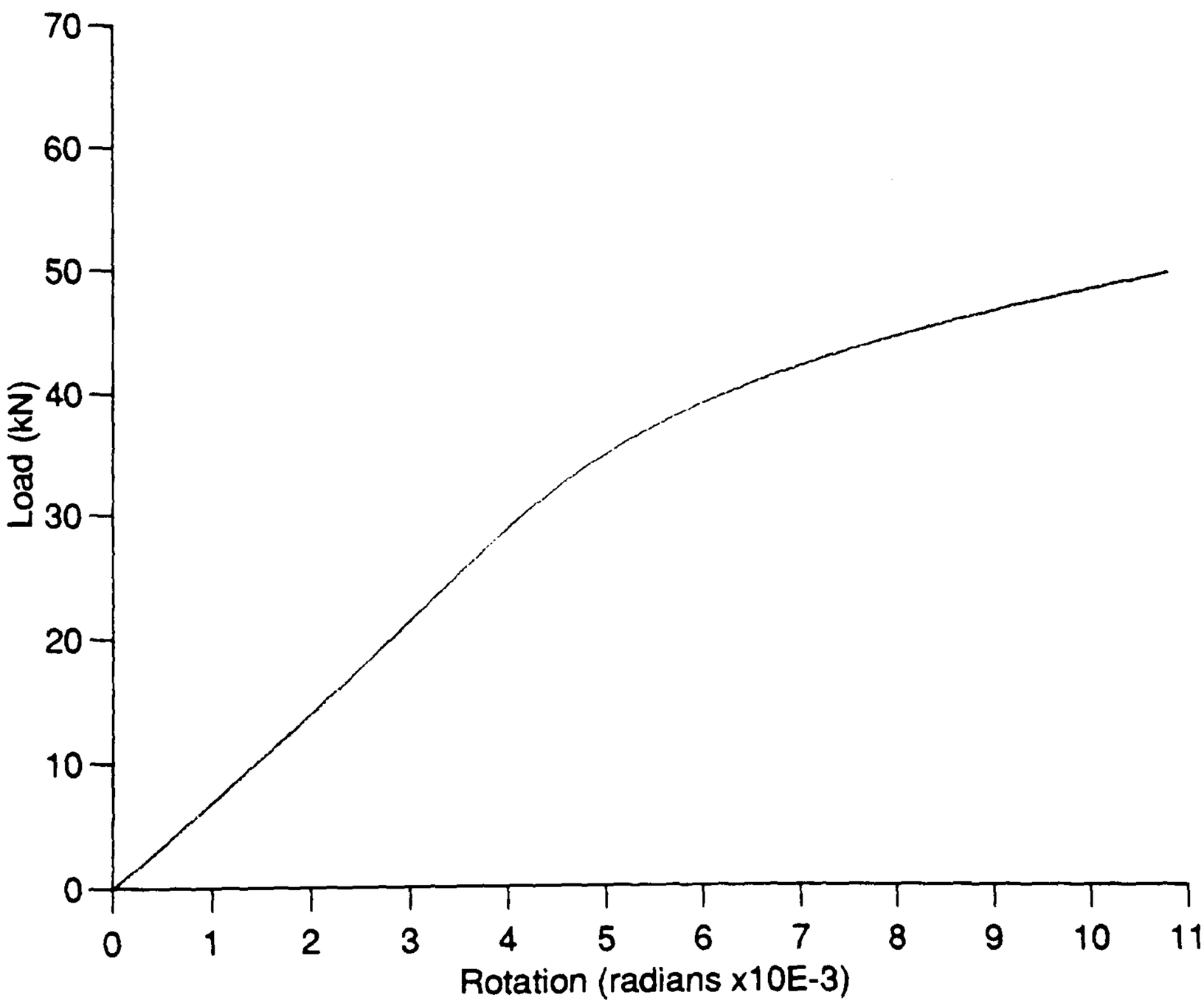


Figure 5.40: Load-rotation relationship for beam EBS1

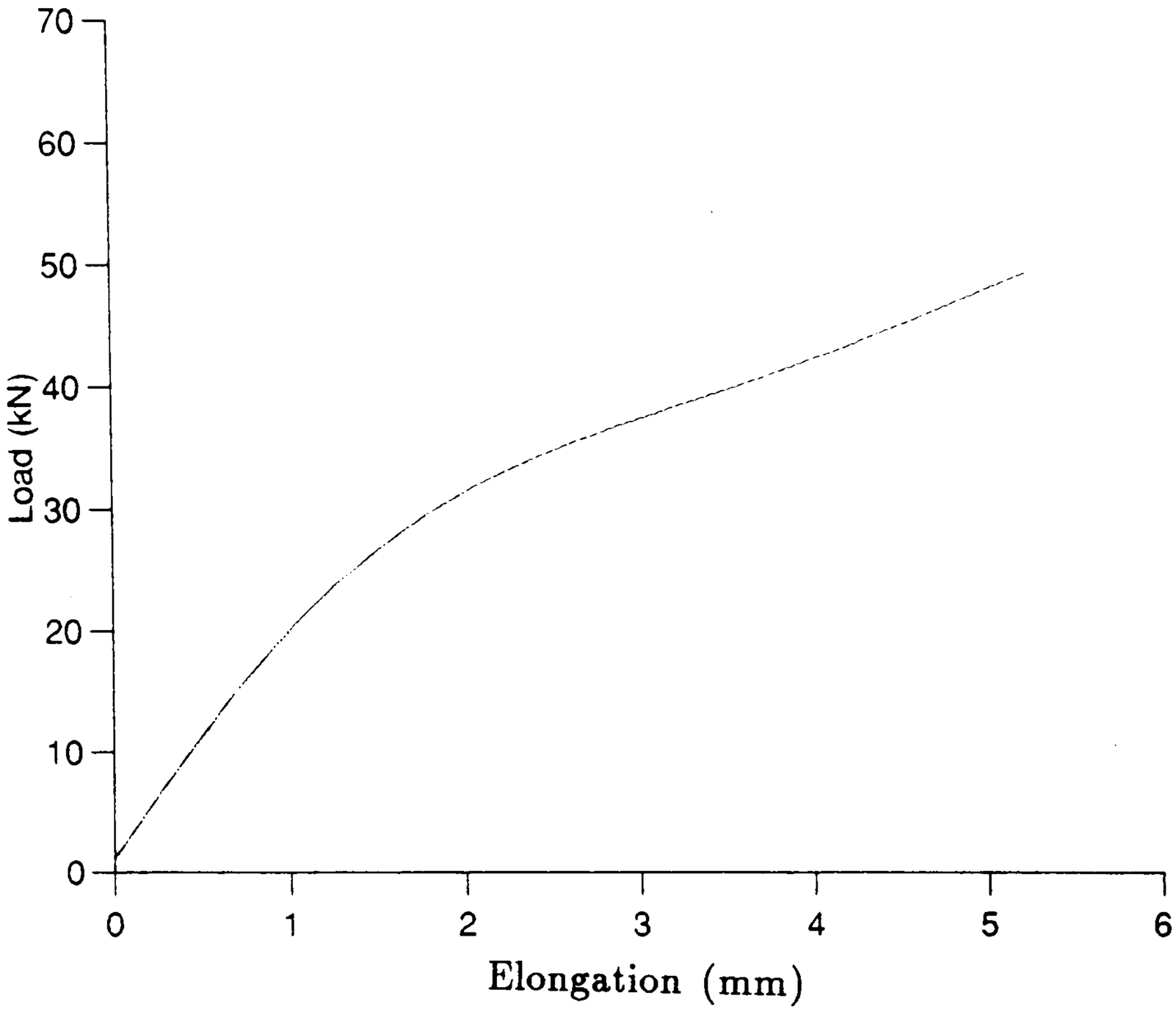


Figure 5.41: Load-elongation relationship for beam EBS1

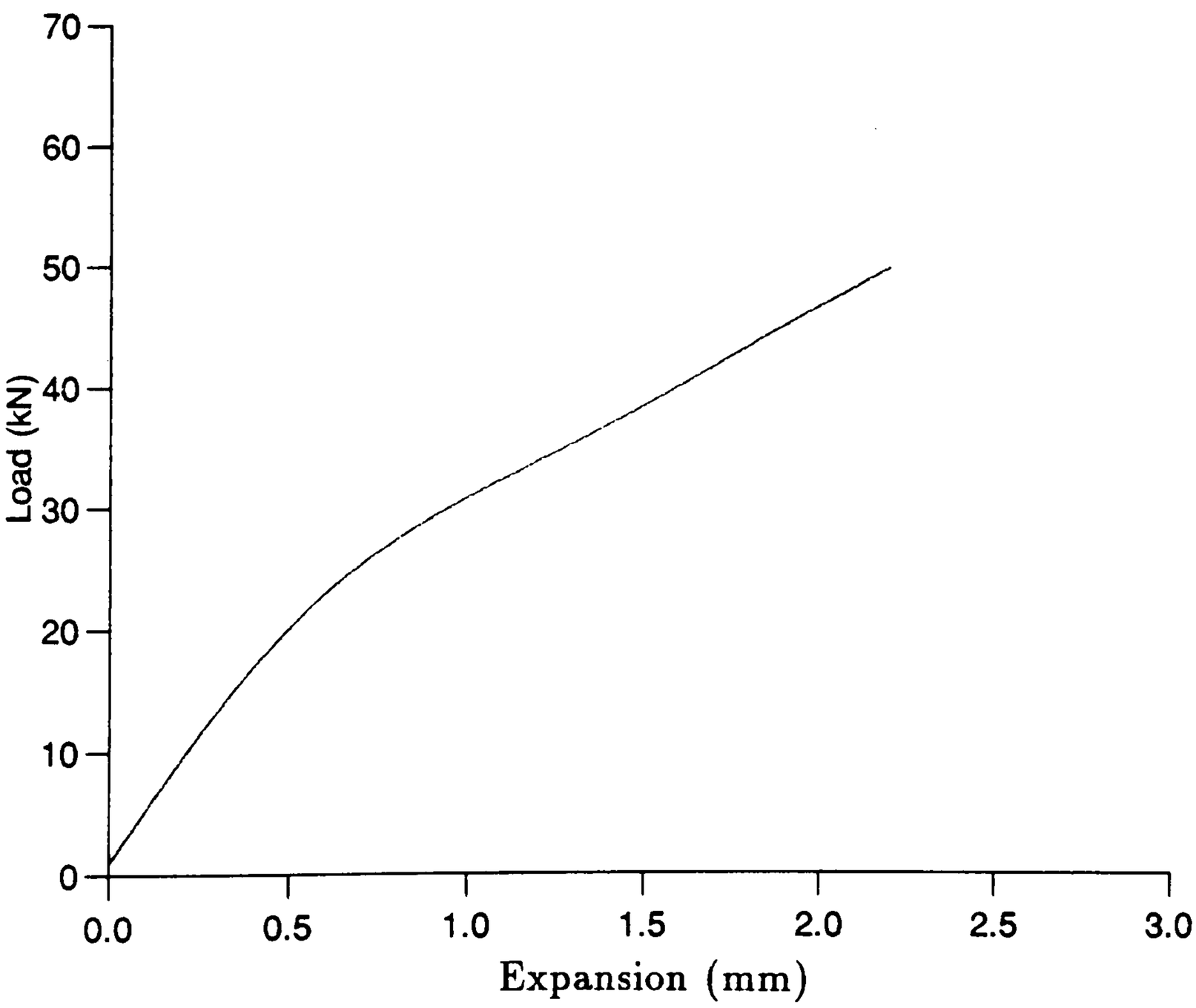


Figure 5.42: Load-expansion relationship for beam EBS1

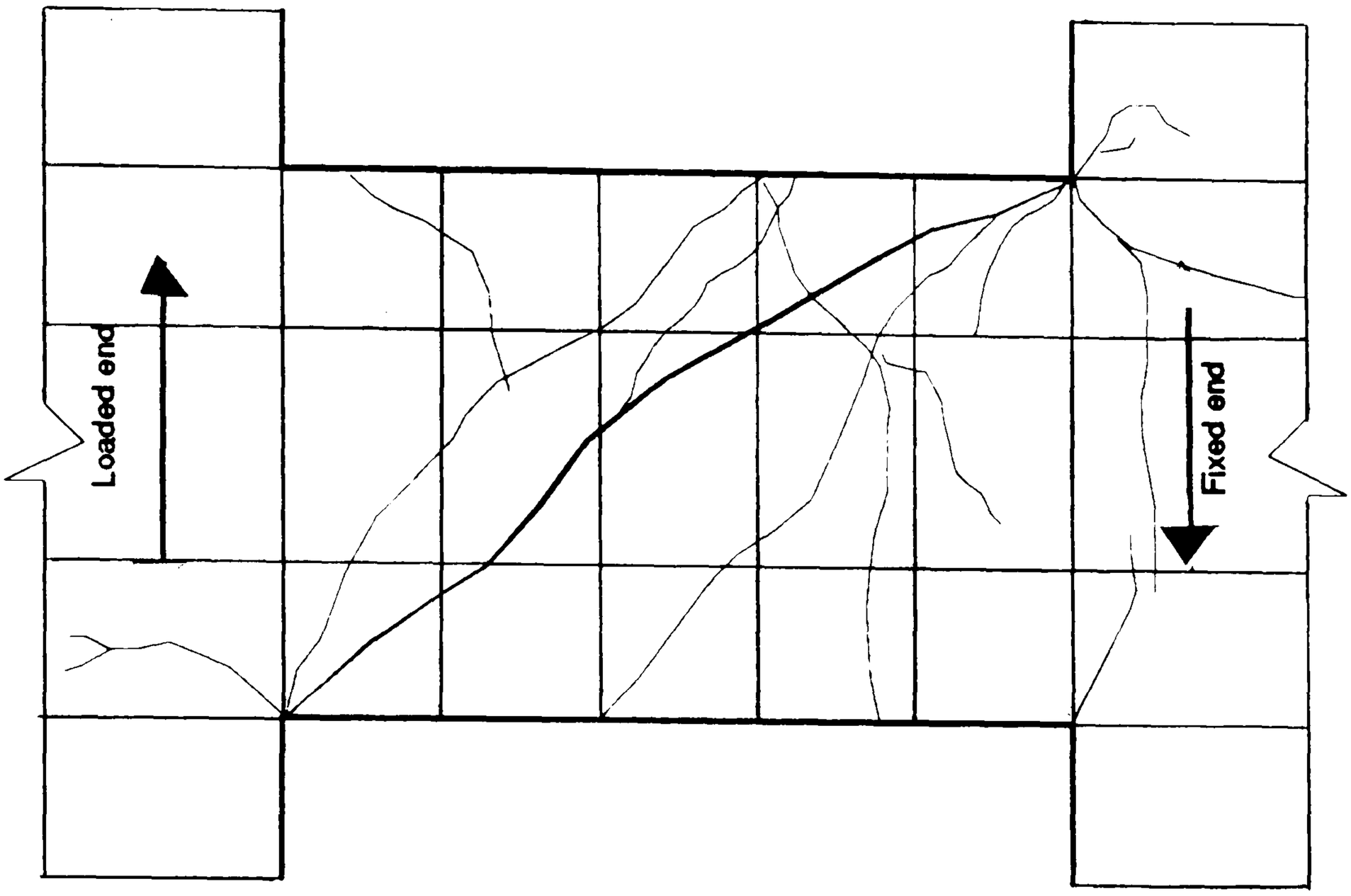


Figure 5.43: Failure mechanism and crack pattern for beam EBS1

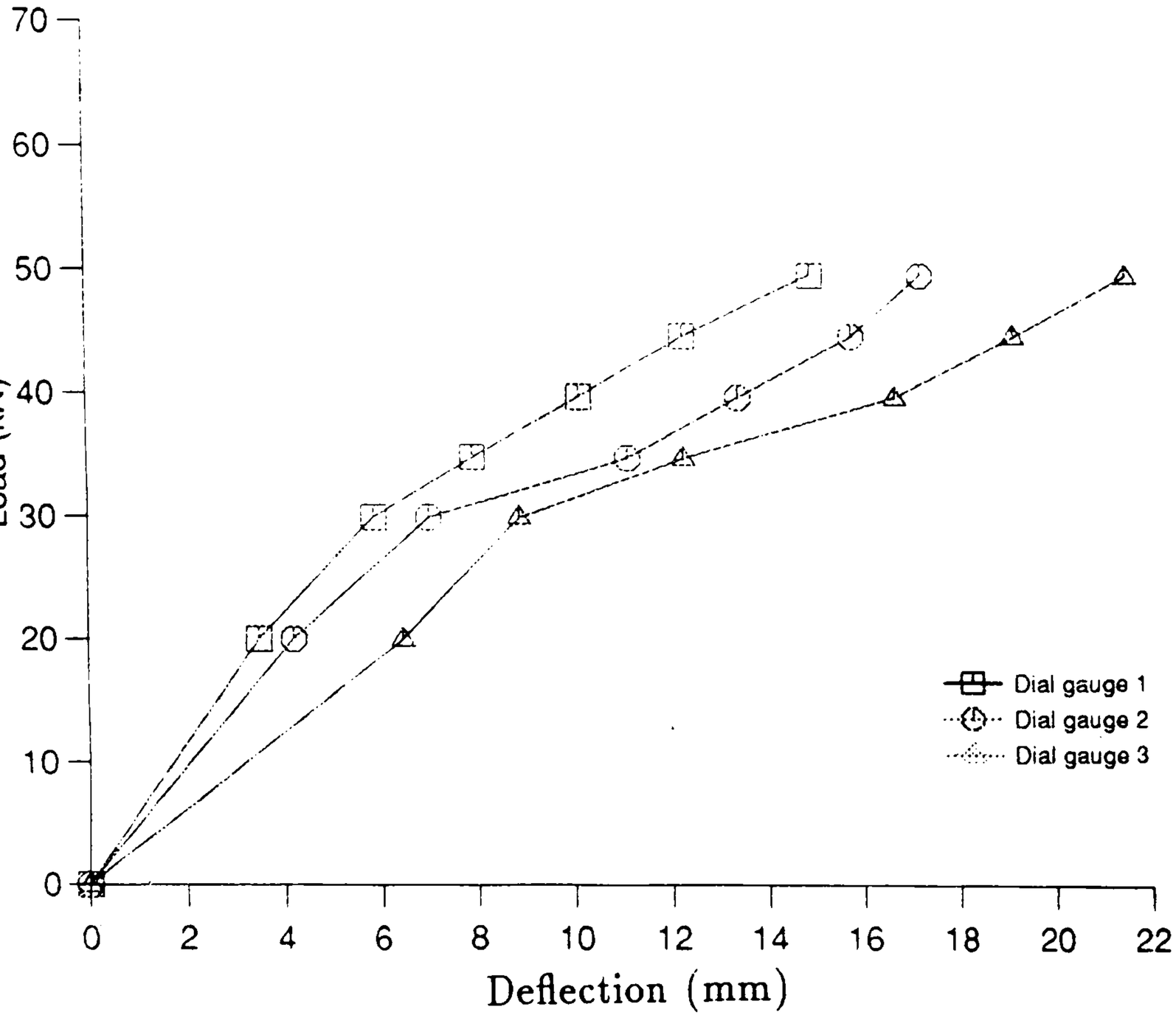


Figure 5.44: Load-deflection relationships for beam EBS2


Figure 5.45: Load-elongation relationship for beam EBS2

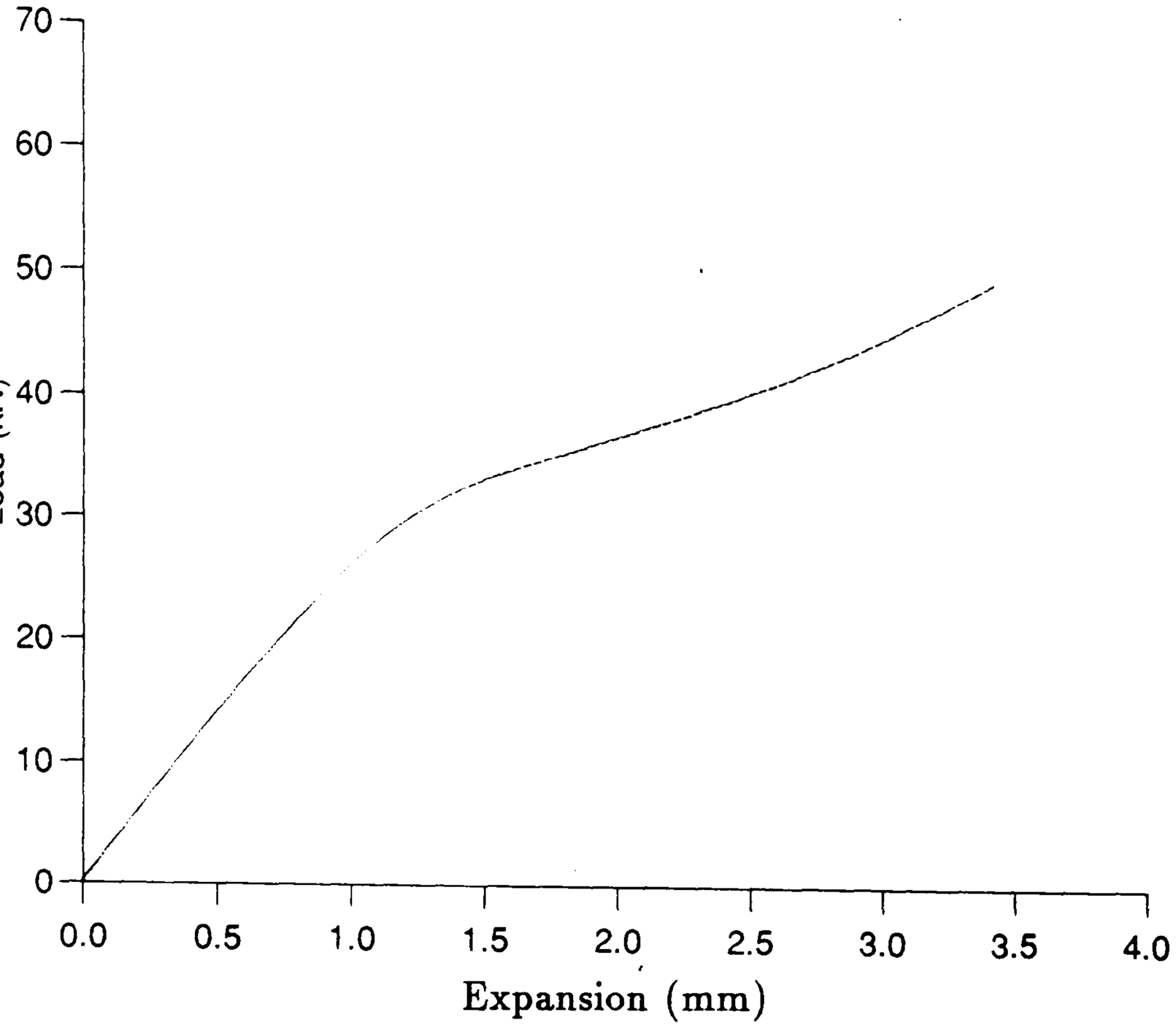


Figure 5.46: Load-expansion relationship for beam EBS2

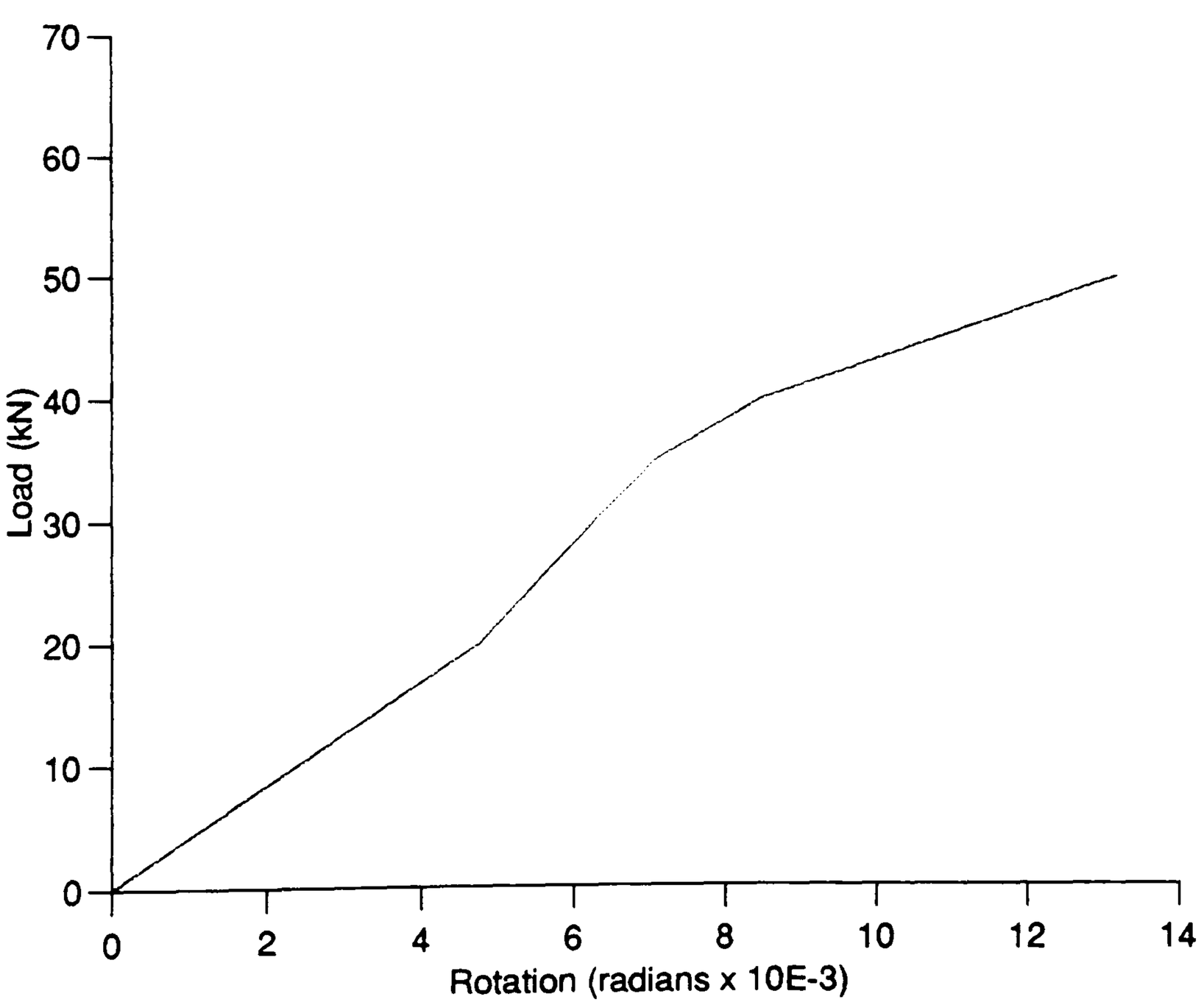


Figure 5.47: Load-rotation relationship for beam EBS2

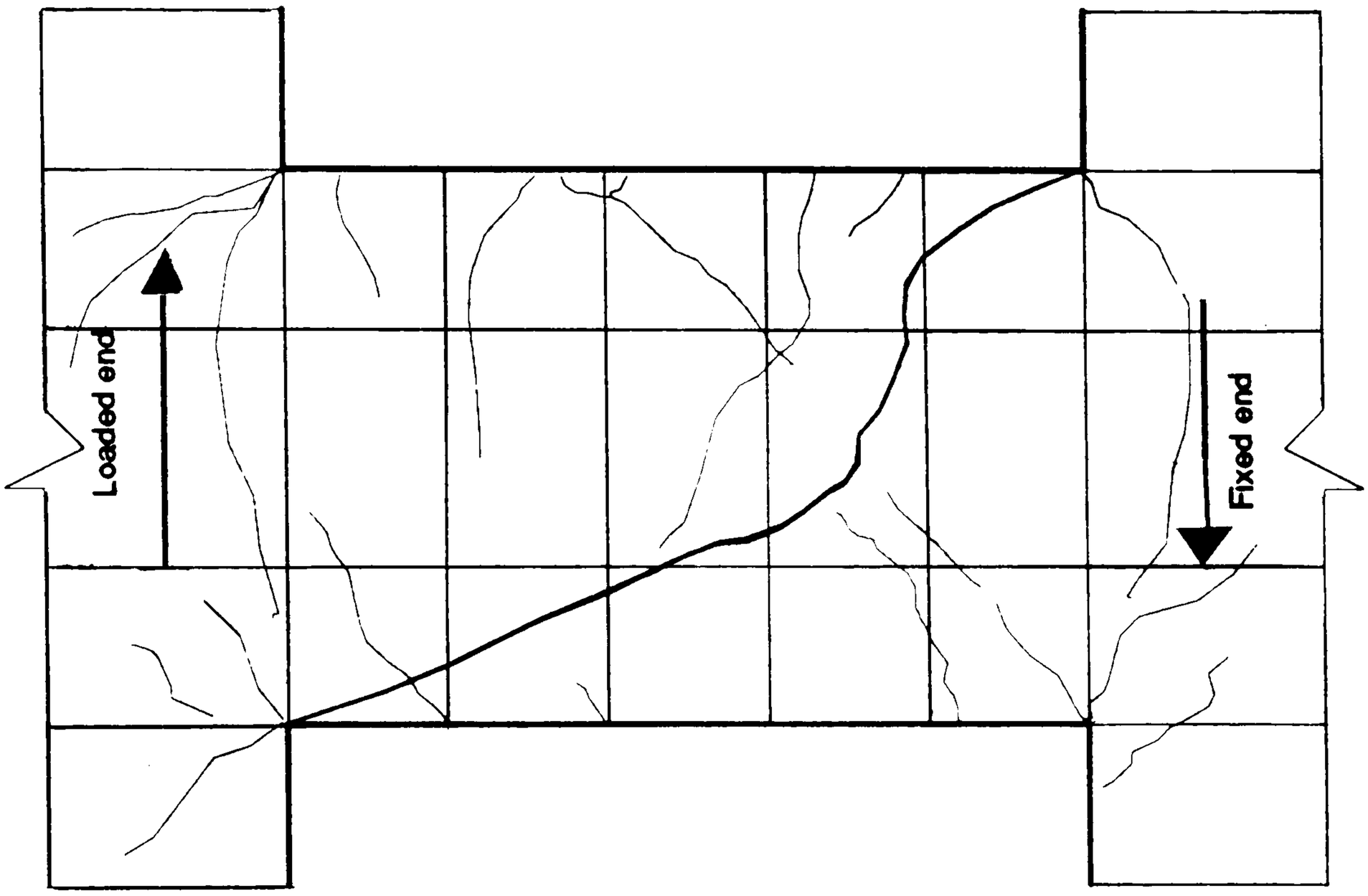


Figure 5.48: Failure mechanism and crack pattern for beam EBS2

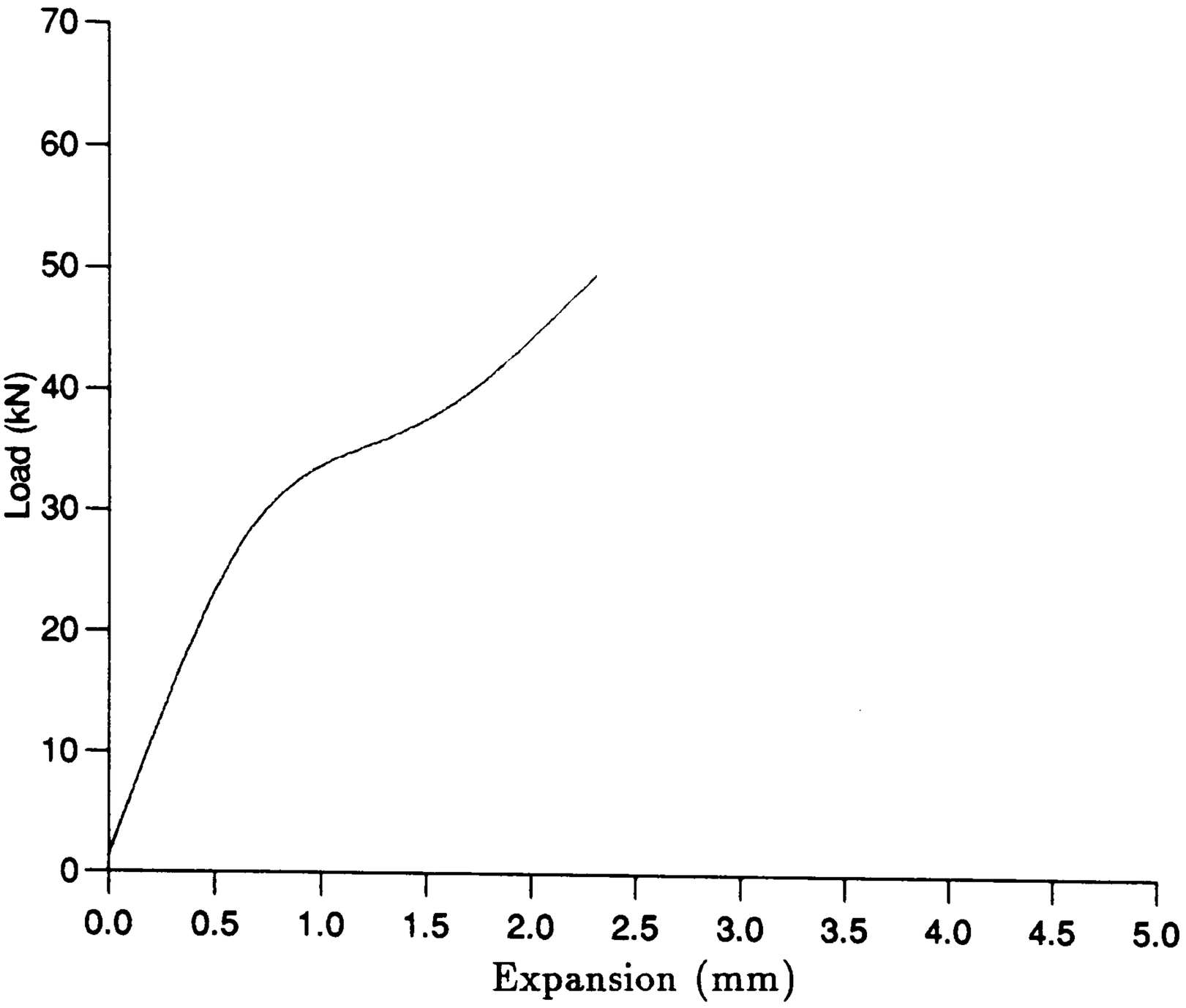


Figure 5.49: Load-expansion relationship for beam DBS2

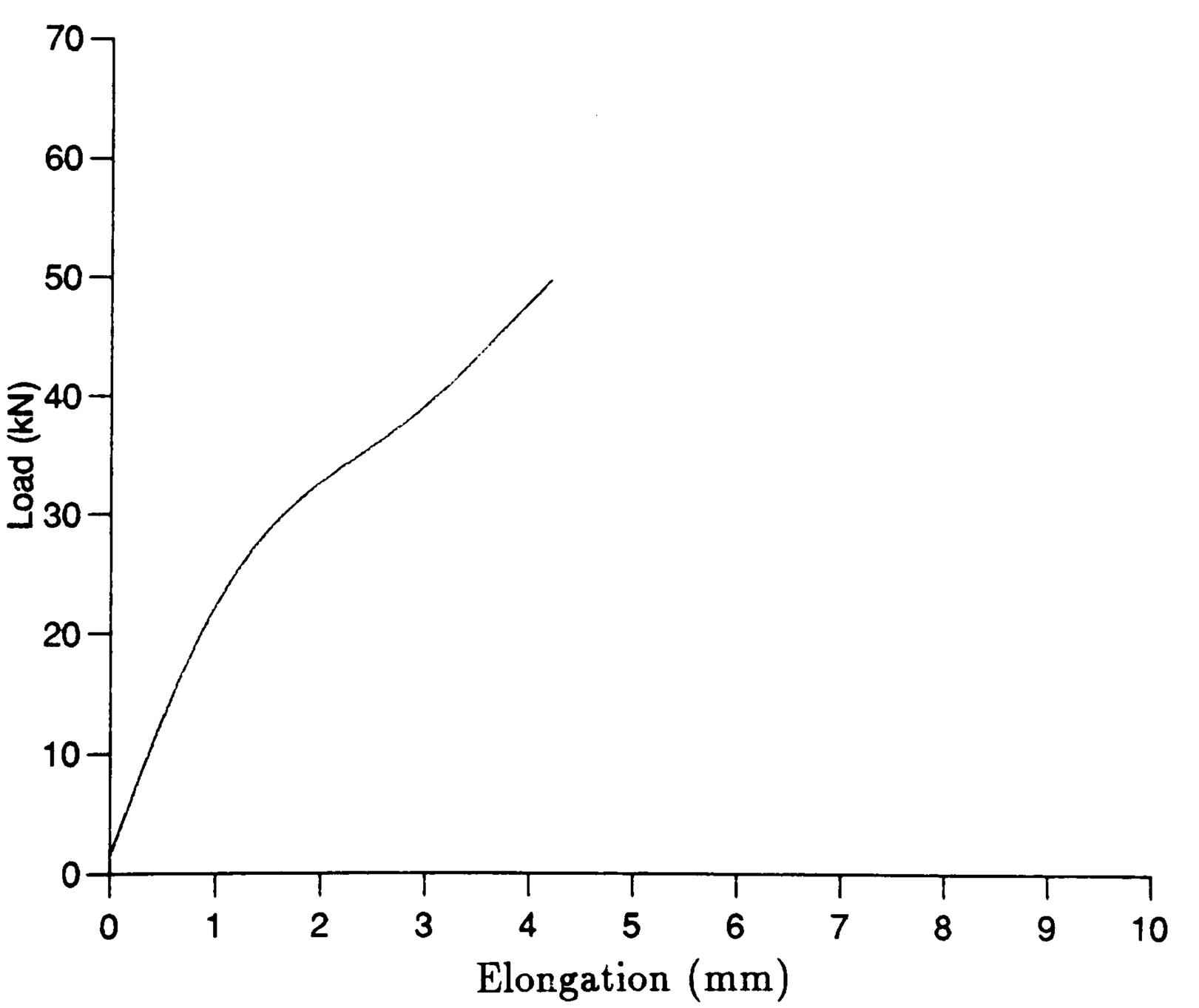


Figure 5.50: Load-elongation relationship for beam DBS2

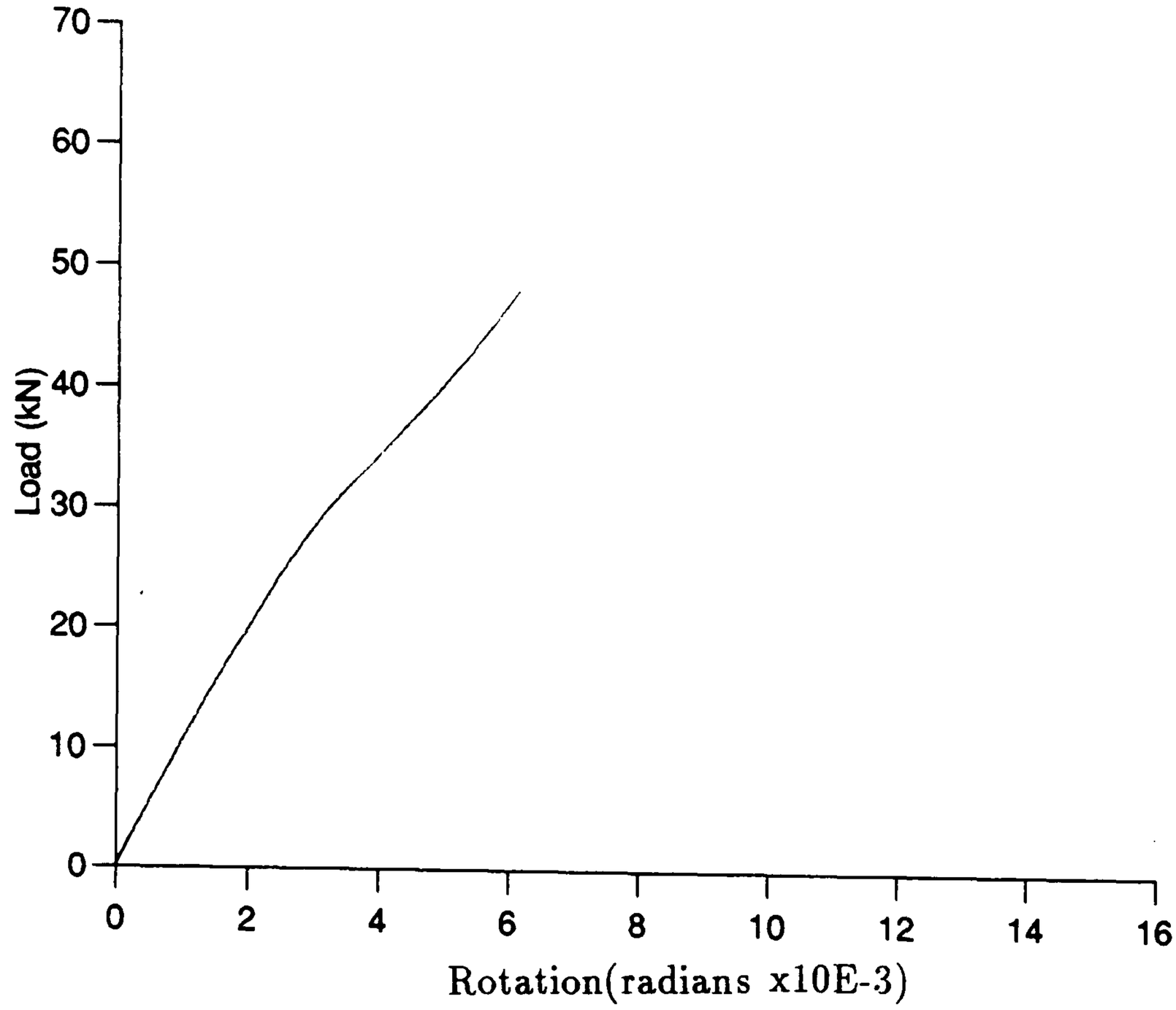


Figure 5.51: Load-rotation relationship for beam DBS2

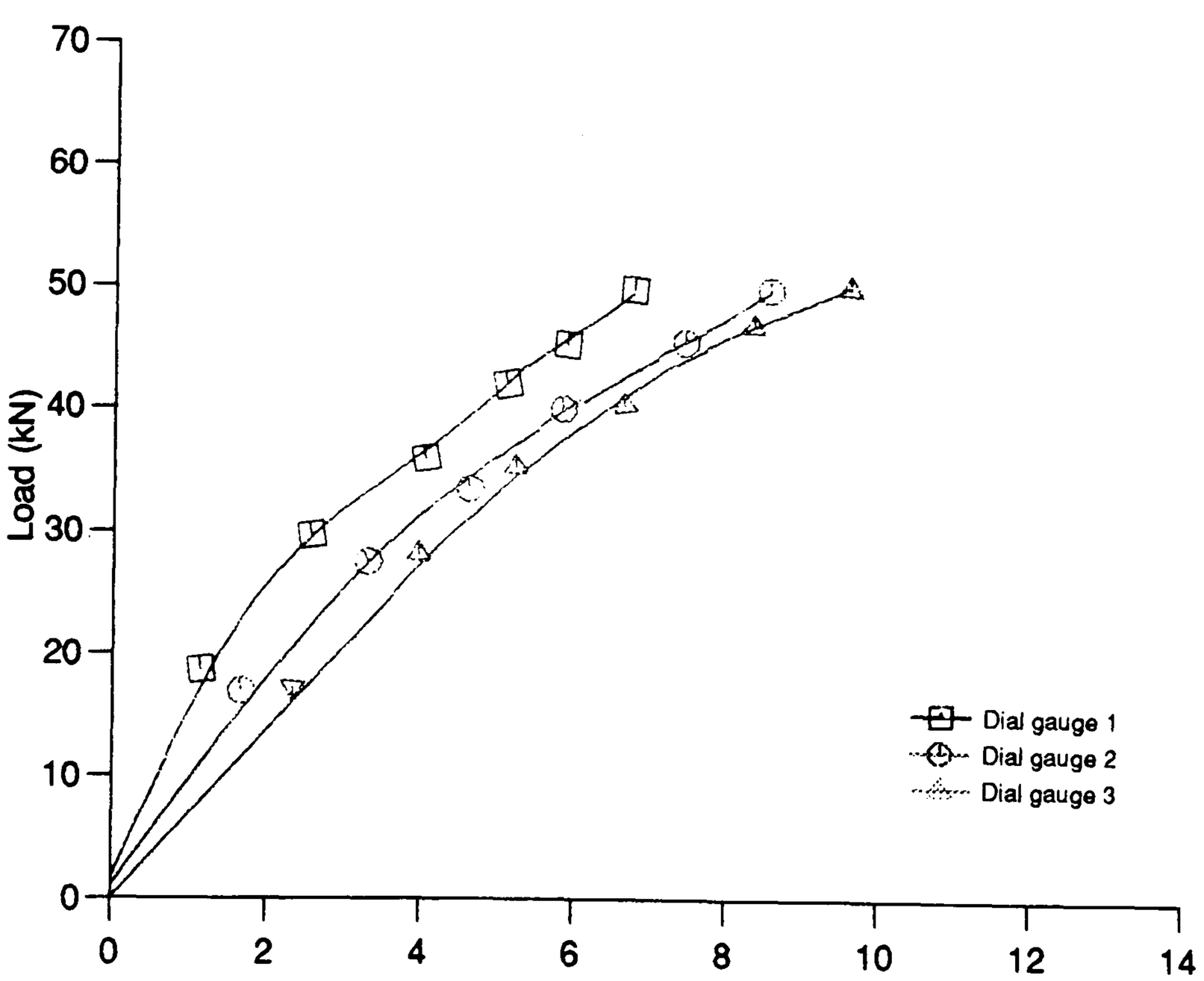


Figure 5.52: Load-deflection relationships for beam DBS2

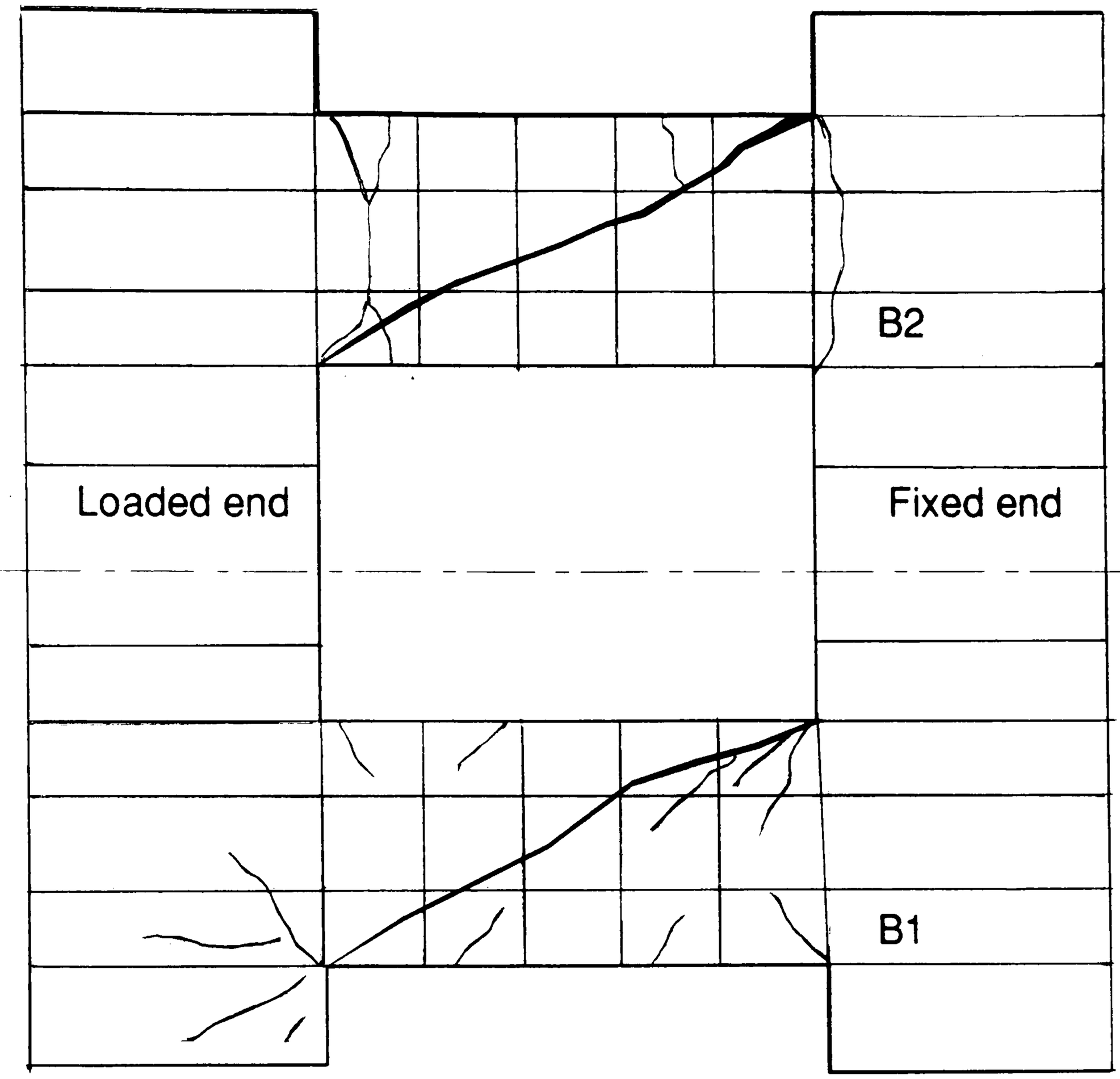


Figure 5.53: Failure mechanism and crack pattern for beam DBS2

# Chapter 6

# ANALYSIS OF BEAMS CBM3 AND EBM3

## 6.1 INTRODUCTION

The tests which are the subject of this Chapter can be regarded as an extension of those described and discussed in the previous Chapter.

The test series in this group consisted of two coupling beams, designated CBM3 and EBM3 which were similar in overall dimensions and in the type of reinforcement used to beams CBM2 and EBM2 respectively described in Chapter 5. The properties of beams CBM3 and EBM3 are given in Chapter 3.

In this case beams CBM3 and EBM3 were designed to investigate the behaviour of the overall structure as well as the behaviour of the web and the longitudinal reinforcement bars.

In particular the test on beam EBM3 was carried out in order to examine in

detail the potential and efficiency of the reinforcement arrangement containing expanded metal mesh as shown in Figure 3.17 in Chapter 3. A total of 30 strain gauges positioned on the main reinforcement bars and the web reinforcement were incorporated in beams CBM3 and EBM3 as shown in Figure 3.11 in Chapter 3. The loading procedures which were used in each case were identical to those used previously. All measurements in these two tests, were recorded up to failure for each load increment during the third load cycle.

## 6.2 BEHAVIOUR OF WEB REINFORCEMENT IN BEAM CBM3

### 6.2.1 Distribution of Strains along the Flexural Reinforcement

The number of strain gauges provided enabled the strains to be measured over the entire clear span of the beam. The distribution of these strains on both the top and bottom reinforcement bars are shown for the last load cycle at the two supports and the middle of the beam as shown in Figure 3.11 in Chapter 3. The load-strain distributions are shown separately for the bottom and top reinforcement within each beam.

Considerable differences were frequently observed between the strains measured on different sides of the beam at the same section because of the relative random formation of cracks. Some cracks extending across the 120 mm width of the beam

did not necessarily cross the corresponding strain gauge length.

Figure 6.1 and Figure 6.2 show that during the third load cycle, the strains at gauge points A', D (situated at the top left hand support) and the strain gauge points C, F' (situated at the bottom right hand support) increased considerably at each increment. At the maximum load the flexural reinforcement yielded first at the supports close to strain gauge point A' where the strain recorded was of the order of 15625 microstrain. At the left hand bottom corner of the beam at strain gauge point A a large strain of the order of 17200 microstrain was found as a results of the appearance of the flexural crack. The large permanent tensile strains observed in the tension zones of the beam at strain gauge point A' shown in Figure 6.1 and at gauge points C and F' shown in Figure 6.6, after load reversal, would suggest that the cracks previously formed could not fully close in the vicinity of the reinforcement bars which had yielded. Therefore one would expect that the tensile and compressive forces in the reinforcement were significant.

The following observations were made from a close examination of the strain distribution curves for the top and bottom reinforcement shown in Figures 6.1 to 6.6:

- The strains in the two reinforcement bars at the top or at the bottom of the beam were generally very similar. They appear to be related to each other.

- The strains were smaller at the centre of the beam at strain gauge points B' and E on the top reinforcement and at gauge points B and E' on the bottom reinforcement i.e. at the point of zero bending moment as shown in Figure 6.2 and in Figure 6.5.

- At higher loads, which are associated with the development of diagonal cracks, the tensile strains were also very large at the point of zero moment. At approximately 30% of the failure load, tensile strains were found over the entire length of the beam in the top and bottom reinforcement bars. Surprisingly at higher loads the flexural reinforcement was also found to be in tension on the "compression zone" of the beam. The maximum strains recorded at the midspan of beam CBM3 were less than 3000 microstrain in the bottom reinforcement and approximately 2000 microstrain in the top reinforcement.

- Near the ultimate load the tensile strains in the two reinforcement bars passing through the "compressive zone"of the beam differed. This may have been due to the development of the major flexural crack shown in Figure 6.20. This unexpected phenomenon is associated with the failure mechanism of the beam.

- The strain distribution along the top and bottom reinforcement at the same section of the beam was, at all levels, nonsymmetrical. The deviations which occurred are due to irregular crack formation rather than due to a change in bending moment.

- During the last loading increment the bars in both layers had extensively yielded near the supports at strain gauge points A and D' due to the development of the flexural crack and at strain gauge points A' and D resulting from the presence of a diagonal crack.

It was noted, that the widest cracks, which formed during the first load cycle, closed during the second load cycle. Indeed they must have closed otherwise the large diagonal compression forces could not have been transmitted. As expected the strains in the compression reinforcement were considerably smaller than the corresponding tensile strains.

### 6.2.2 Behaviour of the Stirrups

Strains were measured close to the corners of the stirrups along the length of their longest leg.

Strain gauges were present on the second strrup on both sides of the beam as can be noted in Figure 3.11 in Chapter 3. Figure 3.11 shows the eighteen strain gauge positions numbered 1 to 18.

The results from these strain gauges are shown in Figures 6.7 to 6.11 for both the top and bottom legs of each stirrup. It should also be noted that strains at the cracks, particularly after the onset of yielding, may be considerably larger than the recorded strains.

The load-strain relationship shown in Figures 6.7 to 6.11 for the top and bottom strain gauge points on stirrups 1 to 8 clearly show that the strain varies significantly along each of the stirrups. After the development of the diagonal cracks the most highly stressed region of each of the stirrups occurred where it was crossed by the main diagonal crack at the position of strain gauge point 10. This crack crossed the beam from the lower right hand corner to the upper left hand corner. It is most probable that strains above strain gauge point 10 on stirrup no. 3 were

considerably higher than that indicated by the curve in Figure 6.10. The first stirrups began to yield in the middle of the beam at stirrup numbers 3 to 5 as shown in Figure 6.9 and in Figure 6.10. This was followed by yielding of the other stirrups in the middle two thirds of the beam and at the supports i.e. at stirrup numbers 1 to 3 and 6 to 8, as the load was increased. During the first and second load cycles up until the end of the last increment of load i.e. 50 kN, small strains of the order of 100 microstrain were found in all the stirrups. It was possible to determine clearly the direction of the diagonal cracking after the loading was applied at the end of initial load cycles.

In each case yielding of the reinforcement was first experienced at the point where the major diagonal crack crossed the stirrups. The steady increase in strain in the stirrups indicated the progression of the diagonal splitting in the concrete.

All load-strain relationships presented in Figures 6.7, 6.8, 6.10 and 6.11 confirmed the widely accepted observation that the stirrups begin to contribute towards shear resistance only after they have been crossed by diagonal cracks. Prior to the formation of cracks, negligible strains, often compressive strains were detected in the stirrups during the first load cycle.

### 6.2.3 Concrete Strains

The strain distribution at a section passing through the supports, the quarter span points and the middle of the beam is shown in Figures 6.12 to 6.16. It can be noted that the strains in the uncracked region of the beam were either very small in tension or were in compression during the early stages of loading of the beam i.e.

during the first load cycle, and thus the results are more affected by inaccuracies in the strain measuring process and the estimation of temperature effects. The measurements during the third load cycle were only taken into consideration to describe the behaviour of the cracked concrete.

After the load reached approximately 30% of the failure load, considerably more difficulty was encountered with the strain measurements in the concrete after a few cracks, particularly the diagonal one, had developed close to a number of the strain gauge lengths.

The strain measurements obtained from beam CBM3 are shown in Figures 6.12 to 6.16 for all load increments during the third load cycle. These measurements indicate that:

- At the supports the concrete strain distribution shown in Figures 6.12 and 6.13 indicates very high strains at gauge points 1 and 13 to 15. This probably resulted from the flexural crack which developed at this section. The magnitude of these strain measurements varied from 9000 to 55000 microstrain in tension.

- At midspan (point of zero moment) near-uniform compression stresses developed after the appearance of diagonal cracking just before failure. These tension strains were of the order of 24384 microstrain at strain gauge point 8. According to the theory of homogeneous, isotropic elastic beams, this section should have been in the state of pure shear.

At the top and the bottom of the beam the tension in the flexural reinforcement dominated the strains, so the concrete cracked at position 8 and the

magnitude of the strain was considerably larger at a load of 150 kN than the measurements recorded during the last load increment of the third load cycle i.e. at a load of 120 kN.

- At the quarter span point the effect of the reinforcement was more pronounced at the "compression edge" as shown in Figure 6.16 for strain gauge point 12. Here the concrete was either in tension or it had cracked. Significant compressive strains were present at strain gauge points 4 and 6.

It should be noted that the principal inclined strains in the beam were larger than those presented for the horizontal direction.

## 6.3 DEFORMATION OF BEAM CBM3

### 6.3.1 Deflections

The displacement of the bottom edge of the beam was measured in the same manner as the beams presented in Chapter 5. The results of the deflection measurements, taken at three positions along the soffit of the beam are shown in Figure 6.17. To be able to estimate the deformed shape of the axis of the coupling beam it was necessary to assume that, the top and bottom edges of the beam deformed in the same way. The curves in Figure 6.17 obtained from the last load cycle in this test show the displacements of the beam edges at three positions along clear span. The maximum deflections recorded were approximately 18.70, 30.10, and 37.90 mm for the three dial gauge positions D1, D2 and D3 respectively at a load of 130 kN.

### 6.3.2 Elongations

As part of the deformation measurements, the elongation of the beam was determined between points A and B using a demec gauge with a gauge length of 150 mm. The elongation measured in this way is larger than the actual extension of the beam, because it also includes the deformations of one half of each end block.

The curve shown in Figure 6.18 indicates clearly when the flexural cracking first became apparent at about 30% to 40% of the ultimate load.

The load-elongation relationship was found to give more useful information with respect to the plastic deformations of the flexural reinforcement.

At a load of 130 kN, the total elongation measured was of the order of 16.90 mm.

### 6.3.3 Transverse Expansions

The deformed shape of the coupling beam, suggests that after diagonal cracking considerable deformations would also occur in the transverse direction. This was also confirmed by the fact that the strains in the stirrups increased as the failure load was approached. The elastic strains in the stirrups extended over a large enough height of the beam to suggest that the transverse expansion of the beam may assume, relative to other types of deformations, to be of significant proportions.

The load-transverse expansion relationship at midspan of the beam was measured in the same way as the elongation between the two points C and D.

The curve in Figure 6.19 indicated that very large transverse deformations occurred in the first stage of loading during the third load cycle and then the in-

crease was proportional to the load after a load of 40 kN was reached. It should be noted that the transverse expansion of the beam between its edges would be larger than that indicated by these measurements. This is particularly so near the supports which was the region in which the largest stirrup strains were found. The expansion measured in beam CBM3 at a load of 130 kN was of the order of 6.30 mm.

### 6.3.4 Rotations

No new features were revealed in the rotations measured in beam CBM3. The behaviour was very similar to that observed in beam CBM2 presented in Section 5.2.2. The total rotation measured at a load of 130 kN was of the order of 12.25 $x10^{-3}$ radians. Detailed information on the rotation for each load increment is reproduced in Figure 6.20. This graph is discussed in greater detail in the next Chapter.

### 6.3.5 Crack Widths and Failure Mechanism

As expected, the first cracks formed at the tension corners of the beam and subsequently propagated in an almost vertical direction. The diagonal cracks developed gradually from flexural cracks which had formed earlier. The main diagonal crack formed at 30% of the failure load. The behaviour of beam CBM3 was characterised by the early appearance of the diagonal crack within the shear span of the beam. This crack then propagated in a different direction with increasing load. The width of these cracks increased as loading progressed i.e. the width of the

major diagonal crack was 0.6mm, 0.8mm and 1.20mm at loads of 40 kN, 60 kN and 70 kN respectively during the third load cycle. Beyond this point the crack widths increased rapidly leading to a major diagonal crack at a loading level of 130 kN where the crack was approximately 3.25 mm in width. This was accompanied by a sudden reduction in sustained load. This indicated that most of the energy dissipation had taken place within the beam. The widths of the minor diagonal cracks remained almost constant over a large range of loading. This is consistent with the strains measured in the stirrups.

it is apparent from Figure 6.21 and Plate A.13 in Appendix A taken at failure, that the beam had separated into two halves along the main diagonal. Failure of the beam was reached at a load of 162 kN.

## 6.4 BEHAVIOUR OF WEB REINFORCEMENT IN BEAM EBM3

### 6.4.1 Distribution of Strain along the Flexural Reinforcement

The distribution of the strains along the top and the bottom reinforcement is shown for the third load cycle in Figures 6.22 to 6.27. The first of these, showing the strain distribution in the third load cycle of loading, enabled a comparison to be made with the results from the earlier beam CBM3. The new features revealed in the distribution of strain in the top and bottom reinforcement are presented in

this Section. In general, the strain distribution was very similar in the direction of the diagonal crack. The difference between the strain in the top and bottom reinforcement was significantly smaller.

The strain in the main flexural reinforcement could be lower over the full length of the beam because of the contribution of the expanded metal mesh to the flexural resistance of the section.

The strain history of the flexural reinforcement in beam EBM3 at both supports, where the failure occurred is shown in Figures 6.24 and 6.25. The strains were recorded at strain gauge points A and D' situated at the left hand bottom corner of the beam and at strain gauge points C'and F situated at the top right hand corner of the beam.

The curves indicate that high tensile strains occurred at the end of the third load cycle. The curves presented in Figure 6.23 for positions at the centre of the top reinforcement confirmed that both strain gauge points B' and E at the same section run close to each other up to a load of 50 kN.

The maximum strains measured in the top and bottom reinforcement at the central strain gauge points did not exceed 2690 microstrain as shown in Figures 6.23 and 6.26. The maximum strain measured at the supports was of the order of 13634.4 microstrain as shown in Figure 6.25. It is considered that the expanded metal mesh which did not fully yield in flexure until the final load increments were applied during the test, prevented the main reinforcement from yielding more extensively. The expanded metal mesh had a restraining or stabilising effect on the behaviour of the beam. The last load increment at the end of the third load

cycle was normally determined by observing the onset of yielding of the flexural reinforcement at the critical strain gauge points A and C' near the supports of the beam. A nonlinear strain distribution in the flexural reinforcement was observed. At maximum load during the third load cycle, the flexural tension reinforcement yielded at the supports at strain gauge points A, D', C' and F where the strain recorded exceeded 13600 microstrain. The permanent tensile strain at gauge point A' observed in the compression zones of the beam, after load reversal, suggests that the cracks, which had formed previously did not fully close in the vicinity of the reinforcement bars which had yielded. Therefore, it was expected that the flexural reinforcement would have to carry significant compression forces.

The strain history of the flexural reinforcement at the right hand support of the coupling beam indicated that at strain gauge points C and F' small compressive strains were indeed present during the third load cycle. This may be noted in Figure 6.27.

The magnitude of the tensile strain was of the order of 2818 microstrain at strain gauge point A' as shown in Figure 6.22 where the flexural crack crossing the depth of the beam had developed.

### 6.4.2 Behaviour of the Expanded Metal Mesh

The full strain history of each of the strands of the expanded metal mesh which were instrumented, during the third load cycle is shown in Figures 6.28 to 6.32 for the sections at the supports, the mid and quarter span points in the beam. When the diagonal crack started to open the strains in the expanded metal mesh

increased steadily at these cracks, as shown in Figure 6.30 for strain gauge points 9 to 12 situated at the middle of the beam.

It may be noted that when yielding occurred, particularly at strain gauge points 13 and 14 shown in Figure 6.32, the strains in the remainder of the expanded metal mesh did not increase significantly with load.

The distribution of the strain along the expanded metal mesh indicated how the beam behaved up to the failure. The maximum strains for each strand of the expanded metal mesh which occur along the main diagonal are represented by curves 13 and 14 in Figure 6.32. The magnitude of the strain did not exceeded 3000 microstrain. This indicates that at the lower left hand quarter span point, the expanded metal mesh experienced higher strains at a greater rate than those near the supports. The first strand of the expanded metal mesh began to yield at the quarter span point in the beam. This was followed by yielding of the other strands along the centre line of the beam with increasing load. Failure occurred when the strands of the expanded metal mesh at the support had also yielded.

The strain history of the expanded metal mesh at strain gauge points 5 to 8 situated approximately at the right hand quarter span point is presented in Figure 6.31 and in Figure 6.32 for the left hand quarter span point. The major diagonal crack which formed under positive loading crossed the expanded metal mesh at strain gauge points 8 and 13. However, during the third load cycle yielding had already occurred at the quarter span of the expanded metal mesh at strain gauge point 13.

At the beginning of the load cycle, a few of the strands of the expanded metal

mesh were in compression but with increased load, tensile strains again began to dominate.

The behaviour of the expanded metal mesh at strain gauge points 1 to 4 and 17 to 18 situated at the boundary of the beam are presented in Figures 6.28 and 6.29. It is interesting to note that after two load cycles this strand of the expanded metal mesh had not yielded extensively at the supports of the beam. This suggests that the diagonal crack did not cross any instrumented strand of the expanded metal mesh at this location. The strains remained small in compression and in tension and their magnitudes did not exceed 1500 microstrain at strain gauge points 1, 2 and 5, 6 because of the absence of a crack at these strain gauge locations. The same phenomenon occurred at strain gauge points 17 and 18 where the magnitude of the strains were less than 500 microstrain.

### 6.4.3 Concrete Strains

The main results obtained from the readings on the side of the beam are presented for five section across the beam in Figures 6.33 to 6.37. The strain distributions do not conform well with the nonsymmetrical load pattern because of the random nature of the crack formations. At strain gauge point 12, the most highly stressed region which is surprisingly located at the quarter span point of the beam, the magnitude of the strain was of the order of 16154 microstrain as shown in Figure 6.37. At the beam supports, the magnitude of the strains did not exceed 3000 microstrain in both the compression and the tension zones as shown in Figure 6.33. At the midspan, the strain was found to be significant as shown in Figure

6.35 where the maximum tensile strain was located in the centre of the beam at strain gauge point 8 and its value was of the order of 10007 microstrain. These strains corresponded with the crack patterns obtained during the test.

As expected, the tensile strains were larger than the compressive strains over the entire span of beam EBM3.

At the right hand support in the beam, the strains measured at strain gauge points 1 to 4 were in compression and their magnitudes were found to be between 660 and 2540 microstrain since no cracks were present in this region.

## 6.5 DEFORMATION OF BEAM EBM3

### 6.5.1 Deflections

The load-deflection relationship curves for beam EBM3 during the last load cycle are shown in Figure 6.38. It can be also noted from Figure 6.38 that the curves for the three different positions were dominated by nonlinear behaviour from the start of the load cycle until failure. The magnitude of the deflections at a load of 130 kN were found to be of the order of 16.50, 28.45 and 34.90 mm for dial gauge positions D1, D2 and D3 respectively.

The measurements again verify the deflection of coupling beam EBM3. The expanded metal mesh was found to contribute towards the strength of the beam because it was subjected to high stresses. The expanded metal mesh appeared to have a significant influence on the crack pattern in the beam. In all conventional beams the diagonal cracks originated from flexural cracks and then gradually propagated into the web. The diagonal crack was the last one to form.

### 6.5.2 Rotations

The rotation of beam EBM3 is shown in Figure 6.39. where the very high stiffness and high strength of the beam can be noted. On the other hand, the rotation experienced by the beam was only 11.20 x $10^{-3}$ radians at a load of 50kN. Towards the end of the load cycle at a load of 130 kN, when the width of the diagonal crack was very significant, the rotation was found to be of the order of 20.40 x $10^{-3}$ radians. The ability of the expanded metal mesh to limit the rotation of the

beam was clearly evident.

### 6.5.3 Elongations

The elongation of beam EBM3 is presented in Figure 6.40. The curve indicated that much less severe elongations were found in this beam compared to that in beam CBM3. The elongation of the beam during the third load cycle was dominated by nonlinear behaviour. During the first two load cycles, the elongation of the beam was negligible. At a load of 130 kN during the third load cycle, the total elongation of the beam was of the order of 14.40 mm. When a large elongation occurred it was difficult to maintain the position of the load.

An increase of at least 25% of the elongation recorded at a load of 130 kN was found just before failure occurred.

At this stage the failure mechanism, initiated by yielding of the flexural reinforcement bars had formed. When failure was approached, the beam experienced large elongations resulting in bending of the expanded metal mesh. Hence, the elongation measurements were no longer meaningful.

### 6.5.4 Transverse Expansions

The introduction of the expanded metal mesh together with the longitudinal reinforcement bars greatly affected the displacement of the beam in the transverse direction. The results obtained from beam EBM3, shown in Figure 6.41, indicate that the presence of the expanded metal mesh led to a decrease in the expansion and an increase in the stiffness of the structure compared to conventionally rein-

forced beams. This also confirmed the effectiveness of this type of reinforcement in resisting shear. The curve indicated that the beam behaved in a more ductile manner. The magnitude of the total expansion measured at a load of 130 kN was 5.90 mm. The observations described previously for the elongations were again appropriate as the load approached failure.

### 6.5.5 Crack Widths and Failure Mechanism

The failure of beam EBM3 is characterised as follows:

At the end of the first load cycle, a crack appeared at an angle of approximately $22^o$ with the horizontal indicating the occurrence of separation between the upper right hand to the lower left hand corners of the beam. A few flexural cracks also appeared during the first load cycle and their width did not exceed 0.10 mm at a load of 50 kN.

After the application of the second load most of the existing cracks closed and new cracks developed. The third load cycle was applied in the same direction as the first load cycle which led to the development of new cracks and increases in the width of the existing cracks after a load of 70kN was reached. In the last load cycle, the diagonal shear crack increased in width at the middle of the beam at each load increment until failure. This was also confirmed by the concrete strain measurements.

A flexural crack also developed in the upper right hand corner of the beam as failure was approached as shown in Figure 6.42 and in Plate A.14 in Appendix A. All the crack widths irrespective of whether they developed as a result of shear

or flexural behaviour varied between 1.0 and 3.50 mm before failure.

The maximum load carried by beam EBM3 was 190 kN. The presence of the expanded metal mesh in beam EBM3 reduced and also delayed the appearance of the cracks. At a load level of 50 kN, the width of the diagonal crack was only 0.20 mm and the width of the flexural cracks was less than 0.10 mm. At a load of 60 kN, the flexural cracks on the face of the beam propagated vertically i.e. perpendicular to the flexural reinforcement which was accompanied by a significant increase in their widths. At a load of 130 kN, the width of the major crack was in excess of 3.25 mm. The test showed that beam EBM3 developed fewer cracks and carried higher external forces. It was therefore, believed that this type of beam would have been stronger and the width of the crack would have been smaller.

Figure 6.42 and Plate A.14 in Appendix A show the crack patterns for the beam after failure. The test results have also shown that the behaviour of beam EBM3 was superior to that of beam CBM3 in terms of strength and crack propagation.

## 6.6 CONCLUSIONS

The most important results obtained from the tests on beams CBM3 and EBM3, relevant to the behaviour of coupling beams have been described in this Chapter. As expected the coupling beams containing conventional reinforcement as well as the expanded metal mesh failed by sliding shear after three cycles of reversed loading, which imposed extensive yielding within the beam.

Beam EBM3 which was reinforced with the expanded metal mesh, behaved very well during the load cycles and the performance of this beam was found to be superior to that of beam CBM3 which contained conventional stirrups, in terms of cracking and strength. Beam EBM3 was 15% stronger than beam CBM3 at failure. It can be concluded that beam EBM3 was stiffer than beam CBM3 throughout their respective loading histories. Both the experimental sets of results and the observations made during each test showed that shear distortions greatly overshadow those resulting from flexure. This needs to be taken into consideration when the stiffness of this type of coupling beam is assessed. The reduction in stiffness, after the cracking of beam CBM3, was considerably more than the reduction experienced in beam EBM3. The stresses along the stirrups and the expanded metal mesh varied significantly. However, localised stress concentrations were not found to affect the ultimate shear strength of the coupling beams. The latter depends on the combined strength of all the stirrups or the section of the expanded metal mesh which was crossed by the potential failure crack. The failure plane normally runs along the main diagonal of the beams.

The new form of reinforcement incorporating expanded metal mesh has been de-

veloped in an attempt to overcome the present deficiency in the design and the detailing of coupling beams. This form of reinforcement presented in Chapter 5 and in this Chapter has been developed for coupling beams under lateral loading. The theoretical approaches upon which this new arrangement has been developed have been described in detail in Chapters 3 and 4. The improved performance of beam EBM3 over beam CBM3 is attributed to the presence of the expanded metal mesh in the central plane of the beam. This reinforcement reduced differential settlements between the most highly stressed regions of the concrete.

The replacement of the stirrups in beam CBM3 by the expanded metal mesh in beam EBM3 was sufficient to reduce the width of the cracks to an acceptable level i.e. the width of crack was less than 0.20 mm at a loading level which corresponded to a load of 50 kN during the first load cycle.

It must be emphasised, that the strains recorded in beam EBM3 for both the concrete and the reinforcement are smaller than those recorded in beam CBM3. This can be also explained by the contribution of the expanded metal mesh towards the resistance to shear and flexure actions.

The test results obtained for beam EBM3 confirmed that the expanded metal mesh is a practical solution which can be used in coupling beam structures. It is anticipated, at this stage, that the proposed reinforcement arrangement will offer a satisfactory solution to the crucial problem of the types of shear wall structures under consideration and that it will, eventually, lead to the development of more practical design solutions for these structures.

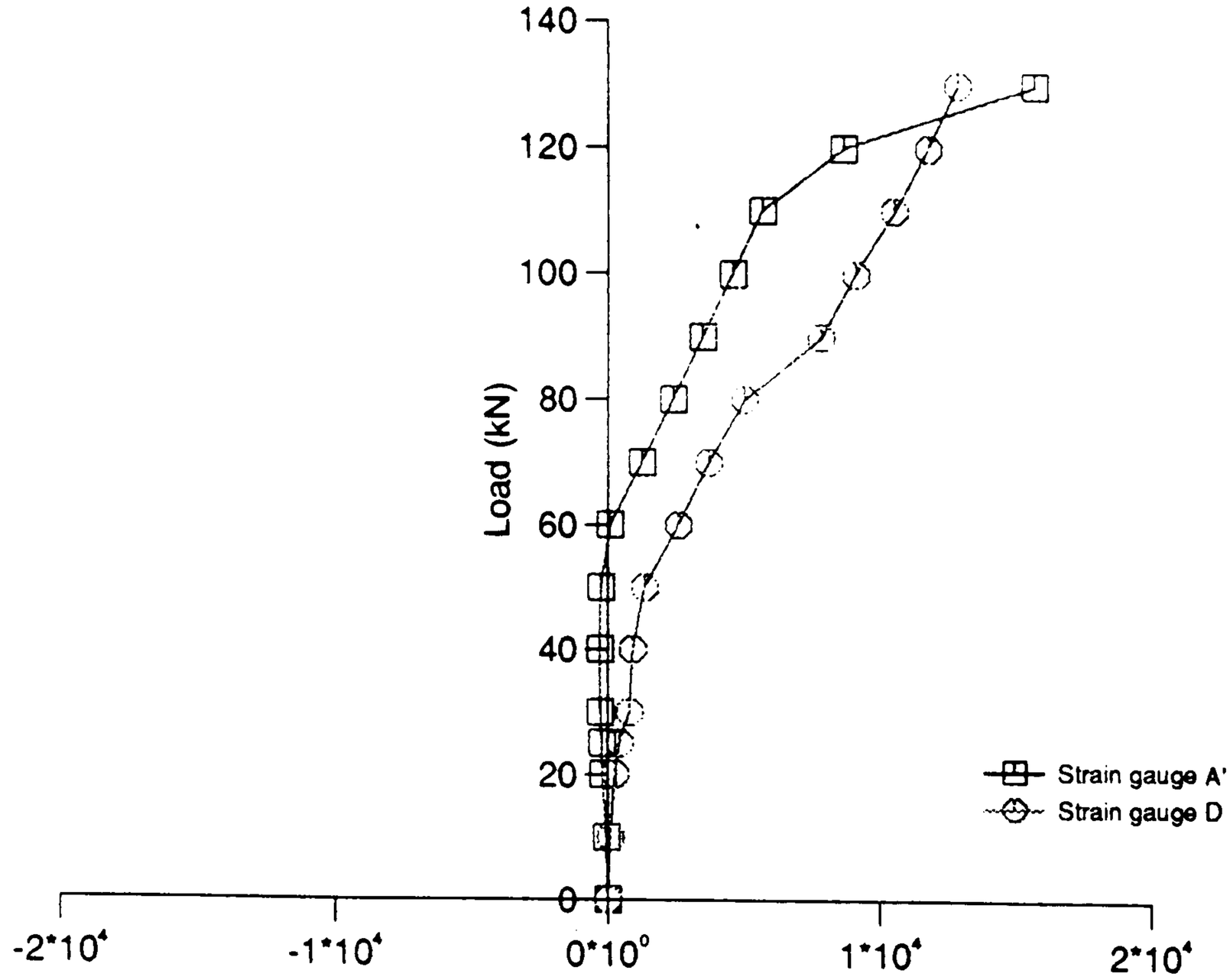


Figure 6.1: Distribution of strain along the top reinforcement at gauge positions A' and D

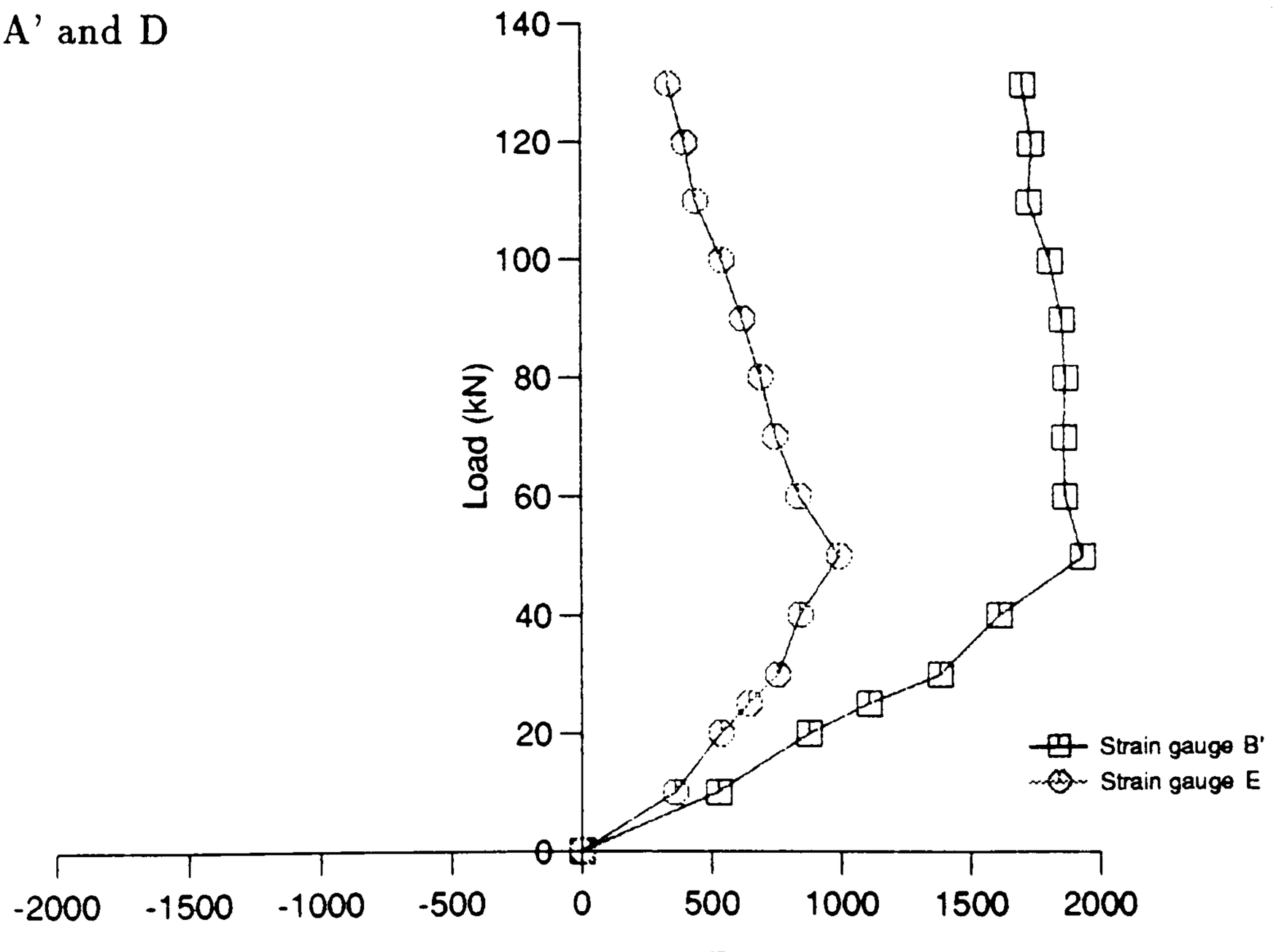


Figure 6.2: Distribution of strain along the top reinforcement at gauge positions B' and E

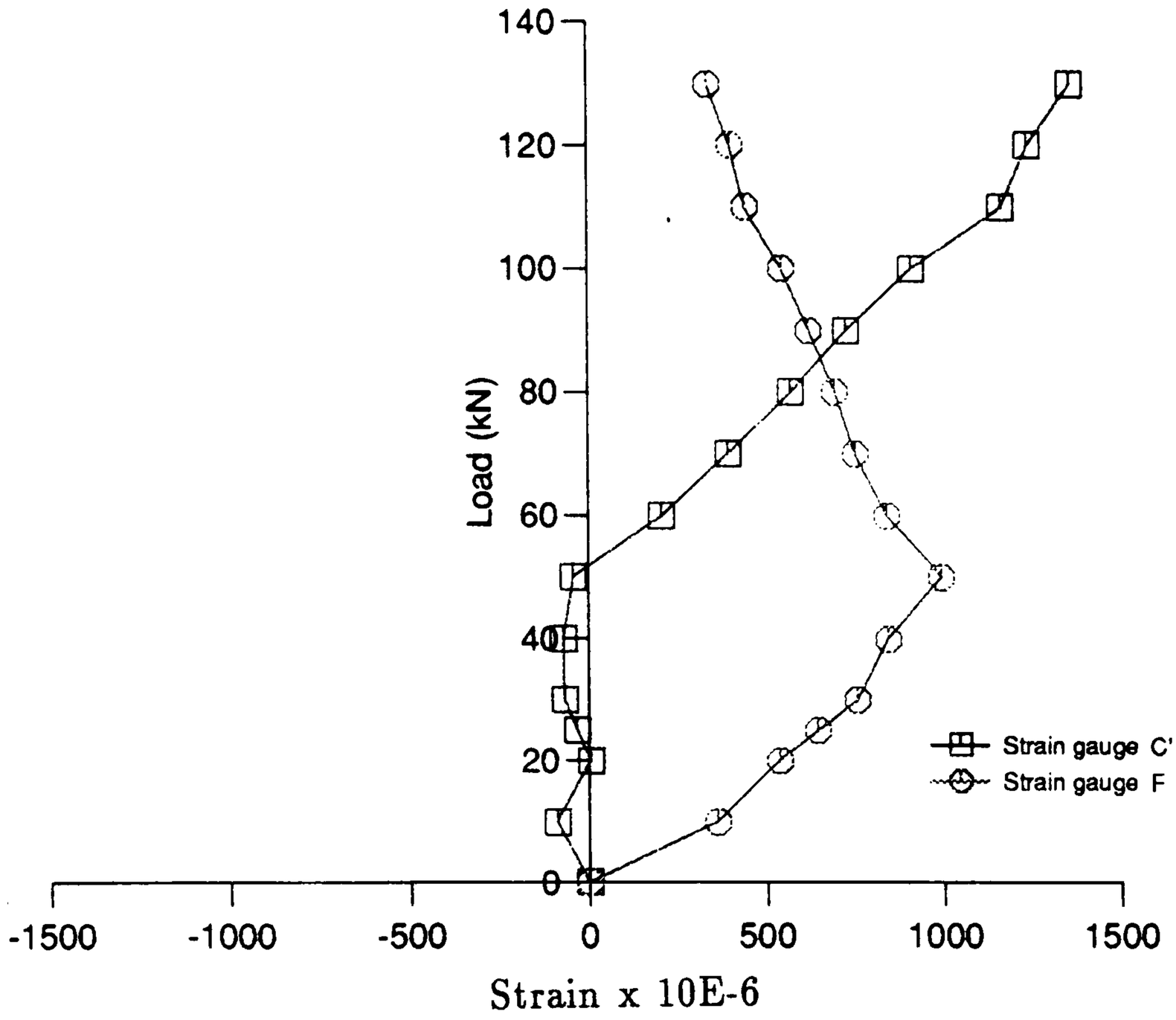


Figure 6.3: Distribution of strain along the top reinforcement at gauge positions C' and F

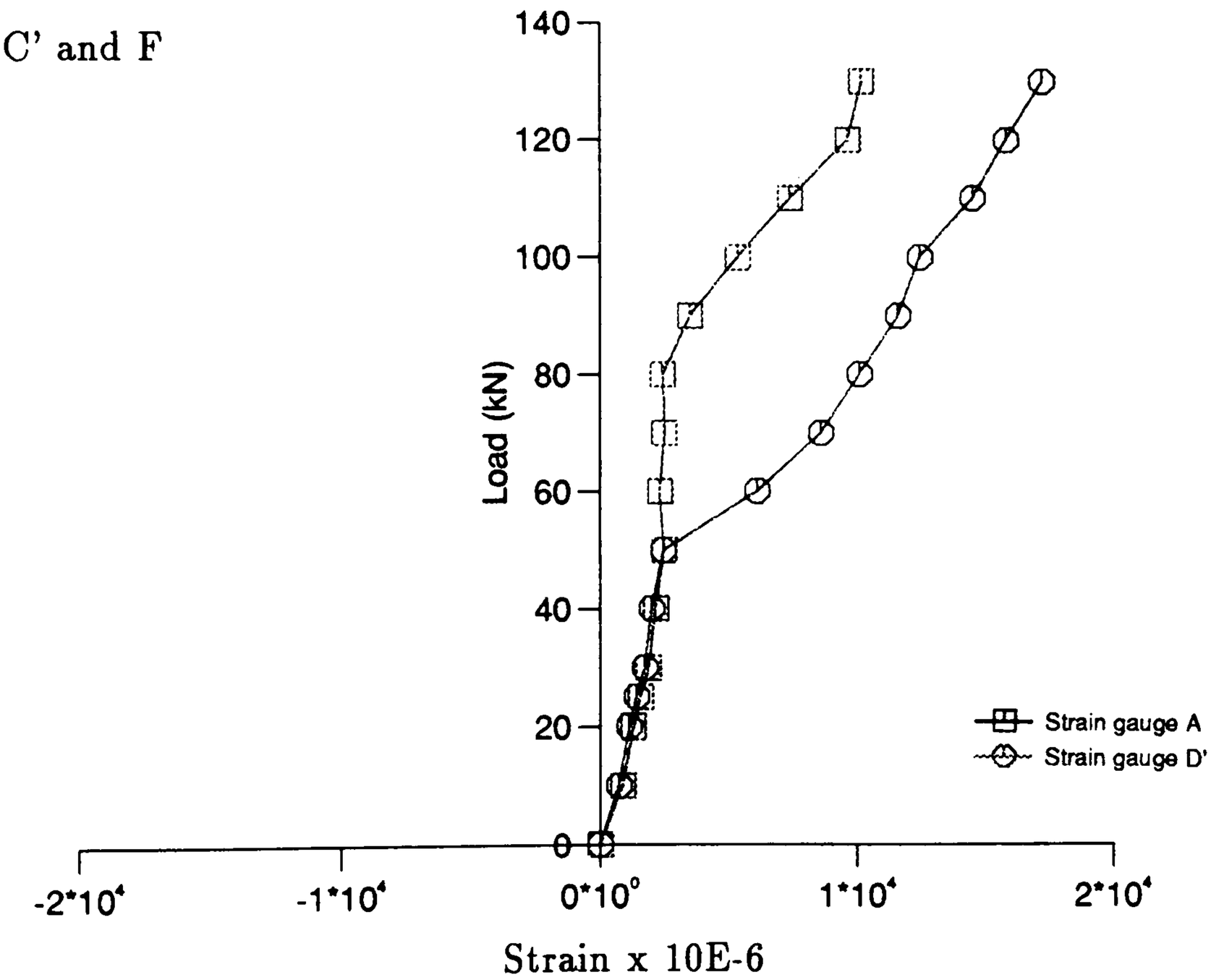


Figure 6.4: Distribution of strain along the bottom reinforcement at gauge positions A and D'

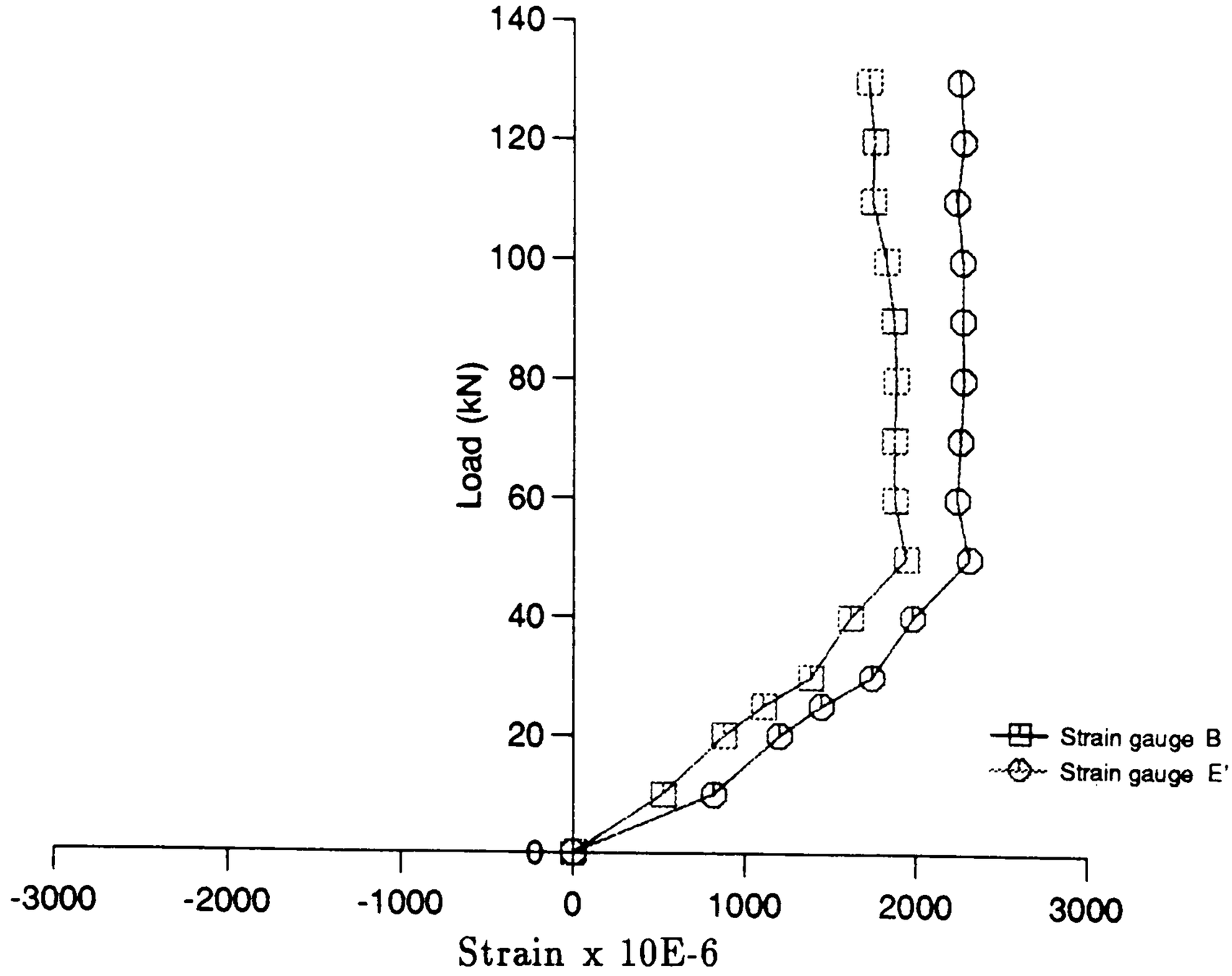


Figure 6.5: Distribution of strain along the bottom reinforcement at gauge positions B and E'

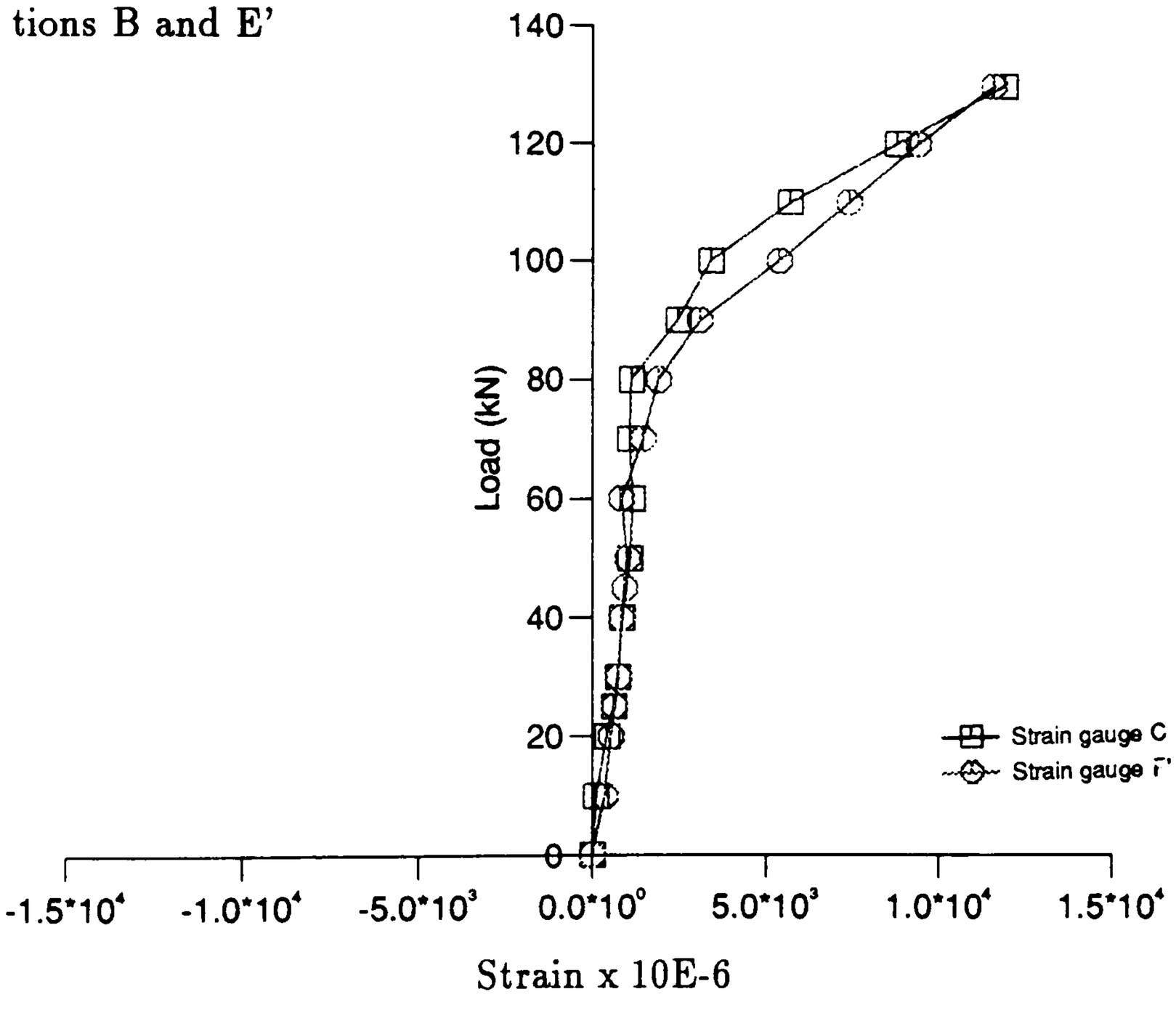


Figure 6.6: Distribution of strain along the bottom reinforcement at gauge positions C and F'

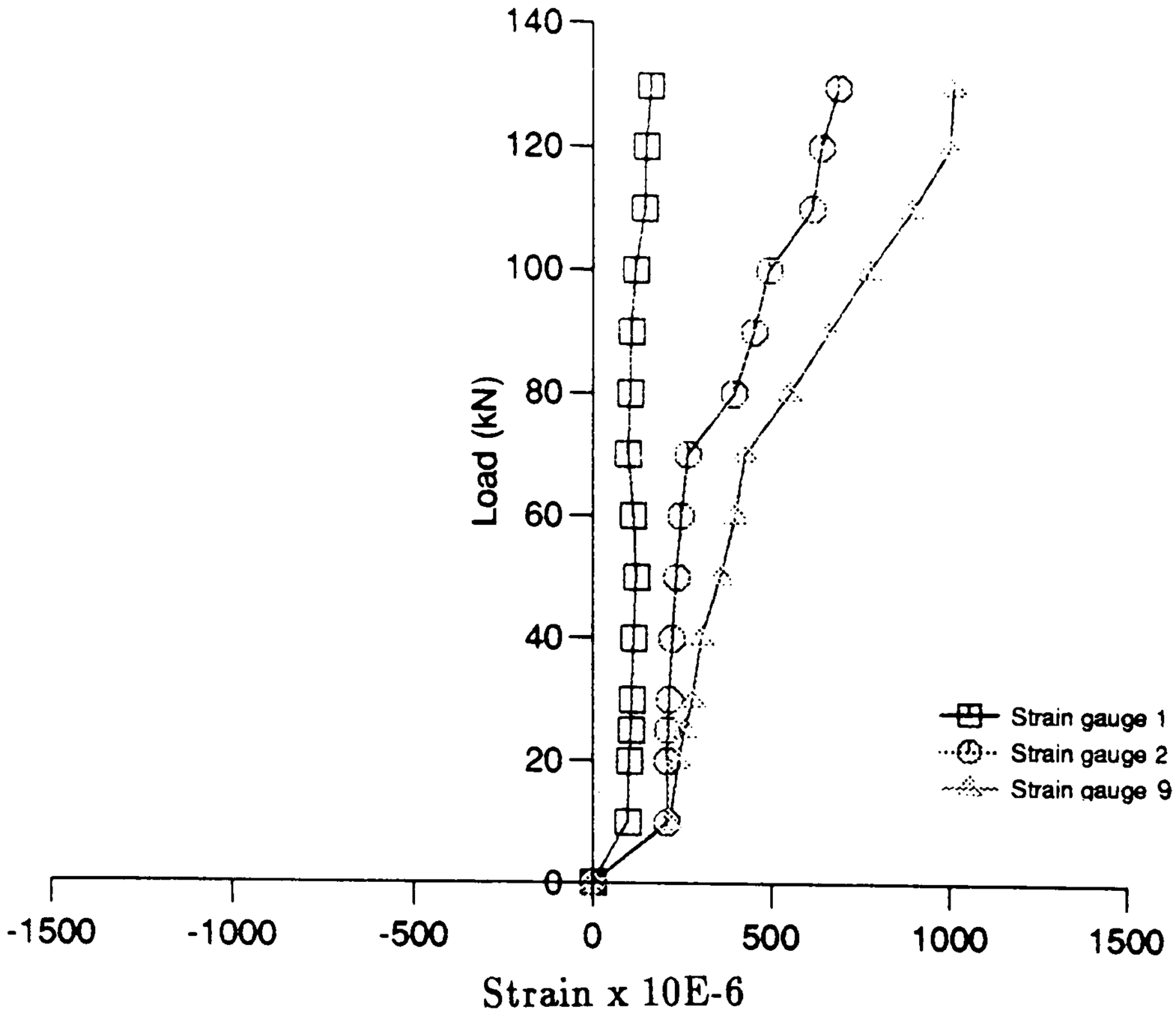


Figure 6.7: Distribution of strain along the stirrups at the right hand support

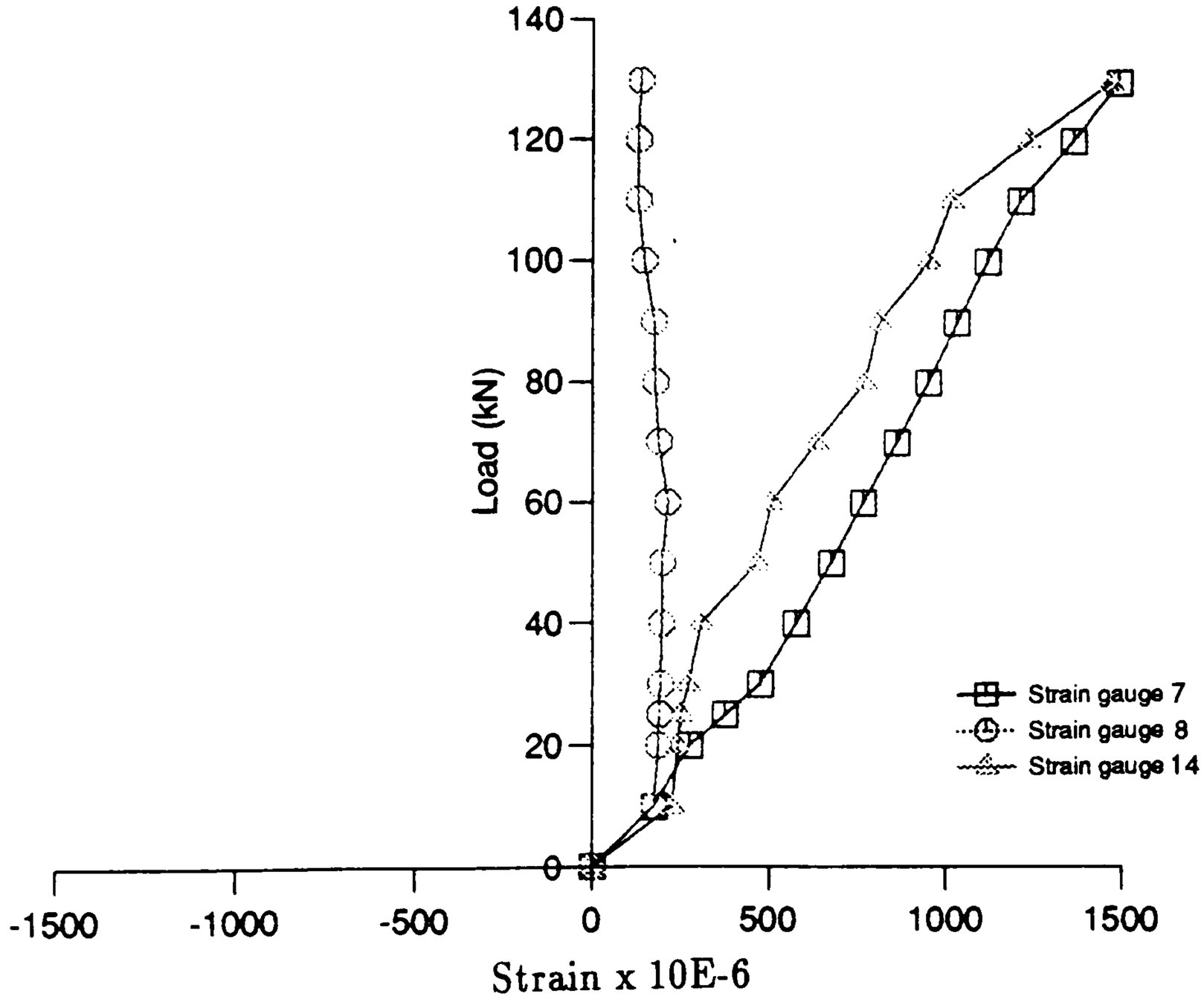


Figure 6.8: Distribution of strain along the stirrups at the left hand support

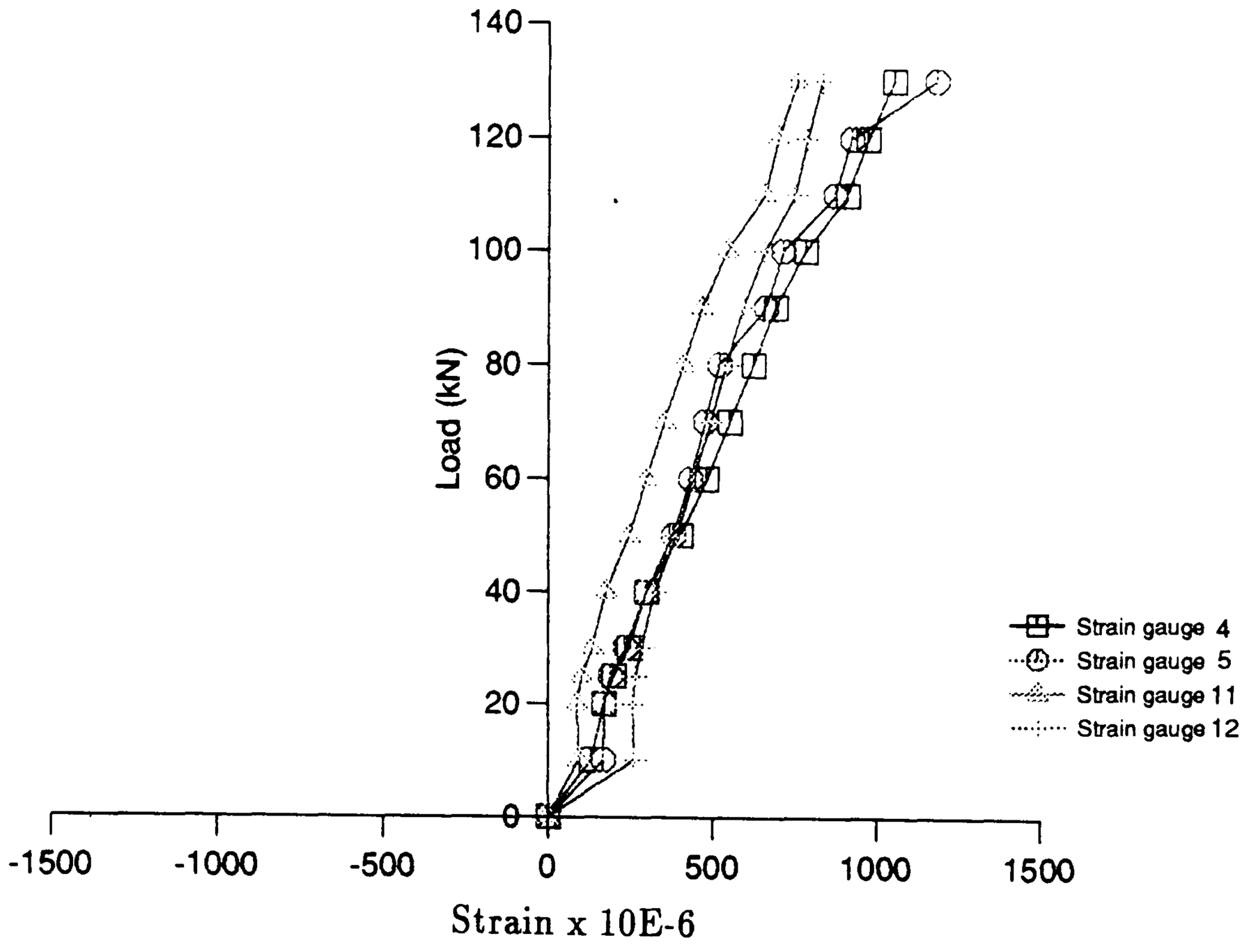


Figure 6.9: Distribution of strain along the stirrups at midspan

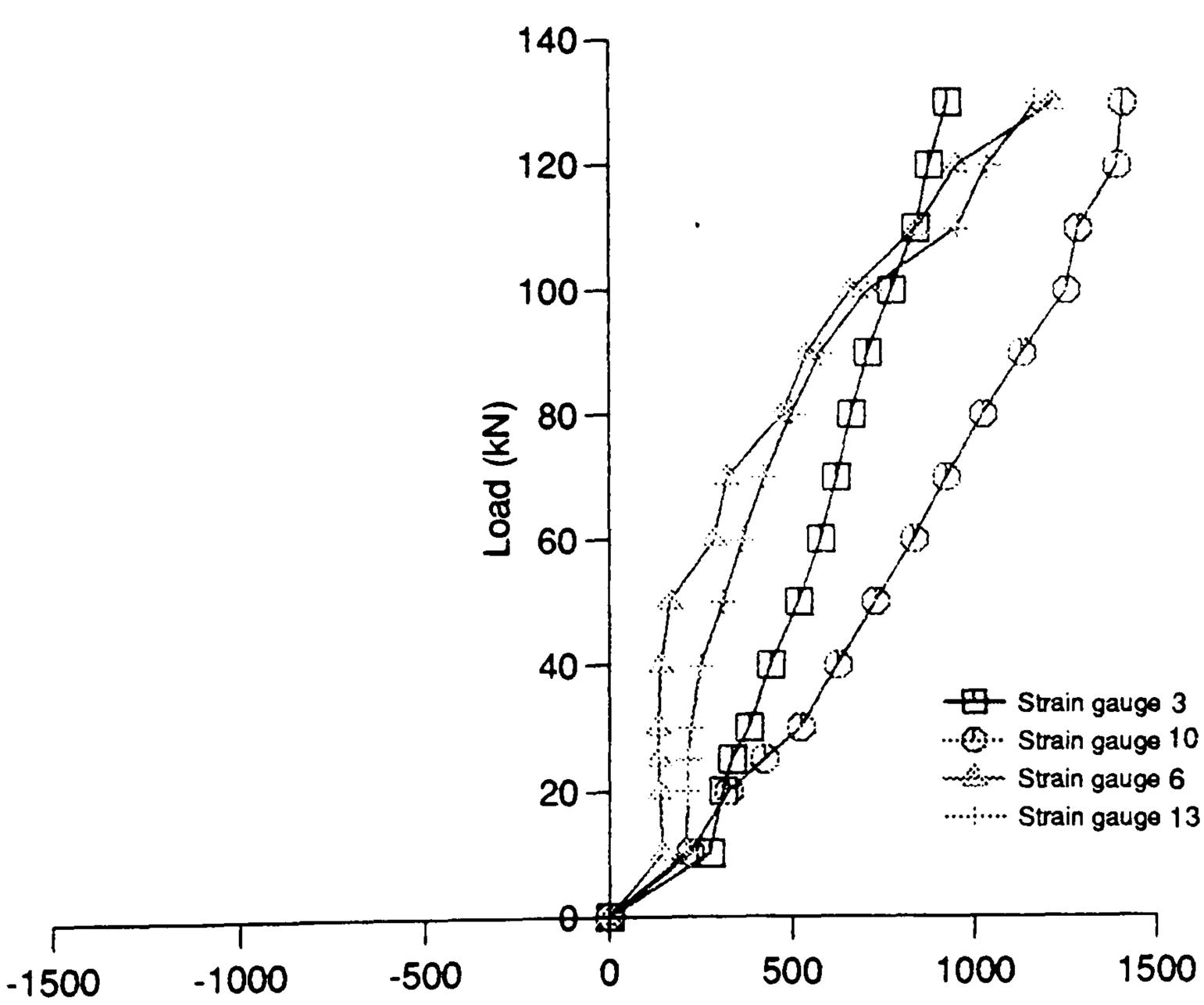


Figure 6.10: Distribution of strain along the stirrups at the quarter span point

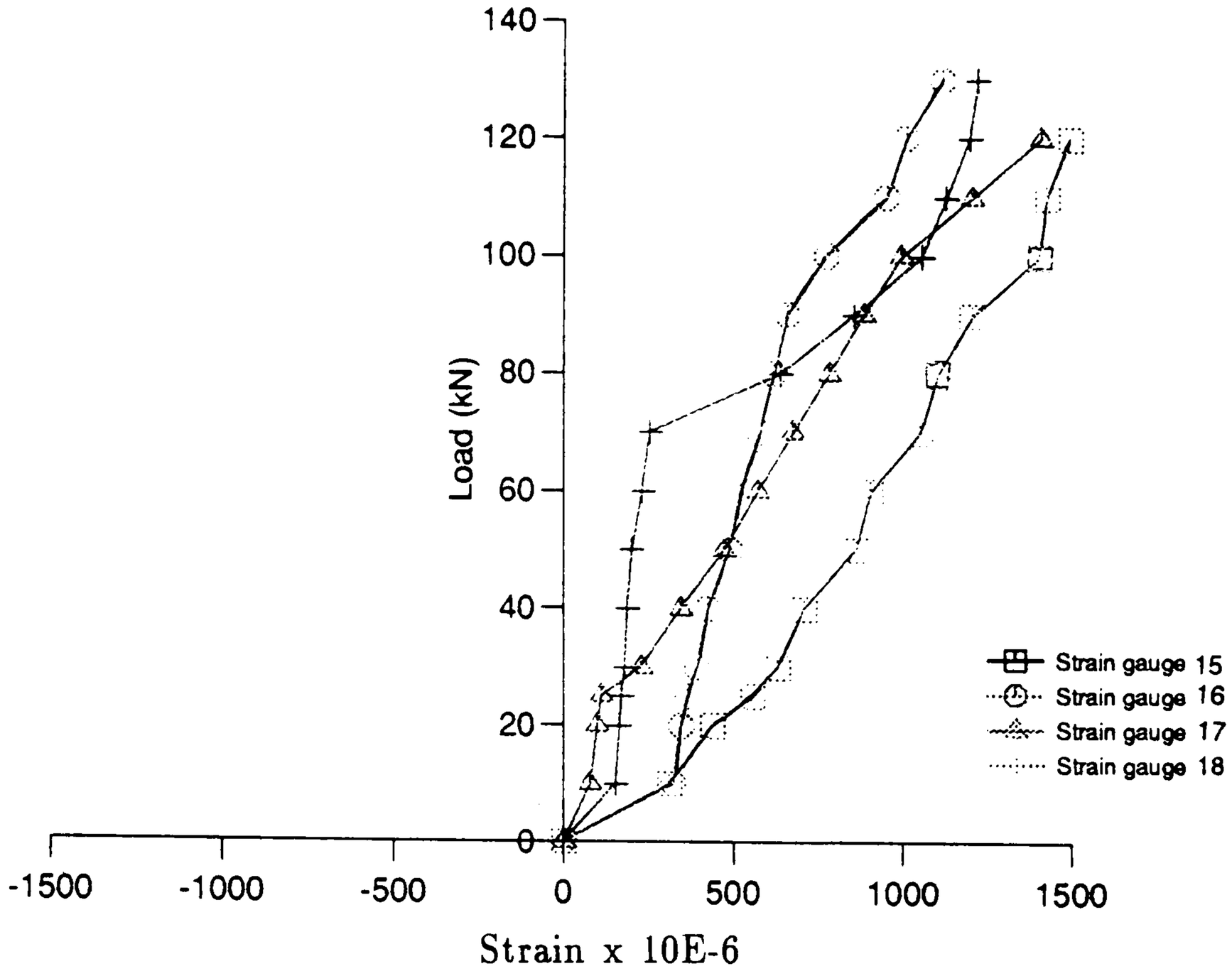


Figure 6.11: Distribution of strain along the second stirrups

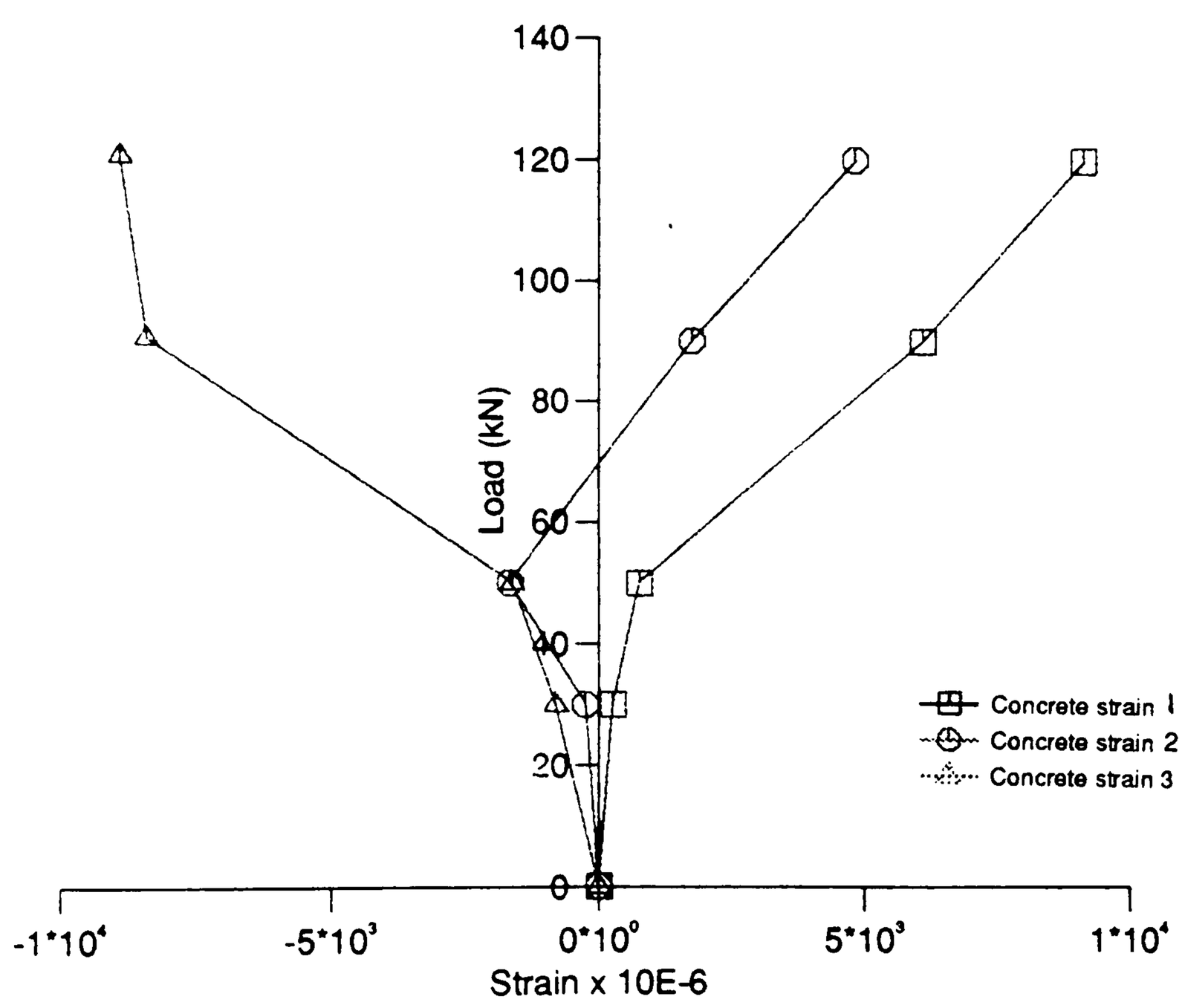


Figure 6.12: Distribution of strain along the concrete at the right hand support

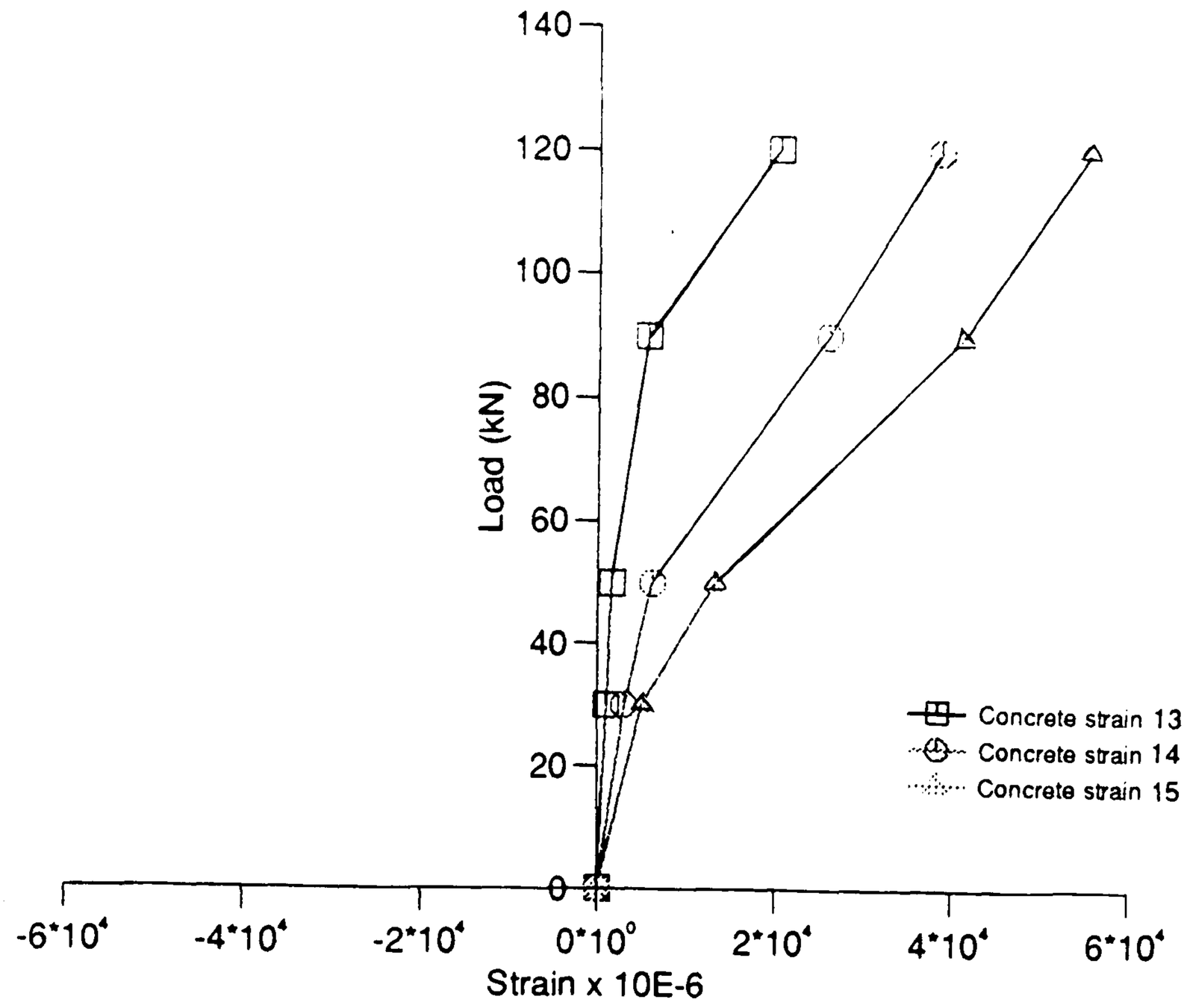


Figure 6.13: Distribution of strain along the concrete at the left hand support

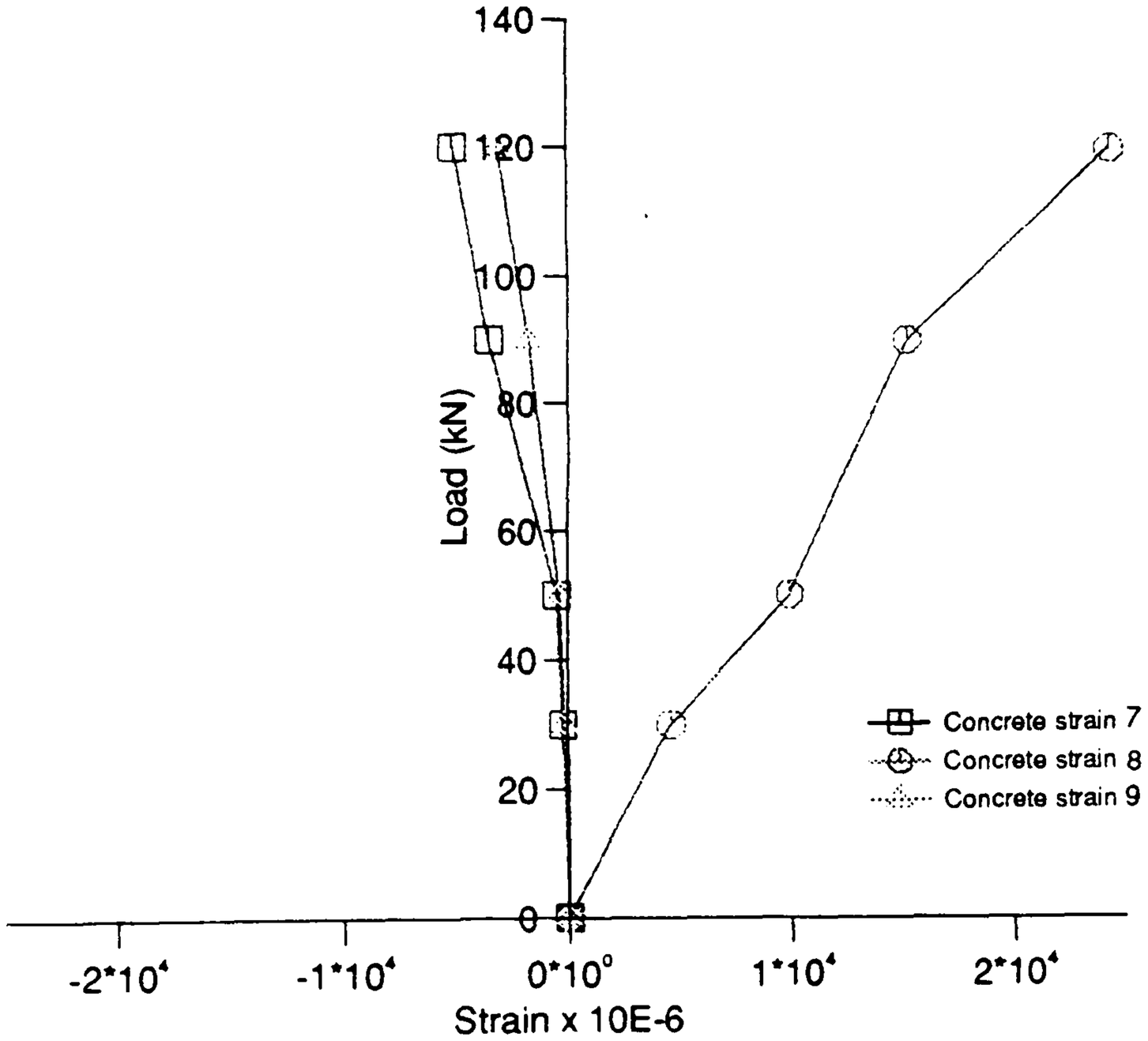


Figure 6.14: Distribution of strain along the concrete at midspan

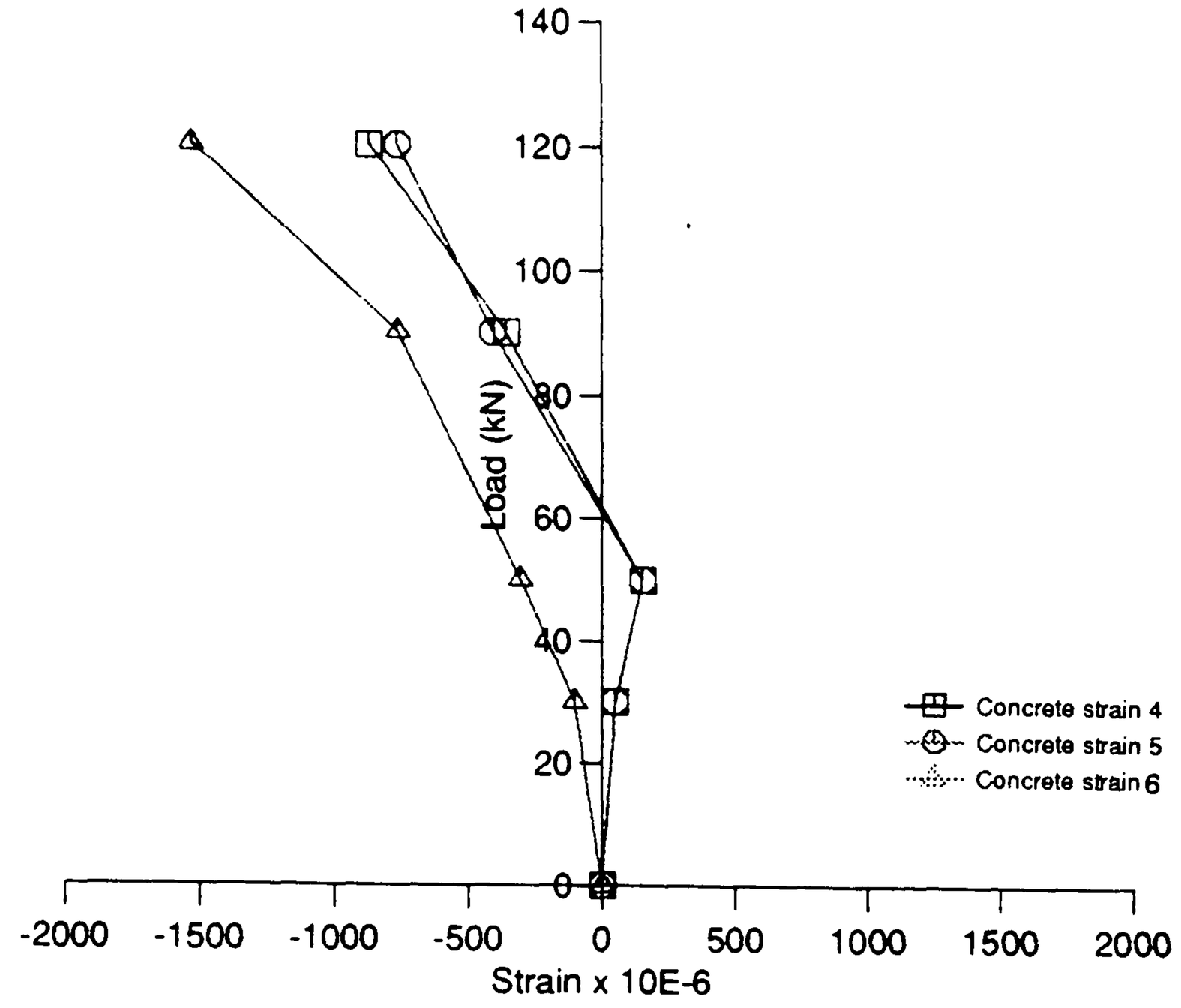


Figure 6.15: Distribution of strain along the concrete at right quarter span point

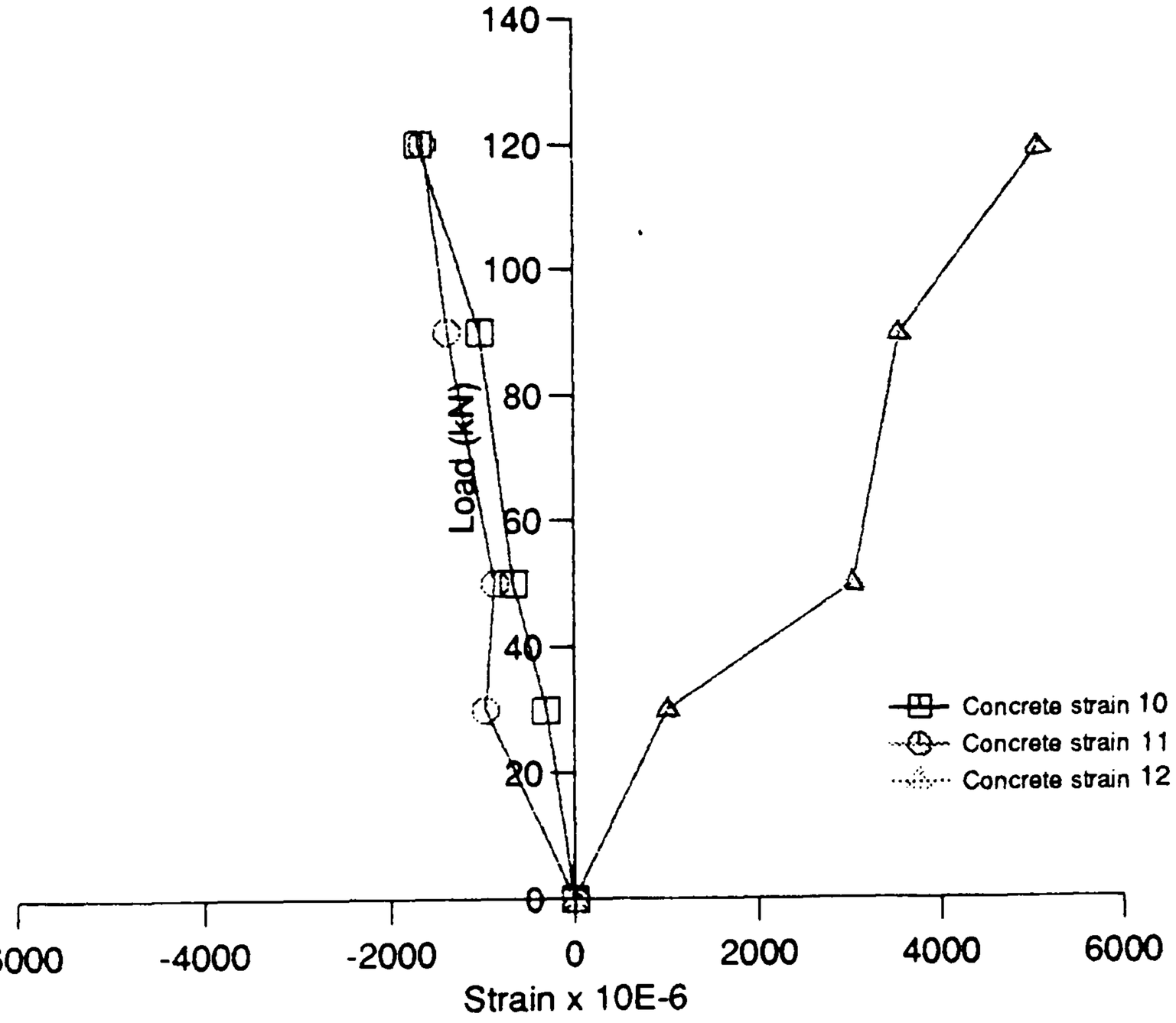


Figure 6.16: Distribution of strain along the concrete at left quarter span point

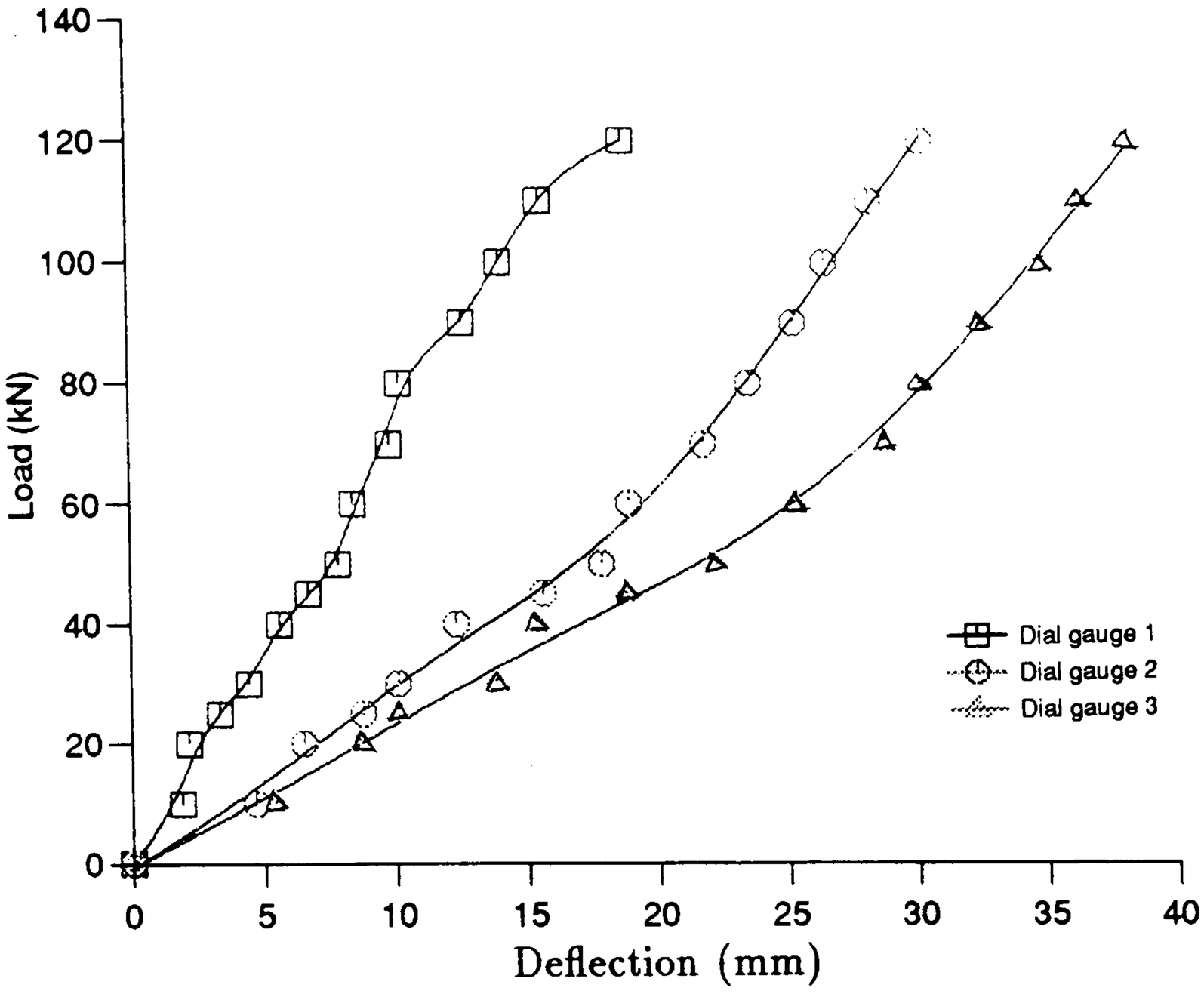


Figure 6.17: Load-deflection relationships for beam CBM3

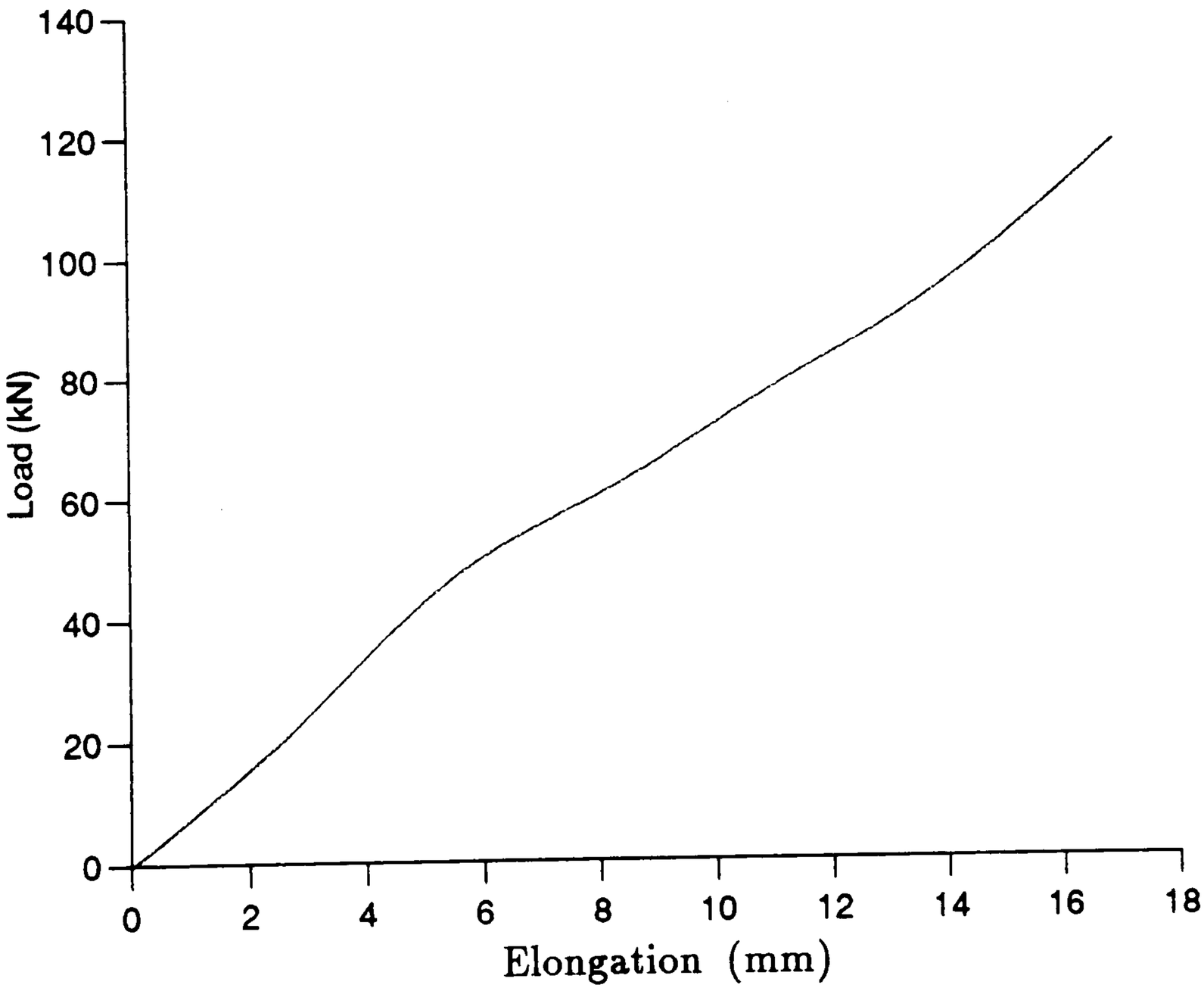


Figure 6.18: Load-elongation relationship for beam CBM3

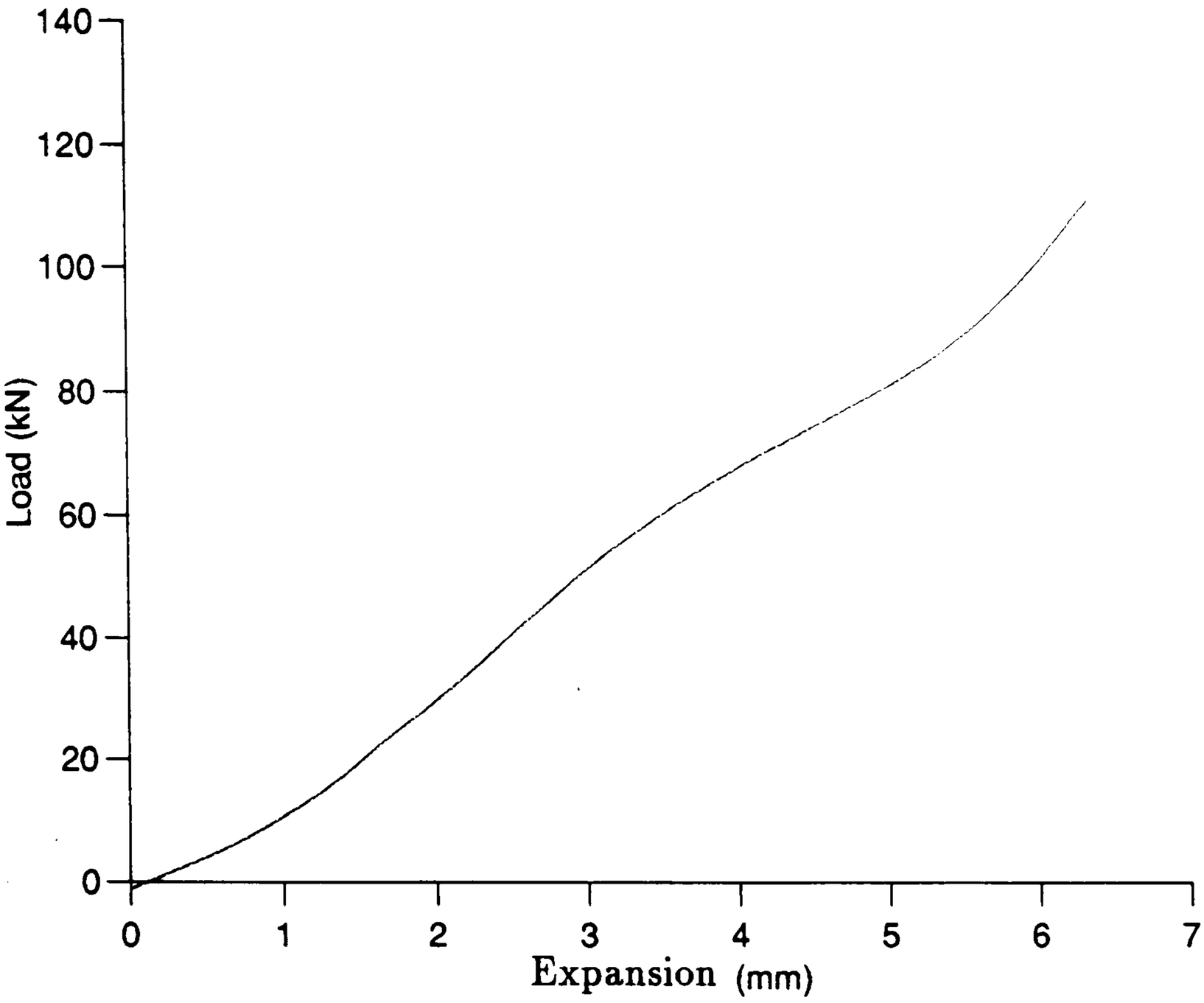


Figure 6.19: Load-expansion relationship for beam CBM3

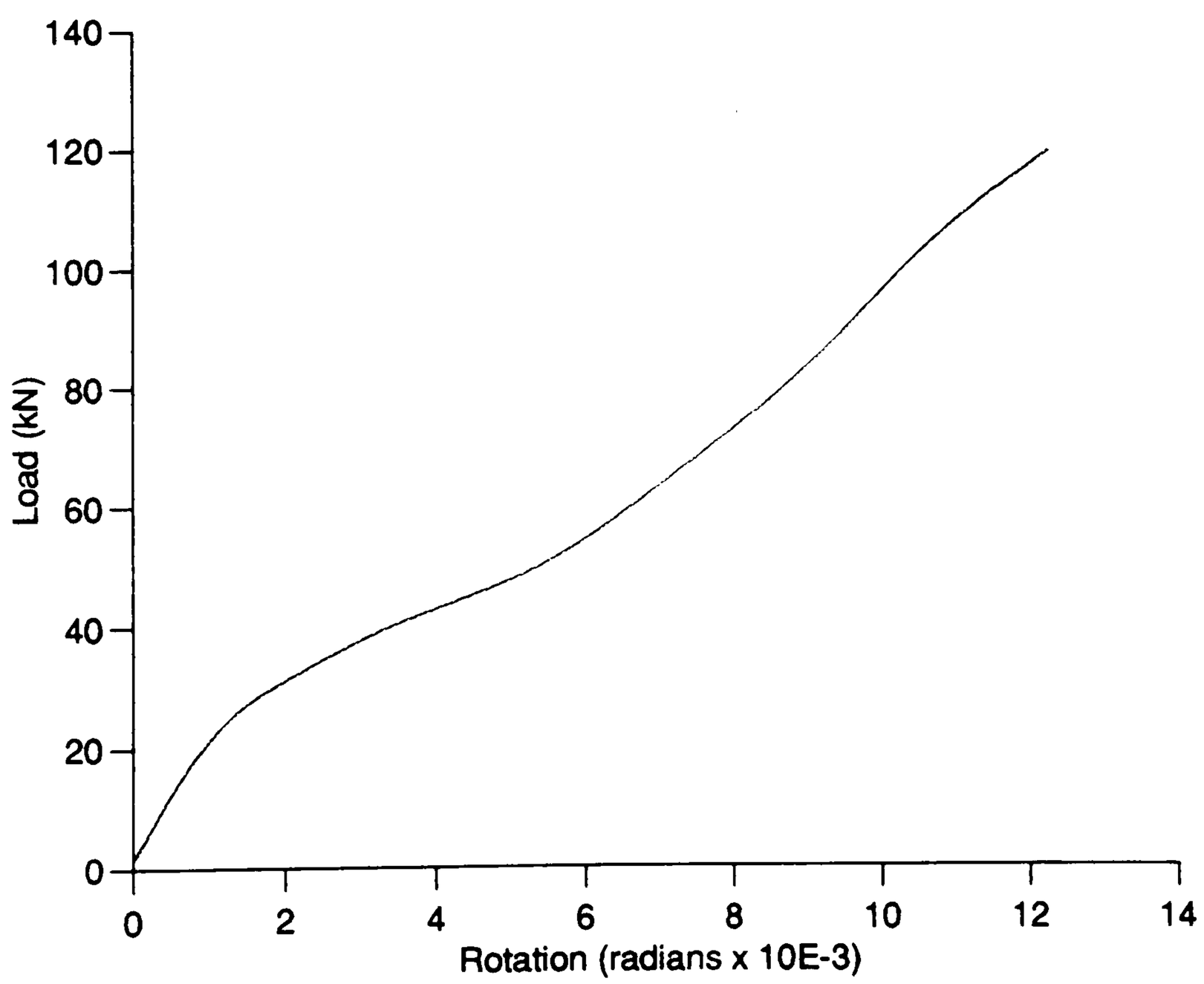


Figure 6.20: Load-rotation relationship for beam CBM3

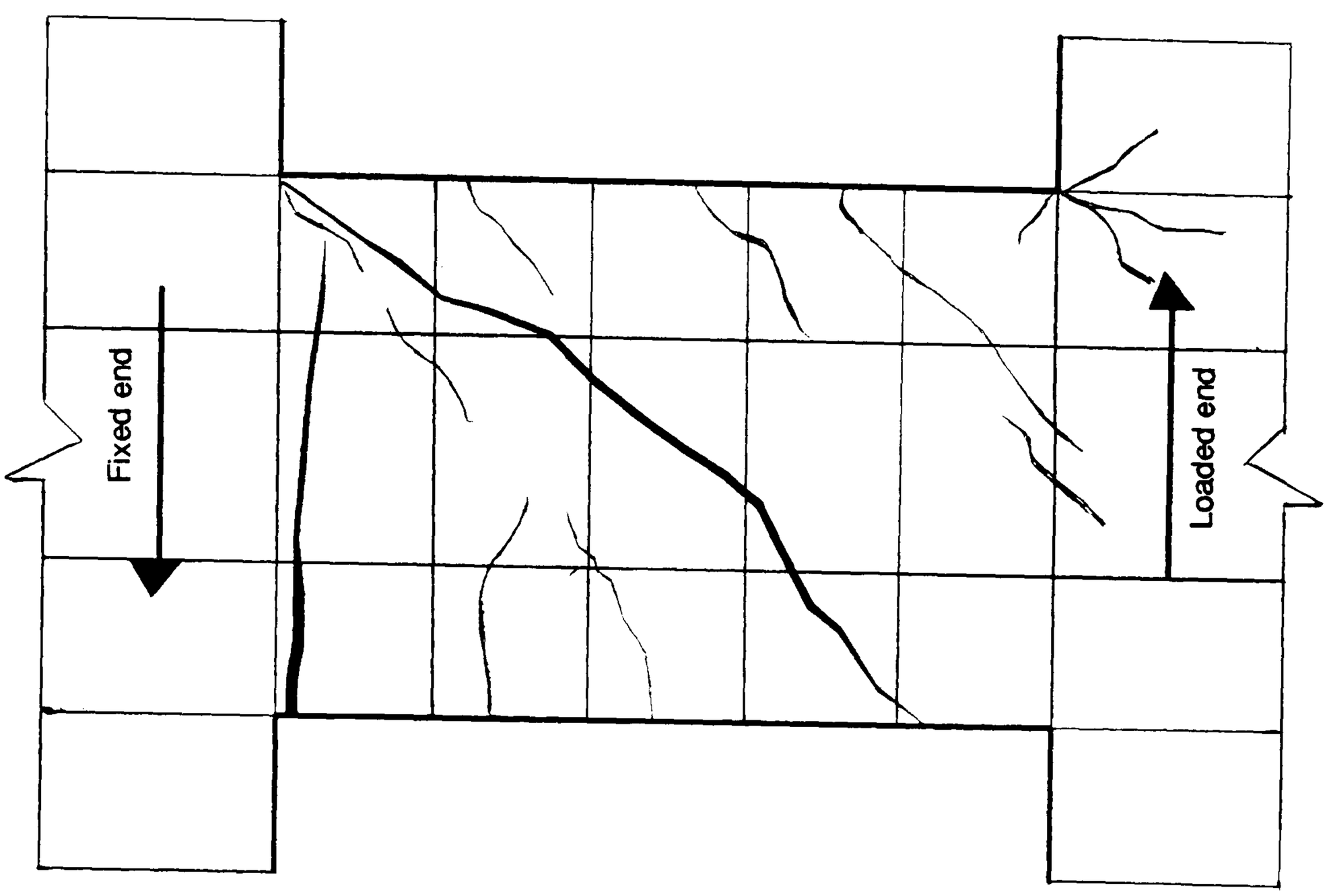


Figure 6.21: Failure mechanism of beam CBM3

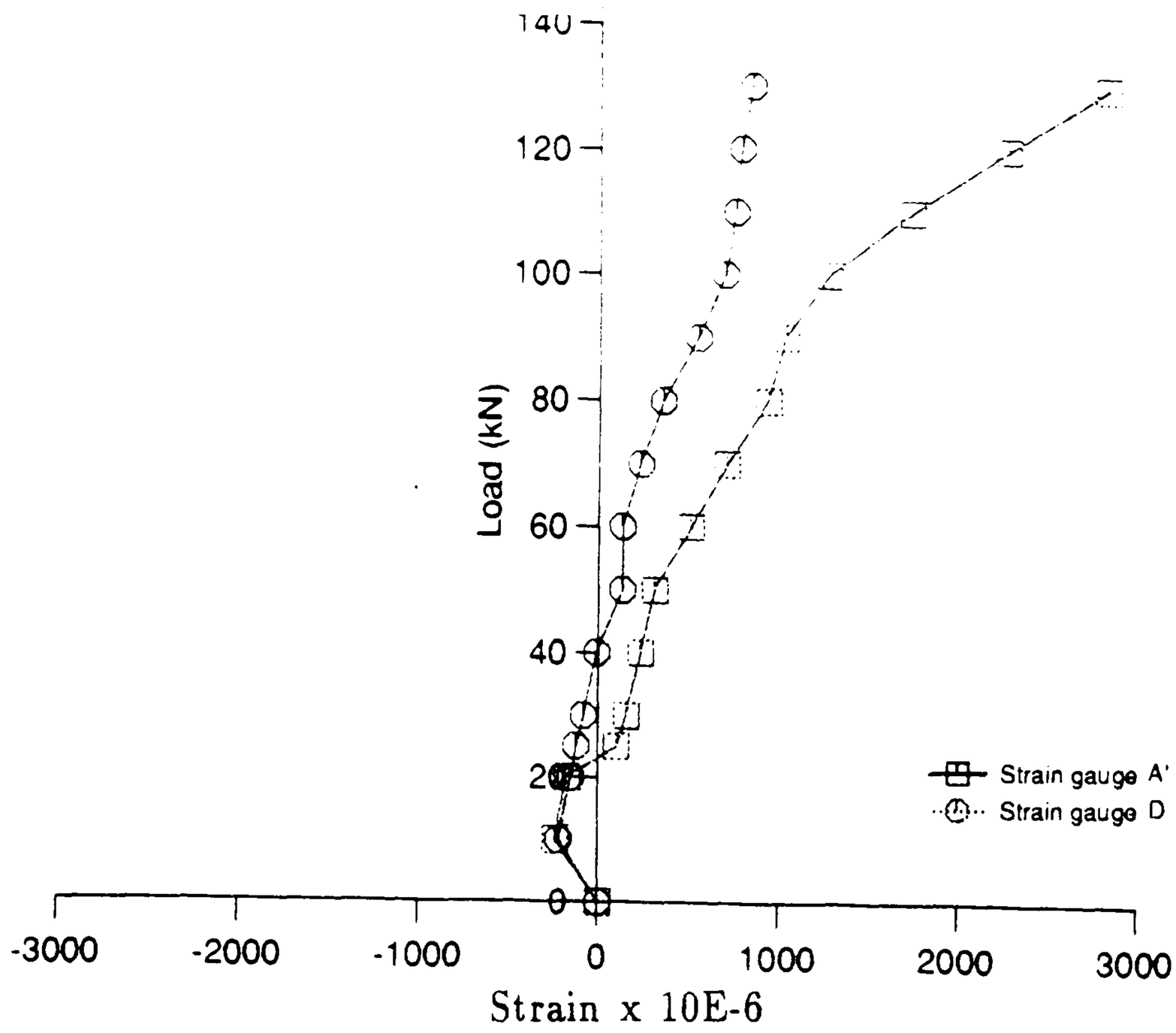


Figure 6.22: Distribution of strain along the top reinforcement at gauge positions A' and D

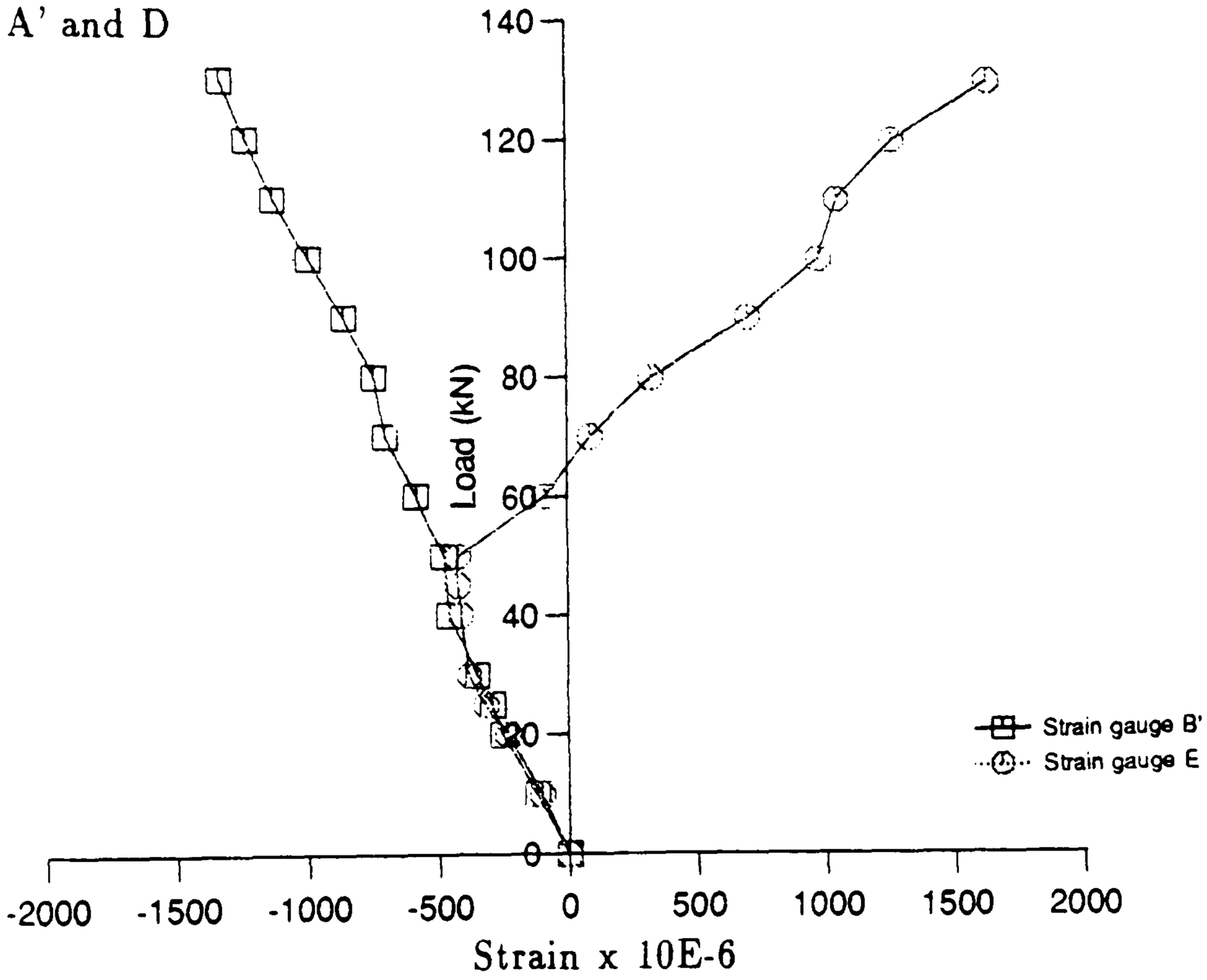


Figure 6.23: Distribution of strain along the top reinforcement at strain gauge positions B' and E

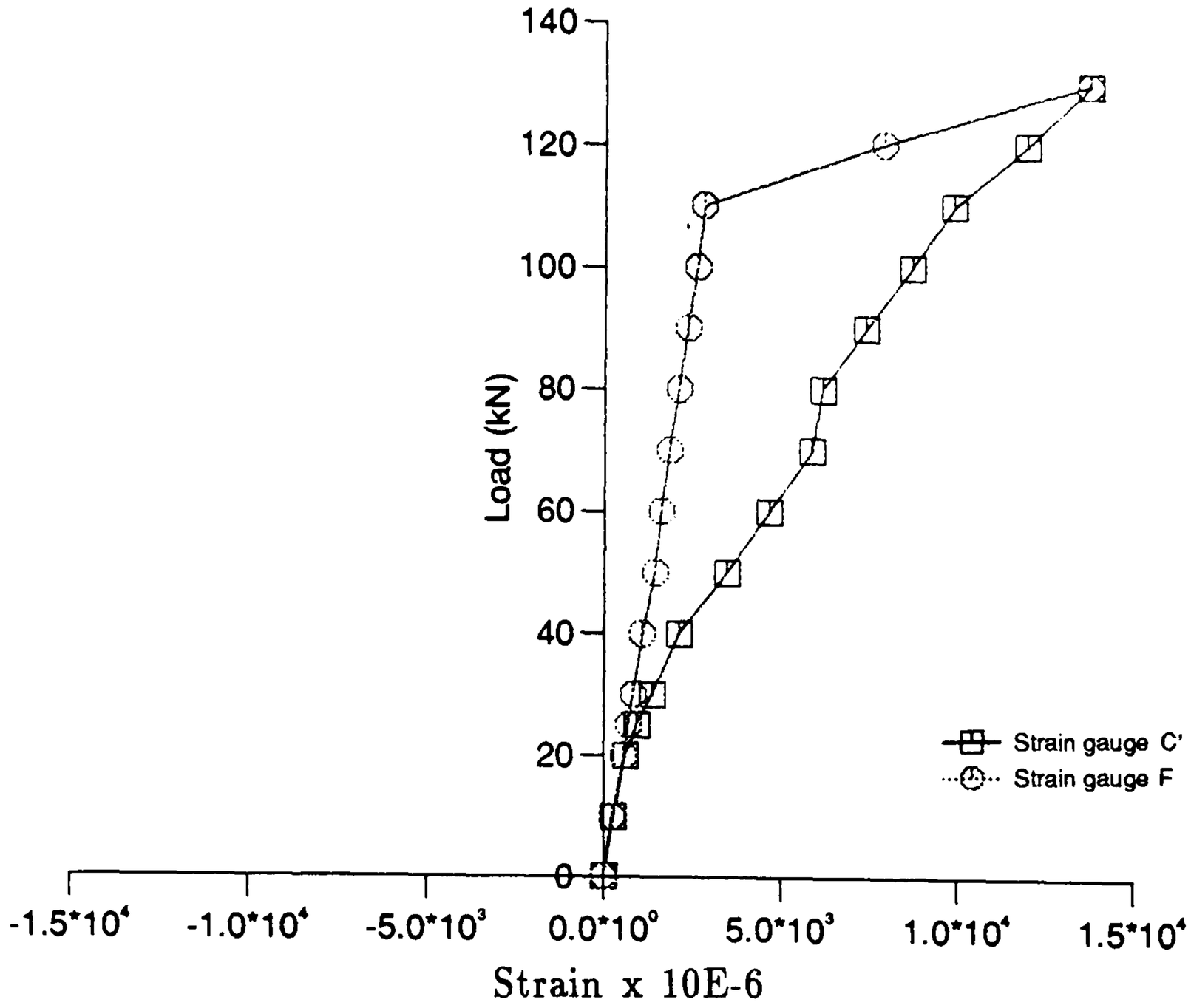


Figure 6.24: Distribution of strain along the top reinforcement at gauge positions C' and F

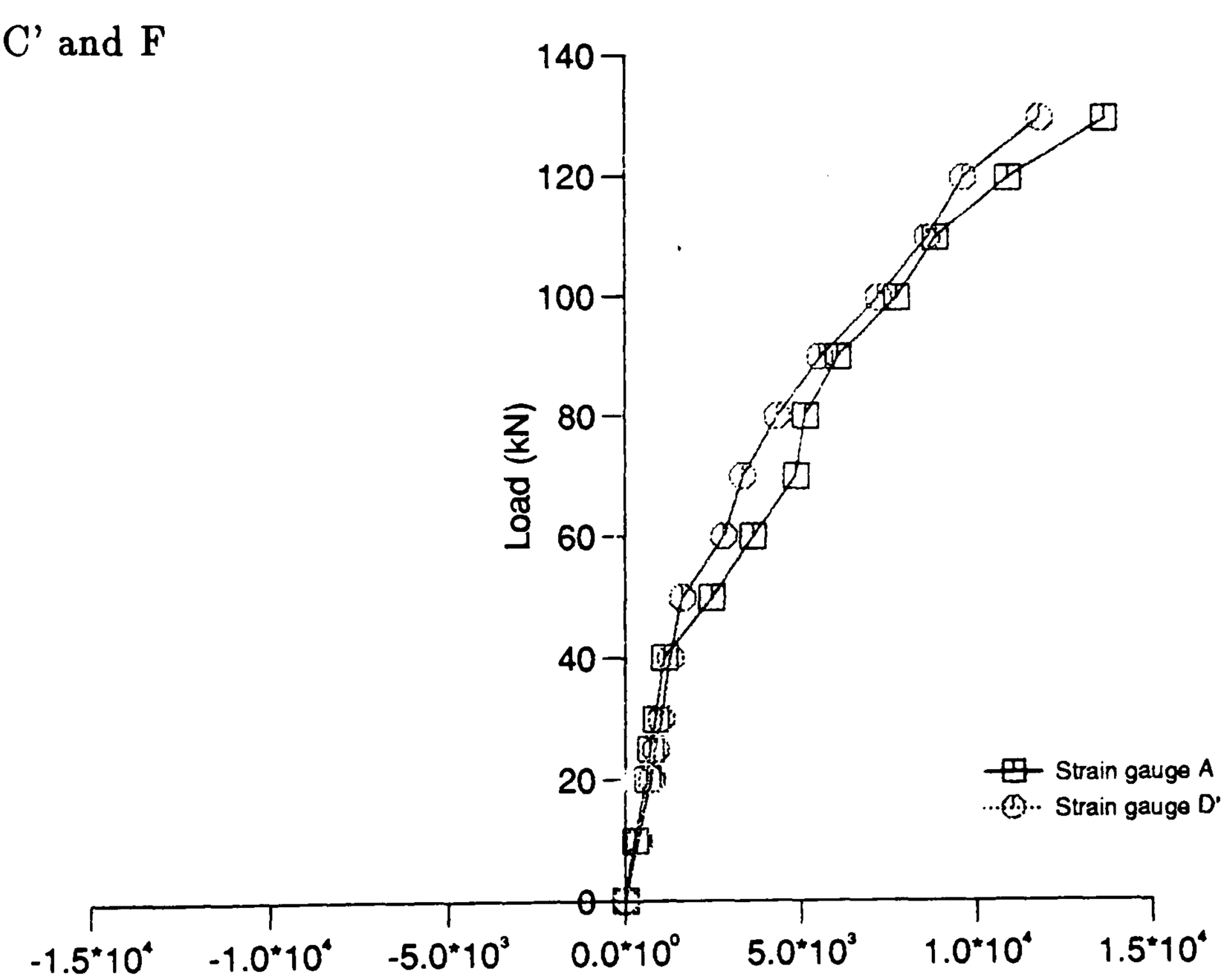


Figure 6.25: Distribution of strain along the bottom reinforcement at gauge positions A and D'

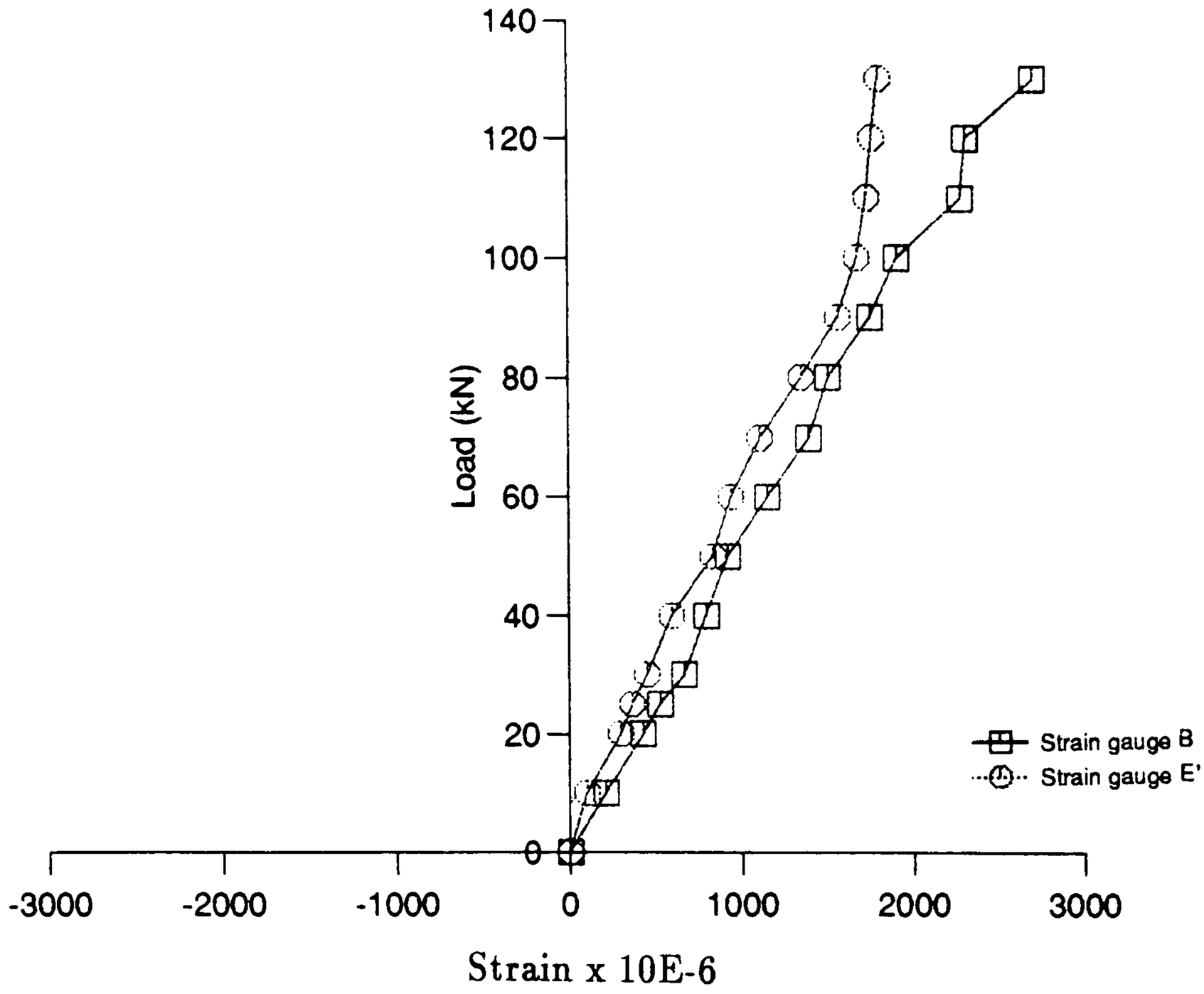


Figure 6.26: Distribution of strain along the bottom reinforcement at gauge positions B and E'

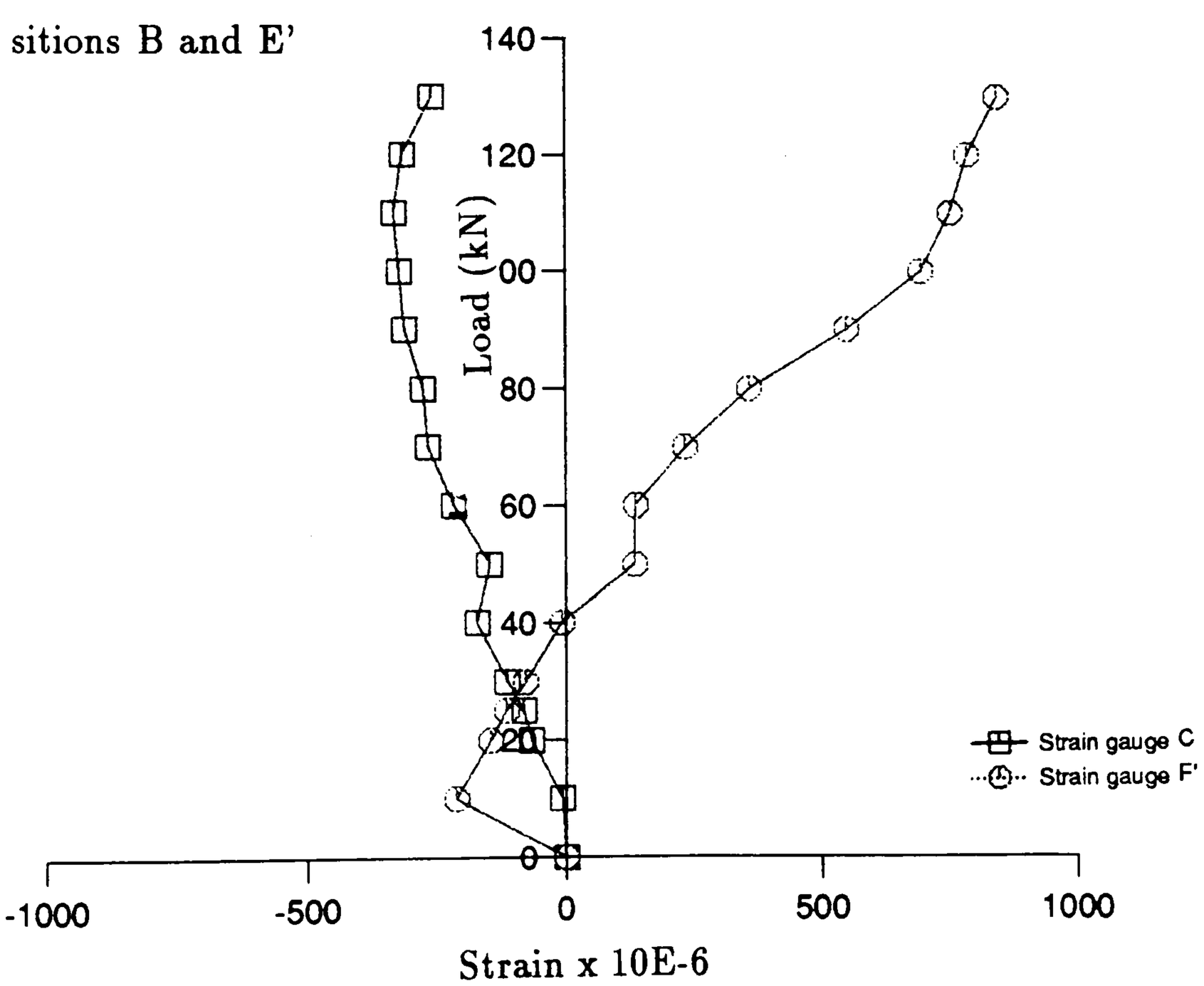


Figure 6.27: Distribution of strain along the bottom reinforcement at gauge positions C and F'

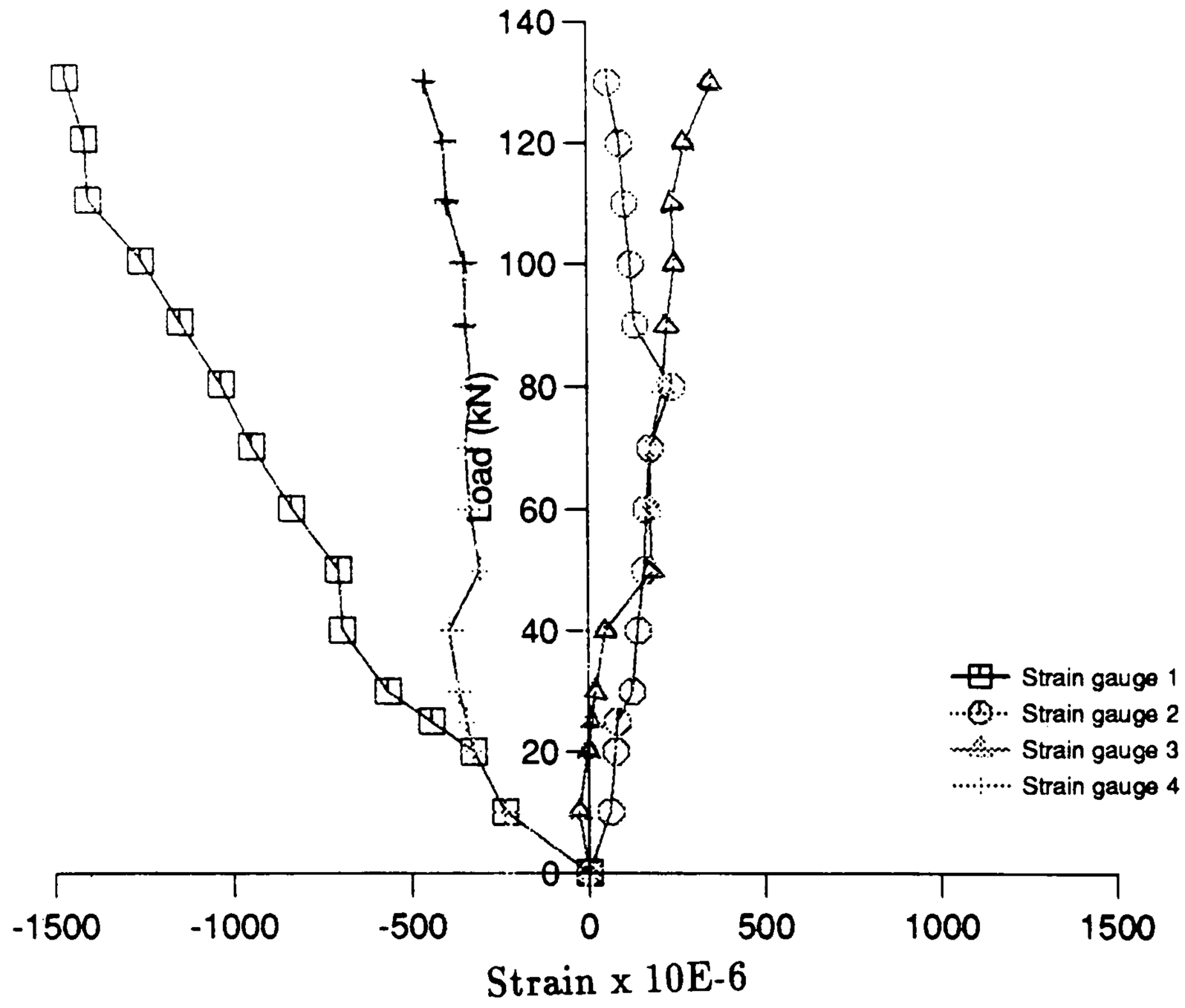


Figure 6.28: Distribution of strain along the mesh at the right hand support

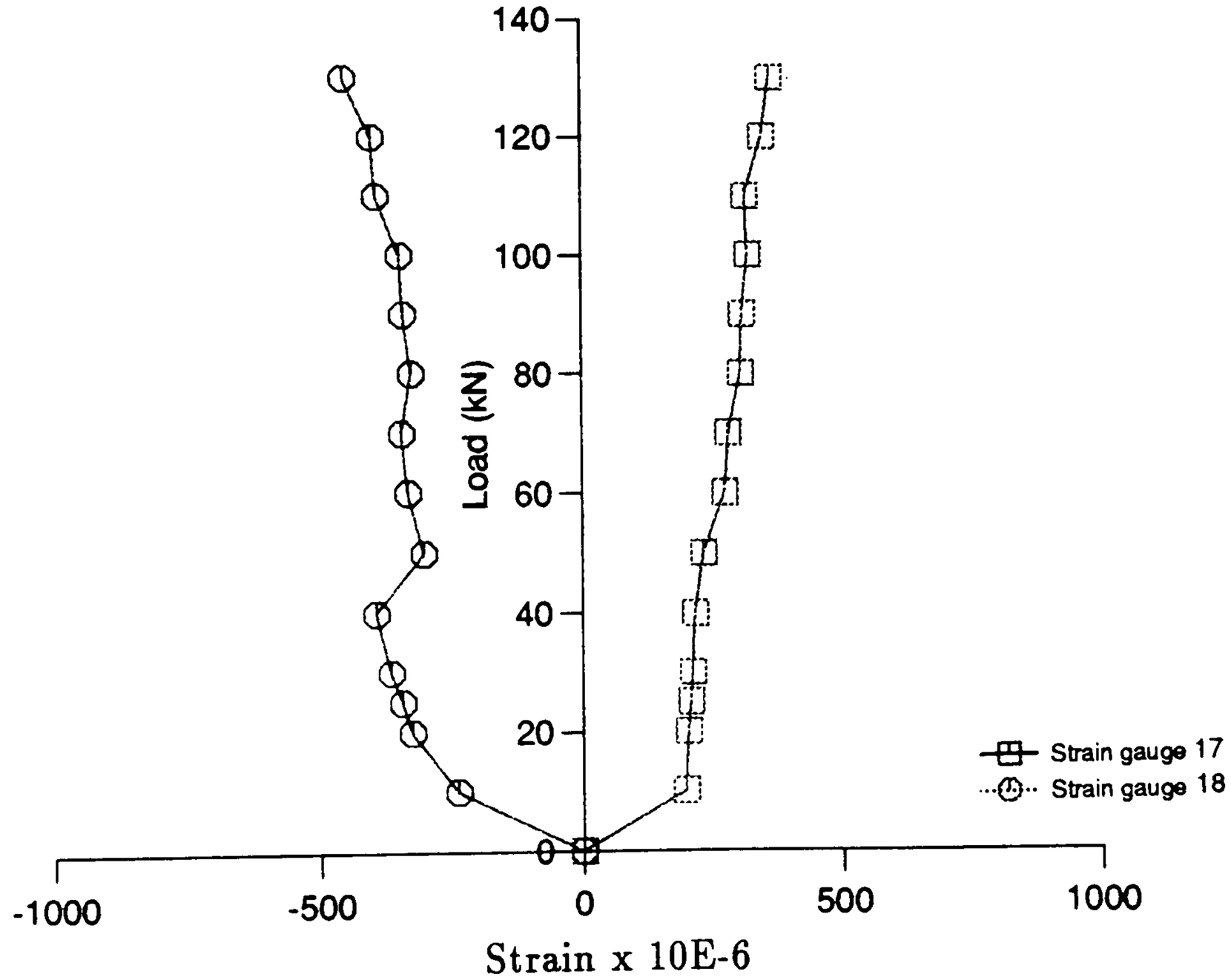


Figure 6.29: Distribution of strain along the mesh at the left hand support

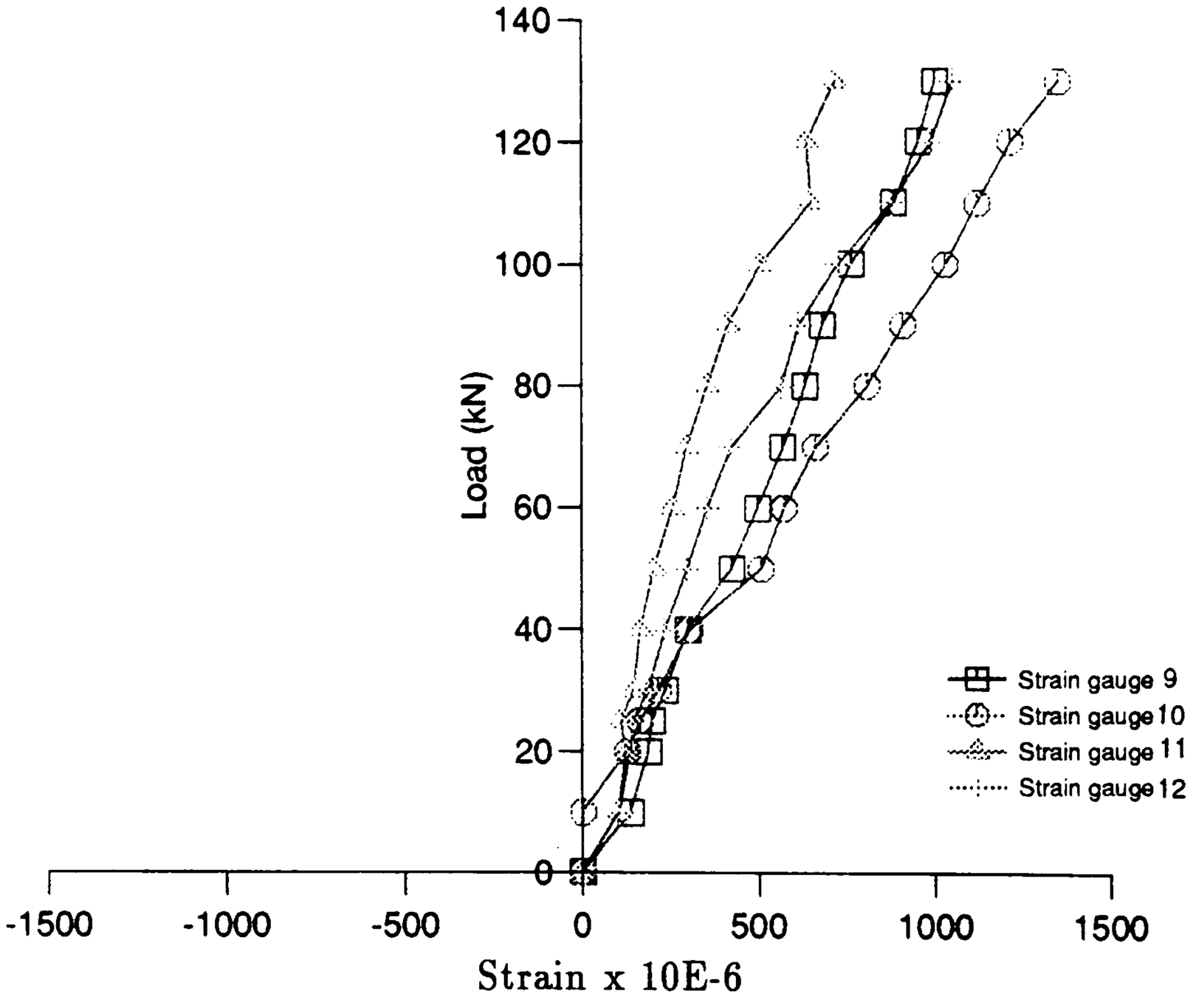


Figure 6.30: Distribution of strain along the mesh at midspan

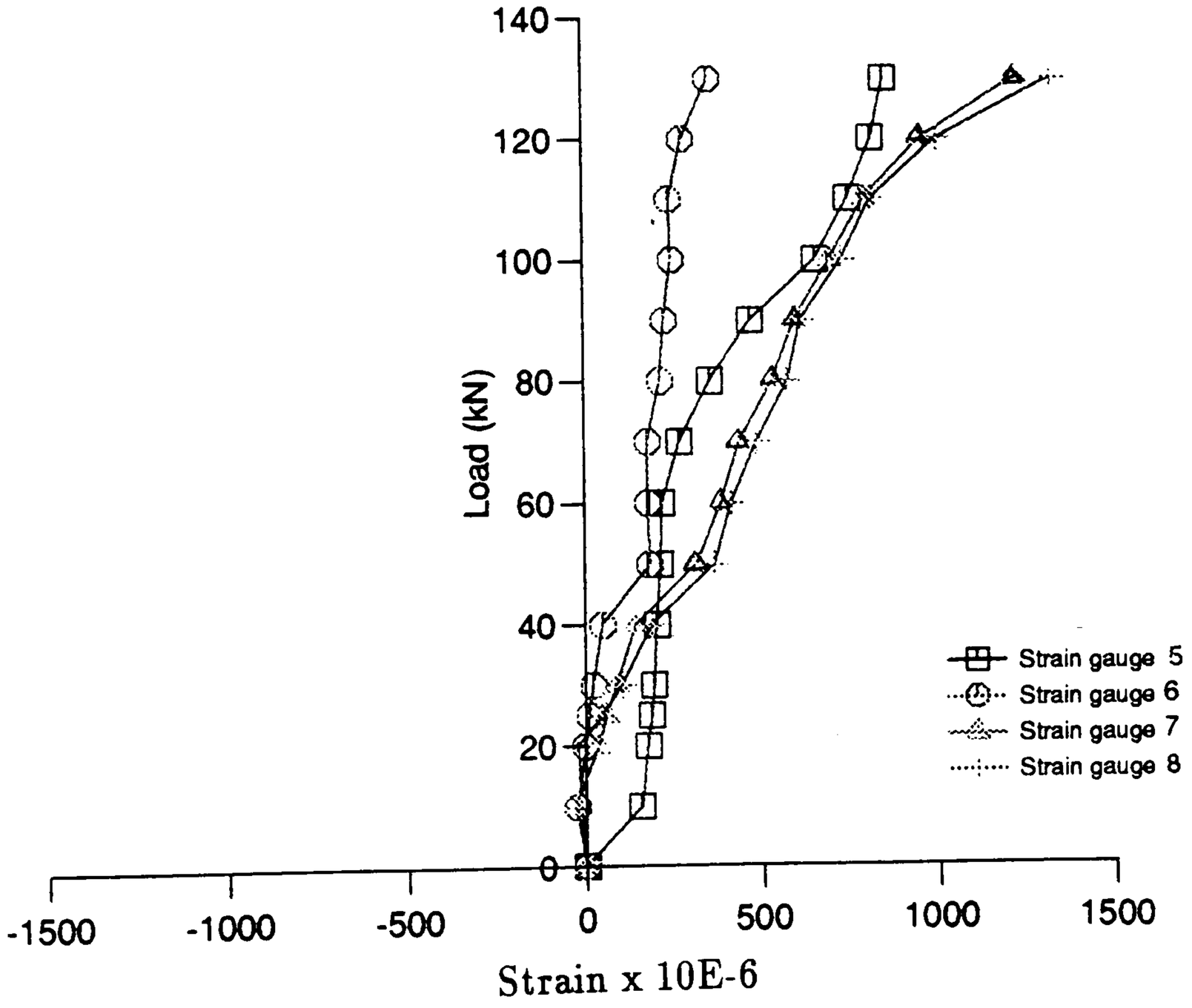


Figure 6.31: Distribution of strain along the mesh at right hand quarter span point

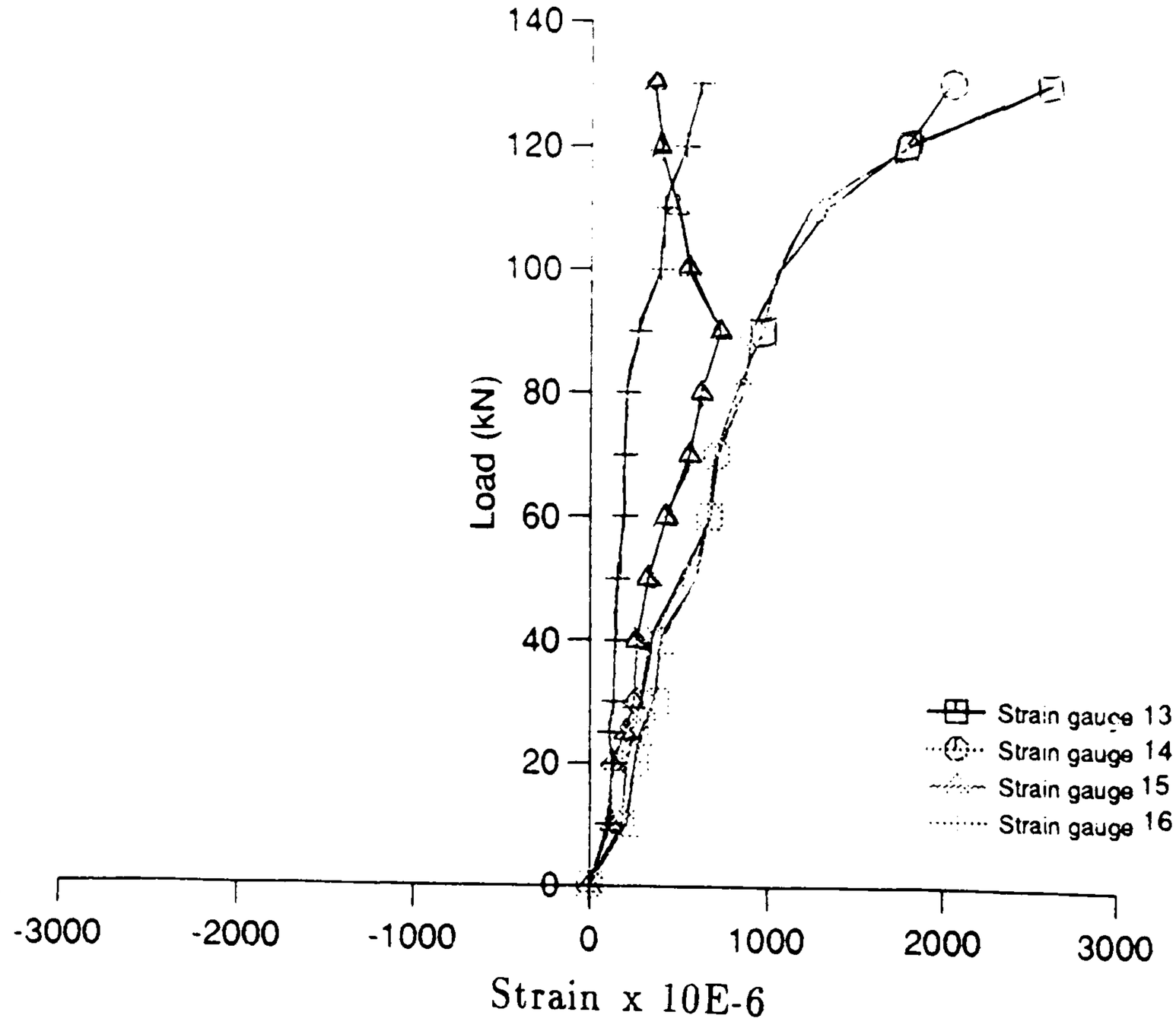


Figure 6.32: Distribution of strain along the mesh at left hand quarter span point

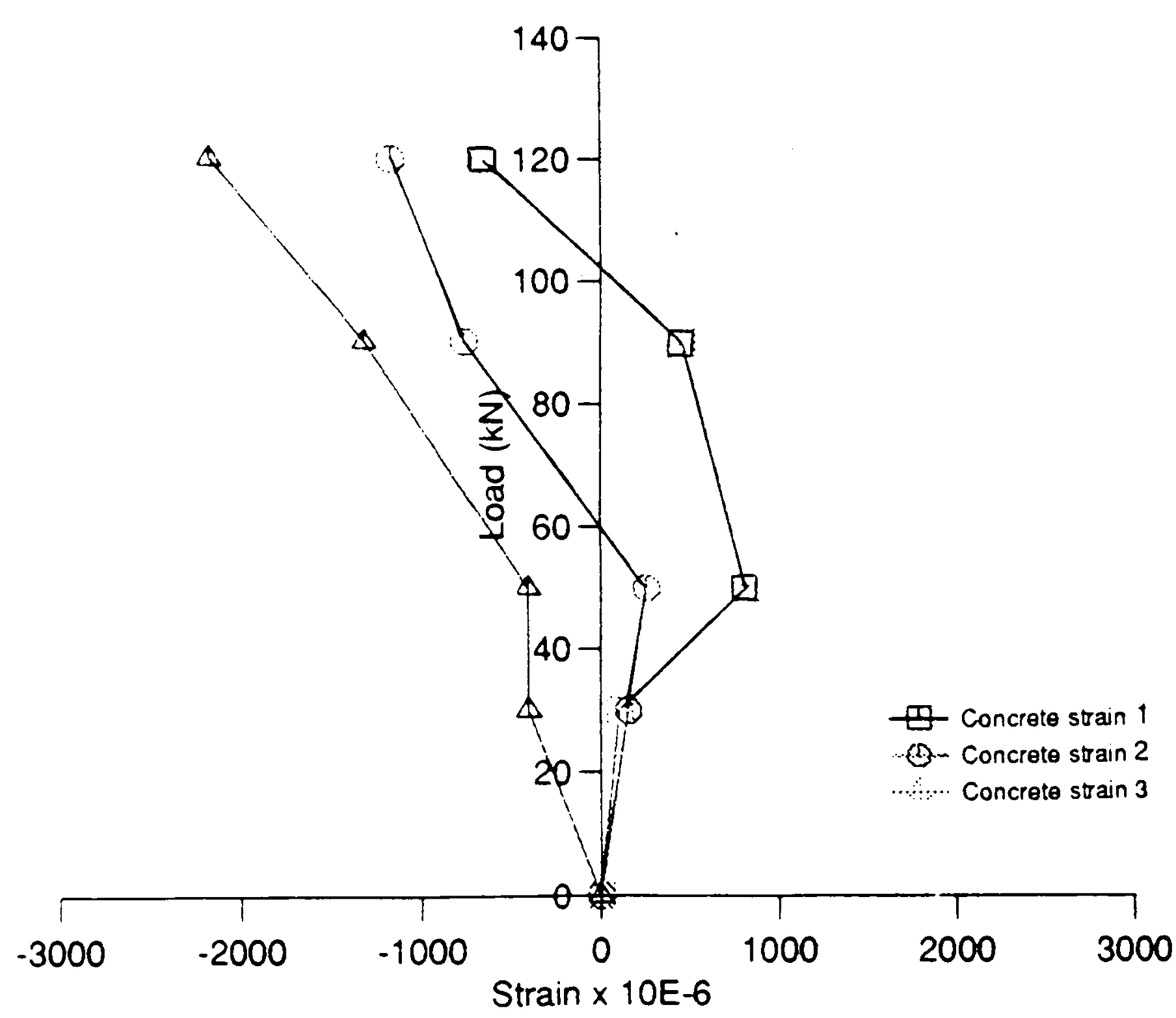


Figure 6.33: Distribution of strain along the concrete at the right hand support

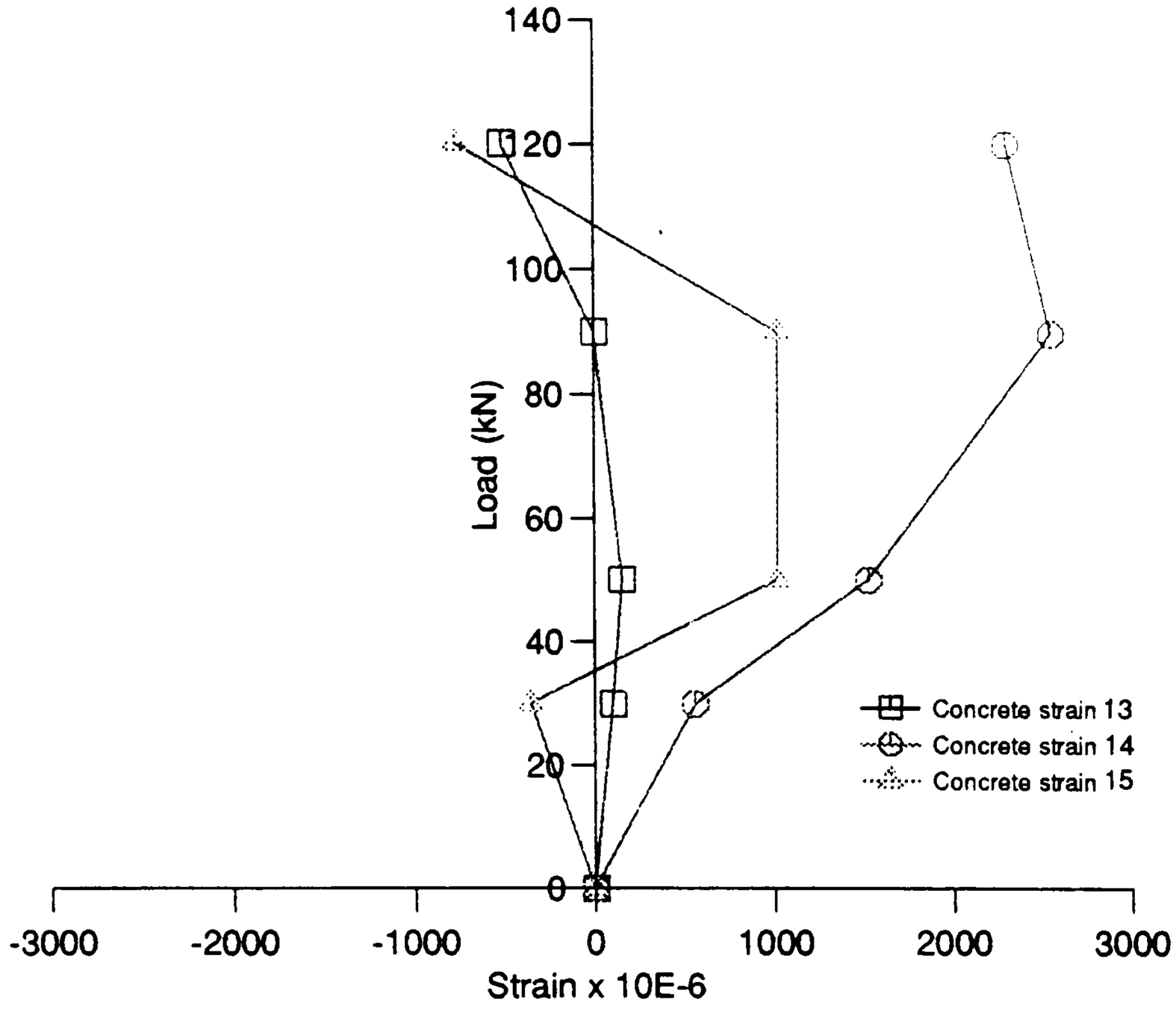


Figure 6.34: Distribution of strain along the concrete at the left hand support

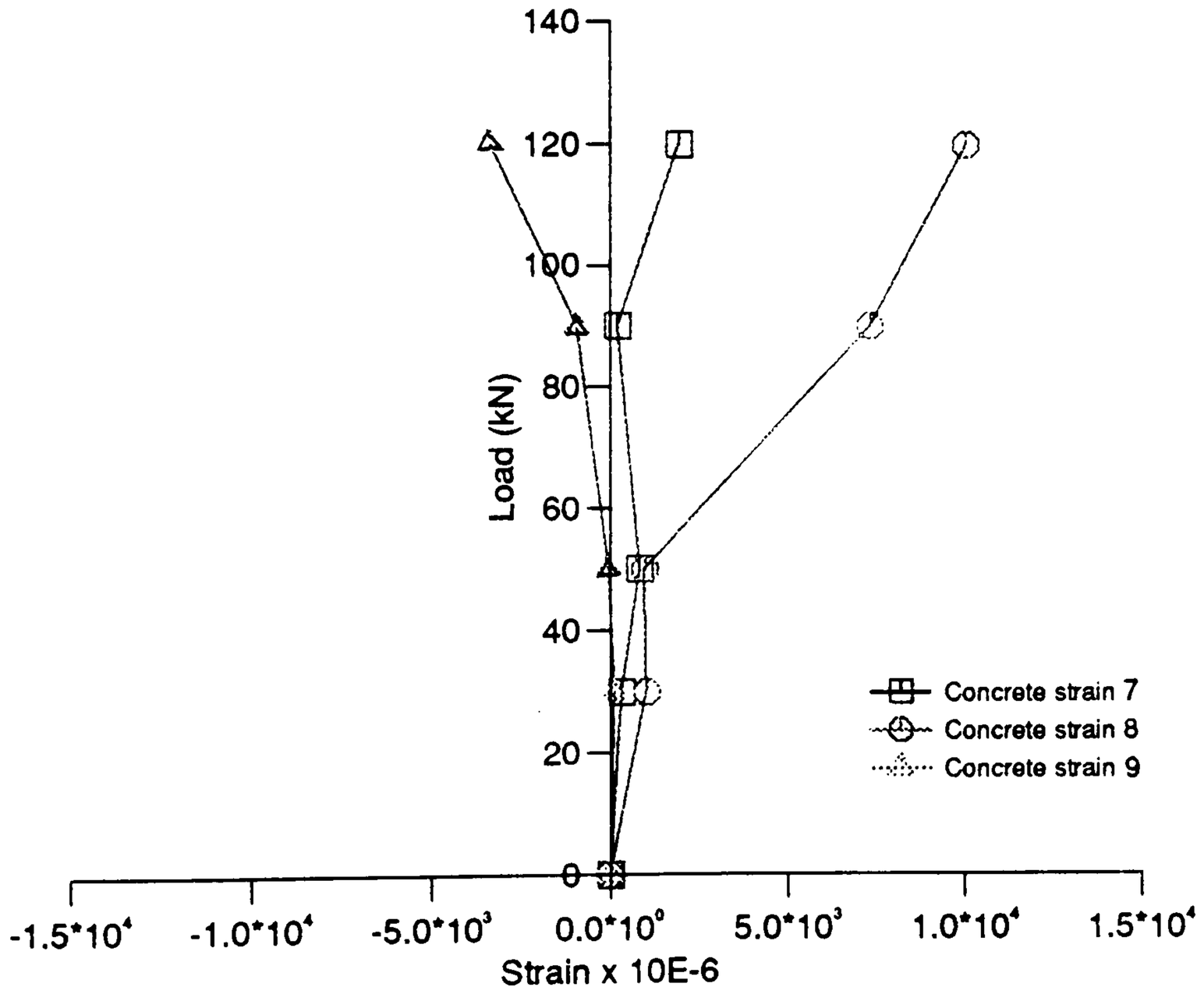


Figure 6.35: Distribution of strain along the concrete at midspan

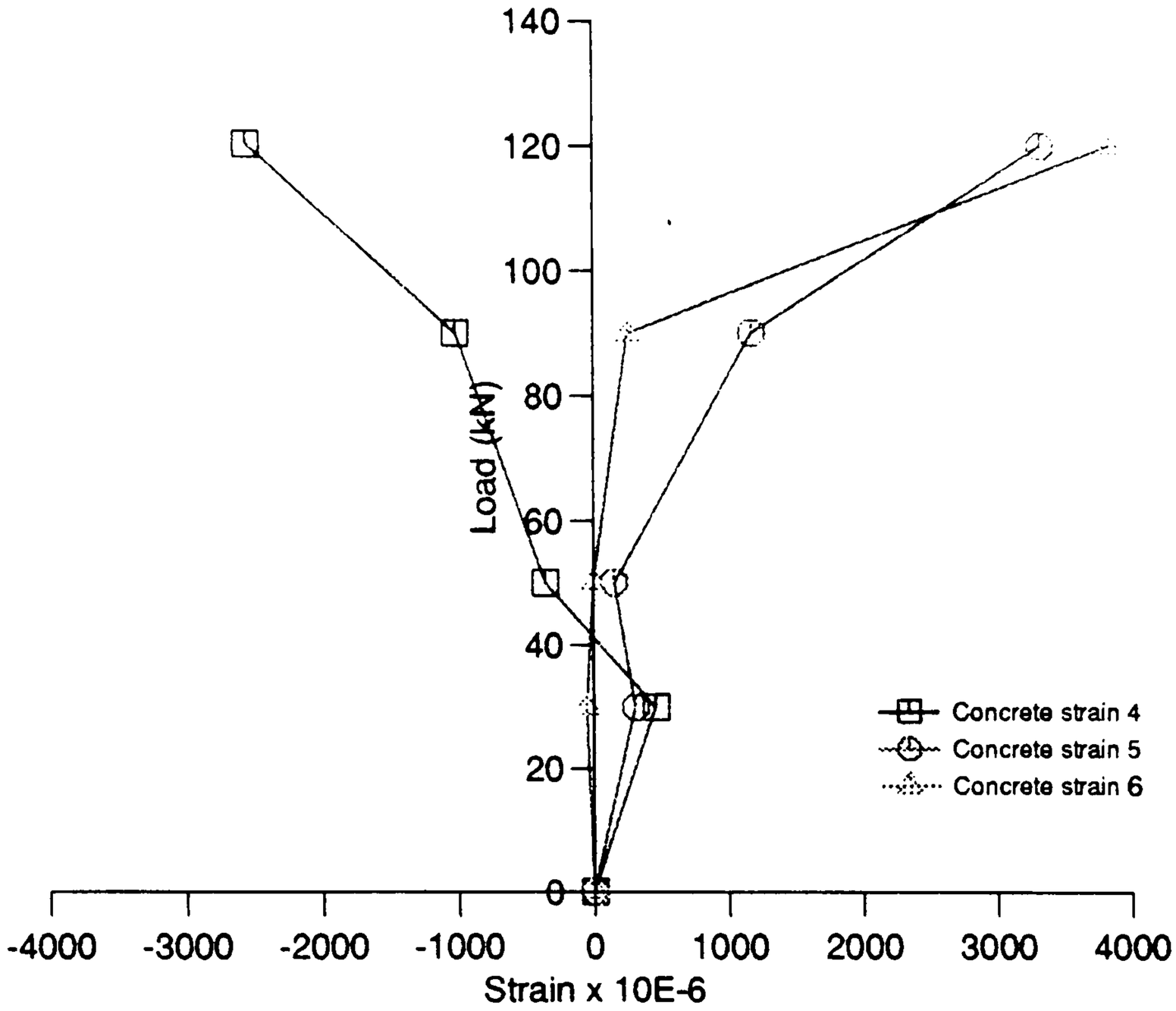


Figure 6.36: Distribution of strain along the concrete at right hand quarter span

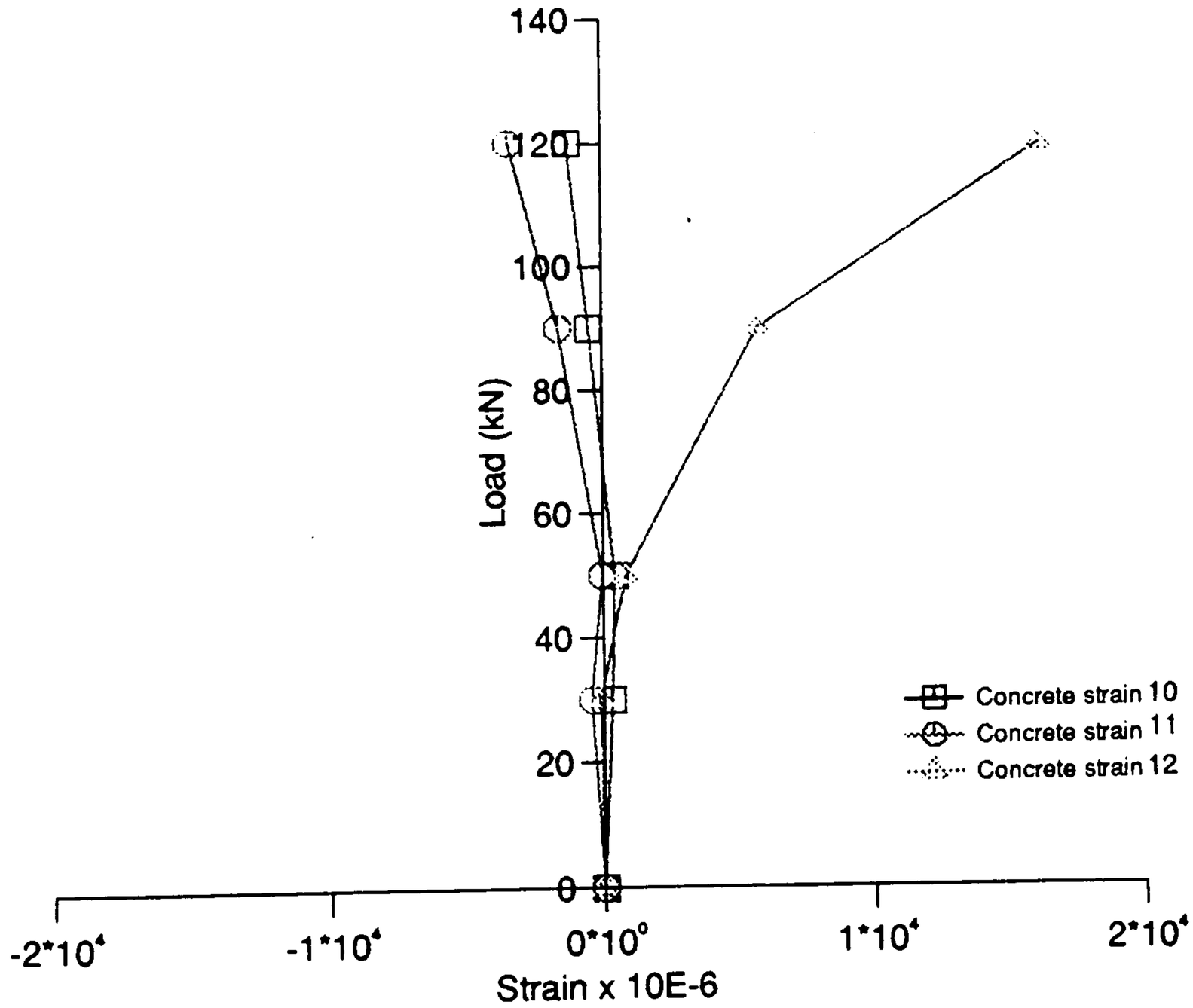


Figure 6.37: Distribution of strain along the concrete at left hand quarter span point

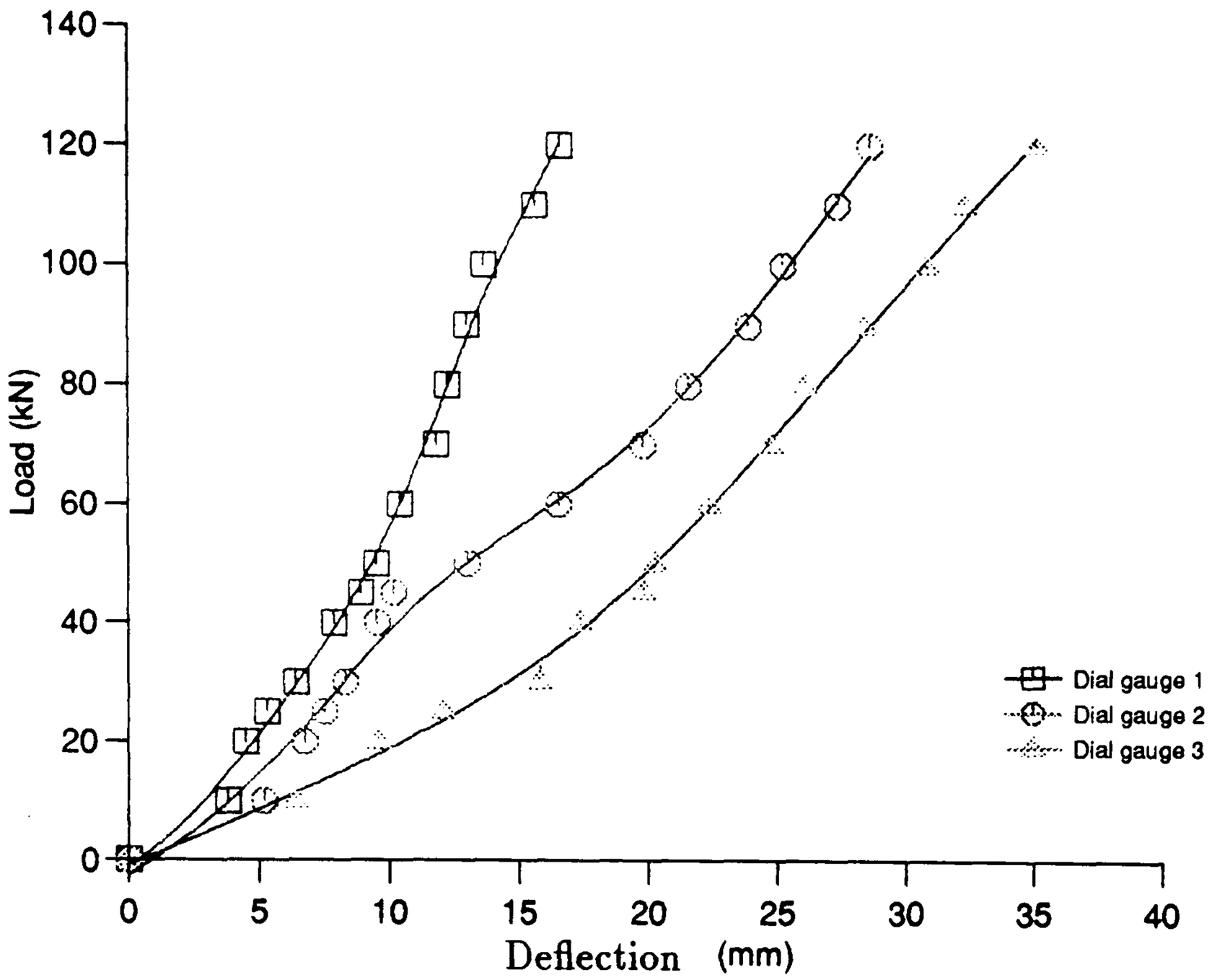


Figure 6.38: Load-deflection relationships for beam EBM3

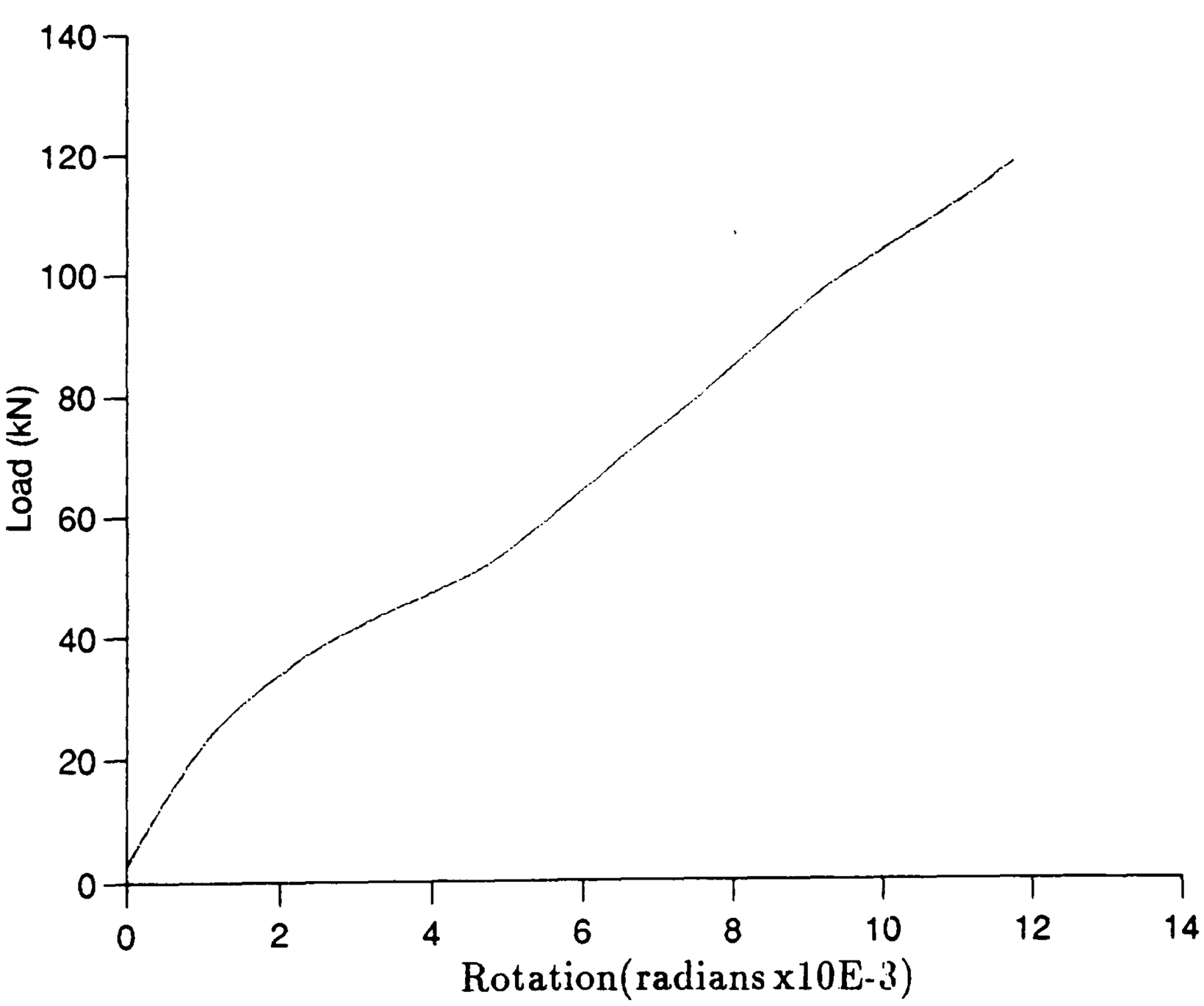


Figure 6.39: Load-rotation relationship for beam EBM3

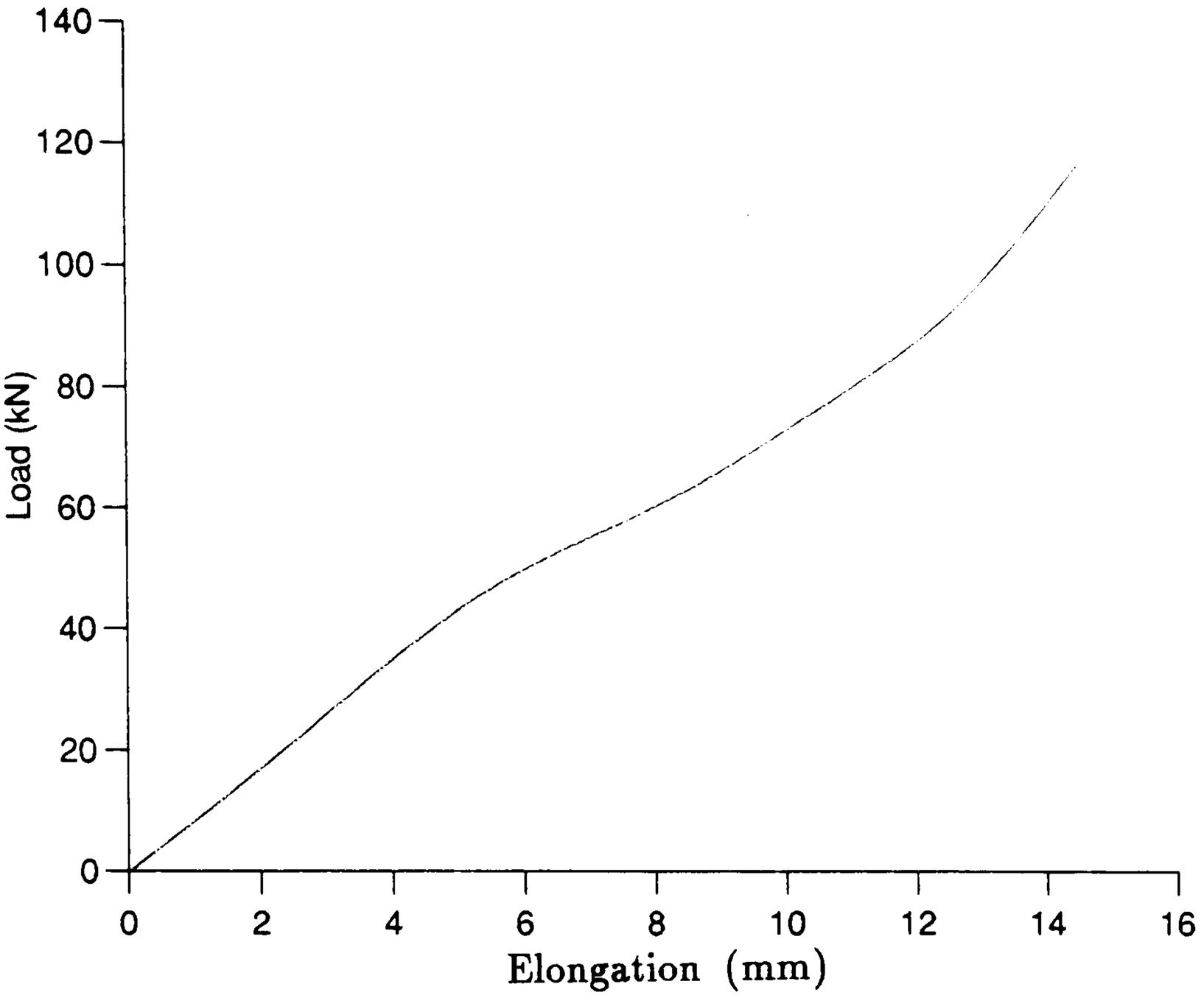


Figure 6.40: Load-elongation relationship for beam EBM3

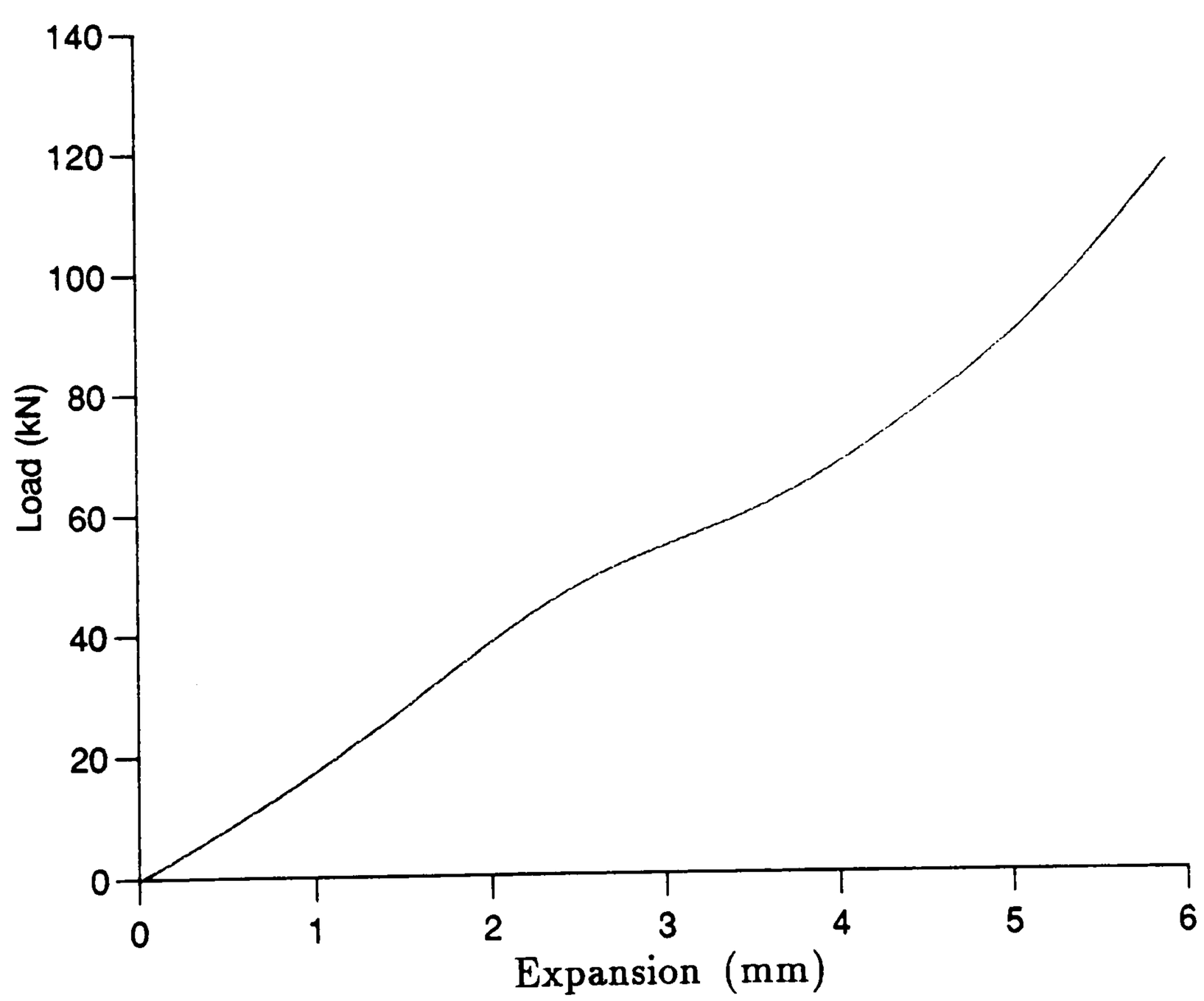


Figure 6.41: Load-expansion relationship for beam EBM3

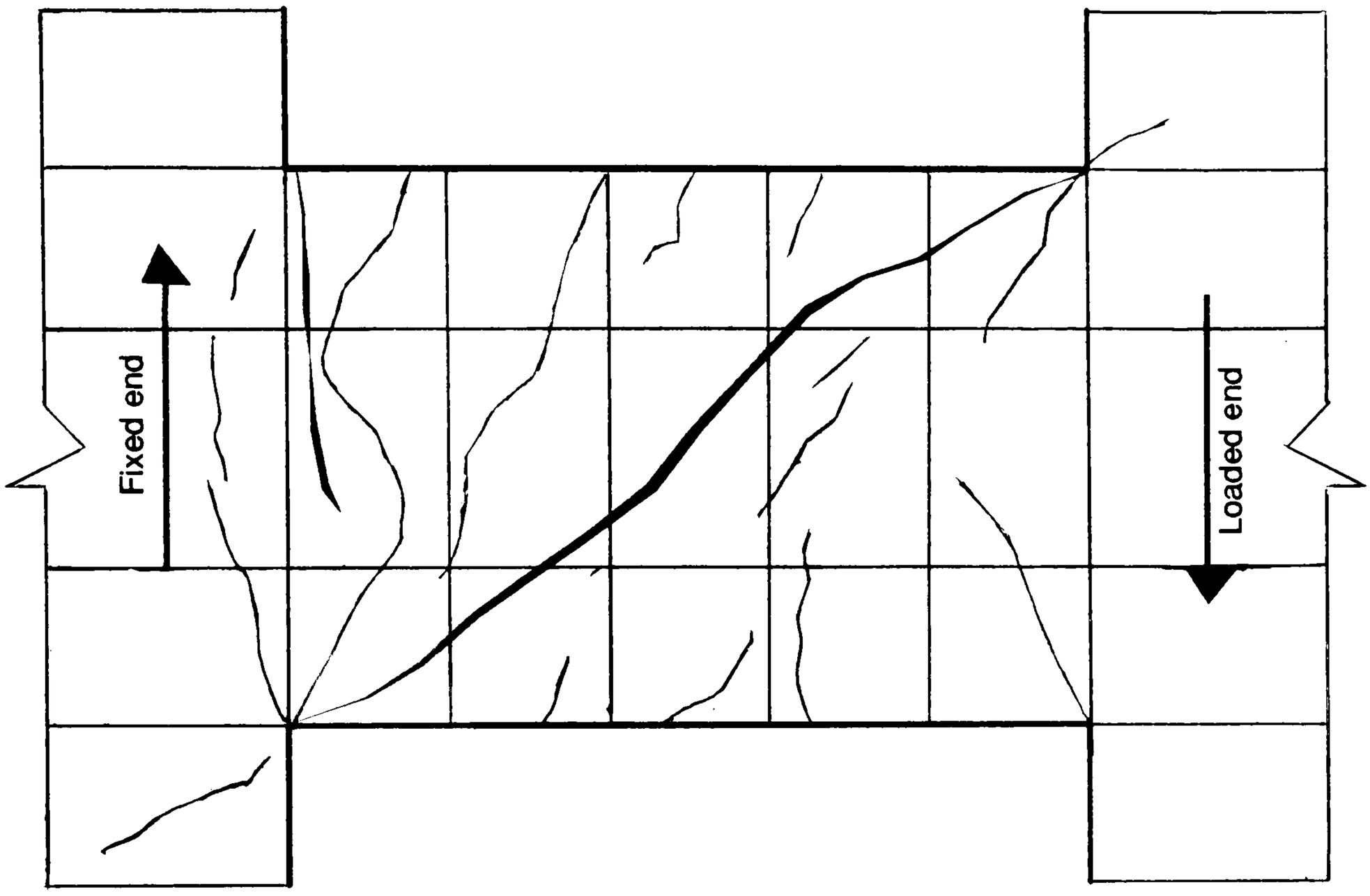


Figure 6.42: Failure mechanism of beam EBM3

# Chapter 7

# COMPARISON OF RESULTS

## 7.1 INTRODUCTION

The nonlinear behaviour of coupling beams in reinforced concrete shear wall structures subject to cyclic loading was examined experimentally and analysed numerically. The theoretical analysis, using the two approaches presented in Chapter 4, gave the predicted maximum load that can be sustained by the beams. The most significant results, from the experimental and theoretical investigations, are given in Chapters 5, 6 and in Appendix B. The results obtained from each beam under load have been discussed separately in Chapters 5 and 6. Emphasis has been given to the load carrying capacity, crack patterns, deformations, and modes of failure of each beam.

A comparison of the results together with the corresponding discussions have been made between the behaviour of the conventional and the expanded metal mesh reinforcement arrangements of the beams for shear span to depth ratios of 1.43

and 2.0.

Beams CBD1 and EBD1 were not considered in the comparison because of the problems encountered during the laboratory tests. The main results from the tests together with information necessary for their interpretation are given in tabular and graphical forms for each beam tested.

The results obtained from the double storey beam DBS2 were only used to check the accuracy of the response of the single beams under load and to provide data for the adjustment of the results obtained from the tests on the single beams.

## 7.2 CONCRETE STRAINS

A comparison of the strain results from the expanded metal mesh reinforced beam EBM3 and the conventionally reinforced beam CBM3 described in Chapter 6, are presented for the three cross sections i.e. at the supports, at the quarter span points and at midspan. The plots indicate that the compressive strains obtained from beam EBM3 at strain gauge points 1 to 3 at the right hand support of the beam were smaller than the strains found in the conventional beam CBM3 at strain gauge points 1 and 2 which were tensile strains. The maximum strain measured in beam EBM3 was at gauge point 12 situated at the quarter span point in the beam. The magnitude of this strain was of the order of 16154 microstrain at a load of 120 kN during the last load cycle. On the other hand, the maximum strain measured in beam CBM3 was located at gauge point 15 which was near the support and its magnitude was of the order of 55372 microstrain at the same load. At the left hand support in beam CBM3 at gauge points 13, 14, and 15

the measurements indicate that this region was entirely in tension, the strains were very high particularly after the appearance of the flexural crack. Since the strain gauges were positioned near to the edge of the supports, local effects may also have influenced the behaviour of the beam, particularly in the compression corners where the localised disturbances were at their maximum.

In the mid section of the beam, significant strains were found in beams CBM3 and EBM3 at strain gauge point 8. It must be pointed out, that the strains found in beam CBM3 were at least 50% higher than the corresponding strains in beam EBM3. This indicated that diagonal splitting of the concrete progressed rapidly in the conventionally reinforced beams. The strains found in the top and bottom points of the mid section of the two beams at strain gauge points 7 and 9, were small in comparison with strain at strain gauge point 8, and were in tension and compression respectively. In the case of strain gauge point 8, however, the entire length of the section was found to be in tension. At the quarter span point in both beams, the strains found at strain gauge points 4 to 6, were compressive in the case of beam CBM3 and their magnitudes were less than 1524 microstrain. In beam EBM3 the strains were found to be tensile in the case of the strain gauges at the same points and their magnitudes were of the order of 3810 microstrain. This phenomenon may have been due to the propagation of the cracks. The results from beam EBM3 indicated that the compression strains at the support were spread over a considerable depth. This was probably caused by the absence of cracks in this region or by the presence of the compressive reinforcement. At a load of 120 kN, the difference in the strains between the two beams was up to

approximately 14000 microstrain at strain gauge point 8. During subsequent load cycles, more pronounced deterioration of the concrete was found at the left hand support of beam CBM3. This was indicated by a large tensile strain of the order of 55372 microstrain at strain gauge point 15.

The development of the strains in beams EBM3 and CBM3 was found to be distinctly nonlinear at all strain gauge points. Apparently the presence of the expanded metal mesh within the middle zone of beam EBM3 prevented further extension of the beam compared to beam CBM3. This was also confirmed by the load-elongation relationships.

## 7.3 BEHAVIOUR OF THE FLEXURAL STRAINS

The results, presented separately in Chapter 6 for beams EBM3 and CBM3, showed the strain distribution along both layers of the longitudinal reinforcement for all load increments in the third positive load cycle. All the strains indicated an increase at locations near to the tension zone of the beam at the supports. It was found that the strains obtained at the same load in the third load cycle for beam CBM3 were higher at strain gauge points A', D and C and F'. In the case of beam EBM3, the maximum strains were located at strain gauge points A, F, C' and D'. The difference in the locations of the maximum strain found in both beams was due to the direction of the development of the diagonal crack. The influence of different web steel contents was insignificant. However, it was noticeable that the strains in the reinforcement were generally smaller in beam EBM3 compared to those in beam CBM3, particularly at high loads. The expanded metal mesh

present in the web of beam EBM3 is believed to be the reason for the development of the particularly low strains.

In the mid section of the two beams, the strains recorded in beam CBM3 were found to be all in tension in both the top and bottom reinforcement at the four locations and their maximum magnitude did not exceed 2237 microstrain. On the other hand, the strains recorded at the same locations on beam EBM3 were found to be tensile and compressive strains and their maximum magnitude did not exceed 2690 microstrain. In beam EBM3 a strain approximately 16% higher than that found in beam CBM3 at the middle section locations was obtained which may have been due to the confinement effect of the expanded metal mesh. In general, the behaviour of the two beams was similar with respect to the direction of the diagonal crack.

## 7.4 BEHAVIOUR OF THE WEB REINFORCEMENT

The strains recorded on the stirrups and on the expanded metal mesh indicated that the web reinforcement in both beams, which was situated at the centre section, were of the order of 1342 microstrain for beam EBM3 and of the order of 1408 microstrain for beam CBM3 at strain gauge point 10, where the diagonal crack passed near to the strain gauge. The distribution of the strains along the expanded metal mesh and the stirrups was not uniform in either of the two beams. A definite strain pattern, consistent with a shear failure mechanism in the beam

was apparent. The contribution of the concrete in beams CBM3 and EBM3 towards the resistance to shear diminished under high intensity alternating loading, even if the stirrups or the expanded metal mesh performed entirely in the elastic range. It needs to be emphasised, that the direction of the critical diagonal crack crossing beam CBM3 was different from the one crossing beam EBM3. It was impossible therefore to carry out a direct comparison of the strains at the same section in the two beams. The results obtained during the experimental investigation and presented in Chapter 6 indicated that the strains recorded in both beams differed significantly at the same locations.

The measurements also indicated that the maximum recorded strains were located at the supports at strain gauge points 13 and 17 in beams EBM3 and CBM3 respectively. The strains in the web indicated, however, that the real weakness in beams CBM3 and EBM3 was in the gradual deterioration of the shear strength at the supports.

The difference in behaviour of beams CBM3 and EBM3 was due to the different roles played by the expanded metal mesh in the one beam and the stirrups in the other.

## 7.5 DEFORMATIONS

In order to simplify the analysis, a direct comparison was made between the deformations from the different beams in each test series. The comparison was based on deflections, rotations, transverse expansions and elongations from the two series of beams with shear span to depth ratios of 1.43 and 2.0. The span to

depth ratio also gave a direct estimation of the enhancement in the strength of the beams.

The behaviour of beams CBM1, CBM2, and CBM3 with a shear span to depth ratio of 1.43 should only be compared with that of the beams reinforced with expanded metal mesh with the same shear span to depth ratio of 1.43 i.e. EBM1, EBM2, and EBM3 respectively. A direct comparison, is therefore, possible between these beams. A similar comparison will be made between the beams with a shear span to depth ratio of 2.0 i.e. beams CBS1 and CBS2 with beams EBS1 and EBS2 respectively.

It has been observed that the crack patterns in the two series of beams were, however, different. This observation was also found in the deformations of the beams. The tests also revealed that fewer cracks appeared in the beams reinforced with expanded metal mesh compared to the beams reinforced conventionally.

The results obtained from the load-deflection relationships at the three dial gauge positions D1, D2, and D3 for the beams with a shear span to depth ratio of 1.43 are shown in Figures 7.1 to 7.3 and in Figures 7.7 to 7.9 for the beams with a shear span to depth ratio ratio of 2.0. The deflection measurements from beam CBM2 for the three dial gauge positions D1, D2, and D3 were at least 18% higher than the deflections found in beam EBM2 and at least 5% higher in beam CBM3 compared to beam EBM3 as shown in Figures 7.13 to 7.15. The 13% difference found in the deflections between beams CBM2 and CBM3 which contained identical reinforcement contents and shear span to depth ratio may be due to the variation in the properties of the materials used and to the time delay before testing took

place. In the case of the diagonally reinforced beams with the same shear span to depth ratio i.e. beams CBM1 and EBM1, the difference in the deflections was less than 18%. Beams CBM2 and EBM2 were compared with beams CBM1 and EBM1 respectively, the deflections found in beams CBM1 and EBM1 were found to be 5% smaller. This reduction is due mainly to the major contribution from the diagonal reinforcement. The other factor which may have contributed to the reduction in the deflections is the presence of the expanded metal mesh in beam EBM1 which accounted for at least 10% of this reduction in comparison with beam CBM1. Approximately the same percentage as quoted above was found in the comparison between the beams with a shear span to depth ratio of 2.0. The influence on the deflections of the increase in the depth of the beams varies from 10% to 15% when the beams with a shear span to depth ratio of 1.43 are compared with the beams with a shear span to depth ratio of 2.0.

The behaviour of beam CBSi should only be compared with that of the beam EBSi reinforced with expanded metal mesh which had an identical shear span to depth ratio as shown in Figures 7.7 to 7.9. It has also been confirmed that the shear span to depth ratio was found to have significant influence on the deflections of the beams as described above. The plots for dial gauge positions D1 to D3 for beam CBS1 show an increase in deflection of at least 10% compared to beam EBS1. In a comparison between beam CBS2 and beam EBS2 in the same test series, the difference in deflection was only 4%. On the other hand, the elongations and transverse expansions shown in Figure 7.10 and Figure 7.11 for the beams with a shear span to depth ratio of 2.0, were significant in comparison

with the beams with a shear span to depth ratio of 1.43 shown in Figure 7.4 and Figure 7.5. The difference in the elongations and the transverse expansions varied from 10% to 30% between beams CBM1, CBM2, EBM1 and EBM2 compared to beams CBS1, CBS2, EBS1 and EBS2 respectively. This may be due to the higher flexibility of the beams with a shear span to depth ratio of 2.0. The decreases in the elongations and the increases in transverse expansions of the diagonally reinforced beams EBM1 and CBM1 compared to beams EBM2 and CBM2 were of the order of 22% and from 15% to 30% respectively. In the case of the beams with a shear span to depth ratio of 2.0, i.e. beams EBS1 and CBS1, compared to beams EBS2 and CBS2, the decreases in the elongation was of the order of 30% and an increase in the expansions from 20% to 40% was found. These differences in the elongations and transverse expansions were manifested by the presence of the factors described above.

The use of the expanded metal mesh resulted also in the reduction in the rotation of the beams. This can be noted from a comparison of the behaviour of beam EBMi with that of beam CBMi with the same shear span to depth ratio shown in Figure 7.6 and the behaviour of beam EBSi with that of beam CBSi with a shear span to depth ratio of 2.0 shown in Figure 7.12. The reduction in rotation varied between 5% to 20%. The lower stiffness found in beams CBMi and CBSi was due to the presence of cracking extending through the full depth of the beams and also the shear deformations. It can be concluded that the stirrups in conventionally reinforced beams were not as efficient as the expanded metal mesh in minimising the shear deformations in the critical sections, especially after the formation of

the cracks running through the full depth of the beam.

The deformation of the beams, in which the expanded metal mesh was introduced together with the diagonal reinforcement bars within the shear span, proved to be superior to that of comparable beams containing a conventional reinforcement arrangement. The failure modes of several of the beams were characterised by the presence of a long and very wide flexural crack together with diagonal cracks as in the case of beams CBD1 and CBM2.

In general, the deformations in the cracked beams were influenced significantly by the presence of the biaxial state of stress. The beneficial influence of the expanded metal mesh is attributed to its role in reducing the cracks and deformations and increasing the strength of the beams.

## 7.6 STIFFNESSES

A comparison of the laboratory based performances of the conventionally reinforced beams, with those containing expanded metal mesh emphasised the superior stiffness of the latter for applications requiring the provision of seismic resistance, where cyclic loading is predominant. After cracking, the loss in stiffness for both types of beams containing no diagonal reinforcement bars was considerably more than the loss encountered in the beams containing diagonal reinforcement bars.

The greatest reduction in stiffness occurred after the formation of the diagonal cracks in all the coupling beams.

Beams CBS2, CBM2 and CBM3 suffered a more dramatic loss in stiffness after

cracking compared to beams CBS1 and CBM1. The same type of behaviour was observed in beams EBM2, EBM3 and CBS1 when compared with the behaviour of beams EBM1 and EBS1.

The response of the beams with shear span to depth ratios of 1.43 and 2.0 are shown in Figures 7.6 and 7.12. It was noted that much more severe rotations were found in the beam with a shear span to depth ratio of 2.0. This was particularly apparent in beam CBS2 where the rotation was 34% higher than the rotation measured in beam CBS1.

The response of beams EBM1 and EBS1, show the characteristic behaviour of the diagonal bars and the expanded metal mesh in the form of a good energy absorption capacity and with a 25% reduction in the loss of strength compared to beams CBM2 and CBS2. It can be noted that there is a significant reduction in stiffness after the first excursion into the post-elastic range during the third load cycle. The load-rotation curves indicate an immediate mobilisation of the diagonal reinforcement bars present in the beams to oppose deformations resulting from load reversals. This is in contrast to conventional beams CBM2 and CBS2 which become very soft at low loads after the initial load cycle. In such beams the large cracks which had formed previously first of all need to be closed before the concrete can transmit diagonal compression. Only a small force is required to do this. The associated rotation may result in very large deflections in the beams before the structure stiffens again. The beneficial contribution of diagonal reinforcement in coupling beams containing expanded metal mesh is again evident in beams EBMi and EBSi in which the strength loss at a given displacement was

found to be much less than in beams CBMi and CBSi.

## 7.7 CRACK PATTERNS

As was expected, all the beams failed after the appearance of diagonal cracks. These occurred, more or less at an inclination of 45° to the horizontal direction in beams EBD1 and CBD1 and at approximately an angle of 35° for the beams with a shear span to depth ratio of 1.43 and at angle of 27° for the beams with a shear span to depth ratio of 2.0.

Beams EBD1, EBMi and EBSi reinforced with the expanded metal mesh presented an advantage because of the continuous and reasonably closely integrated mesh. This provided continuity of reinforcement in all directions and is naturally efficient in the reduction in cracking. This was confirmed through a comparison with the conventionally reinforced beams i.e. beams CBD1, CBMi and CBSi. In general, the expanded metal mesh reinforced beams showed only minor cracks and less loss of strength compared to those conventionally reinforced, especially during the first and second load cycles. This is due to the effectiveness of the expanded metal mesh in binding the beam together.

The expanded metal mesh in the beams also proved to be very efficient during a limited number of loading cycles, until the appearance of significant diagonal cracking. This was confirmed by the resulting crack patterns for each beam. Crack width measurements indicated that the diagonal cracks became wider when the reinforcement bars were in tension.

## 7.8 FAILURE OF THE BEAMS

The strength of the beam was dependent on either the number of stirrups, the diagonal bars or the amount of expanded metal mesh encountered along the line of the potential failure crack which followed the main diagonal.

In general, the failure mechanism observed in the tests on the two groups of beams was of a typical shear type. This is characterised by the opening of one diagonal crack. In beams reinforced with expanded metal mesh i.e. beams EBMi and EBSi, the critical diagonal cracks appeared in the first positive load cycle during the last load increments before reaching a load of 50 kN. On the other hand, in the beams reinforced with conventional stirrups i.e. beams CBMi and CBSi, the diagonal crack appeared at an early stage during the first load cycle before a load of 30 kN was reached. In all the beams included in this investigation a diagonal tension (separation) failure occurred along the diagonal connecting opposite corners of the beams. The strength of beams CBMi and CBSi deteriorated more rapidly during cyclic loading than in the case of beams EBMi and EBSi.

The last two coupling beams CBM3 and EBM3 which were reinforced differently, failed also by separation after three load reversals resulting in yielding of the flexural reinforcement. It has to be noted, that a deep flexural crack also developed in beam CBM3 near the support which contributed to the rapid deterioration of this beam. Beams EBM1, EBS1, CBM1 and CBS1 failed in a more ductile manner than beams EBM2, EBS2, CBM2 and CBS2. This was due to the presence of diagonal bars.

It should also be noted that, in all the cases investigated, the concrete never

failed in compression within the beams before the limiting load carrying capacity had been attained. The entire shear span of beams CBM3 and EBM3, increased in length because the flexural reinforcement was in tension. Therefore, it can be concluded that, the expanded metal meshes incorporated in beams EBMi and EBSi did reduce these elongations and contributed to the ultimate flexural strength of the beams. The expanded metal mesh tended to produce a more uniform crack spacing. The inclusion of diagonal reinforcement bars was also found to have a beneficial influence on the failure mechanism of the beams.

In all beams the performance of the expanded metal mesh was satisfactory, even when large deformations were imposed. The tests have also shown, however, that the real weakness in the overall structure was in the shear carrying capacity of the zones containing the plastic hinges.

The replacement of the stirrups by the expanded metal mesh showed clearly that the deterioration in the shear strength was inevitable, but the confining action afforded by the expanded metal mesh did minimise the damage to the beam.

## 7.9 CONCLUSIONS

The findings from this investigation have the following implications with respect to coupling beams:

The improvement in the behaviour of the beams which contained the expanded metal mesh i.e. beams EBMi and EBSi, compared to the conventionally

reinforced beams CBMi and CBSi, was characterised by the increase in strength and the reduction in cracking.

The strength of beams EBM1, CBM1, CBS1 and EBS1 under load was increased significantly due to the introduction of diagonal reinforcement bars along the shear span of the beams. The presence of these bars prevented brittle failure in the beams and also resulted in much improved ductility. This is supported by the findings of Paulay and Santhakumar [52], who carried out tests on coupling beams containing diagonal reinforcement bars. In their investigation [52], they found that the diagonal reinforcement bars had a significant influence on the behaviour of coupling beams.

A substantial increase in strength in beams EBD1, EBMi and EBSi due to the presence of the expanded metal mesh was apparent, however, the rate of increase in strength of the coupling beams tends to increase as the shear span to depth ratio decreases. Increasing the depth of the beams was found to have a beneficial influence on the strength of the beams in which both types of reinforcement were present.

In general, the beams which contained expanded metal mesh had three major advantages over the ones which were conventionally reinforced. Firstly, they were stronger, secondly they had smaller crack widths and thirdly they failed in a more ductile manner.

Finally, the results obtained from the beams investigated in this test programme have confirmed that the introduction of expanded metal mesh can be considered to be an effective and efficient way of reinforcing coupling beams.

## 7.10 COMPARISON OF EXPERIMENTAL AND THEORETICAL RESULTS

The beams described in the previous Chapters are directly comparable, therefore, an experimental comparison between them has been made in terms of strength (or efficiency).

By comparing the performance of the conventionally reinforced coupling beams CBMi and CBSi with the performance of the beams containing expanded metal mesh i.e. beams EBMi and EBSi, the superior behaviour of the latter with respect to shear capacity is evident.

In Table 7.1, the comparison of the results obtained from the analytical approaches and the laboratory based investigation are presented. The values predicted by the two approaches were in reasonable agreement with the failure loads obtained from the tests. An examination of the beams reinforced with diagonal bars with a shear span to depth ratio of 1.43 i.e. beams CBM1 and EBM1, showed that their corresponding efficiencies varied between 20 to 40%. Therefore, the predicted failure loads of these two beams were much smaller than the actual failure loads. This was also found to be the case for the other beams with different shear span to

depth ratios. The results confirmed that the ultimate load predicted using the two approaches provide a reasonable lower bound value.

It may also be noted in Table 7.1, that the maximum load sustained by beam CBM2 was 153 kN whereas, the theoretical ultimate load capacity was 135.06 kN based on the approach developed by Subedi [2] and 136.96 kN using the Compressive Force Path approach. The resulting efficiency of the beams was approximately 10%.

Beam EBM2 failed in shear at a loading level of 185 kN, which corresponds to an efficiency of only 22% based on the approach developed Subedi [2] and 5% for the Compressive Force Path approach. The difference in the efficiency between the two analytical approaches is due to the difference in the steel strength used in each approach i.e. the Compressive Force Path approach uses the ultimate strength and the approach developed by Subedi [2] uses the yield strength of the reinforcement.

It was noted that the size of the coupling beam structures had a significant effect on the ultimate strength of the structural assembly. The beams in the first test series i.e. beams CBMi and EBMi with a shear span to depth ratio of 1.43 exhibited a strength approximately 20% to 40% higher than the strength of beams CBSi and EBSi with a shear span to depth ratio of 2.0.

It was also found that all beams included in this investigation failed in shear before their theoretical flexural capacity had been attained. The failure load for each beam shown in Appendix A confirms the above statement.

It can therefore be noted that, the behaviour of the beams reinforced with ex-

panded metal mesh together with diagonal reinforcement bars was superior in all aspects compared to the conventionally reinforced beams i.e. in terms of cracking, ductility, deformations and strength. However, more experimental work on the expanded metal mesh alternative is needed to confirm the degree of confidence in the reported gain in strength of the coupling beams.

In general the results from the laboratory based investigation and the theoretically derived values presented in Table 7.1 agree reasonably well with each other. It is necessary to point out that the modified form of the test arrangement did restrain the test beams more effectively during testing i.e. the end blocks did rigidly restrain the beam against rotation and against lateral displacement.

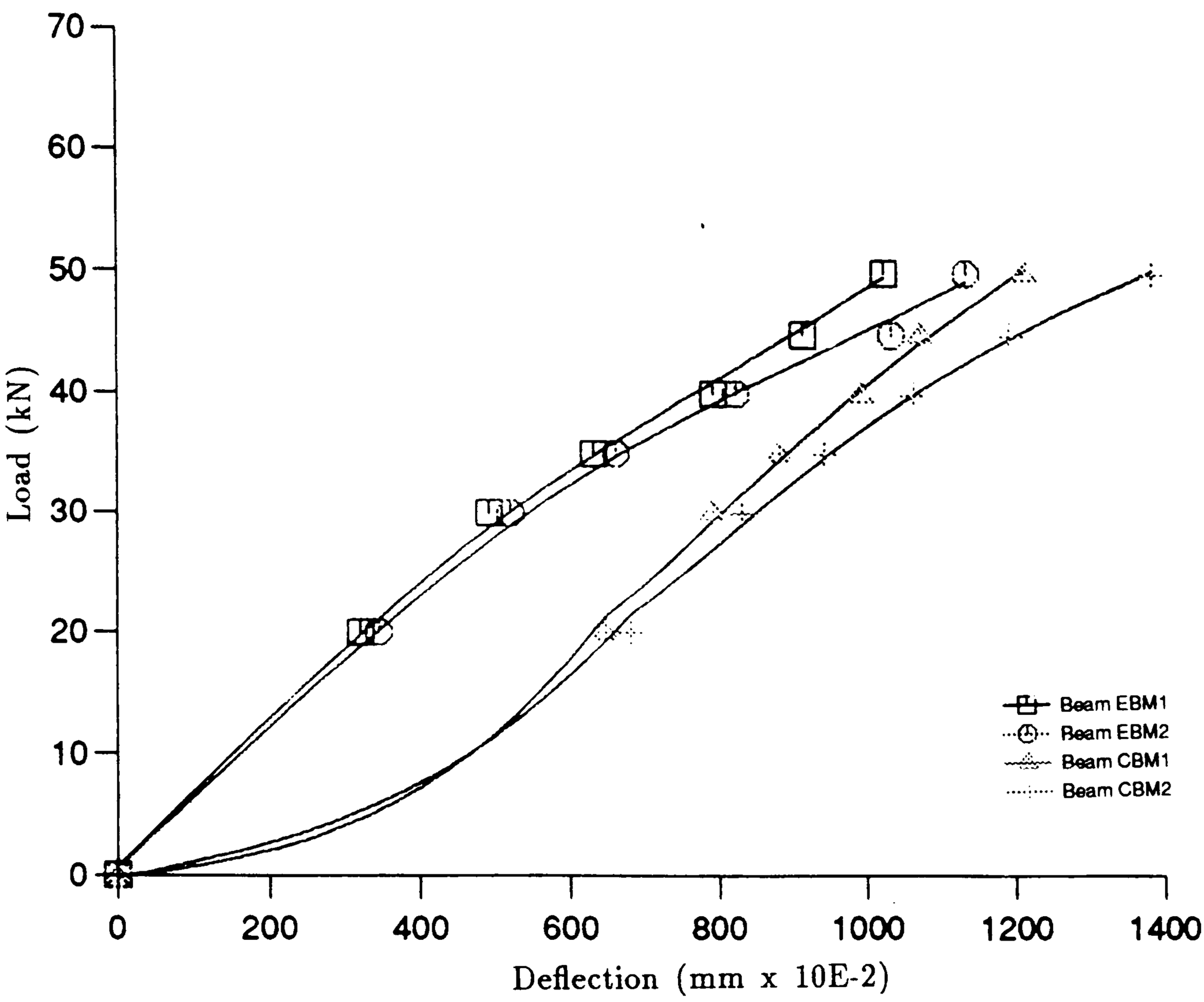


Figure 7.1: Deflections of beams with a shear span to depth ratio of 1.43 at the position of dial gauge D1

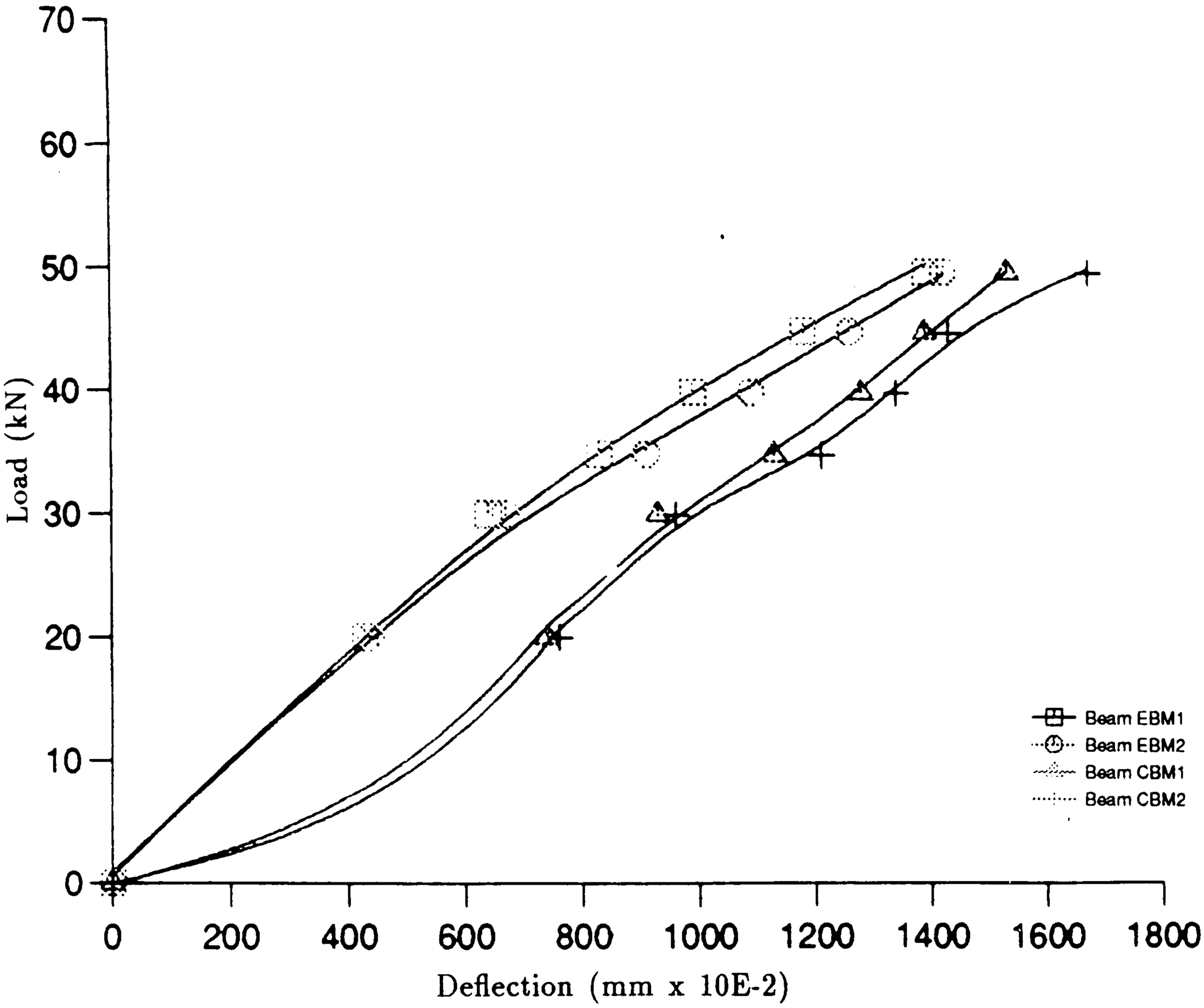


Figure 7.2: Deflections of beams with a shear span to depth ratio of 1.43 at the position of dial gauge D2

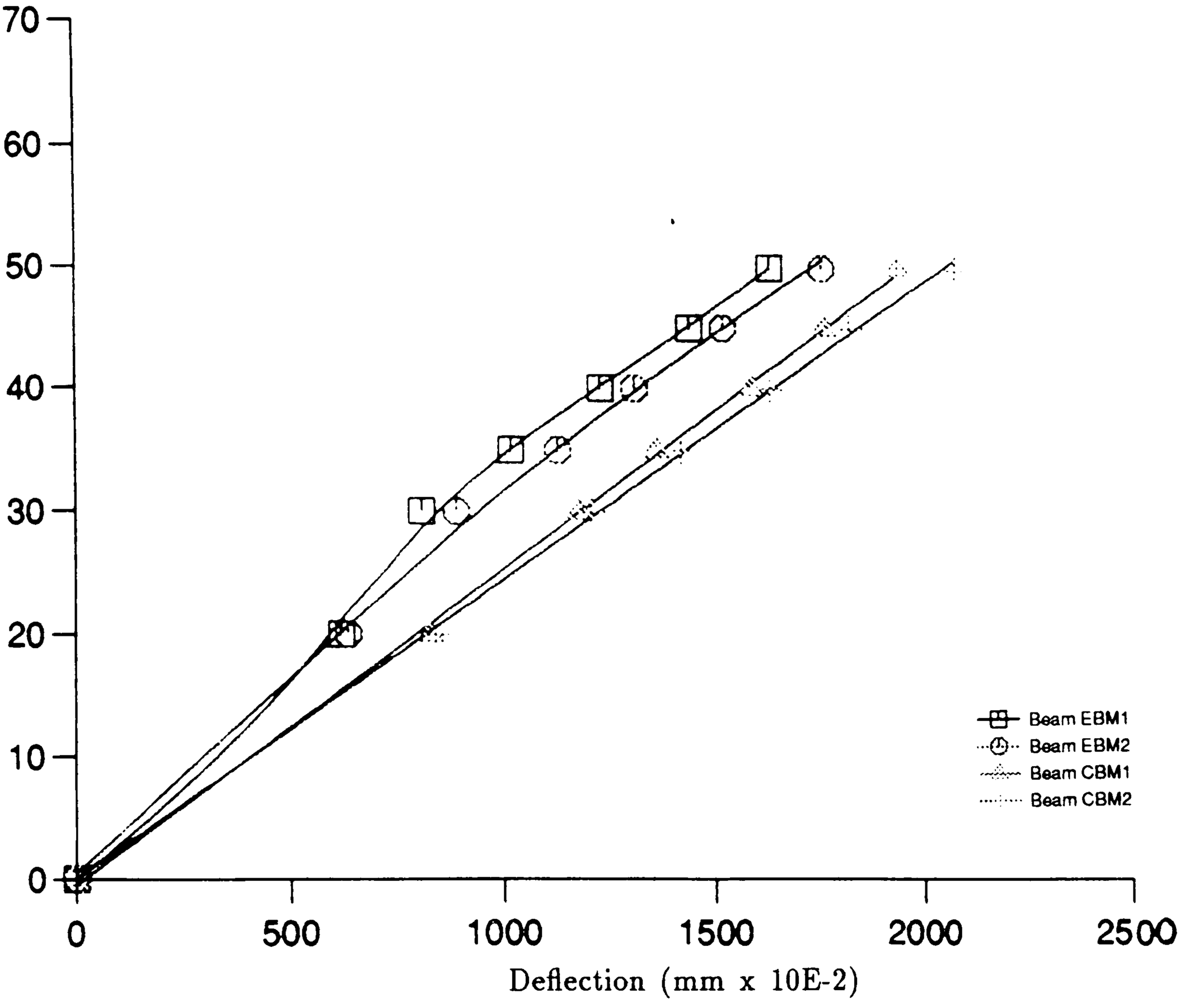


Figure 7.3: Deflections of beams with a shear span to depth ratio of 1.43 at the position of dial gauge D3

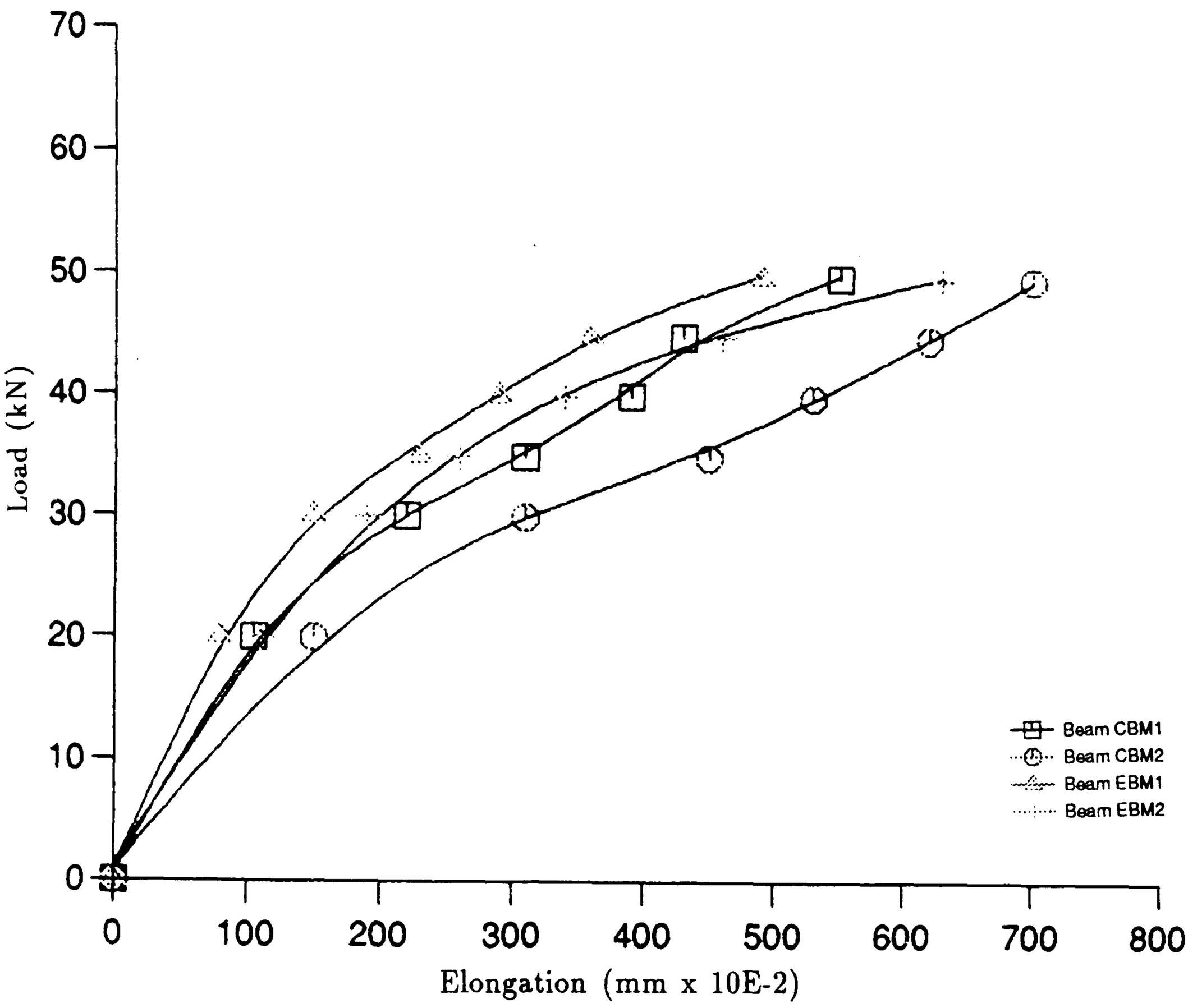


Figure 7.4: Elongations of beams with a shear span to depth ratio of 1.43

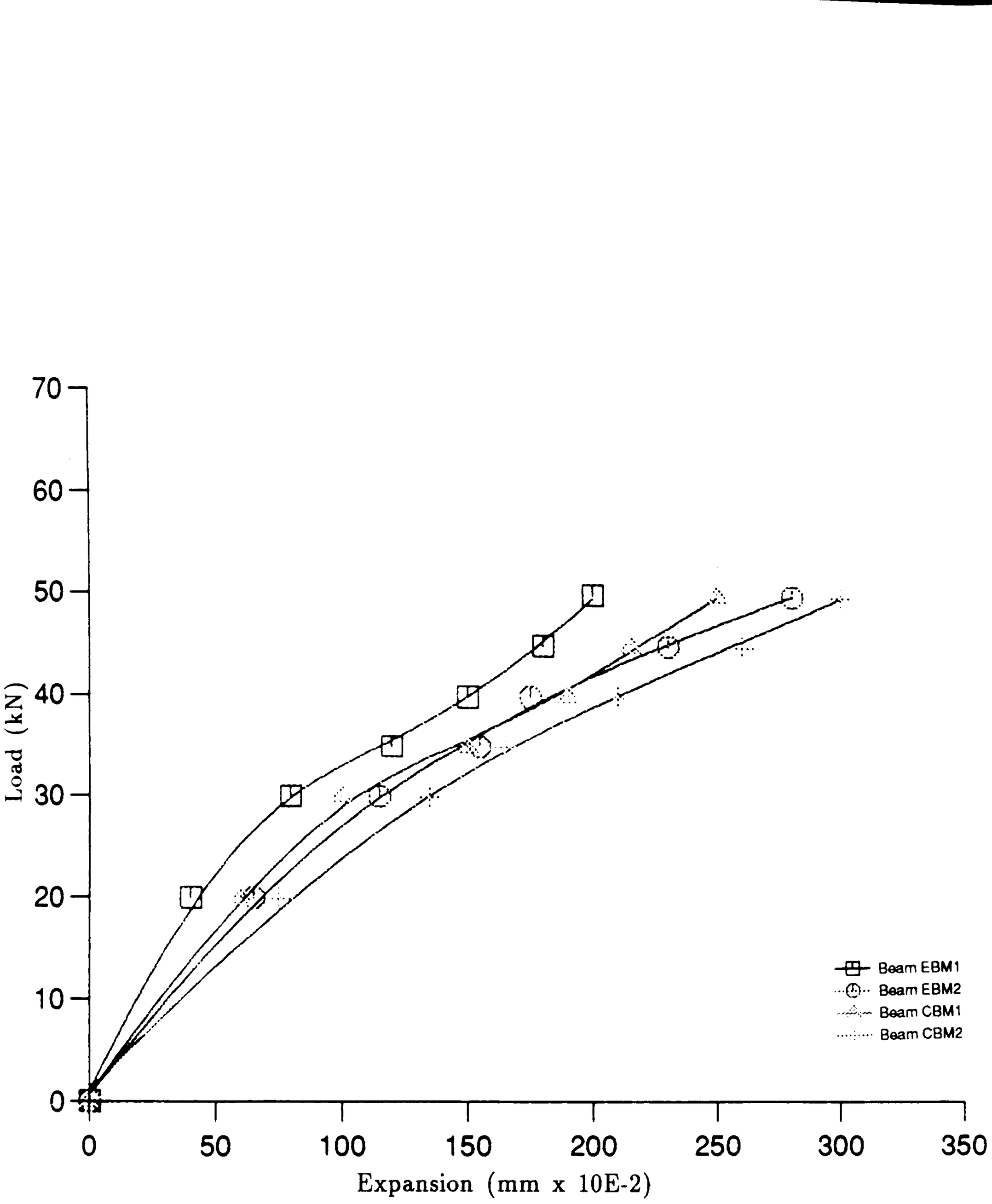


Figure 7.5: Transverse expansions of beams with a shear span to depth ratio of 1.43

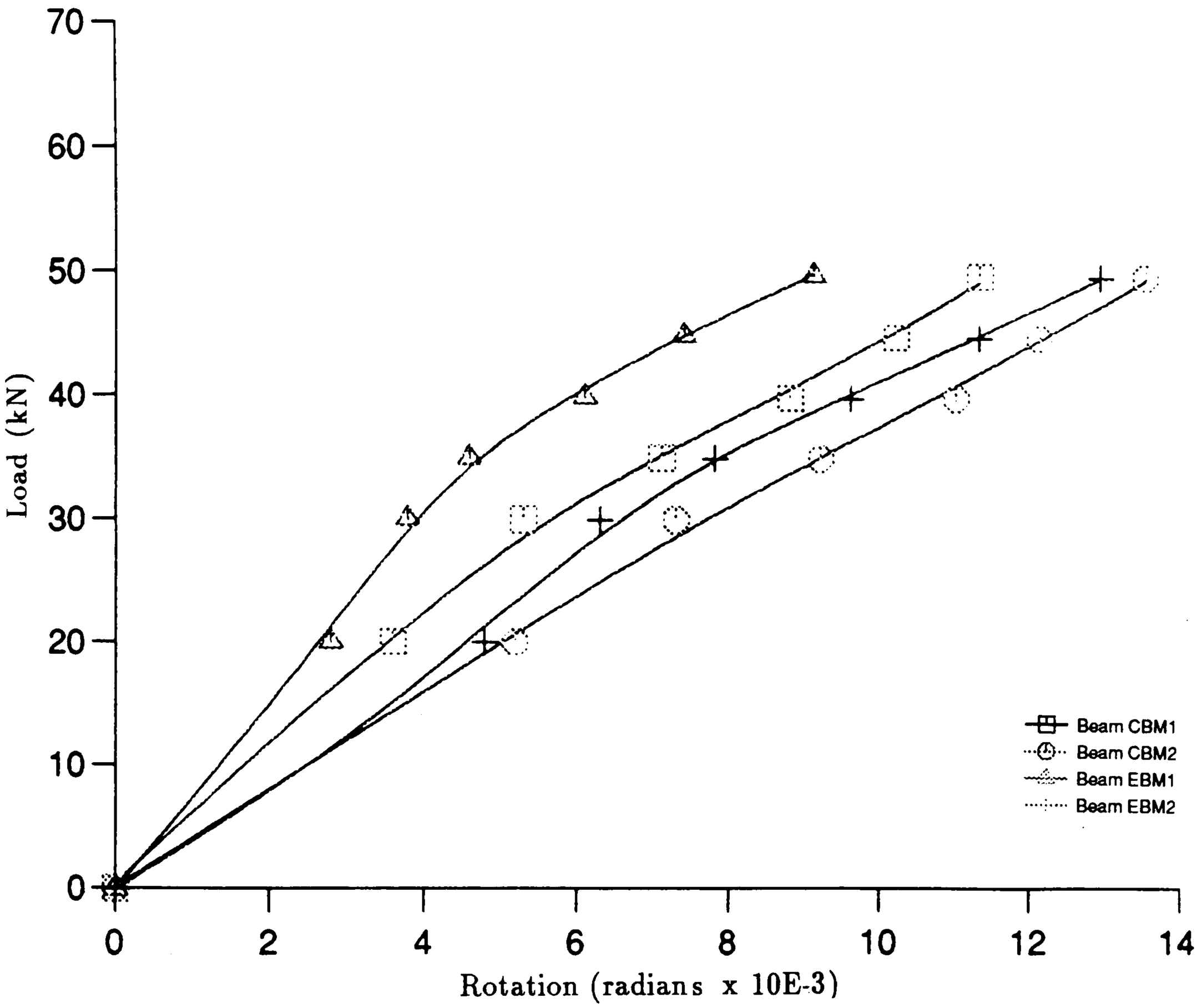


Figure 7.6: Rotations of beams with a shear span to depth ratio of 1.43

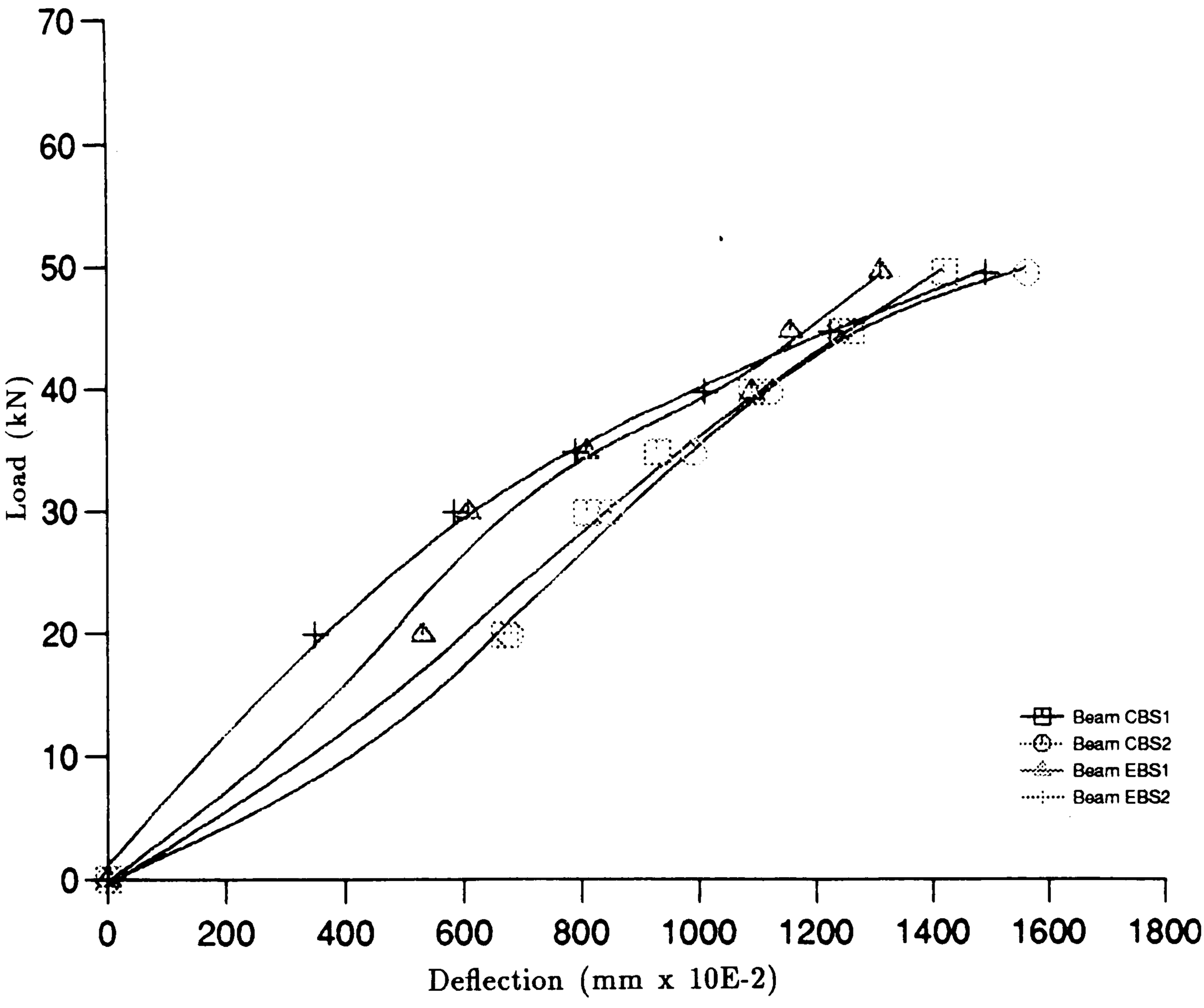


Figure 7.7: Deflections of beams with a shear span to depth ratio of 2.0 at the position of dial gauge D1

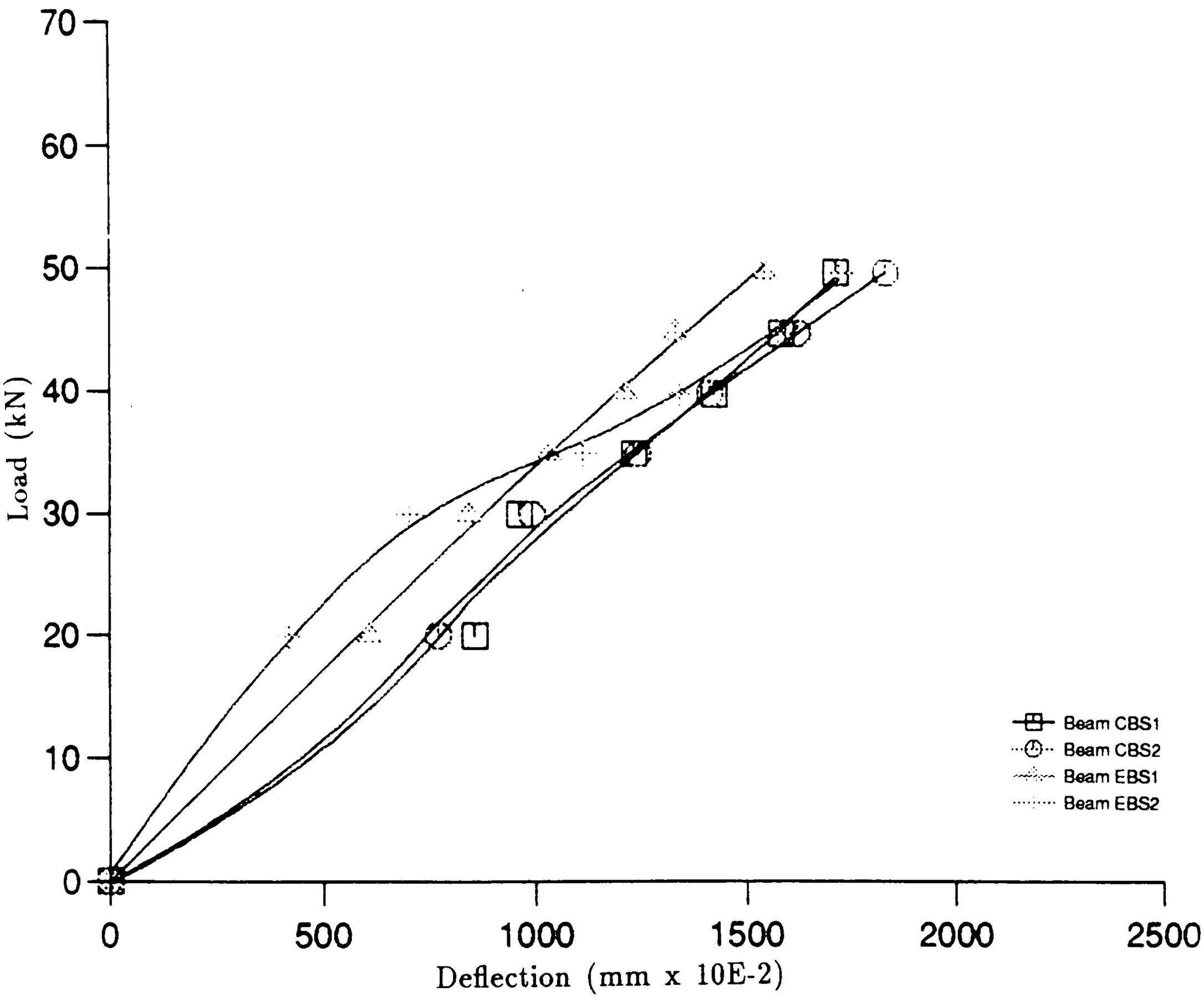


Figure 7.8: Deflections of beams with a shear span to depth ratio of 2.0 at the position of dial gauge D2

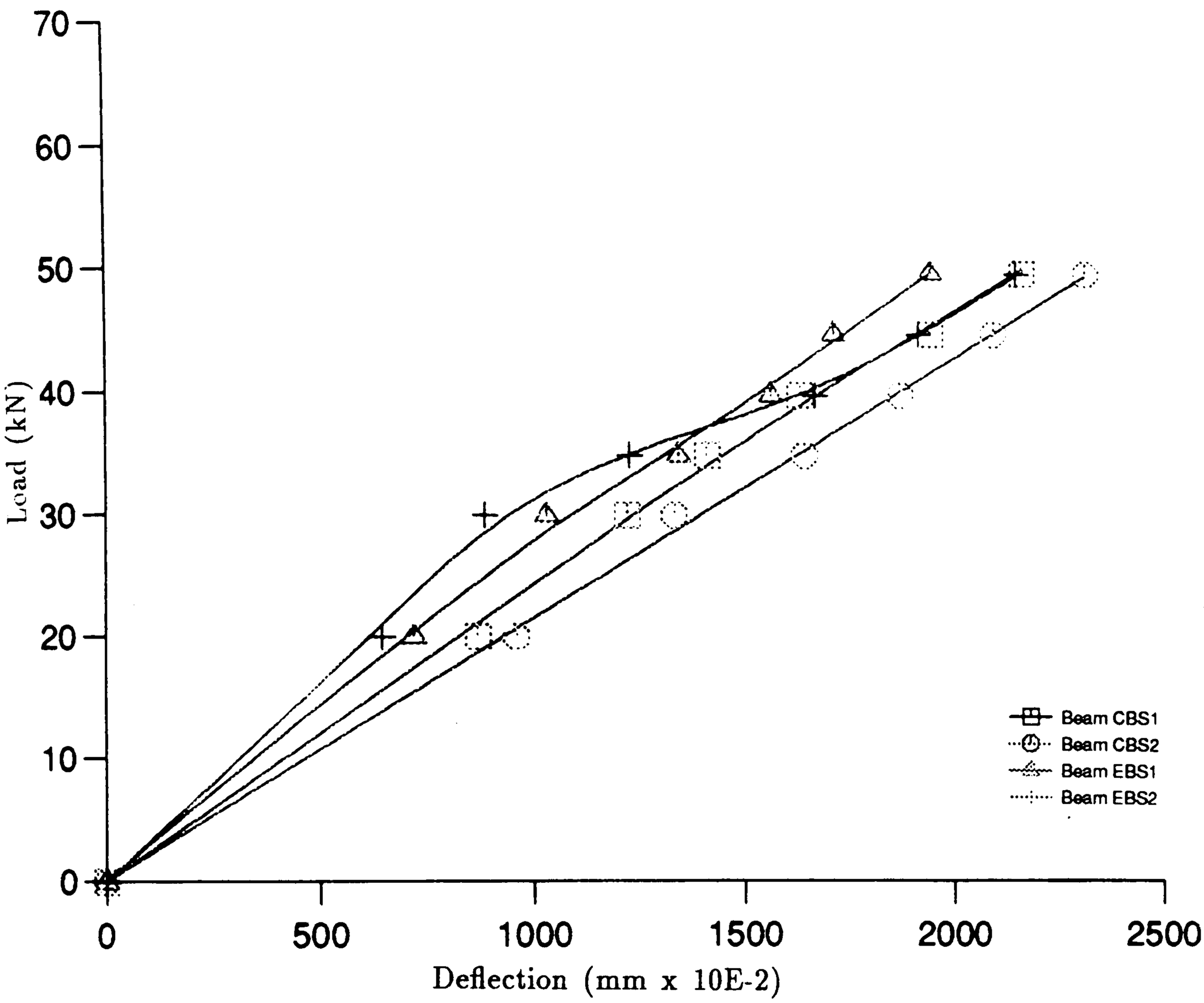


Figure 7.9: Deflections of beams with a shear span to depth ratio of 2.0 at the position of dial gauge D3

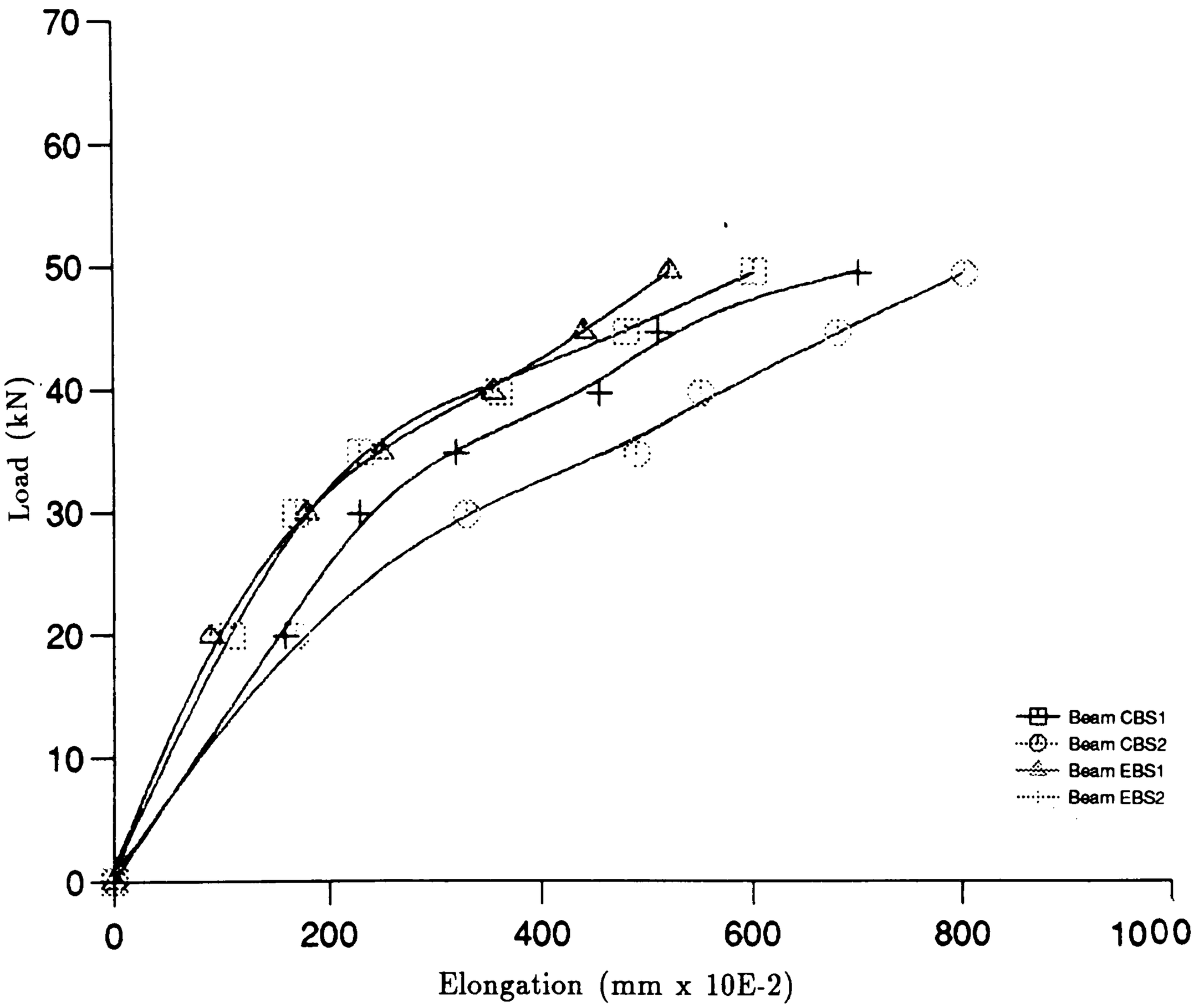


Figure 7.10: Elongations of beams with a shear span to depth ratio of 2.0

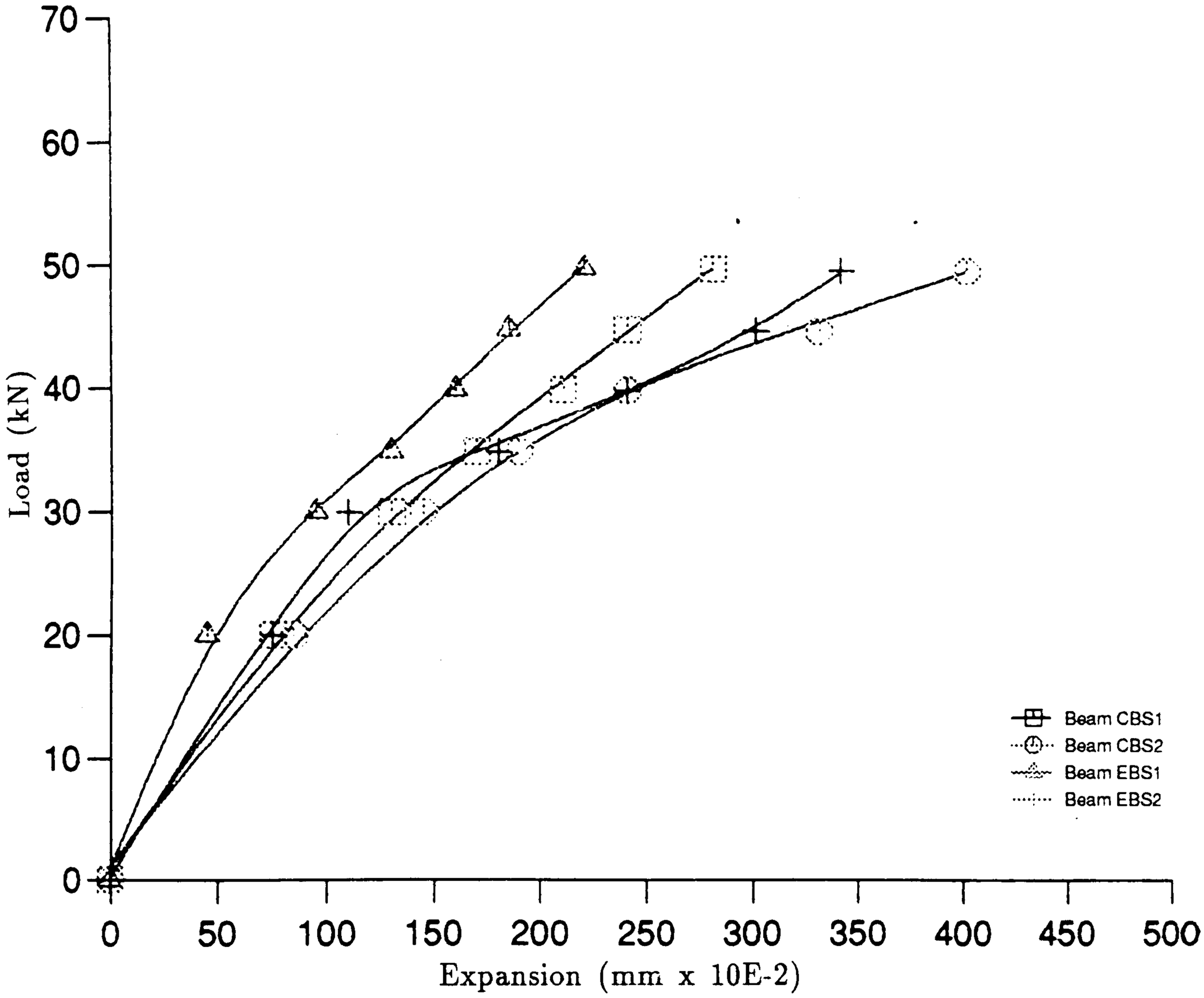


Figure 7.11: Transverse expansions of beams with a shear span to depth ratio of 2.0

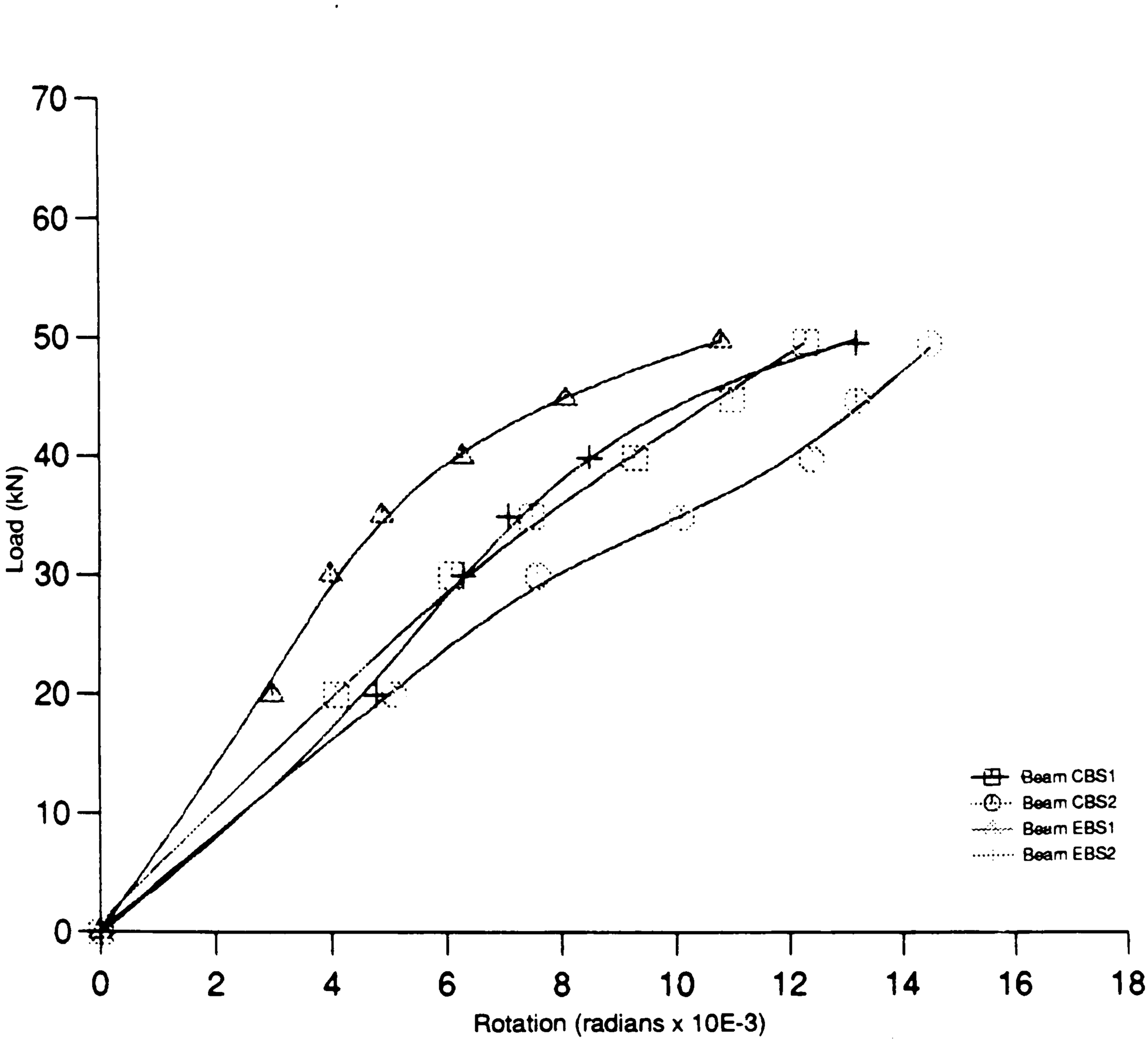


Figure 7.12: Rotations of beams with a shear span to depth ratio of 2.0

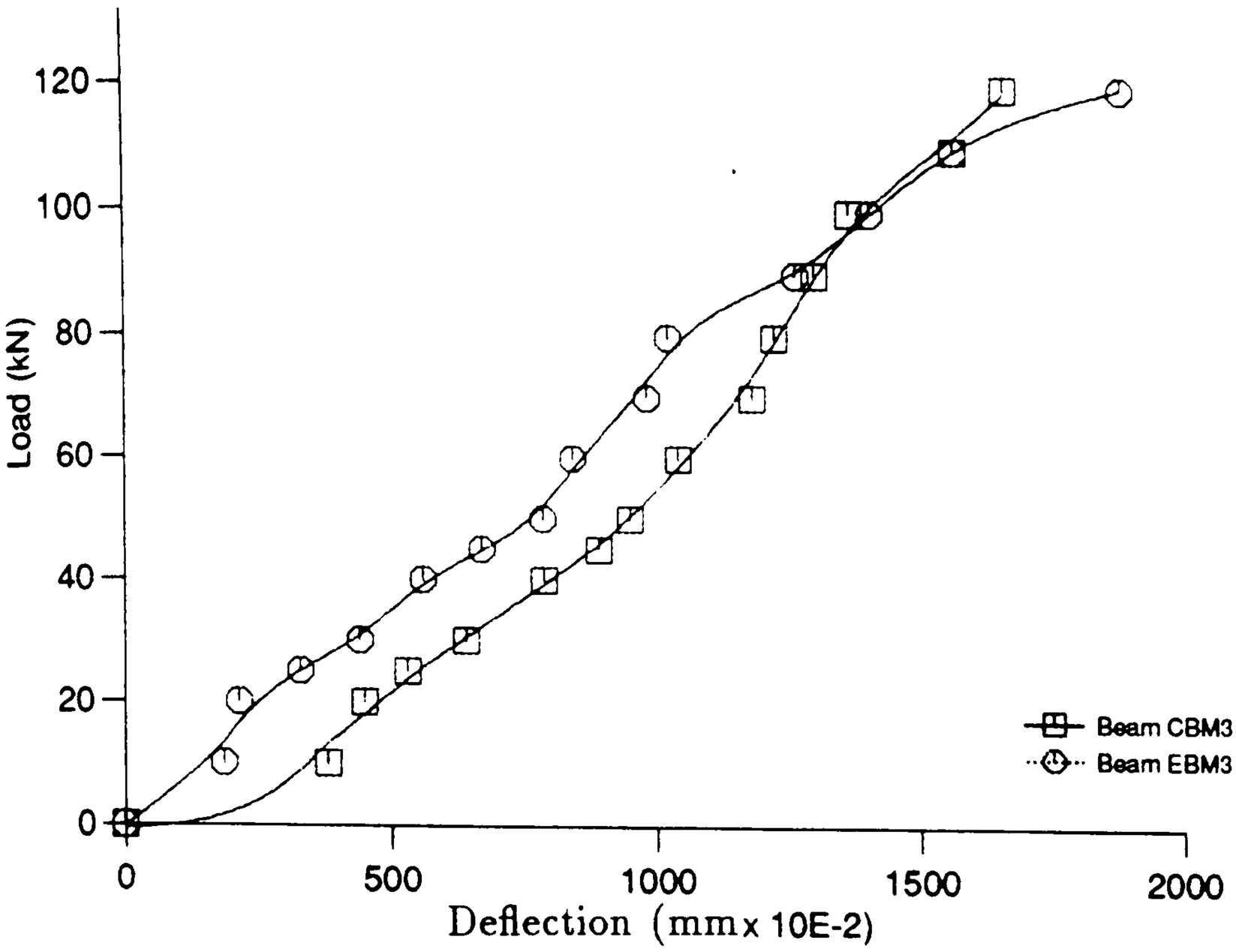


Figure 7.13: Deflections of beams CBM3 and EBM3 at the position of dial gauge D1

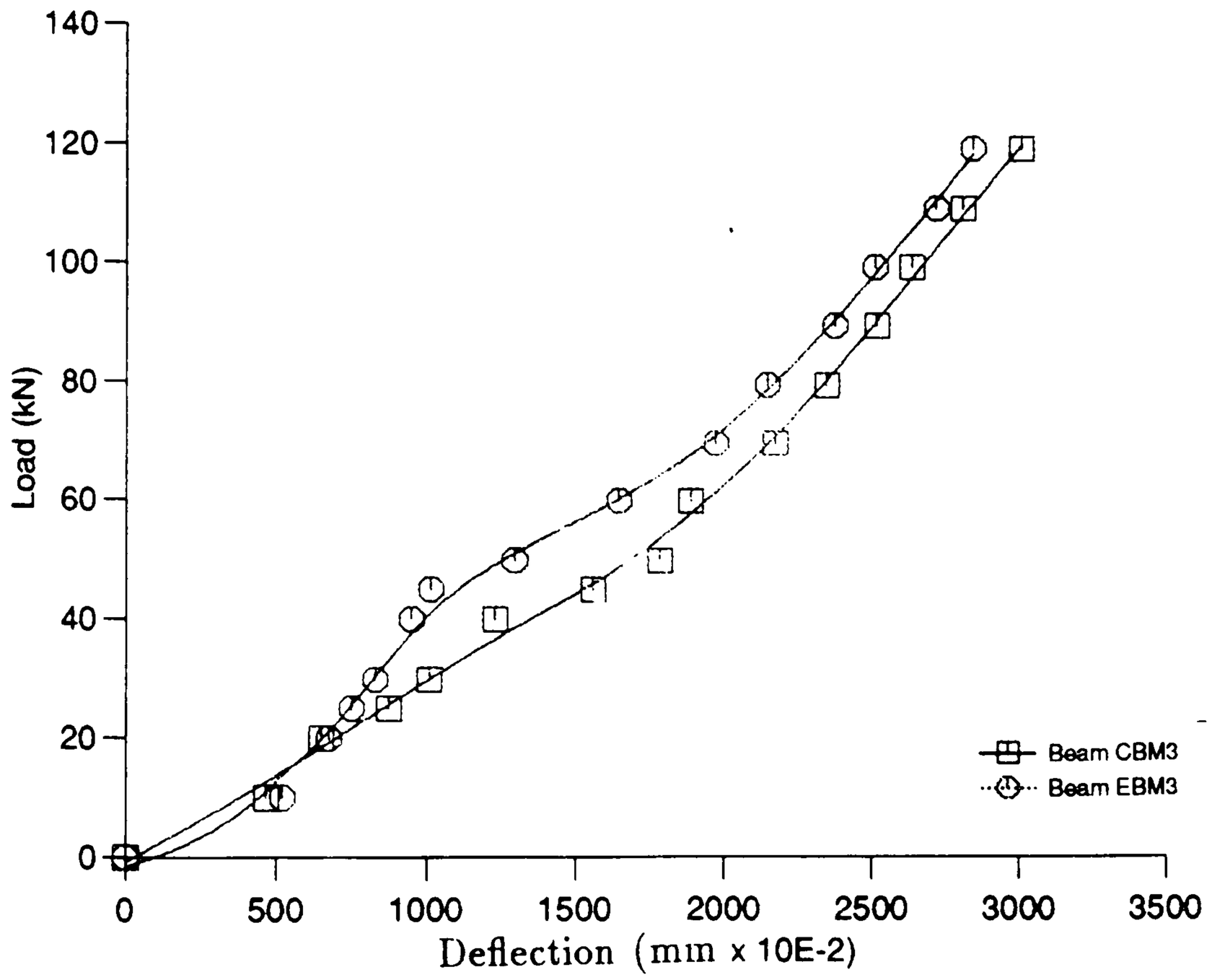


Figure 7.14: Deflections of beams CBM3 and EBM3 at the position of dial gauge D2

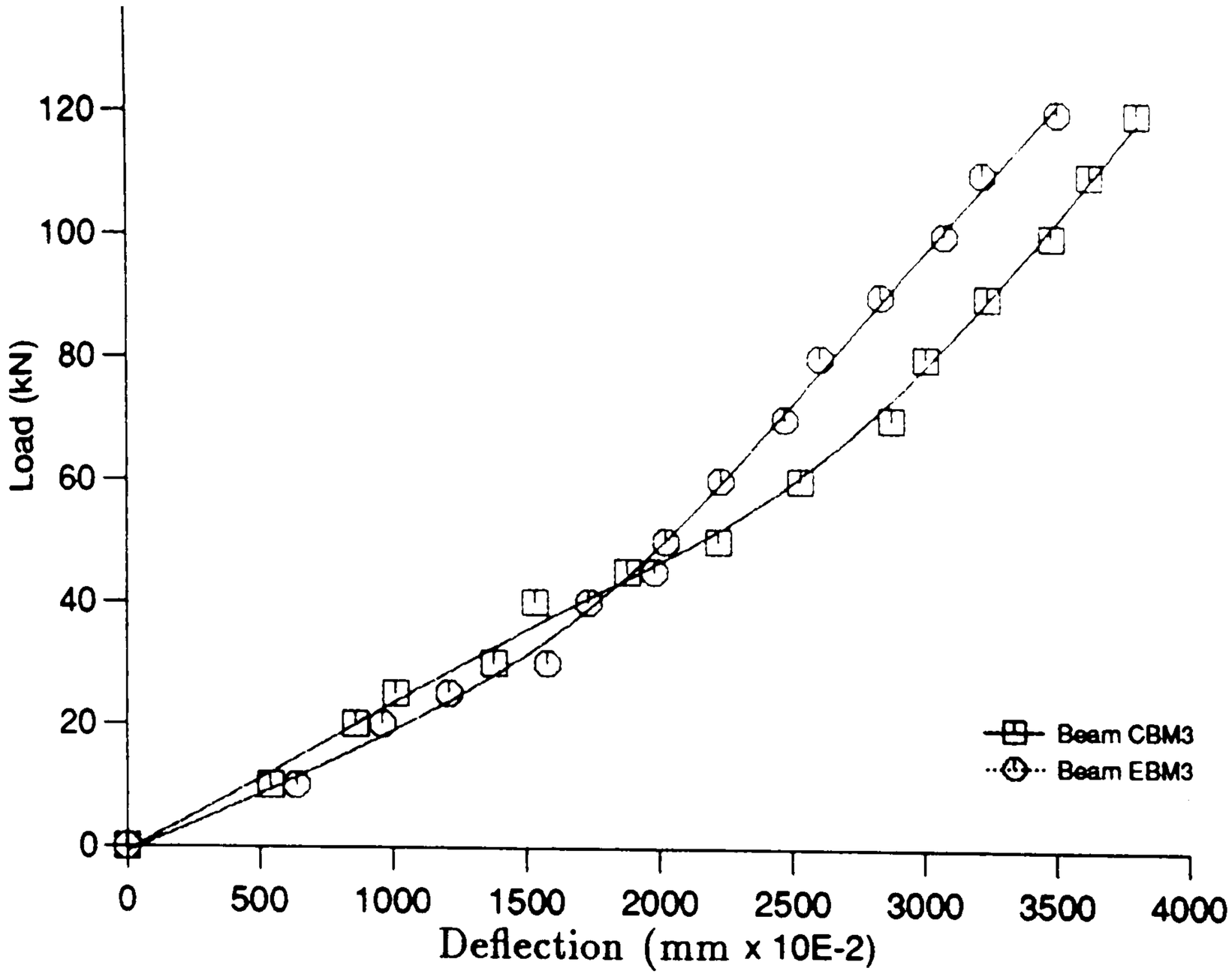


Figure 7.15: Deflections of beams CBM3 and EBM3 at the position of dial gauge D3

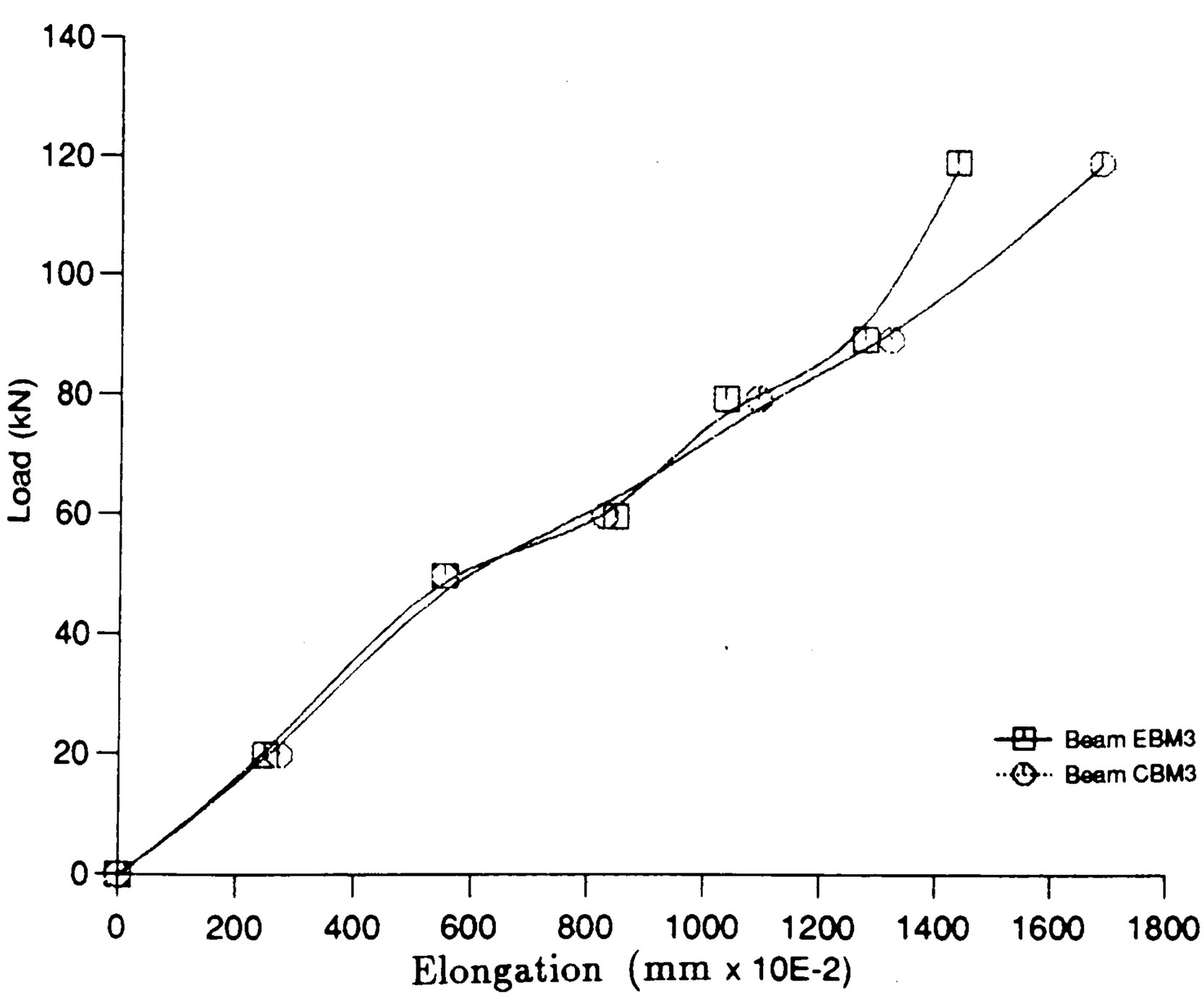


Figure 7.16: Elongations of beams CBM3 and EBM3

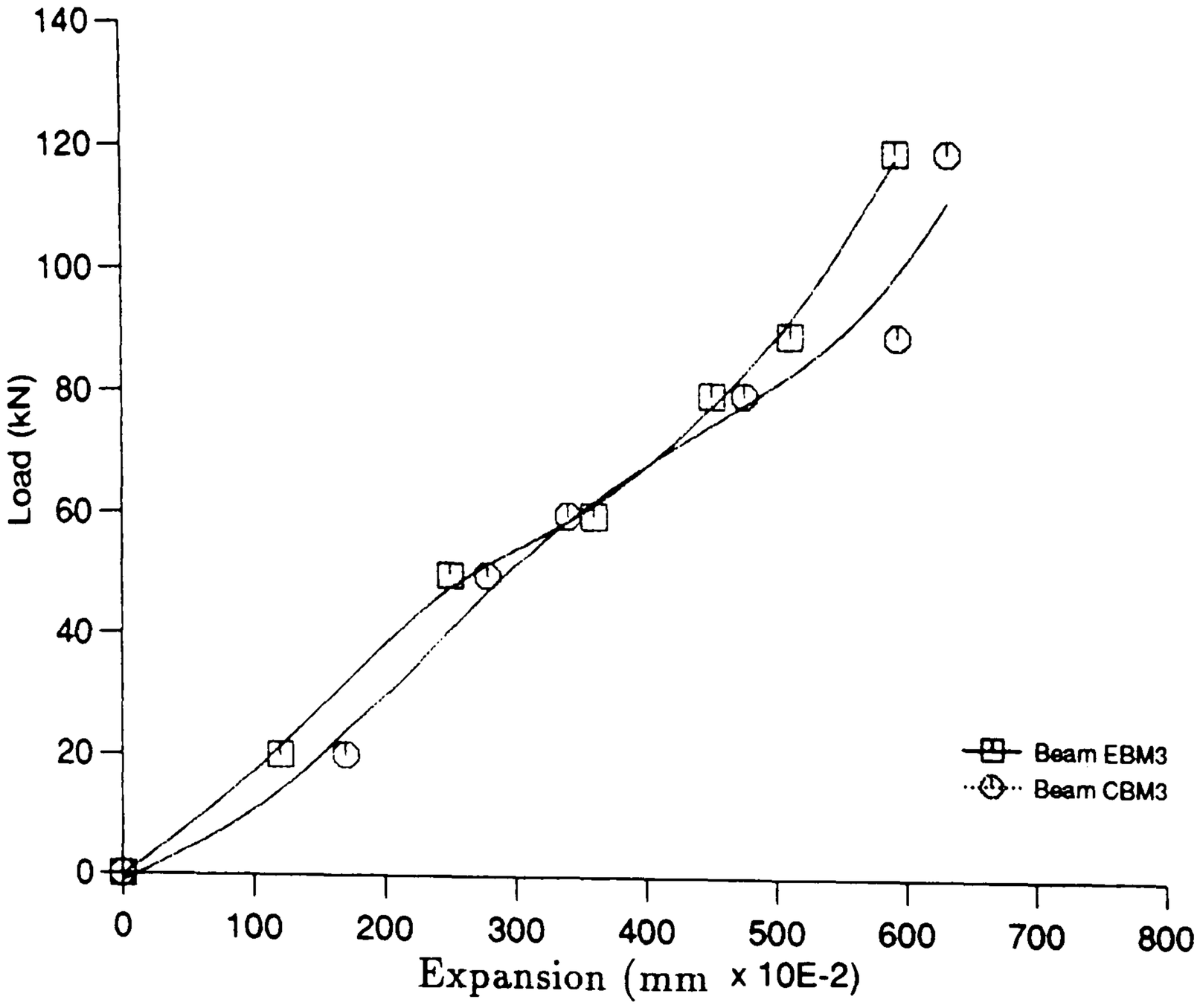


Figure 7.17: Transverse expansions of beams CBM3 and EBM3

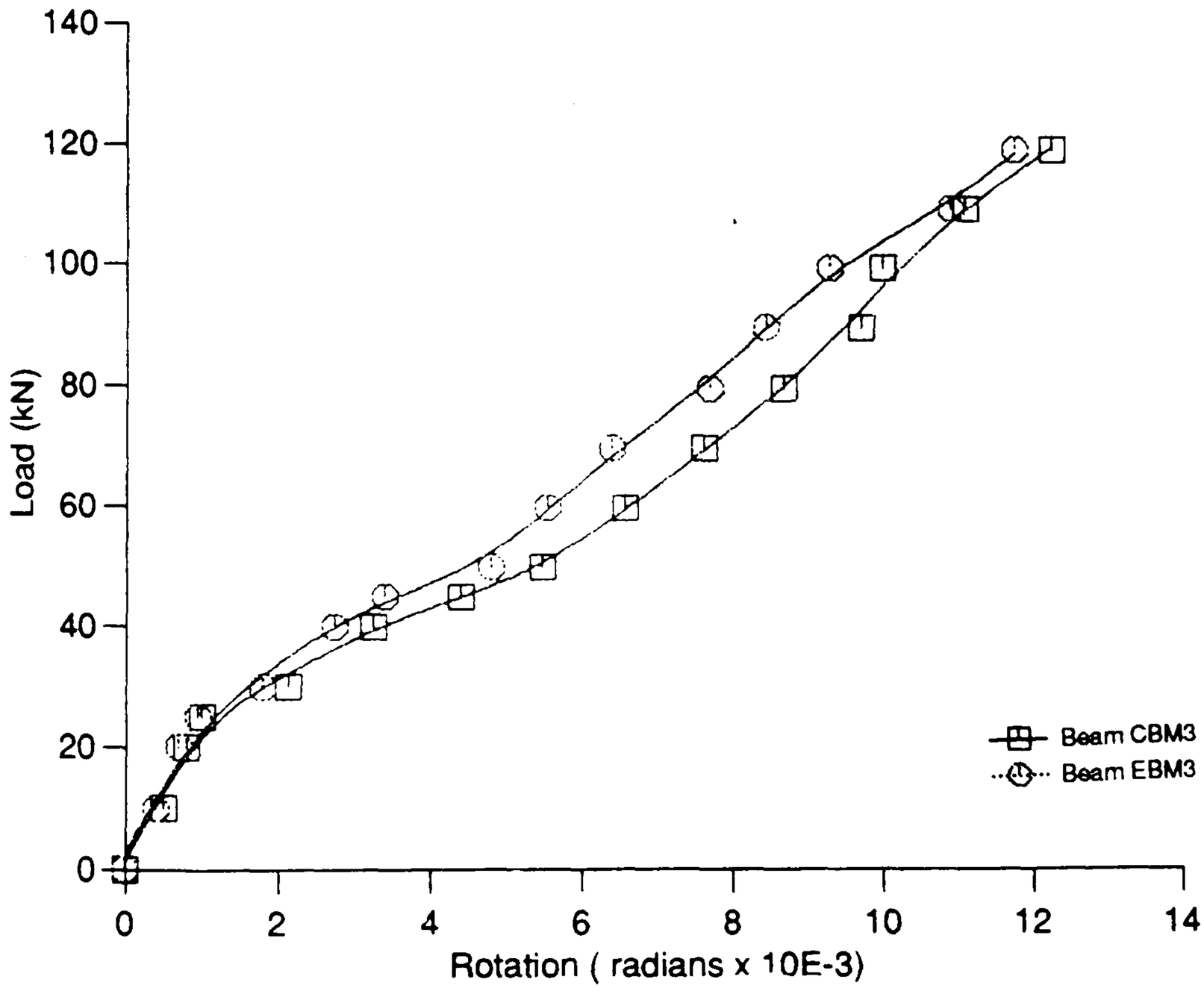


Figure 7.18: Rotations of beams CBM3 and EBM3

| Total Sustained load in kN | | | | |
|---|---|---|---|---|
| Beam | Reinforcement | Subedi's approach | C.F.P approach | Measured |
| CBM2 | Conventional | 135.06 | 136.96 | 153.00 |
| EBM2 | Mesh | 145.27 | 176.32 | 185.00 |
| CBM1 | Conv + diag | 153.81 | 182.08 | 225.00 |
| EBM1 | Mesh + diag | 165.17 | 237.64 | 280.00 |
| CBM3 | Conv + diag | 135.79 | 136.48 | 162.00 |
| EBM3 | Mesh + diag | 144.44 | 179.04 | 190.00 |
| CBS1 | Conv + diag | 110.95 | 125.88 | 142.00 |
| CBS2 | Conventional | 78.33 | 92.65 | 115.00 |
| EBS1 | Mesh + diag | 96.78 | 152.36 | 175.00 |
| EBS2 | Mesh | 93.83 | 122.52 | 145.00 |
| CBD1 | Conv + diag | 246.50 | 263.12 | 360.00 |
| EBD1 | Mesh + diag | 330.42 | 395.69 | 480.00 |

Table 7.1: Predicted and measured loadings

# Chapter 8

# CONCLUSIONS AND SUGGESTIONS FOR FUTURE WORK

## 8.1 INTRODUCTION

A procedure for reinforcing coupling beams using expanded metal mesh has been proposed as a means of reducing the extent of the problems encountered in coupled shear wall structures under the action of full load reversals. This approach has been successfully investigated for the static analysis of such structures [72].

The investigation has not included all aspects of the behaviour of coupling beams but it has addressed what is believed to be the most important aspect with respect to structural concrete design, i.e. the ultimate strength of the beam.

## 8.2 CONCLUSIONS

The following conclusions can be made from the actual and predicted performance of the coupling beams included in this investigation:

1. In Chapter 1, it was shown that it was not only structural design considerations which control the construction of coupled shear wall buildings, but a number of additional concepts such as the sociological aspects and human reactions to such buildings have to be accommodated.

2. The encouraging results which were obtained from this investigation were a consequence of the use of expanded metal mesh which made a significant contribution to the stiffness of the beams especially in the cracked sections. It is anticipated that the use of expanded metal mesh will result in high efficiencies because of its confining influence. It is believed that this form of reinforcement will be less effective in very large scale coupling beams with respect to the bond between concrete and steel.

3. Suitable construction and test procedures have been developed to study the behaviour of single storey height sections of walls coupled by beams. These procedures can be extended to structures which have more than two walls and are more than two storeys high.

4. A number of expanded metal mesh reinforced concrete coupling wall beams have been tested and, from the results, it has been shown that this form of reinforcement can enhance the shear performance of the beams and limit

the formation and propagation of cracking when compared with beams reinforced with conventional stirrups.

5. The results obtained from the laboratory tests and the analytical approaches indicate that, the loss in stiffness of coupling beams resulting from diagonal cracking was greater in the beams conventionally reinforced compared to those which contained the expanded metal mesh.

6. It has been demonstrated that the shear mode of failure can be contained using the improved reinforcing details introduced into beams EBMi, EBSi and EBD1, thus making it possible to obtain more ductile behaviour in the beam under load.

7. There was a reduction in the probability of cracks appearing in any part of the beams with higher span to depth ratios heavily reinforced with expanded metal mesh and conventional reinforcement.

8. Confining reinforcement, consisting of closely spaced strands of expanded metal mesh, introduced into the beams, especially at the corners, can prevent rapid deterioration of the beams during cyclic loading and can lead to significant increases in their strengths.

9. Diagonally reinforced coupling beams are capable of sustaining much larger forces during cyclic loading when compared to beams conventionally reinforced.

10. The failure in diagonally reinforced beams generally resulted from buckling of the compression bars leading to breaking away of the surrounding concrete. The transient nature of the load developed during seismic disturbances means that buckling of the compression reinforcement bars does not result in a complete loss of strength of the beam. During loading reversals buckled bars may straighten and contribute fully towards the tensile strength requirement of the beam, although some sliding shear is present during a change in the loading direction.

11. To prolong the effective contribution of coupling beams during catastrophic earthquakes, the confinement of the concrete within the cage of the diagonally placed group of bars is imperative.

12. The omission of the conventional horizontally positioned flexural reinforcement in diagonally reinforced coupling beams facilitates relatively easy assembly of the prefabricated cage required to reinforce the complete beam. The placement of this cage into the coupled shear wall structure, without undue congestion of the reinforcement bars where the wall and beam intersect, can also be accomplished.

13. The tests included in this investigation confirmed conclusively the superior performance of coupled shear walls containing expanded metal mesh combined with diagonal reinforcement bars in the following respects:

a) improved stiffness characteristics were evident at low loads so this form of reinforcement is desirable in minimising nonstructural damage during mod-

erate earthquakes;

b) less damage to coupling beams;

c) better energy absorption, which is essential in ensuring survival during catastrophic ground shaking.

14. The failure of the reinforced concrete coupling beams with symmetrically placed top and bottom reinforcement is characterised by localised crushing of the concrete at the corners, which are highly stressed in compression.

15. The test results have established that the expanded metal mesh reinforced beam containing diagonal reinforcement bars is a feasible proposition for use in structures. On the question of economy, expanded metal meshes can be obtained directly from suppliers and any additional work to the expanded metal mesh will be minimal. A preliminary estimate discussed in Chapter 3 suggests that expanded metal mesh provides an economical alternative to conventional reinforcement, which involves the cost of material, bar bending and fixing.

16. The investigation has shown that the main problem associated with the expanded metal mesh is the bond between the expanded metal mesh and the concrete. There is, however, some degree of mechanical fixing by virtue of the holes in the expanded metal mesh.

17. A comparison of the results from the theoretical approaches and the laboratory based tests in terms of the load carrying capacity of the beams during the third load cycle highlighted the ability of the analytical approaches to predict usable design information.

18. The results from this investigation indicate that with careful detailing, particularly in areas where yielding can occur, coupled beam structures can be made to possess all the desirable features of an effective earthquake resistant structure.

19. It can be claimed from consideration of the experimental evidence and theoretical comparisons that the investigation has achieved its ultimate objectives. These objectives were the development of effective and efficient design methods to permit the use of conventional and diagonal reinforcement bars in conjuction with expanded metal mesh in coupling beams.

## 8.3 SUGGESTIONS FOR FUTURE WORK

Although many papers and much work has been published relating the theoretical and experimental analysis of coupled shear walls, there still remains a large number of aspects which require detailed investigation. Some of the areas which could benefit from further work are:-

1. In order to gain further information on the behaviour of expanded metal mesh in coupling shear wall structures it is recommended that an experimental investigation on multi-storey beam-wall structures, based on the findings from the present investigation, be carried out.

2. To supplement the experimental findings from this investigation it would be useful to repeat some of the tests using different forms of expanded metal mesh, with different parameters including large scale specimens, in order to study the problem of the bond between the concrete and reinforcement.

3. The performance of beams which were reinforced with expanded metal mesh could have been improved if additional stirrups at the supports had been included. It is recommended that further testing is also necessary to examine the behaviour of the test beams containing a combination of expanded metal mesh and stirrups at the supports.

   The respective form of these two reinforcement arrangements allows for such a combination to be accommodated relatively easily.

4. The improved strength of the beams detailed in accordance with the reinforcement arrangement incorporating expanded metal mesh could have advantages with respect to earthquake resistant applications. However, a more detailed investigation to confirm the apparent improvement would be useful and will require to be investigated.

5. The size of expanded metal mesh may have a significant influence on the behaviour of coupling beams. Further research is therefore, necessary in

order to quantify the apparent positive influence of the size of the expanded metal mesh on the shear strength of this type of beam so that it can be fully exploited in design. It is also recommended that such research should be carried out using the different combinations of expanded metal mesh and stirrups.

6. In seismically active areas it is essential that coupling beams remain ductile and that the walls do not fail. An investigation into the detailing of the reinforcement in the walls and the coupling beams using expanded metal mesh at their junctions would provide useful information on their behaviour.

7. While designing coupled shear walls with known static indeterminacy, it is desirable to proportion the reinforcement to result in an advantageous sequence of hinge formations so that the damage occurs initially in repairable and less critical areas. The detailed study of the behaviour of the walls together with the coupling beams, similar to the types investigated in the present investigation, to determine the overall structural behaviour would be useful.

It is recommended that all horizontal reinforcement should pass along the full span of the coupling beam without cut-offs or laps, and be generously anchored into the adjoining walls over a distance of at least three quarters of the beam span. It should be noted that the concrete in the anchorage zones may be subjected to transverse tensile strains and may thus contain cracks in the anchorage region of the reinforcement.

8. In conventionally reinforced beams, it is possible that the concentration of stirrups at the supports may be useful in preventing or in delaying the destructive shear displacements across the cracked compression zones of the coupling beams since these regions are subjected to high intensity cyclic loading. This could be achieved by carrying out a series of tests with only the spacing of the stirrups being varied or with the introduction of additional stirrups at the supports.

# Appendix A

# PHOTOGRAPHIC RECORD OF THE INVESTIGATION

Figure A.1: Data logging system

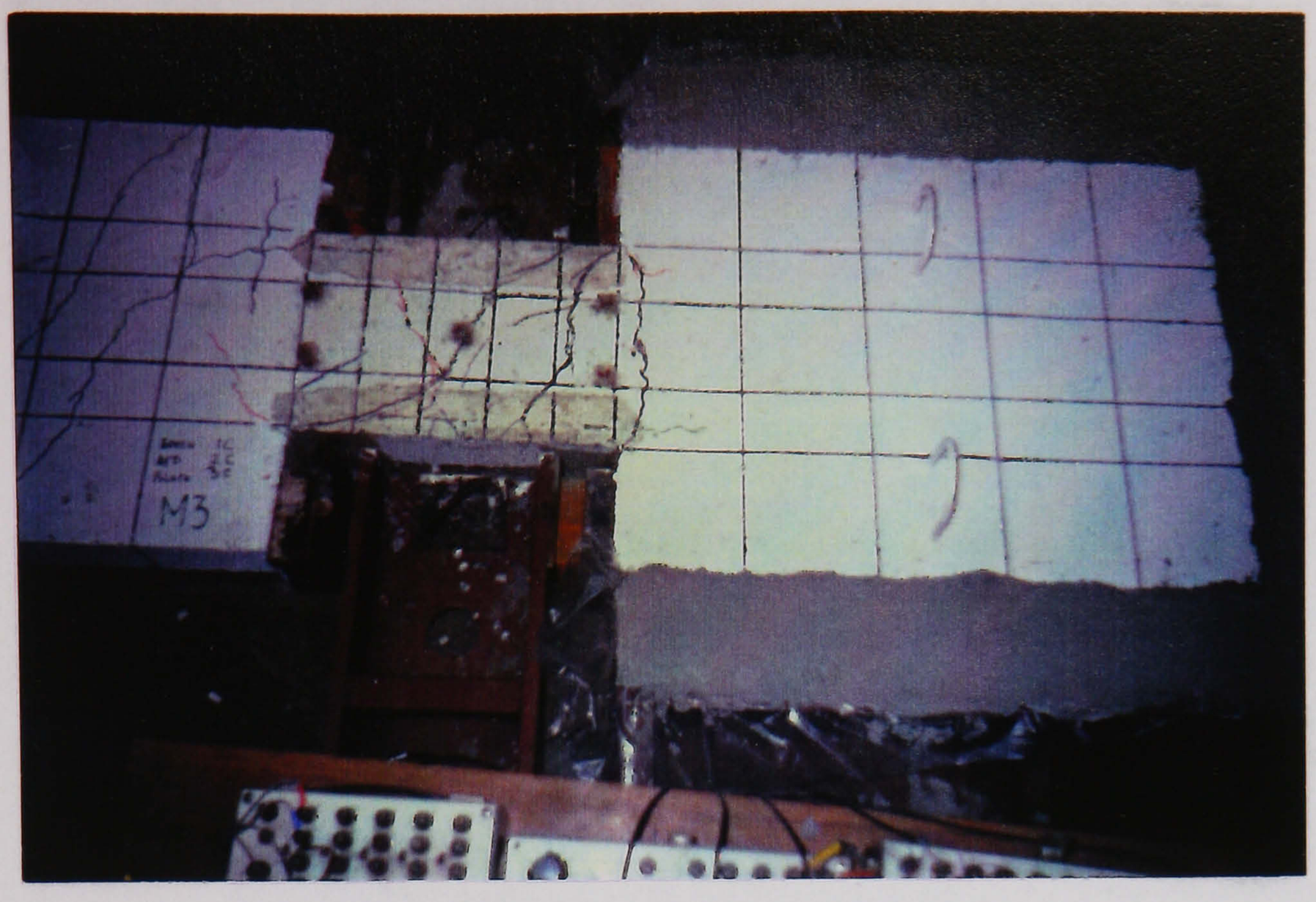


Figure A.2: Beam CBM1 at failure




Figure A.3: Beam CBM2 at failure

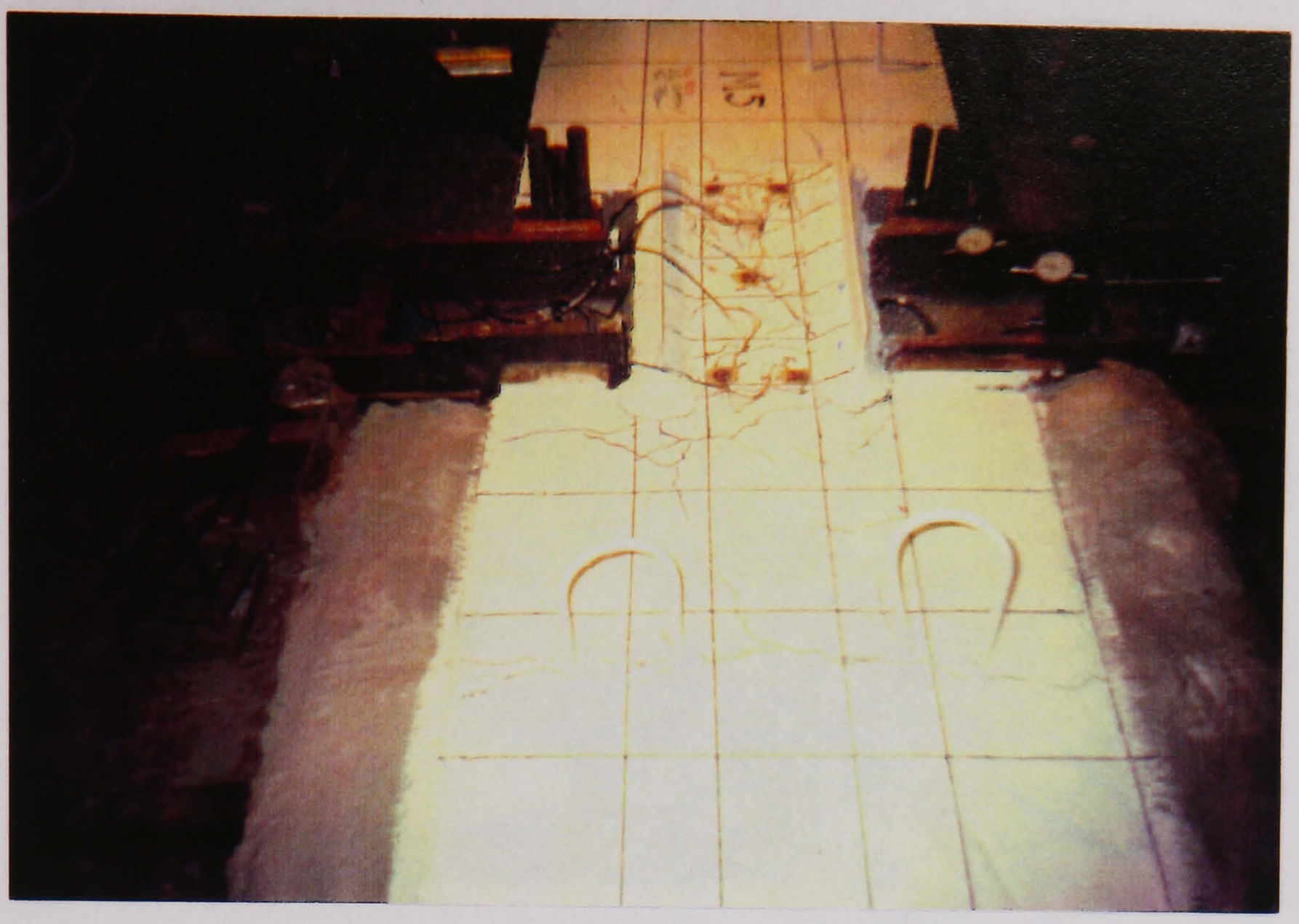

Figure A.4: Beam EBM1 at failure


Figure A.5: Beam EBM2 at failure

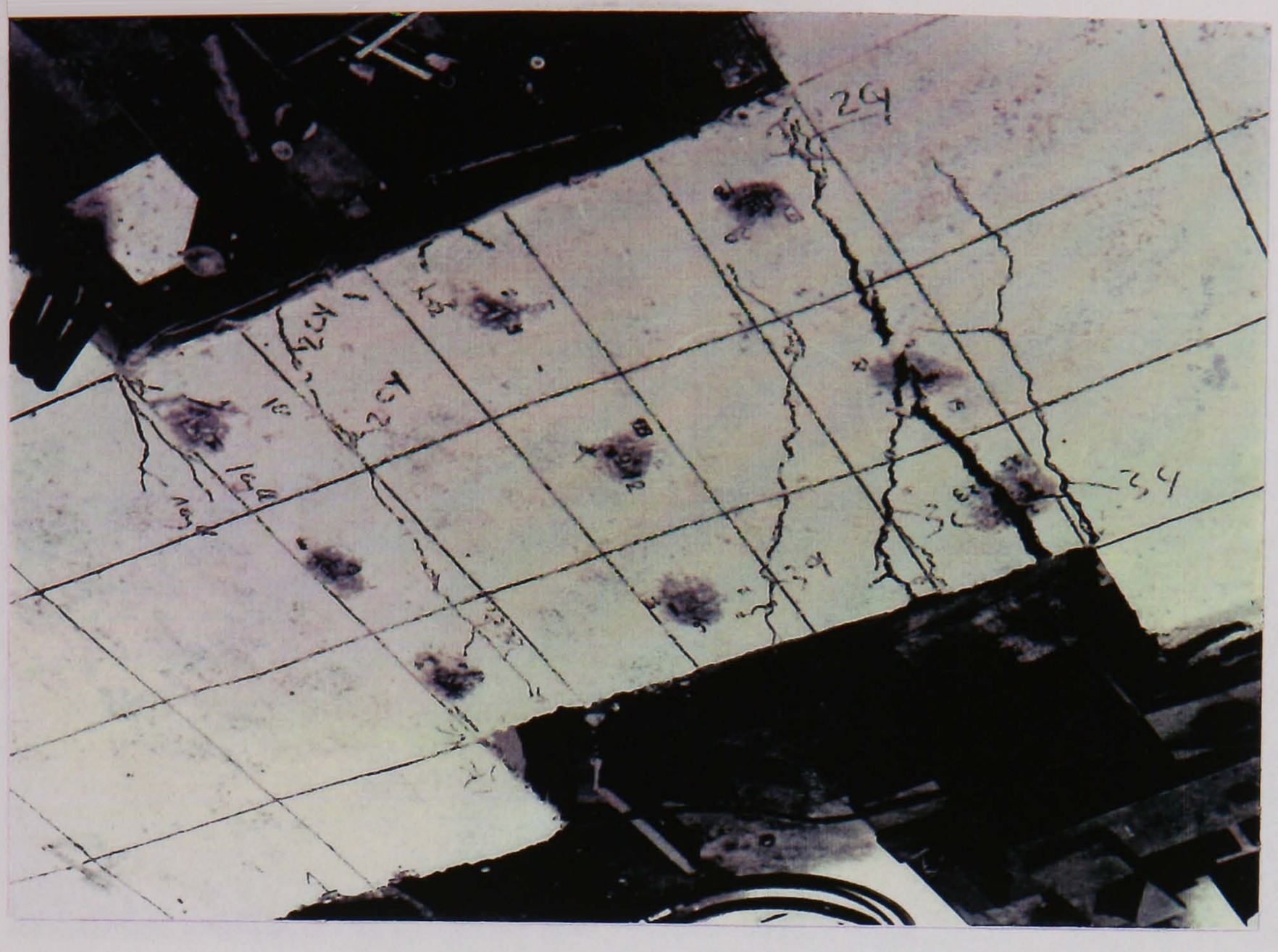

Figure A.6: Beam CBD1 at failure

Figure A.7: Beam EBD1 at failure

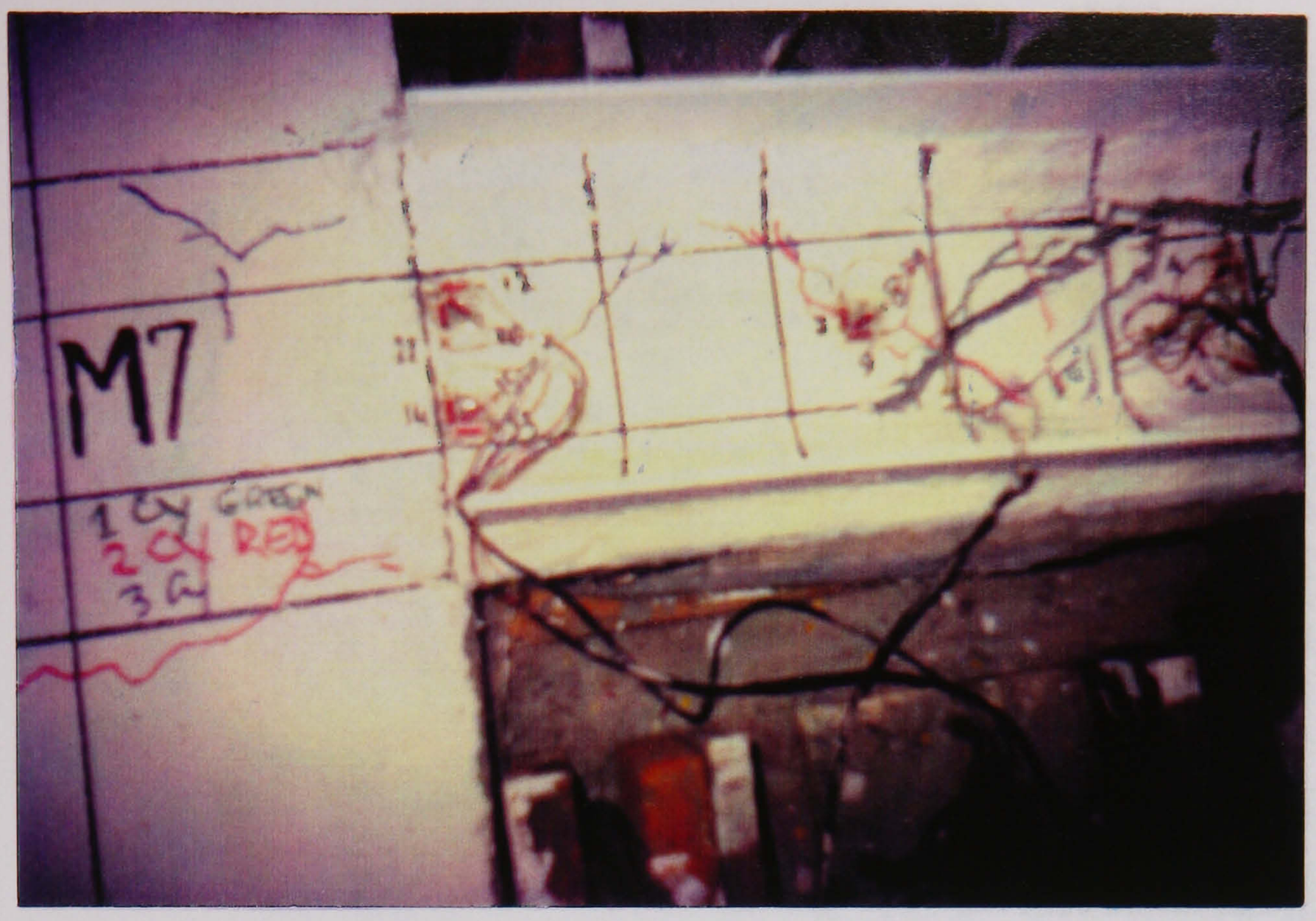


Figure A.8: Beam CBS1 at failure

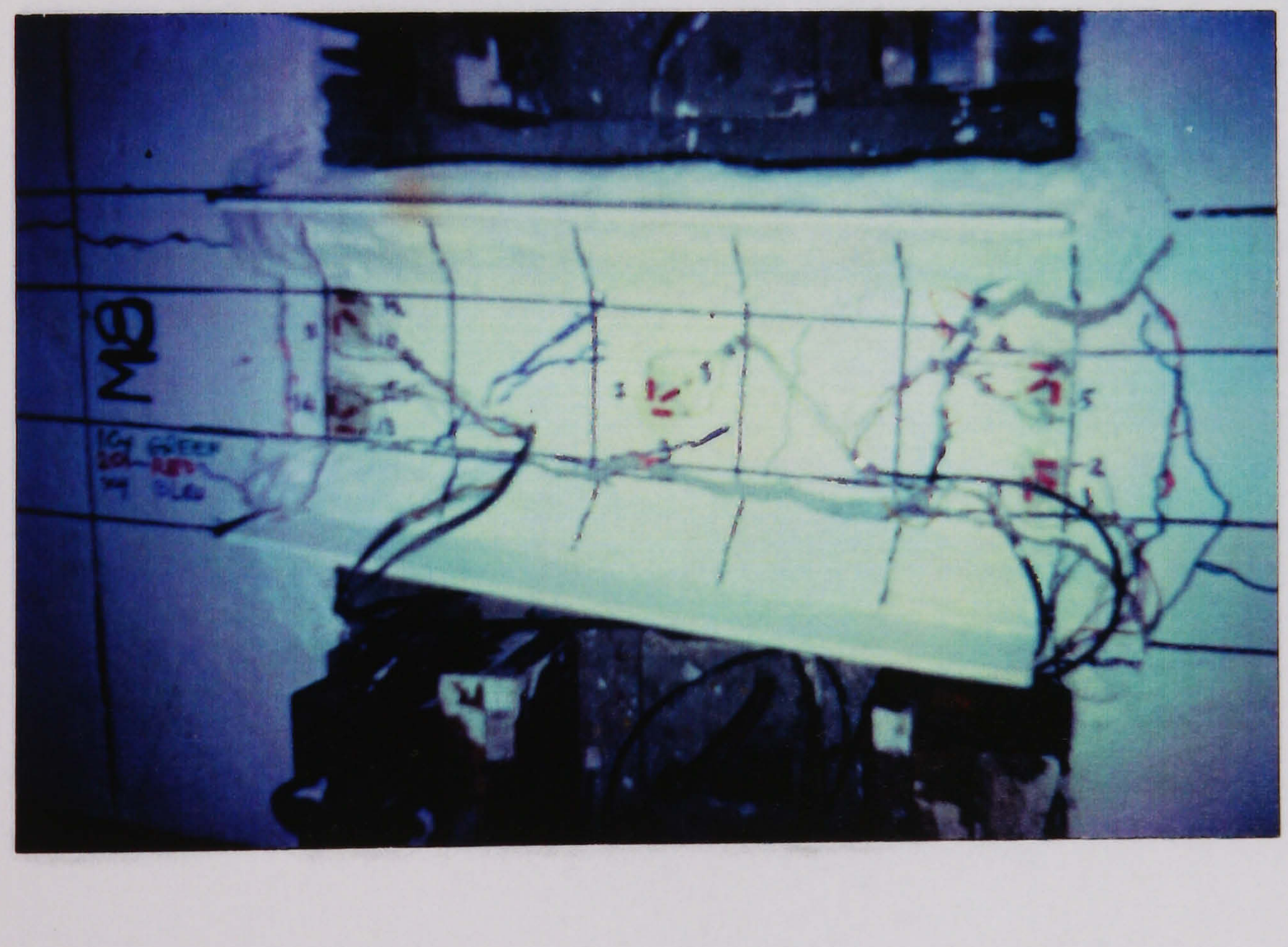


Figure A.9: Beam CBS2 at failure

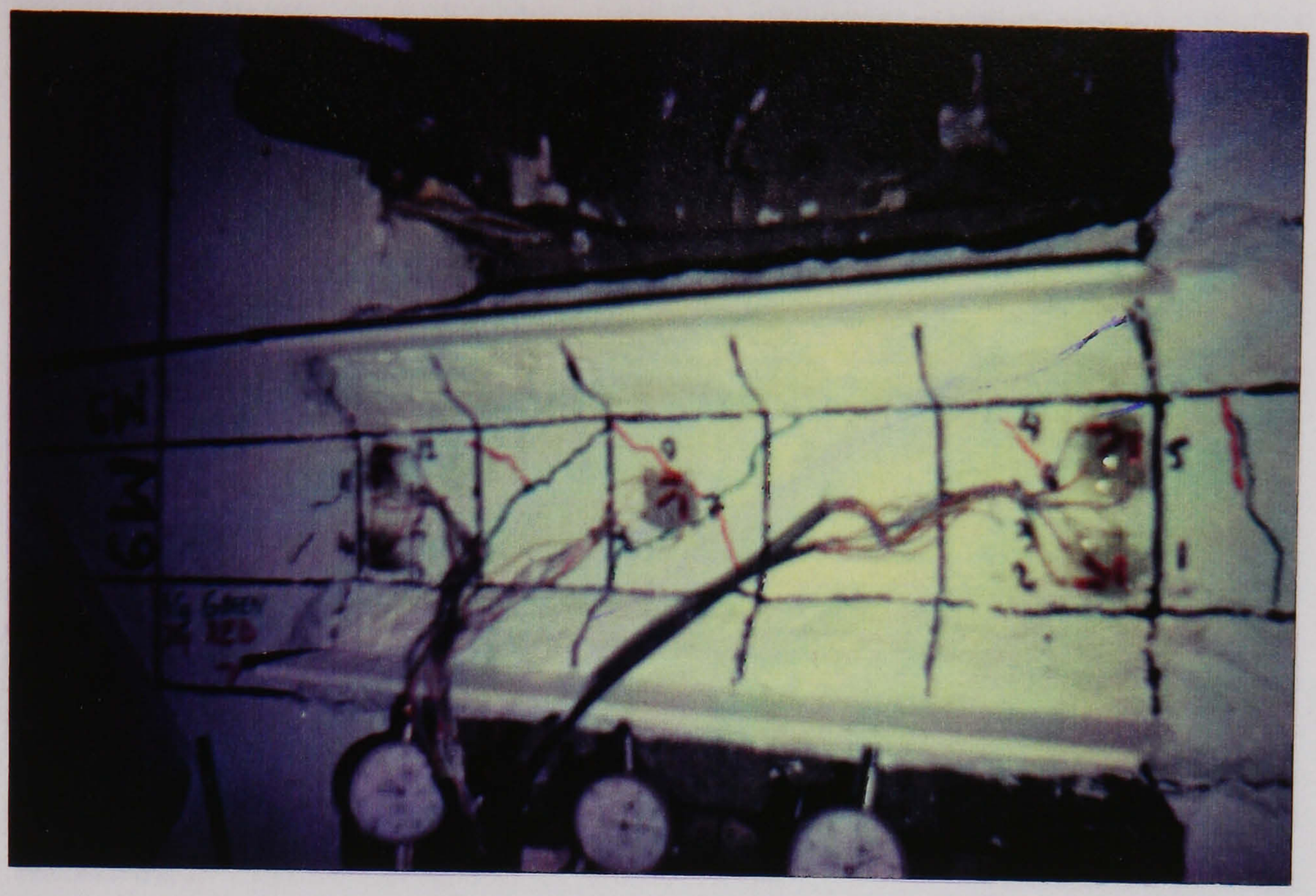

Figure A.10: Beam EBS1 at failure

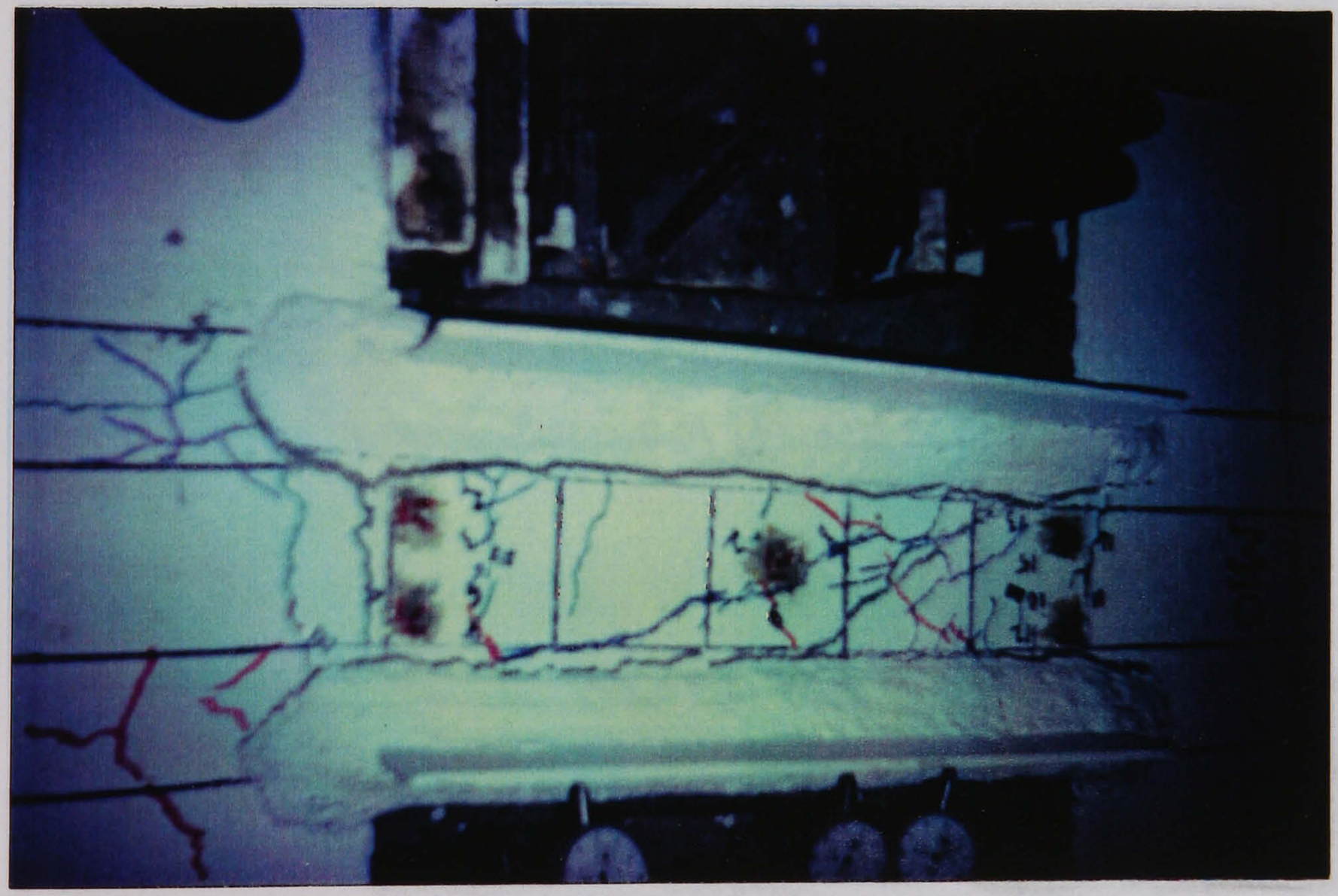

Figure A.11: Beam EBS2 at failure

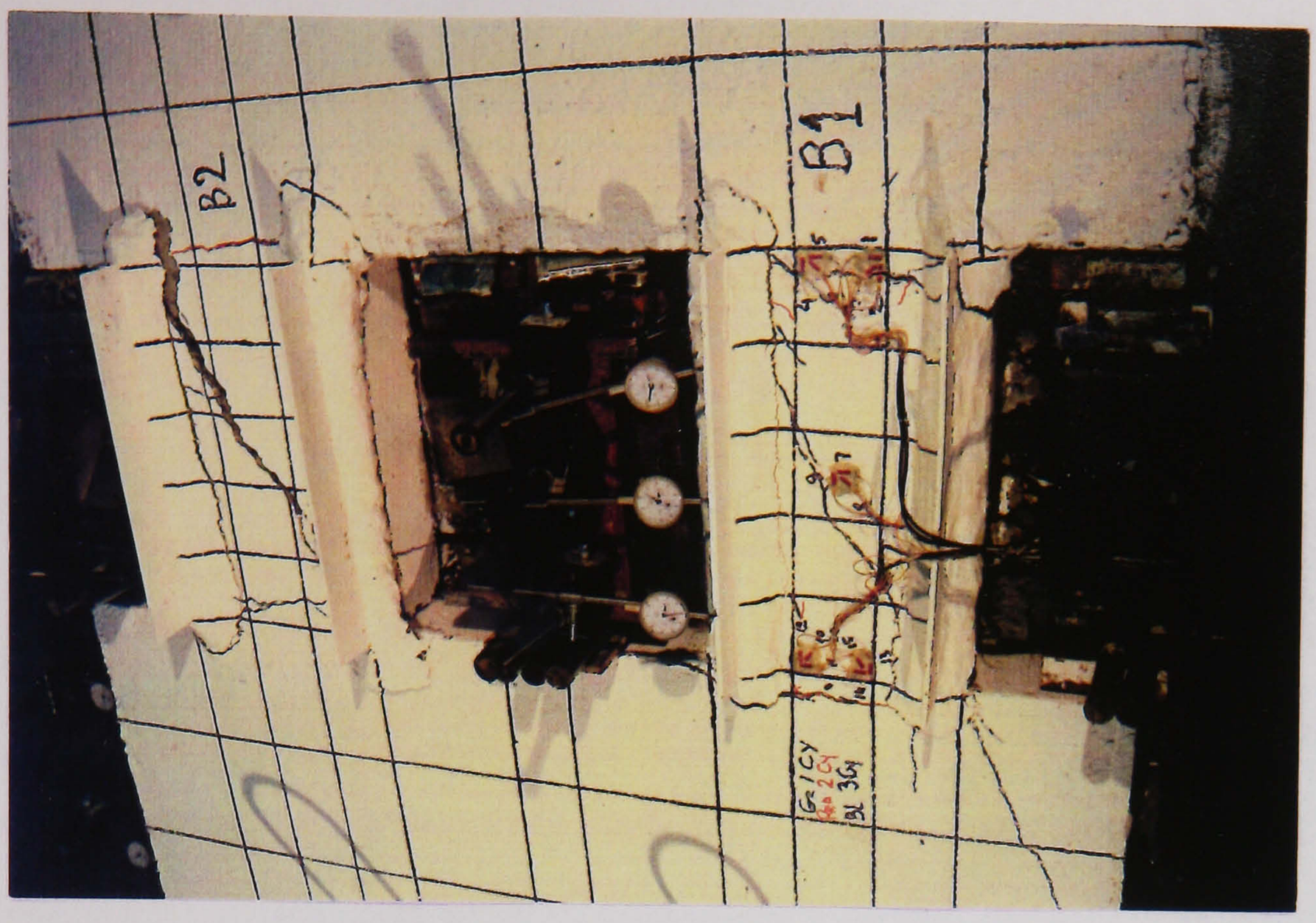


Figure A.12: Beam DBS2 at failure

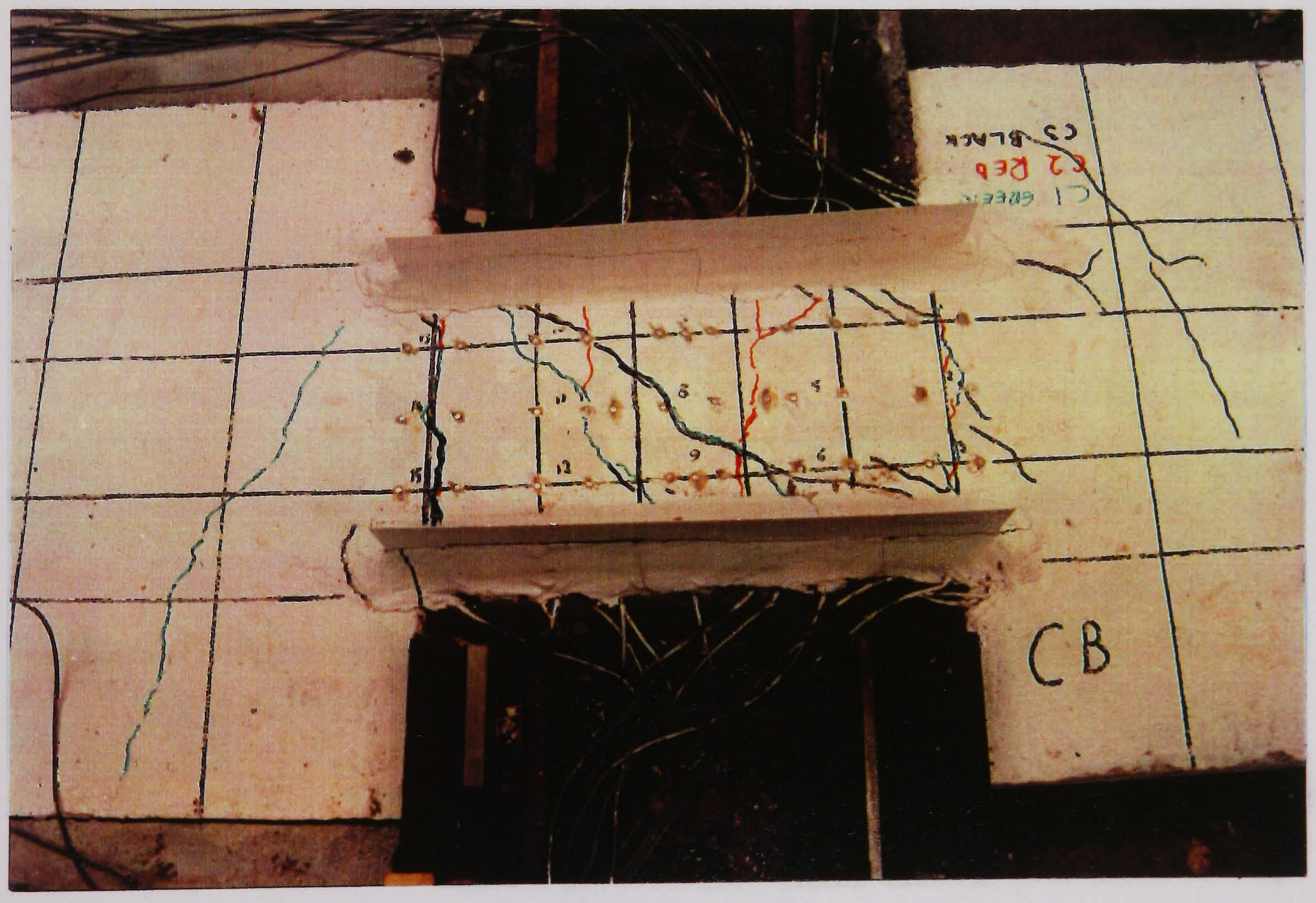


Figure A.13: Beam CBM3 at failure

Figure A.14: Beam EBM3 at failure


EBM3

# Appendix B

# DESIGN CALCULATIONS

The design calculations described below are intended not only to provide evidence of the applicability of the proposed design methods but also to compare them with the experimental results.

## B.1 BEAM DETAILS

The data relating to the properties of the materials used in the test specimens, the cross sectional dimensions and the reinforcement details of the coupling beams included in the test programme have been given in Chapter 3. Only additional data relating to the detailing of the reinforcement and the strength characteristics of the concrete will be presented in this Appendix.

The three series of coupling beams with span to depth ratios of 1.1, 1.43 and 2.0 were analysed theoretically using the two approaches presented in Chapter 4. The beams had a clear span L = 500 mm between the supports for the coupling beams with span to depth ratios of 1.43 and 2.0 and were equally loaded at the

supports. The beams with a span to depth ratio of 1.1 had a clear span L = 1000 mm. The form and dimensions of these coupling beams have been also presented in Figures 3.15 to 3.17 in Chapter 3. All the coupling beams were reinforced in flexure along their top and bottom faces with two 12 mm diameter high-yield steel bars. To eliminate the possibility of anchorage failure, the reinforcement bars were extended a distance equal to the clear span beyond the support.

Six conventionally reinforced coupling beams i.e. beams CBM1, CBM2, CBM3, CBS1, CBS2 and CBD1 contained transverse reinforcement comprising of 8 mm diameter mild steel links at a spacing of 70 mm within the portion of the shear span between the supports. The other six coupling beams i.e. beams EBM1, EBM2, EBM3, EBS1, EBS2 and EBD1 were reinforced with expanded metal mesh and the double storey test beam DBS2 was reinforced in a similar manner to beam CBS2. Beam CBD1 had a span to depth ratio of 1.1 and additional stirrups were introduced into this beam.

# B.2 COMPRESSIVE FORCE PATH APPROACH

## B.2.1 Design Calculations for Beam CBM2

### Flexural Capacity

$T = f_u A_{st}$ $T = 495 * 226.08N$

$T = 111.90$ kN

Since T = C,

Then $A_c = 113040/23.60 = 4789.83mm^2$

Thus T * z = C * z

0.875 $f_y$ $A_{st}$ z = 0.45 $f_{cu}$ b x z

x = 0.875 ($f_y$ $A_{st}$) /(0.45 $f_{cu}$ b )

x = 51.16 mm

z = d - 0.45 x

z = 306.97 mm

Hence the flexural capacity is:

$M_f$ = T * z = 34.24 kN.m

The maximum sustained point load which can be applied is :

$V_a = M_f$ / s = 136.96 kN

The applied load to be considered in the analysis is $V_a$ = 136.96 kN

## B.2.2 Design Calculations for Beam EBM2

### Flexural Capacity

$T_t = T_{bars} + T_{mesh} cos\theta$

$T_t = 480 * 226.08 + 360 * 15.08 * 2 * 9 * cos27^o$ N

$T_t = 195.56$ kN

Since T = C,

$A_c = T_t / f_{cu} = 5439.01 mm^2$

Thus T * z = C * z

$0.875[f_y A_{st} + f_{ym} A_m/2]z = 0.45 f_{cu}$ b x z

x = 68.97 mm

z = d - 0.45 x

z = 299.9 mm

Hence the flexural capacity is:

$M_f = M_{f(bars)} + M_{f(mesh)}$

$M_f = T_{bar} * z + T_{mesh} cos\theta z/2$

$M_f = 44.08$ kN.m

The maximum sustained point load which can be applied is :

$V_a = M_f$ / s = 176.32 kN

The applied load to be considered in the analysis is $V_a = 176.32$ kN

### B.2.3 Design Calculations for Beam CBM1

#### Flexural Capacity

$T_t = T_{bars} + T_{d.bars}$

$T_t = 110.77 + 85.3$ kN

$T_t = 196.07$ kN

Since T = C,

Thus T * z = C * z

$0.875\ [f_y A_{st} + (f_{yd} A_{st} cos\alpha)/2]z = 0.45 f_{cu}$ b x z

x = 72.90 mm

z = d - 0.45 x

z = 297.19 mm

Hence the flexural capacity is:

$M_f = M_{f(bars)} + M_{f(d.bars)}$

$M_f = 32.89 + 12.66$ $M_f = T * z + T_{dbars}$ z/2

$M_f = 45.55$ kN.m

The maximum sustained point load which can be applied is :

$V_a = M_f$ / s = 182.20 kN

The applied load to be considered in the analysis is $V_a = 182.20$ kN

### B.2.4 Design Calculations for Beam EBM1

**Flexural Capacity**

$$T_t = T_{h.bars} + T_{d.bars}cos\alpha + T_{mesh}cos\theta$$

$$T_t = f_u A_{st} + f_{ud} A_d cos\alpha + 2 f_{um} A_m n cos\theta$$

$T_t = 289.73$ kN

Since T = C,

Thus T * z = C * z

$$0.875\ [f_y A_{st} + f_{ym} A_m n + (f_{yd} A_{st})/2]z = 0.45 f_{cu}\ \text{b x z}$$

x = 76.46 mm

z = d - 0.45 x

z = 295.59 mm

Hence the flexural capacity is:

$$M_f = M_{f(bars)} + M_{f(d.bars)} + M_{f(mesh)}$$

$$M_f = T * z + T_{dbars} z/2 + T_{mesh} z/2$$

$$M_f = 33.35 + 12.86 + 13.20$$

$M_f = 59.41$ kN.m

The maximum sustained point load which can be applied is :

$V_a = M_f$ / s = 237.64 kN

The applied load to be considered in the analysis is $V_a = 237.64$ kN

## B.2.5 Design Calculations for Beam CBM3

### Flexural Capacity

$T_t = T_{bars}$

$T_t = 110.78$ kN

Since T = C,

Thus T * z = C * z

0.875 $f_y A_{st} z = 0.45 f_{cu}$ b x z

x = 47.60 mm

z = d - 0.45 x

z = 308.57 mm

Hence the flexural capacity is:

$M_f = M_{f(bars)}$

$M_f = 34.12$ kN

The maximum sustained point load which can be applied is :

$V_a = M_f$ / s = 136.48 kN

The applied load to be considered in the analysis is $V_a = 136.48$ kN

## B.2.6 Design Calculations for Beam EBM3

### Flexural Capacity

$T_t = T_{h.bars} + T_{mesh} cos\theta$

$T_t = f_u A_{st} + 2 f_{um} A_m n cos\theta$

$T_t = 199.12$ kN

Since T = C,

Thus T * z = C * z

$0.875\ [f_y A_{st} + f_{ym} A_m n]z = 0.45 f_{cu}$ b x z

x = 67.63 mm

z = d - 0.45 x

z = 299.56 mm

Hence the flexural capacity is:

$M_f = M_{f(bars)} + M_{f(mesh)}$

$M_f = T * z + T_{mesh} z/2$

$M_f = 31.79 + 12.97$ kN

$M_f = 44.76$ kN.m

The maximum sustained point load which can be applied is :

$V_a = M_f$ / s = 179.04 kN

The applied load to be considered in the analysis is $V_a = 179.04$ kN

## B.2.7 Design Calculations for Beam CBS1

### Flexural Capacity

$T_t = T_{bars} + T_{d.bars} cos\alpha$ $T_t = 109.64 + 97.07$ kN

$T_t = 206.72$ kN

Since T = C,

Thus T * z = C * z

$0.875\ [f_y A_{st} + (f_{yd} A_{st})/2]z = 0.45 f_{cu}$ b x z

x = 67.93 mm

z = d - 0.45 x

z = 199.43 mm

Hence the flexural capacity is:

$M_f = M_{f(bars)} + M_{f(d.bars)}$

$M_f = T * z + T_{dbars} z/2 + T_{mesh} z/2$

$M_f$ = 31.47 kN.m

The maximum sustained point load which can be applied is :

$V_a = M_f$ / s = 125.88 kN

The applied load to be considered in the analysis is $V_a$ = 125.88 kN

## B.2.8 Design Calculations for Beam CBS2

### Flexural Capacity

$T_t = T_{bars}$

$T_t = f_u A_{st}$

$T_t$ = 111.90 kN

Since T = C,

Thus T * z = C * z

0.875 $[f_y A_{st}] z = 0.45 f_{cu}$ b x z

x = 50.18 mm

z = d - 0.45 x

z = 207.41 mm

Hence the flexural capacity is:

$$M_f = M_{f(bars)}$$

$$M_f = T * z$$

$$M_f = 23.16 \text{ kN.m}$$

The maximum sustained point load which can applied is :

$$V_a = M_f \ / \ \text{s} = 92.65 \text{ kN}$$

The applied load to be considered in the analysis is $V_a = 92.65$ kN

## B.2.9 Design Calculations for Beam EBS1

$$T_t = T_{bars} + T_{d.bars} cos\alpha + T_{mesh} cos\theta$$

$$T_t = 108.5 + 88.75 + 87.06 \text{ kN}$$

$$T_t = 284.31 \text{ kN}$$

Since T = C,

Thus T * z = C * z

$$0.875 \ [f_y A_{st} + f_{ym} A_m n + (f_{yd} A_{st})/2]z = 0.45 f_{cu} \text{ b x z}$$

$$\text{x} = 79.33 \text{ mm}$$

$$\text{z} = \text{d - } 0.45 \text{ x}$$

$$\text{z} = 194.29 \text{ mm}$$

Hence the flexural capacity is:

$$M_f = M_{f(bars)} + M_{f(d.bars)} + M_{f(mesh)}$$

$$M_f = T * z + T_{dbars} z/2 + T_{mesh} z/2$$

$$M_f = 21.05 + 8.60 + 8.44 \text{ kN}$$

$$M_f = 38.09 \text{ kN.m}$$

The maximum sustained point load which can be applied is :

$V_a = M_f$ / s = 152.36 kN

The applied load to be considered in the analysis is $V_a$ = 152.36 kN

## B.2.10 Design Calculations for Beam EBS2

### Flexural Capacity

$T_t = T_{h.bars} + T_{mesh} cos\theta$

$T_t$ = 110.77 + 89.48 kN

$T_t$ = 200.25 kN

Since T = C,

Thus T * z = C * z

0.875 $[f_y A_{st} + f_{ym} A_m n]z = 0.45 f_{cu}$ b x z

x = 71.31 mm

z = d - 0.45 x

z = 197.9 mm

Hence the flexural capacity is:

$M_f = M_{f(bars)} + M_{f(mesh)}$

$M_f = T * z + T_{mesh} z/2$

$M_f$ = 30.63 kN.m

The maximum sustained point load which can be applied is :

$V_a = M_f$ / s = 122.52 kN

The applied load to be considered in the analysis is $V_a$ = 122.52 kN

## B.2.11 Design Calculations for Beam CBD1

### Flexural Capacity

$T_t = T_{bars} + T_{d.bars} cos\alpha$

$T_t = 117.56 + 78.124$ kN

$T_t = 195.68$ kN

Since T = C,

Thus T * z = C * z

$0.875\ [f_y A_{st} + (f_{yd} A_{st})/2]z = 0.45 f_{cu}$ b x z

x = 87.40 mm

z = d - 0.45 x

z = 840.67 mm

Hence the flexural capacity is:

$M_f = M_{f(bars)} + M_{f(d.bars)}$

$M_f = T * z + T_{dbars} z/2$

$M_f = 131.56$ kN.m

The maximum sustained point load which can be applied is :

$V_a = M_f$ / s = 263.12 kN

The applied load to be considered in the analysis is $V_a = 263.12$ kN

## B.2.12 Design Calculations for Beam EBD1

### Flexural Capacity

$T_t = T_{h.bars} + T_{d.bars} cos\alpha + T_{mesh} cos\theta$

$T_t = 113.04 + 78.76 + 174.35\text{kN}$

$T_t = 366.15$ kN

Since T = C,

Thus T * z = C * z

$0.875\ [f_y A_{st} + f_{ym} A_m n + (f_{yd} A_{st})/2]z = 0.45 f_{cu}$ b x z

x = 114.035 mm

z = d - 0.45 x

z = 828.68 mm

Hence the flexural capacity is:

$M_f = M_{f(bars)} + M_{f(d.bars)} + M_{f(mesh)}$

$M_f = T * z + T_{dbars} z/2 + T_{mesh} z/2$

$M_f = 197.81$ kN.m

The maximum sustained point load which can be applied is :

$V_a = M_f$ / s = 395.69 kN

The applied load to be considered in the analysis is $V_a = 395.69$ kN

# B.3 APPROACH DEVELOPED BY SUBEDI

## B.3.1 Design Calculations for Beam CBM2

### Flexural Strength

The flexural capacity of the beam can be evaluated by taking into account the main reinforcement only and is derived as follows:

For beam CBM2: $f_{tc} = 1.67N/mm^2$ and $f_s = 16.7N/mm^2$

$Q_{flex} = A_{st} f_y 2h'/l$

$Q_{flex} = 2(330/500) * 410 * 226.08 * 10^{-3}$ kN

$Q_{u(flex)} = 2Q_{flex} = 244.71$ kN

### Shear Strength

a) Determine control of the web

The total horizontal component of the web splitting force

$H = f_{tc} bh' + A_h f_s$

$A_h = 0$, then no horizontal contribution

H = 55.11 kN

$A_h f_{yw} = 0$ then $H > A_h f_{yw}$

The total vertical component of the web splitting force

$V = f_{tc} bl + A_v f_s$

V = 96.92 kN

$A_v f_s = 233.11$ kN then $V < A_v f_{yw}$

Using the criteria test given in Table 4.1 in Chapter 4. The controlling parameter of beam CBM2 is the concrete i.e. $f_{tc}$ will contribute and $P_v = A_v f_s$ and $P_h = A_h f_s$

The ultimate load can be found from:

$Q_{u(shear)} = 2Q_{shear}$

$Q_{shear} = [f_{tc}bl + 2C + P_h]h'/l$

$P_h = 0$

$Q_{u(shear)} = 2Q_{shear} = 135.06$ kN

The ultimate strength and the predicted mode of failure of the beam is determined by comparing the shear and the flexural strengths.

$Q_{u(flex)} = 244.71$ kN and $Q_{u(shear)} = 135.06$ kN

Therefore $Q_{analysis}$ =135.06 kN i.e. the predicted mode of failure is shear.

## B.3.2 Design Calculations for Beam EBM2

### Flexural Strength

The flexural capacity of the beam can be evaluated by taking into account the main reinforcement and the expanded metal mesh and is derived from Equation 4.35 for Q in Chapter 4.

For beam EBM2: $f_{tc} = 1.73N/mm^2$ and $f_s = 17.3N/mm^2$

Using Equation 4.35 for Q in Chapter 4, we have

$Q_{u(flex)}) = 2Q_{flex} = 284.23$ kN

## Shear Strength

a) Determine control of the web

The total horizontal component of the web splitting force is

H = $f_{tc}bh' + A_h f_s$

$A_h = 2nA_m cos\theta$ horizontal contribution from the expanded metal mesh.

H = 61.27 kN

$A_h f_{yw}$ = 68.92 kN then $H < A_h f_{yw}$

The total vertical component of the web splitting force

V = $f_{tc}bl + A_v f_s$

$A_v = 2nA_m sin\theta$

V = 88.63 kN

$A_v f_{yw}$ = 35.12 kN then $V > A_v f_{yw}$

Using the criteria test given in Table 4.1 in Chapter 4. The controlling parameter for beam EBM2 is the concrete i.e. $f_{tc}$ will contribute and $P_v = A_v f_s$ and $P_h = A_h f_s$

The ultimate load can be found from:

$Q_{u(shear)} = 2Q_{shear}$

$Q_{shear} = [f_{tc}bl + 2C + P_h]h'/l$

$P_h = A_h f_s$

$Q_{u(shear)} = 2Q_{shear}$ = 145.27 kN

The ultimate strength and the predicted mode of failure of the beam is determined by comparing the shear and the flexural strengths.

$Q_{u(flex)}$ = 284.23 kN and $Q_{u(shear)}$ = 145.27 kN

Therefore $Q_{analysis}$ =145.27 kN i.e. the predicted mode of failure is shear.

## B.3.3 Design Calculations for Beam CBM1

### Flexural Strength

The flexural capacity of the beam can be evaluated by taking into account the main reinforcement and the diagonal reinforcement bars and is derived from Equation 4.23 for Q in Chapter 4.

For beam CBM1: $f_{tc} = 1.61N/mm^2$ and $f_s = 16.1N/mm^2$

Using Equation 4.23 for Q in Chapter 4, we have

$Q_{u(flex)} = 2Q_{flex} = 335.57$ kN

### Shear Strength

a) Determine control of the web

The total horizontal component of the web splitting force

H = $f_{tc}bh' + A_h f_s$

$A_h = A_d cos\alpha$ horizontal contribution by the diagonal bars.

H = 54.18 kN

$A_h f_{yw} = 71.01$ kN then $H < A_h f_{yw}$

The total vertical component of the web splitting force

V = $f_{tc}bl + A_v f_s$

$A_v = A_d sin\alpha + \sum A_s$

V = 95.42 kN

$A_v f_{yw} = 283.3$ kN then $V < A_v f_{yw}$

Using the criteria test given in Table 4.1 in Chapter 4. The controlling parameter of beam CBM1 is the reinforcement i.e. $f_{tc}$ will not contribute and $P_v = A_v f_{yw}$ and $P_h = A_h f_{yw}$

The ultimate load can be found from:

$$Q_{u(shear)} = 2Q_{shear}$$

$$Q_{shear} = [0 + 2C + P_h]h'/l$$

$$P_h = A_h f_{yw}$$

$$Q_{u(shear)} = 2Q_{shear} = 153.81 \text{ kN}$$

The ultimate strength and the predicted mode of failure of the beam is determined by comparing the shear and the flexural strengths.

$Q_{u(flex)} = 335.57$kN and $Q_{u(shear)} = 153.81$kN

Therefore $Q_{analysis}$ =153.81 kN i.e. the predicted mode of failure is shear.

## B.3.4 Design Calculations for Beam EBM1

### Flexural Strength

The flexural capacity of the beam can be evaluated by taking into account the main reinforcement, the diagonal bars and the expanded metal mesh and is derived from Equation 4.48 for Q in Chapter 4.

For beam EBM1: $f_{tc} = 1.91 N/mm^2$ and $f_s = 19.1 N/mm^2$

Using Equation 4.48 for Q in Chapter 4, we have

$$Q_{u(flex)} = 2Q_{flex} = 417.30\text{kN}$$

**Shear Strength**

a) Determine control of the web

The total horizontal component of the web splitting force

$H = f_{tc}bh' + A_h f_s$

$A_h = A_d cos\alpha + 2nA_m cos\theta$

Horizontal contribution by the diagonal bars and the expanded metal mesh.

H = 71.28 kN

$A_h f_{yw}$ = 135.28kN then $H < A_h f_{yw}$

The total vertical component of the web splitting force

$V = f_{tc}bl + A_v f_s$

$A_v = A_d sin\alpha + 2nA_m sin\theta$

V = 100.198 kN

$A_v f_{yw}$ = 78.21kN then $V > A_v f_{yw}$

Using the criteria test given in Table 4.1 in Chapter 4. The controlling parameter of beam EBM1 is the concrete i.e. $f_{tc}$ will contribute and $P_v = A_v f_s$ and $P_h = A_h f_s$

The ultimate load can be found from:

$Q_{u(shear)} = 2Q_{shear}$

$Q_{shear} = [f_{tc}bl + 2C + P_h]h'/l$

$P_h = A_h f_s$

$Q_{u(shear)} = 2Q_{shear}$ = 165.17 kN

The ultimate strength and the predicted mode of failure of the beam is determined by comparing the shear and the flexural strengths.

$Q_{u(flex)}$ = 417.3kN and $Q_{u(shear)}$ = 165.17kN

Therefore $Q_{analysis}$ =165.17 kN i.e. the predicted mode of failure is shear.

## B.3.5 Design Calculations for Beam CBM3

### Flexural Strength

The flexural capacity of the beam can be evaluated by taking into account the main reinforcement and diagonal bars and is derived from Equation 4.13 for Q in Chapter 4.

For beam CBM3: $f_{tc} = 1.68N/mm^2$ and $f_s = 16.8N/mm^2$

Using Equation 4.13 for Q in Chapter 4, we have

$Q_{u(flex)} = 2Q_{flex} = 241.72$kN

### Shear Strength

a) Determine control of the web

The total horizontal component of the web splitting force

H = $f_{tc}bh' + A_h f_s$

$A_h = 0$

H = 55.44 kN

$A_h f_{yw} = 0$ then $H > A_h f_{yw}$

The total vertical component of the web splitting force

V = $f_{tc}bl + A_v f_s$

$A_v = \sum A_s$

V = 98.30 kN

$A_v f_{yw} = 233.11$kN then $V < A_v f_{yw}$

Using the criteria test given in Table 4.1 in Chapter 4. The controlling parameter of beam CBM1 is the concrete i.e. $f_{tc}$ will contribute.

The ultimate load can be found from:

$Q_{u(shear)} = 2Q_{shear}$

$Q_{shear} = [0 + 2C + P_h]h'/l$

$P_h = A_h f_{yw} = 0$

$Q_{u(shear)} = 2Q_{shear} = 135.79$ kN

The ultimate strength and the predicted mode of failure of the beam is determined by comparing the shear and the flexural strengths.

$Q_{u(flex)} = 241.72$kN and $Q_{u(shear)} = 135.79$kN

Therefore $Q_{analysis}$ =135.79 kN i.e. the predicted mode of failure is shear.

### B.3.6 Design Calculations for Beam EBM3

#### Flexural Strength

The flexural capacity of the beam can be evaluated by taking into account the main reinforcement, the diagonal bars and the expanded metal mesh and is derived from Equation 4.35 for Q in Chapter 4.

For beam EBM3: $f_{tc} = 1.72N/mm^2$ and $f_s = 17.2N/mm^2$

Using Equation 4.35 for Q in Chapter 4, we have

$Q_{u(flex)} = 2Q_{flex} = 285.03$kN

**Shear Strength**

a) Determine control of the web

The total horizontal component of the web splitting force

$H = f_{tc}bh' + A_h f_s$

$A_h = 2nA_m cos\theta$

Horizontal contribution by the diagonal bars and the expanded metal mesh.

H = 60.94 kN

$A_h f_{yw}$ = 70.13kN then $H < A_h f_{yw}$

The total vertical component of the web splitting force

$V = f_{tc}bl + A_v f_s$

$A_v = 2nA_m sin\theta$

V = 88.113 kN

$A_v f_{yw}$ = 35.74kN then $V > A_v f_{yw}$

Using the criteria test given in Table 4.1 in Chapter 4. The controlling parameter of beam EBM1 is the concrete i.e. $f_{tc}$ will contribute and $P_v = A_v f_s$ and $P_h = A_h f_s$

The ultimate load can be found from:

$Q_{u(shear)} = 2Q_{shear}$

$Q_{shear} = [f_{tc}bl + 2C + P_h]h'/l$

$P_h = A_h f_s$

$Q_{u(shear)} = 2Q_{shear}$ = 144.44 kN

The ultimate strength and the predicted mode of failure of the beam is determined by comparing the shear and the flexural strengths.

$Q_{u(flex)} = 285.03$kN and $Q_{u(shear)} = 144.44$kN

Therefore $Q_{analysis}$ =144.44 kN i.e. the predicted mode of failure is shear.

## B.3.7 Design Calculations for Beam CBS1

### Flexural Strength

The flexural capacity of the beam can be evaluated by taking into account the main reinforcement and the diagonal bars and is derived from Equation 4.23 for Q in Chapter 4.

For beam CBS1: $f_{tc} = 1.71N/mm^2$ and $f_s = 17.1N/mm^2$

Using Equation 4.23 for Q in Chapter 4, we have

$Q_{u(flex)} = 2Q_{flex} = 232.90$kN

### Shear Strength

a) Determine control of the web

The total horizontal component of the web splitting force

H = $f_{tc}bh' + A_h f_s$

$A_h = A_d cos\alpha$ horizontal contribution by the diagonal bars.

H = 42.86 kN

$A_h f_{yw} = 72.28$kN then $H < A_h f_{yw}$

The total vertical component of the web splitting force

V = $f_{tc}bl + A_v f_s$

$A_v = A_d sin\alpha + \sum A_s$

V = 100.77 kN

$A_v f_{yw}$ = 273.3kN then $V < A_v f_{yw}$

Using the criteria test given in Table 4.1 in Chapter 4. The controlling parameter of beam CBS1 is the reinforcement i.e. $f_{tc}$ will not contribute and $P_v = A_v f_{yw}$ and $P_h = A_h f_{yw}$

The ultimate load can be found as:

$Q_{u(shear)} = 2Q_{shear}$

$Q_{shear} = [0 + 2C + P_h]h'/l \; P_h = A_h f_{yw}$

$Q_{u(shear)} = 2Q_{shear}$ = 110.95 kN

The ultimate strength and the predicted mode of failure of the beam is determined by comparing the shear and the flexural strengths.

$Q_{u(flex)}$ = 232.90kN and $Q_{u(shear)}$ = 110.95kN

Therefore $Q_{analysis}$ =110.95 kN i.e. the predicted mode of failure is shear.

## B.3.8 Design Calculations for Beam CBS2

### Flexural Strength

The flexural capacity of the beam can be evaluated by taking into account the main reinforcement only and is derived from Equation 4.13 for Q in Chapter 4.

For the beam CBS2: $f_{tc} = 1.66N/mm^2$ and $f_s = 16.6N/mm^2$

Using Equation 4.13 for Q in Chapter 4, we have:

$Q_{flex} = A_{st} f_y 2h'/l$

$Q_{u(flex})) = 2Q_{flex}$ = 166.39kN

## Shear Strength

a) Determine control of the web

The total horizontal component of the web splitting force

$H = f_{tc}bh' + A_h f_s$

$A_h = 0$

No horizontal contribution

H = 38.18 kN

$A_h f_{yw} = 0$ then $H > A_h f_{yw}$

The total vertical component of the web splitting force

$V = f_{tc}bl + A_v f_s$

V = 96.35 kN

$A_v f_s = 237.13$kN then $V < A_v f_{yw}$

Using the criteria test given in Table 4.1 in Chapter 4. The controlling parameter of beam CBS2 is the concrete i.e. $f_{tc}$ will contribute and $P_v = A_v f_s$ and $P_h = A_h f_s$

The ultimate load can be found from:

$Q_{u(shear)} = 2Q_{shear}$

$Q_{shear} = [f_{tc}bl + 2C + P_h]h'/l$

$P_h = 0$

$Q_{u(shear)} = 2Q_{shear} = 78.33$ kN

The ultimate strength and the predicted mode of failure of the beam is determined by comparing the shear and the flexural strengths.

$Q_{u(flex)} = 168.47$kN and $Q_{u(shear)} = 78.33$kN

Therefore $Q_{analysis} = 78.33$ kN i.e. the predicted mode of failure is shear.

## B.3.9 Design Calculations for Beam EBS1

### Flexural Strength

The flexural capacity of the beam can be evaluated by taking into account the main reinforcement, the diagonal bars and the expanded metal mesh and is derived from Equation 4.48 for Q in Chapter 4.

For beam EBS1: $f_{tc} = 1.91N/mm^2$ and $f_s = 19.1N/mm^2$

Using Equation 4.48 for Q in Chapter 4, we have

$Q_{u(flex)} = 2Q_{flex} = 326.80\text{kN}$

### Shear Strength

a) Determine the web control

The total horizontal component of the web splitting force

$\text{H} = f_{tc}bh' + A_h f_s$

$A_h = A_d cos\alpha + 2nA_m cos\theta$

Horizontal contribution by the diagonal bars and the expanded metal mesh.

$\text{H} = 52.27$ kN

$A_h f_{yw} = 141.38\text{kN}$ then $H < A_h f_{yw}$

The total vertical component of the web splitting force

$\text{V} = f_{tc}bl + A_v f_s$

$A_v = A_d sin\alpha + 2nA_m sin\theta$

$\text{V} = 99.81$ kN

$A_v f_{yw} = 67.45\text{kN}$ then $V > A_v f_{yw}$

Using the criteria test given in Table 4.1 in Chapter 4. The controlling parameter of beam EBM1 is the concrete i.e. $f_{tc}$ will contribute and $P_v = A_v f_s$ and $P_h = A_h f_s$

The ultimate load can be found from:

$Q_{u(shear)} = 2Q_{shear}$

$Q_{shear} = [f_{tc}bl + 2C + P_h]h'/l$

$P_h = A_h f_s$

$Q_{u(shear)} = 2Q_{shear} = 96.78$ kN

The ultimate strength and the predicted mode of failure of the beam is determined by comparing the shear and the flexural strengths.

$Q_{u(flex)} = 326.8$kN and $Q_{u(shear)} = 96.78$kN

Therefore $Q_{analysis} = 96.78$ kN i.e. the predicted mode of failure is shear.

## B.3.10 Design Calculations for Beam EBS2

### Flexural Strength

The flexural capacity of the beam can be evaluated by taking into account the main reinforcement and the expanded metal mesh is derived from Equation 4.35 for Q in Chapter 4.

For beam EBS2: $f_{tc} = 1.904N/mm^2$ and $f_s = 19.04N/mm^2$

Using Equation 4.35 for Q in Chapter 4, we have

$Q_{u(flex)} = 2Q_{flex} = 266.99$kN

## Shear Strength

a) Determine control of the web

The total horizontal component of the web splitting force

$H = f_{tc}bh' + A_h f_s$

$A_h = 2nA_m cos\theta$

Horizontal contribution by the expanded metal mesh.

H = 48.4 kN

$A_h f_{yw} = 71.35$kN then $H < A_h f_{yw}$

The total vertical component of the web splitting force

$V = f_{tc}bl + A_v f_s$

$A_v = 2nA_m sin\theta$

V = 97.54 kN

$A_v f_{yw} = 36.35$kN then $V > A_v f_{yw}$

Using the criteria test given in Table 4.1 in Chapter 4. The controlling parameter of beam EBM2 is the concrete i.e. $f_{tc}$ will contribute and $P_v = A_v f_s$ and $P_h = A_h f_s$

The ultimate load can be found from:

$Q_{u(shear)} = 2Q_{shear}$

$Q_{shear} = [f_{tc}bl + 2C + P_h]h'/l$

$P_h = A_h f_s$

$Q_{u(shear)} = 2Q_{shear} = 93.83$ kN

The ultimate strength and the predicted mode of failure of the beam is determined by comparing the shear and the flexural strengths.

$Q_{u(flex)} = 266.99\text{kN}$ and $Q_{u(shear)} = 93.83\text{kN}$

Therefore $Q_{analysis}$ =93.83 kN i.e. the predicted mode of failure is shear.

## B.3.11 Design Calculations for Beam CBD1

### Flexural Strength

The flexural capacity of the beam can be evaluated by taking into account the main reinforcement and the diagonal bars and is derived from Equation 4.23 for Q in Chapter 4.

For beam CBD1: $f_{tc} = 1.49N/mm^2$ and $f_s = 14.9N/mm^2$

Using Equation 4.23 for Q in Chapter 4, we have

$Q_{u(flex)} = 2Q_{flex} = 435.37\text{kN}$

### Shear Strength

a) Determine control of the web

The total horizontal component of the web splitting force

$\text{H} = f_{tc}bh' + A_h f_s$

$A_h = A_d cos\alpha$

Horizontal contribution by the diagonal bars.

$\text{H} = 133.53$ kN

$A_h f_{yw} = 59.72$ kN then $H > A_h f_{yw}$

The total vertical component of the web splitting force

$\text{V} = f_{tc}bl + A_v f_s$

$A_v = A_d sin\alpha + \sum A_s$

V = 165.78 kN

$A_v f_{yw}$ = 542.25kN then $V < A_v f_{yw}$

Using the criteria test given in Table 4.1 in Chapter 4. The controlling parameter of beam CBS1 is the concrete i.e. $f_{tc}$ will contribute and $P_v = A_v f_s$ and $P_h = A_h f_s$

The ultimate load can be found from:

$Q_{u(shear)} = 2Q_{shear}$

$Q_{shear} = [f_{tc} bl + 2C + P_h]h'/l$

$P_h = A_h f_s$

$Q_{u(shear)} = 2Q_{shear}$ = 246.50 kN

The ultimate strength and the predicted mode of failure of the beam is determined by comparing the shear and the flexural strengths.

$Q_{u(flex)}$ = 435.37kN and $Q_{u(shear)}$ = 246.50kN

Therefore $Q_{analysis}$ = 246.50 kN i.e. the predicted mode of failure is shear.

## B.3.12 Design Calculations for Beam EBD1

### Flexural Strength

The flexural capacity of the beam can be evaluated by taking into account the main reinforcement, the diagonal bars and the expanded metal mesh and is derived from Equation 4.48 for Q in Chapter 4.

For beam EBD1: $f_{tc} = 1.53N/mm^2$ and $f_s = 15.3N/mm^2$

Using Equation 4.48 for Q in Chapter 4, we have

$Q_{u(flex)} = 2Q_{flex}$ = 671.03kN

**Shear Strength**

a) Determine the web control

The total horizontal component of the web splitting force

$$H = f_{tc}bh' + A_h f_s$$

$$A_h = A_d cos\alpha + 2nA_m cos\theta$$

Horizontal contribution by the diagonal bars and the expanded metal mesh.

H = 144.64 kN

$A_h f_{yw}$ = 198.43kN then $H < A_h f_{yw}$

The total vertical component of the web splitting force

$$V = f_{tc}bl + A_v f_s$$

$$A_v = A_d sin\alpha + 2nA_m sin\theta$$

V = 160.71 kN

$A_v f_{yw}$ = 122.89kN then $V > A_v f_{yw}$

Using the criteria test given in Table 4.1 in Chapter 4. The controlling parameter of beam EBM1 is the concrete i.e. $f_{tc}$ will contribute and $P_v = A_v f_s$ and $P_h = A_h f_s$

The ultimate load can be found from:

$$Q_{u(shear)} = 2Q_{shear}$$

$$Q_{shear} = [f_{tc}bl + 2C + P_h]h'/l$$

$$P_h = A_h f_s$$

$$Q_{u(shear)} = 2Q_{shear} = 330.42 \text{ kN}$$

The ultimate strength and the predicted mode of failure of the beam is determined by comparing the shear and the flexural strengths.

$Q_{u(flex)} = 671.03$kN and $Q_{u(shear)} = 330.42$kN

Therefore $Q_{analysis}$ =330.42 kN i.e. the predicted mode of failure is shear.

# Appendix C

# PRESENTATION OF RESULTS OBTAINED DURING FIRST AND SECOND LOAD CYCLES

| First cycle of loading | | | | |
|---|---|---|---|---|
| Load | Deflections (mm) | Rotation | Expansion | Elongation |
| (kN) | D1 - D2 - D3 | (rad) | (mm) | (mm) |
| 0.0 | 0.00-0.00-0.00 | 0.00 | 0.00 | 0.00 |
| 20.0 | 2.30-2.70-3.05 | 1.20 | 0.20 | 0.35 |
| 30.0 | 2.60-3.15-3.65 | 1.65 | 0.35 | 0.65 |
| 35.0 | 2.95-3.65-4.25 | 1.95 | 0.40 | 0.85 |
| 40.0 | 3.40-4.25-4.90 | 2.35 | 0.55 | 1.05 |
| 45.0 | 3.75-4.55-5.65 | 2.80 | 0.65 | 1.35 |
| 50.0 | 4.10-4.70-6.20 | 3.30 | 0.85 | 1.65 |

Table C.1: Beam CBM1

| Second cycle of loading | | | | |
|---|---|---|---|---|
| Load | Deflections (mm) | Rotation | Expansion | Elongation |
| (kN) | D1 - D2 - D3 | (rad) | (mm) | (mm) |
| 0.0 | 0.00-0.00-0.00 | 0.00 | 0.00 | 0.00 |
| 20.0 | 2.65-3.15-3.85 | 1.40 | 0.30 | 0.45 |
| 30.0 | 3.65-4.05-4.90 | 1.95 | 0.45 | 0.75 |
| 35.0 | 4.10-4.80-5.85 | 2.65 | 0.65 | 0.95 |
| 40.0 | 4.80-5.95-7.05 | 3.55 | 0.85 | 1.20 |
| 45.0 | 5.75-6.75-9.30 | 4.05 | 1.05 | 1.45 |
| 50.0 | 6.70-8.40-11.30 | 4.65 | 1.30 | 1.95 |

Table C.2: Beam CBM1

| First cycle of loading | | | | |
|---|---|---|---|---|
| Load | Deflections (mm) | Rotation | Expansion | Elongation |
| (kN) | D1 - D2 - D3 | (rad) | (mm) | (mm) |
| 0.0 | 0.00-0.00-0.00 | 0.00 | 0.00 | 0.00 |
| 20.0 | 2.45-2.95-3.10 | 1.35 | 0.35 | 0.55 |
| 30.0 | 2.75-3.45-4.20 | 1.80 | 0.45 | 0.95 |
| 35.0 | 3.20-4.10-4.95 | 2.25 | 0.65 | 1.20 |
| 40.0 | 3.90-4.60-5.55 | 2.75 | 0.85 | 1.50 |
| 45.0 | 4.20-4.95-6.10 | 3.50 | 0.95 | 1.85 |
| 50.0 | 4.95-5.30-6.70 | 4.10 | 1.20 | 2.05 |

Table C.3: Beam CBM2

| Second cycle of loading | | | | |
|---|---|---|---|---|
| Load | Deflections (mm) | Rotation | Expansion | Elongation |
| (kN) | D1 - D2 - D3 | (rad) | (mm) | (mm) |
| 0.0 | 0.00-0.00-0.00 | 0.00 | 0.00 | 0.00 |
| 20.0 | 2.85-3.35-4.20 | 1.55 | 0.45 | 0.65 |
| 30.0 | 3.90-4.25-5.10 | 2.25 | 0.60 | 0.85 |
| 35.0 | 4.60-5.30-6.30 | 2.95 | 0.95 | 1.05 |
| 40.0 | 5.50-6.25-7.95 | 3.65 | 1.25 | 1.30 |
| 45.0 | 6.35-7.90-9.80 | 4.25 | 1.35 | 1.60 |
| 50.0 | 7.30-9.40-12.00 | 4.95 | 1.65 | 2.10 |

Table C.4: Beam CBM2

| First cycle of loading | | | | |
|---|---|---|---|---|
| Load | Deflections (mm) | Rotation | Expansion | Elongation |
| (kN) | D1 - D2 - D3 | (rad) | (mm) | (mm) |
| 0.0 | 0.00-0.00-0.00 | 0.00 | 0.00 | 0.00 |
| 20.0 | 1.90-2.05-2.65 | 0.95 | 0.15 | 0.30 |
| 30.0 | 2.30-2.80-3.45 | 1.30 | 0.30 | 0.55 |
| 35.0 | 2.65-3.30-3.95 | 1.60 | 0.35 | 0.75 |
| 40.0 | 3.05-3.55-4.50 | 2.05 | 0.45 | 0.90 |
| 45.0 | 3.45-3.80-5.10 | 2.45 | 0.55 | 1.25 |
| 50.0 | 3.80-4.50-6.70 | 3.05 | 0.65 | 1.40 |

Table C.5: Beam EBM1

| Second cycle of loading | | | | |
|---|---|---|---|---|
| Load | Deflections | Rotation | Expansion | Elongation |
| (kN) | D1 - D2 - D3 | (rad) | (mm) | (mm) |
| 0.0 | 0.00-0.00-0.00 | 0.00 | 0.00 | 0.00 |
| 20.0 | 2.20-2.80-3.40 | 1.05 | 0.25 | 0.35 |
| 30.0 | 2.60-3.10-3.90 | 1.15 | 0.40 | 0.65 |
| 35.0 | 3.10-3.75-4.70 | 1.35 | 0.55 | 0.95 |
| 40.0 | 3.95-4.65-5.90 | 2.20 | 0.65 | 1.25 |
| 45.0 | 4.65-5.30-6.75 | 3.10 | 0.70 | 1.45 |
| 50.0 | 5.30-6.50-8.90 | 3.80 | 0.80 | 1.60 |

Table C.6: Beam EBM1

| First cycle of loading | | | | |
|---|---|---|---|---|
| Load | Deflections | Rotation | Expansion | Elongation |
| (kN) | D1 - D2 - D3 | (rad) | (mm) | (mm) |
| 0.0 | 0.00-0.00-0.00 | 0.00 | 0.00 | 0.00 |
| 20.0 | 2.10-2.50-2.80 | 1.05 | 0.25 | 0.45 |
| 30.0 | 2.50-3.10-3.65 | 1.45 | 0.50 | 0.85 |
| 35.0 | 2.90-3.80-4.05 | 1.95 | 0.60 | 1.25 |
| 40.0 | 3.25-4.10-4.90 | 2.45 | 0.70 | 1.35 |
| 45.0 | 3.85-4.60-5.75 | 2.95 | 0.80 | 1.55 |
| 50.0 | 4.30-5.90-9.10 | 3.55 | 0.95 | 1.75 |

Table C.7: Beam EBM2

| Second cycle of loading | | | | |
|---|---|---|---|---|
| Load | Deflections | Rotation | Expansion | Elongation |
| (kN) | D1 - D2 - D3 | (rad) | (mm) | (mm) |
| 0.0 | 0.00-0.00-0.00 | 0.00 | 0.00 | 0.00 |
| 20.0 | 2.40-2.90-3.80 | 1.25 | 0.30 | 0.55 |
| 30.0 | 2.95-3.35-4.45 | 1.55 | 0.65 | 0.95 |
| 35.0 | 3.35-4.10-5.60 | 2.35 | 0.75 | 1.35 |
| 40.0 | 4.10-5.25-7.10 | 3.10 | 0.90 | 1.55 |
| 45.0 | 5.05-6.30-9.05 | 3.65 | 1.10 | 1.70 |
| 50.0 | 5.60-7.80-10.10 | 4.20 | 1.35 | 1.90 |

Table C.8: Beam EBM2

| First cycle of loading | | | | |
|---|---|---|---|---|
| Load | Deflections | Rotation | Expansion | Elongation |
| (kN) | D1 - D2 - D3 | (rad) | (mm) | (mm) |
| 0.0 | 0.00-0.00-0.00 | 0.00 | 0.00 | 0.00 |
| 20.0 | 2.50-3.10-3.45 | 1.15 | 0.35 | 0.45 |
| 30.0 | 2.90-3.65-4.25 | 1.85 | 0.65 | 0.75 |
| 35.0 | 3.25-4.10-4.90 | 2.35 | 0.85 | 0.95 |
| 40.0 | 3.90-4.85-5.90 | 2.90 | 0.95 | 1.35 |
| 45.0 | 4.40-5.20-6.65 | 3.45 | 1.15 | 1.65 |
| 50.0 | 4.80-6.60-7.80 | 4.10 | 1.25 | 1.95 |

Table C.9: Beam CBS1

| Second cycle of loading | | | | |
|---|---|---|---|---|
| Load | Deflections | Rotation | Expansion | Elongation |
| (kN) | D1 - D2 - D3 | (rad) | (mm) | (mm) |
| 0.0 | 0.00-0.00-0.00 | 0.00 | 0.00 | 0.00 |
| 20.0 | 3.20-3.90-4.25 | 1.55 | 0.45 | 0.65 |
| 30.0 | 3.70-4.25-5.30 | 2.05 | 0.80 | 0.95 |
| 35.0 | 4.90-5.60-6.70 | 2.95 | 1.05 | 1.25 |
| 40.0 | 5.45-7.10-8.20 | 3.40 | 1.25 | 1.65 |
| 45.0 | 6.30-8.05-10.30 | 4.05 | 1.35 | 1.85 |
| 50.0 | 7.10-9.75-13.10 | 4.90 | 1.50 | 2.10 |

Table C.10: Beam CBS1

| First cycle of loading | | | | |
|---|---|---|---|---|
| Load | Deflections | Rotation | Expansion | Elongation |
| (kN) | D1 - D2 - D3 | (rad) | (mm) | (mm) |
| 0.0 | 0.00-0.00-0.00 | 0.00 | 0.00 | 0.00 |
| 20.0 | 2.70-3.30-3.90 | 1.40 | 0.45 | 0.60 |
| 30.0 | 3.10-3.95-4.55 | 2.05 | 0.75 | 0.95 |
| 35.0 | 3.60-4.50-5.40 | 2.55 | 0.95 | 1.25 |
| 40.0 | 4.30-5.30-6.35 | 3.25 | 1.25 | 1.45 |
| 45.0 | 4.65-5.70-7.25 | 3.80 | 1.35 | 1.85 |
| 50.0 | 5.30-6.25-8.35 | 4.35 | 1.50 | 2.15 |

Table C.11: Beam CBS2

| Second cycle of loading | | | | |
|---|---|---|---|---|
| Load | Deflections | Rotation | Expansion | Elongation |
| (kN) | D1 - D2 - D3 | (rad) | (mm) | (mm) |
| 0.0 | 0.00-0.00-0.00 | 0.00 | 0.00 | 0.00 |
| 20.0 | 3.30-4.10-4.60 | 1.65 | 0.55 | 0.75 |
| 30.0 | 4.10-4.90-5.90 | 2.40 | 0.95 | 1.05 |
| 35.0 | 5.30-6.10-7.10 | 3.10 | 1.15 | 1.45 |
| 40.0 | 6.10-7.30-9.70 | 3.90 | 1.35 | 1.85 |
| 45.0 | 7.05-8.70-12.10 | 4.60 | 1.50 | 2.05 |
| 50.0 | 7.60-10.20-14.20 | 5.20 | 1.80 | 2.35 |

Table C.12: Beam CBS2

| First cycle of loading | | | | |
|---|---|---|---|---|
| Load | Deflections | Rotation | Expansion | Elongation |
| (kN) | D1 - D2 - D3 | (rad) | (mm) | (mm) |
| 0.0 | 0.00-0.00-0.00 | 0.00 | 0.00 | 0.00 |
| 20.0 | 2.20-2.80-3.20 | 1.30 | 0.35 | 0.45 |
| 30.0 | 2.40-3.10-3.90 | 1.65 | 0.55 | 0.60 |
| 35.0 | 2.90-3.85-4.50 | 2.05 | 0.70 | 0.80 |
| 40.0 | 3.40-4.40-5.30 | 2.55 | 0.85 | 1.05 |
| 45.0 | 3.85-4.85-6.10 | 3.15 | 1.05 | 1.45 |
| 50.0 | 4.50-5.70-7.25 | 3.90 | 1.15 | 1.75 |

Table C.13: Beam EBS1

| Second cycle of loading | | | | |
|---|---|---|---|---|
| Load | Deflections | Rotation | Expansion | Elongation |
| (kN) | D1 - D2 - D3 | (rad) | (mm) | (mm) |
| 0.0 | 0.00-0.00-0.00 | 0.00 | 0.00 | 0.00 |
| 20.0 | 3.00-3.50-4.00 | 1.45 | 0.40 | 0.55 |
| 30.0 | 3.50-4.10-4.90 | 1.95 | 0.70 | 0.80 |
| 35.0 | 4.50-5.30-5.90 | 2.80 | 0.95 | 1.05 |
| 40.0 | 5.10-6.90-7.10 | 3.30 | 1.15 | 1.35 |
| 45.0 | 5.95-7.50-8.70 | 3.90 | 1.25 | 1.60 |
| 50.0 | 6.50-8.20-12.10 | 4.50 | 1.35 | 1.85 |

Table C.14: Beam EBS1

| First cycle of loading | | | | |
|---|---|---|---|---|
| Load | Deflections | Rotation | Expansion | Elongation |
| (kN) | D1 - D2 - D3 | (rad) | (mm) | (mm) |
| 0.0 | 0.00-0.00-0.00 | 0.00 | 0.00 | 0.00 |
| 20.0 | 2.60-3.25-3.60 | 1.40 | 0.40 | 0.60 |
| 30.0 | 3.10-3.90-4.50 | 1.85 | 0.70 | 0.90 |
| 35.0 | 3.40-4.30-5.20 | 2.40 | 0.90 | 1.15 |
| 40.0 | 4.10-5.10-6.30 | 3.10 | 1.15 | 1.60 |
| 45.0 | 4.60-5.45-7.10 | 3.90 | 1.25 | 1.80 |
| 50.0 | 5.10-5.90-8.60 | 4.20 | 1.35 | 2.10 |

Table C.15: Beam EBS2

| Second cycle of loading | | | | |
|---|---|---|---|---|
| Load | Deflections | Rotation | Expansion | Elongation |
| (kN) | D1 - D2 - D3 | (rad) | (mm) | (mm) |
| 0.0 | 0.00-0.00-0.00 | 0.00 | 0.00 | 0.00 |
| 20.0 | 3.30-4.10-4.50 | 1.60 | 0.50 | 0.70 |
| 30.0 | 3.95-4.60-5.60 | 2.15 | 0.95 | 1.05 |
| 35.0 | 5.20-5.90-7.10 | 3.20 | 1.25 | 1.35 |
| 40.0 | 5.70-7.40-9.30 | 3.95 | 1.30 | 1.70 |
| 45.0 | 6.50-8.70-11.30 | 4.10 | 1.40 | 1.90 |
| 50.0 | 7.30-10.05-13.40 | 4.35 | 1.45 | 2.30 |

Table C.16: Beam EBS2

| First cycle of loading | | | | |
|---|---|---|---|---|
| Load | Deflections | Rotation | Expansion | Elongation |
| (kN) | D1 - D2 - D3 | (rad) | (mm) | (mm) |
| 0.0 | 0.00-0.00-0.00 | 0.00 | 0.00 | 0.00 |
| 20.0 | 1.40-1.60-2.00 | 0.65 | 0.20 | 0.35 |
| 30.0 | 1.65-2.00-2.30 | 0.95 | 0.40 | 0.50 |
| 35.0 | 1.85-2.25-2.90 | 1.30 | 0.60 | 0.60 |
| 40.0 | 2.20-2.60-3.10 | 1.60 | 0.75 | 0.70 |
| 45.0 | 2.40-2.90-3.80 | 1.85 | 0.80 | 0.90 |
| 50.0 | 2.60-3.30-4.40 | 2.05 | 0.90 | 1.05 |

Table C.17: Beam DBS2

| Second cycle of loading | | | | |
|---|---|---|---|---|
| Load | Deflections | Rotation | Expansion | Elongation |
| (kN) | D1 - D2 - D3 | (rad) | (mm) | (mm) |
| 0.0 | 0.00-0.00-0.00 | 0.00 | 0.00 | 0.00 |
| 20.0 | 1.65-2.00-2.40 | 0.85 | 0.30 | 0.35 |
| 30.0 | 1.90-2.50-3.20 | 1.25 | 0.45 | 0.60 |
| 35.0 | 2.30-3.00-3.60 | 1.50 | 0.60 | 0.75 |
| 40.0 | 3.05-3.50-4.30 | 2.00 | 0.70 | 0.95 |
| 45.0 | 3.60-4.30-6.20 | 2.40 | 0.80 | 1.05 |
| 50.0 | 3.90-5.10-7.20 | 2.60 | 0.95 | 1.15 |

Table C.18: Beam DBS2

| First cycle of loading | | | | |
|---|---|---|---|---|
| Load | Deflections | Rotation | Expansion | Elongation |
| (kN) | D1 - D2 - D3 | (rad) | (mm) | (mm) |
| 0.0 | 0.00-0.00-0.00 | – | 0.00 | 0.00 |
| 40.0 | 5.20-7.10-9.20 | – | 0.20 | 0.40 |
| 45.0 | 6.30-8.40-10.40 | – | 0.35 | 0.55 |
| 50.0 | 7.90-9.90-11.50 | – | 0.45 | 0.65 |
| 55.0 | 8.75-10.40-13.60 | – | 0.60 | 0.75 |
| 60.0 | 9.60-11.60-15.30 | – | 0.75 | 0.90 |
| 65.0 | 10.20-12.10-16.90 | – | 0.85 | 1.05 |
| 70.0 | 11.60-13.50-17.80 | – | 0.90 | 1.15 |
| 80.0 | 12.40-15.00-19.10 | – | 1.00 | 1.35 |
| 90.0 | 13.50-16.10-20.30 | – | 1.10 | 1.55 |
| 100.0 | 14.10-16.90-21.60 | – | 1.25 | 1.85 |
| 110.0 | 14.90-17.50-23.05 | – | 1.30 | 2.15 |
| 120.0 | 15.60-18.70-24.10 | – | 1.40 | 2.45 |

Table C.19: Beam CBD1

| Second cycle of loading | | | | |
|---|---|---|---|---|
| Load | Deflections | Rotation | Expansion | Elongation |
| (kN) | D1 - D2 - D3 | (rad) | (mm) | (mm) |
| 0.0 | 0.00-0.00-0.00 | – | 0.00 | 0.00 |
| 40.0 | 7.10-9.10-12.40 | – | 0.30 | 0.60 |
| 45.0 | 8.30-10.60-14.10 | – | 0.60 | 0.85 |
| 50.0 | 10.20-11.65-15.20 | – | 0.70 | 1.05 |
| 55.0 | 11.40-13.40-16.60 | – | 0.80 | 1.35 |
| 60.0 | 12.60-15.60-18.30 | – | 0.90 | 1.60 |
| 65.0 | 13.60-17.10-19.90 | – | 1.15 | 1.75 |
| 70.0 | 14.60-17.90-22.10 | – | 1.35 | 1.85 |
| 80.0 | 16.10-19.30-24.10 | – | 1.45 | 2.35 |
| 90.0 | 17.30-20.60-25.30 | – | 1.65 | 2.65 |
| 100.0 | 18.10-22.10-27.30 | – | 1.80 | 2.85 |
| 110.0 | 19.50-23.30-29.05 | – | 1.95 | 3.15 |
| 120.0 | 20.30-24.70-30.10 | – | 2.10 | 3.45 |

Table C.20: Beam CBD1

| First cycle of loading | | | | |
|---|---|---|---|---|
| Load | Deflections | Rotation | Expansion | Elongation |
| (kN) | D1 - D2 - D3 | (rad) | (mm) | (mm) |
| 0.0 | 0.00-0.00-0.00 | – | 0.00 | 0.00 |
| 40.0 | 3.60-5.10-6.20 | – | 0.15 | 0.35 |
| 45.0 | 4.30-6.40-7.30 | – | 0.25 | 0.45 |
| 50.0 | 4.90-7.40-8.50 | – | 0.40 | 0.55 |
| 55.0 | 5.70-8.90-9.60 | – | 0.55 | 0.70 |
| 60.0 | 6.60-9.60-10.70 | – | 0.70 | 0.85 |
| 65.0 | 7.50-10.10-12.10 | – | 0.80 | 1.00 |
| 70.0 | 8.10-11.50-13.20 | – | 0.85 | 1.10 |
| 80.0 | 8.10-11.90-14.10 | – | 1.00 | 1.30 |
| 90.0 | 9.50-12.55-15.20 | – | 1.05 | 1.45 |
| 100.0 | 10.10-13.20-16.30 | – | 1.10 | 1.65 |
| 110.0 | 11.05-14.50-17.05 | – | 1.15 | 1.85 |
| 120.0 | 11.60-14.80-18.20 | – | 1.20 | 2.15 |

Table C.21: Beam EBD1

| Second cycle of loading | | | | |
|---|---|---|---|---|
| Load | Deflections | Rotation | Expansion | Elongation |
| (kN) | D1 - D2 - D3 | (rad) | (mm) | (mm) |
| 0.0 | 0.00-0.00-0.00 | – | 0.00 | 0.00 |
| 40.0 | 5.10-6.20-9.30 | – | 0.20 | 0.55 |
| 45.0 | 6.10-7.40-10.50 | – | 0.30 | 0.85 |
| 50.0 | 7.30-8.50-12.10 | – | 0.55 | 0.95 |
| 55.0 | 8.80-9.40-13.70 | – | 0.70 | 1.15 |
| 60.0 | 9.40-10.60-15.40 | – | 0.85 | 1.35 |
| 65.0 | 10.60-11.90-16.80 | – | 0.95 | 1.50 |
| 70.0 | 11.20-12.80-17.60 | – | 1.15 | 1.75 |
| 80.0 | 12.10-14.10-19.40 | – | 1.25 | 1.95 |
| 90.0 | 13.05-15.30-21.10 | – | 1.35 | 2.20 |
| 100.0 | 14.80-16.20-22.20 | – | 1.45 | 2.40 |
| 110.0 | 15.50-17.10-23.00 | – | 1.60 | 2.65 |
| 120.0 | 15.90-18.50-24.60 | – | 1.75 | 2.95 |

Table C.22: Beam EBD1

| First cycle of loading | | | | |
|---|---|---|---|---|
| Load | Deflections | Rotation | Expansion | Elongation |
| (kN) | D1 - D2 - D3 | (rad) | (mm) | (mm) |
| 0.0 | 0.00-0.00-0.00 | 0.00 | 0.00 | 0.00 |
| 20.0 | 0.80-0.90-1.30 | 1.05 | 0.25 | 0.40 |
| 30.0 | 1.35-2.45-3.60 | 1.35 | 0.35 | 0.70 |
| 35.0 | 2.00-3.65-4.10 | 1.75 | 0.55 | 0.90 |
| 40.0 | 2.75-3.90-4.70 | 2.25 | 0.75 | 1.10 |
| 45.0 | 3.10-4.20-5.50 | 2.95 | 0.80 | 1.40 |
| 50.0 | 4.10-5.60-6.80 | 3.70 | 1.10 | 1.75 |

Table C.23: Beam CBM3

| Second cycle of loading | | | | |
|---|---|---|---|---|
| Load | Deflections | Rotation | Expansion | Elongation |
| (kN) | D1 - D2 - D3 | (rad) | (mm) | (mm) |
| 0.0 | 0.00-0.00-0.00 | 0.00 | 0.00 | 0.00 |
| 20.0 | 1.50-2.45-3.90 | 1.35 | 0.35 | 0.50 |
| 30.0 | 2.20-3.40-4.70 | 1.85 | 0.55 | 0.70 |
| 35.0 | 2.80-4.20-5.50 | 2.30 | 0.80 | 0.95 |
| 40.0 | 3.40-5.40-6.30 | 2.90 | 1.10 | 1.20 |
| 45.0 | 4.10-6.10-8.10 | 3.60 | 1.30 | 1.45 |
| 50.0 | 6.55-8.80-11.50 | 4.20 | 1.50 | 1.85 |

Table C.24: Beam CBM3

| First cycle of loading | | | | |
|---|---|---|---|---|
| Load | Deflections | Rotation | Expansion | Elongation |
| (kN) | D1 - D2 - D3 | (rad) | (mm) | (mm) |
| 0.0 | 0.00-0.00-0.00 | 0.00 | 0.00 | 0.00 |
| 20.0 | 1.85-2.20-2.70 | 1.00 | 0.20 | 0.40 |
| 30.0 | 2.10-2.95-3.20 | 1.35 | 0.40 | 0.80 |
| 35.0 | 2.80-3.60-3.95 | 1.85 | 0.55 | 1.20 |
| 40.0 | 3.10-3.80-4.20 | 2.35 | 0.70 | 1.30 |
| 45.0 | 3.60-4.10-5.20 | 2.85 | 0.80 | 1.40 |
| 50.0 | 4.10-5.10-8.80 | 3.40 | 0.90 | 1.60 |

Table C.25: Beam EBM3

| Second cycle of loading | | | | |
|---|---|---|---|---|
| Load | Deflections | Rotation | Expansion | Elongation |
| (kN) | D1 - D2 - D3 | (rad) | (mm) | (mm) |
| 0.0 | 0.00-0.00-0.00 | 0.00 | 0.00 | 0.00 |
| 20.0 | 2.10-2.80-3.70 | 1.20 | 0.25 | 0.45 |
| 30.0 | 2.80-3.30-4.30 | 1.45 | 0.55 | 0.85 |
| 35.0 | 3.10-3.90-5.10 | 2.20 | 0.70 | 1.25 |
| 40.0 | 3.90-4.70-6.10 | 3.00 | 0.90 | 1.45 |
| 45.0 | 4.80-5.90-7.80 | 3.50 | 1.05 | 1.65 |
| 50.0 | 5.10-7.20-9.60 | 4.10 | 1.25 | 1.85 |

Table C.26: Beam EBM3

# Bibliography


[1] Kotsovos M. D. Compressive force path: Basis for ultimate limit state reinforced concrete design. *ACI Structural Journal*, Vol. 85(No.1):pp. 68–75, Jan.–Feb. 1988.

[2] Subedi N. K. Reinforced concrete beams with plate reinforcement for shear. *Proceedings. Institution of Civil Engineers*, Vol. 87(Part:2), pp. 377–399, Sept. 1989.

[3] Dowding C. H. Blast vibration monitoring and control. *Prentice-Hall Inc*, USA, 1985.

[4] Irwin A.W. Analysis of tall shear wall buildings including in-plane floor deformation. *Build. International Applied Science Publishers*, London, 1975.

[5] Coull A. and Irwin A. W. Model investigation of shear wall structure. *ASCE Proceedings. Journal of the Structural Division*, Vol. 52(No. ST6), pp. 1223–1237, Jun. 1972.

[6] Irwin A. W. Static and dynamic tests on model shear-wall. *Proceedings. Institution of Civil Engineers*, Vol. 51, pp. 701–710, Apr. 1972.

[7] Irwin A. W. Analysis of shear wall structures. *Internal Research Report - Heriot-Watt University*, No.3, Feb. 1976.

[8] Cassaro M. K. and Romero E. M. The Mexico earthquakes-1985. *American Society of Civil Engineers*, USA, 1987.

[9] Irwin A. W. Human response to dynamic motion of structures. *The Structural Engineer*, Vol. 56A(No. 9), pp. 237–244, Sept. 1978.

[10] Winokur A. and Gluck J. Ultimate strength analysis of coupled shear walls. *ACI Structural Journal*, Vol. 65, pp. 1029–1036, Dec. 1968.

[11] Paulay T. Coupling beams of reinforced concrete shear walls. *ASCE Proceedings. Journal of the Structural Division*, Vol. 97(No. ST3), pp. 843–864, Mar. 1971.

[12] Chitty L. On the cantilever composed of a number beams interconnected by cross bars. *Magazine and Journal of Science*, Vol. 38, pp. 685–699, Oct. 1947.

[13] Green N. B. Bracing walls for multistorey buildings. *ACI Structural Journal*, Vol. 49(No. 18), pp. 233–248, Apr. 1952.

[14] Beck H. Ein neues berechnungverfahren fuer gegliederte scheiben, dargestellt am beispiel der vierendeeltraegers. *Heft 12*, Vol.31, pp. 443–463, 1956. In German.

[15] Beck H. Contribution to the analysis shear walls. *ACI Structural Journal*, Vol. 59(No. 08), pp. 1055–1069, Aug. 1962.

[16] Rosman R. Beitrag zur statischen berechnung waagrecht belaster quewaende bei hochbauten. *Der Bauingenieur*, Heft 4(part I), pp. 133–136, 1960. In German.

[17] Rosman R. Approximate analysis of shear wall subjected to lateral loads. *ACI Structural Journal*, Vol. 61(No. 06), pp. 717–733, 1964.

[18] Naumann W. and Walters H. Bericht zur statischen berechnung waagrecht belasteter quuerwande bei hochbauten. Vergleichende betrachtung zu den berluntersuchung. *Der Bauingenieur (Berlin)*, Vol. 36, pp. 311–313, 1961. In German.

[19] Dechauchy A. Wind bracing of tall buildings. *Annales de l'institut du batiment et des travaux public*, Vol. 17, pp. 93–108, 1964. In French.

[20] Albiges M. and Goulet J. Wind bracing of tall buildings. *Annales de l'Institut du batiment et des Travaux publics*, Vol. 149, pp. 437–500, May 1960. In French.

[21] Coull A. and Choudhury R. J. Analysis of coupled shear wall. *ACI Structural Journal*, Vol. 64(No. 9), pp. 587–593, Sept. 1967.

[22] Coull A. and Choudhury R. J. Stresses and deflections in coupled shear walls. *ACI Structural Journal*, Vol. 64(No. 2), pp. 65–72, Feb. 1967.

[23] Coull A. and Puri R. D. Analysis of pierced shear wall. *ASCE Proceedings. Journal of the Structural Division*, Vol. 94(No. ST1), pp. 71–82, Jan. 1968.

[24] Coull A. and Irwin A.W. Analysis of load distribution in multi-storey shear wall structures. *The Structural Engineer*, Vol. 48(No. 8), pp. 301–306, Aug. 1970.

[25] Coull A. Stiffening of coupled shear walls against foundation movement. *The Structural Engineer*, Vol. 52(No. 1), pp. 23–26, Jan. 1974.

[26] Chan H.C. and Kuang J.S. Effect of single deep beam on twin shear walls with rational coupling. *Proceedings. Institution of Civil Engineers*, Vol.85(Part 2), pp. 503–515, 1988.

[27] Coull A. Stresses and deflections in coupled shear walls. *ACI Structural Journal*, Vol. 64, pp. 587–593, 1967.

[28] Ngo D. and Scordelis A.C. Finite element analysis of reinforced concrete. *ACI Structural Journal*, Vol. 65(No. 9), pp. 757–766, Sept. 1968.

[29] Cervenka V. and Gerstle K. H. Inelastic analysis of reinforced concrete panels. *IABSE Publication*, Vol. 31(II–Part:1), pp. 32–43, 1971.

[30] Cervenka V. and Gerstle K. H. Experimental verification and application. *IABSE Publication*, Vol. 30(II– Part:2), pp. 25–37, 1971.

[31] Yuzugullu O. and Schnobrich W.C. A numerical procedure for the determination of the behaviour of shear wall frame systems. *ACI Structural Journal*, Vol. 70(No. 74), pp. 474–479, Jul. 1973.

[32] Umemura H., Aoyama H. and Liao Ming H. Studies on reinforced concrete shear wall and frame masonry shear walls. *Research Report*, University of Tokyo, Jun. 1964.

[33] Darwin D. and Pecknold D.A. Analysis of reinforced concrete shear panels under cyclic loading. *ASCE Proceedings. Journal of the Structural Division*, Vol. 102(No. ST2), Feb. 1976.

[34] Mamet J.C., Mufti A.A. and Jaeger L.J. New development in the analysis of shear wall buildings. *Department of Civil Engineering and Applied Mechanics McGill University Montreal, Quebec*, pp. 203–205, 1973.

[35] Bhatt P. Effect of beam-shear wall junction deformations on the flexibility of the connecting beams. *Building Science*, Vol. 8, pp. 149–151, 1973.

[36] Hall A. S. Joint deformations in building frames. *Proceedings. Institution of Civil Engineers* , pp. 60–62, 1969. Australia.

[37] Macleod I.A. Structural analysis of wall system. *The Structural Engineer*, Vol. 55(No. 11), pp. 487–497, Nov. 1977.

[38] Cheung Y.K. Chapter 38 : Tall building 2. *Handbook of Structural concrete*, pp. 487–497, 1983. Pitman London. Edited F.K. Kong et al.

[39] Macleod I.A. and Hosny H. M. Frame analysis of shear wall cores. *Proceedings. Institution of Civil Engineers* , Part 2, pp. 280–299, June 1991.

[40] Vlasov V.Z. Thin walled elastic beams. *This was translated for the Russian/Israeli program for scientific translation*, Jerusalem, Feb. 1961.

[41] Nobuaki S. Inelastic analysis of reinforced concrete shear wall structures: Application and experimental verification. *IABSE Colloquium Delft 1981,87-700*, pp. 687–700, 1981.

[42] Duen H. and Chi Ho. L. Analysis of shear wall and shear core assembly subjected to lateral and torsional loading. *Proceedings. Institution of Civil Engineers*, Vol. 79(Part 2), pp. 119–133, Mar. 1985.

[43] Ha K.H. and Desbois M. Finite element for tall building analysis. *Computers and Structures*, Vol. 33(No. 1), pp. 249–255, 1989.

[44] Kwan A. K. H. Analysis of coupled wall-frame structures by frame method with shear deformation allowed. *Proceedings. Institution of Civil Engineers.*, Vol. 91, pp. 273–297, Part 2 1991.

[45] Kwan A. K. H. Analysis of coupled wall/frame structures by frame method with shear deformation allowed. *Computers and Structures*, Vol. 48(No. 4), pp. 615–625, 1993.

[46] Paulay T. Elasto-plastic analysis of coupled shear walls. *ACI Structural Journal*, Vol. 67(No. 60), pp. 915–922, Nov. 1970.

[47] Gluck J. Elasto-plastic analysis of coupled shear walls. *ASCE Proceedings. Journal of the Structural Division*, (No. ST8), pp. 1743–1760, Aug. 1973.

[48] Pekau O.A. Elasto-plastic analysis of coupled shear walls. *Journal of Structural Engineering*, Vol. 3(No. 2), pp. 87–95, 1981.

[49] Branzan I. Berechnung von stahlbetonscheiben mit einer offnungsreihe in plastishen bereich. *Die Bautecnick*, Vol. 46, pp. 415–418, Dec. 1969. In German.

[50] Paulay T. and Binney J.R. Diagonal reinforced coupling beams of shear walls. *ACI Structural Journal*, Vol. SP–42(No. 26), Jun. 1975.

[51] Yamada M., Kawamura H. and Katagihara K. Reinforced concrete shear walls with openings. *ACI Structural Journal*, Vol. SP–42(No. 25), Jun. 1975.

[52] Paulay T. and Santhakumer A.R. Ductile behaviour of shear walls. *ASCE Proceedings. Journal of the Structural Division*, Vol. 102(No. ST1), Jan. 1976.

[53] Irwin A.W. and Young R.W. Tests on reinforced concrete model shear wall buildings. *Proceedings. Institution of Civil Engineers.*, Vol. 61(Part 2), pp. 363–177, Mar. 1976.

[54] Paulay T. Design aspects of shear walls for seismic areas. *Canadian Journal of Civil Engineering*, Vol. 2, pp. 321–342, 1975.

[55] Chana P.S. Analytical and experimental studies of shear failures in reinforced concrete beams. *Proceedings. Institution of Civil Engineers*, Vol. 85(Part 2), pp. 609–628, Dec. 1988.

[56] Subedi N. K. Ultimate strength analysis of reinforced concrete coupling beams. *The Structural Engineer*, Vol. 68(No. 3), Feb. 1990.

[57] Kotsovos M. D. Designing RC beams in compliance with the concept of the compressive force path. *The Structural Engineer*, Vol. 67, pp. 177–184, 1989.

[58] Kotsovos M. D., Bobrowski J. and Eibl J. Behaviour of RC T-beams in shear. *The Structural Engineer*, Vol. 65B(No. 1), pp. 1–10, Mar. 1987.

[59] Bobrowski J. and Bardham-Roy B. K. Method of calculating the ultimate strength of reinforced and prestressed beams in combined flexure and shear. *The Structural Engineer*, Vol. 47, pp. 197–209, 1969.

[60] Kotsovos M. D. and Lefas I. D. Behaviour of rc beams designed in compliance with the compressive force path. *ACI Structural Journal*, Vol. 87(No. 2), pp. 127–139, Mar.–Apr. 1990.

[61] Kotsovos M. D. and Bobrowski J. Design model for structural concrete based on C.F.P. *ACI Structural Journal*, Vol. 90, pp. 12–20, Jan.–Feb. 1993.

[62] Kotsovos M. D. and Newman J. D. Effect of the boundary conditions on the behaviour of the concrete under concentrations of load. *Magazine of Concrete Research*, Vol. 33, pp. 161–170, Sept. 1981.

[63] Kotsovos M. D. A fundamental explanation of the behaviour of reinforced concrete beams in flexure based on the properties of concrete under multiaxial stress. *Material and Structures*, Vol. 15, pp. 529–539, 1982.

[64] British Standards Institution. Method of making and curing test specimens. *BS 1881 : Part 5*, 1970.

[65] British Standards Institution. Method of testing concrete for strength. *BS 1881 : Part 4*, 1970.

[66] Expanded metal steel and aluminium meshes. *Leaflet No. IP2h*, Dec. 1984.

[67] Expanded Metal Ltd. Expanded metal meshes. *Leaflet No. CI/SfB (Hh2) (Jh4)*, Jun. 1985.

[68] Irwin A. W. Design of shear wall buildings. *CIRIA Report 102, 1984.*

[69] Subedi N. K. Reinforced concrete deep beams method of analysis. *Proceedings. Institution of Civil Engineers*, Vol. 85(Part:2), pp. 1–30, Mar. 1988.

[70] Kong F. K. Reinforced concrete deep beams. *Van Nostrand Reinhold*, USA, 1990.

[71] Kotsovos M. D. Mechanism of shear failure. *Magazine of Concrete Research*, Vol. 35(No. 123), pp. 99–106, Jun. 1983.

[72] Abid S. Analysis of concrete structures with conventional and expanded metal reinforcement. *Thesis for degree of MSc*, Heriot-Watt University, Sept. 1988.

[73] Ziara M. M. The influence of confining the compression zone in the design of structural concrete beams. *Thesis for degree of Ph.D*, Heriot-Watt University, 1993.

[74] Collins M. P. Towards a rational theory for RC members in shear. *Journal of Structural Division*, ASCE, Vol. 104(No.4), April 1978, pp. 649–666.

[75] Vecchio F. J. and Collins M. P. The response of reinforced concrete to in-plane shear and normal stresses. *Technical Report Publication* No. 82-03, Department of Civil Engineering, University of Toronto, March 1982, 332 pp.

[76] Vecchio F. J. and Collins M.P. Predicting the response of the reinforced concrete beams subjected to shear using modified compression field. *ACI Structural Journal*, Vol. 85(No.3), May-June 1988, pp. 235–268.

[77] Schlaich D. and Shafer K. Design and detailing of structural concrete using strut-and-tie models. *The Structural Engineer*, Vol. 69(No.6), March 1991.

[78] Kotsovos M. D. A fundamental explanation of the behaviour of reinforced concrete beams in flexure based on the properties of concrete under multiaxial stress. *Materials and Structures*, Reasearch and Testing (RILEM, Paris) Vol. 15(No. 90), Nov-Dec. 1982, pp. 529–537.